University of Nottingham
Department of Civil Engineering

Numerical Modelling of Connections in Composite Frames

by

Bashir Ahmed
B.Sc., M.Sc.

Thesis submitted to the University of Nottingham for the degree of Doctor of Philosophy

November 1996

Dedicated to:

my father Mr. Nazir Ahmed,
mother Mrs. Nurjahan Ahmed
and wife Mrs. Ferdous Akhter

Their constant love, support and encouragement
made it possible.

Contents

List of Figures

Chapter 1

Chapter 2

Chapter 5

Chapter 6

Chapter 8

Chapter 9

List of Tables

Acknowledgements

I am greatly indebted my supervisor Professor D. A. Nethercot, Head of Civil Engineering, University of Nottingham, for his constant guidance, generous help, continued encouragement and unfailing enthusiasm throughout the process of completing this thesis.

Thanks are due to the Commonwealth Scholarship Commission for sponsoring the research work, Manchester Computer Centre for allowing the use of the super computer, Cripps Computer Centre and Department of Civil Engineering, University of Nottingham for the local computing facilities.

I would like to thank Dr. T. Q. Li, research associate; University of Nottingham, for providing all his published and unpublished test results for verifying the numerical models and for his suggestions during the finite element modelling. Thanks are due to Dr. Jean-Pierre Jaspart - University of Liege, Belgium and Mr. Klaus Weynand - Institute of Steel Construction, RWTH Aachen, Germany for providing the SERICON database of composite connection test results, Professor Roberto Leon - Georgia Institute of Technology, USA for providing his published and unpublished test results, Dr. David Moore - BRE, UK for providing the test results of Dr. Jarrett and Professor David Anderson - University of Warwick, UK for providing the test results of Dr. Najafi, A. A. - all these results were used to verify the proposed design procedures of composite endplate, finplate and angle cleated connections.

I would like to thank Bangladesh University of Engineering and Technology (BUET) for the study leave provided for the course of research.

Finally thanks are due to my wife Polash for her patience, support and encouragement throughout the duration of research. It would have been impossible for me to complete this thesis in such a manner without her support.

Declaration

I declare that this thesis is the result of my own work. No part of this thesis has been submitted to any other University or other educational establishment for a Degree, Diploma or other qualification (except for publication).

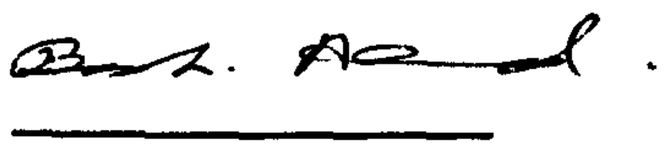

(Bashir Ahmed)

ABSTRACT

The main objective of this thesis was to develop numerical modelling procedures for composite connections and to use results generated in conjunction with data from other sources as the basis for the preparation of design procedures.

The finite element method has been used for the numerical simulation of composite endplate connections. The developed model was verified by comparing both local measures of response and overall behaviour with test results. The validated model was then used in conjunction with theoretical analysis to study the behaviour of composite endplate connections for variable shear to moment ratios. This permitted the identification of those cases for which changes in the shear to moment ratio affects the connection's moment capacity. The model was also used in conjunction with theoretical analysis to study the effect of varying levels of axial column loading on the connection moment capacity. Results of both studies indicated a need for modifications to the equations of EC3 (for bare steel connections but which are also applicable to composite connections) that consider the interaction with column loading. These are: the equations for column web compression resistance, column web shear resistance and the bolt force. Using the FEM results, available test results and EC3 and EC4 equations for the determination of basic component forces, design procedures for composite flush endplate, finplate and angle cleated connections are proposed.

Predictions from the design method have been compared with a total of 53 test and finite element results for the flush endplate connections (32 laboratory tests from 7 different sources plus a further 21 numerical results) so as to provide validation over the full range of parameters. These comparisons gave an overall prediction to test ratio of 0.99 with a standard deviation of 0.14, thereby demonstrating that the proposed method can accurately predict the resistance of composite flush endplate connections under a variety of different connection arrangements and loading conditions. Similarly,

the prediction from the design method was compared with 6 finplate test results which gave an average prediction to test ratio of 1.06 with a standard deviation of 0.18. Comparisons for the angle cleated connection using 16 test results from 4 different sources gave an average prediction to test ratio of 0.98 with a standard deviation of 0.13.

Theoretical studies have been performed to develop equations to predict the initial stiffness for composite endplate connections and these have been verified against test results. Suggestions to predict the available rotation capacity of flush endplate connections have also been made. This two methods has been combined with the moment capacity model to develop a prediction method for the overall behaviour of the flush endplate connections.

The finite element method has also been used to develop a numerical simulation of non-sway composite frames. Comparisons of results show good agreement with the observed test behaviour. It has been found that it is possible to model the non-sway frames in a way that can predict the frame moment distribution, connection moment - rotation response and the beam load displacement history with sufficient accuracy. This provides an economic tool to study different aspects of the behaviour of composite non-sway frames. A numerical model has been developed for un-braced steel frames by simplifying the composite frame model. This model was verified using numerical results selected from the work of other researchers. Using the model for steel frames, studies were conducted for sway behaviour which provide guidance on behaviour suitable as a basis for developing design procedures.

Notation

τ	Column web shear stress
ϕ	Connection rotation
Φ	Curvature of beam
η	Ratio of beam loads on two sides of the connection
β	To be taken as 1.25
Δ	Sway deflection
Δ_b	Elongation of bolt
Δ_c	Compression deformation of column web
Δ_b	Elongation of bolt
Δ_n	Non dimensional sway
Δ_b	Elongation of bolt
Δ_{pin}	Sway of a frame with pin connections
γ_{Mo}	Material safety factor
σ_m	von - Mises stress
σ_n	Applied column stress
σ_x	Horizontal stress in the column web due to applied load
σ_y	Vertical stress in the column web due to applied load
τ_{xy}	Developable column web shear stress due to applied load
a	Throat thickness of weld
A_b	Area of one bolt
A_r	Reinforcement area
A_v	Area of column resisting the shear
b_{bf}	Width of beam flange
b_{cf}	Width of column flange
b_{eff}	Effective depth of column web resisting transverse compression
$b_{eff\text{-}b}$	Effective depth of column web for calculating buckling resistance

d_{bi}	Distance of centreline of i th bolt row from bottom flange centreline
$d_{c,bw}$	Depth of compression of the beam web
d_o	Diameter of Bolt
d_h	Diameter of Bolt hole
D_c	Depth of column section
D_{fp}	Depth of finplate
D_r	Distance of rebar from the bottom flange centreline
e	Distance of outer bolt from the column flange end
E	Young's modulus
$f_{a,bw}$	Available compressive stress of the beam web considering shear
f_b	Ultimate strength of bolt
f_{bf}	Beam flange ultimate strength
f_c'	Cylinder compressive strength of concrete
f_{cw}	Ultimate strength column web
f_{cf}	Ultimate strength of column flange
f_u	Ultimate strength of reinforcement
f_{bw}	Beam web ultimate strength
f_{usc}	Seating cleat ultimate strength
f_{uw}	Ultimate strength of weld
f_{uwc}	Finplate or web cleat ultimate strength
$f_{y,cw}$	Yield strength column web
$f_{y,cf}$	Yield strength column flange
f_{yb}	Yield strength of beam
f_p	Ultimate strength of endplate
$F'_{c,bf}$	Final compressive force in the bottom flange
F_b	Developable bolt force
F_b'	Final bolt force
$F_{c,b}$	Developable beam compressive force

$F_{c,bf}$	Developable compression force in bottom flange
$F_{c,bfl}$	Developable compression force in bottom flange of the far side of the connection
$F_{c,buckle}$	Column web buckling force
$F_{c,bw}$	Beam web compressive force
$F_{c,cw}$	Attainable connection compressive force
F_{cj}	Connection compression force
F_c	Compression force required for balancing equilibrium
$F_{c.Rd}$	Transverse compressive force in the column web
$F_{cs,shear}$	Effective shear force in the column web
F_{cs}	Column web shear resistance under non-symmetric loading
F_h	Horizontal shear present in the column web
F'_r	Final rebar force
F_r	Developable rebar tensile force
F_R	Reduction factors to calculate the available shear strength and compression resistance
F_R	Strength reduction factors
H_1	Height of the lower storey of a frame
H_b, h_s	Depth of steel beam
H_T	Total height of a frame
h_c	Depth of concrete slab
h_{cs}	Effective depth of concrete slab
h_{sc}	Depth of column section
I	Moment of inertia
k, k_1, k_2	Reduction factor for shear stud force
K	Total number of bolt rows present in a connection
K_b	Stiffness of the bolt
K_{col}	Stiffness of the column

K_i	Initial stiffness of the connection
K_n	Non dimensional connection stiffness
K_r	Stiffness of rebar, reduction factor for column flange resisting moment in tension
K_{rb}	Reduction factor for bolt force observed in the FE analyses
K_s	Stiffness of shear studs
L_2	Span of beam
m	Distance of the bolt from column web
M	Connection moment capacity
M_{c2}	Moment present on the far side of the connection
M_u	Ultimate moment of a composite beam
M_y	First yield moment of a composite beam
n	Number of shear connectors
N_b	Number of bolt rows in tension, no of span
N_{bw}	Number of bolts connecting the web cleat or the finplate to the beam web. For a connection with double web cleats the bolts will be in double shear so the value is twice the actual number of bolts
N_{cb}	Number of bolts connected to the beam flange and seating cleat
N_{con}	Number of connections in a frame
N_{cs}	Number of bolts connecting the seating cleat to the column flange
N_{cw}	Number of bolts connecting the web cleat (or cleats) to the column flange
P	Applied vertical load
p	Bolt pitch, shear stud pitch
P_r, P_l	Horizontal compression forces on the two sides of column web
P_u	Ultimate load capacity
P_v	Attainable beam shear force
R_{Rd}	Shear resistance of a single shear stud
t_{bf}	Thickness of beam flange

t_{cf}	Thickness of column flange
t_{cw}	Thickness of column web
t_{fp}	Thickness of the finplate
t_p	Thickness of endplate
$t_{sc.h}$	Thickness of the horizontal leg of the seating cleat
$t_{sc.v}$	Thickness of the vertical leg of the seating cleat
$t_{wc.b}$	Thickness of the web cleat connected to the beam web
$t_{wc.c}$	Thickness of the web cleat connected to the column flange
V_{Rd}	Column web shear resistance
x	Distance of applied load from column flange
x_1	Distance of centreline of bolts connected to beam web from column flange
y	Distance of neutral axial from bottom flange centreline

Chapter 1

Introduction and review of literature

1.1 Introduction

The traditional method of analysing and hence designing a composite frame structure assumes the beam-column connections to be either pinned or rigid. The actual behaviour of the connection is neither completely pinned nor fully rigid; it is somewhere in between. This behaviour of the connection is known as semi-rigid.

Figure 1-1 shows the moment diagram for a beam loaded with a uniformly distributed load W, having span of L with different support conditions. It is clear from Figure 1-1 that the assumption of a pin connection overestimates the span moment and deflections and underestimates the support moment. A rigid connection assumption underestimates the mid span moment and deflection, while it overestimates the support moment.

Figure 1-2 shows a composite beam and the stress distribution for hogging and sagging bending. It is known that in the hogging region the concrete slab is not effective due to cracking. To produce the necessary tensile force, a significant contribution from the reinforcement is required, resulting in a large depth of steel beam, when a fixed end connection is assumed. This also produces a larger moment capacity in the sagging region, since the concrete is in compression in this region and will never be fully utilised.

From Figure 1-1 it can be seen that the sum of the connection moment and the span moment is always equal to $\frac{W.L^2}{8}$. So if it is possible to know the connection moment capacity, then it should be possible to design the members more efficiently. After the formation of a plastic hinge at the connection, the moment may be redistributed to the mid span, in such a way so that the sum of the connection moment and the mid span moment is still $\frac{W.L^2}{8}$.

The formation of the plastic hinge at the beam-to-column connection (referred to as joint or connection later on) requires that the connection must posses sufficient rotation capacity. This means that two things in addition to the connection moment capacity are to be known, they are: the rotation required (required rotation capacity) to achieve the desired degree of moment redistribution and the actual rotation that can be achieved (available rotation capacity) from the connection used. It is therefore also necessary during the design phase to select a percentage of moment redistribution for which the required rotation is less than the available rotation capacity. Clearly the total moment at the beam mid span after the redistribution cannot be greater than the beam sagging moment capacity. So for an efficient design the following properties need to be known:

- Connection moment capacity
- Beam sagging moment capacity
- Connection rotation capacity
- Required rotation capacity for the selected moment redistribution

1.2 Types of composite connection in use

Before the introduction of composite beams in the 1970's frames were designed as bare steel frames. With the introduction of composite beams the design of composite frames

started. Figure 1-3 shows a few type of connections that are used to form the joint between the beam and the column. Figure 1-4 shows the typical composite details. The connection types that are used in composite construction are:

a. Endplate

b. Finplate

c. Angle cleats

Endplate connections can be:

i Flush endplate

ii Extended endplate

iii Partial depth endplate

Angle cleated connections can be:

i Web side cleat (single or double)

ii Top or bottom cleat

ii Combination of web and top or bottom cleat

1.3 Study on composite connections and frames

The study of semi-rigid composite connections started in 1970. Since then approximately 200 composite connections have been tested all over the world. Using the test results, attempts were made to produce simplified prediction methods. Equations for moment capacity and rotation capacity, and mechanical models to predict the response have been proposed on the basis of the test results. Numerical studies have also been performed, but in a very limited way. A few tests have been performed on full scale composite frames. Due to the complicated characteristics and the limitation of the computing facilities, no structural design code at present covers the detailed design approaches for frames with semi-rigid composite connections. The

next sections describe briefly the experimental and analytical work carried out in this field to study the moment capacity and rotation capacity of composite connections.

1.4 Tests on composite connections and frames

The interaction between the composite slab and the components of the steel connection makes the connection behaviour more complicated than the bare steel connections. To clearly understand such response the direct method is to carryout full scale tests. The results of experimental work not only provide understanding of the response of the composite connections, but also supply the necessary information for comparison against analytical work. The first tests on semi-rigid composite connections were conducted by Johnson and Hope-Gill [1-1] in 1972. They conducted five tests on composite cleated connections, with flat slabs. Since then more than 200 connection specimens have been tested in different countries all over the world. Zandonini (1989) carried out a review [1-2] of tests on connections up to 1987, which is summarised in Table 1-1. Xiao (1994) made a review [1-3] of tests from 1985 to 1994, which is summarised in Table 1-2. From these tables it can be observed that connection moment capacity can vary from 20 kN•m to 600 kN•m, ultimate rotation values can vary from 7.2 mrad to more than 70 mrad. Failure in a composite connection can be either non ductile (bolt failure, reinforcement fracture, slab failure in shear etc.) or ductile (excessive deformation of connection components). From the conducted tests 14 different failure modes have been identified (as shown in Figures 7-1b, 8-1a and 8-1b). These are:

i Yield of column flange in bending

ii Yield or local buckling of column web in transverse compression

iii Yield or local buckling of column web panel in shear

iv Yield or buckling of beam flange in compression

v Yield or buckling of beam web in compression and shear

vi Yield or fracture of slab reinforcement in tension

vii Anchorage failure of reinforcement of the external connections

xi Yield or fracture of connecting bolts in tension

viii Failure of slab in shear

ix Crushing failure of concrete slab against column face on the lower moment side of the connection (highly non-symmetrically loaded connections)

x Shear connector failure or local failure of concrete around the shear connectors

xi Web side plate twisting

xii Yield of endplate in bending

xiii Weld failure between steel beam and connected part

xiv Excessive connection deformation

Behaviour of bare steel connections: a composite connection is a combination of the bare steel connection and a reinforced concrete slab acting together and sharing the loads. It is therefore essential to understand the behaviour of the bare steel connection in order to properly understand the behaviour of the composite connections. A large number of tests have been performed on bare steel connections since the 1930's. Nethercot and Zandonini (1989) made a review of the prediction methods [1-4] for the bare steel connections. Generally, the extended endplate connection gives the highest moment capacity and stiffness and the web cleat connections provides the lowest. Typical M-θ curves are shown for these connections in Figure 1-5 for the same beam and column combination. The reason for the high moment capacity of the extended endplate connection is that the lever arm is largest for this connection. The moment-rotation curves shown in the figure are idealised, in reality they may not be so smooth due to the slip of the bolts and local buckling of components. Figure 1-6 shows the effect of local buckling on the moment-rotation behaviour of the connection.

Behaviour of composite connections: Composite connections may be regarded as simply the addition of the reinforced concrete slab with a proper shear transfer mechanism between the steel beam and the concrete slab. All the test results have shown that the addition of reinforcement near the column increases the moment capacity and the stiffness of the connections. This is also due to the increase in the lever arm of the internal forces in the connections. But the percentage increase may be different for different types of connections for the same percentage increase of reinforcement. For example in Benussi's test (1989) on composite header plate connections [1-5], the increase in moment capacity was higher with respect to the composite endplate connections, although the increase in reinforcement ratio was high for the endplate connection. But the basic behaviour of the connection remains the same, for example in Anderson's test [1-6,1-7] for the same reinforcement ratio the composite extended endplate connection had more moment capacity (11%) than the composite flush endplate connection; this trend is the same as for the bare steel connections.

Xiao's (1994) test SCJ8, SCJ9 and SCJ10 used endplates at the top, middle and at the bottom of the beam respectively. It was observed that SCJ8 gave the lowest moment capacity whereas SCJ10 gave the highest moment capacity. This is due to the fact that the position of the endplate controls the length of lever arm.

Leon [1-8] performed a few tests on sub-assemblage composite frames. Li *et al* [1-9] performed the first full scale 3D test on a composite non-sway two bay, two-storey frame (which had two frames), to obtain the frame moment distribution. It was observed that the interaction in the non-sway frame is not significant, since when one frame was loaded moment transfer to the other frame was very low. The test results indicated that the external connections can also be designed as semi-rigid connections. From this test it was also evident that the moment capacity of a connection depend on the "other side" connection moment.

1.5 Main factors that influence the moment capacity of composite connections

The moment capacity of a composite connection as observed in the tests is affected by: reinforcement ratio, symmetry and non-symmetry of the applied load, degree of shear interaction provided (using shear studs), shear to moment ratio, column characteristics, column axis connection.

1.5.1 Reinforcement ratio

Usually, up to a certain limit, the higher the reinforcement ratio the higher the moment capacity of the connection. Tests by Benussi *et al* [1-5], Anderson and Najafi [1-6, 1-7], Xiao [1-10, 1-11] have confirmed this. Results reported by Li *et al* [1-12], show that SJS-1 and CJS-1 had the same steel detailing, the later had a composite beam with 1% reinforcement (767 mm^2) but the moment capacity was increased to 181 kN•m from 62.8 kN•m. Xiao's test SCJ3 and SCJ4 had the same steel detailing but the reinforcement ratios were 0.2% and 1% and the moment capacity was increased by 136%.

From this it is clear that a small amount of reinforcement can dramatically increase the moment capacity of the composite connections, due to the increase in lever arm. However, the reinforcement can affect the joint characteristics in a different way, e.g. if the rebars have smaller diameter and are evenly distributed, it can prevent the formation of large cracks will be replaced by well distributed hair cracks. But wire mesh [1-6, 1-11, 1-13, 1-14] has limited ductility and it has been suggested that its contribution is not reliable without the presence of reinforcing bars at the connection. It is however evident also from the test SCJ3 [1-10] that wire mesh alone also increases the moment capacity in a way similar to the reinforcing bars.

Li *et al* [1-12] observed that the concrete crack width did not exceed 0.3 mm until the connection moment reached about 50% of the ultimate connection moment capacity. All their tests showed that the rebar stress corresponding to this crack width was less than 150 N/mm^2. So they concluded that by controlling the rebar stress to be less than 150 N/mm^2 or limiting the connection moment to be less than 50 % of the connection moment capacity the crack width can be limited to 0.3 mm.

1.5.2 Load application procedure

The studies and analyses of the joints is of course, undertaken with the eventual aim of using such joints in frames. In a real structure the joint is usually loaded non-symmetrically. Most of the tests on composite connections have been symmetrical. But tests by Puhali *et al* [1-15] indicated that non-symmetric application of the load affects the behaviour of the composite joints. Tests by Benussi *et al* [1-5] and Law [1-16] showed that unbalanced moments on the two sides of the column also affects the connection behaviour. Tests by Li *et al* [1-12], showed that the effect of non-symmetrical moment on the connection moment capacity is significant only when the non-symmetrical moment ratio is quite high compared with the column web shear resistance or the concrete strength.

1.5.3 Shear connectors

Most of the tests on composite connections have been carried out using a uniform distribution of shear connectors and full shear connection between the reinforced slab and the steel beam top flange. This makes it difficult to interpret the exact role played by the shear connectors in the composite connections. Tests conducted by Law [1-16] employed uniformly distributed shear connectors on one side of the connection and a non uniform distribution of shear connectors on the other side of the connection. Results of his tests indicate that a different interaction between the steel beam and the

concrete slab affects the connection behaviour slightly in the early stage but significantly in the non-linear part. Najafi and Anderson [1-7] conducted tests with partial shear interaction and full shear interaction. Results indicated that the partial strength connections have low moment capacity and initial stiffness with respect to the full interaction. It was also observed from the tests that by increasing the amount of transverse reinforcement the crushing of the concrete around the shear connectors can be prevented. Tests C1, C2 and C3 of Aribert and Lachel [1-17] on flush endplate connections and D2, D3 and D4 on angle cleated connections also showed similar effects. It was observed from these tests that changing to a composite connection dramatically increased the initial stiffness and the moment capacity, while the variation in the degrees of shear interaction caused similar effects (i.e., increase or decrease) in both moment capacity and initial stiffness of the composite connections.

1.5.4 Shear to moment ratio at the connection

Studying the internal equilibrium of horizontal forces a joint it can be seen that the moment capacity is governed by the magnitude of the internal forces. It appears that wherever the load is applied to the beam these values will be constant and hence the moment capacity will be constant. However, as the load is moved nearer to the connection, for the same level of moment the magnitude of the shear must be increased, so this indicates that shear force transmitted to the connection must be increased. This may change the failure mode of the connection and may also lead to the buckling of the beam web or column web if the stiffening effect of transverse beams on the column web is absent. Echeta and Owens [1-18] conducted tests with two loads on each beam and by adjusting the ratio of the two loads they obtained the pre determined shear to moment ratio. The test results did not indicate any noticeable effect of this ratio on the connection moment capacity. Xiao [1-3] conducted two tests SCJ4 and SCJ6, both with the same connection detail but with different magnitudes of shear to moment ratio. These results however indicated that the shear to moment ratio effect

was significant. Both of these tests failed by local buckling of the column web. To investigate this effect, Li *et al* [1-12] conducted three tests CJS-1, CJS-4 and CJS-5 with variable shear to moment ratios and having the same detailing for all specimens. It was observed that initially the moment capacity was reduced, but CJS-5 with the highest shear to moment ratio achieved the largest moment. The conclusion from the tests was that shear force has little effect on the moment capacities of composite flush endplate connections.

1.5.5 Concrete slab and column interaction

The rebar force for an external column connection or the difference in rebar force for the internal column connection when the connection is loaded non-symmetrically must be balanced through the compressive force between the slab and the column face. Xiao *et al*'s [1-11] test failed by the crushing of the concrete outside the column, and the conclusion was drawn that these connections should be designed as pinned connections. Echeta's [1-18] test also failed by the crushing of the concrete on the lateral face of the column.

1.5.6 Column characteristics

If the column web is weak with respect to the other components of the connection, it may lead to the buckling of its web if no stub beam is attached to the column web. Also the thickness of the column web determines the compressive force that can be sustained by a column web. Xiao's [1-11] test SCJ4 reached its ultimate capacity due to the buckling of the column web. But at the same time test SCJ6, which had a web stiffener, developed an increased moment capacity of 19%.

1.5.7 Column axial loading for bare steel connections

Only a few tests have been conducted with column axial loading on the bare steel connections. Zoetemeijer's observations [1-19] lead to the formulation of equations [1-20, 1-21] for reducing the bolt force and column web compressive strength. Recently, Jaspart [1-22] conducted some tests on bare steel connections. These indicated that the compression capacity is not affected by the column axial loading but the bolt forces are significantly affected by the presence of the column axial loading.

1.5.8 Effect of column axis connection

Xiao *et al* [1-11] conducted a total of four tests (SCJ13, SCJ14, SCJ18 and SCJ19) with column minor axis connection. The equivalent connections for SCJ13 and SCJ14 for major axis connections are SCJ10 and SCJ8. For SCJ10 the moment capacity was 147.8 kN•m and for SCJ13 the moment capacity was 181.4 kN•m. The reason for the increased moment capacity of SCJ13 is that SCJ10 reached its ultimate moment due to buckling of the column web, which was prevented in this case. For SCJ14 the moment capacity was 89.8 kN•m. and for SCJ8 it was 84 kN•m - both connections reached their ultimate moment capacity due to buckling of the beam web. It appears that as long as the compressive forces can be resisted and the column web buckling can be prevented by means of stub beams, there is no effect of this factor on the moment capacity of composite cruciform connections. Tests SCJ18 and SCJ19 were cantilever joints; both the connections failed due to the insufficient anchorage of the reinforcement which produced failure of the concrete slab.

1.6 Prediction methods for moment and rotation capacity and initial stiffness of composite connections

1.6.1 Prediction of moment, rotation and stiffness behaviour using equations

Using the simple equilibrium model in Figure 1-7, Johnson and Hope-Gill [1-1] in 1972 proposed the calculation of plastic moment capacity of the connection as:

$$M_P = A_S . f_y . d_f$$

The method considers the strength of the rebar only, any contributions from the other components are neglected.

Johnson and Law (1981) proposed a formula for the ultimate moment capacity of the composite connection [1-23] by summing the plastic moment capacity of the steel connection and the resistance moment given by the yield strength of the reinforcement. According to their formulation:

$$M_P = M_{P,S} + A_r . f_{yr} . d_f$$

Where:

M_P is the plastic moment capacity of the composite connection

$M_{P,S}$ is the plastic moment capacity of the steel connection

d_f is the depth of lever arm of tensile force

f_{yr} is the yield stress of the tensile reinforcement

A_r is the area of reinforcement

They also proposed a formula for calculation of the rotation capacity:

$$\phi = \frac{M_u}{K_s}\left(1 - \frac{Qd_f}{R}\right) - \frac{C_o d_f \sinh\sqrt{RL}}{K_S}$$

Where:

ϕ is the connection rotation

C_O is the initial parameter to decide tensile force

L is the length of the hogging moment region

K_S is the elastic stiffness of the steel connection

M_u is the ultimate moment resistance of the connection

Q is the shear resistance of the shear stud

Elastic stiffness of the composite connection is given by:

$$K=C.d_b^2$$

The connection coefficient C is:

$$C=\frac{1}{0.5\left[\left(1/C_b\right)+\left(1/C_c\right)\right]\left(d_b/d\right)^2+1/C_P}$$

Where:

C_b is the stiffness of the bolts

C_c is the stiffness of the column flange

C_P is the stiffness of the endplate

The model for determining the elastic stiffness is shown in Figure 1-8a, Comparison of predicted and experimental results is shown in Figure 1-8b.

From eight tests Aribert (1992) has proposed a simple form of M-ϕ relation [1-17]. This is suitable only for flush endplate connections. The deformation relationship is shown in Figure 1-9. The moment rotation relation is:

$$M = S_a \phi + F D$$

Where:

F is the axial force in the reinforcing bars

S_a is the stiffness of the corresponding steel connection

The initial stiffness of the composite connection is defined as:

$$S_{ac} = S_a + \frac{D}{\frac{h}{2E_r A_r D} + \frac{\alpha}{Nkh_b}}$$

Where:

E_r is the elastic modulus of the reinforcement

A_r is the section area of the reinforcing bars

D is the distance from the reinforcement to the centre of the bottom flange

N is the number of active shear studs

h_b is the depth of the steel beam

h is the depth of the steel column

k is the secant stiffness of one shear connector

α is the increase factor, taken ≈2

Rotation of the beam can be obtained from the condition of strain compatibility at the column face as:

$$\phi = \frac{\Delta}{D} + \frac{s}{h_b}$$

Where:

Δ is the elongation for the rebar over half the depth of the column

s is the slip of the shear studs near the connection

$=\alpha F/(Nk)$

Whilst the model is simple, its accuracy is doubtful. It is similar to the Johnson and Law proposal as the total moment for a composite connection is taken as the sum of the reinforced slab resistance and the bare steel resistance. The comparison between the predicted and tested initial stiffness had large discrepancies, sometimes more than 100%.

The SCI (1992) prepared a document [1-24] in which the rotation capacity of the composite connection is calculated using the elongation of the rebar, with the assumption that the compression zone is located at the bottom flange of the steel beam (the model is similar to the one in Figure 1-8a). The assumed ultimate reinforcement strain was assumed to be 2%.

$$\Delta l = 0.02\left(p_1 + \frac{D_c}{2}\right) + 0.02\frac{(n-1)p_2}{2}$$

$$\phi_{ult} = \frac{\Delta l}{D + D_r}$$

Where:

p_1 is the distance of the column flange to the first shear connector

p_2 is the pitch of the shear connectors

n is the number of shear connectors needed to resist the longitudinal force

D_c is the depth of the column

D is the depth of the beam

D_r is the distance of the reinforcement from the top of steel beam

Xiao (1994) tested nineteen composite connections and used the findings to develop a mathematical model [1-3] to predict both moment capacity and rotation capacity of composite cleated connections, composite finplate connections, and composite flush

endplate connections. Reduction factors according to EC4 clause 4.4.3 [1-25] and BS5950 Part 1, Clause 4.2.6 [1-26] were recommended for use when high beam shear was present. Separate equations were proposed to calculate the moment capacity of the connection when its compressive capacity was governed by the column.

Xiao *et al* (1994) have proposed a method [1-27] similar to the SCI method, to calculate the available rotation capacity of composite connections. By calculating the extension of the rebar, the rotation capacity was defined as:

$$\phi_u = \frac{\Delta L}{D + D_r}$$

Where:

D is the depth of the beam

D_r is the distance of the upper flange of the beam to the centre of the reinforcement

The elongation of reinforcement ΔL consists of two parts: deformation of the reinforcement in the plastic zone (L_1) and deformation of reinforcement in the remaining elastic zone (L_2). It was concluded later on by Xiao [1-3] that the elongation of the reinforcement in the elastic zone has no effect on the rotation capacity and should be neglected. The elongation in the plastic zone was calculated as:

$$L_1 = \varepsilon\left(p_1 + p + \frac{D}{2}\right)$$

Where:

p_1 is the distance of the column flange to the first shear stud

p is the pitch of the shear studs

ε is the plastic strain of reinforcement taken as 0.005

Xiao [1-3] used the location of the neutral axis to determine the rotation capacity of composite connections. The rotation capacity also considers the slip of the shear studs. The rotation capacity was defined considering four different location of neutral axis, i.e., neutral axis in the concrete slab, neutral axis in the top flange, neutral axis between the top flange and the top bolt row and finally neutral axis below the top bolt row. The model is similar to the one in Figure 7-12 of Chapter 7. Among these possibilities the last one is the most likely one and hence is described in detail. The rotation capacity for the last case is given by:

$$\phi_u = \frac{L_1}{d_c + p_1 + ip + \frac{2}{3}p} + \frac{L_2}{p_1 + ip + \frac{2}{3}p}$$

Where:

p is the bolt pitch

p_1 is the distance of the top bolt row from the top flange

d_c is the depth of the concrete slab

i is the number of tension bolts that yielded and is given by the integer part of the following expression:

$$i = integer\ part\ of\ \frac{p_y t_{bf} b_{bf} - F_s + p_y t_{bw}\left(D - p_1 - t_{bf} + \frac{1}{3}p\right)}{2F_t + p_y t_{bw} p}$$

Where:

p_y is the yield strength

$$F_s = min\begin{cases} capacity\ \ of\ \ rebar \\ capacity\ \ of\ \ stud \end{cases}$$

$$F_t = (p_t A_t - Q_t)$$

p_t is allowable bolt tensile stress from BS5950

A_t is tensile area of bolt

Q_t is the prying force

$$L_2 = \frac{F_s}{N\ k}$$

Where:

N is the number of shear studs

k is the secant stiffness of a shear stud, taken as 30 kN/mm

The main drawback of the above formula is that the depth considered for the calculation of rotation capacity becomes larger than the depth of beam and sometimes greater than the combined beam and slab depth, when compared with the test results - this is not acceptable. This depth will mean that the beam is rotating without even having any physical contact with the column at the level of its bottom flange. It can be easily visualised from the equation that for a connection with two rows of bolts where the top row has yielded the considered depth can easily be larger than the beam depth. A typical example is test CJS-1 of reference 1-12, where the top row of bolts developed a force of 180 kN, i.e., yielded, for this connection d_c = 90 mm, p_1 = 49 mm, p = 157 mm, D = 257 mm. The calculated depth corresponding to rotation is 90 + 49 + 157 +2/3*157 = 400 mm, which is greater than the distance between the bottom flange centreline and reinforcement.

Li *et al* (1994) tested six composite flush endplate connections as a way of studying the effects of both a variable shear to moment ratio and unequal moments on either side of a cruciform joint [1-12, 1-28]. The comprehensive test records included full moment-rotation curves as well as various strain and stress histories and stress - strain curves for the basic materials. Examination of the test results lead to a method to predict the moment capacity of non-symmetrically loaded connections, that included the effect of the shear to moment ratio by assuming a shear and using it to reduce the

available compressive strength of the beam web. Reductions for column load were included according to the EC3 [1-20, 1-21] rules for bare steel connections.

Anderson and Najafi (1994) have proposed a model [1-29] to predict the moment capacity of the connection using simple concepts of plastic analysis (the model is similar to the one in Figure 7-1c of Chapter 7). When the total tensile resistance (bolt and rebar) exceeds the bottom flange compressive force, a plastic stress block is assumed in the lower part of the web. The moment resistance of the connection is given by:

$$M = R_r D_r + R_b D_b - \left(R_r + R_b - R_f\right)\left(\frac{x}{2} + \frac{T}{2}\right)$$

Where:

R_r is the rebar force

R_b is the bolt force

R_f is the compression in bottom flange

x is the depth of web compression

T is the thickness of beam flange

A relation between the moment and the rotation of a composite connection was also proposed by Anderson and Najafi. The model assumed a rotation of the beam web about the bottom flange, but at the same time considered the slip of the studs. The method assumes that the developed moment is due to rebar and bolt force only. It does not account for any possible compressive force that may develop in the beam web and not applicable to mesh reinforced connections. The relationship is:

$$M = \left(\frac{K_r K_s D D_r}{K_r + K_s} + K_b D_b{}^2\right)\phi$$

Where M is the moment and ϕ is the rotation, subscripts r, s and b indicate rebar shear stud and bolt. D represents distance from bottom flange centre line, and K represent the stiffness of the associated member. Where:

$$K_r = \frac{2E_r A_r}{D_c}$$

After the initial model verification, when the flexibility of the shear studs was taken into account, it was proposed by the authors to increase the length of rebar up to the first row of studs.

K_s is taken as 200 kN/mm

$$K_b = \frac{C_s}{D_b^2}$$

The stiffness C_s (in the range of 0-50 kN-m) can be calculated for steelwork endplate joints from EC3 or using other prediction methods or from tests.

The above formulae do not consider the yield of the column web, or the column web stiffness or, more importantly, the influence of the different numbers of studs present in connections is not properly reflected.

Ren and Crisinel (1995) developed a relation [1-30] for the moment capacity of composite connections which is the same as that proposed by Anderson and Najafi. The relation between the moment and the rotation of the composite flush endplate connections was also used to predict the initial stiffness by them. The derivation of the formula used a basic assumption that the moment capacity of a composite connection is the sum of the rebar capacity and the bare steel connection capacity. The method considers the deformation of the column web at beam bottom flange level due to the compression. The relationship is:

$$M = \frac{D^2}{\frac{1}{K_r} + \frac{1}{K_s} + \frac{1}{K_c}} \phi$$

Where:

D is the distance of rebar from bottom flange centre

$$K_r = \frac{E_r A_r}{2\eta(60 + 1.3\,k\,s)}$$

η is taken as 0.35

k is 1 for pure tension, 0.5 for simple bending

s spacing distance between the reinforcement

$$K_s = min\begin{cases} \frac{0.6 R_r}{\Delta\ u} \\ \frac{0.6 R_s}{\Delta\ u} \end{cases}$$

$\Delta\ u$ is the interface slip taken as 0.5 mm for 19x100 mm welded shear connectors

R_r, R_s are the resistance of reinforced concrete slab and shear connectors over the composite beam length of hogging moment respectively

$$K_c = min\begin{cases} \frac{EA_{wc}}{L} \\ \frac{EA_b}{L} \end{cases}$$

$$A_{wc} = 2t_{wc}\left(2\left(t_p + t_{fc}\right) + t_{fb}\right)$$

A_b is the cross sectional area of the steel beam

It can be seen that while Anderson & Najafi and Ren's method deals with the stiffness of components to determine the initial stiffness of a composite connection, Aribert's method adds the stiffness of the steel beam to the contribution of rebars and shear studs towards the stiffness. The Anderson & Najafi method was not directly developed for initial stiffness but its main objective was to trace the M- ϕ curve.

1.6.2 Simplified method by curve fitting the test results using mathematical expressions

Moment rotation curves are the basic and most important characteristics of semi-rigid connections. A number of M-ϕ curve fitting methods have been proposed [1-4] for bare steel connections. These are Frye-Morris polynomial, Jones-Kirby-Nethercot B-spline curve, Ang-Morris power curve, Lui and Chen's exponential curve etc.

1.6.3 Mechanical model

The principle of this method is to divide the connection into a set of mechanically connected components, representing the behaviour of elemental parts. The behaviour of each element is then described by general constitutive relations, either in stress space or strain space. Finally, the general connection behaviour can be combined together from these separate element relationships by considering force equilibrium and deformation compatibility.

Tschemmernegg (1988) suggested a model to describe the deformational characteristics of the steel connection, using the above philosophy of a component-based approach in combination with empirical relationships for the components [1-31]. The mechanical model is shown in Figure 1-10, where spring set A represents the load transfer from the beam to the column and B models shear deformation of the column web panel. The spring properties were derived from data obtained from experiments by the author. The connection M-ϕ relationship was obtained by imposing two sets of

springs together. After further modification, this was extended to model the composite connections shown in Figure 1-11. The column web is in the unstiffened condition and is assumed to govern the overall connection behaviour. This enables the composite connection to be dealt with by means of a mechanical model almost identical to the set-up for the bare steel connection.

Recently, Tschemmernegg (1992) has proposed a new spring model for composite connections [1-32]. The procedure is the same as the previous one except that an additional compressive spring was introduced. The tension force is simulated by the truss model shown in Figure 1-12. The load spring simulates the flexibility of the truss system. The tension spring simulates the flexibility of reinforcement on both sides. An external spring and an internal spring introduces the load in the compression zone, as shown in Figure 1-13. The shear deformation of the column web panel is described by a shear spring shown in Figure 1-14. The full model is shown in Figure 1-15. Comparisons of the test results and predictions using the model are shown in Figure 1-16. The model cannot account for slip between concrete and steel and does not consider shear lag in the composite beam. Also, it cannot consider any tension in the column flange, which is possible for low reinforcement ratios.

Madas (1993) proposed the mechanical model [1-33] shown in Figure 1-17. The proposed model is capable of predicting the behaviour of steel and composite connections of web angle, top and seat angles, partially welded flush endplate and fully welded connections. His formulation considered non-linear behaviour of the connecting elements and connected members, bolt extension and slippage, shear connector flexibility, coupled moment - axial force behaviour, but did not consider shear force in the connecting elements. The model was incorporated into ADAPTIC, an existing computer program. The results were compared with Echeta's and Leon's tests for monotonic and cyclic loading respectively. The accuracy of the predictions is

reasonably high. This is the most comprehensive mechanical model available, at present.

1.6.4 Numerical modelling

Although the experimental measurements of strain and displacements with increasing load provide valuable insight into the problem, in many cases important local effects cannot be measured at all or cannot be measured with the necessary accuracy. This is due to the fact that the necessary measuring process is either impractical or is too expensive. Numerical studies thus provide a low cost-effectiveness ratio. Also the number of geometric and mechanical parameters which can reasonably be expected to influence the connection behaviour is significant. In such cases numerical modelling is a very effective method for including more variables than could be contained in the limited scope of an experimental program. For developing simple prediction methods the extensive parametric studies required can only realistically be carried out by means of numerical simulation. The most suitable tool available at present for studying such a complicated problem is the Finite Element Method (FEM).

The first study using FEM, into the connection behaviour by Bose *et al* (1972) was related to welded beam column connections [1-34] shown in Figure 1-18. They performed a study on the critical load level. Patel and Chen (1984) also investigated welded two way connections [1-35], where the beam was fully welded to the column or welded at the flange. Bathe *et al* (1974) modelled [1-36] a full connection assembly using a general purpose program NONSAP. Atamaz-Sibai (1988) studied the one way unstiffened connection [1-37]. Lipson and Hague (1978) made an FE analysis [1-38] of single-angle bolted welded connections. The main aim of their study was not to obtain a moment-rotation curve but to improve the understanding of the behaviour of single angle bolted connections, already tested by Lipson. The connection was modelled as a rigidly supported elastic-plastic plate (Figure 1-19a) subjected to a load distribution

simulating the bolt plate interaction (Figure 1-19b). Richard and his associates (1983) carried out numerical work [1-39] on single web plate connections. The finite element model included part of the beam as well as the whole connection system. To simulate the bolt action, an inelastic finite element was developed. Patel and Chen (1985) adopted a very simple equivalent bar system [1-40] in order to account for the bolt action. They simulated the response of the fully bolted moment connection shown in Figure 1-20, using NONSAP. A plane stress isoparametric element was used to model beam, column and connection plates, while three bar elements were used to simulate bolt action, two for pre-tension in bolts and one formulating shear carrying behaviour. Krishnamurthy (1980) developed a FE model [1-41] that physically modelled bolts during modelling a bare steel end plate connection. In his model the support of the end plate was considered rigid. The model can simulate bolt pre-loading, the FE mesh used by Krishnamurthy is shown in Figure 1-21.

All the FE analyses described above were performed on simple connections, none of them included any composite action. The first numerical study on composite connections was undertaken by Leon and Lin (1986) [1-42]. They used a general purpose FE software ADINA to model the connection. In the model concrete was considered to have no tensile resistance, and was ignored. They modelled a connection tested by Leon. To develop the three dimensional model they used a two step procedure. First they developed a 3D FE model for the behaviour of cleat segments subjected to either a tension or compression force acting along one leg, which included the effect of slip due to the bolt hole clearance. From the result of this model multi-linear stress-strain constitutive laws were formed for equivalent truss elements. Then the composite connection was modelled by using twenty noded three dimensional elements for the I beam, very stiff beam elements for shear connectors and truss elements for angles and reinforcements. The model is shown in Figure 1-22. Although the contribution due to the deformation of bolts and column and flexibility of shear

studs was not considered, comparison between experimental and FE M-ϕ curves as shown in Figure 1-23, indicated fairly close agreement.

Puhali and Zandonini (1990) carried out a non-linear finite element analysis of one composite connection [1-15] using a general purpose FE software named ABAQUS. The adopted model was a quasi-truss, in which the slab and steel beam were modelled by beam type elements. The model is shown in Figure 1-24. Multi-linear material constitutive laws were used for steel, concrete and shear connectors. The shear connection flexibility was allowed for by non-linear springs. Compression deformation of column web was also taken into account in the analysis. Figure 1-25 gives a comparison between the experimental result and the FE analysis result. The authors concluded that even when the beam-slab connection is designed to ensure full interaction, the slip between the steel beam and the concrete slab in the vicinity of the connection, even though modest, is sufficient to affect remarkably the steel beam stress state and, hence its curvature.

Aribert *et al* (1994) developed a simple finite element method [1-43] to represent the composite connection to obtain the moment-rotation curves as in test. They used a composite element for this purpose which is composed of two parallel beam elements, one to represent the steel beam and the other for the slab. These two are linked by means of two nodal elements simulating the force-slip behaviour of the shear connectors. To introduce semi-continuity (due to interaction with a semi-rigid connection or/and local buckling) an intermediate spring element was combined with the composite element. The intermediate element has to include three components one is a rotational spring with variable stiffness to control the sum of internal moments, second one is a linear spring with variable stiffness to control the axial force and third one is for buckling. This modelling approach is similar the one described in reference 1-15. The approach is simple but doubtful.

Li, Nethercot and Choo (1991) modelled [1-44] one composite flush endplate connection using ABAQUS. The modelling included steel beam, endplate, column by using 9 noded shell elements, concrete using 20 noded solid elements with reinforcement, shear connection and bolts included as connection elements. The contact relationships of the slab to the steel beam and endplate to column flange were described. To represent the cracking and post-cracking behaviour of the concrete, a smear cracking model was used to describe the tension stiffness change. The FE mesh is shown in Figure 1-26. Test SCJ5 of Xiao [1-3] was used to compare with the modelling result. This is the most detailed model so far attempted. But in the inelastic range it showed considerable differences. Comparison of test and FE results is shown in Figure 1-27. The model gave less rotation and moment than the actual test result. The reason was explained that the actual composite slab was modelled as a solid slab and the column deformation was neglected.

Ren and Crisinel developed a macro element model [1-45] using finite elements as shown in Figure 1-28. Their macro element consisted of four types of finite elements. Element I is a deep beam element which may model the elastic-plastic behaviour of shear deformation of column panel zone. Element II is the spring block element including three kinds of spring which simulate respectively axial, transverse and rotational characteristics of the steelwork connection, including the effect of bolts, endplate, cleats etc. Element III is a beam element for modelling the reinforced concrete slab action above the steel connection. Element IV is a partial shear connection composite member element which is used to model the composite beam behaviour. It permits a consideration the effect of degree of shear connection between the slab and the steel beam. The formulation of the elements are described by the authors. The model was compared with eleven composite connection specimens tests. According to the authors moment-rotation curves were generally in good agreement with the test results.

Huang and Morris (1991) conducted computer analyses [1-46] of bare steel frames by using the moment - rotation curves of the connections generated by functions based on connection test data to study the effect of connection properties on lateral drift.

Colson and Bjorhovde (1991) undertook computer analyses [1-47] of a two storey, two span bare steel frame using a computer program PEP-Micro, the analysis assumed pin connections for the beam-to-column connection for the exterior columns and semi-rigid connections for the interior beam-to-column connections. Obviously it will not represent the true frame behaviour as the assumption of a pin connection for the exterior beam-to-column connections will produce a moment distribution in the frame far from the true one.

Deierlein (1991) conducted computer analyses [1-48] of semi-rigid bare steel frames using a computer program CU-STAND, in which all the beam-to-column connections were modelled by zero-length rotational springs to account for their non-linear moment-rotation behaviour. The interior and exterior joints had the same moment-rotation characteristics, which is not the true behaviour.

Li *et al* (1995) analysed a two-span, two-story semi-rigid bare steel frame [1-49] using the general purpose finite element software ABAQUS. They studied the effect of connection length on the moments at different sections corresponding to different connection stiffness levels. It was observed that when the connection/beam stiffness ratio is greater than 2.0, the effect of connection length on external column moments is small (less than 10%), whereas the internal column moments, when the frame layout and loading are symmetrical, was not affected by the assumption of zero connection length. It was concluded that the zero connection length will lead to underestimates of the external column moments and slight underestimates of the internal column moments. On the other hand, the beam end moments are significantly overestimated, especially for beam ends on the external column side. The beam span moments are moderately overestimated by this assumption. It was also observed that zero

connection length leads to moderate overestimation of the horizontal displacements of the frame. The connection length/span ratio and drift with zero connection length/drift with finite connection length was observed to have a linear relation. The effect of connection element length on column buckling load was analysed for a two story single bay unbraced frame. It was concluded that column buckling loads are significantly affected by zero connection length assumption for sway frames, and almost unaffected by zero connection length assumption for non-sway frames.

Ye Mei-xin *et al* (1995) proposed a finite element model for composite frames [1-50] using the general purpose software ABAQUS. The method is similar to the Li *et al* method, the difference being the inclusion of the composite beams through a simplified procedure via the inclusion of the moment curvature of the composite beam determined from reference 1-51.

1.7 Design equations to reduce strength for the interaction of column loading and high shear

To consider the interaction with column loading present in a frame structure, EC3 provides equations to reduce the column web compressive strength, shear strength and the bending resistance of the column flange in tension - for calculating the reduced bolt force for column loading. These were based on the early tests of Zoetemeijer [1-19], which were believed to be the reflection of column loading on the buckling resistance of the column web. Hence these equations (column web compressive strength and bending resistance of column flange in tension) need proper investigation and modification or total change. Also the calculation of column web shear strength considering the interaction of column loading is a constant value whatever the magnitude of column loading. This equation is based on Jaspart's [1-52] proposal. It is essential to investigate the actual interaction that may take place in a composite connection. To consider the effect of high shear on the moment capacity of composite

beams EC4 (DD ENV 1994-1-1:1994, revised 30 Jun, 1994) introduces a reduction factor. If the shear force is greater than 50 % of the design plastic shear resistance $V_{pl.Rd}$ according to Clause 4.4.3:

$$M_{Sd} \leq M_{f.Rd} + \left(M_{Rd} - M_{f.Rd}\right)\left[1 - \left(\frac{2V_{Sd}}{V_{pl.Rd}} - 1\right)^2\right]$$

Where:

M_{Sd} and V_{Sd} are the design moment and shear values

$V_{pl.Rd}$ is the plastic shear resistance

M_{Rd} is the design bending resistance given by 4.4.1

$M_{f.Rd}$ is the design plastic bending resistance of a cross section consisting of the flanges only, with effective sections as used in the calculation of M_{Rd}

It is necessary to investigate the effect of high shear on the moment capacity of composite connections.

1.8 Calculation of sway of unbraced steel frames

Ammerman and Leon [1-53] proposed an equation to calculate the lateral deflection of one floor of any frame with multiple stories and multiple bays as:

$$\Delta = \frac{PH^3}{\alpha E \sum I_{col}}$$

Where:

P is the total lateral load on the floor

H is the story height

$\sum I_{col}$ is the sum of the inertia for all the columns on that floor

To determine α for buildings with restraint provided to the column tops by beams acting in conjunction with semi-rigid connections, a convenient equation (Ammerman and Leon, 1990) which provides good results is:

$$\alpha = 3 + 9e^{-GF}$$

$$GF = \frac{\frac{E\sum I_{col}}{H}}{\frac{\sum \beta_\beta EI_{cb}}{L}}$$

$$\beta_\beta = \frac{1}{1+\frac{2EI_{cb}}{LC}}$$

If the base floor is assumed to be fixed and the tops of the columns do not rotate with respect to the floor α is 12 (Figure 1-29a), and α is 3 if the tops are free to rotate (Figure 1-29b). However, the proposed formula for α was purely empirical, and was based on their frame studies. The equation was merely intended to provide a smooth transition between the case where the columns are free to rotate ($\alpha = 3$) and the case where the columns are fixed ($\alpha = 12$). This expression was intimately tied to the frames studied by them, hence the expression for α was not a generalised one.

1.9 Objectives of the study

From the above review it was understood that a considerable number of tests have been conducted on semi-rigid composite connections. However, for practical application of the semi-rigid connections, a large amount of research work remains to be done in different areas. Some of these are listed below as they form the main content of this thesis.

(i) Development of a numerical model to accurately represent the composite connection behaviour

Understanding of the detailed aspects of the connection behaviour has, thus far, largely relied on test evidence and the subsequent development of behavioural models. Because of the large number of variables and potential failure modes associated with composite connections, such an approach isnever likely to be able to thoroughly examine all aspects of the problem. It is therefore natural to explore the possibility of using alternative numerical approaches. Of these, the finite element method, which has previously been used successfully to model several different forms of bare steelwork connection, was selected. Although some initial work in this area has been undertaken by other researchers, a successful approach to the finite element modelling of composite connections has yet to be developed. One of the objectives of this study was to utilise the available test data and the test results as a basis for numerically simulating the behaviour of semi-rigid composite connections. Once an extensively validated and reliable model is developed, it can then be used to carry out parametric studies, with the aim of providing a through knowledge of the load transfer mechanism in a variety of composite connections.

(ii) Effect of shear to moment ratio on connection moment capacity

The number of tests conducted with variable shear to moment ratio was not sufficient to gain a clear picture of the role of this parameter on composite connection moment capacity. It was observed in the review part that results from the tests were contradictory to some extent regarding the effect of this parameter. Hence there was a need for some theoretical and numerical work on the shear to moment ratio. This work forms a part of the investigation in this thesis.

(iii) Effect of column loading on connection moment capacity

Although columns are subjected to axial loads in a frame structure, no tests have been reported on the composite connection to simulate its effect on the connection moment capacity. It was observed that for the bare steel connections the Structural Eurocodes provide some guide to evaluate this effect, but further studies were required to complete the understanding, which can be resolved through proper theoretical and numerical work. The investigation of the effect of column loading on composite connection moment capacity also forms a part of this thesis.

(iv) Development of design methods for composite connections

A few methods have been proposed to calculate the moment capacity of composite connections. It was observed that none of the methods provided a complete coverage of all the important parameters that affects the connection moment capacity. It was observed that none of the methods actually relate the loading position with the connection shear capacity, although some include this parameter in an indirect way. Besides this, the methods allow for column axial loading effect on moment capacity by using the approach of the Structural Eurocodes. The present work includes the development of a design procedure for composite flush endplate connections that includes these effects (symmetric and non-symmetric loading, shear to moment ratio, column axial loading etc.) and at the same time is able to predict the probable failure mode when the connection reaches its ultimate moment capacity. Besides this, design procedures for composite finplate and angle cleated connections were also developed.

(v) Initial stiffness, rotation capacity and overall behaviour of flush endplate connections

Another important aspect of the behaviour of semi-rigid composite connections concerns their initial stiffness and available rotation capacity. It was observed in the

literature review that there was a need to develop a method to estimate the connection stiffness and available rotation capacity of composite flush endplate connections. This thesis includes work on this topic as well as the overall behaviour.

(vi) Development of a numerical model to faithfully represent the composite frame behaviour

Another objective of this thesis was to develop a reliable FE model for composite frames and to verify this against available test results. The moment - rotation result of the connection test was used as the input data for FE model for the frames. This was done as the aim was to develop a cost (computer time) effective but yet reliable analysis procedure for the composite non-sway frames. It was demonstrated that it is possible to obtain an accurate frame moment distribution, connection moment - rotation curve and beam - load deflection history with the developed frame model.

(vii) Sway in unbraced steel frames

From the literature review, it was observed that the available equations to predict the sway of steel frames were empirical and tied to the relevant frame tests. A finite element model for steel frames was developed that was verified using the numerical results of other researchers. This model was utilised to study the sway behaviour of steel frames with different conditions. This provided an initial method which can be used for further study and development of design rules for sway frames.

1.10 Conclusions

It is possible to design a structure economically provided the connection moment capacity, rotation capacity and the required rotation to produce the necessary degree of moment redistribution are known. Different attempts have been made to represent the connection behaviour by evaluating the test results. Mathematical formulae and

mechanical models have been proposed on the basis of test results. Many tests have now been performed, but the number of variables to be covered is too large for complete coverage. Preliminary models using FE packages by various researchers demonstrated that it is possible to numerically model the semi-rigid composite connections. The existing test results can be used to verify the FE model. The model can then be used to study the connection behaviour and the results used to develop prediction methods for moment capacity, rotation capacity and initial stiffness of the connection.

1.11 References

1-1 Johnson, R. P. and Hope-Gill, M. (1972) *Semi-rigid joints in composite frames*, IABSE Ninth Congress, Prelim Report, Amsterdam, pp. 133-144.

1-2 Zandonini, R. (1989) *Semi-Rigid Composite Joints*, Structural Connections and Strength, Chapter 3, ed R. Narayanan, Elsevier Applied Science, pp. 63-120.

1-3 Xiao, Y. (1994) *Behaviour of Composite Connections in Steel and Concrete*, Ph.D. thesis, University of Nottingham, UK.

1-4 Nethercot D. A. and Zandonini. R. (1989) *Methods of Prediction of Joint Behaviour: Beam to Column Connections*, Chapter 2, ed R. Narayanan, Elsevier Applied Science, pp. 23-62.

1-5 Benussi, F. Puhali, R., Zandonini, R. (1989) *Semirigid joints in steel-concrete composite frames*, Construzioni Metalliche n. 5.

1-6 Anderson, D. and Najafi, A. A. (1991) *Semi-continus composite frames in Eurocode4*, Connections in steel structures II: Behavior, Strength, and Design.

Proceedings of the second international workshop, Pittsburg, USA. pp. 142-151.

1-7 Anderson, D. and Najafi, A. A. *Composite connection with structural steel endplates, Reports to Steel Construction Institute*, No. 2 to No. 4, Department of Engineering, University of Warwick, UK.

1-8 Leon, R. T. *Behavior of semi-rigid composite frame*, Composite steel Structures: Advance, design and Construction, ed. R Narayanan, Elsevier Applied Science, London, pp. 145-153.

1-9 Li, T. Q., Moore, D. B., Choo, B. S. and Nethercot, D. A. *The Experimental Behaviour of a Full-scale Semi-rigidly Connected Composite Frame: Overall Considerations*, Journal of construction Steel Research (under review).

1-10 Xiao, Y., Nethercot, D. A. and Choo, B. S. (1993) *Composite connections in steel and concrete*, Final report to Building Research Establishment, Department of Civil Engineering, University of Nottingham, UK.

1-11 Xiao, Y., Choo, B. S. and Nethercot, D. A. (1994) *Composite connections in steel and concrete (I) Experimental behaviour of composite beam-to-column connections*, Journal of construction Steel Research, Vol. 31, pp. 3-30.

1-12 Li, T. Q., Nethercot, D. A. and Choo, B. S. (1996) *Behaviour of flush end plate composite connections with unbalanced moment and variable shear/moment ratios: part 1: experimental behaviour*, Journal of Constructional Steel Research, Vol. 38, No. 2, pp. 125-164.

1-13 Davison, J. B., Lam, D. and Nethercot, D. A. (1990) *Semi-rigid Action of Composite Joints*, The Structural Engineer, Volume 68 No. 24 December, pp. 489-499.

1-14 Uth, H. J. (1987) *Continuous composite beams in buildings - local instability in negative moment regions*, Dr-Ing. dissertation, University of Kaiserlautern, pp. 137.

1-15 Puhali, R., Smotlak, I. and Zandonini, R. (1990) *Semi-Rigid Composite Action: Experimental Analysis and a Suitable Model*, Journal of Constructional Steel Research Vol.15, pp. 121-151.

1-16 Law, C. L. C. (1983) *Plannar no-sway frames with semi-rigid beam - to - column joints*, Ph.D. thesis, University of Warwick, UK.

1-17 Aribert, J. M. and Lachal, A. (1992) *Experimental investigation of composite connection and global interpretation.* Proceedings of the COST C1 conference on Semi-Rigid joints, Strasbourg, France, pp. 158-169.

1-18 Echeta, C. B. and Owens, G. W. *A semi-rigid connection for composite frames: initial test results*, Proceedings of International conference on Joints in Structural Steelwork (ed. J. H. Howlett *et al.*), Pentech Press, London, pp. 3.20-3.38.

1-19 Zoetemeijer (1975) *Influence of normal- bending - and shear stresses in the web of European rolled sections*, Report N° 6-75-18, Stevin Laboratory, Delft University of Technology, The Netherlands.

1-20 Eurocode No 3 (1992) *Design of Steel Structures, Part 1.1: General Rules for Buildings*, DD ENV 1993-1-1, April 1992, European Committee for Standardisation (CEN).

1-21 CEN/TC 250 (1994) New Revised Annex J of Eurocode 3: Part 1.1, CEN document N419E.

1-22 Stephane, G. and Jaspart, J. P. (1996) *Influence of Structural Frame Behaviour on Joint Design,* Connections in Steel Structures III: Behaviour, Strength and Design, Edited by Reidar Bjorhovde, Andre Colson, Riccardo Zandonini, Proceedings of the Third International Workshop, Trento University, 29-31 May, 1995, pp. 321-330.

1-23 Johnson, R. P. and Law, C. L. C. (1981) *Semi-Rigid Joints for Composite Frames*, Proceedings of international conference on Joints in Structural Steelwork (ed J.H. Howlett), Pentech Press, London, pp. 3.3-3.19.

1-24 SCI report (1992) *Partial strength moment resisting connections in composite frames,* Document No. SCI-RT-275, Revision 0, April.

1-25 Eurocode No 4 (1992) *Design of Composite Steel and Concrete Structures,* March, European Committee for Standardisation (CEN).

1-26 BSI, BS5950 (1985) *Structural use of Steelwork in Buildings, Part 1: Code of Practice for Design of simple and Continuous Construction: Hot Rolled Sections,* British Standars Institution, London, UK.

1-27 Xiao, Y., Nethercot, D. A. and Choo, B. S. (1994) *Design of semi-rigid composite beam-column connections*, Building the future; Innovation in

Design, Materials and Construction, Edited by F. K Garas *et al*, E & FN Spon, London, First edition, pp. 391-406.

1-28 Li, T. Q. (1994) *The Analysis and Ductility Requirements of Semi-Rigid Composite Frames*, Ph.D. thesis, University of Nottingham, UK.

1-29 Anderson, D. and Najafi, A. A. (1994) *Performance of Composite Connections: Major Axis End Plate Joints*, Journal of Construction Steel Research, Vol. 31, No 1, pp. 31-57.

1-30 Ren, P. and Crisinel, M. (1996) *Prediction method for moment-rotation behaviour of composite beam to steel column connections*, Connections in Steel Structures III: Behaviour, Strength and Design, Edited by Reidar Bjorhovde, Andre Colson, Riccardo Zandonini, Proceedings of the Third International Workshop, Trento University, 29-31 May1995, pp. 33-46.

1-31 Tschemmernegg, F. (1988) *On the Nonlinear Behaviour of Joints in Steel Frames,* Connections in Steel Structures: Behaviour, Strength and Design (ed. R.Bjorhovde *et al*). Elsevier Applied Science Publishers, London, pp. 158-165.

1-32 Tschemmernegg, F. (1992) *A New Spring Model for Composite Joints*, Proc. of COST C1 Conference on Semi-Rigid Joints, Strasbourg, France, pp. 356-368.

1-33 Madas, P. J. (1993) *Advanced Modelling of Composite Frames Subjected to Earthquake Loading*, Ph.D. thesis, University of London, UK.

1-34 Bose, S. K., McNeice, G. M. and Sherbourne, A. N. (1972) *Column webs in steel beam to column connections. Part I, Formulation and verification*, Computers and Structures, Vol.2 (February), pp. 253-72.

1-35 Patel, K. V. and Chen, W. F. (1984) *Nonlinear analysis of steel moment connections*, ASCE, Journal of Structural Engineering, Vol.110(8), pp. 1861-75.

1-36 Bathe, K. J., Wilson, E. L. and Iding, R. H. (1974) *NONSAP: A Structural Analysis Program for Static and Dynamic Response of Nonlinear Systems.* Structuctural Engineering Laboratory, University of California, Berkeley, USA.

1-37 Atamaz Sibai, W. and Frey, F. (1988) *Numerical simulation of the behaviour up to collapse of two welded unstiffened one-sided flange connections,* Connections in Steel Structures: Behaviour, Strength and Design (ed. R. Bjorhovde *et al.*). Elsevier Applied Science Publishers, London, pp. 85-92.

1-38 Lipson, S. L. and Hague, M. I. (1978) *Elasto-plastic analysis of single-angle bolted welded connections using the finite element method*, Computers and Structures,Vol.9(6), pp. 533-45.

1-39 Richard, R. M, Rabern D. A., Hornby, D. E. and Williams, G. C. (1983) *Analytical models for steel connections*, In Behavoiur of Metal Structures Proc. W.H. Munse Symposium, (ed. W.J. Hall & M.P. Gaus). American Society of Civil Engineers. May.

1-40 Patel, K. V. and Chen, W. F. (1985) *Analysis of a fully bolted moment connection using NONSAP*, Computers and Structures, Vol.21(3), pp. 505-11.

1-41 Krishnamurthy, N. (1980) *Modelling And Prediction of Steel Bolted Connection Behaviour*, Comput. Structures Vol.11 pp. 75-82.

1-42 Leon, R. and Lin, J. (1986) *Towards the Development of an Analytical Model for Composite Semi-Rigid Connections*, Report to AISC, Struct. Eng. Report. No86-06, University of Minnesota, Minneapolis, p 83.

1-43 Aribert, J. M. and Lachal, A., Muzeau, J. P. and Racher, P. (1994) *Recent tests on steel and composite connections.* Proceedings of the COST C1 conference on Semi-Rigid joints, Strasbourg, France, pp. 61-74.

1-44 Li, T.Q., Nethercot, D. A. and Choo, B.S. (1991) *Continuity Effects in Composite Frames*, Progress report No.2 to SERC, SR92006, University of Nottingham, UK.

1-45 Ren, P. and Crisinel, M. (1994) *Effect of Reinforced Concrete Slab on the Moment-Rotation Behaviour of Standard Steel Beam-to-Column Joints. Experimental study and Numerical Analysis.* 2nd workshop COST C1.

1-46 Huang, J. and Morris, G. (1991) *Analysis of flexibly connected frames under non - proportional loading,* Proceedings of the second international workshop on connections in steel structures, 10-12 April, Pennsylvania, USA, pp. 236-243.

1-47 Colson, A. and Bjorhovde, R. (1991) *Connection Moment - Rotation curves for Semi - rigid frame design,* Proceedings of the second international workshop on connections in steel structures, 10-12 April, Pennsylvania, USA, pp. 282-294.

1-48 Deirlein, G. G. (1991) *An Inelastic Analysis and Design System for Steel Frames with Partially Restrained Connections,* Proceedings of the second international workshop on connections in steel structures, 10-12 April, Pennsylvania, USA, pp. 408-415.

1-49 Li, T. Q., Choo, B.S. and Nethercot, D. A. (1995) *Connection Element Method for the Analysis of Semi-rigid Frames,* Journal of Constructional Steel Research,Vol 32, pp. 143-171.

1-50 Ye Mei-xin, Nethercot, D. A. and Li, T. Q. (1996) *Non Linear Finite Element Analysis of Composite Frames*, Proceedings of the Instution of Civil Engineers, Structures & Buildings, Vol. 116, pp. 244-247.

1-51 Li, T. Q., Choo, B.S. and Nethercot, D. A. (1995) *Determination of Rotation Capacity Requirements for Steel and Composite Beams*, Journal of Constructional Steel Research,Vol. 32, pp. 303-332.

1-52 Jaspart, J. P. (1991) *Etude de la semi-rigidite' des noeuds poutre-colonne et son influence sur la re' sistance et la stabilite' des ossatures en acier*, Ph.D. Thesis, Department MSM, University of Lie'ge, Belgium.

1-53 Ammerman, D. J. and Leon, R. T. (1990) *Unbraced Frames with Semi-Rigid Composite Connections,* Engineering Journal/American Institute of Steel Construction, first quarter pp. 12-21.

Table 1-1 Composite connection tests before 1987 (ref. 1-3)

Author	Specimen	Connection type *	Column orientation **	Test M (kN•m)	M/M_p	M/M_{p-}	M/M_{p+}	ϕ_u (mRad)	Failure mode ***
Johnson &Hope-Gill 1972	HB50	CL	IN(F)	101	1.24	0.84	0.67	>60	G
	HB51	CL	IN(F)	105	0.56	0.47	0.35	>70	A
	HB52	CL	IN(F)	222	1.21	0.89	0.77	>65	A
	HB53	CL	IN(F)	254	1.45	0.89	0.84	30	K
	HB54	CL	IN(F)	303	1.35	0.89	0.79	33	E.F
Van Dalen &Godoy 1982	CB1	CL	IN(F)	120	1.19	0.98	0.57	47	A
	CB2	CL	IN(F)	163	1.44	1.15	0.77	36	A
	CB3	CL	IN(F)	157	1.39	1.1	0.74	10	A
	CB4	CL	IN(F)	138	1.37	1.12	0.65	22	A
	CB5	CL	IN(F)	162	1.26	1.14	0.77	14	A
Echeta & Owens 1983	1B	CL	IN(F)	111	1.06	0.8	0.56	>32	A
	2BS	CL	EX(F)	65	0.62	0.52	0.33	>34	B
	3BS	CL	EX(F)	72	0.46	0.39	0.37	>30	A
	4BS	CL	EX(F)	68	0.43	0.37	0.35	>50	I
	5BS	CL	EX(F)	50	0.45	0.38	0.29	>45	A
Law &Johnson 1983	JX1	FE	IN(F)	354	0.87	0.66	0.55	24	A
	JX2	FE	IN(F)	370	0.9	0.68	0.57	35	A
	JY1	FE	IN(F)	384	0.94	0.71	0.59	10	A
	JY2	FE	IN(F)	600	1.47	1.11	0.93	88	E.F
	JC1	FE	IN(F)	449	1.1	0.83	0.69	19	B
	JC2	FE	IN(F)	530	1.3	0.94	0.82	18	B
Ammerman &Leon.1987	SRCC1ML	CL	IN(F)	235	0.94	0.64	0.53	30	A
	SRCC1MR	CL	IN(F)	305	1.22	0.84	0.69	39	J
Benussi. Puhali &Zandonini 1986	SJA-10	PE	IN(F)	165	0.91	0.67	0.43	>21	A
	SJA-14	PE	IN(F)	221	1.22	0.81	0.58	>23	A
	SJB-10	FE	IN(F)	208	1.15	0.84	0.54	>22	A
	SJB-14	FE	IN(F)	261	1.44	0.96	0.68	24	E.F

* Connection type: Flush endplate(FE), Partial depth endplate(PE),
Cleated (CL), Finplate(FN), Extended endplate(EE)

** Column orientation: IN(internal joint), EX(external joint), F(major axis), W(minor axis)

*** Failure modes: A. Test terminated for excessive joint deformation B. Fracture of slab reinforcement
C. Excessive deformation of column flange D. Local buckling of column web
E. Buckling of beam flange F. Buckling of beam web
G. Shear connector failure H. Web side plate twisting
I. Anchorage failure of reinforcement J. Failure of connecting bolts
K.Failure of slab in shear

Table 1-2 Recent tests (ref. 1-3)

Author	Specimen	Connection type	Column orientation	Test M (kN•m)	M/M_p	M/M_{p-}	M/M_{p+}	ϕ_u (mRad)	Failure mode
Kemp &Clercq 1985	C1	PE	IN(F)	292	2.10	1.51	1.07	22.6	E.F
	C2	PE	IN(F)	330	1.48	1.31	0.89	29.9	E.F
	C3	EE	IN(F)	253	1.82	1.57	0.93	>34.3	G
Lam, Davison &Nethercot 1989	C1	CL	EX(F)	29.5	0.15	0.13	0.07	22.5	I
	C2	CL	EX(F)	50	0.25	0.16	0.13	21.5	I
	C3	CL	EX(F)	60	0.18	0.13	0.11	20.5	I
	C4	CL	EX(F)	14	0.04	0.03	0.03	28	I
	C5	CL	EX(W)	94	0.28	0.30	0.24	18	I
	C6	CL	IN(F)	31.5	0.16	0.10	0.08	10	B
	C7	CL	IN(F)	140	0.71	0.46	0.35	31	C
	C8	CL	IN(F)	181	0.91	0.59	0.45	32.5	C
	C9	CL	IN(W)	160	0.81	0.53	0.39	15	B
	C10	CL	IN(W)	175	0.53	0.37	0.29	23	A
	C11	CL	IN(W)	200	0.60	0.46	0.35	12	A
MacGinley 1989	Test1	PE	IN(F)	117	0.94	0.72	0.54	38	A
	Test2	CL	IN(F)	71	0.57	0.43	0.32	25	A
Puhali, Smotlak &Zandonini 1990	SJA14/1	PE	IN(F)	165	1.36	0.78	0.61	34	A
	SJA14/2	PE	IN(F)	221	1.34	0.76	0.60	47	A
	SJA14/4	PE	IN(F)	208	1.33	0.73	0.59	24	A
	RJ14	WE	IN(F)	261	1.52	0.87	0.68	18	E,F
Altmann, Maquoi &Jaspart 1990	30x3c.2	CL	IN(F)	253	2.94	0.99	0.70	40	A,D
	30x3c.3	CL	IN(F)	288	1.95	0.98	0.80	10	D
	30x3c.1	CL	IN(F)	322	1.35	0.94	0.89	23	D
	30x3c.6	CL	IN(F)	293	3.34	1.14	0.81	43	A
	30x3c.8	CL	IN(F)	287	1.94	0.95	0.80	18	D
	30x3c.7	CL	IN(F)	328	1.37	0.95	0.91	19	D
	30x2c.2	CL	IN(F)	208	2.41	0.81	0.58	28	A
	30x2c.1	CL	IN(F)	262	1.77	0.89	0.73	21	J
	30x2c.3	CL	IN(F)	322	1.35	0.94	0.89	20	D
	30x2c.5	CL	IN(F)	203	2.11	0.79	0.56	40	A
	30x2c.6	CL	IN(F)	297	2.00	0.99	0.82	26	D
	30x2c.7	CL	IN(F)	322	1.35	0.94	0.89	21	D
	36x3c.1	CL	IN(F)	288	3.34	0.77	0.56	27.2	D
	36x3c.2	CL	IN(F)	334	2.25	0.80	0.65	16	D
	36x3c.3	CL	IN(F)	370	1.55	0.79	0.73	17	D
	36x3c.5	CL	IN(F)	295	3.42	0.79	0.58	35.4	D
	36x3c.6	CL	IN(F)	357	2.41	0.85	0.70	14	D
	36x3c.7	CL	IN(F)	395	1.65	0.84	0.78	20	B
	36x2c.2	CL	IN(F)	250	2.90	0.67	0.49	43	D
	36x2c.1	CL	IN(F)	343	2.32	0.82	0.67	46	D
	36x2c.3	CL	IN(F)	367	1.54	0.78	0.72	17	A
	36x2c.7	CL	IN(F)	252	2.92	0.67	0.49	61	D
	36x2c.6	CL	IN(F)	346	2.34	0.83	0.68	21	D
	36x2c.5	CL	IN(F)	364	1.52	0.77	0.71	25	D

Table 1-2 Recent tests (continued, ref. 1-3)

Leon 1990	SRCC4M	CL	IN(F)	508.4	0.97	0.69	0.53	12.3	A
	SRCC5M	CL	IN(F)	377.8	0.72	0.50	0.39	39	A
	SRCC9M	CL	IN(F)	450.9	0.86	0.61	0.47	45	A
	SRCC10M	CL	IN(F)	418.4	0.79	0.56	0.43	48.3	A
Anderson & Najafi 1992	Test1	FE	IN(F)	262	1.35	0.96	0.78	28	B
	Test2	EE	IN(F)	291	1.50	1.07	0.86	20	E
	Test3	FE	IN(F)	179	0.92	0.69	0.53	15.7	B
	Test4	FE	IN(F)	243	1.25	0.82	0.72	9.2	G
	Test5	FE	IN(W)	293	1.51	1.07	0.87	22.5	B
	Test6	FE	IN(W)	138	0.71	0.63	0.41	2.8	B
	Test7	FE	IN(F)	302	1.57	1.06	0.89	22.7	E,F
	Test8	FE	IN(W)	207	1.06	0.86	0.61	4.8	B
	Test10	FE	IN(F)	416	1.22	0.92	0.68	14	B
Xiao, Nethercot & Choo 1992	SCJ1	CL	IN(F)	43.1	0.21	0.20	0.12	14.3	B
	SCJ2	FN	IN(F)	29.6	0.15	0.14	0.07	16.4	B
	SCJ3	FE	IN(F)	85.7	0.42	0.39	0.23	7.2	B
	SCJ4	FE	IN(F)	202.9	0.99	0.66	0.55	23.4	C,D
	SCJ5	FE	IN(F)	240.8	1.18	0.78	0.62	26	G,E
	SCJ6	FE	IN(F)	157.6	0.79	0.53	0.41	11.5	C,D
	SCJ7	FE	IN(F)	204.5	1.03	0.67	0.56	26.5	G,D
	SCJ8	PE	IN(F)	84	0.42	0.30	0.24	29	F
	SCJ9	PE	IN(F)	107.5	0.54	0.39	0.31	27	F
	SCJ10	PE	IN(F)	147.8	0.74	0.53	0.50	16.5	C,D
	SCJ11	CL	IN(F)	169.5	0.85	0.63	0.48	14.3	C,D
	SCJ12	FN	IN(F)	101.3	0.51	0.38	0.29	39	H
	SCJ13	PE	IN(W)	181.4	0.84	0.60	0.45	19.3	A
	SCJ14	PE	IN(W)	89.8	0.42	0.30	0.25	34.4	F
	SCJ15	FE	IN(F)	185.5	0.86	0.59	0.48	23.2	A
	SCJ16	FN	IN(F)	224.7	0.29	0.24	0.18	27.1	H
	SCJ17	FN	IN(F)	97.4	0.45	0.34	0.25	44.1	H
	SCJ18	PE	EX(W)	85.5	0.40	0.28	0.22	17.9	I
	SCJ19	PE	EX(W)	60.8	0.28	0.20	0.18	41.6	I
Aribert & Lachal 1992	A2	FE	IN(F)	296	0.99	0.90	0.70	26	B,J
	A3	FE	IN(F)	152	1.51	0.77	0.74	36	B,J
	A4	FE	IN(F)	297	1.00	0.71	0.70	35	B,J
	B2	EE	IN(F)	376	1.27	1.18	0.89	38	B,J
	B3	EE	IN(F)	392	1.31	1.07	0.93	40	J,B
	C1	FE	IN(F)	344	1.15	0.84	0.82	28	J
	C2	FE	IN(F)	326	1.09	0.83	0.77	29	G
	C3	FE	IN(F)	288	0.97	0.78	0.68	21	G
Li, Nethercot &Choo 1993	CJS-1	FE	IN(F)	181	1.91	0.94	0.65	54	E,F
	CJS-2	FE	IN(F)	173	1.83	0.90	0.62	63	E,F
	CJS-3	FE	IN(F)	149	1.57	0.77	0.54	78	E,F
	CJS-4	FE	IN(F)	160	1.68	0.83	0.58	60	E,F
	CJS-5	FE	IN(F)	195	2.05	1.01	0.70	51	K
	CJS-5	FE	IN(F)	174	1.84	0.91	0.63	84	E,F

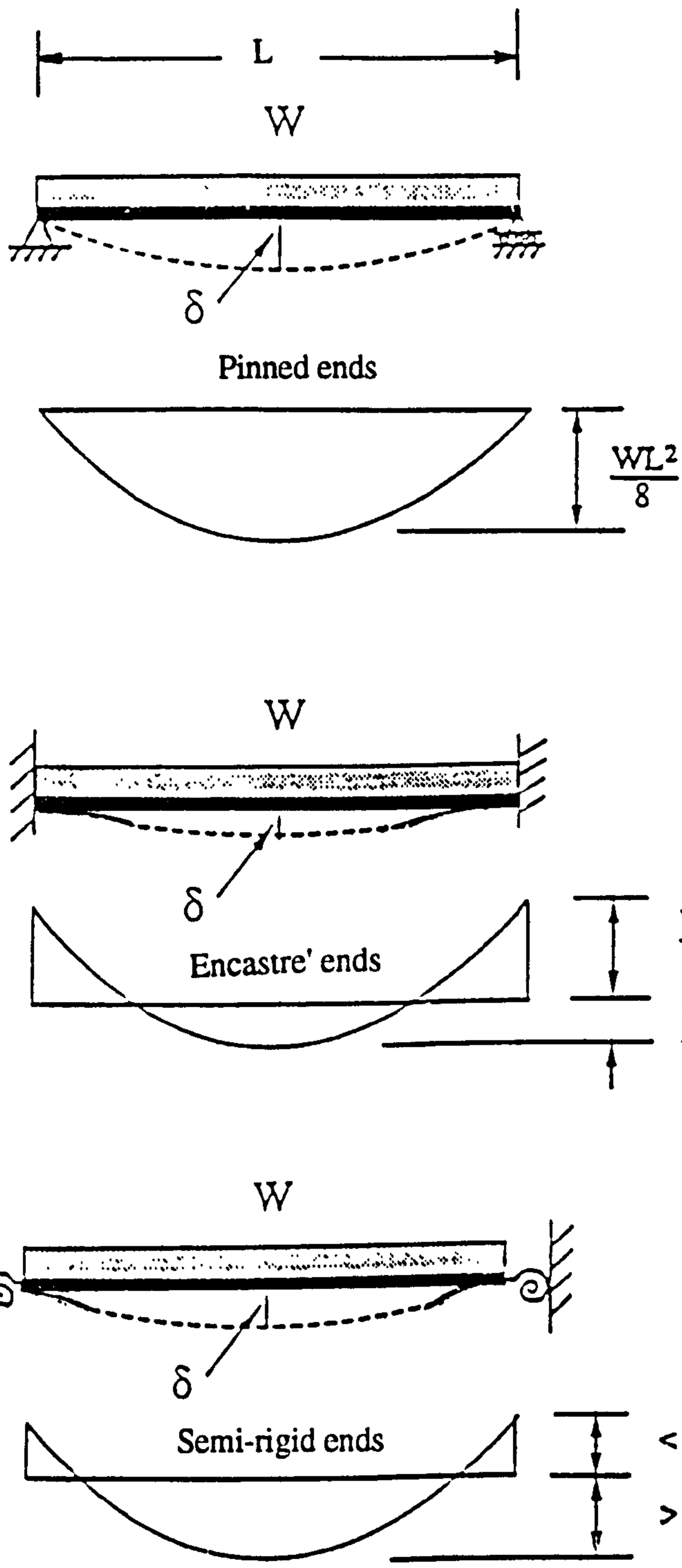

Figure 1-1 Moment diagram of a beam with uniformly distributed load and different support conditions

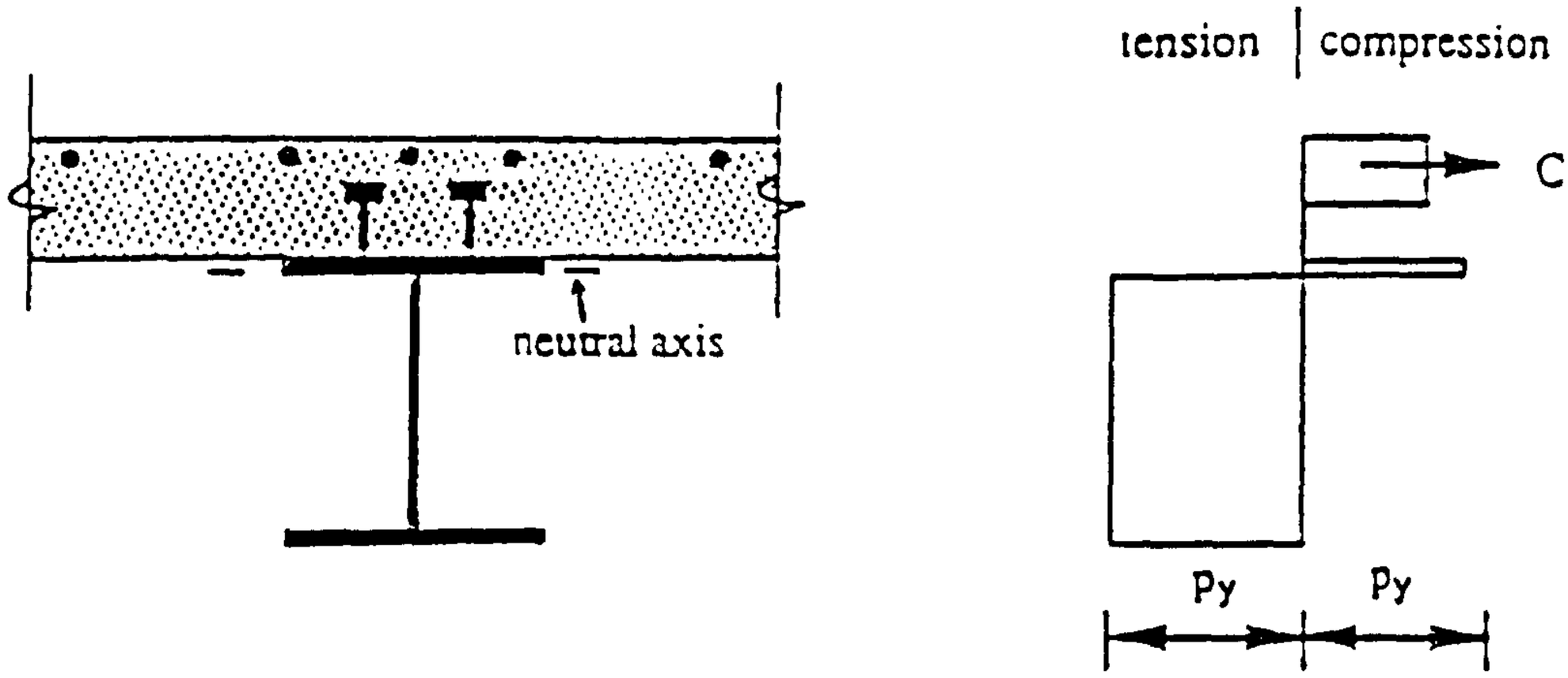

(a) Sagging bending (mid-span)

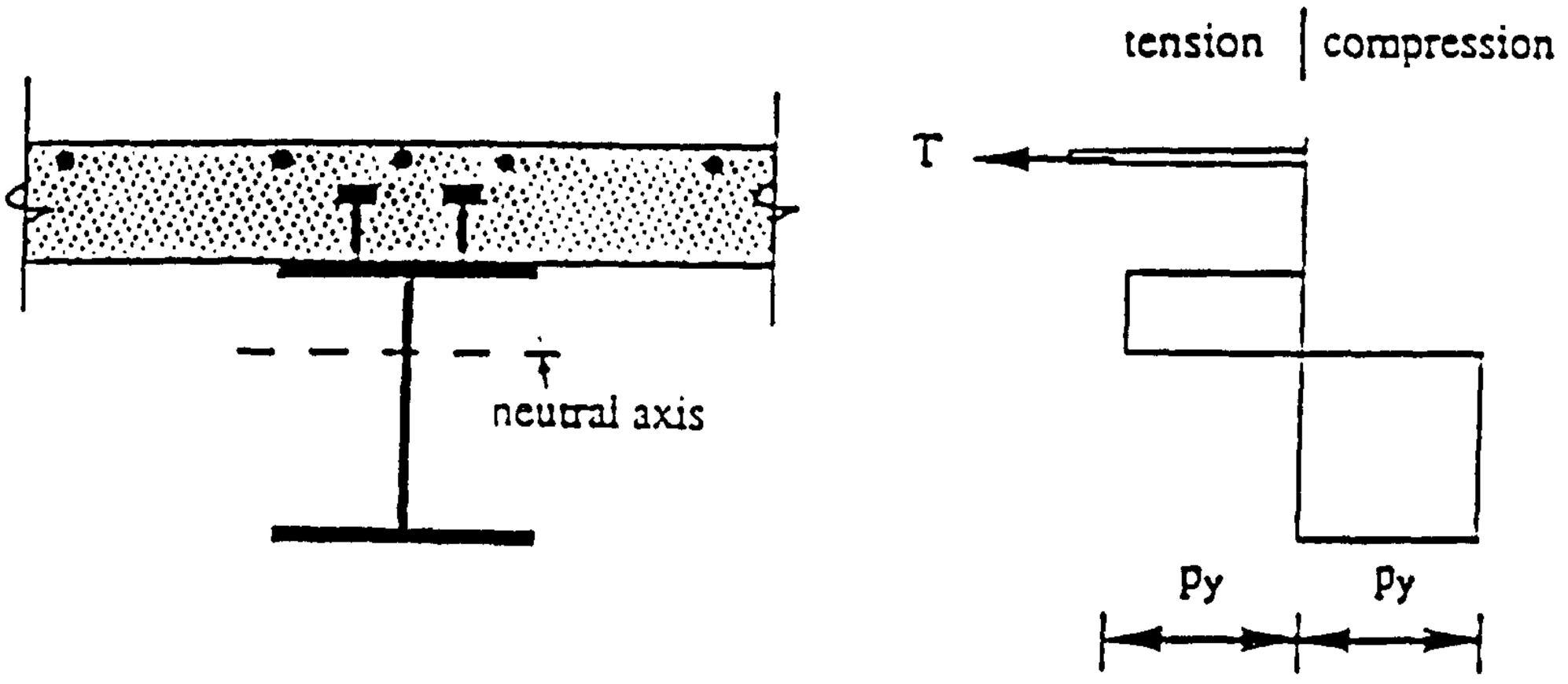

(b) Hogging bending (support)

Figure 1-2 Composite beam in sagging and hogging bending

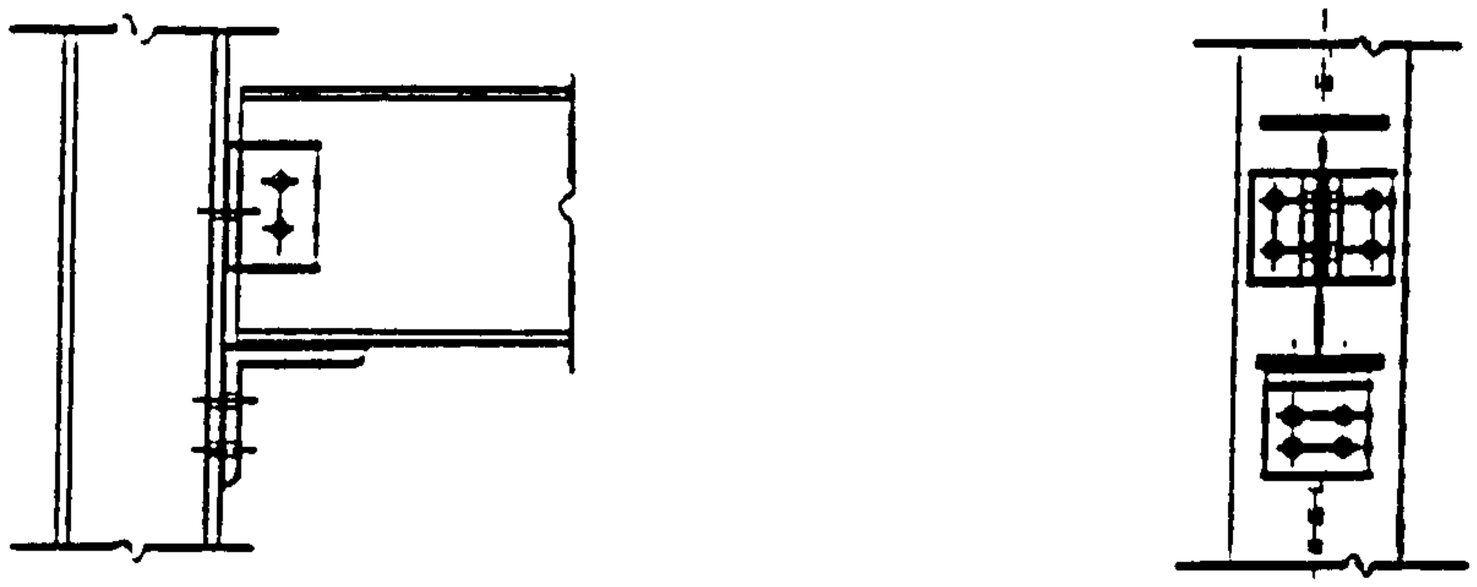

(a) Type I Seating cleat joint

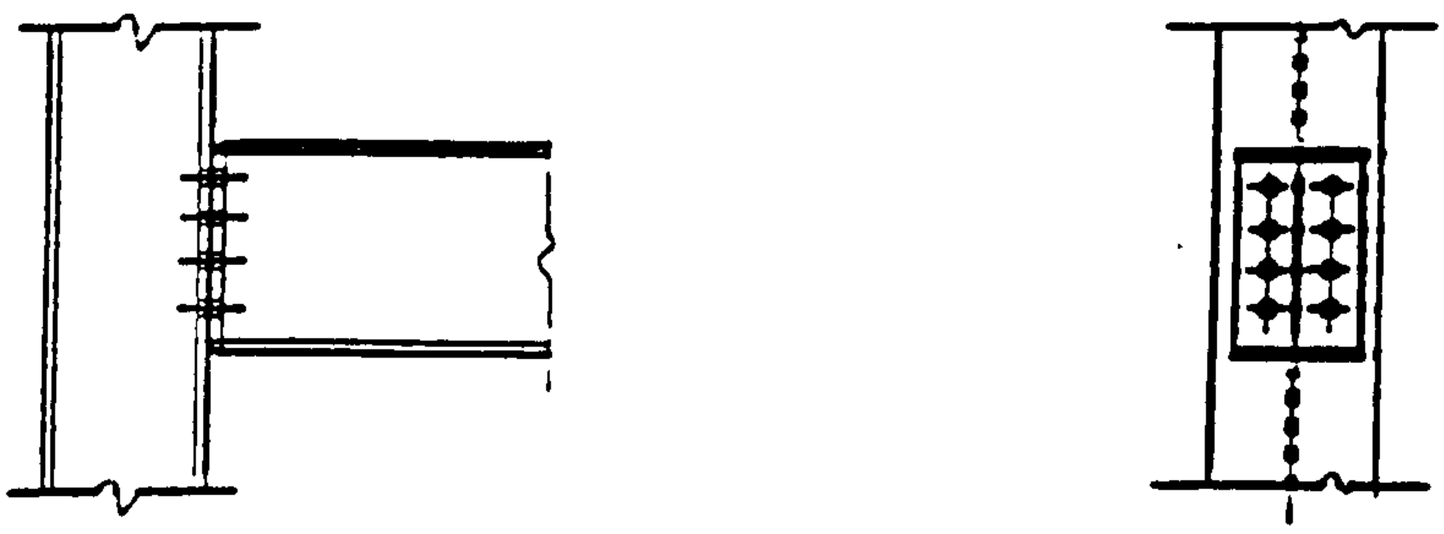

(b) Type II Flush endplate joint

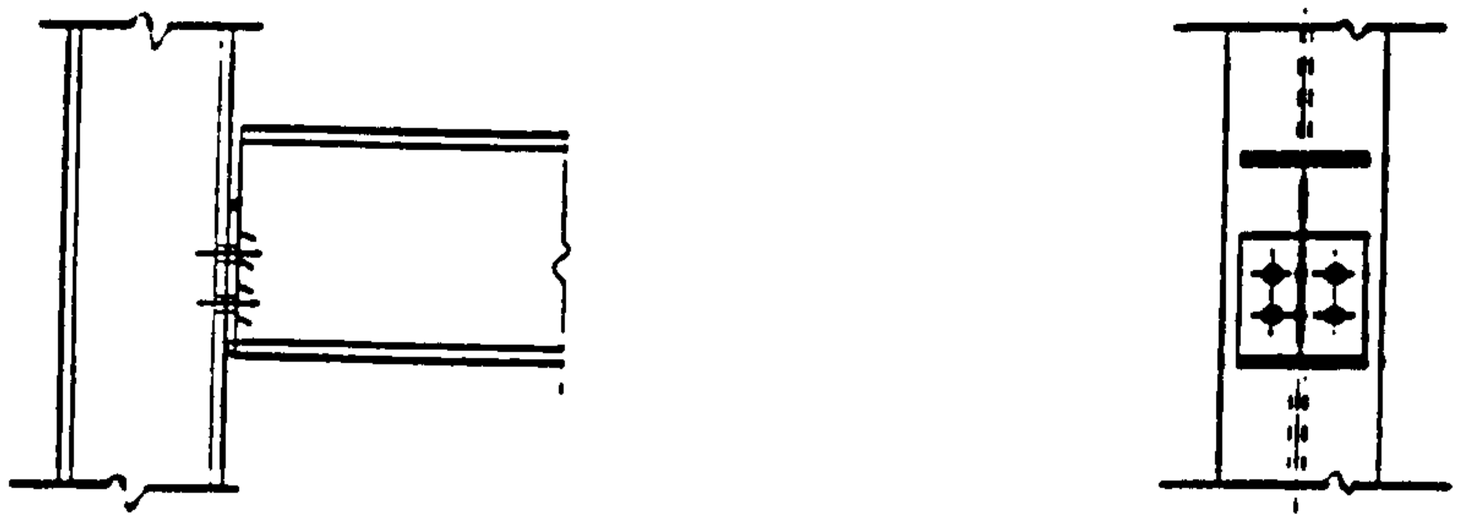

(c) Type III Partial depth endplate joint

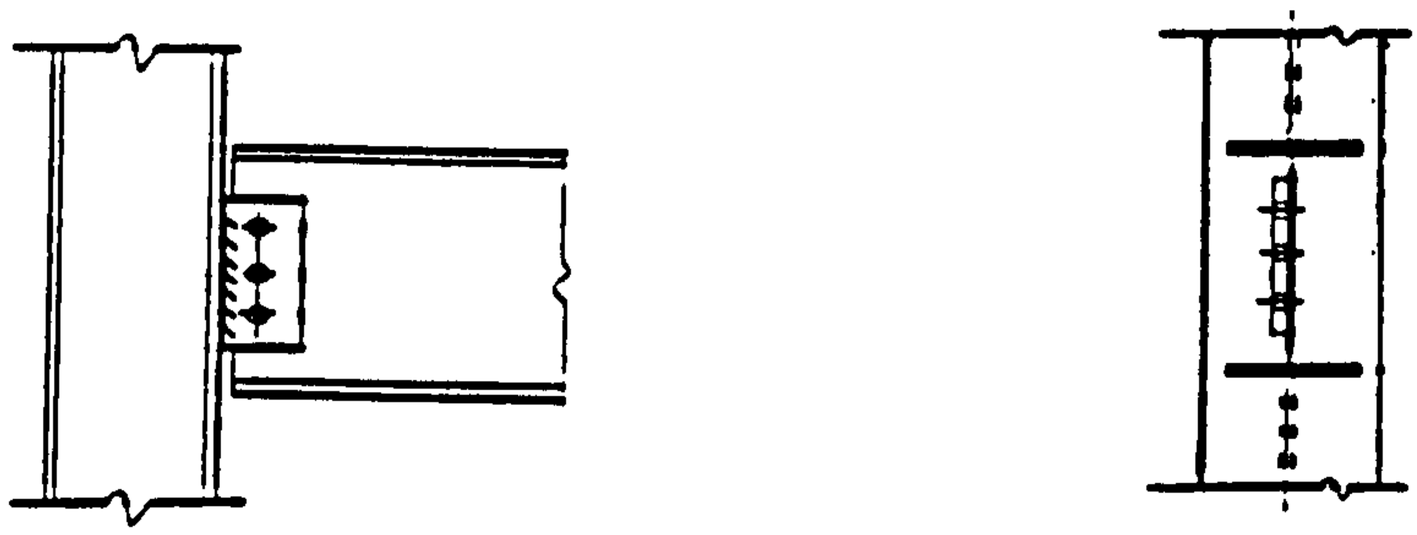

(d) Type IV Finplate joint

Figure 1-3 Four types of beam - to - column connections

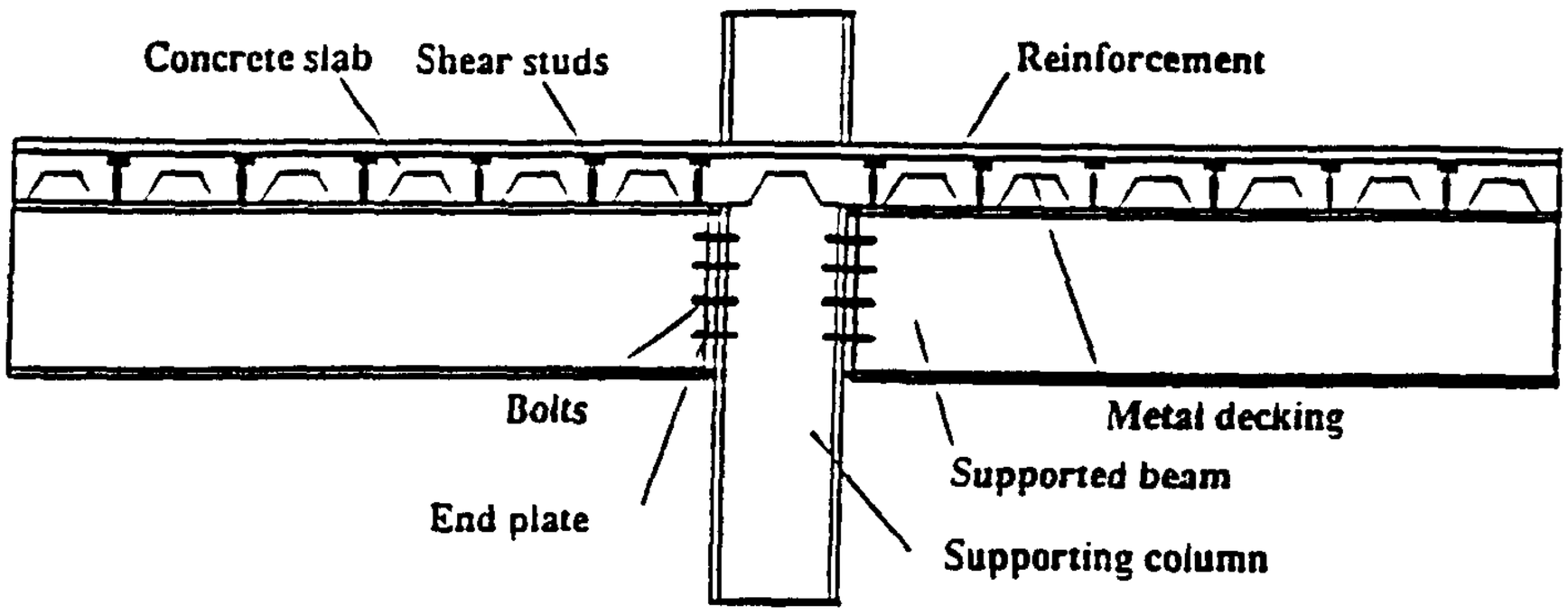

(a) Composite flush endplate connection

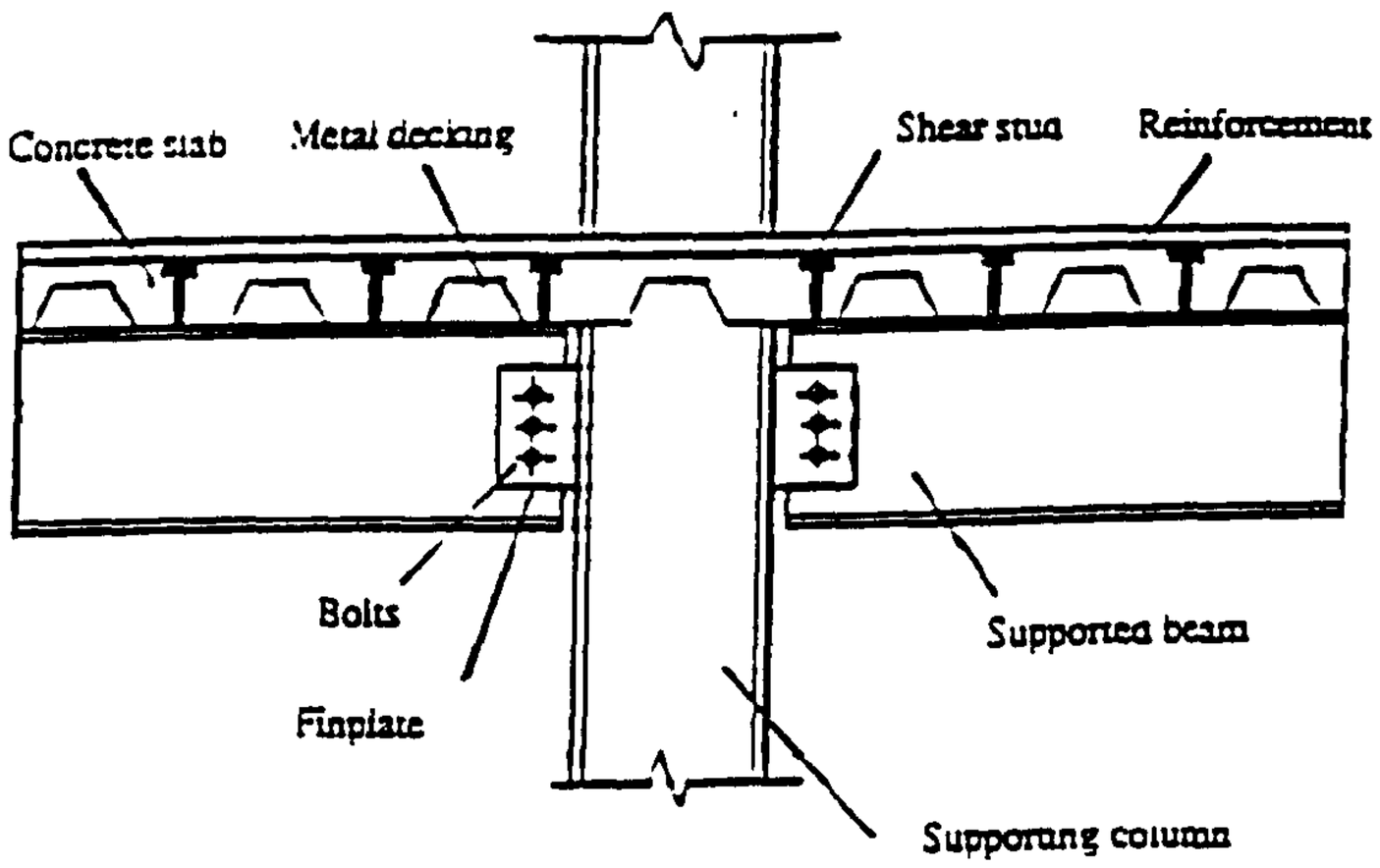

(b) Composite finplate connection

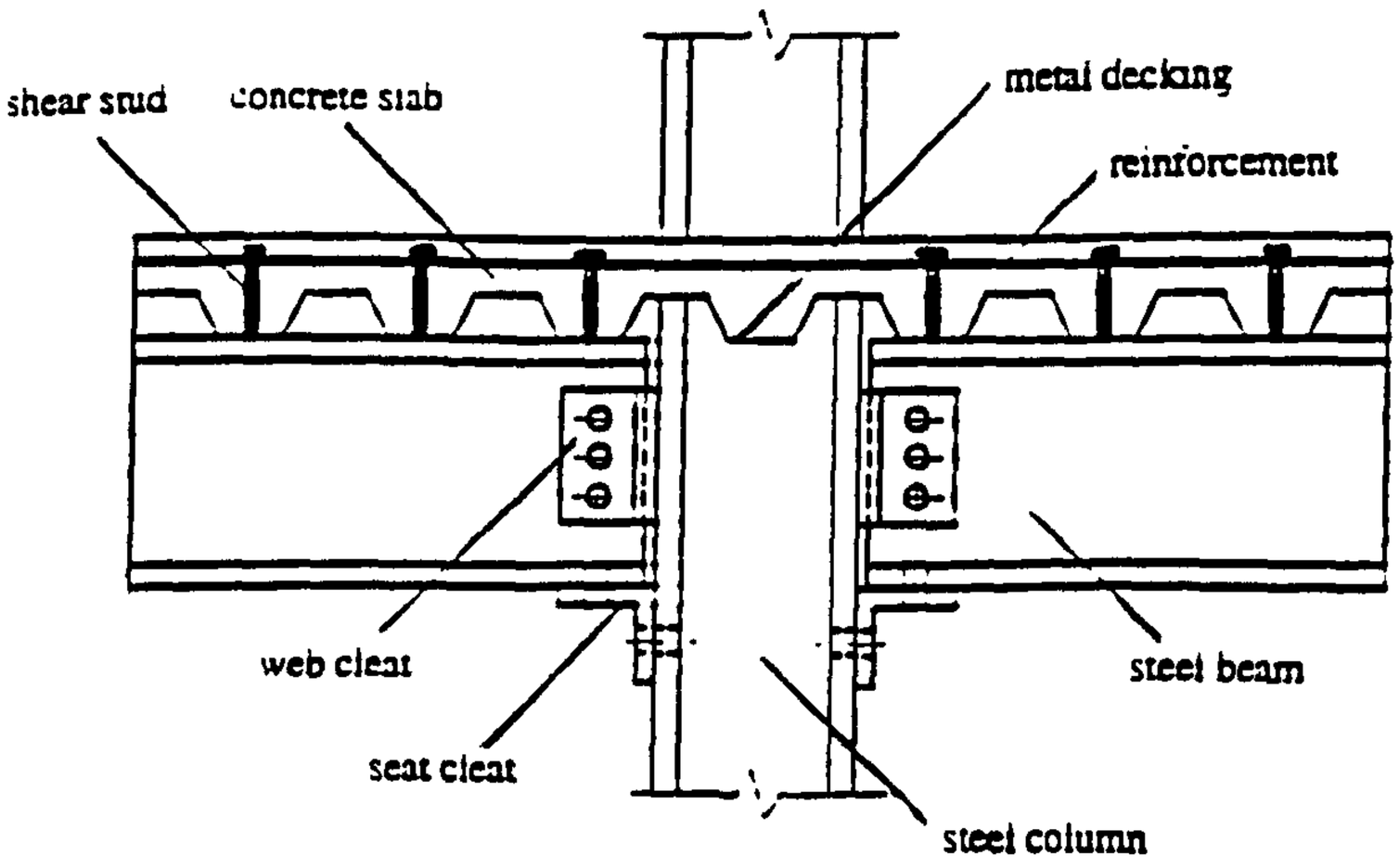

(c) Composite angle cleated connection

Figure 1-4 Composite connections with components

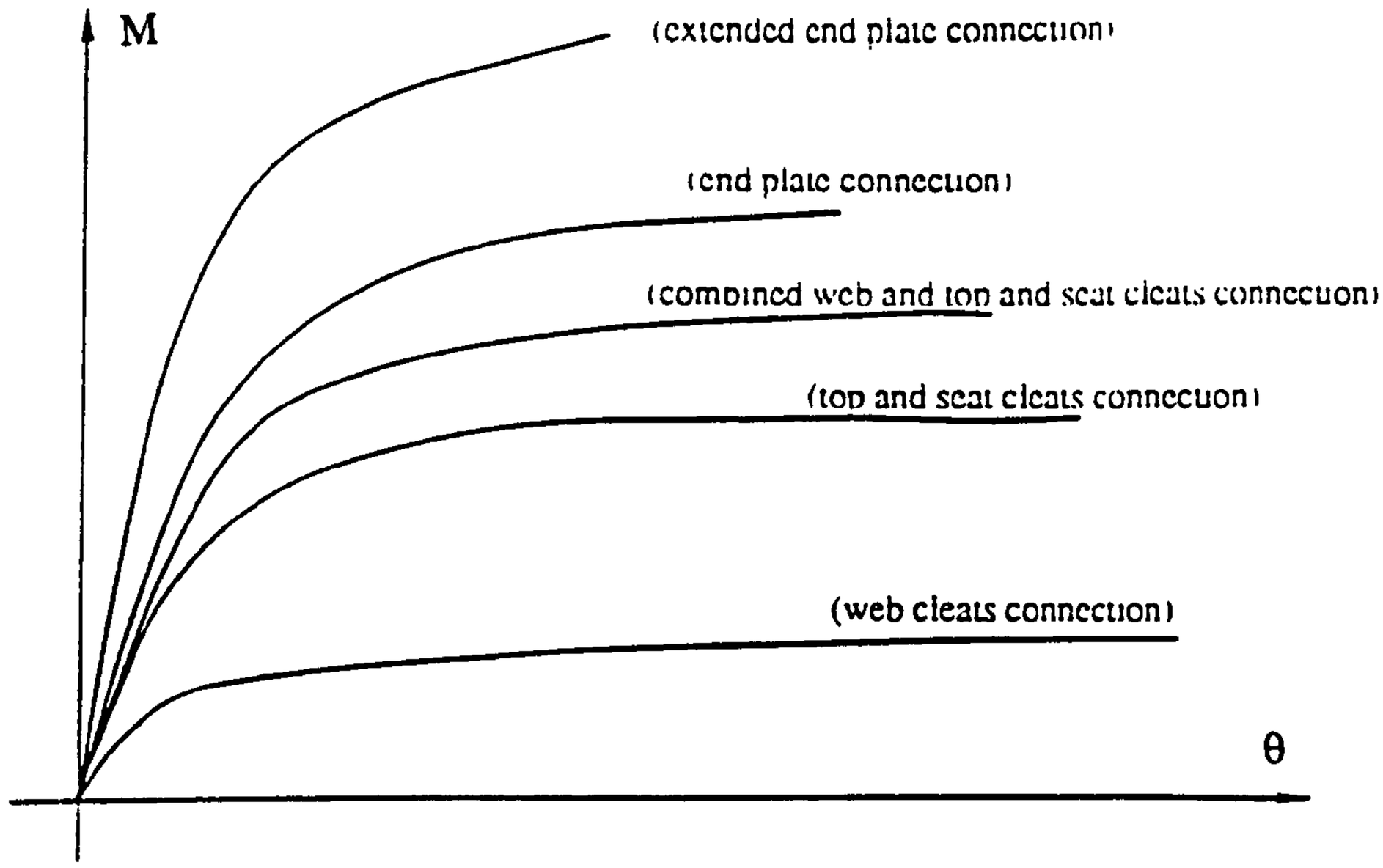

Figure 1-5 Typical moment - rotation curves of commonly used steel connections

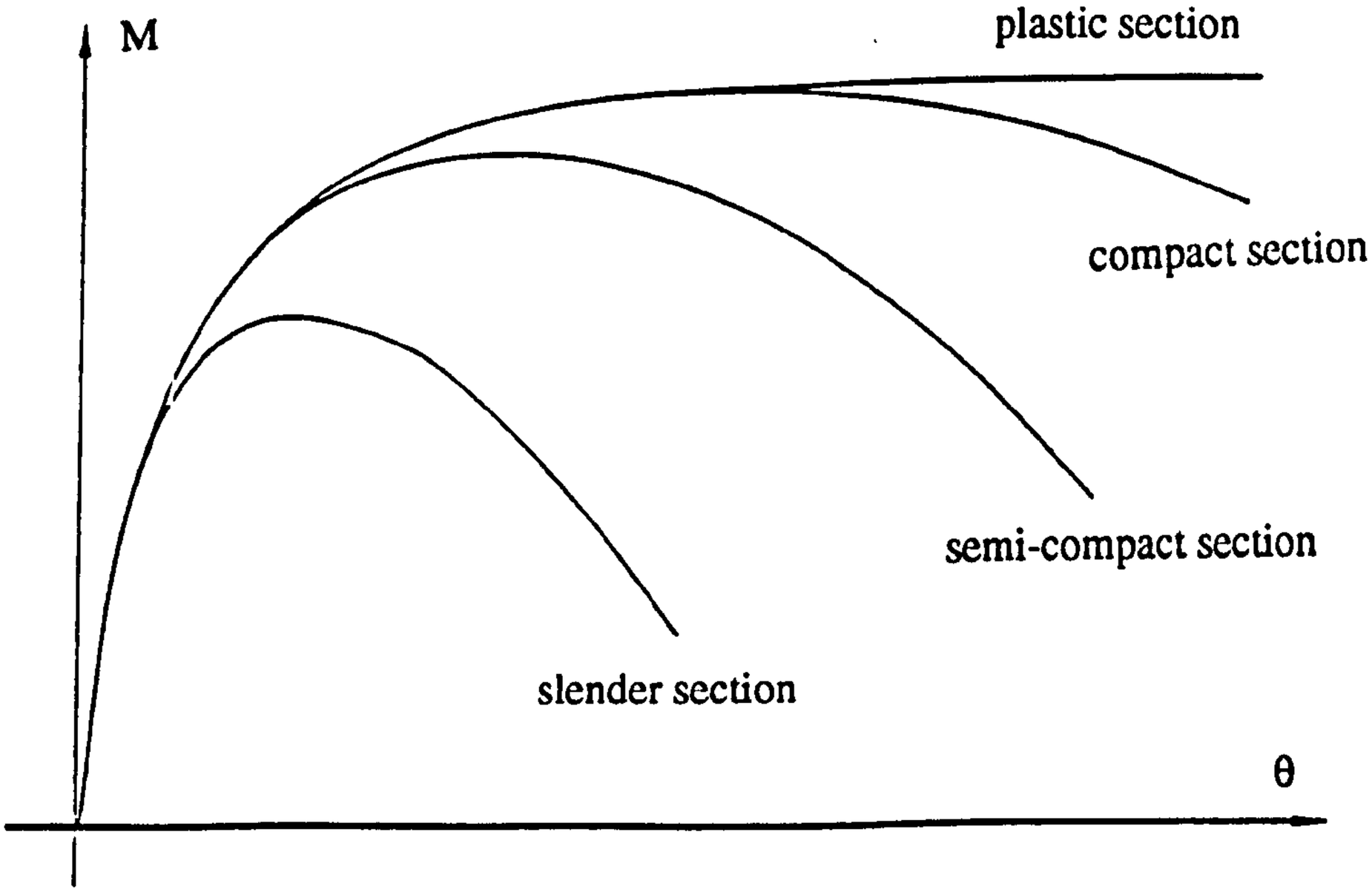

Figure 1-6 The effects of steel beam section classes on connection moment - rotation curves

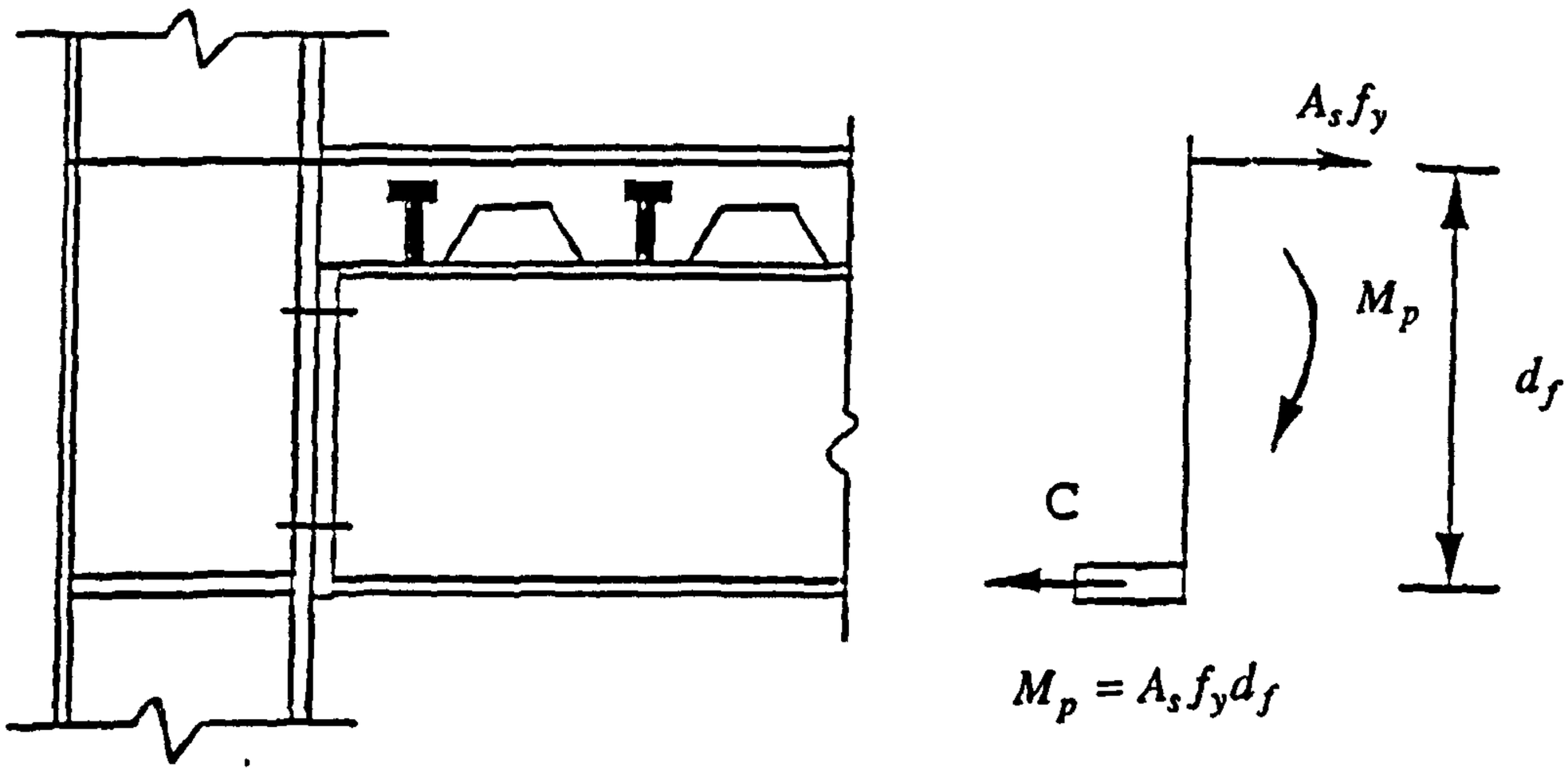

Figure 1-7 Load transfer in a composite connection (Johnson & Hope-Gill, ref. 1-1)

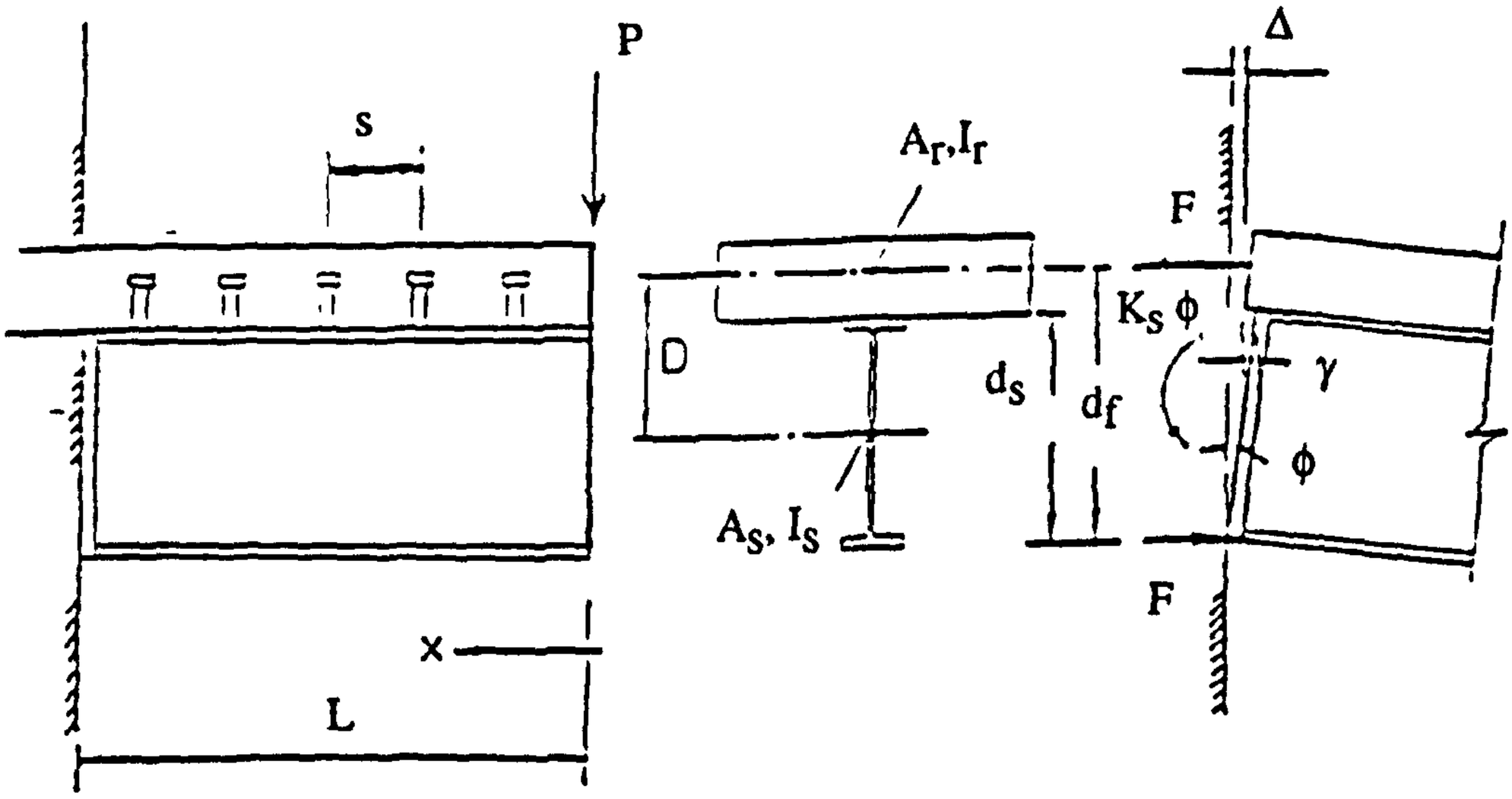

1-8a The model for determining the elastic stiffness in Johnson and Law's method (ref. 1-23)

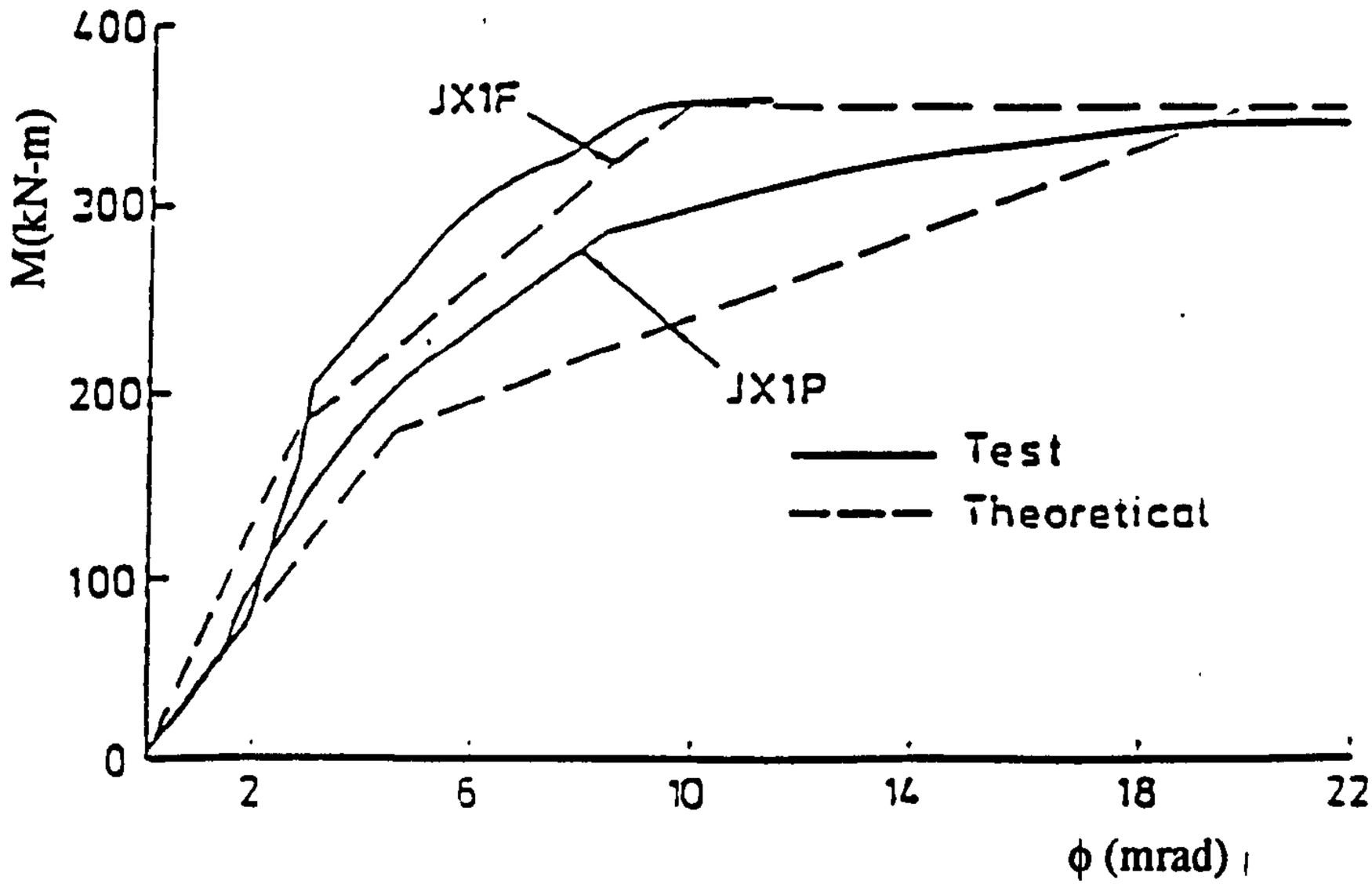

1-8b Comparison of experimental and predicted results in Johnson and Law's method (ref. 1-23)

Figure 1-8 Johnson and Law's method (ref. 1-23)

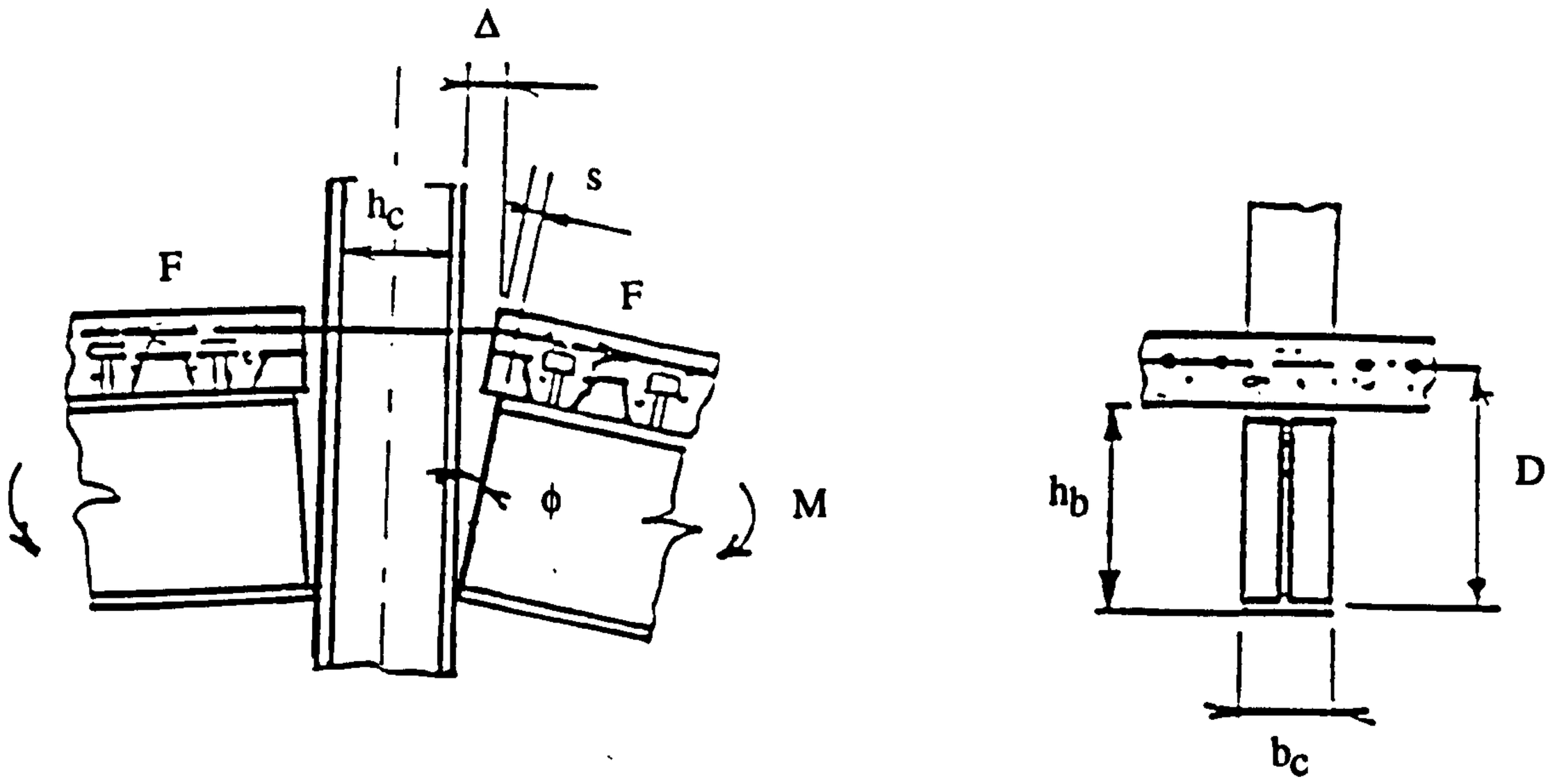

Figure 1-9 Model for establishing relationship of deformation and force in Aribert's model (ref. 1-17)

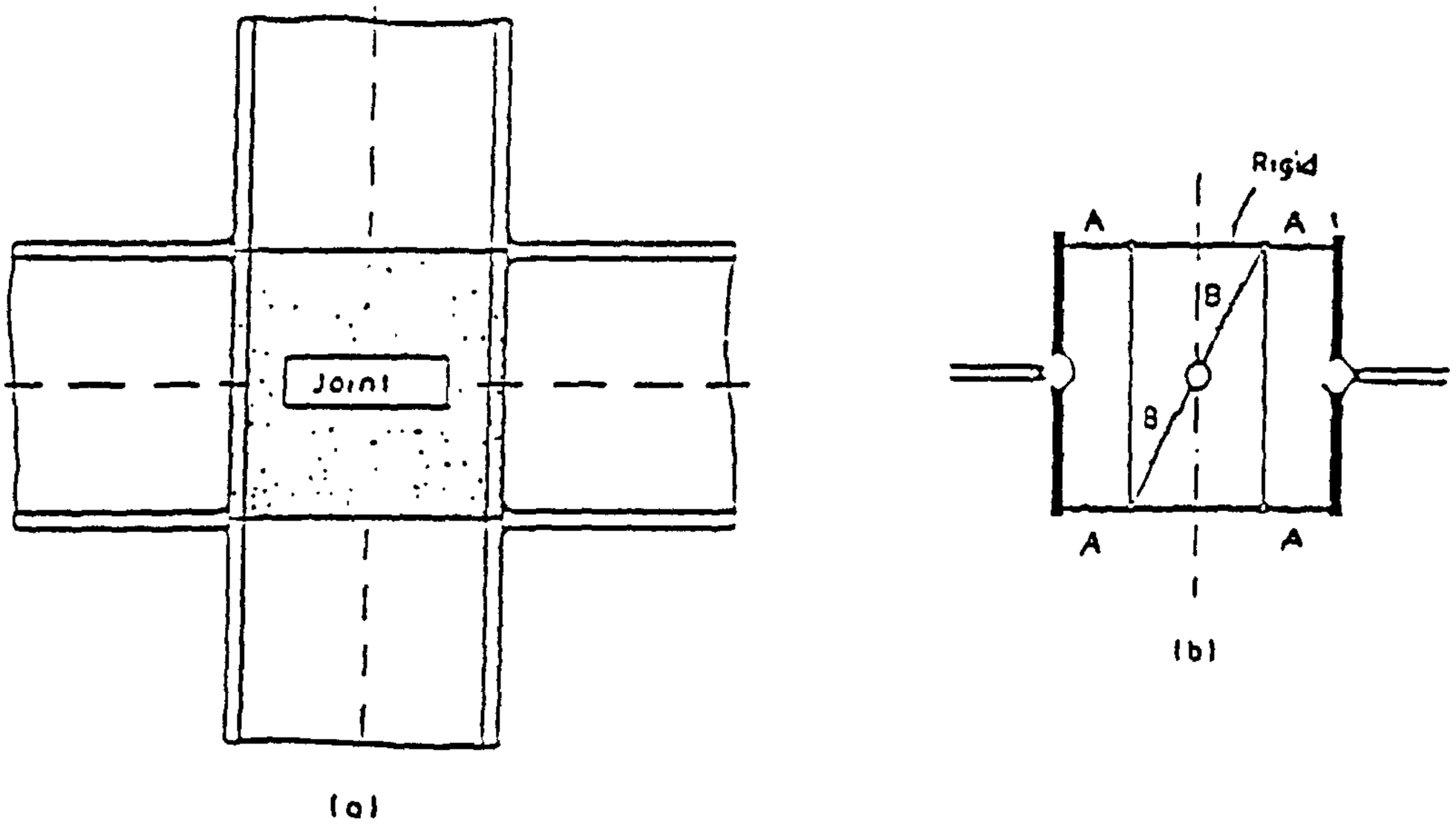

Figure 1-10 Mechanical model of a full welded joint (Tschemmernegg, ref. 1-31)

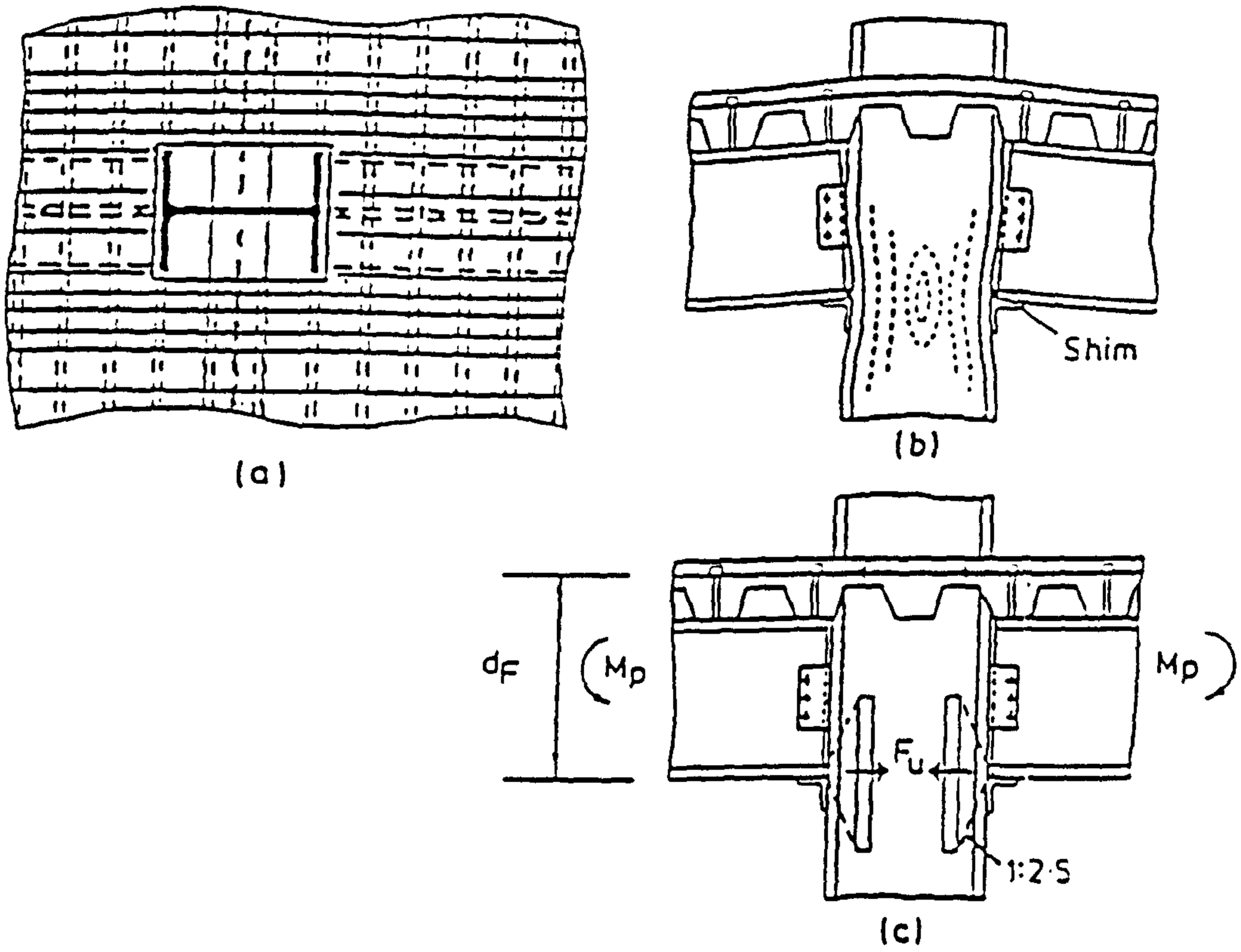

Figure 1-11 Joint action considered in prediction model by Tschemmernegg (ref. 1-31)

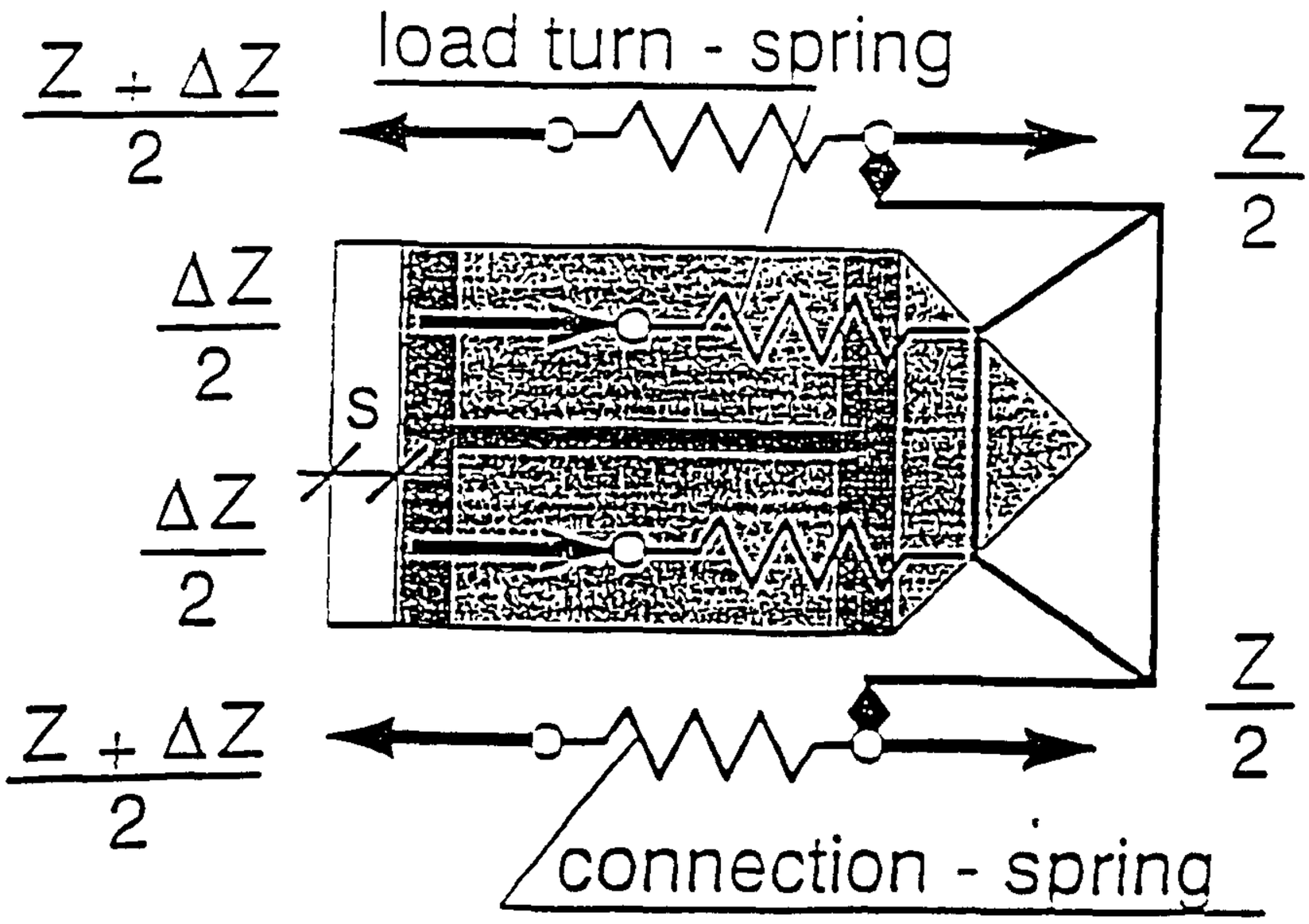

Figure 1-12 Truss model for tension zone of composite joint

(Tschemmernegg, ref. 1-32)

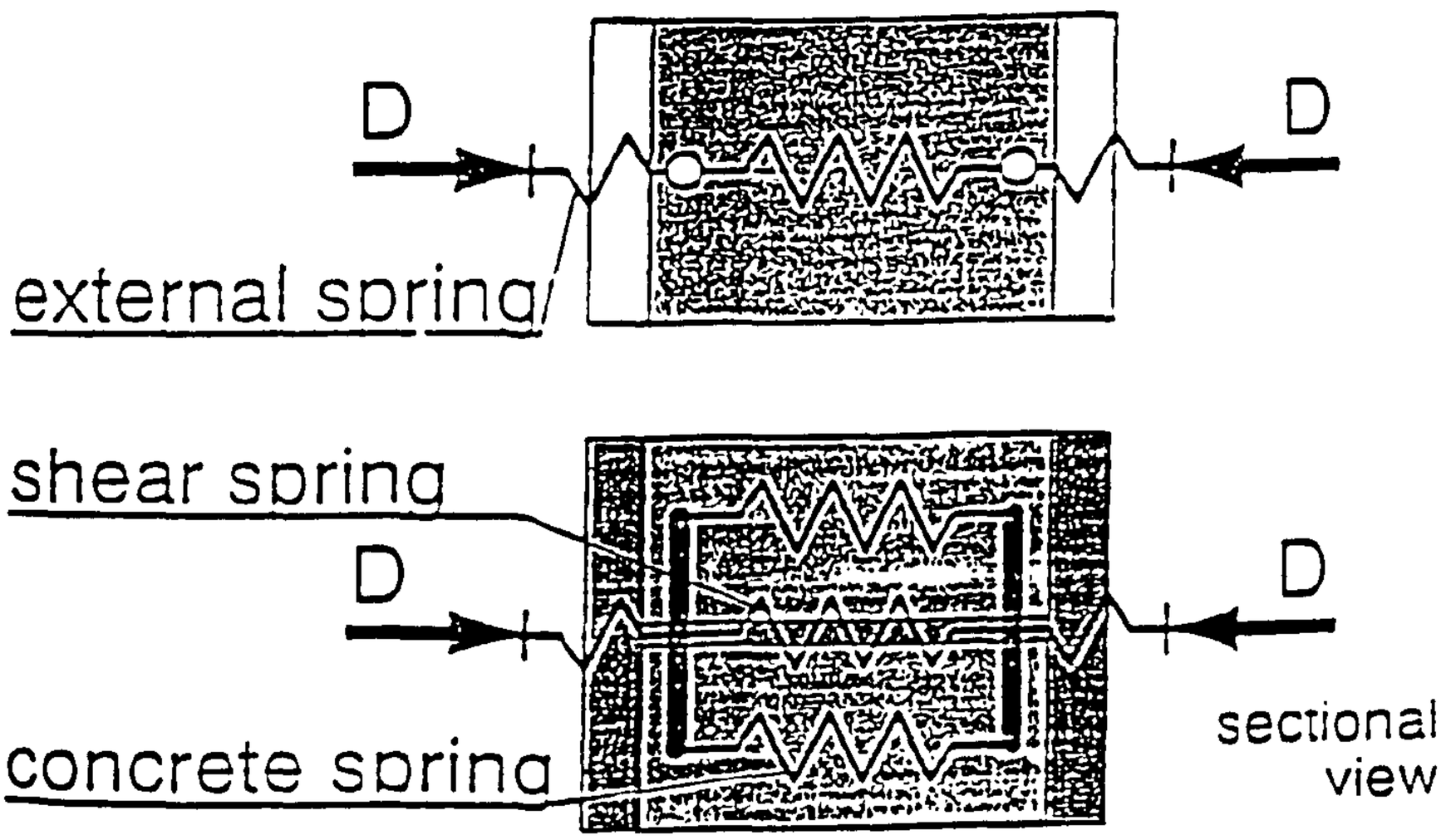

Figure 1-13 Spring model for compression zone of composite connections

(Tschemmernegg, ref. 1-32)

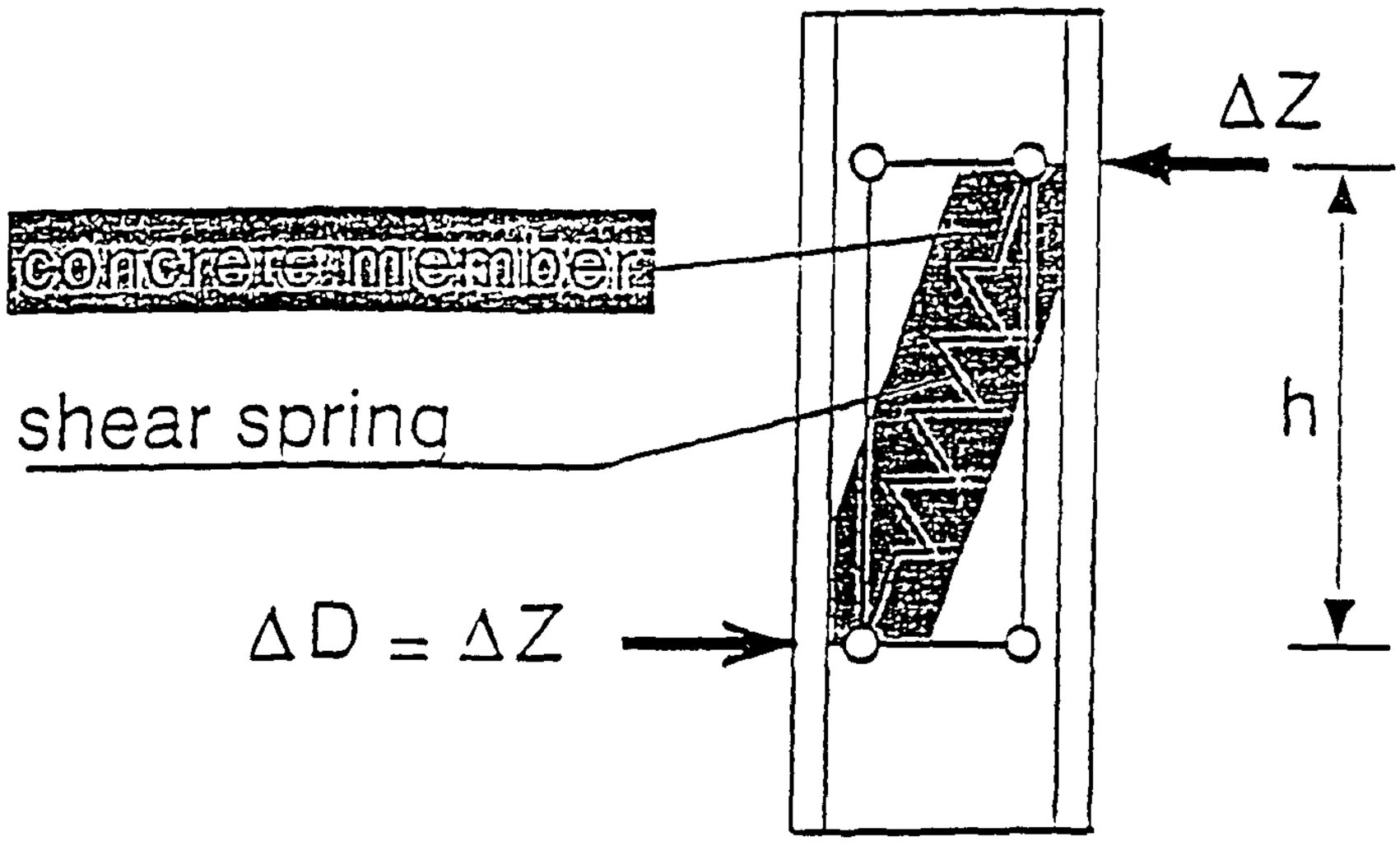

Figure 1-14 Spring model for shear zone of composite connections

(Tschemmernegg, ref. 1-32)

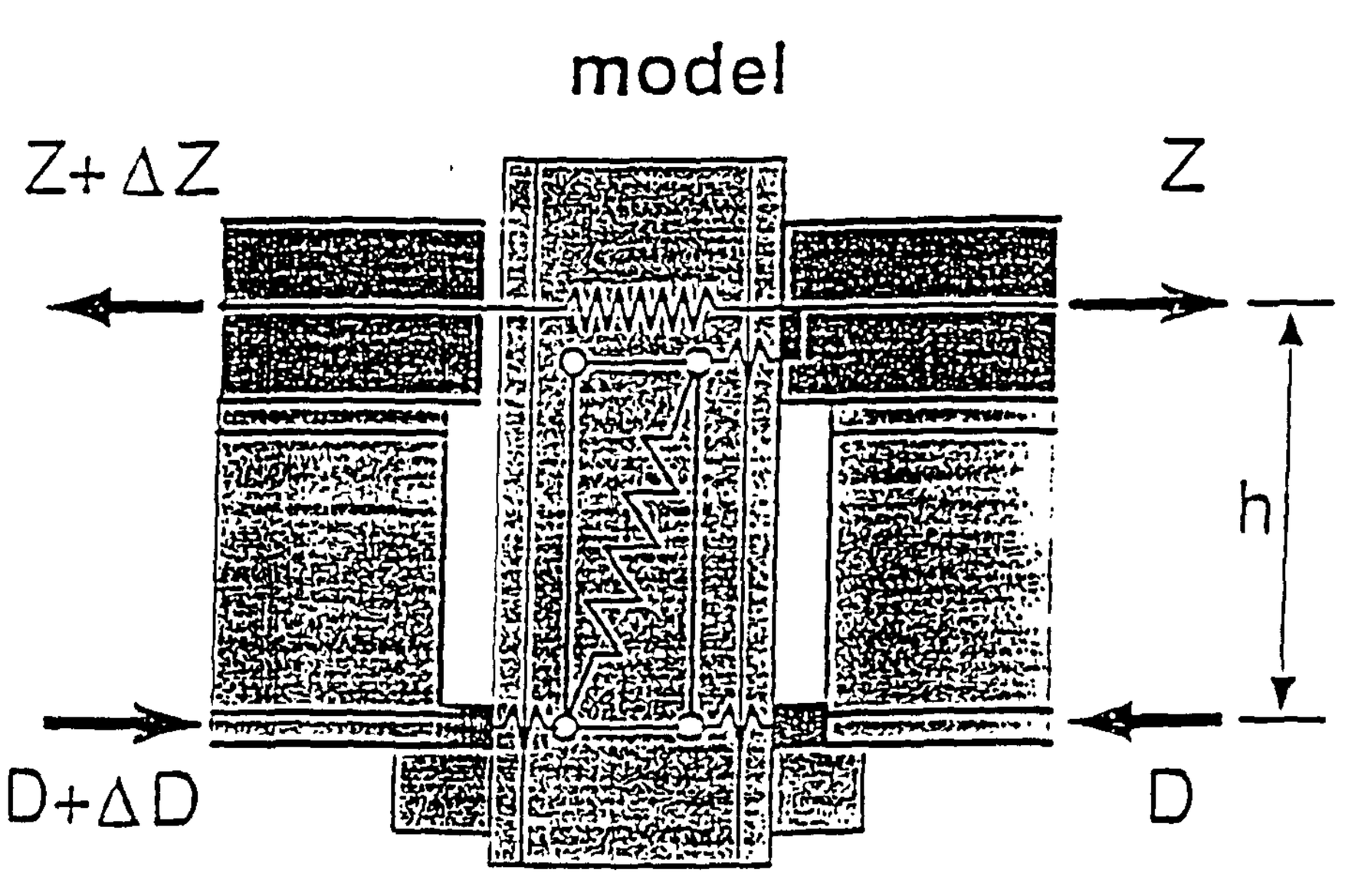

Figure 1-15 Assembly of the full model for composite connections

(Tschemmernegg, ref. 1-32)

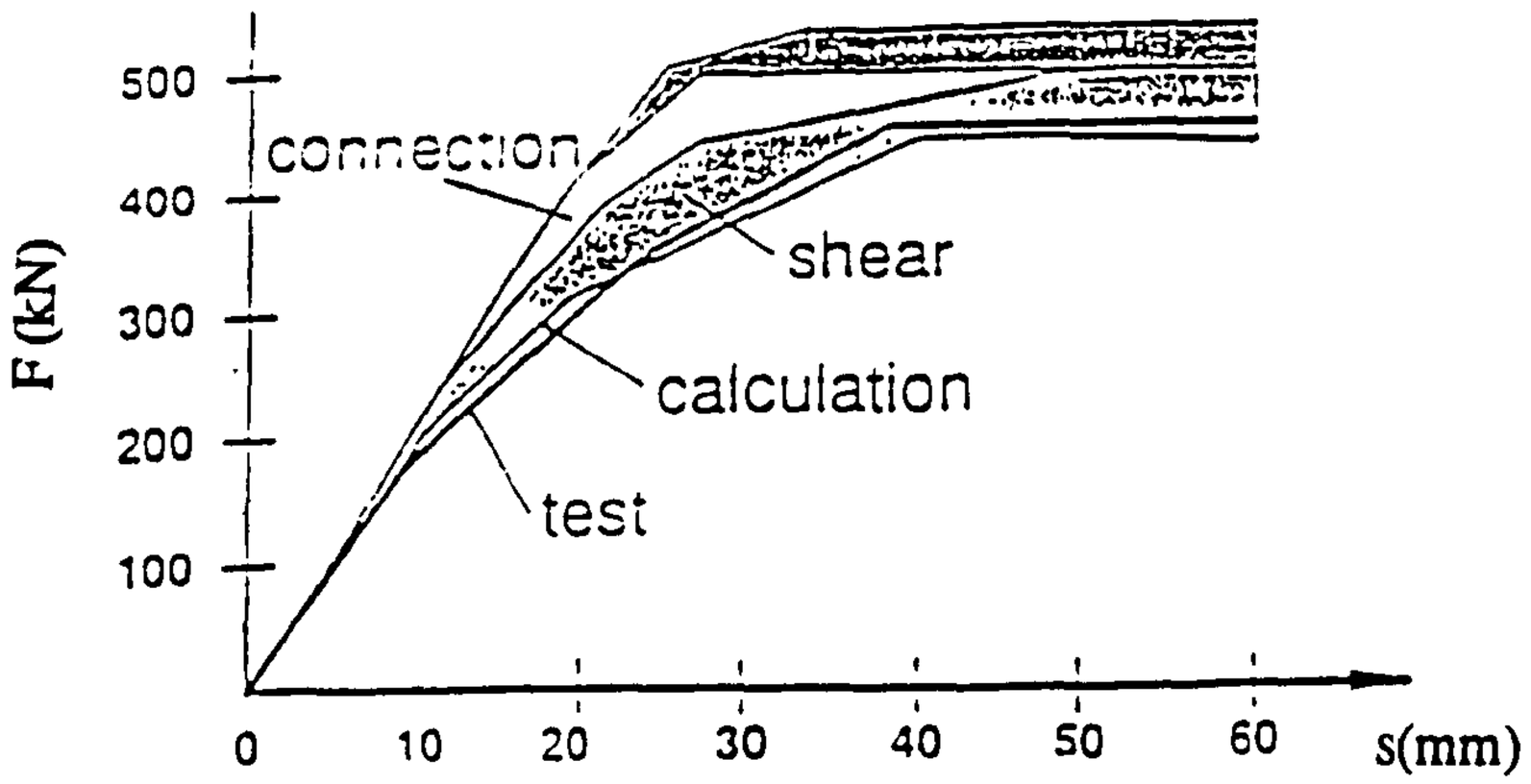

Figure 1-16 Comparison of load deformation curves from calculation and test (Tschemmernegg, ref. 1-32)

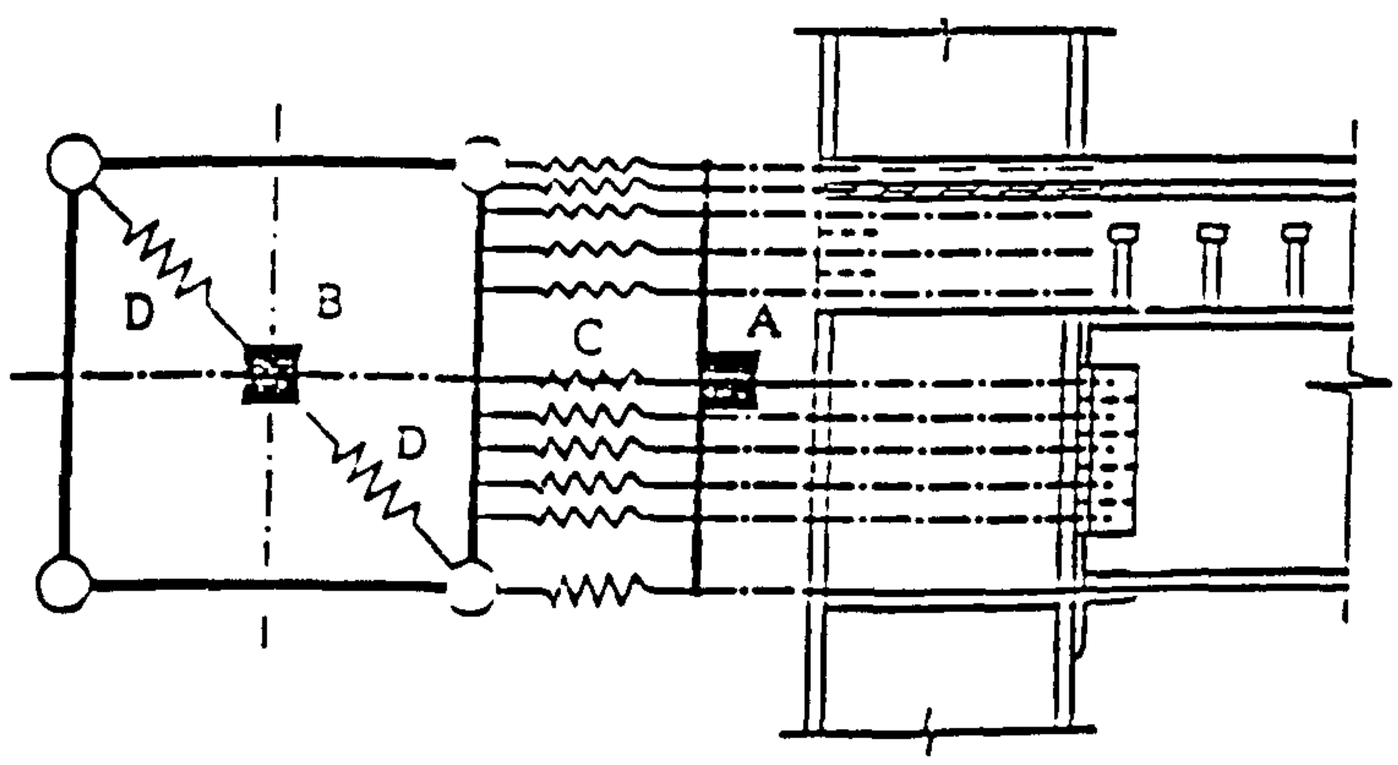

(a) Un-deformed mechanical analogue

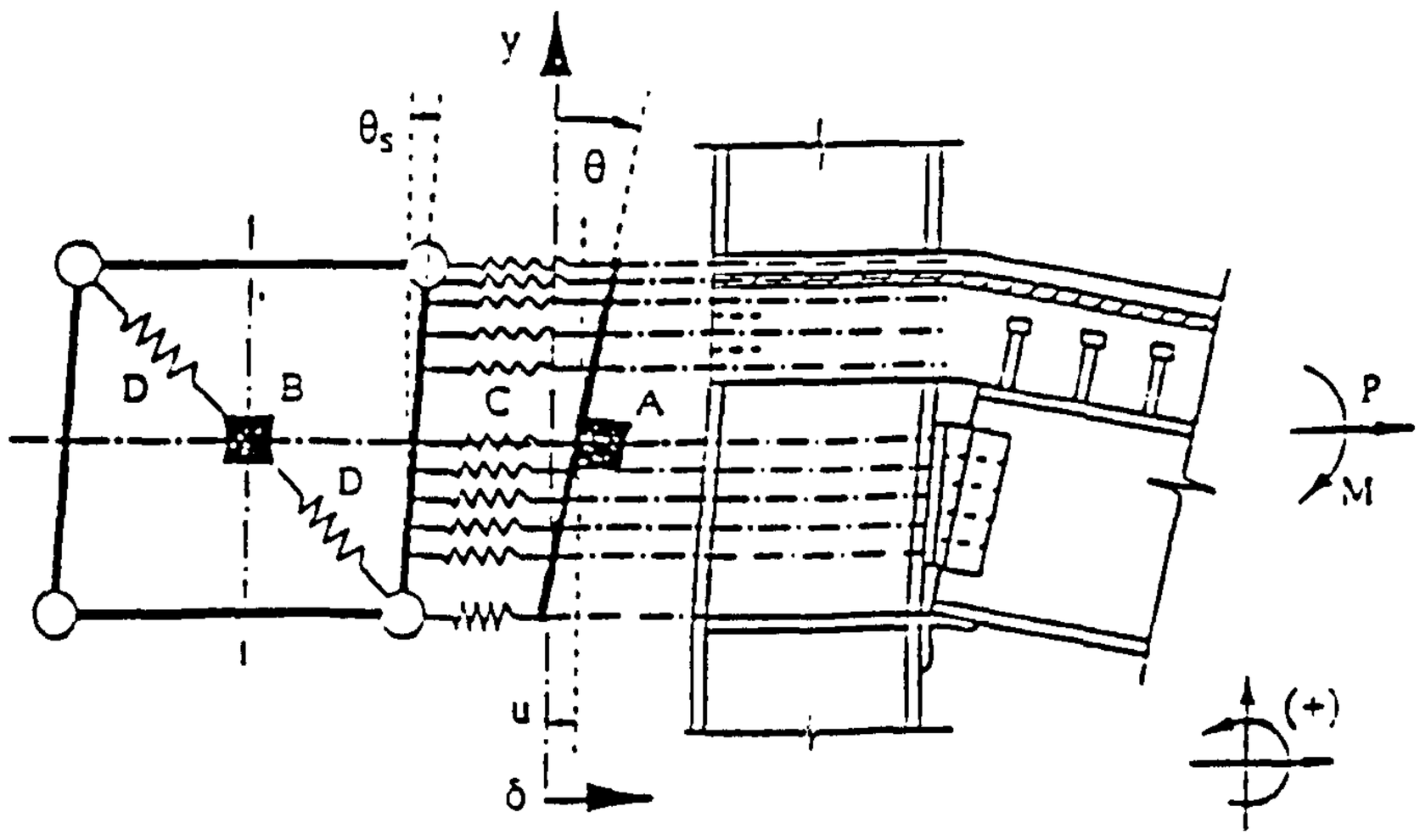

(b) Deformed mechanical analogue

Figure 1-17 Idealisation of connection by the proposed model (Madas, ref. 1-33)

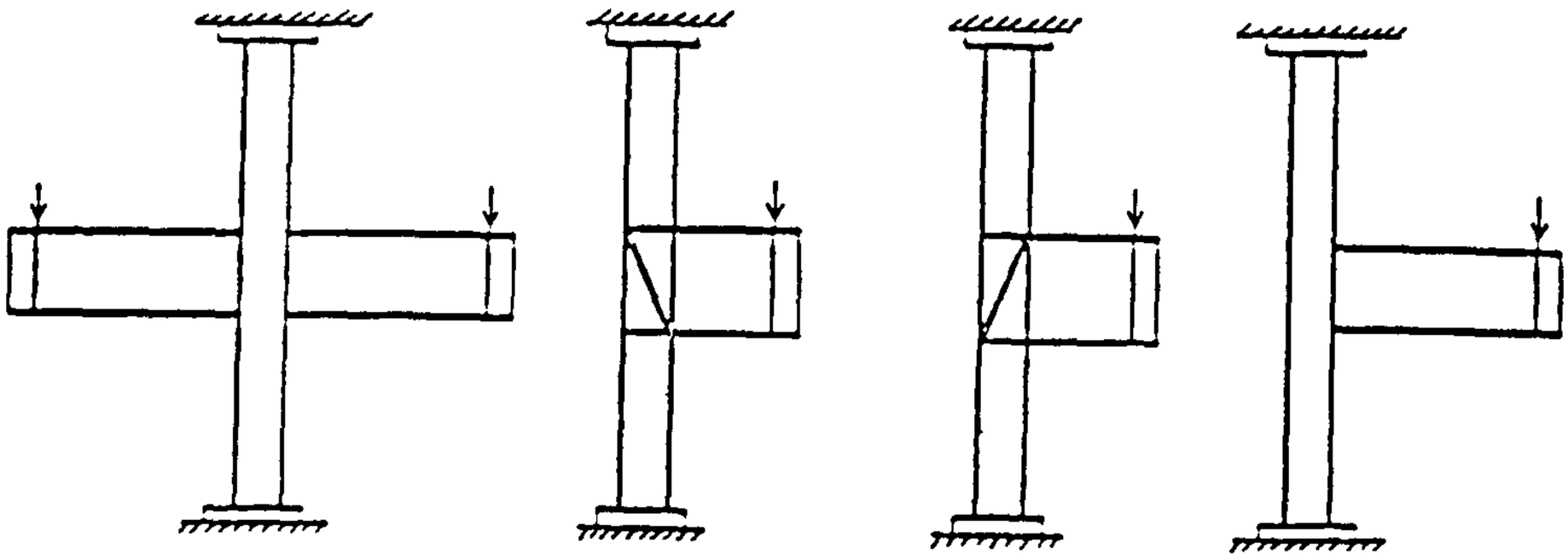

Figure 1-18 Fully welded connections analysed by various authors using FE technique

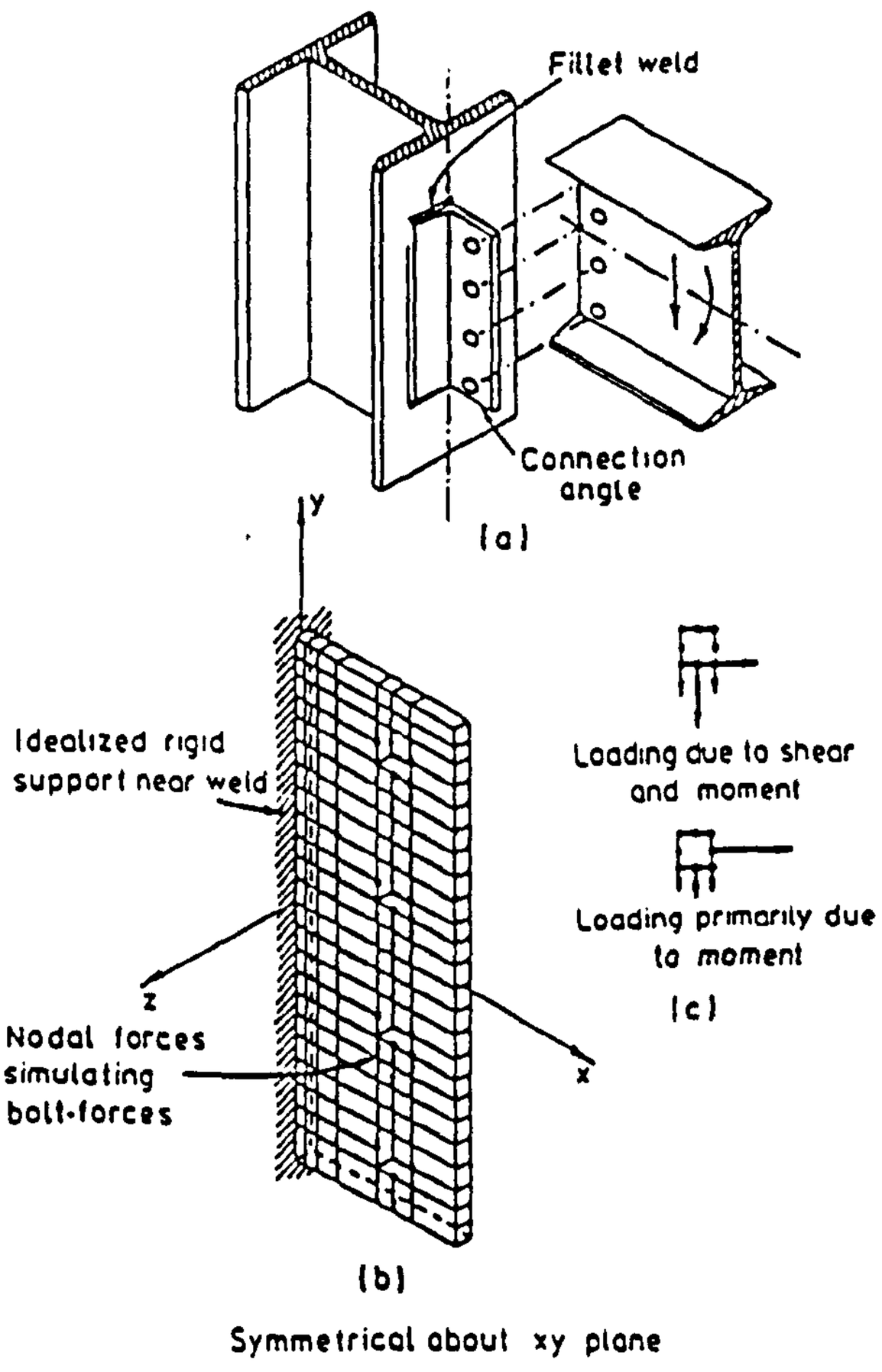

Figure 1-19 FE analysis of a single-angle bolted-welded connection

(Lipson & Hague, ref. 1-38)

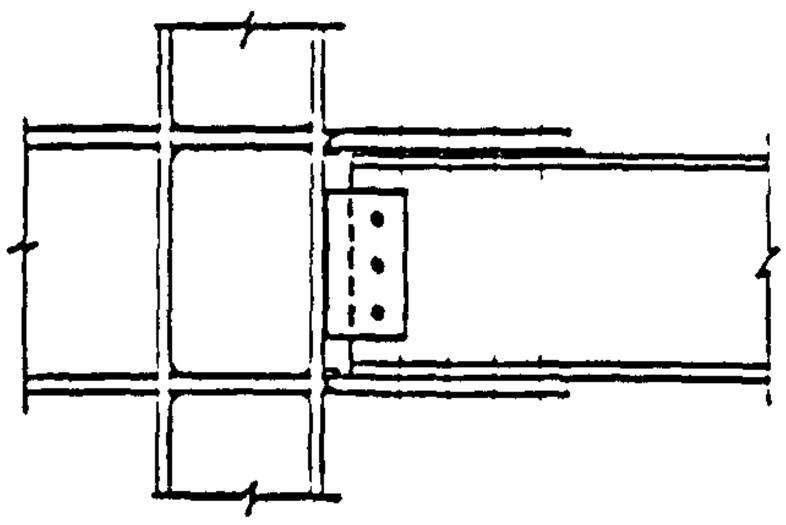

(a)

The bolted moment connection analysed

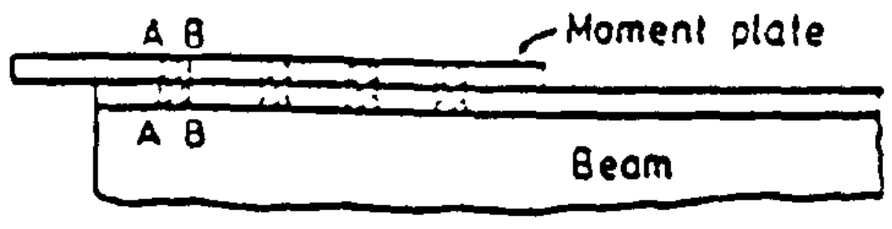

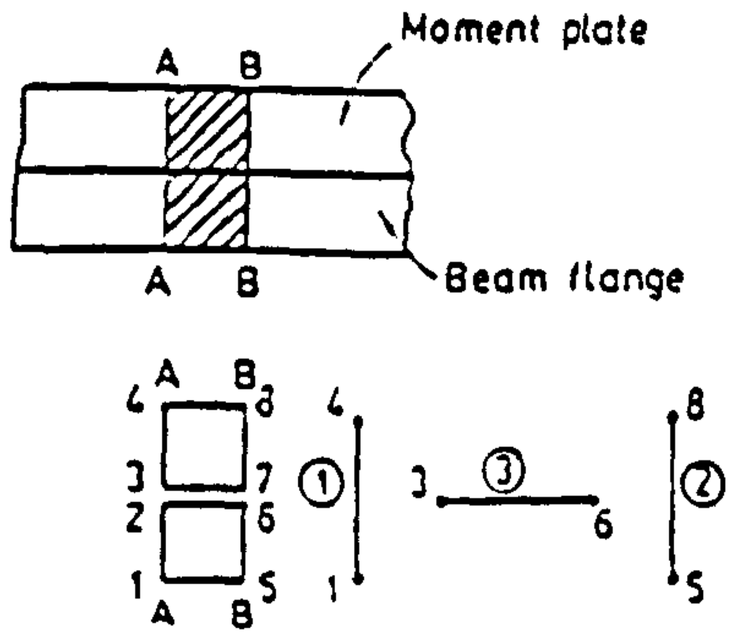

(b)

The equivalent truss system

Figure 1-20 FE analysis of a bolted moment connection using the truss system to simulate bolt behaviour (Patel & Chen, ref. 1-40)

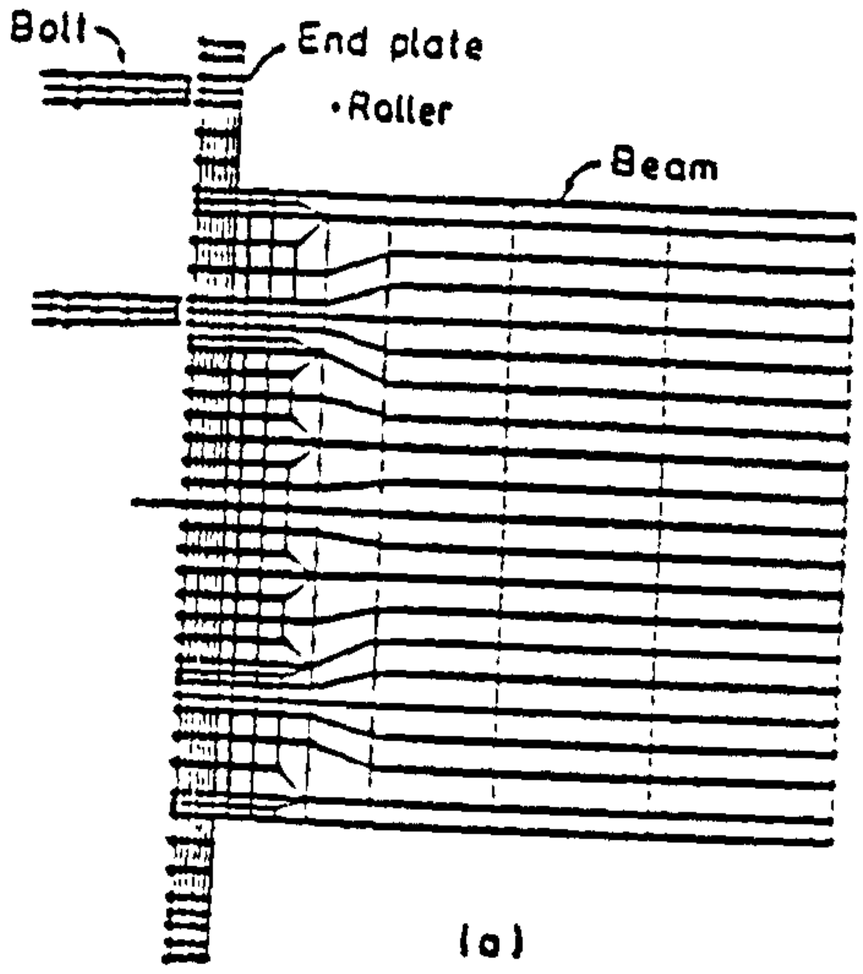

Finite element mesh for the 2-D analysis

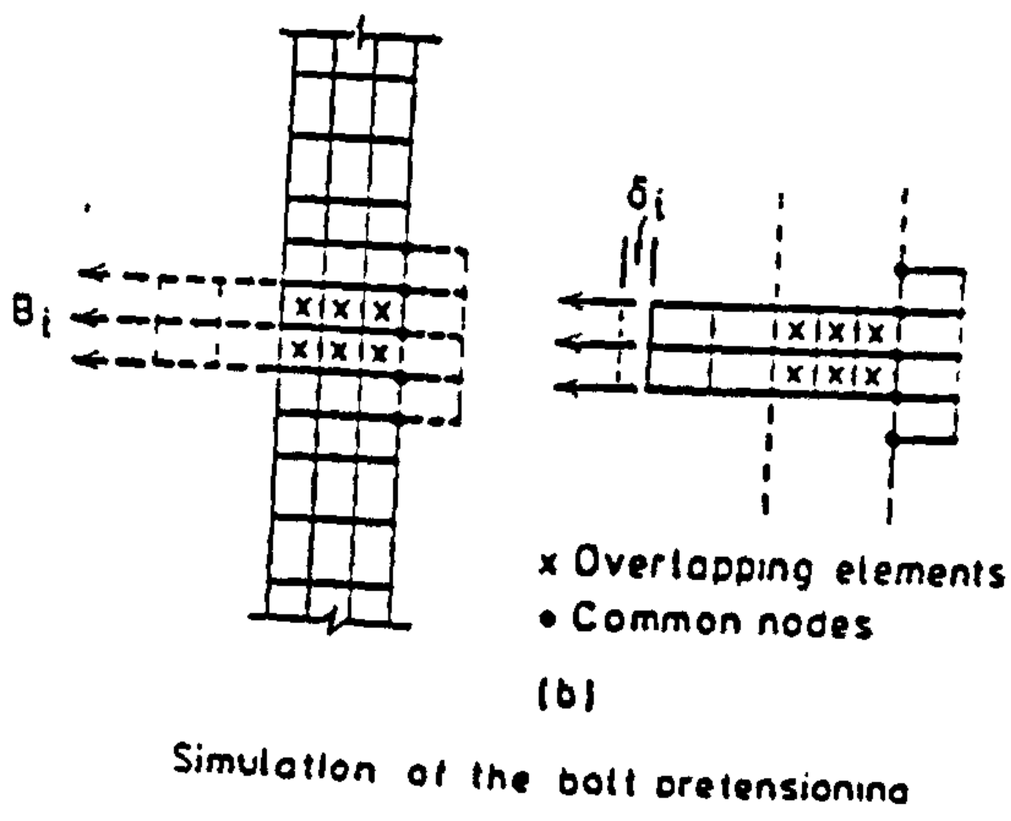

Figure 1-21 FE analysis of extended endplate connections

(Krishnamurthy et al., ref. 1-41)

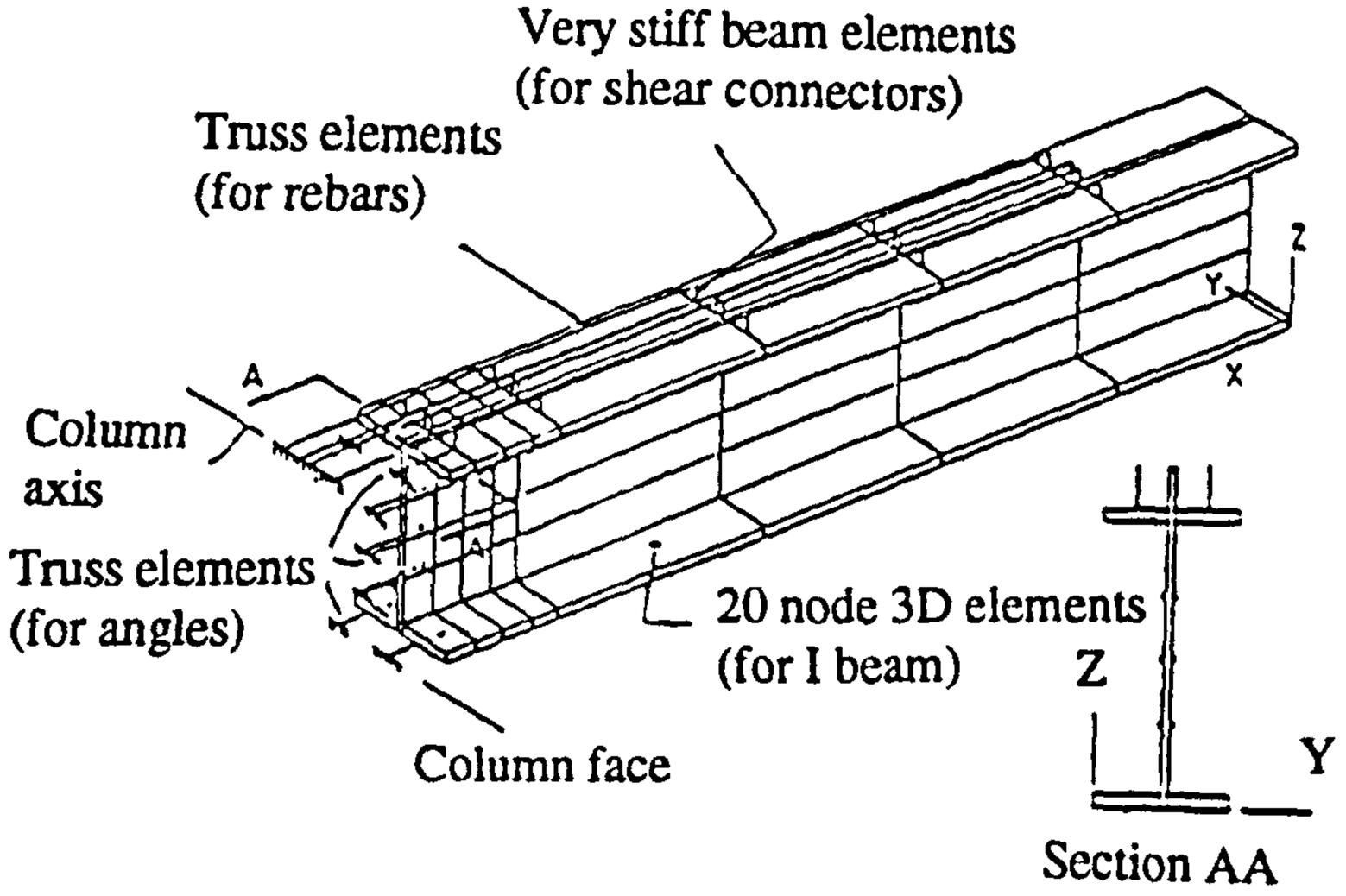

Figure 1-22 FE mesh for the joint and the beam (Leon & Lin, ref. 1-42)

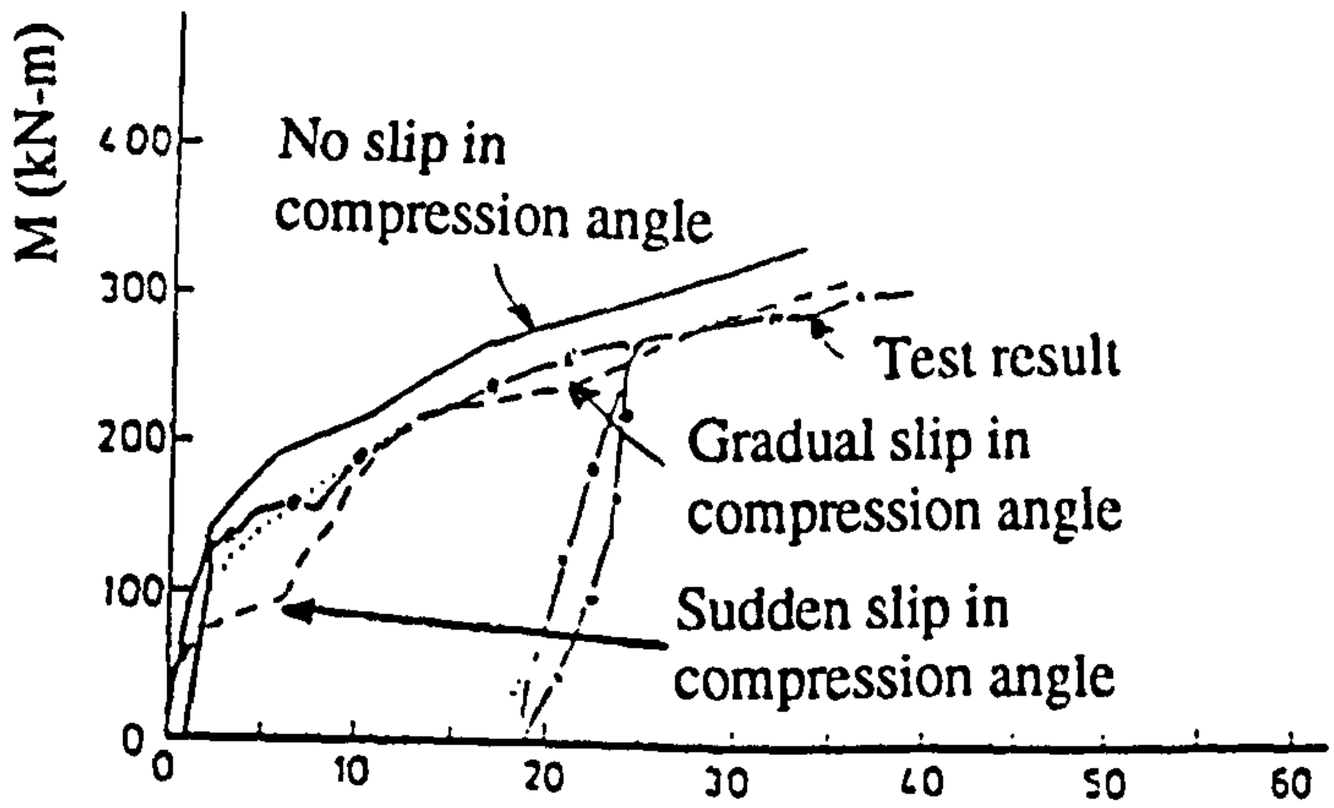

Figure 1-23 Comparison between test results and numerical M-ϕ curves for different slip model (Leon & Lin, ref. 1-42)

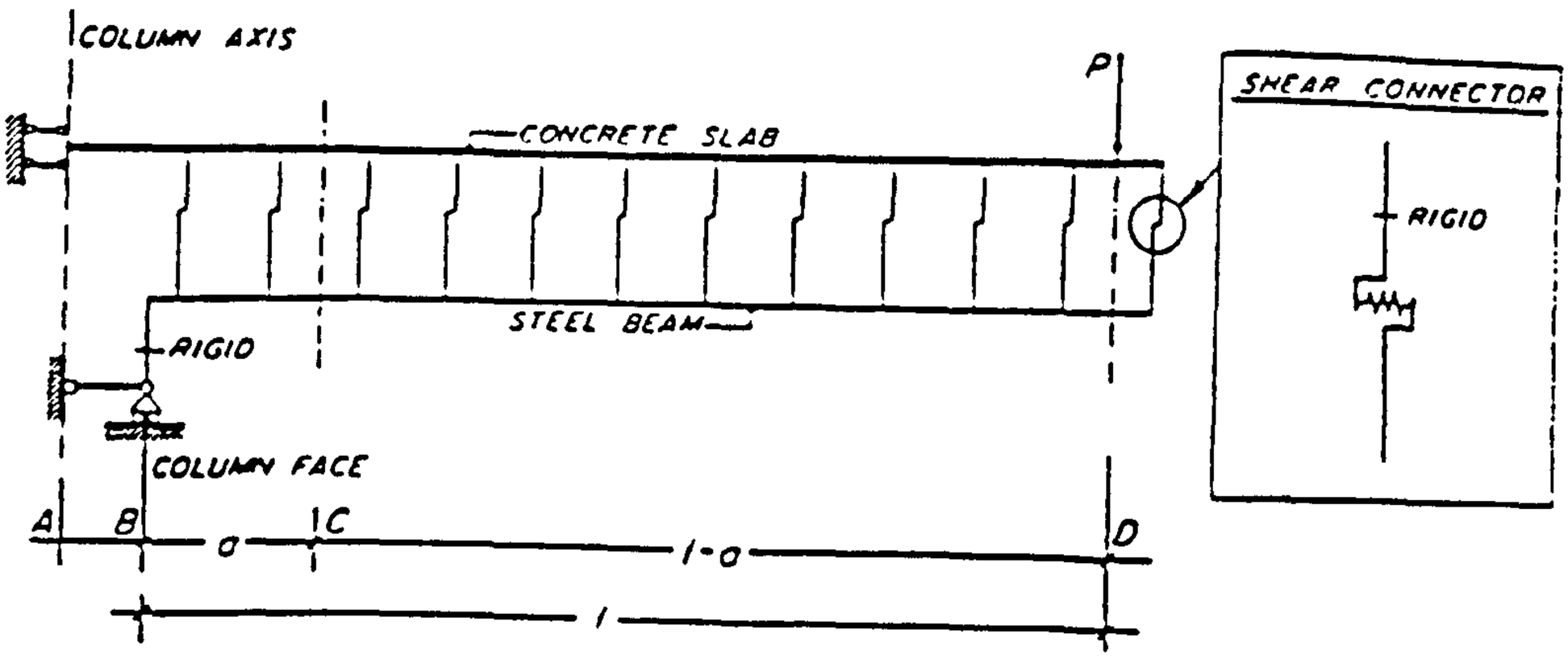

Figure 1-24 FE model by Zandonini considering shear slip (ref. 1-15)

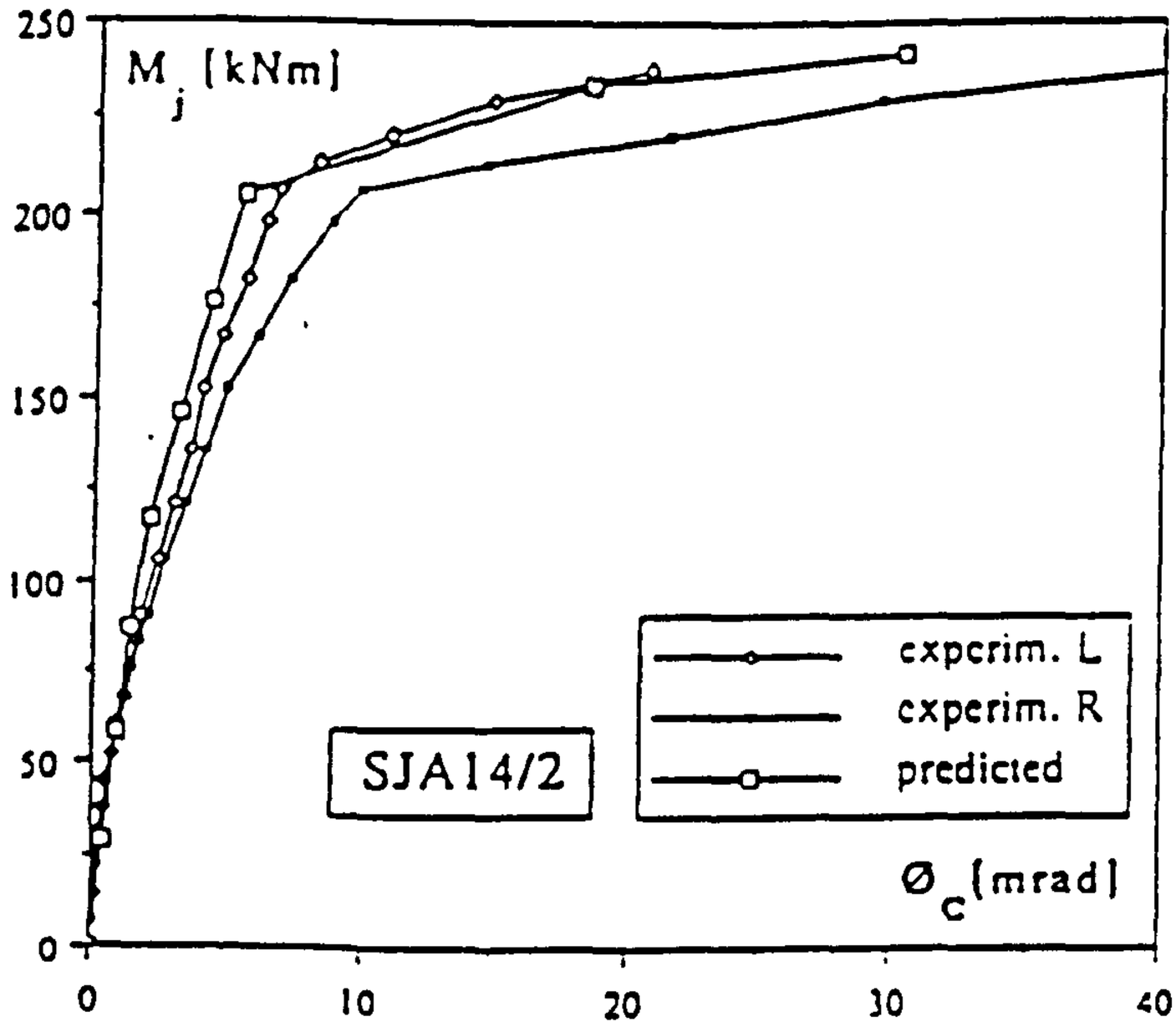

Figure 1-25 Comparison of the analytical and the experimental results (Zandonini, ref. 1-15)

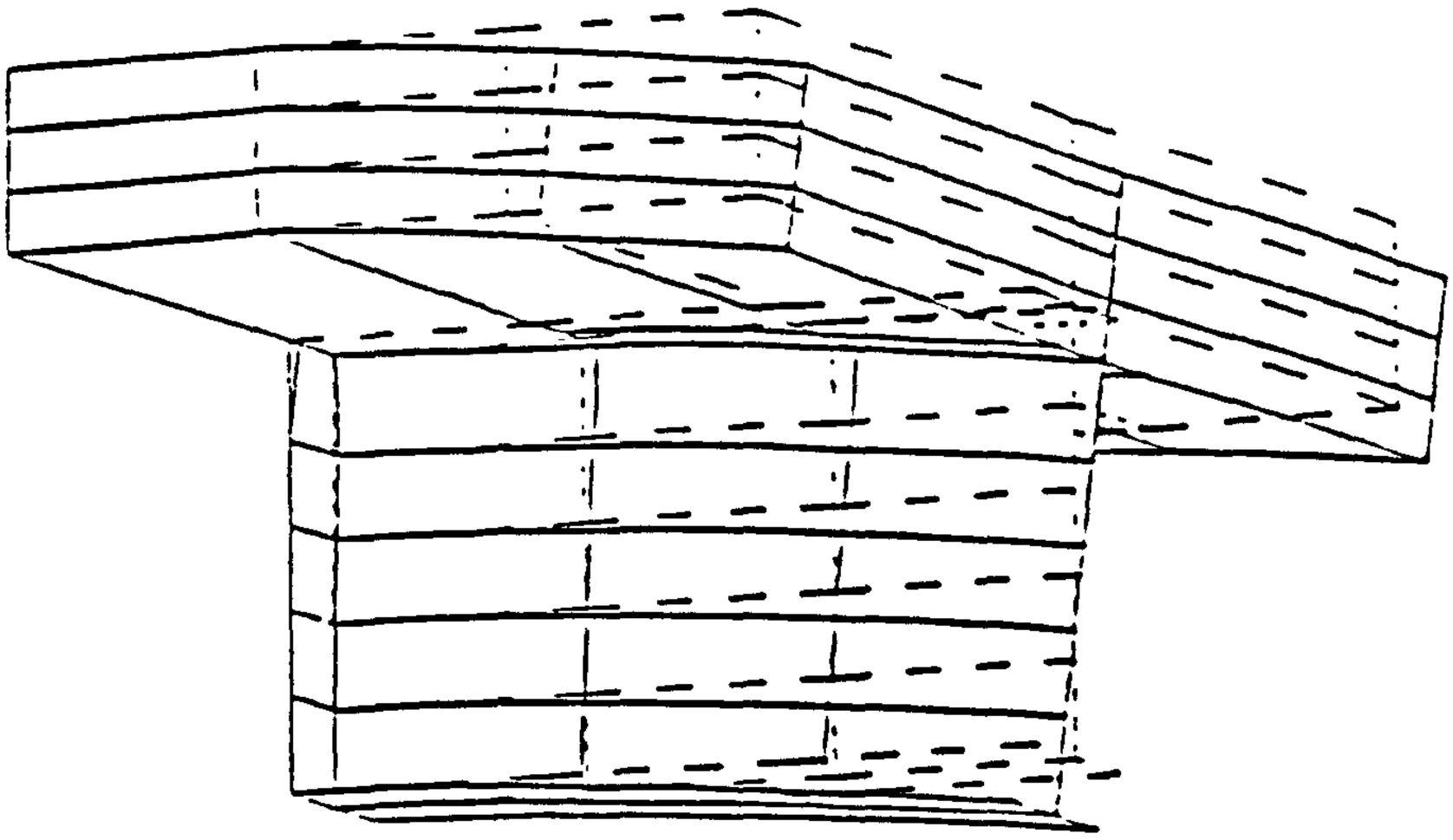

Figure 1-26 Composite connection mesh (Li et al, ref. 1-44)

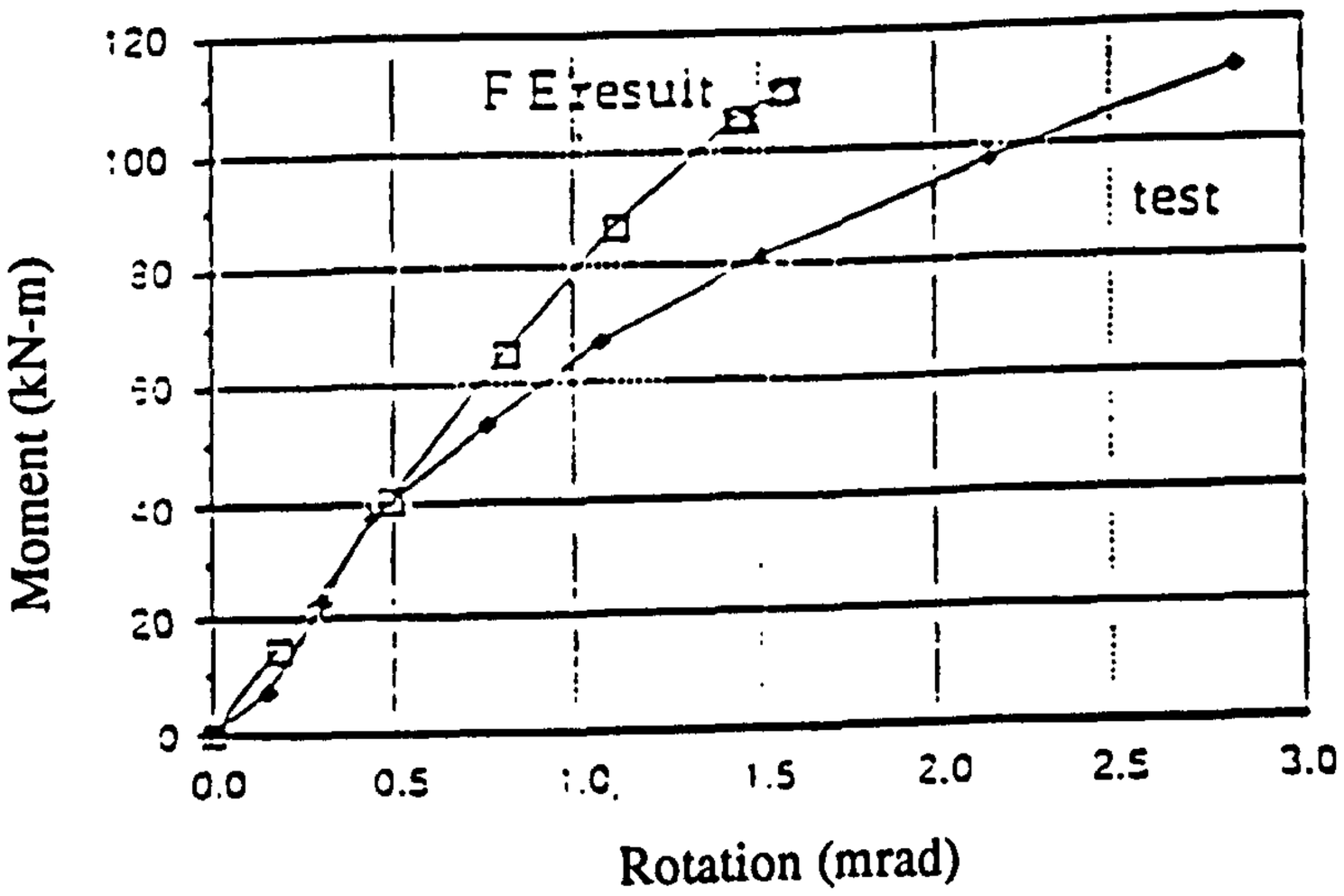

Figure 1-27 Comparison of the analytical and the experimental results (Li et al, ref. 1-44)

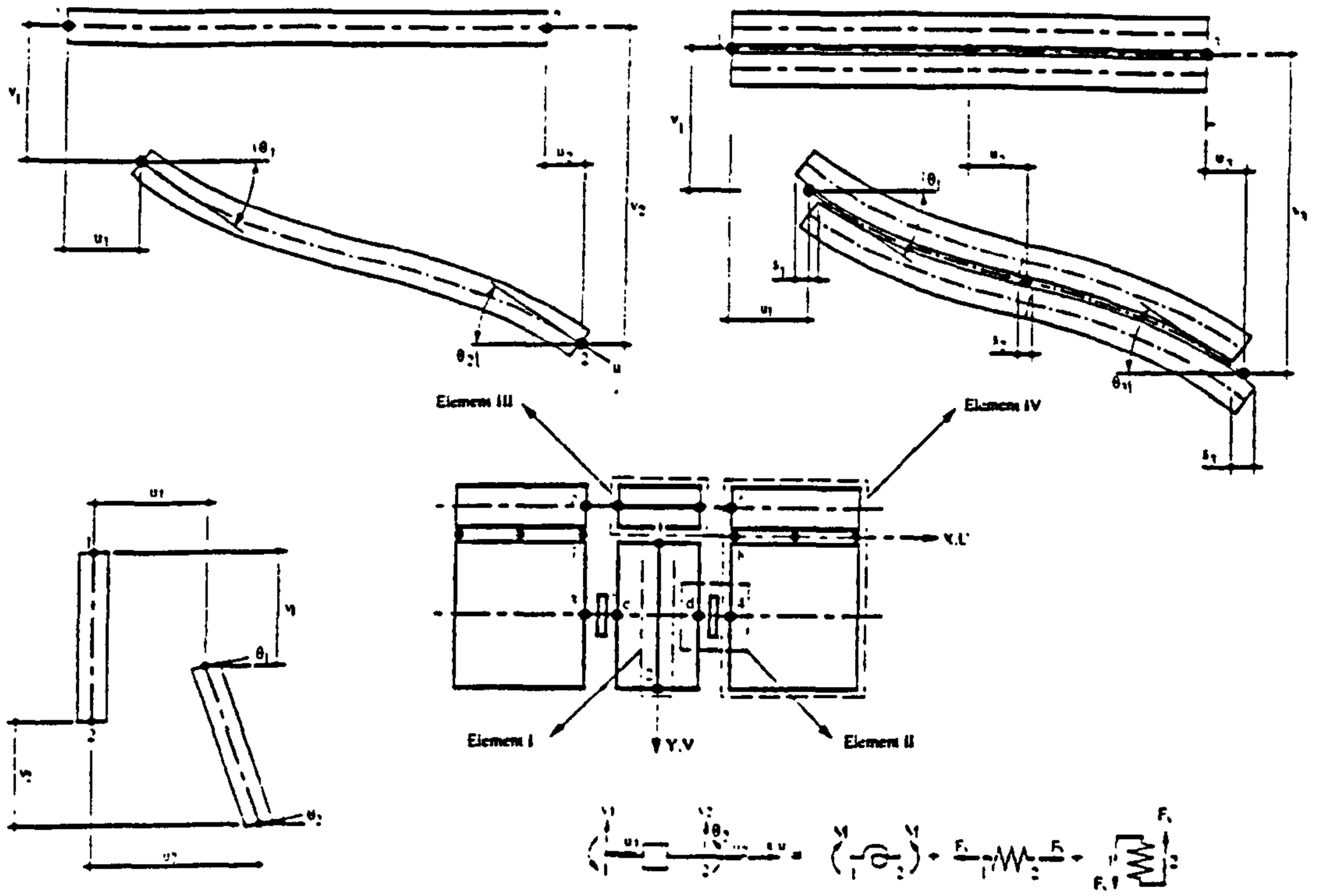

Figure 1-28 Macro element model for composite connection (Ren & Crisinel ref. 1-45)

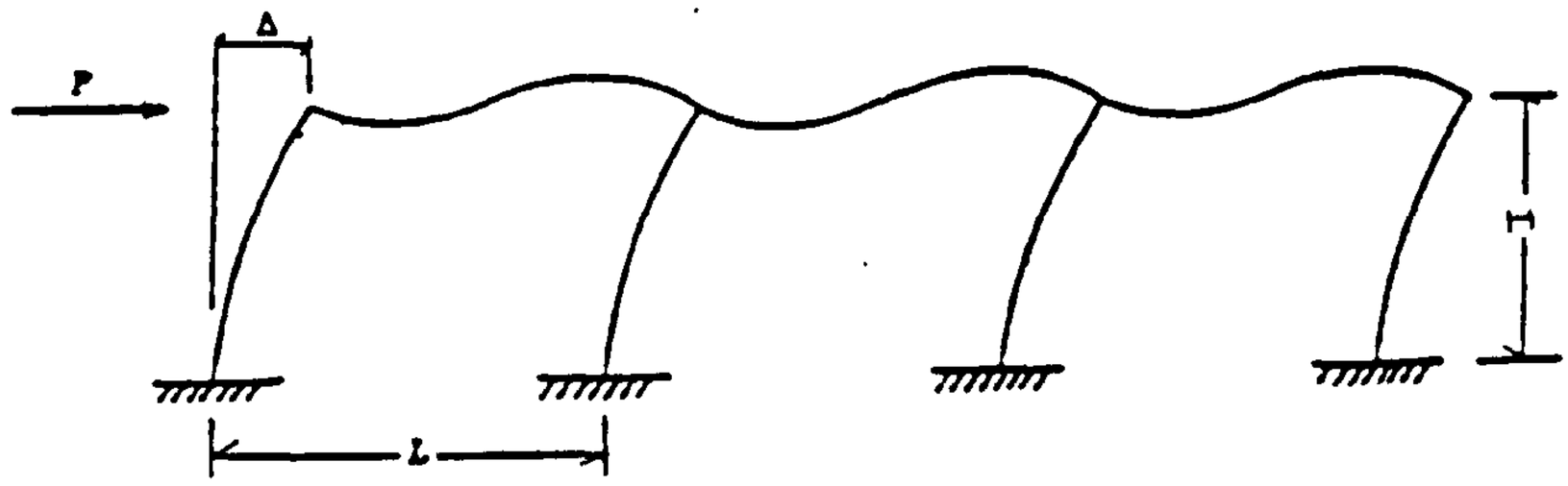

(a) Beams with no flexural rigidity

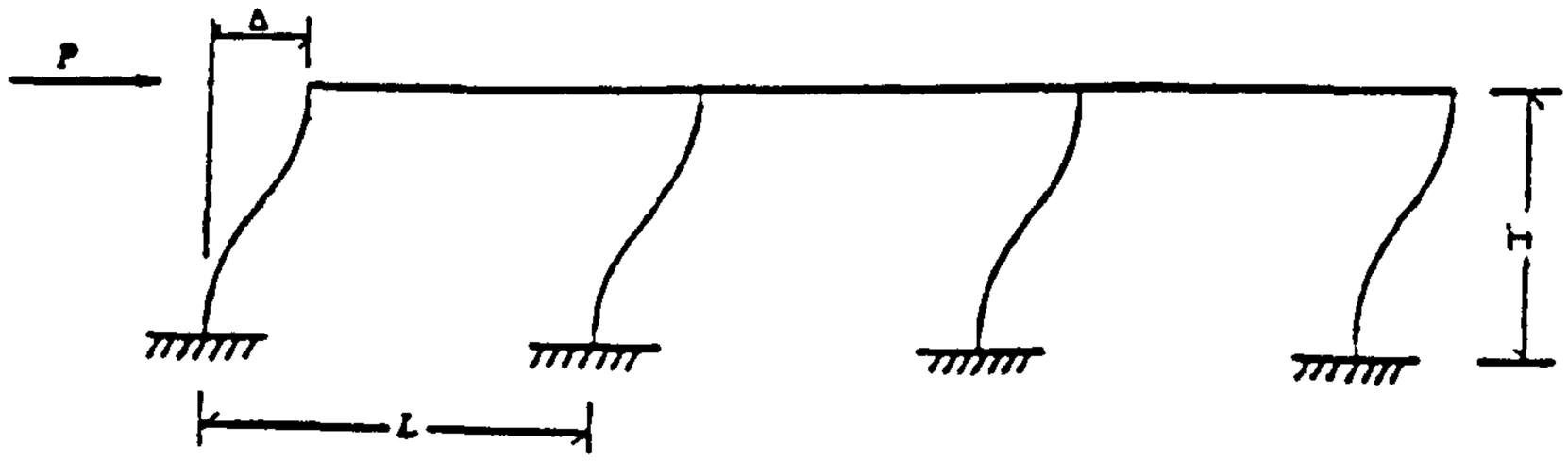

(b) Rigid beams and connections

Figure 1-29 Effect of connection and beam rigidity on sway

(Ammerman & Leon ref. 1-53)

Chapter 2

Finite element method and its application

2.1 Introduction

Modelling of a composite connection requires the successful representation of all the different components associated with the connection. To model a component properly it is essential to chose a proper element type and size and to correctly represent all the key material properties. Since it is difficult to assess the actual behaviour of any particular component in a model that contains several different components, it is essential to verify each component model before assembling them into the complete composite connection model. In a semi-rigid composite connection the following major components must be considered:

i Reinforced concrete slab

ii Steel beam and column

iii Bolts

iv Shear studs

v Endplate

vi Interface of endplate and column flange

vii Welds

This chapter first describes the finite element method in general terms and than goes on to discuss the elements and other aspects of the modelling that will be used for the study of semi-rigid composite connections. Verification of all stages in the build-up of the model are also reported in this and the next chapter.

The semi-rigid composite connection can be considered as the combined action of a bare steel connection and the reinforced concrete slab over it connected by the shear studs. Figure 2-1 shows a composite connection together with the bare steel connection and reinforced concrete slab. To simulate the actual behaviour of the composite connection it is essential to first verify that the model of a bare steel connection works properly and that the model of a reinforced concrete beam works properly. Once this has been achieved, the modelling of the complete composite connection can be attempted. In this chapter a bare steel connection SJS-1 tested in Nottingham University [ref. 2-1] is modelled. In parallel to this the modelling of a reinforced concrete beam is described; this has been verified using theoretical results.

2.2 Finite element method

The Finite Element method is a numerical technique for analysing structures in which the solution domain is divided into small (finite) elements. The behaviour of the variables in each type of element is defined by a suitable shape function. From the shape function, for each element the stiffness matrix is developed. Then the stiffness matrices are assembled into the global stiffness matrix. The applied load is arranged in a matrix known as the load matrix. Using the basic equation: $[F] = \Sigma[K][d]$ the displacement at every nodal point is calculated. From the displacements, element stresses and nodal stresses are calculated.

2.2.1 Non-linear finite element analysis

In linear analysis the behaviour of the structure is assumed to be reversible, i.e. the body returns to its original un-deformed state upon the removal of the applied load. But in cases of buckling or failure analysis or for large deformation, including those beyond the elastic limit, it is not possible to superimpose the solution from several load

cases to obtain the solution for a higher load case. In such cases non-linear finite element analysis is required. In practice four types of non-linearity can be identified:

i Material non-linearity (non-linear stress-strain relation but linear strain-displacement relation). An example of this is the elastic-plastic behaviour in materials.

ii Geometric non-linearity (non-linear strain - displacement relation but linear stress-strain relation). An example of this is elastic post buckling of structures.

iii Combined material and Geometric non-linearity. An example of this is the deformation of rubber - like materials.

iv Boundary non-linearity (when the deformations and stresses at contacting bodies are not linearly dependent on the applied load). This is due to the fact that the extent of the contact area changes with the applied load.

Semi-rigid composite connections possess material, geometric and boundary non-linearity.

2.2.2 The stiffness matrix in non-linear problems

In linear problems, the overall stiffness matrix [K] is a function of geometry and material properties, not the boundary conditions or the applied load. Therefore the element stiffness matrix [K_e] remains constant for linear problems, and hence is calculated once as:

$$[K_e]=\int_v [B]^T [D][B]dv$$

Where:

$[D]$ is the material property matrix

$[B]$ is the shape function matrix

In non-linear problems, the overall stiffness matrix $[K]$ is a function of the current state of stress and strain. Therefore $[K_e]$ must be updated to take into account the changing material properties and/or the geometry with the current stress and strain. For non-linear problems, $[K_e]$ can be written as:

$$[K_e] = f(F,u)$$

Where:

F is the external forces

u is the displacement

Figure 2-2 shows the basic effect of variation of the stiffness matrix in linear and non-linear problems.

2.2.3 Numerical procedure in non-linear problems

Usually there are two solution techniques for non-linear problems. They are:

i The incremental procedure

ii The iterative procedure

In the incremental procedure the total load is divided into small increments and for each increment a new $[K]$ is used. The non-linearity is therefore treated as piece-wise linearity. In the iterative procedure a constant $[K]$ is used in all increments. At first the full load is applied and iterations are performed to check that equilibrium is satisfied (i.e. external load is balanced). After each iteration the "unbalanced" portion of the external force is estimated and applied in the next increment. The two methods are explained in Figure 2-3. The Finite element software, ABAQUS [2-2] that will be used

for numerical modelling uses a combination of these two methods. In addition it allows the use of the modified RIKS method which assists in obtaining a solution for potentially numerically unstable cases, that are associated with buckling and/or yielding.

2.3 Steps in creating and analysing a finite element analysis

This section describes the methods used to establish a finite element model of the semi-rigid composite connection as described in chapter 3. Particular reference is made to the ABAQUS FE package as it was used for the analysis. To develop the model, it is necessary to define the geometry of the model, material properties, boundary conditions, the load and to request the results of interest.

2.3.1 Developing the model geometry

To construct the geometry of the model, all the nodes must first be defined. This is done by giving each node a number and then identifying the co-ordinates of the node. But it is not essential to write down all the nodes and their co-ordinates, since it is possible to give the co-ordinates of the principal nodes and their numbers and then to generate the intermediate nodes through some special commands (*NGEN, *NFILL, *NCOPY). After the node definition the next step is to define the elements. To define the elements the required input is the element number, type of the element and the numbers of the nodes forming the element. As in the case of generating nodes, elements can also be generated from the master element, through special commands (*ELCOPY, *ELGEN). When using these special commands, the numbering of the nodes and elements must be maintained in a regular fashion. The defined geometry of the model can be viewed through the use of special software (EMUTEK, ABAQUS POST).

It is also possible to develop the geometric model through the use of appropriate packages such as FEMGEN (Femview Limited 1990) [2-3] and SDRC-IDEAS (1990) [2-4]. These can be used to generate meshes onto a system of geometry. The user inputs key geometric points which are then connected via lines and arcs, which are in-turn used to generate surfaces. The user can then select certain surfaces or parts of the surface and generate elements onto them. These packages have the ability to transfer the nodal co-ordinates and the elements to the input file of the major FE Suite (i.e. ABAQUS).

2.3.2 Material properties

To define the properties of the materials it is essential to divide the elements into specific sets. Then for each set of elements it is possible to assign individual material properties. Material properties for modelling purposes can be obtained from coupon tests of the material. From the test it is possible to obtain Young's modulus of elasticity, Poisson's ratio and the stress-strain curve. To define ultimate static strength, the user must provide elastic and plastic yield strength and can also define the strain hardening properties. All properties come from the material's uniaxial $\sigma-\epsilon$ curve.

2.3.3 Boundary conditions

To define the support condition or to establish symmetry, appropriate restraints on nodes or node sets are required. Nodes can be restrained for any/all displacements or any/all rotations, or for both.

2.3.4 Loads

The magnitude, type (distributed, concentrated, line etc.), direction and the node number or the node set or element over which load acts must be given. It is also possible to define the initial values of applied load. The condition for terminating the

analysis can also be defined (at a certain displacement/rotation at certain node, load magnitude etc.).

2.3.5 Output request

After defining the model geometry, material properties, boundary conditions and the loads, the results from the analysis can be obtained in different formats. Outputs can be created in TEXT format (.DAT) or in ASCII format (.FIL, .RES) which can be post processed. Through the use of the *RESTART option, it is possible to create a graphic results file (.RES) for any required result (displaced shape, rotation contour, stress contours etc.).

2.4 Mesh fineness

There are no hard and fast rules to decide how fine the mesh should be in order to obtain an accurate result from the FE analysis. It must be decided by the user through a few initial runs. Results from each run can be compared and a mesh density can be identified, beyond which making a finer mesh will not affect the results of the analysis.

In general it is possible to decide through inspection where stress concentrations will occur and the location of points of interests. At these areas the mesh should be finer, elsewhere it can be made gradually coarser. In this study the area at which the beam and column is connected had a finer mesh and gradually the element size was increased away from it. It is worth mentioning that in a composite or bare steel connection, besides these the location of endplate and the bolts will also govern the size of the elements of the column flange, endplate and beam.

To produce accurate results it is a good practice to keep the aspect ratio of the elements (for shell elements the ratio of length to width, for solids the ratio of largest

and smallest dimension) close to unity. Usually if the aspect ratio is larger than five, in the region of interest the results may be inaccurate. In general long and thin elements should be avoided. Sometimes it becomes essential to break this rule in less important regions of the model, to reduce the number of elements (to control the extent of calculation and the CPU time).

2.5 Main elements in use

The semi-rigid composite connections which are under investigation, with their complicated geometry and behaviour, require the use of several types of element to define the model geometry. The elements that are used for modelling purposes are described.

2.5.1 Shell elements

These are the main elements used to model the semi-rigid composite connections. The column web and flange, beam web, flange and the plate (endplate/finplate) were all modelled through the use of shell elements. Their use requires a smaller number of nodes to model the steel beam, column or the plate, than solid elements with a proper aspect ratio. Also, numerical problems were encountered during an analysis of the bolts, in which one plate was fixed at one end while the other one was pulled, when the plate and the bolt were modelled using solid elements.

These elements generally have five degrees of freedom per node; if the in-plane rotation is considered, the degrees of freedom per node becomes six. The elements are divided into five layers through their thickness and only one node is required through the thickness. The structure of the shell finite element is shown in Figure 2-4. Several types of shell element are available within the ABAQUS suite including four, eight and nine noded quadrilateral elements and various forms of triangular elements. In the case

of four noded shells there is one integration point whereas in nine noded shells there are four integration points. Figure 2-5 shows the configuration of four and nine noded shell elements. These are available as thick (6 degrees of freedom per node) or thin (5 degrees of freedom per node) shells. The number of layers within the shell can be determined by the user, but the ABAQUS manual recommends five layers for static analysis of non-linear problems. In this study four and nine noded thick shells were used.

2.5.2 Beam element

These elements allow for bending and stretching actions. They are available in two different formats, in the ABAQUS software, in-plane (two displacement and in-plane rotation per node), and three-dimensional (six degrees of freedom are active at each node). They can be of various cross sections, i.e. rectangular, circular, I-section, L-section, and general section. Three dimensional beam elements with circular and rectangular cross sections were used in this study to model the shear studs in the connections.

2.5.3 Truss elements

Truss elements allow for axial force only. They are therefore most suitable for modelling the reinforcement in the simpler model for composite connections described in chapter 3. They are also available as plane and space elements. These elements have three degrees of freedom (displacements) per node.

2.5.4 Solid elements

Many types of solid element are available in the software. Among the three dimensional solids, eight noded and twenty noded solid elements were selected for

modelling the concrete slab of the connection. The nodes of these elements have three displacement degrees of freedom only. The elements are shown in Figure 2-6.

2.5.5 Interface elements

These elements are used to model contact problems and are essential for modelling the interaction between the endplate and the column flange, beam web and finplate etc. They use pressure (S_{11}) and shear stress (S_{12}) between the contacting surfaces as the basic variable. The property of the interface elements used in this study is the default one, which is that no pressure (i.e. no tension) can be transmitted when there is no contact and any magnitude of pressure can be transmitted from one surface to the other (i.e. compression) when in contact. When four noded shell elements are used, eight noded interface elements (INTER4) are required and when nine noded shell are used then eighteen noded interface elements (INTER9) are necessary. Figure 2-7 shows both types of element. In addition to these elements being used to model the contact between the beam bottom flange and the column flange, two noded interface elements (INTER1) will be used in case of finplate connections to model the interaction of the bottom flange of the beam and the column flange. It is also possible to change the default property of the interface elements, so that they can transmit some degree of tension. In addition to this it is possible to define the frictional coefficient, through an appropriate command (*FRICTION).

2.5.6 Joint elements

This is a special type of element with two nodes. The co-ordinates of the two nodes are to be close to each other. They are used to model joints between separate parts of a structure. Basic input for these elements is the load deformation property of the joint. The element is shown in Figure 2-8. In this study the joint elements (JOINTC) were used for two reasons:

i To model the bolts

ii To model the slip between the reinforcement and the steel beam

Since shell elements will be used to model the column, beam and plates it was not possible to model the bolts physically by using solid elements. The bolt load-deformation curves were therefore obtained from a separate modelling of the bolts, or from available test results, or from elastic solutions.

2.6 Multi-point constrains (MPC) and EQUATION

Multi-point constraints allows constraints to be imposed between different degrees of freedom of a finite element model. These constraints may be non-linear and non homogeneous. The use of MPC helps to impose the known displacement relation between the nodes or to simplify a model. Three types of MPC are used in this thesis these are: LINEAR, BEAM and SLIDER. The Linear MPC is a standard method for mesh refinement of first-order elements. The MPC is shown in Figure 2-9 (a). This MPC constrains each degree of freedom at node **p** to be interpolated linearly from the corresponding degrees of freedom at nodes **a** and **b** (see Figure 2-9 (a)). The BEAM type MPC provides a rigid beam between two nodes to constrain the displacement and rotation at the first node **a** to the displacement and rotation at the second node **b**, corresponding to the presence of a rigid beam between the two nodes **a** and **b** (see Figure 2-9 (b)). The SLIDER type MPC keeps a node **q1** on a straight line defined by two other nodes **c** and **d**, but allow the possibility of moving along the line, and the line to change length (see Figure 2-9(c)).

The EQUATION option allows direct input of a linear multi-point constraint in the form:

$$A_1u_1 + A_2u_2 + \ldots\ldots\ldots + A_Nu_N = u_p$$

Where u_p is a prescribed value which may vary with load, u_i are the nodes and A_i are the relation between the corresponding degrees of freedom.

2.7 Failure criteria

The failure criterion is used to relate the point at which failure will occur when the material is subjected to a combined stress system with the behaviour of a material subjected to simple tension or compression tests. Several theories have been proposed to correlate the yielding in uniaxial tests with that in a more complex state of loading. They are:

a) The maximum principal stress theory (Rankine)

b) The maximum principal strain theory (Saint Venant)

c) The maximum shear stress theory (Tresca)

d) The von-Mises yield theory

The von-Mises yield theory gives results that are in good agreement with the test results for ductile materials. The strength of the material obtained from the uniaxial test is the value of the Mises stress at which failure will occur due to the action of the combined stresses. This failure criterion was used for the analyses.

2.8 Modelling the individual components of the composite connection

2.8.1 Modelling of a reinforced concrete beam

To develop the model for the behaviour of the reinforced concrete slab in the composite connection, a reinforced concrete cantilever beam was used, since they are similar to each other. Two types of element were used to model the concrete: eight noded and twenty noded 3D solids, in two separate models. The reinforcement was introduced through a special command (*REBAR) available in the ABAQUS software.

It is mentioned in the user guide for the software that this command can simulate some interaction between the concrete and the reinforcement. The stress-strain curve for the concrete was modelled through the *CONCRETE option. To define the shape of the failure surface, * FAILURE RATIO option was used. The ratio of the ultimate biaxial compressive stress to the uniaxial compressive ultimate stress was selected as 1.16. The absolute value of the ratio of uniaxial tensile stress at failure to the uniaxial compressive stress at failure was taken as 0.08. To define the retained tensile stress normal to a crack as a function of the deformation in the direction normal to the crack, *TENSION STIFFENING parameter was used. The model was fixed at one end by keeping all nodes at that end fixed (i.e. restraining all displacements at those nodes). The load was applied on the other end. The depth of the beam was 508 mm, width of section was 254 mm, and the length of the beam was 3048 mm. Area of reinforcement was 1290 mm^2. The reinforcement was divided into two parts and located at 95.25 mm, from the top of the beam and 63.5 mm from the edges. The model using twenty noded solids had 192 elements and the model with eight noded solids had 1536 elements. The stress-strain curve used in the analysis is shown in Figure 2-10. The FE mesh for twenty noded elements is shown in Figure 2-11. Before performing the FE analysis, a hand calculation was made for the beam, using elastic theory with uncracked and cracked sections. Strain at any point was calculated as:

$$\varepsilon = \frac{\sigma}{E} = \frac{M.Y}{I.E}$$

Where:

Y is the distance of the point of interest from the neutral axis

M is the moment at the section considered

I is the second moment of area

E is the modulus of elasticity

The deflection values were calculated by:

$$\delta = \frac{P.x^3}{3E.I}$$

Where:

P is the applied load

x is the distance of the point of interest from the support

Location of neutral axis was calculated as

$$\bar{y} = \frac{(b.h - A_S).h/2 + n.A_s.(h - h')}{b.h} \tag{2-1}$$

Where:

n is the modular ratio

b, h are breadth and depth of section

A_S is the steel area

h' is the distance of reinforcement from the top

The moment of inertia of the section was calculated as:

$$\bar{I} = \frac{b.h^3}{12} + n.A_S\left(h - h' - \bar{y}\right)^2 \tag{2-2}$$

And the failure load was calculated by assuming a rectangular stress block, assuming the tensile force equal to the compressive force and applying a safety factor of 1. The formula for ultimate load capacity was:

$$P_u = \frac{A_s f_y}{L}\left(h - h' - \frac{A_s f_y}{2bf_c'}\right) \tag{2-3}$$

Where:

P_u is the ultimate load capacity

L is the span of the beam

f_c' is the cylinder compressive strength of the concrete

The deflected shape of the beam is plotted in Figure 2-12; to make the shape clear the displacements are magnified 25 times. Figure 2-13 compares the load deflection curve at the free end of the beam. To calculate the theoretical deflection values the moment of inertia of the cracked section was used at the ultimate load value. It appears that the estimated ultimate load and the estimated deflections are quite reasonable. Figure 2-14 shows the comparison of the stress - strain curve from FE analysis and theoretical analysis at the bottom part of mid span. Figure 2-15 shows the stress (S_{11}) contours for different load values. From the contour plots the variation of depth of the tension zone can be observed.

2.8.2 Modelling of a steel beam

Like the concrete slab, a separate model was created to study the steel beam, using the FE method. Four noded shells with six degrees of freedom were used to model the beam. The dimensions of the beam were: flange thickness = 8.4 mm, web thickness = 6.1 mm, depth of section = 257 mm, and flange width = 99.7 mm, length = 675 mm. In the model the beam web had 15 divisions along the axis of the beam, 14 divisions in the vertical direction, each flange had eight divisions across the width and 15 divisions along the axis of the beam. To make a simple analysis, the stress-strain curve used for the beam was chosen as a simple one as shown in Figure 2-16. The FE mesh is shown in Figure 2-17. Like the previous case, at first theoretical calculations were done. The second moment of area of the I section is:

$$I = \frac{t_w.h^3}{12} + \frac{1}{2}b.t_f.\left(D - t_f\right)^2 \qquad (2\text{-}4)$$

Where:

t_w is the web thickness

t_f is the flange thickness

D is the depth of section

b is the flange width

$$h = D-2t_f$$

The flexural and shear displacements were calculated as:

$$\delta = \frac{P.x^3}{3.E.I} + \frac{P.x}{G.D.t} \tag{2-5}$$

The ultimate load capacity was calculated from the plastic moment capacity of the section:

$$P_u = \frac{M_P}{L}$$

$$P_u = \frac{\sigma_p}{L}\left[b_f t_f \left(D - t_f\right) + \frac{1}{4} t_w h^2\right] \tag{2-6}$$

The elastic rotation was calculated as:

$$\phi = \frac{P}{2EI}.\left(2.L.x - x^2\right) \tag{2-7}$$

To take into account of shear simplified equation used is:

$$\phi = \frac{P}{2EI}.\left(2.L.x - x^2\right) + \frac{P}{GDt} \tag{2-8}$$

The displaced shape is plotted in Figure 2-18, displacements are magnified by 25 times. The load displacement curve at the free end is plotted in Figure 2-19. The moment-rotation curve is plotted in Figure 2-20, the moment is calculated at the support, while the rotations are calculated 375 mm away from the beam support. The results of the FE analysis as shown in the above mentioned figures are close to the simple theory. Figure 2-21 shows the von-Mises stress contours. The propagation of plastic stress from these figures can be easily observed. From the von-Mises stress contour plot the plastic hinge can be observed at the failure load.

The modelling of the column is similar that of the steel beam, so it is not described here.

2.8.3 Modelling of bolts

Since it was decided to use JOINTC elements for modelling the bolts, the bolt property had to be equivalently transferred to the property of these elements. One bolt and two plates were modelled by using solid elements with six and eight nodes. The finite element mesh is shown in Figure 2-22. One of the plates at one end was kept fixed and the other plate was pulled. Interface elements were used between the bolt and the plates, and also between the plates. From the results of this model, the load shear deformation property of the bolt was obtained. For load-axial deformation property, one end of the bolt was kept fixed while the other end was pulled. Results of the analysis are shown in Figure 2-23. These load deformation curves were used as the basic property input for the JOINTC elements.

2.8.4 Modelling of welds

Modelling of welds can be done by using shell elements for the welds or solid elements for the weld. Although mixing different types of elements does not seems to be compatible, ABAQUS allows it and results of FE analysis by Crockett [2-5] show good agreement. In this study shell elements for welds were selected, and the analysis was also conducted ignoring the welds and making the connection continuous at that region.

2.8.5 Modelling the interface of the endplate and column flange

To model the interface between the endplate and the column flange, interface elements are used. When four node shell elements are used an eight node interface element must be used and when a nine node shell element is used an eighteen node interface element

is used. The interface property used was that it can transfer any magnitude of compression but can separate without transferring any tensile force, zero frictional coefficient was used - to make a true representation of the connection as the shear is transmitted through the bolts in a composite connection.

2.8.6 Modelling of shear studs

Shear studs were modelled by a combination of two elements, one of which is a beam element while the other is a spring element. The spring element was used to introduce the test load slip curve for the shear studs. The beam element was connected to the steel beam top and the spring element. The spring element connects the beam element to the reinforcement. To model the shear slip JOINTC elements were used. The properties (Figure 3-5 of chapter 3) of these elements were obtained from the available test results [2-6, 2-7, 2-8, 2-9 and 2-10]. These elements are used in chapter 3 where the composite connection model is described.

2.9 Numerical modelling of a bare steel connection

2.9.1 Representation of the experiment

To obtain an accurate result from the finite element analysis, it is necessary to make the test set-up and the FE model comparable, i.e. the model in the FE analysis should represent the experimental procedure used in the laboratory as closely as possible. This section describes the experimental set-up and results, and the FE model.

2.9.2 Test Set-up and results

Figure 2-24 shows the experimental set-up for the test SJS-1 [2-1] with a bare steel cruciform flush endplate connection. The steel beam used in the test was 254x102UB 25, the column used was 203x203UC46 and the endplate dimension was 280x130x10 mm. The endplate was bolted to the column flange by four bolts, the diameter of the

bolt holes was 22 mm (bolt diameter 20 mm). The bolts were vertically 175 mm centre to centre, and horizontally 70 mm centre to centre. Length of the column was 1800 mm, and the beam was 1590 mm long. Both the top and the bottom of the column were bolted. The load was applied at 1473 mm from the column face using load cells. The specimen failed at a load of 42.63 kN, the moment at failure was 62.8 kN•m. In the test at first the endplate yielded at 54% of the final load (it was determined by the deformed shape of the endplate), bolts yielded at 95% of the final load and finally the column web horizontal stress reached yield, and the von-Mises stress value exceeded the yield stress at the column web.

2.9.3 The FE mesh

The FE mesh used in the analysis is shown in Figure 2-25. Since it was a cruciform test, by taking advantage of symmetry only half the connection was modelled, with proper boundary conditions. The full length of the beam was modelled. Since the main interest of the modelling was the overall behaviour of the connection the column length was not fully modelled. Length of the column modelled was 150 mm on each side of the beam. The analysis used a fine mesh, with half the column web width divided into four vertical divisions. From the bottom of the column to the bottom of the beam flange there were five divisions, also from the top of the beam flange to the top of the column there were five divisions. The vertical and horizontal number of divisions in the connection were selected so as to represent the locations of bolts, beam flange and plate size in the most suitable way. The column flange for that condition had fourteen divisions, the plate had ten divisions and the beam flanges had eight divisions in the horizontal direction. Vertically the plate had sixteen divisions and the beam had fourteen divisions. Also, provision was made for the bolt holes. Along the beam near the connection the divisions were fine but away from it they gradually became more coarse.

To model the beam, column and the plate, four noded shell elements with six degrees of freedom were used. As mentioned earlier JOINTC elements were used for modelling the bolts. The JOINTC elements were used in such a way that they also accounted for the bolt heads. To model one bolt twelve JOINTC elements were used.

In the model the nodes used to define the beam top and bottom flange had the co-ordinates of the centreline of the flanges so that after the thickness was introduced, it achieved the real dimensions. To model the interface between the endplate and the column flange, interface elements were used (INTER4), these elements can model the separation and closure of contacting bodies.

2.9.4 Material properties

The stress strain curves as reported in ref. 2-1, are shown in Figure 2-26. The tests were conducted on some coupons randomly selected from the test specimens.

2.9.5 Boundary conditions

Since the advantage of symmetry was used to reduce the problem size, it was essential to address the problem with proper boundary conditions. The nodes at the column web centreline were restrained from movement along direction 1, (see Figure 2-25) i.e. the direction of the beam axis, and also restrained from any rotation about the column centreline and about the line perpendicular to the column centreline. The nodes at the top and bottom of the column were restrained to move along the beam axis and the line perpendicular to the column centreline, in addition the nodes at the base were restrained to move vertically. Using equations, the nodes at the free edge of the beam flange were made to have the same vertical displacement, (but both flanges are not made equal to each other). Multi point constraints were used at the nodes of the free end of the beam web to keep them on a line which can rotate (*MPC, type SLIDER).

2.9.6 Application of load

The test ultimate load was applied at the beam end, by dividing it equally between ten nodes. Using the available method the suggested initial increment was 0.05 times the applied load, and minimum load to carry out a further analysis was 10^{-8} times the applied load.

2.9.7 Comparison of test results and FE results

The FE results and the test results in terms of the moment rotation (rotation at beam web centreline, 180 mm from the column face) curve are shown in Figure 2-27. The results of the test and the FE analysis are very close to each other. The column web stress S_{11} is shown in Figure 2-28(a), at this stage of load the compressive stress in the column web at beam bottom flange level reached 544 N/mm^2. The von-Mises stress for the same load level is plotted in Figure 2-28(b), the von-Mises stress reached a value of 472 N/mm^2. These results are consistent with the description of the test behaviour. The von-Mises stress for the total connection is shown in Figure 2-28(c). Deflected shape is shown in Figure 2-28(d). From the deflected shape the separation of the endplate from the column web at the beam top flange level can be observed. This is also consistent with the test, which is shown in Figure 2-29.

2.10 Conclusions

This chapter gave a brief introduction to the finite element method and its use for modelling semi-rigid composite connections. The elements which are used to develop the model of semi-rigid composite connections described in chapter 3 have also been described.

This chapter covered the development of the modelling of the individual components of the semi-rigid composite connection and the checking of their behaviour against

alternative analysis methods. From the success in modelling the separate elements of the connection, encouragement has been given for the modelling of the complete semi-rigid composite connection.

The method of modelling a semi-rigid bare-steel connection has been described and the results compared against test results. The comparison indicates that the modelling approach is correct. So now the modelling can be extended to composite connections as described in next chapter 3. Modelling of semi-rigid composite non-sway frame and bare steel sway frame will be described in chapter 9.

2.11 References

2-1 Li, T. Q. (1994) *The Analysis and Ductility Requirements of Semi-Rigid Composite Frames*, Ph.D. thesis, University of Nottingham, UK.

2-2 *ABAQUS user manual*, Version 5.3.1 (1994) Hibbitt, Karlsson & Sorensen, inc., 1080 Main Street, Pawtucket, RI 02860-4847, USA.

2-3 Femview Limited (1989), '*FEMGEN/FEMVIEW user's manual*'.

2-4 SDRC (1990) '*IDEAS-FEM Finite element modelling user's guide*'.

2-5 Crockett, P. (1994) *Finite Element Analysis of welded Tubular Connections*, Ph.D. thesis, University of Nottingham, UK.

2-6 Chapman, J. C. and Balakrishna, S. (1964) *Experiments on Composite Beams*, The Structural Engineer, November 1964, No. 11, Vol. 42, pp. 369-383.

2-7 Lloyd, R. M. and Wright, H. D. (1990) *Shear Connection between Composite Slabs and Steel Beams*, Journal of Construction Steel Research, Vol. 15, pp. 255-285.

2-8 Lam, D., Elliot, K. S. and Nethercot, D. A. *Push off tests on studs with hollow cored floor slabs* (in preparation).

2-9 Razaqpur, A. G. and Nofal, M. (1989) *A Finite Element for Modelling the Nonlinear behaviour of Shear Connectors in Composite Structures*, Computer & Structures Vol. 32, No. 1, pp. 169-174.

2-10 Mistakidis, E. S., Thomopolos, K. T., Avdelas, A. and Panagiotopoulos, P. D. (1995) *Analysis of composite beams with shear connectors allowing for softening*, Steel Structures - Eurosteel 95, Kounadis (ed. Balkema), Rotterdam, pp. 73-80.

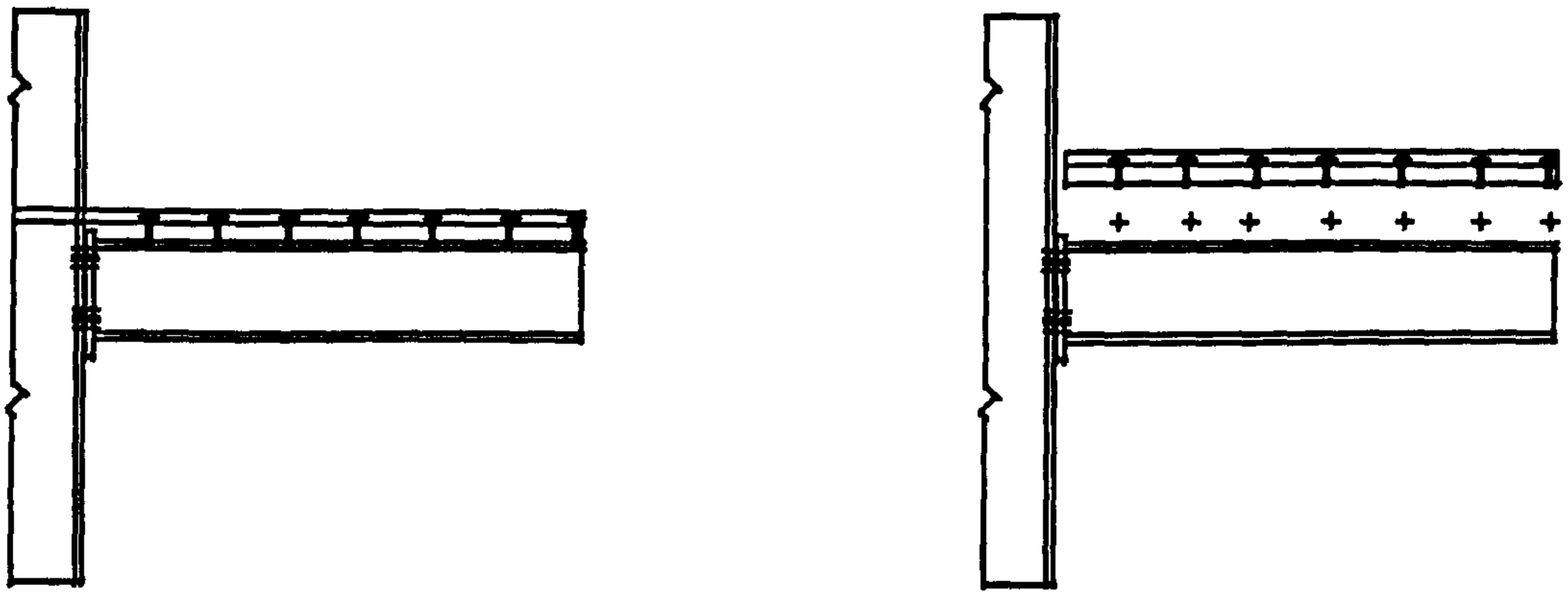

(a) (b)

(a) Composite connection

(b) Bare steel connection and reinforced concrete slab added with proper shear connection

Figure 2-1 Separating a composite beam into two components

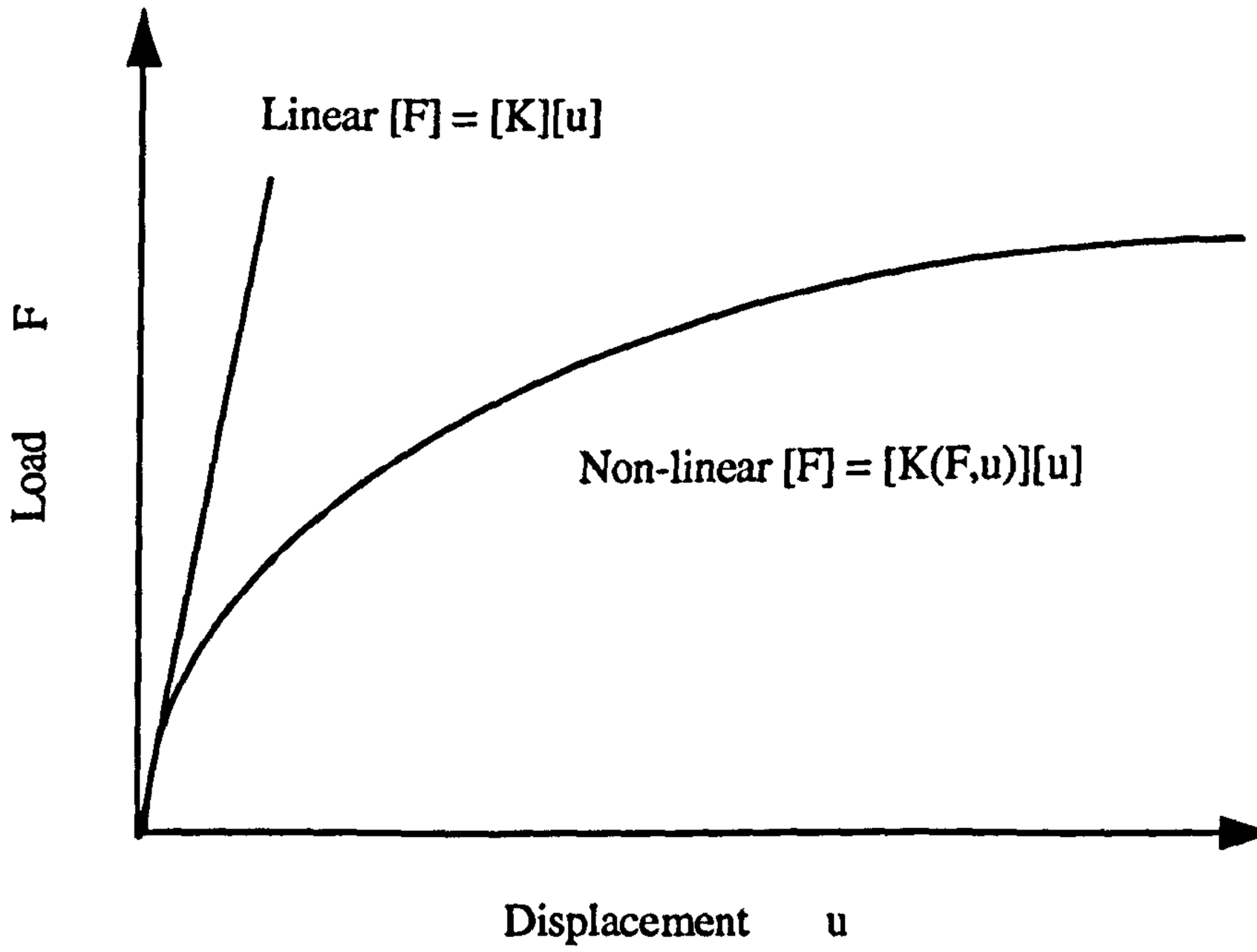

Figure 2-2 Stiffness-matrix in non-linear problems

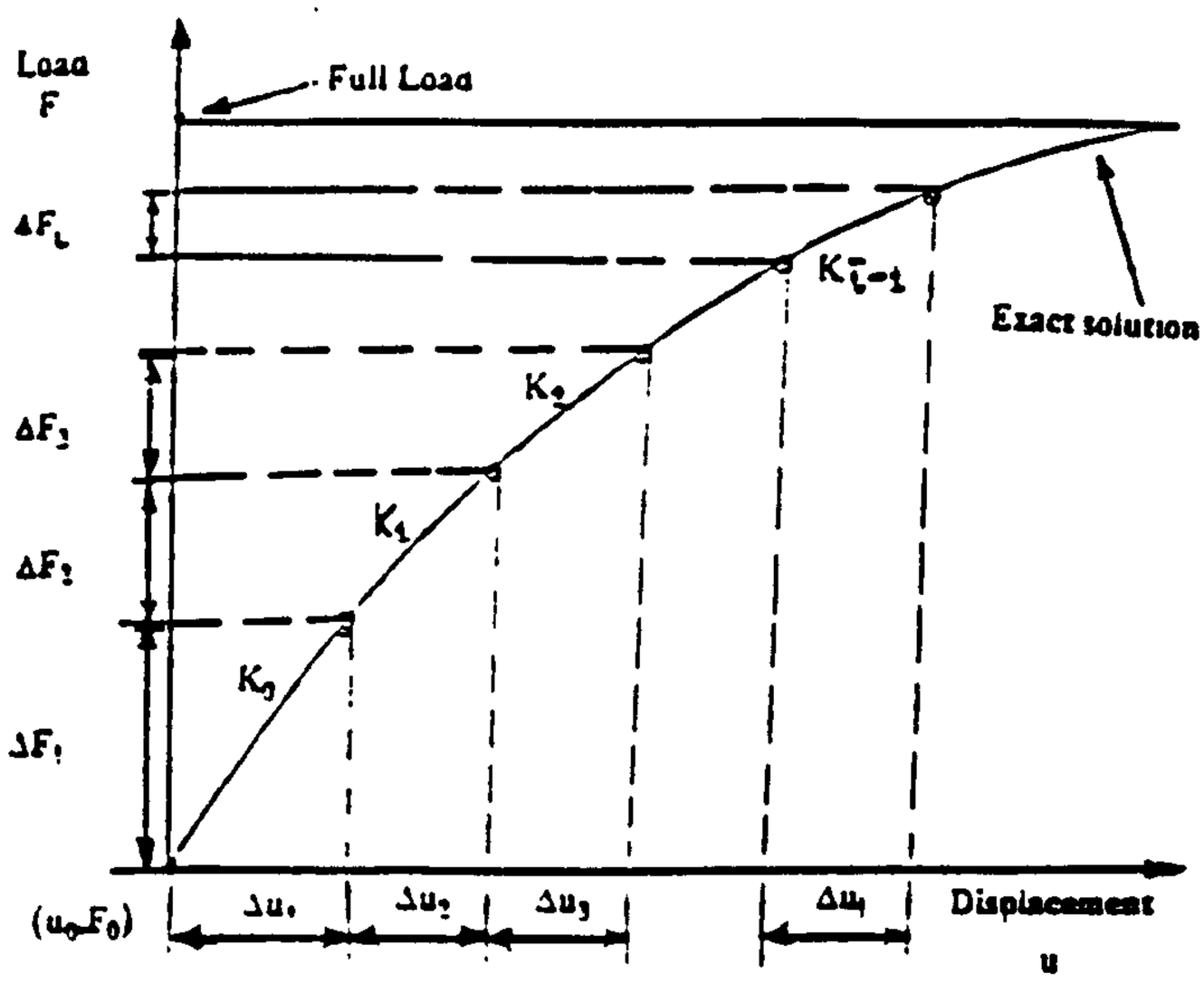

(a) Incremental procedure

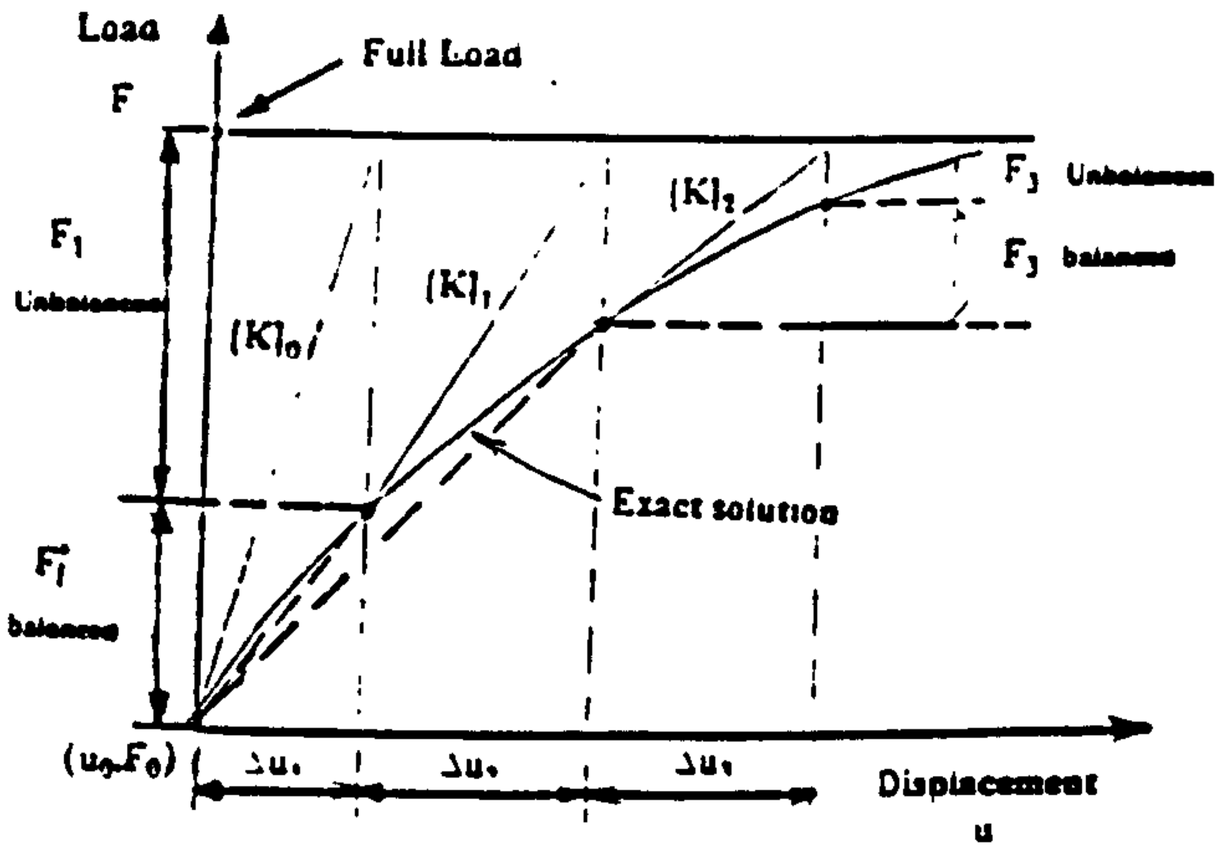

(b) Iterative procedure

Figure 2-3 Solution techniques in non-linear problems

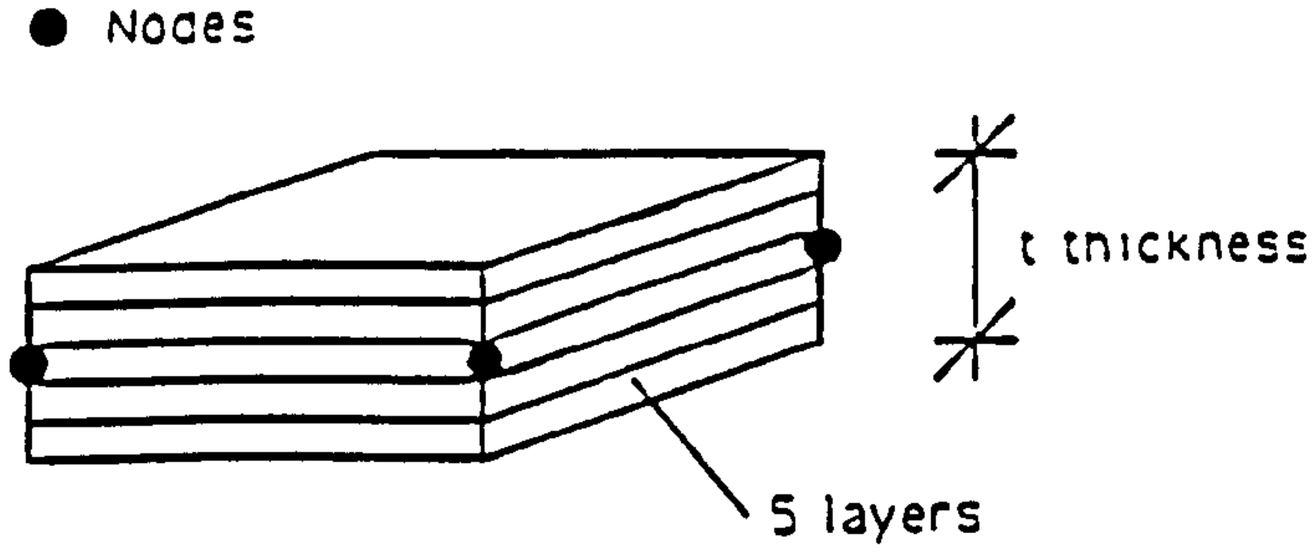

Figure 2-4 Structure of a shell finite element

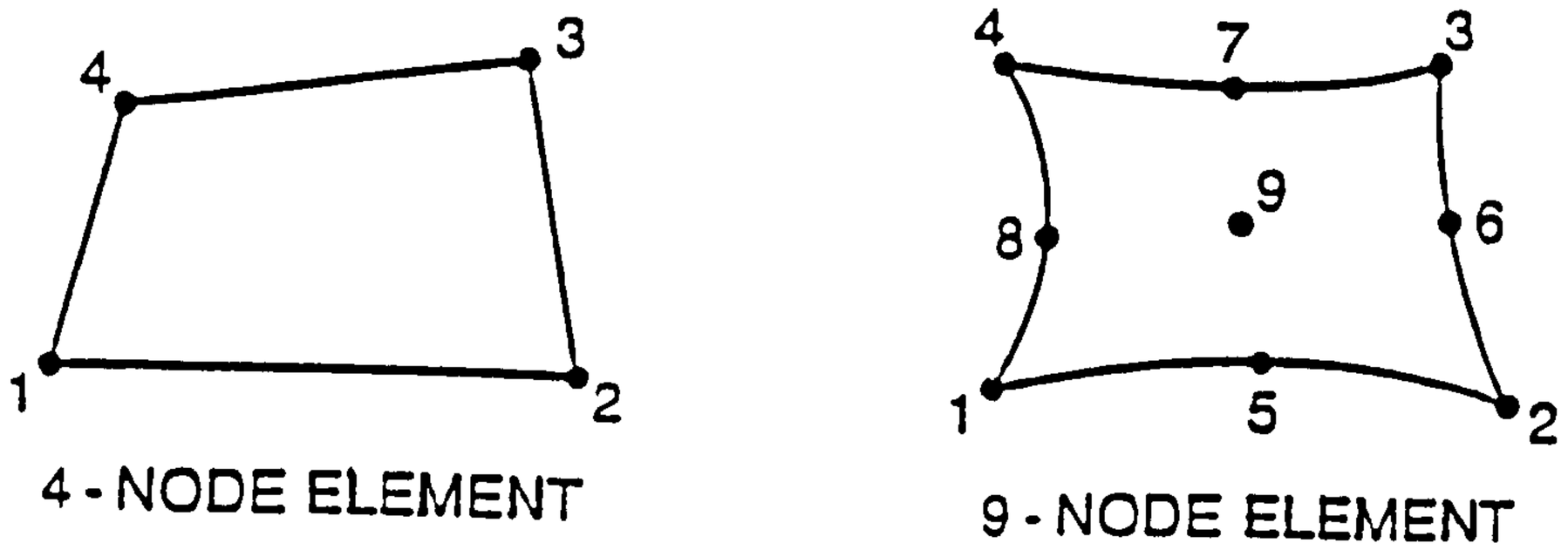

Figure 2-5 Configuration of four and nine noded shell elements

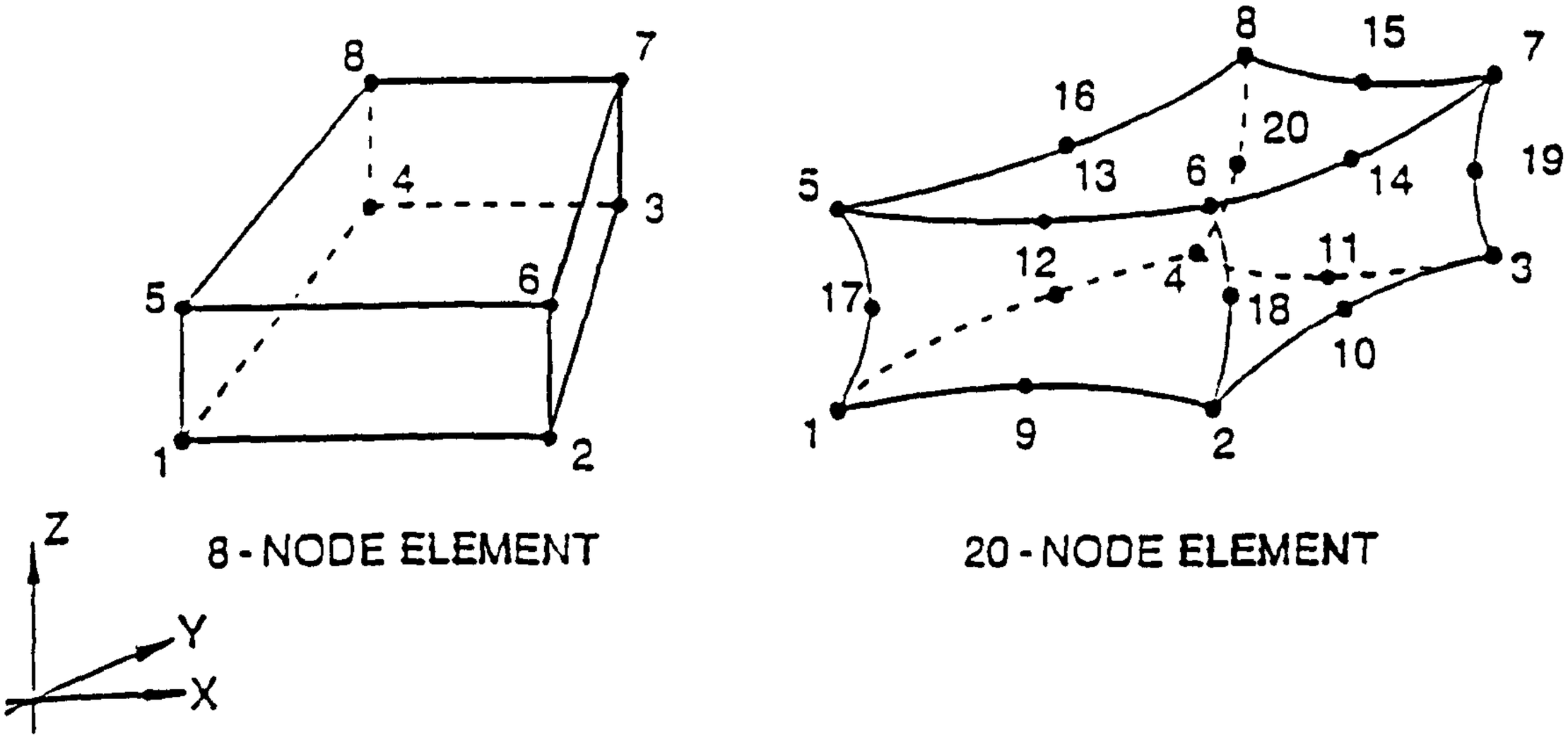

Figure 2-6 Solid elements

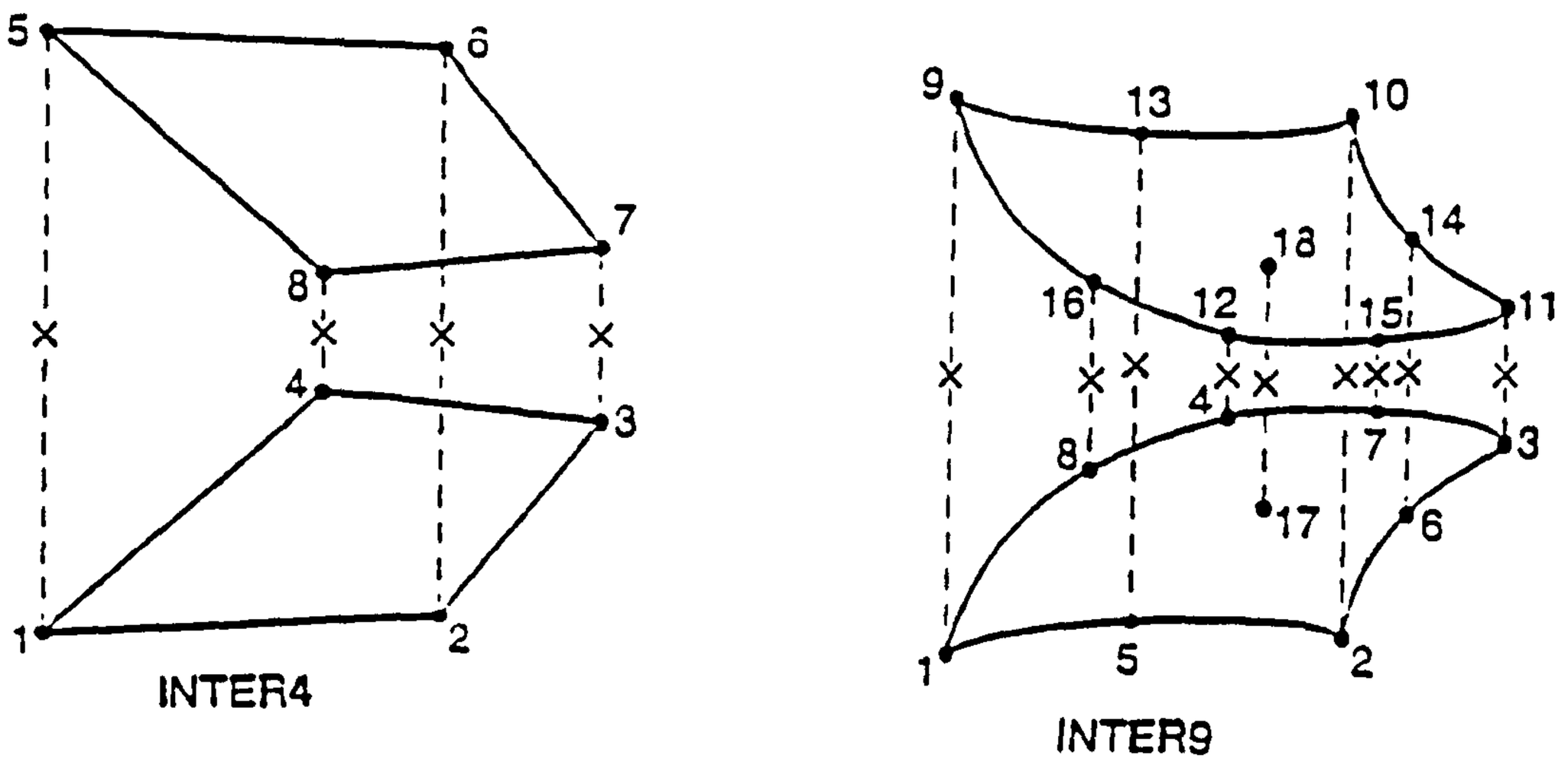

Figure 2-7 Interface elements

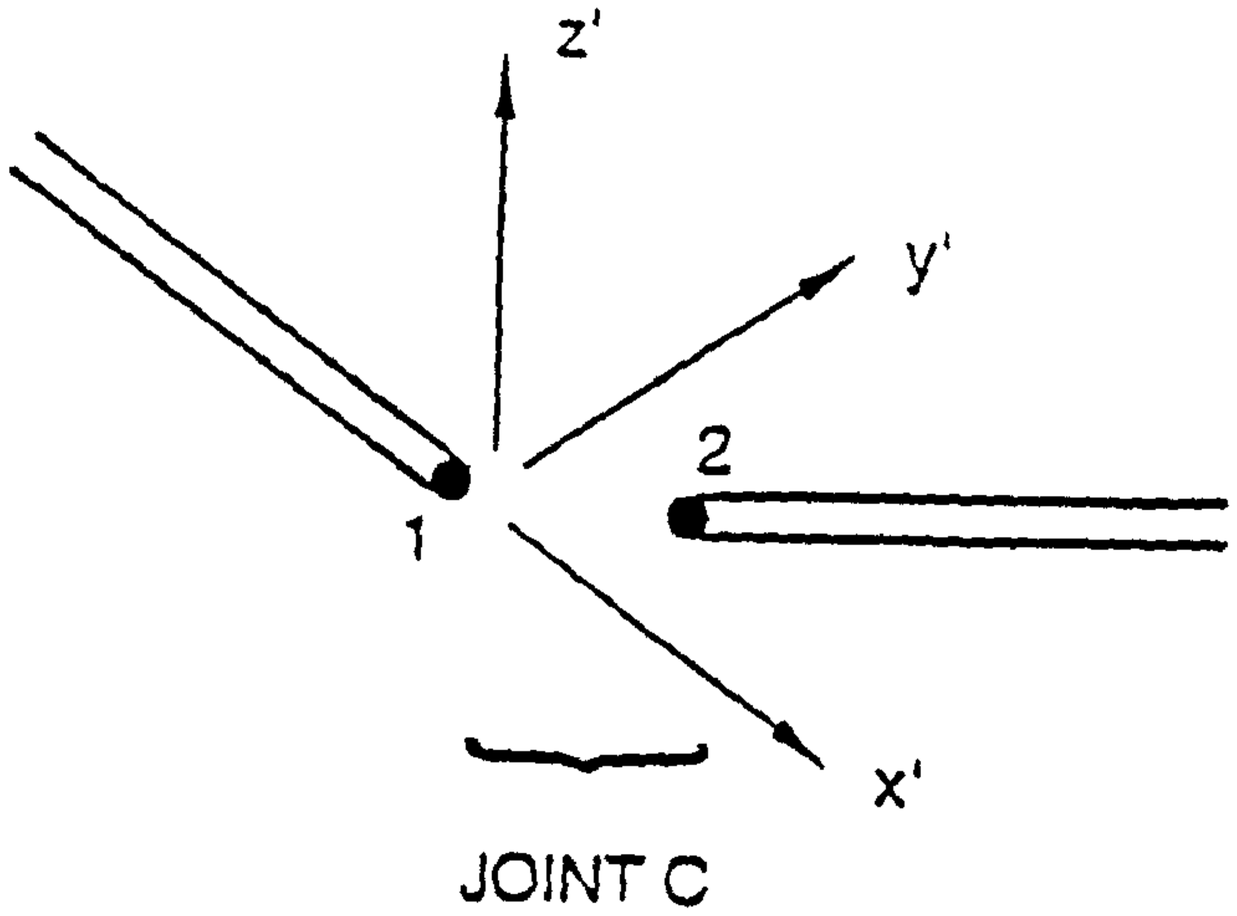

Figure 2-8 Joint elements

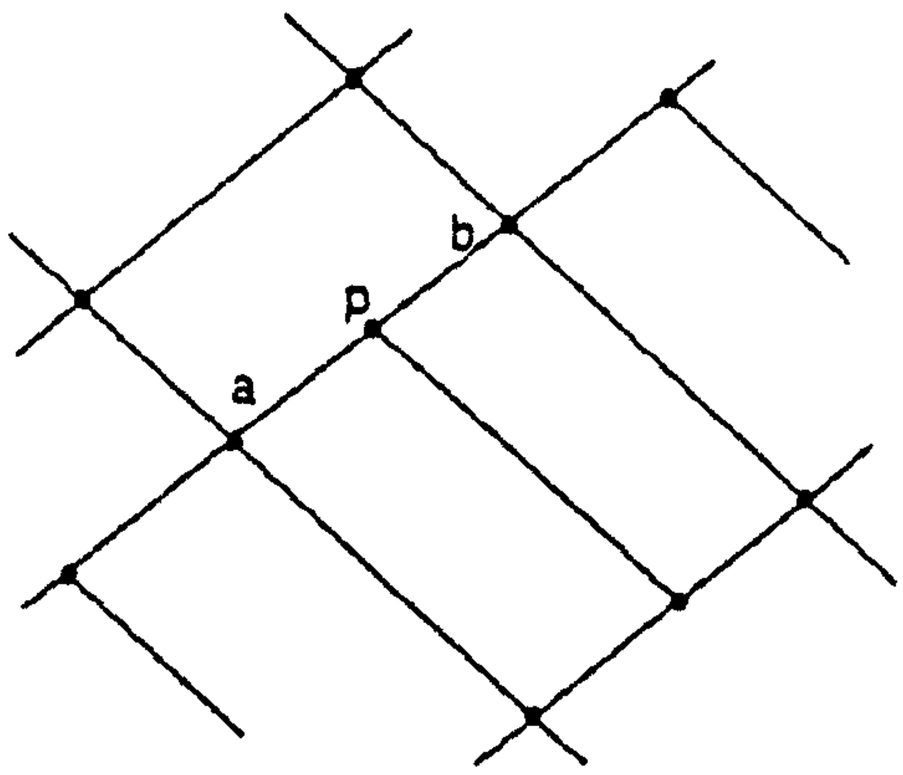

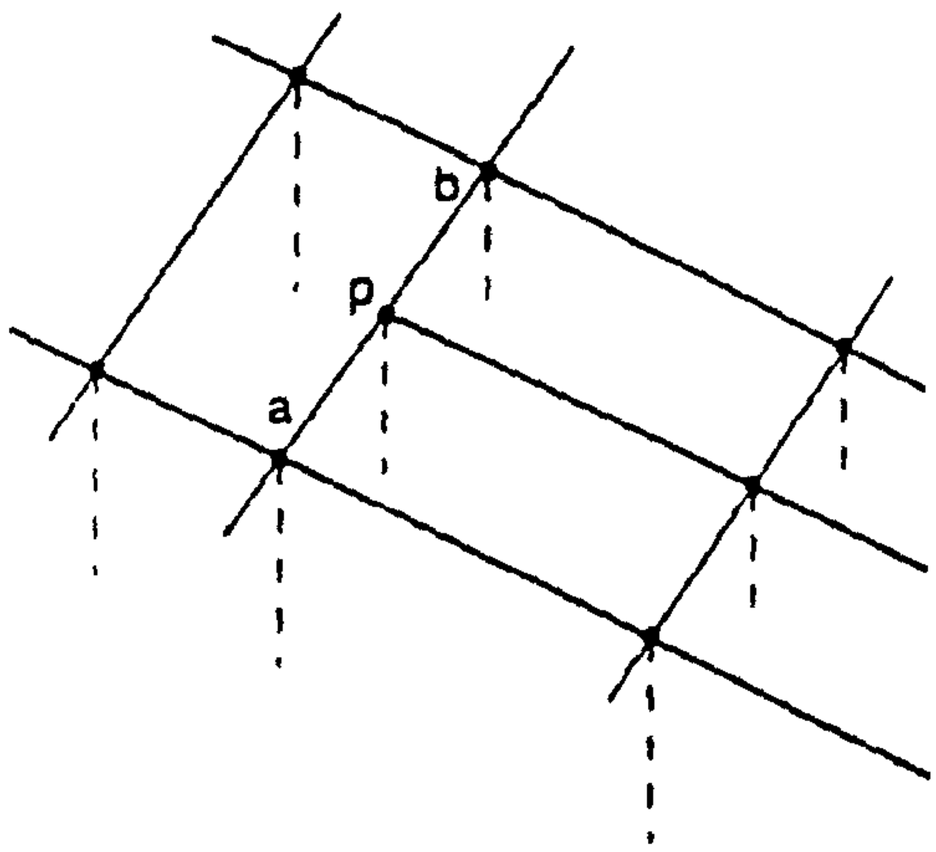

2-9(a) LINEAR type MPC.

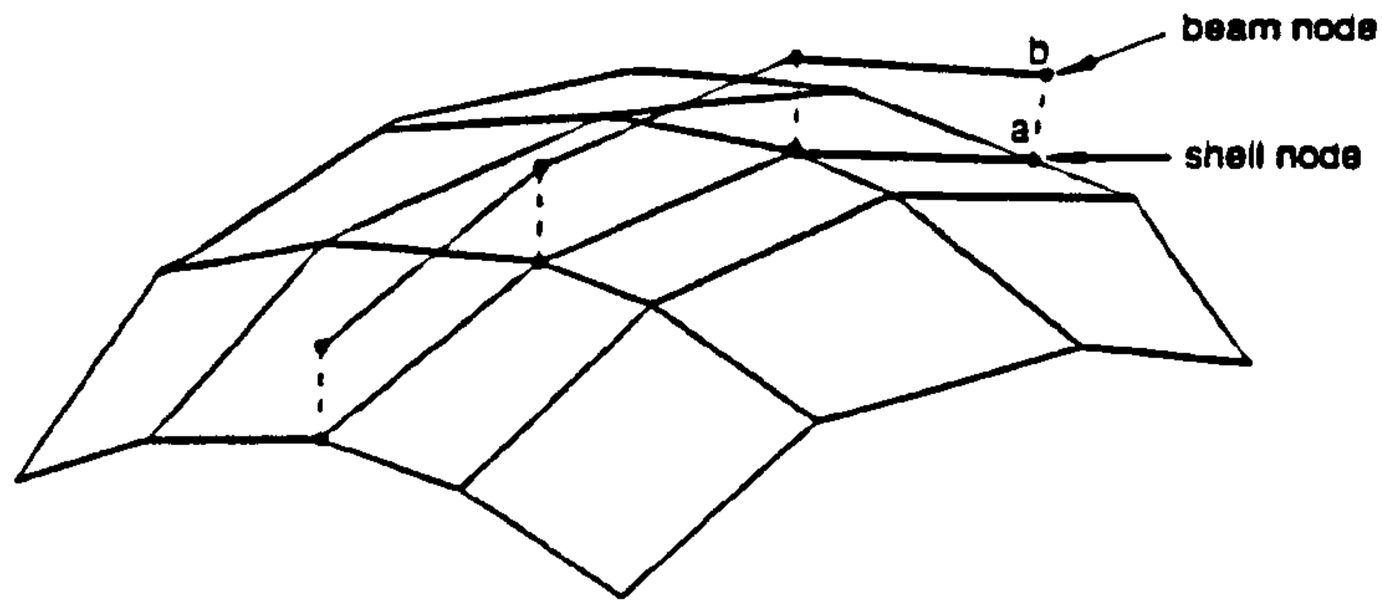

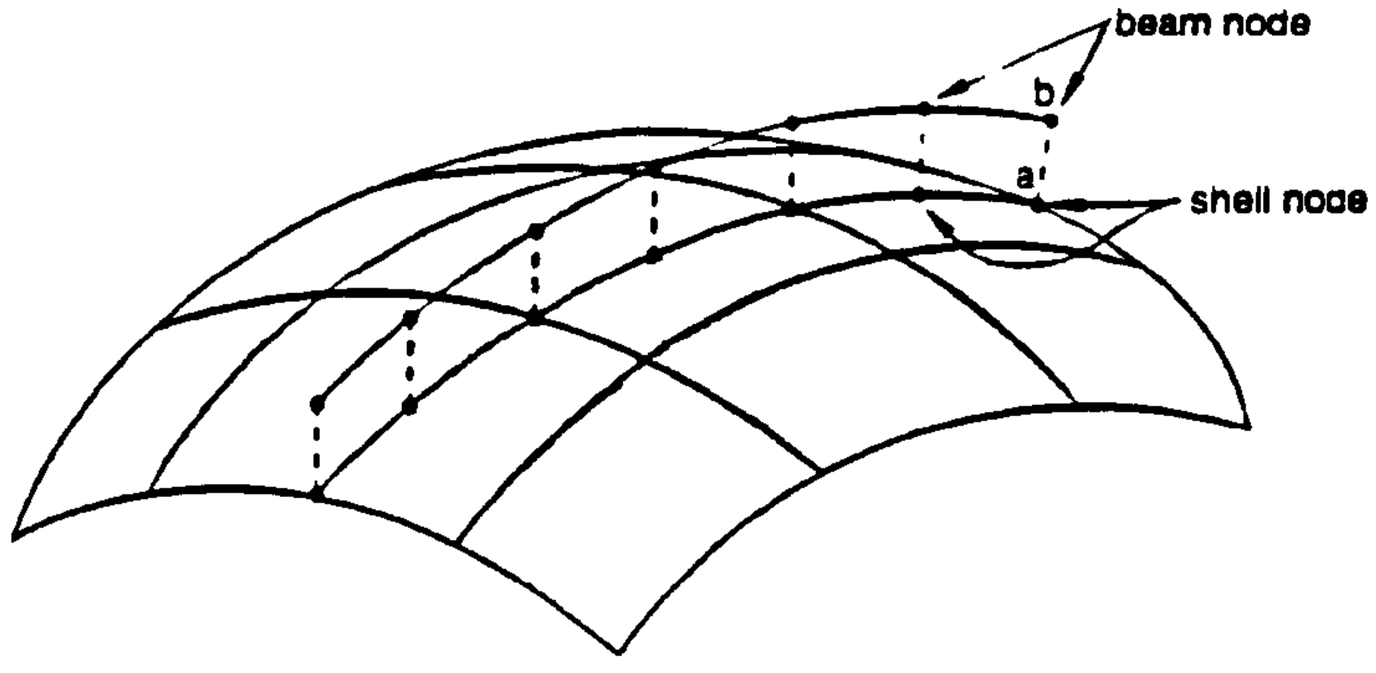

2-9(b) BEAM type MPC.

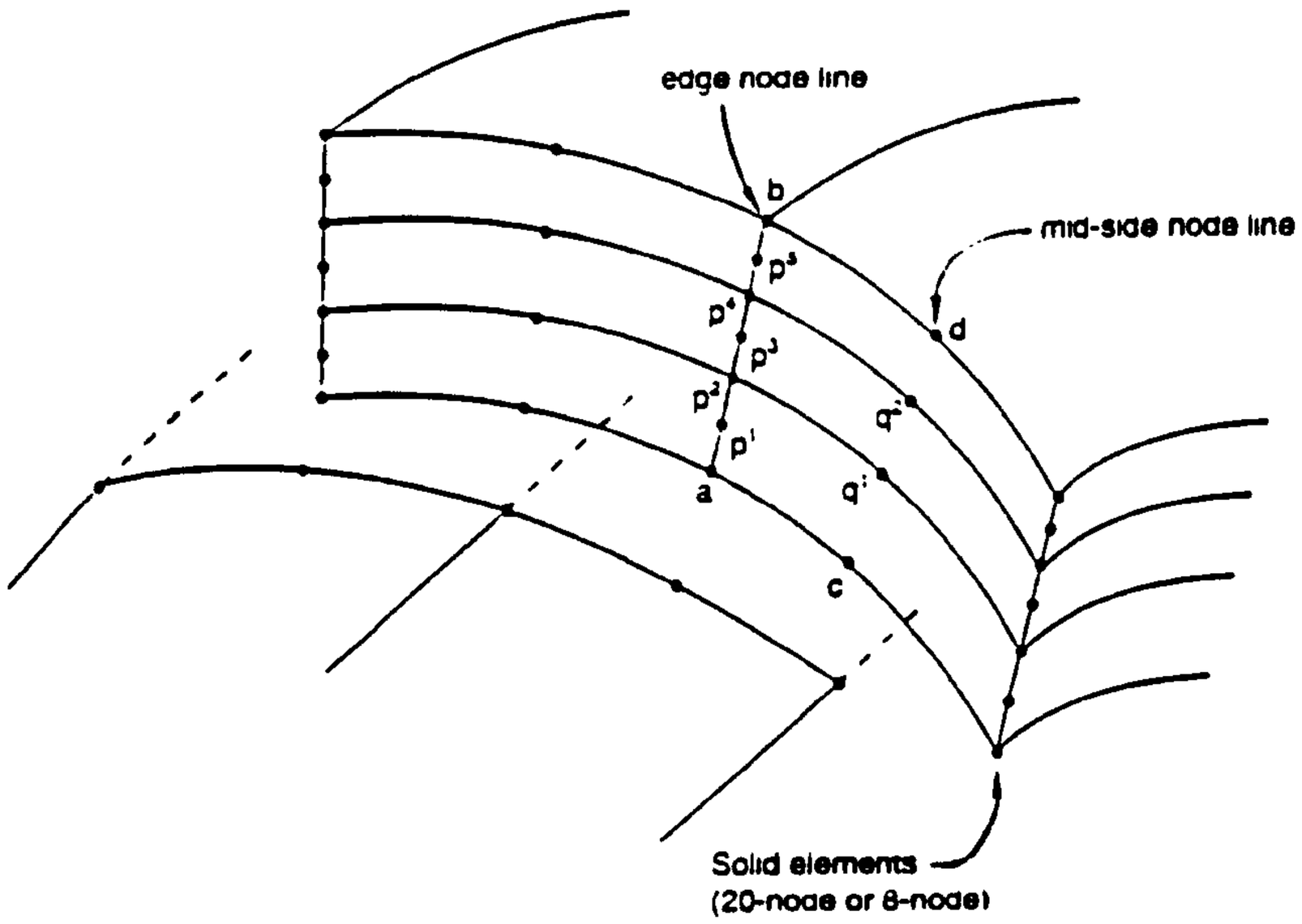

2-9(c) SLIDER type MPC

Figure 2-9 Different types of MPC

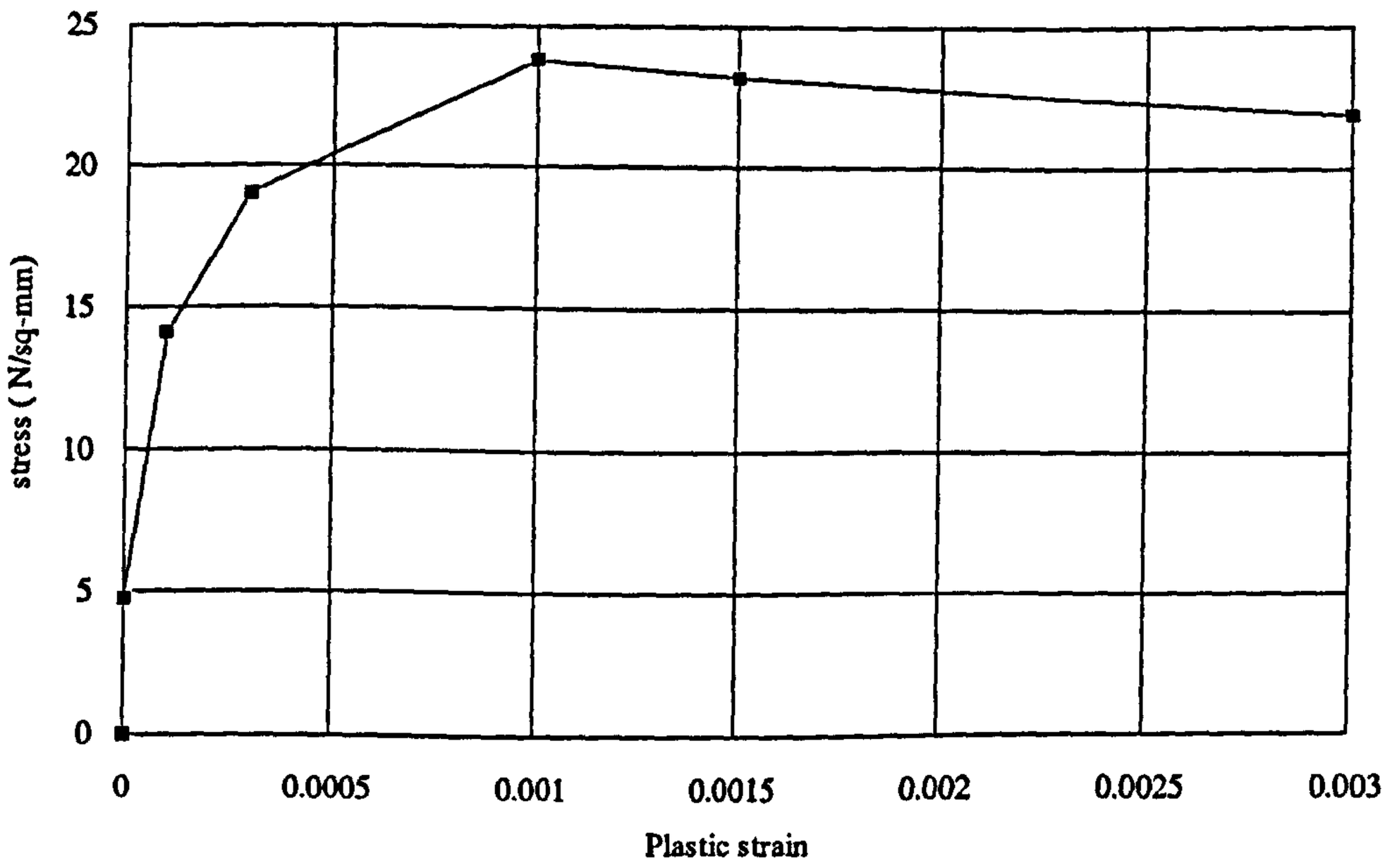

Figure 2-10 Stress strain curve used for concrete

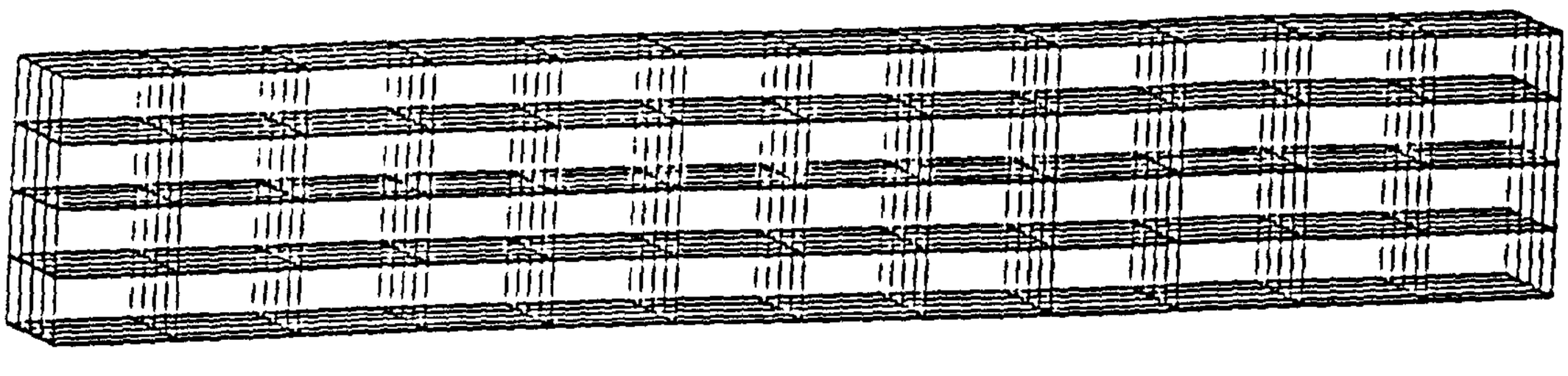

Figure 2-11 FE mesh for reinforced concrete beam

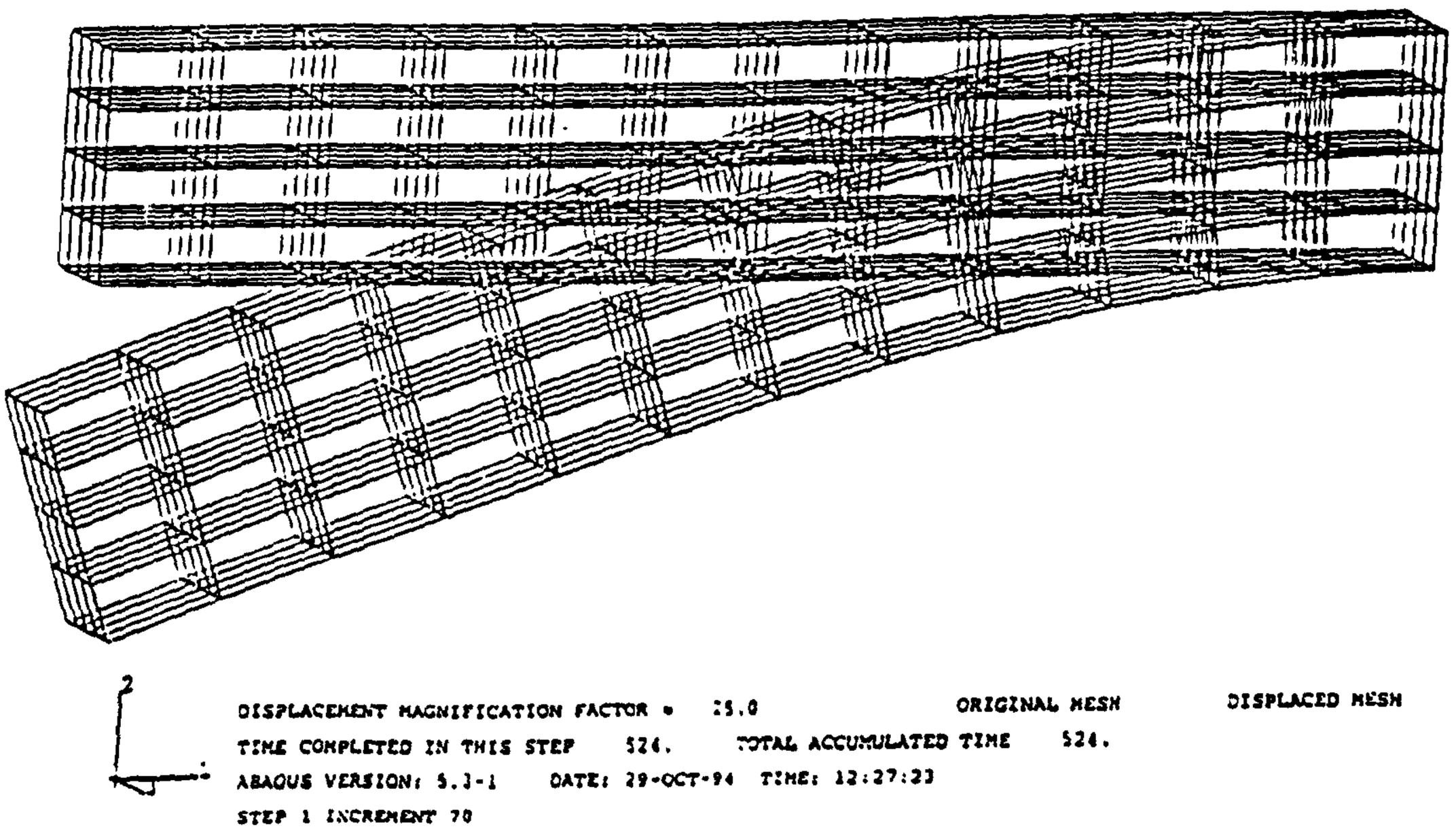

Figure 2-12 Deflected shape of the reinforced concrete beam at ultimate load

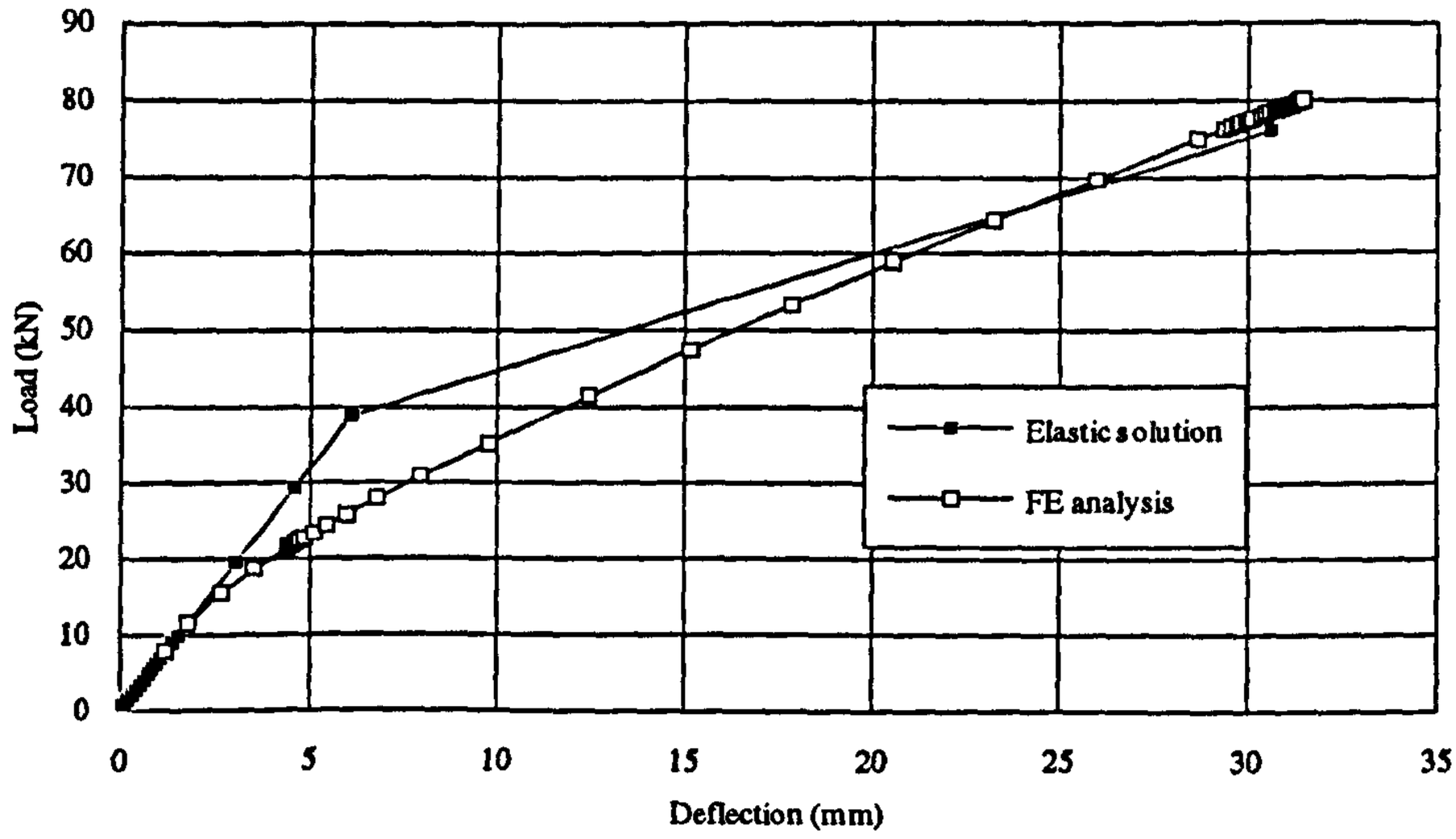

Figure 2-13 Comparison of load deflection curves

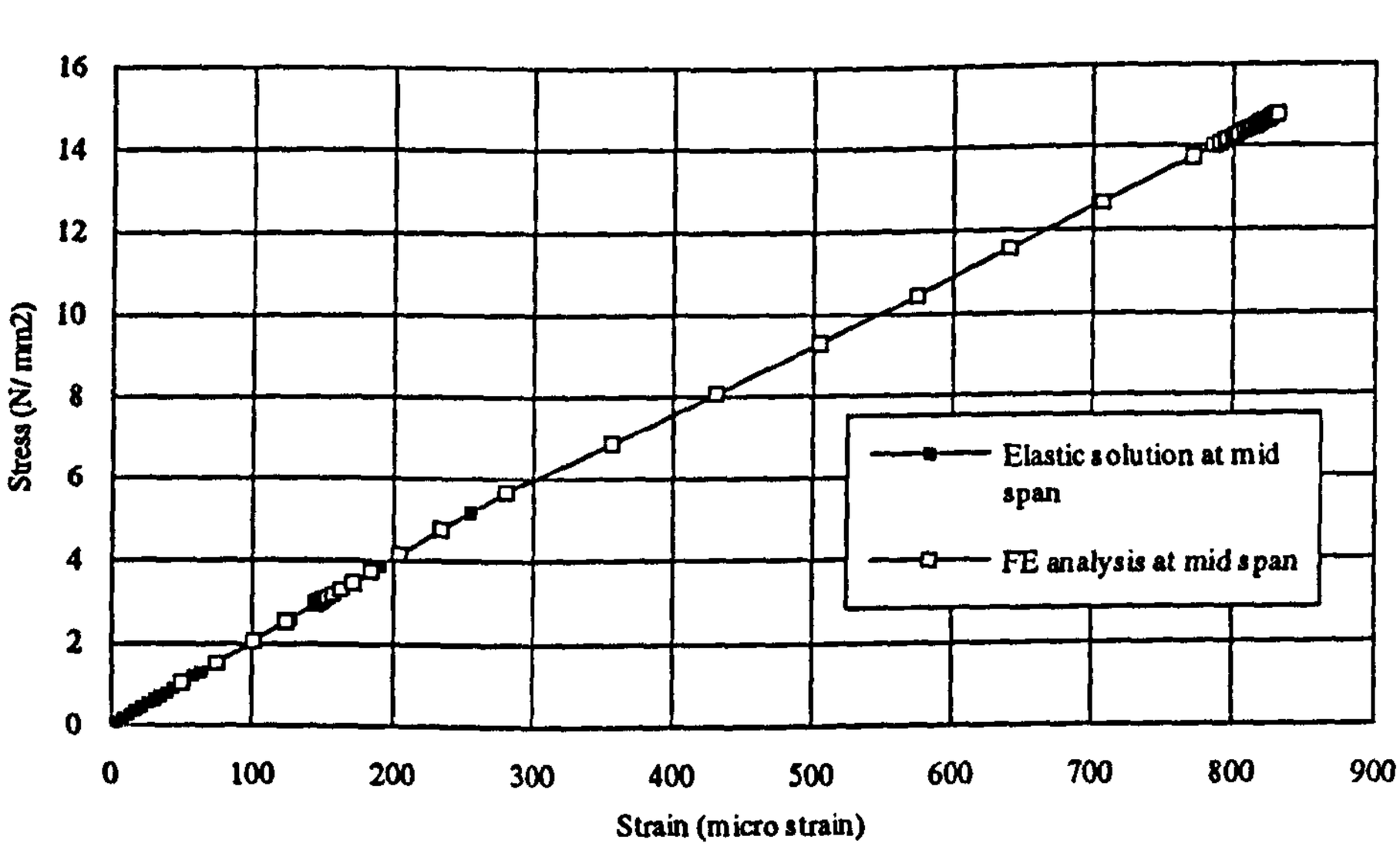

Figure 2-14 Comparison of stress-strain curves at the bottom of the concrete beam

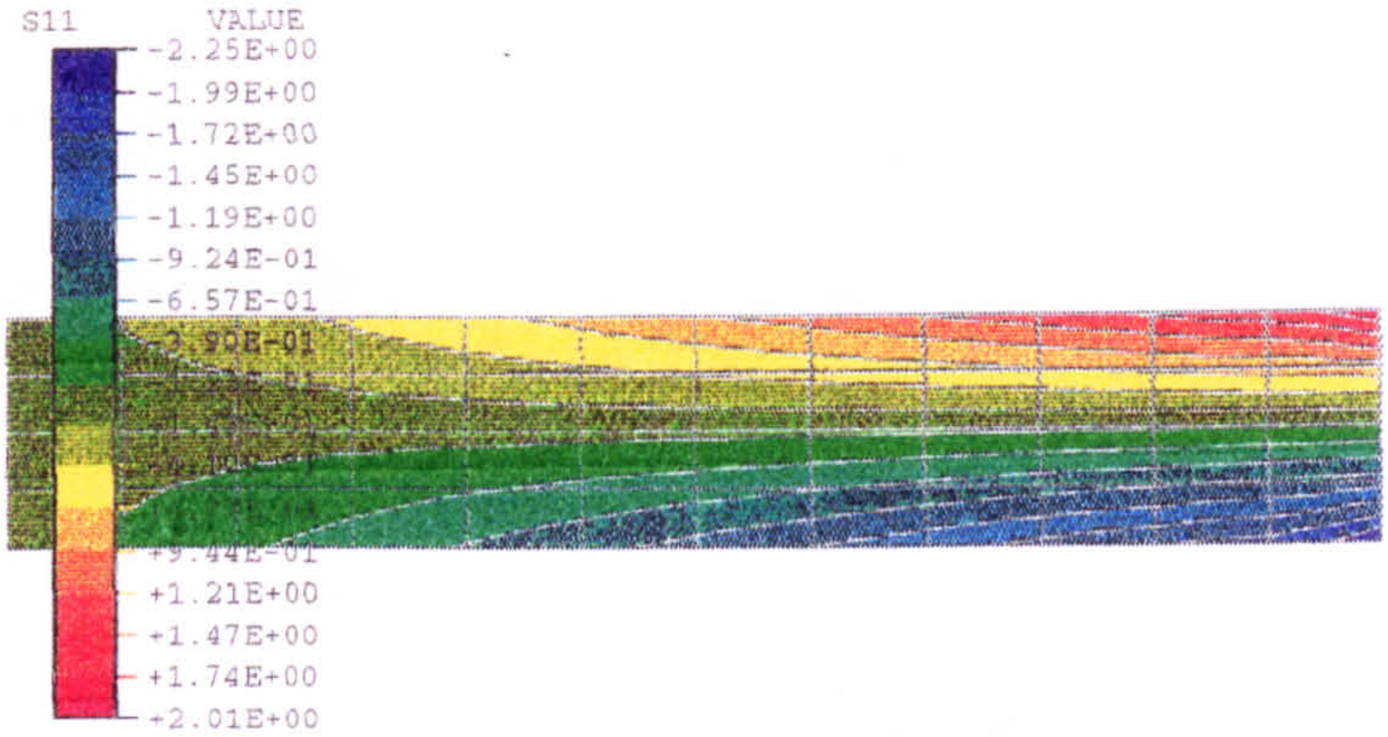

(a) Normal stress contour at 2.5% of ultimate load

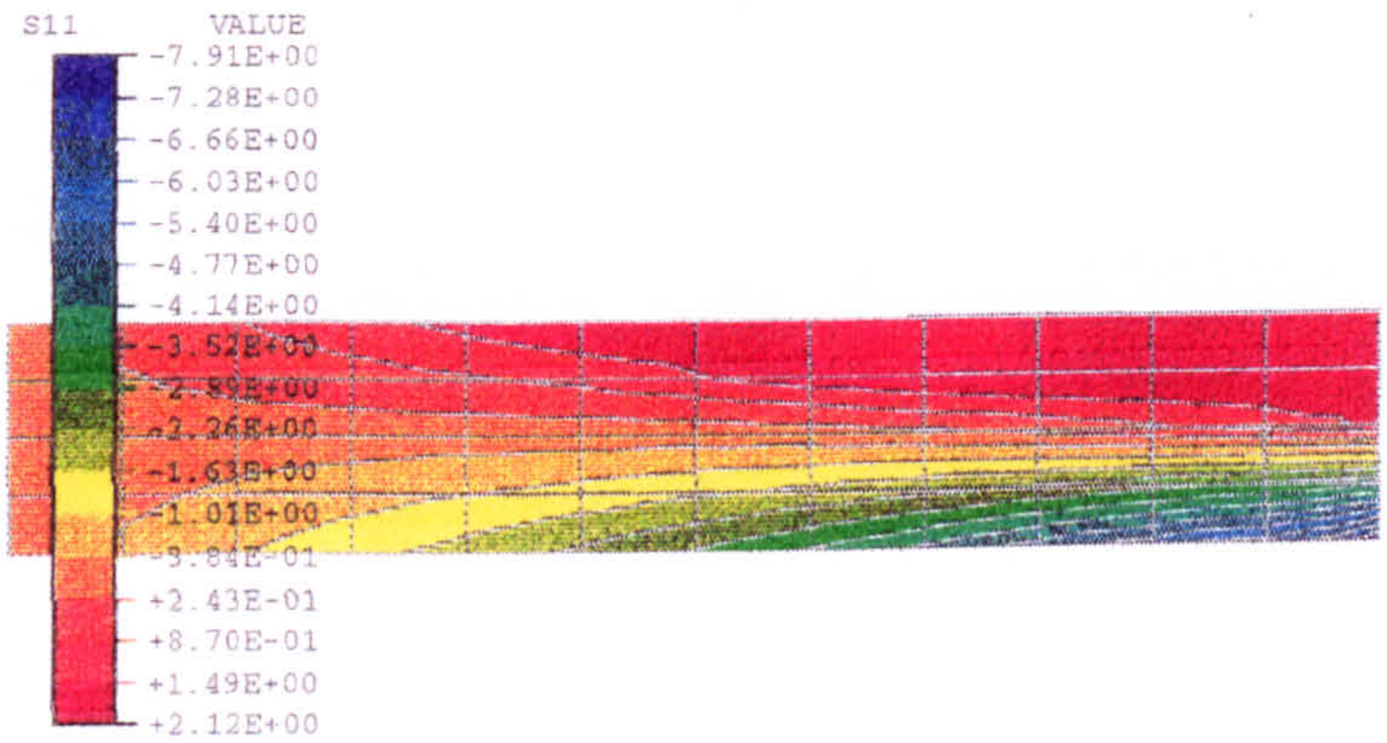

(b) Normal stress contour at 10% of ultimate load

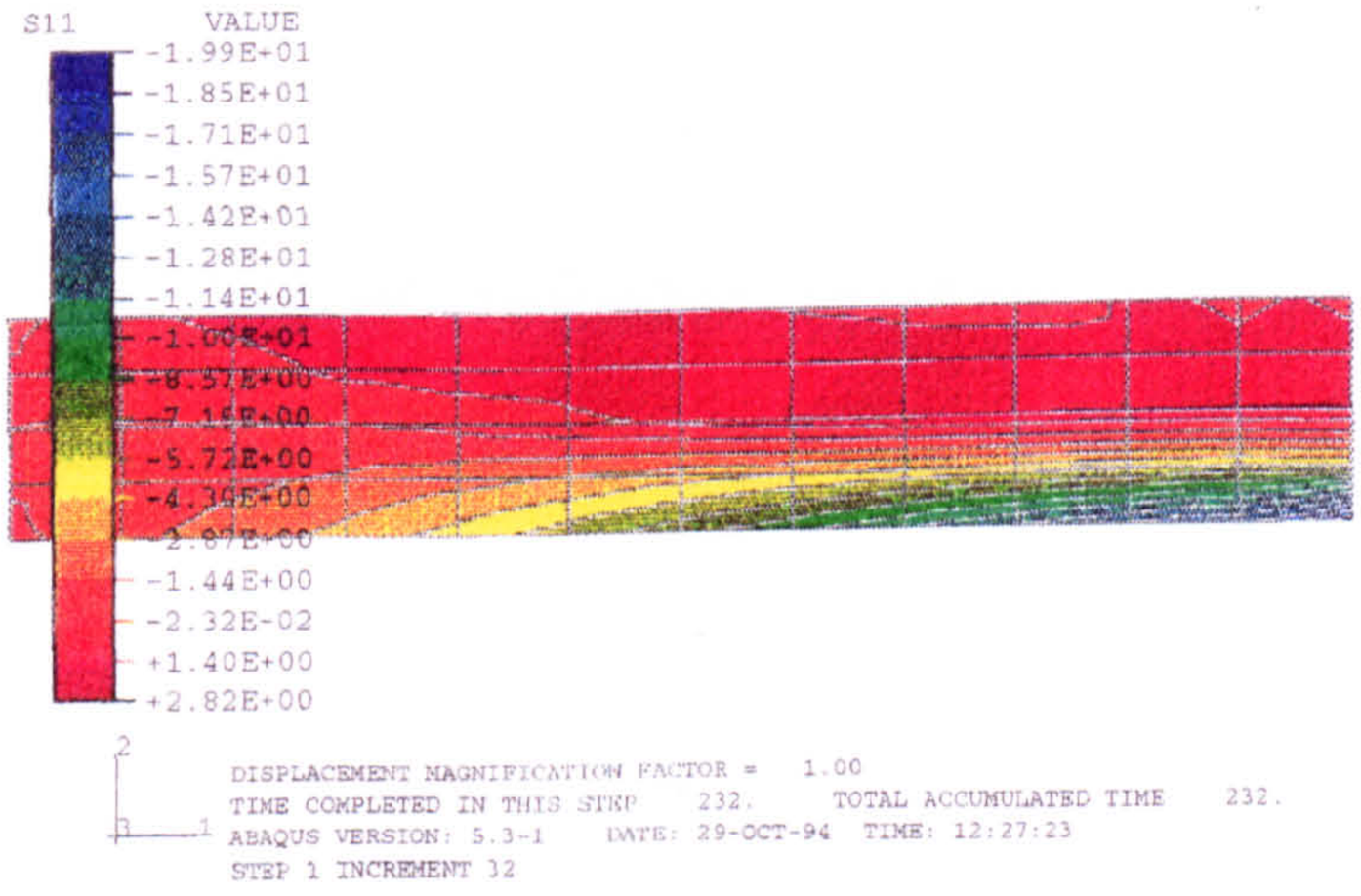

(c) Normal stress contour at ultimate load

Figure 2-15 Normal stress contour at different load levels

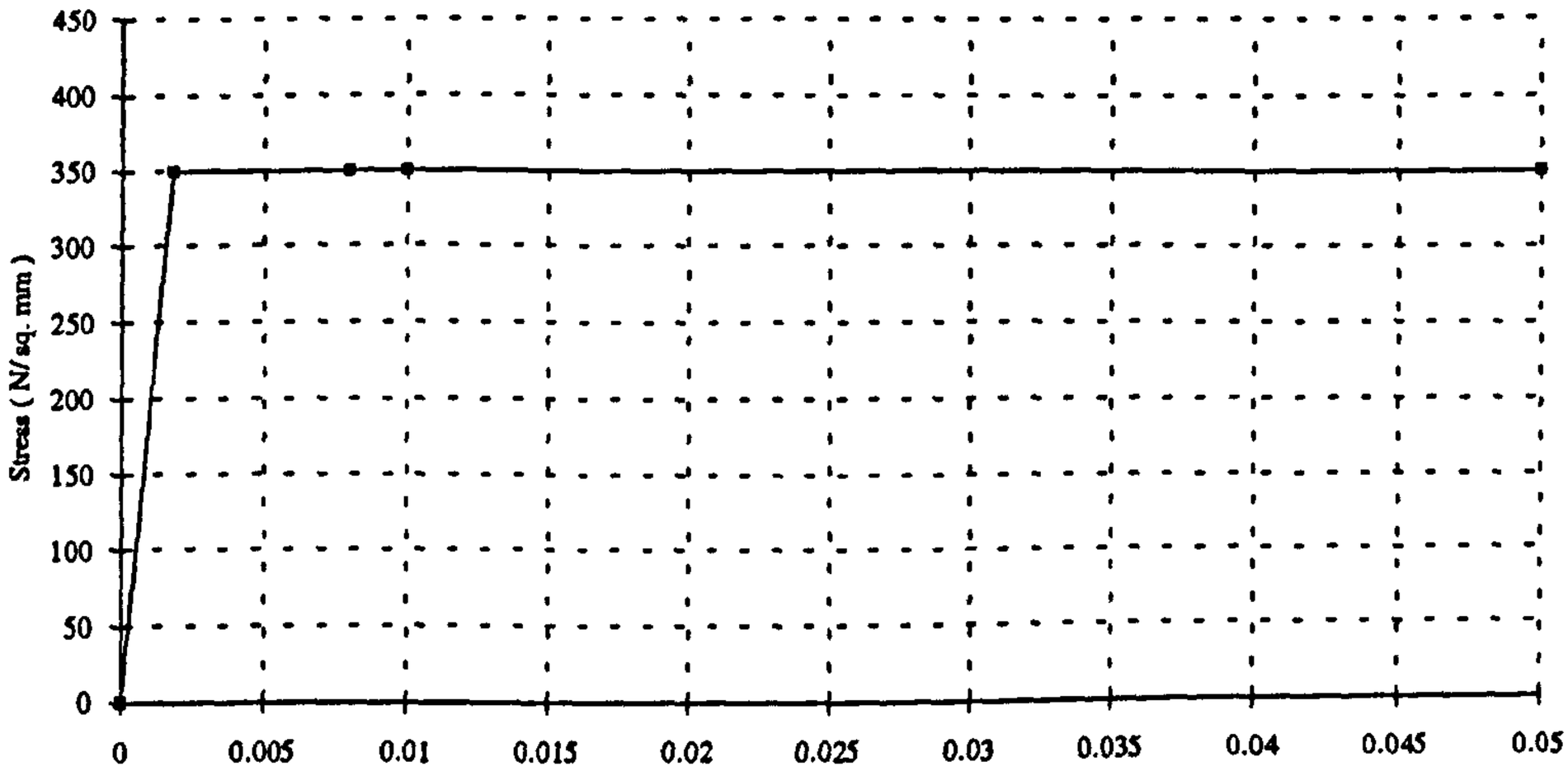

Figure 2-16 Stress strain curve of steel used for the I beam model

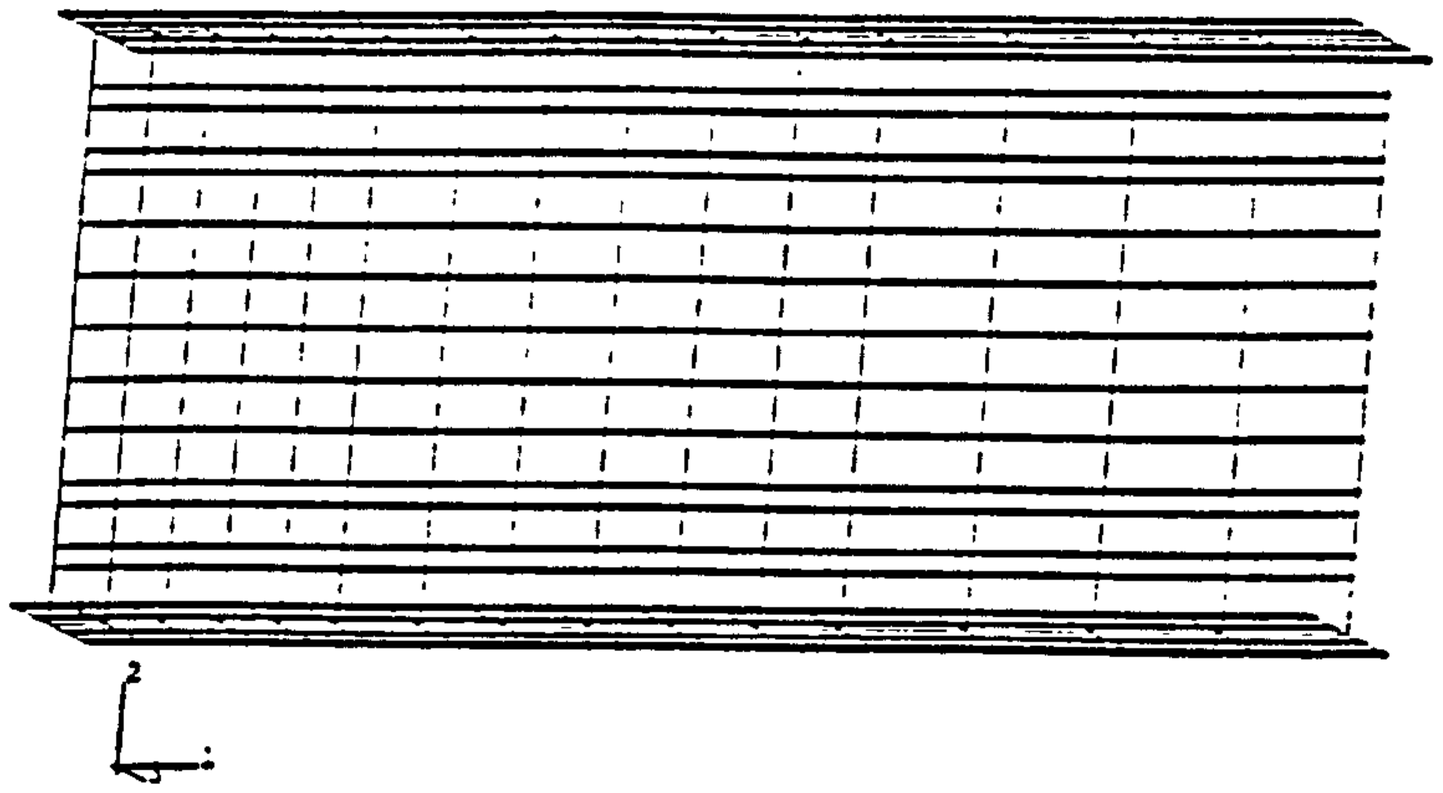

Figure 2-17 FE mesh for steel I beam

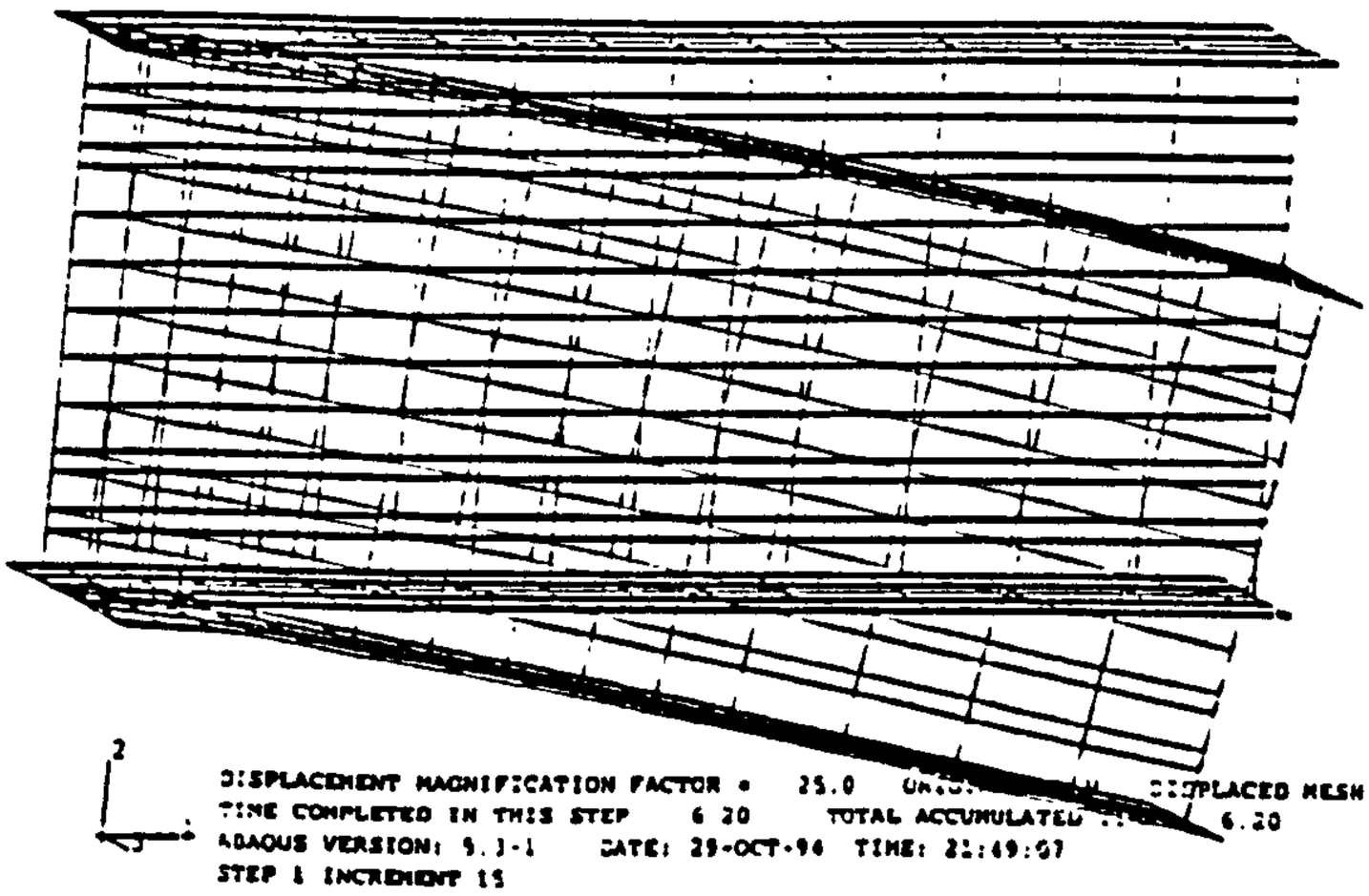

Figure 2-18 Deflected shape of the I beam at ultimate load

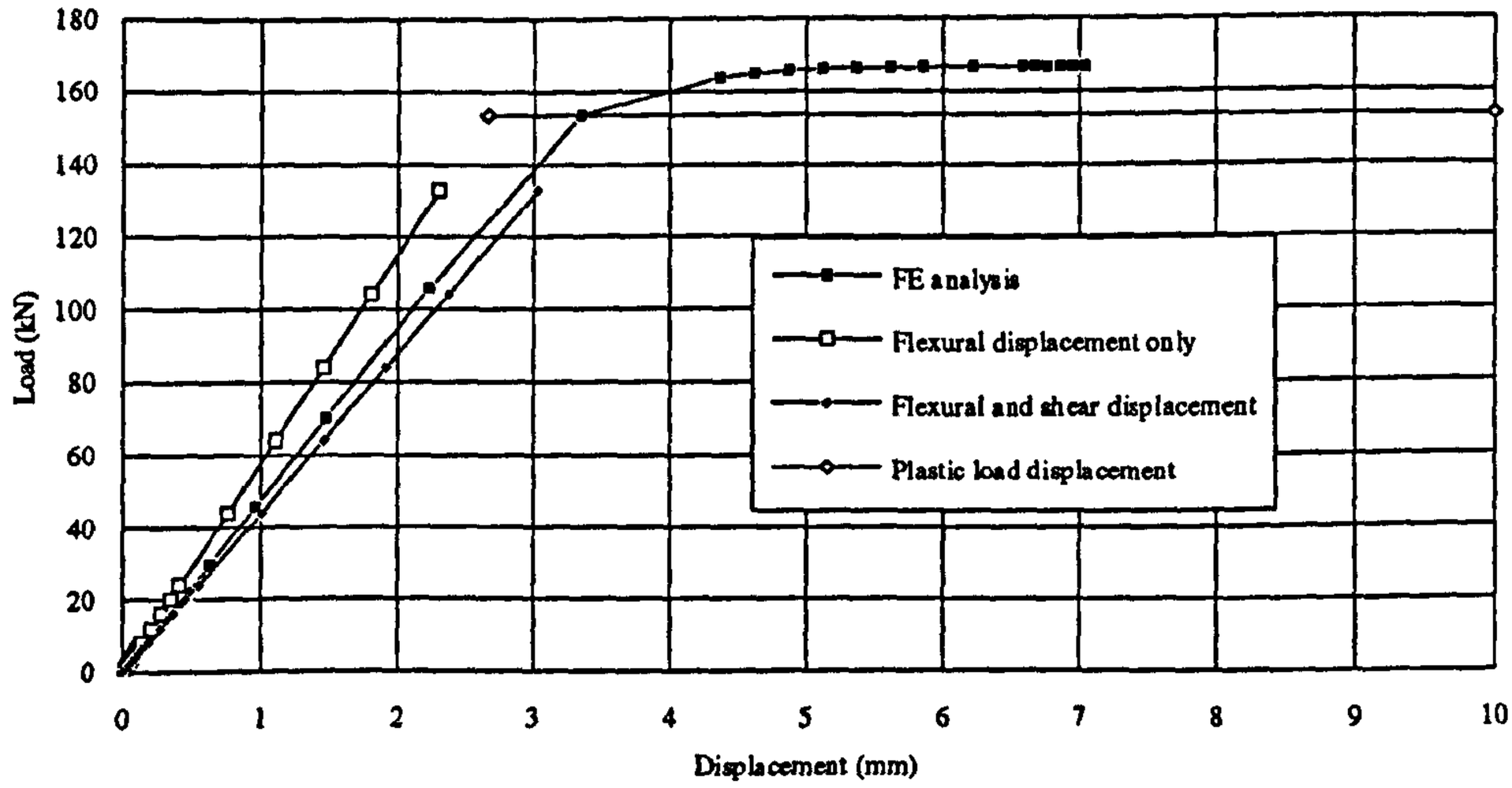

Figure 2-19 Load displacement curves for the steel I beam

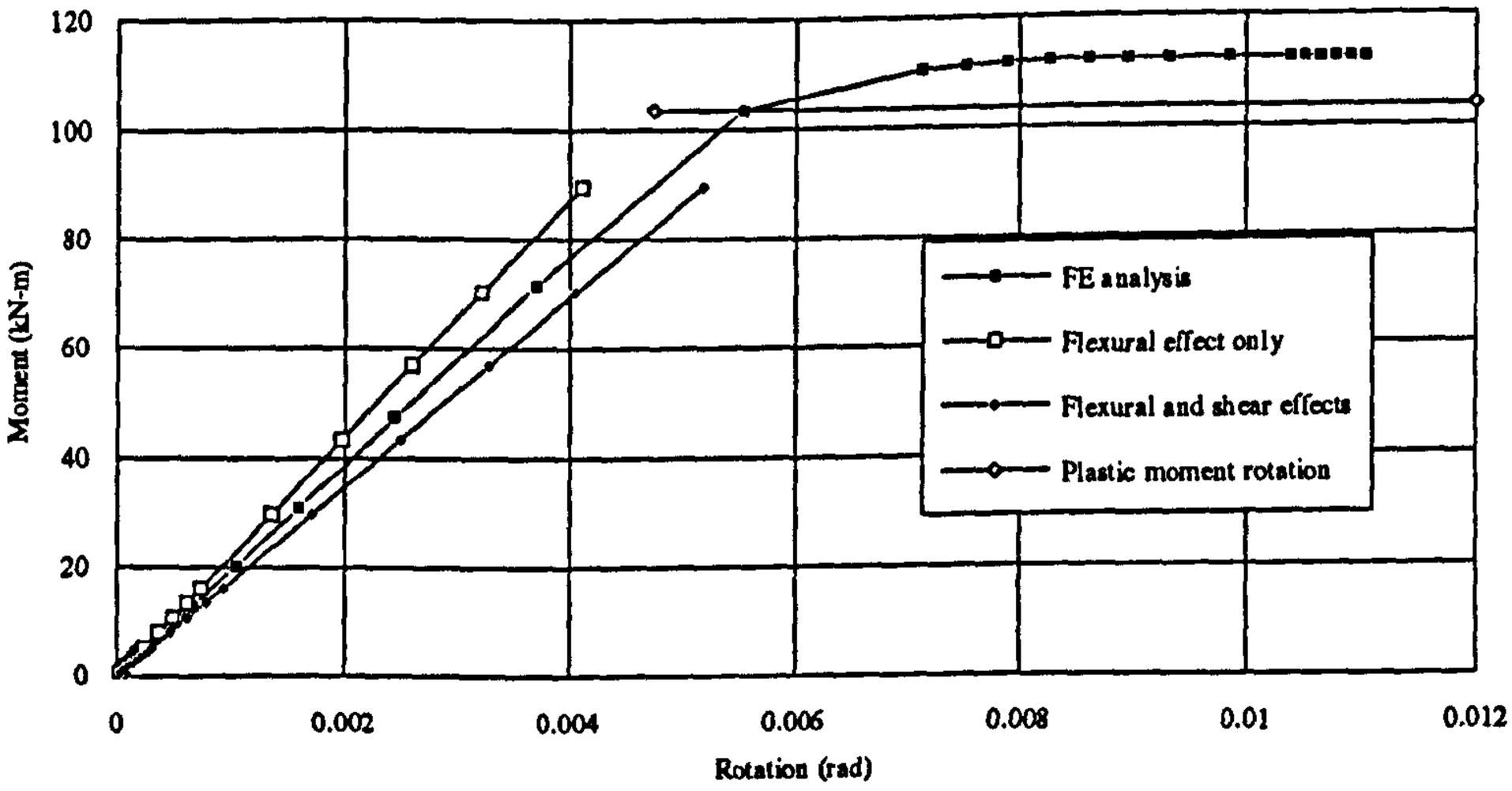

Figure 2-20 Moment-rotation curves for the steel I beam

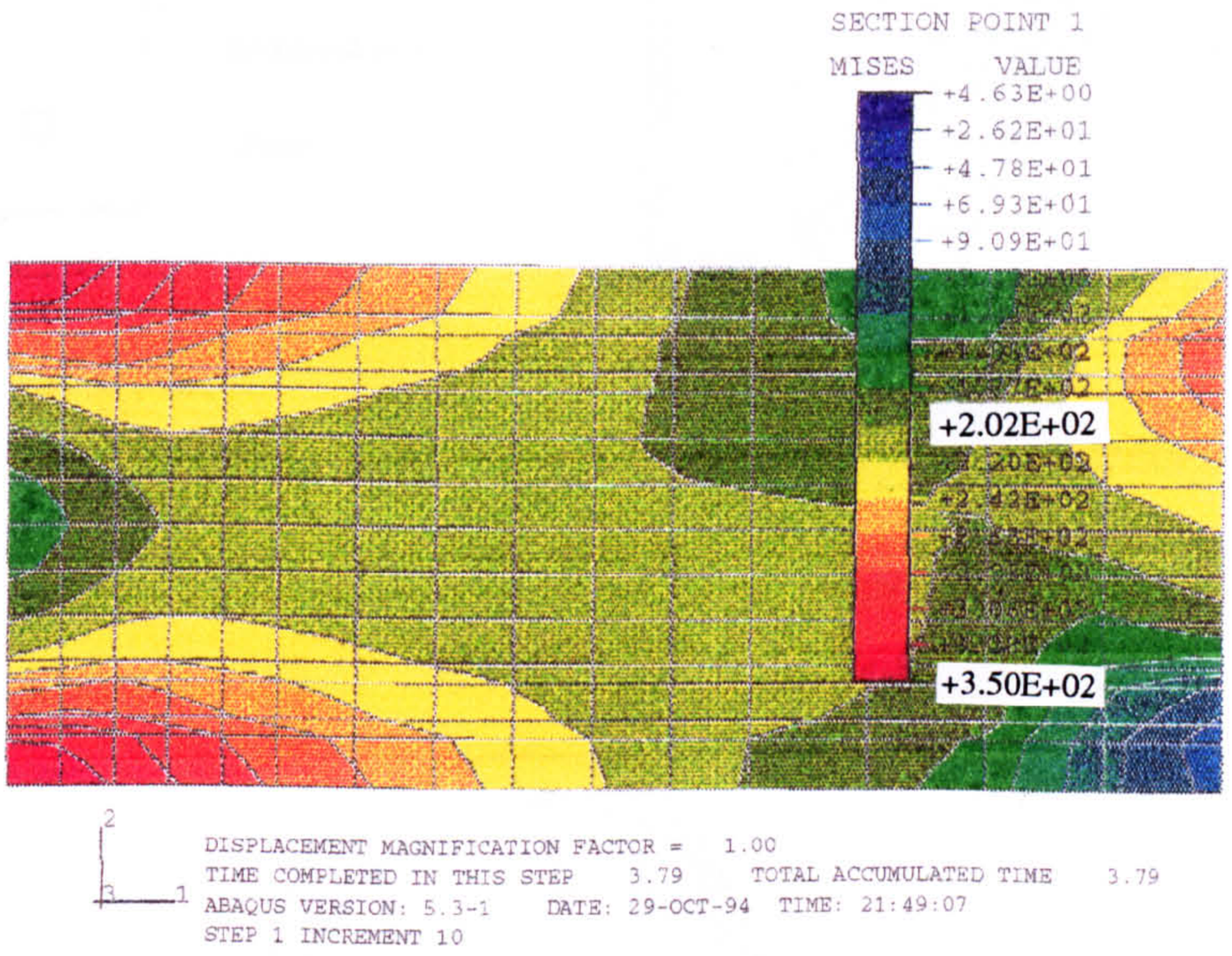

(a) von-Mises stress contour at 60% of ultimate load

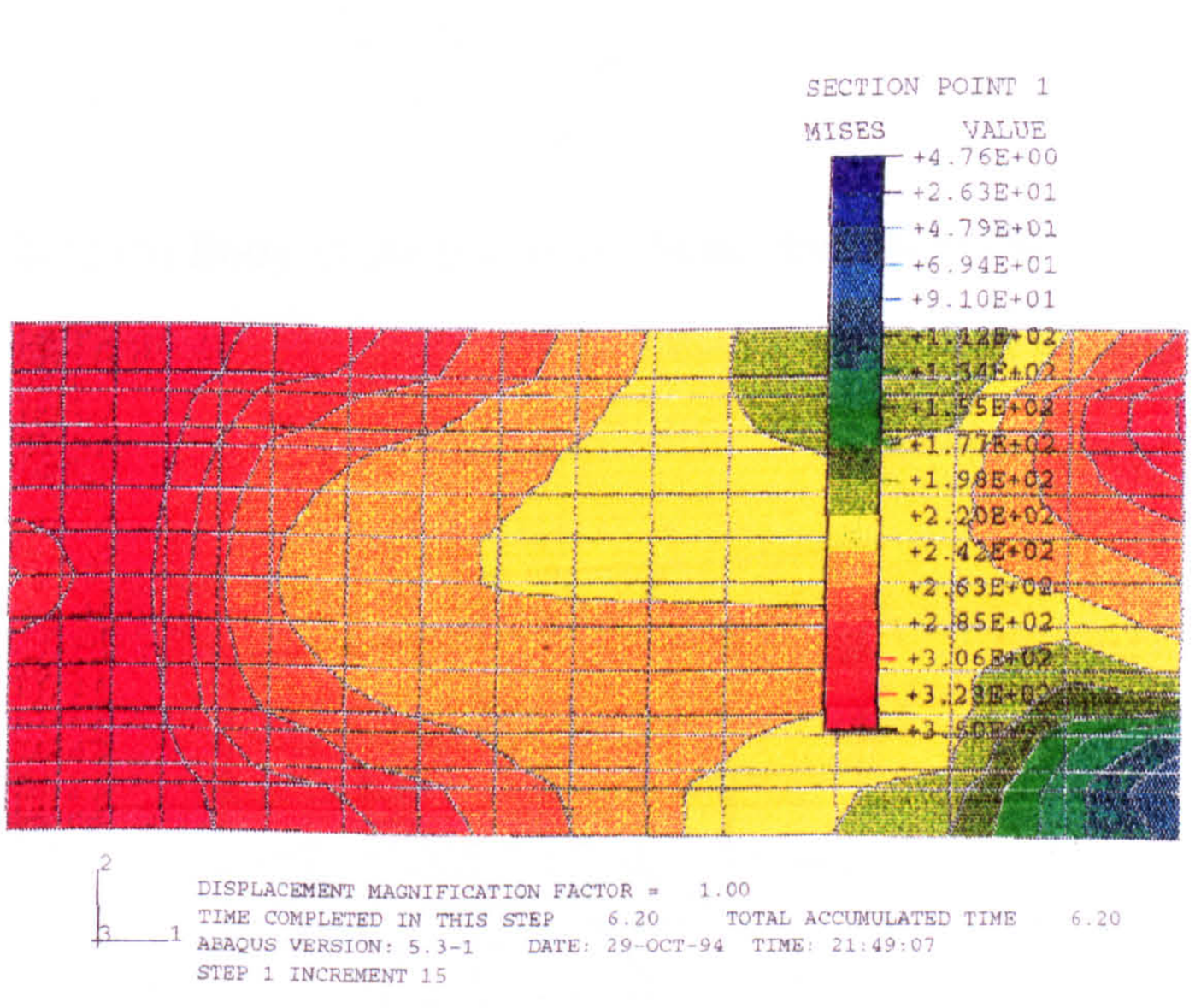

(b) von-Mises stress contour at ultimate load

Figure 2-21 Von-Mises stress contours at different load level

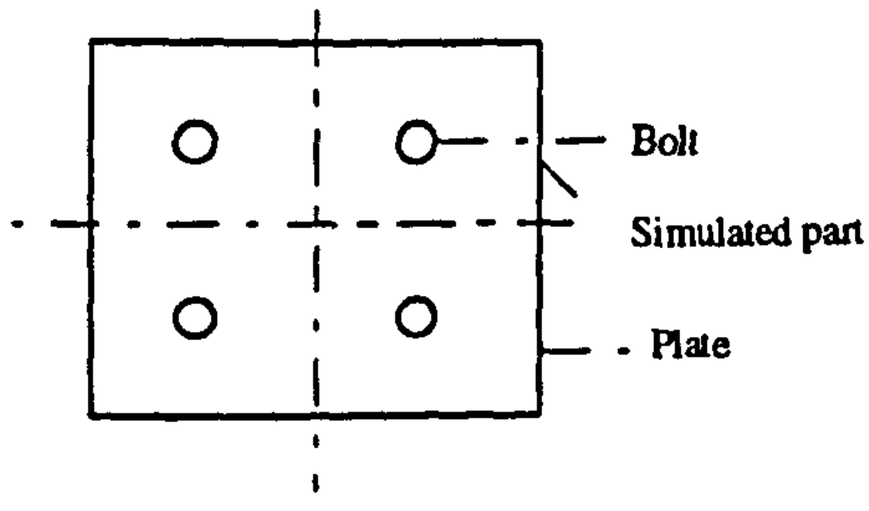

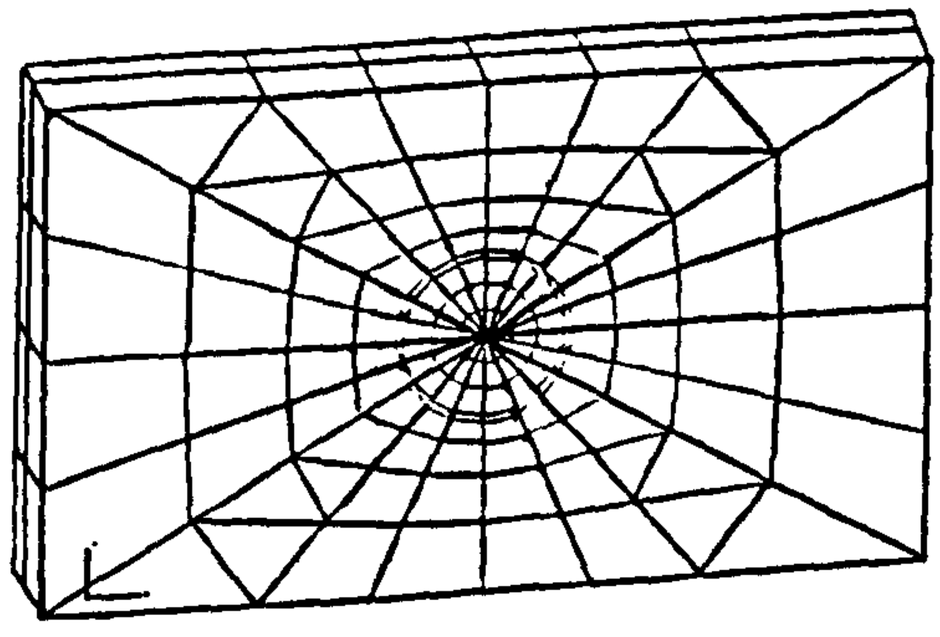

2-22 (a) Plate with bolt and its finite element representation

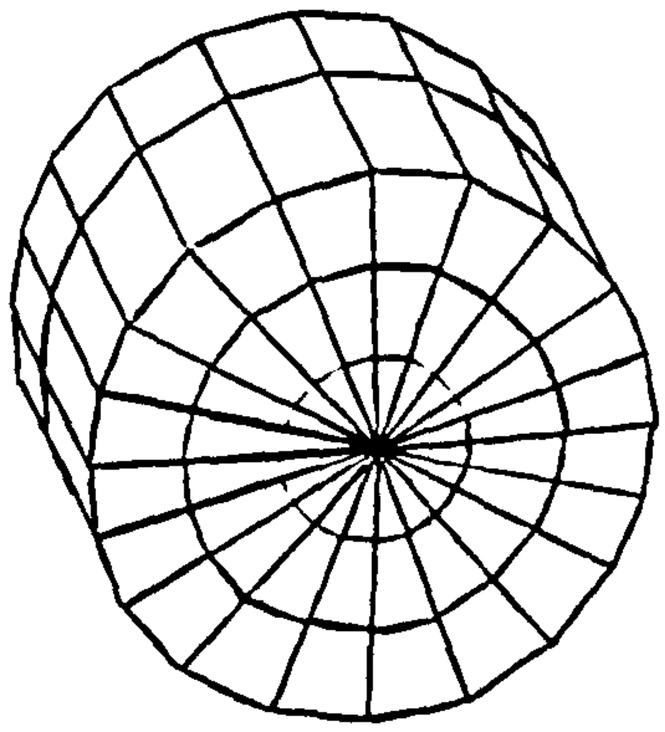

2-22 (b) Body of the bolt in the finite element model

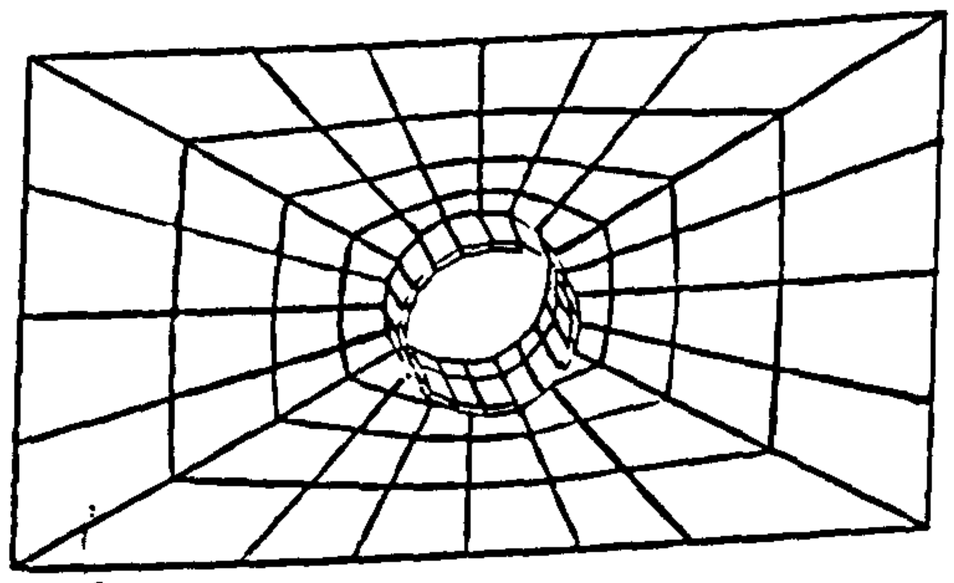

2-22 (c) Interface elements between the two plates and between the plates and bolt

Figure 2-22 FE mesh for bolt analysis

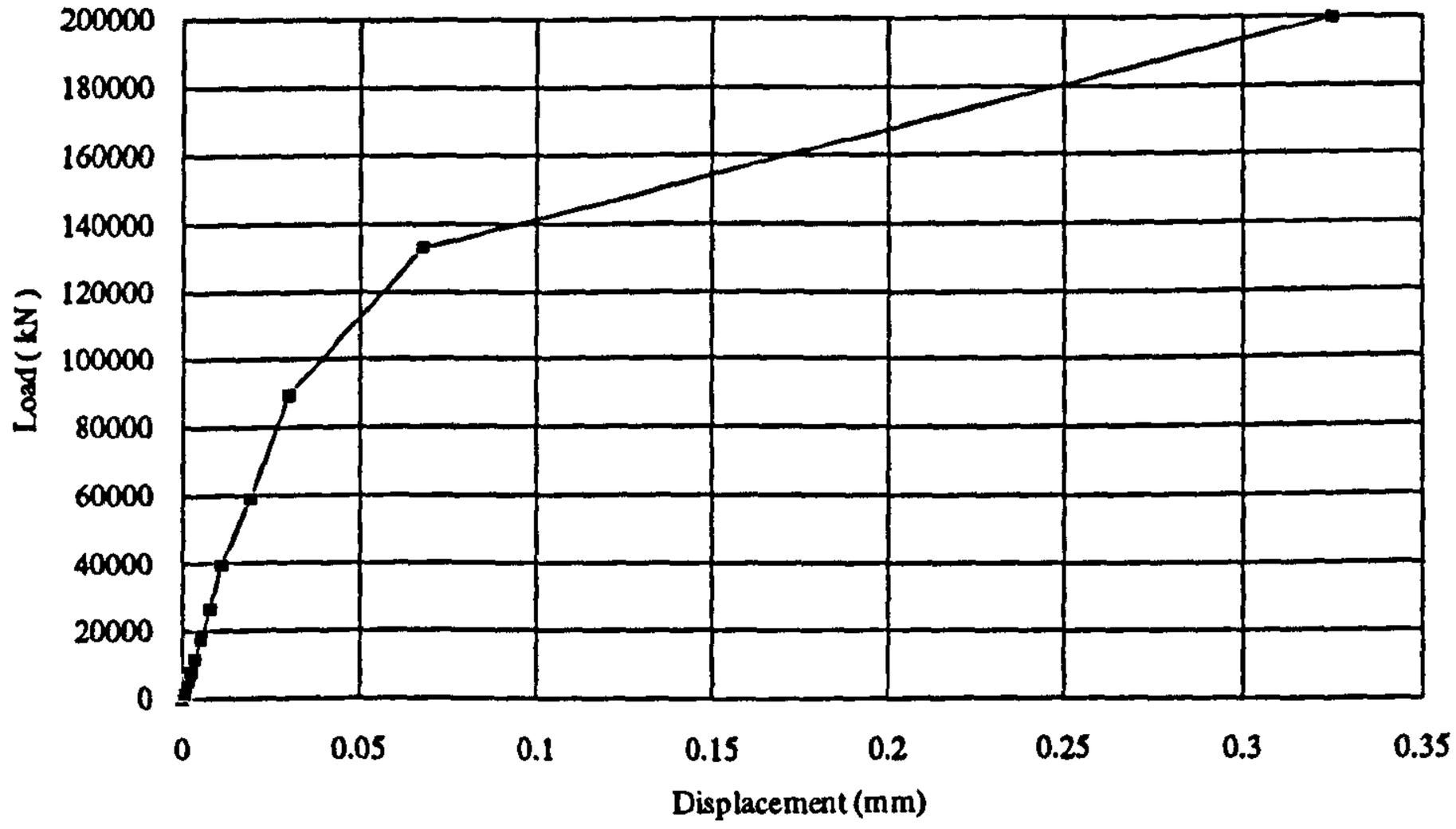

2-23 (a) Load shear deformation curve for bolt

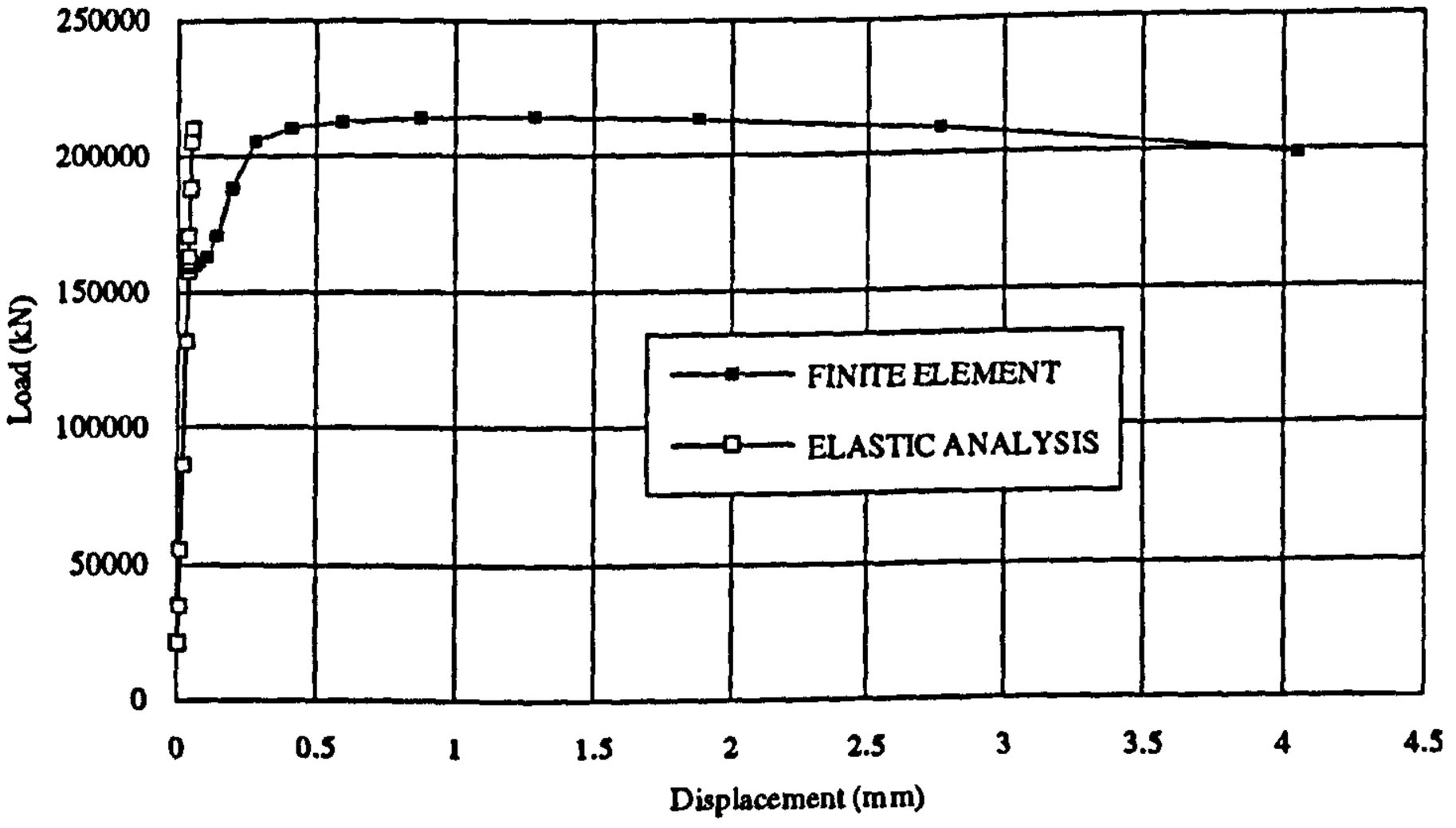

2-23 (b) Load axial deformation curves for bolt

Figure 2-23 Load deformation curves for bolt

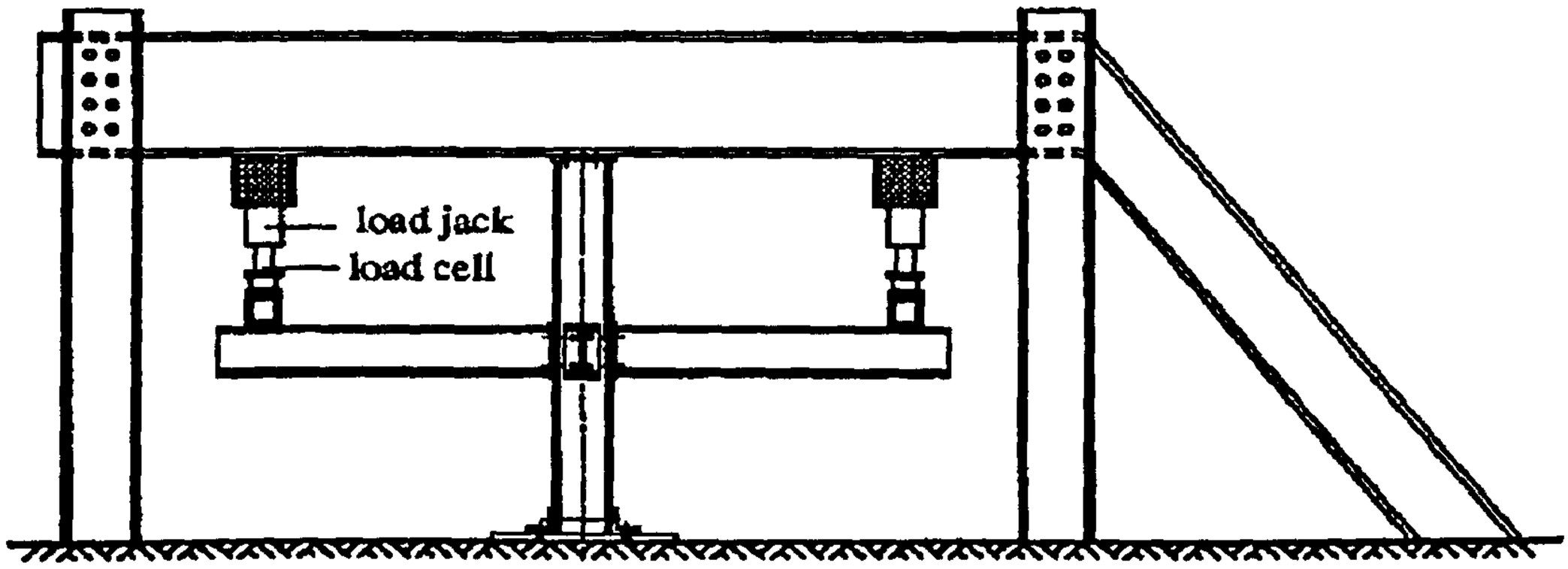

Figure 2-24 Test rig and specimen (SJS-1) set-up (Li, ref. 2-1)

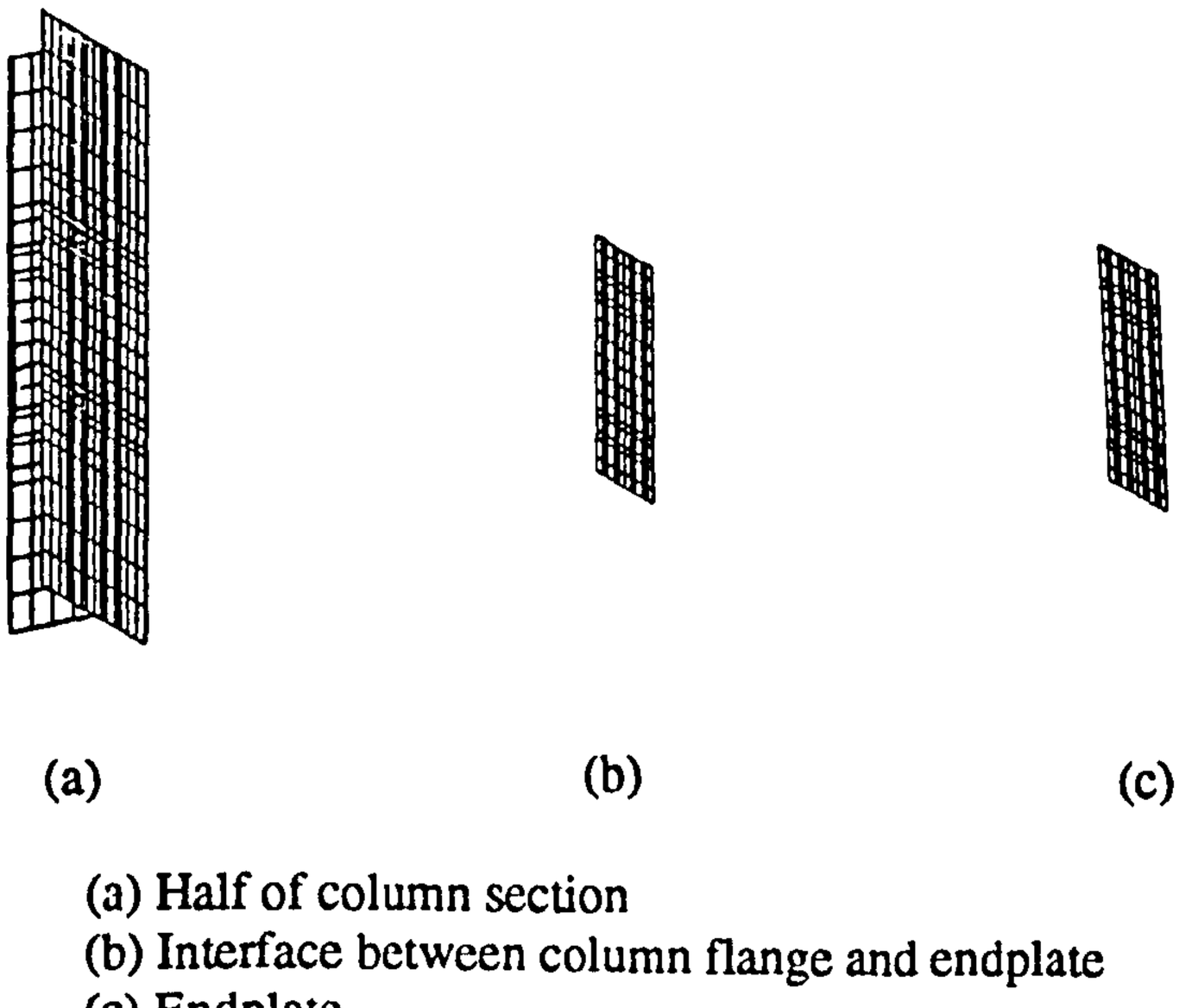

(a) (b) (c)

(a) Half of column section
(b) Interface between column flange and endplate
(c) Endplate

(d) Steel beam

(e) Connection SJS-1

Figure 2-25 FE mesh for test SJS-1

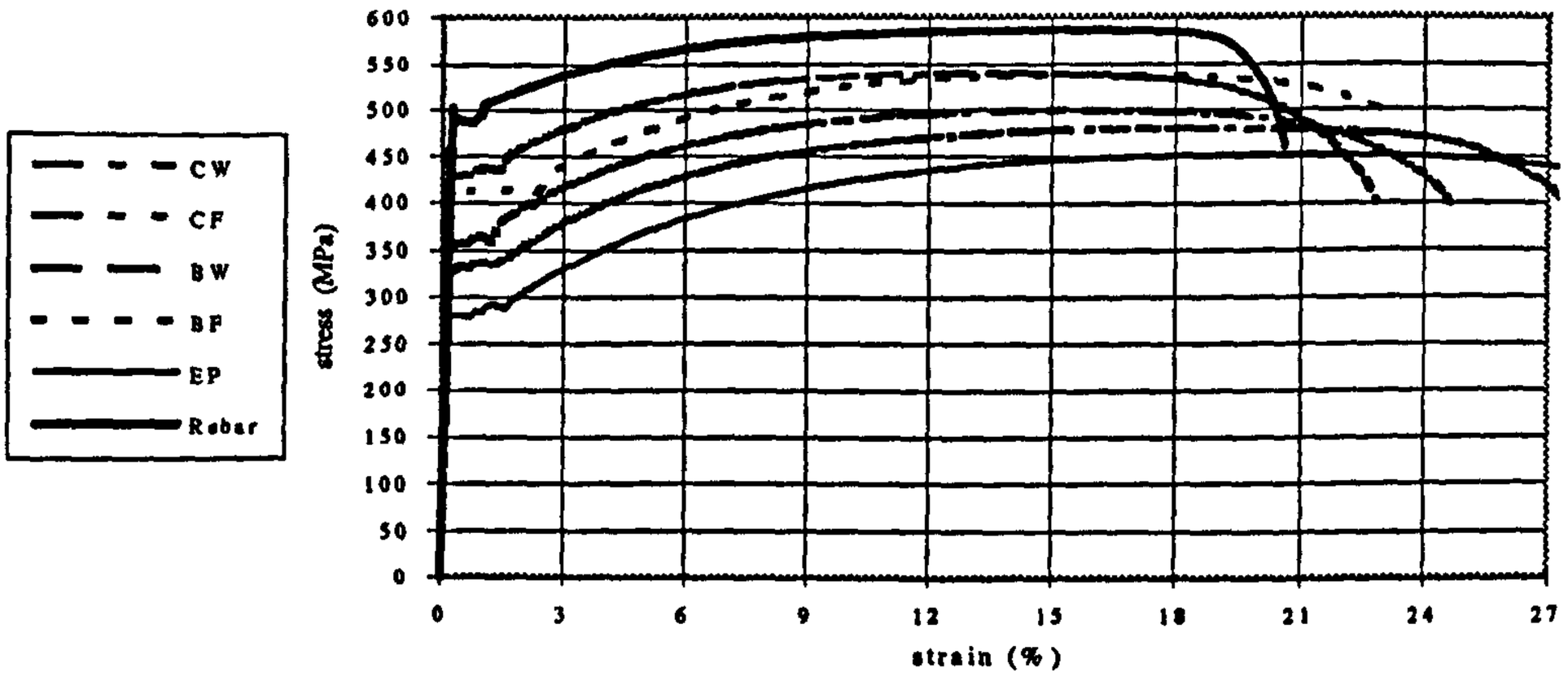

Note: CW is column web, CF is column flange, BW is beam web, BF is beam flange
EP is endplate and Rebar is reinforcement

Figure 2-26 Typical stress-strain curves of steel specimens (Li, ref. 2-1)

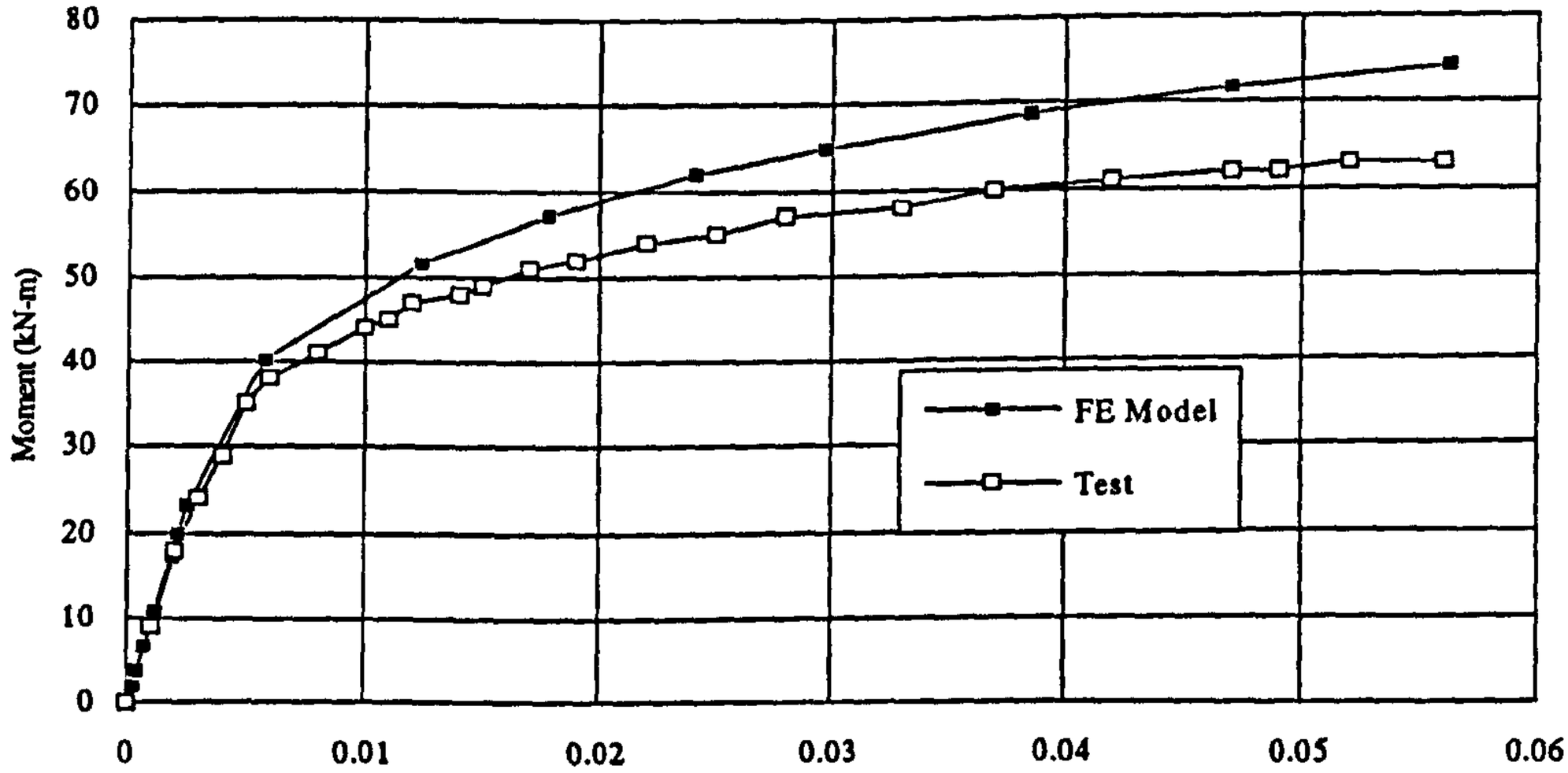

Figure 2-27 Comparison of moment-rotation curves

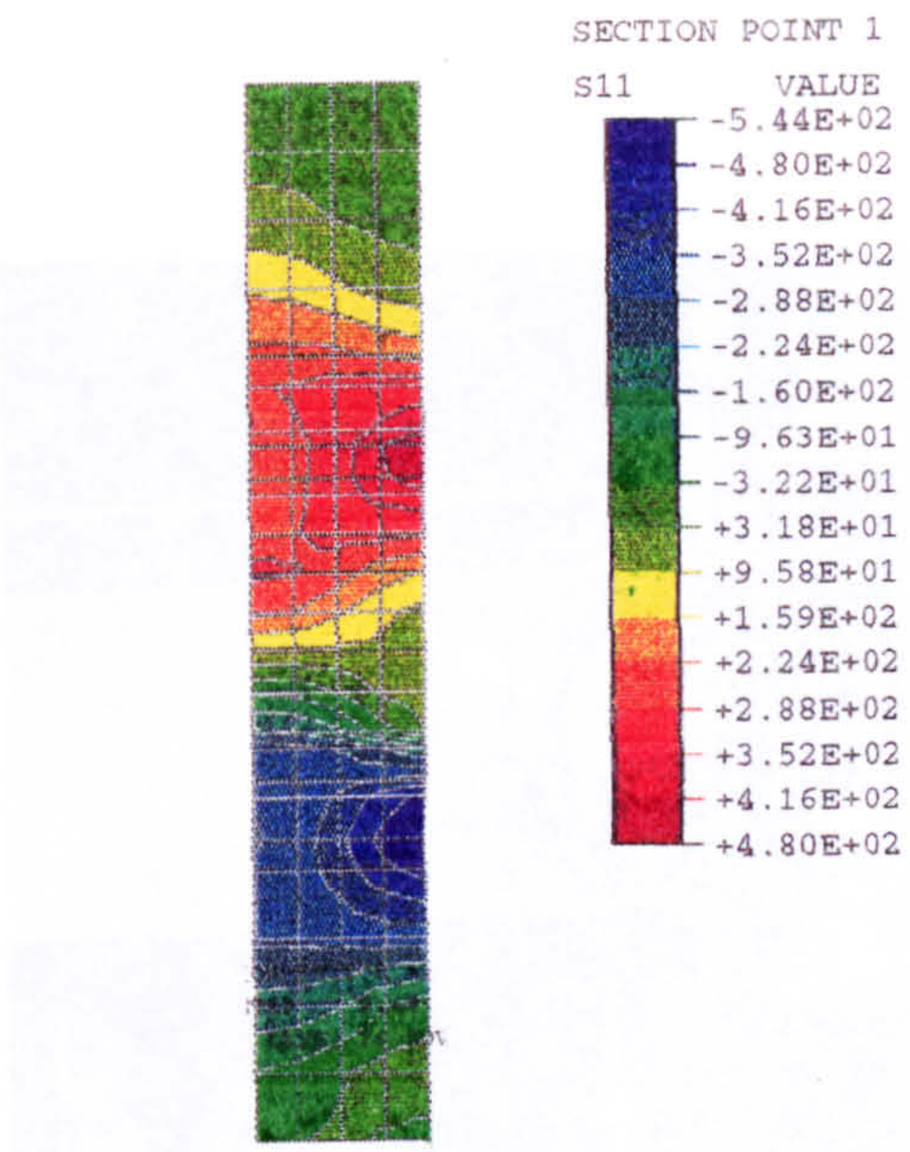

(a) Column web horizontal stress

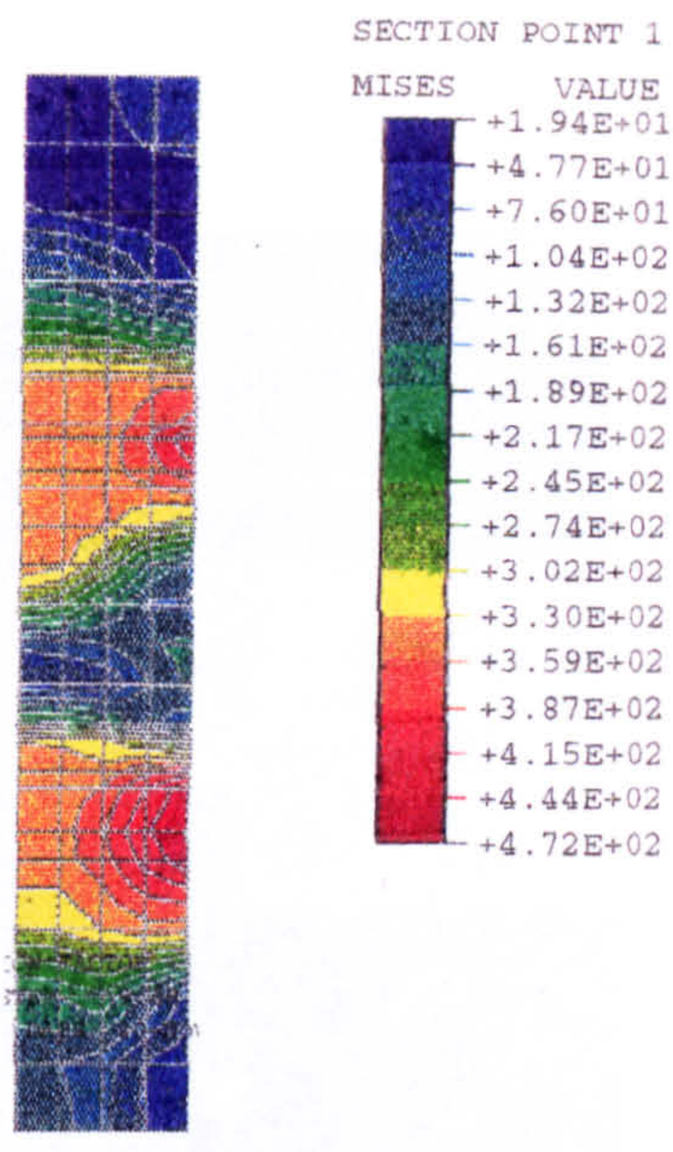

(b) Column web von-Mises stress

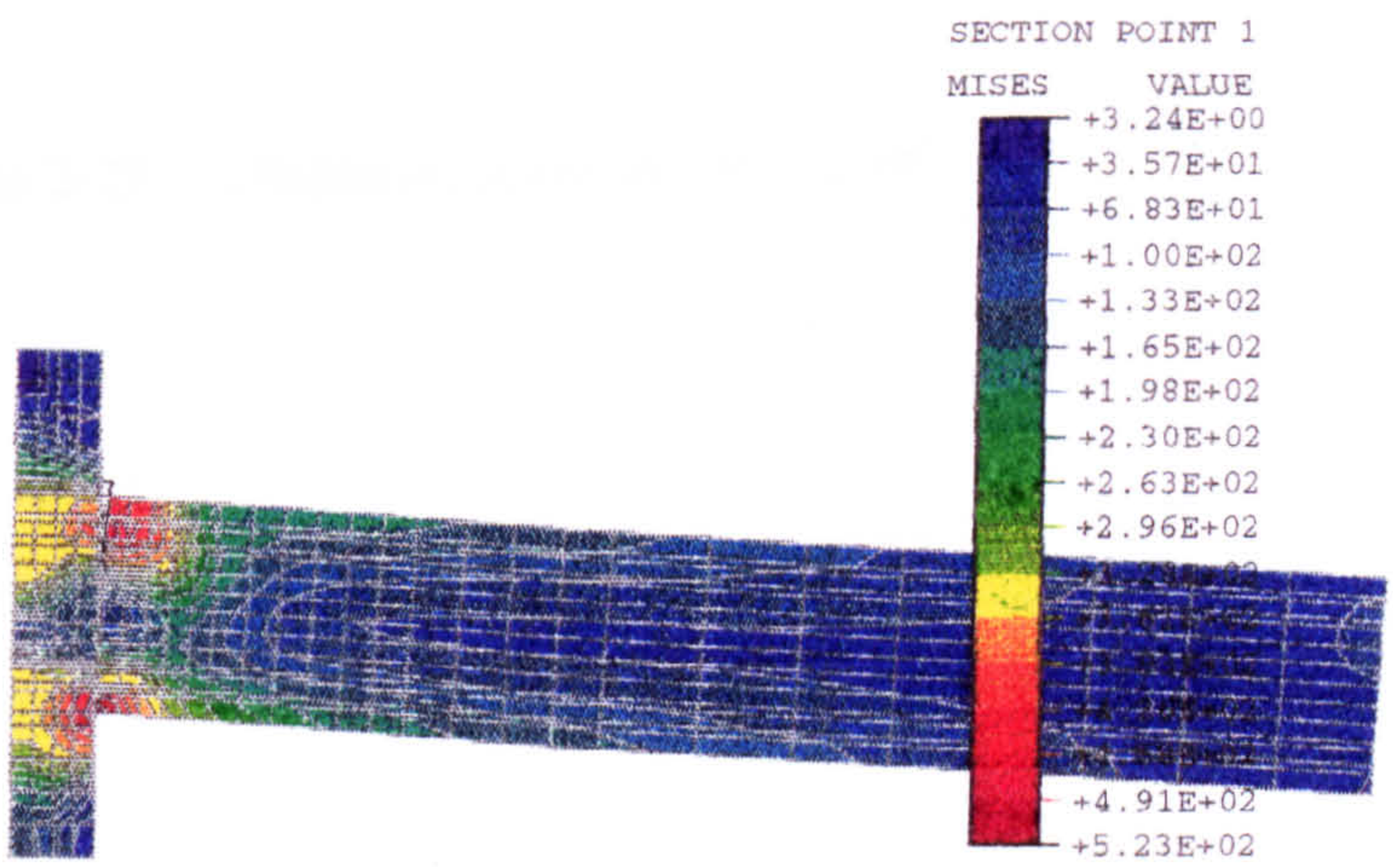

(c) Von-Mises stress for the complete connection

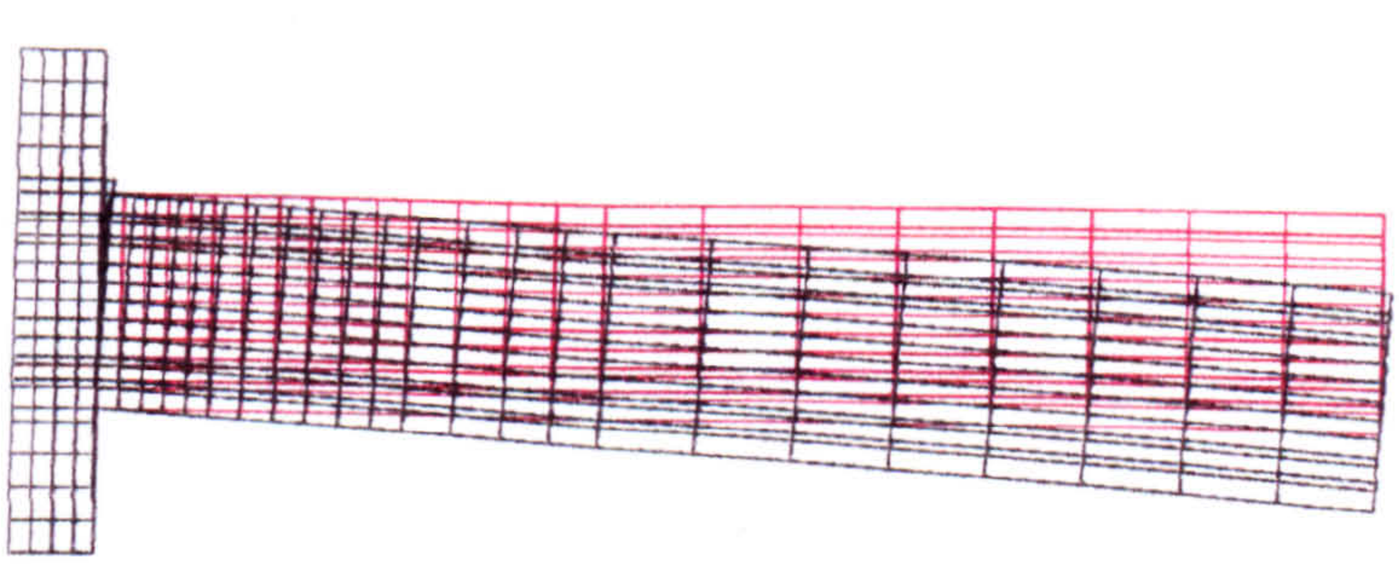

(d) Displaced shape of the connection

Figure 2-28 FE results for SJS-1

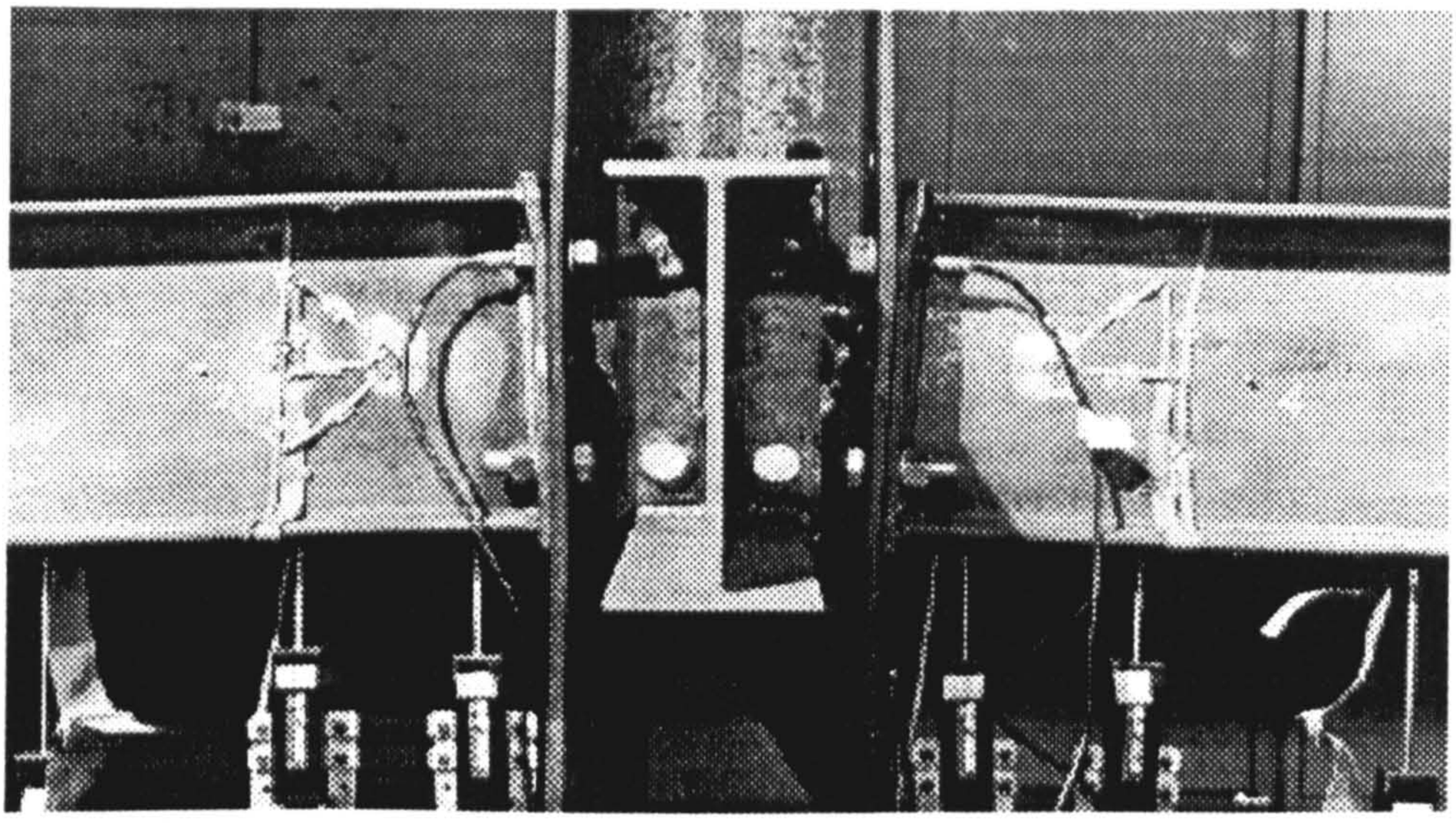

Figure 2-29 Displaced shape in test (Li, ref. 2-1)

Chapter 3

Modelling of composite connections

3.1 Introduction

This chapter describes the modelling of a composite connection CJS-1, tested in the University of Nottingham [3-1, 3-2]. The test arrangement was identical to the one described in chapter 2, except that a composite connection with 1.2% reinforcement (area 767 mm^2) was used. For this reason the only change to the model was to introduce the effect of the tensile reinforcement. The method of introducing the reinforcement and shear studs is described in this chapter. When it was clear that parameters such as the area of reinforcement, the shear studs and the load application position were modelled properly, modelling of the bolts was refined. The detailed approach for modelling the bolts is also described. Finally, a comparison of FE results with test results (test CJS-1, CJS-4 and CJS-5), which address the problem of shear to moment ratio of cruciform composite connections, is reported. Besides this, the modelling of tests SCJ3, SCJ4, SCJ10, SCJ11 (web cleat with seat cleat) and SCJ12 (finplate) from reference 3-4 is also described in this chapter.

3.2 The finite element model for CJS-1

This section describes the technique used for modelling a composite connection, CJS-1. The problems associated with modelling concrete and the approach devised to represent the test properly neglecting the concrete are also described.

3.2.1 The finite element model with concrete

The finite element mesh used for the analysis is shown in Figure 3-1. The concrete slab that rests directly on the steel beam was modelled with the full reinforcement. All the material properties are given in the previous chapters. The model gives the moment rotation values only in the initial region; when the concrete reached its tensile capacity, numerical problems were encountered. These were similar to those reported in ref. 3-3. The displaced shape at this stage is shown in Figure 3-2. It appeared from the results that the concrete part, although working well when modelled separately, causes the solution to stop. The reason behind this is that the solution scheme in ABAQUS assumes that when some part of the model cracks extensively or fails the model reaches its ultimate state, which is not true for this specific case. Thus this effect must be modelled in a different way.

3.2.2 Alternate model for CJS-1

Realising the fact that the concrete slab in the tests contributes in carrying the tensile force in the initial un-cracked region only, and after cracking it does not take any tensile force but only helps to transfer the force to the reinforcement, attempts were made to separately model concrete and reinforcement, but it did not work. It was decided to remove the concrete and the *REBAR command for modelling the reinforcement. Axial force elements were chosen to represent the reinforcement. The shear studs can be modelled by beam elements and joint elements at the top of the beam elements to introduce the stud capacity. The resulting FE model is shown in Figure 3-3. The problem was to make the studs act in a way that corresponds to the test. Neglecting the concrete and modelling in the above mentioned way produced a load capacity of only 62% of the test load. The stiffness of the shear studs and their capacity was changed but this failed to produce any significant change. Reinforcement and shear studs were modelled in two rows, but this also made no significant change.

The number of elements in a stud was also varied but it had no effect on the load capacity. The concrete was transformed into an equivalent steel area and modelled as shell elements connecting the steel beam top flange and the reinforcements. This produced a load carrying capacity very close to the test, but the moment-rotation curve was too stiff with respect to the test. Then the concrete equivalent area was removed from the model. Reinforcement was modelled by using truss elements with two nodes per element as illustrated in Figure 3-4. Shear studs were modelled by a combination of two elements, one of which was a beam element while the other was a spring element. The spring element, which was located between the beam element and the reinforcement, was used to introduce the test load - slip curve for the shear studs as shown in Figure 3-4. This simulates the shear slip that occurs in the test, also the maximum load carrying capacity of the studs. To model the load deformation property of the stud, at the top of the rigid studs JOINTC elements with the properties in Figure 3-5 were used. The beam element was connected directly to the steel beam top flange.

*EQUATION option was used to introduce the relation between displacements of the reinforcement nodes and the corresponding steel beam nodes. This too produced a moment-rotation curve much stiffer then the test. *MPC (type = linear) was used to keep the nodes of the reinforcement and the nodes of the steel beam at a particular cross-section in a straight line; this also resulted in a stiffer moment-rotation curve. To make the connection flexible the slope of the stress-strain curve was given as E/50 but it created a model that carried increasing load without failing.

*MPC (type = slider) was used at the beam end, for nodes in the beam web and the reinforcement node; this did not consider the effect of internal shear studs but produced a moment-rotation curve similar to the test. CJS-4, CJS-5 of references 3-1 and 3-2, and SCJ3, SCJ4, SCJ12 of ref. 3-4 were modelled. But in the parametric study phase CJS-1 exhibited problems; some reinforcement ratios produced results that were not sensible. The reason found was that the *MPC (type = slider) actually allows

the movement of nodes along their connecting line, and thus makes the particular problem unstable. Later on this MPC was discarded and at the stud section *MPC (type = beam) was used, which produced results that are acceptable when compared with tests.

3.2.3 Simplified FE model of CJS-1

The simplified model (with beam MPC) consists of the FE mesh already shown in Figure 3-3, with stud and reinforcement model shown in Figure 3-4. Material properties for the steel sections are the same as those used in Chapter 2 (Figure 2-26), and the stud properties as shown in Figure 3-5. The bolt load displacement properties were that shown in Figure 2-23. Since the concrete is neglected, it is assumed that the model will give less (but not significantly) stiffness in the linear region, but the ultimate load capacity should be correctly obtained and the rotations should be comparable. In fact the tests were terminated due to excessive deformation with constant load, samples did not actually fail, so the final rotation values from the model should be greater than the test. The moment - rotation curves for the test and the model are compared in Figure 3-6. The displaced shape is shown in Figure 3-7. As expected the model has slightly less stiffness in the linear region, but in the non-linear region the moment and corresponding rotations are almost the same and the rotation is also higher then the test. It was observed from the results at this stage that the bolt forces were about twice (shown in Figure 3-12, curve 12b) the test results although the moment rotation curves show close agreement. Hence the modelling of the bolts required special attention.

3.3 Modelling bolts in composite connections

The modelling of composite connections requires the proper modelling of the bolts to properly simulate the actual behaviour of components, although it is possible to

produce an overall moment-rotation curve that is very similar to that obtained in a test without properly modelling the bolts. In the previous sections it has been clearly shown that the other features of a composite connection may be accurately modelled. This section deals with the development of the modelling procedure for the bolts. The effect of a simplified bolt model is that the interaction between the endplate and the column flange may not represent to that of a real test, as the bolts transfer tensile force to the column flange. Therefore to achieve proper transmission of force at the interface of column flange and endplate so that the internal forces in the column flange and column web are reliable, it is essential to model the bolts in a simplified way but with sufficient accuracy. To find a realistic modelling approach for the bolts in composite connections the following eight approaches were considered:

3.3.1 Analysis i: The first attempt treated the body of the bolt and its head using joint elements; twelve joint elements were used. The bolt is of 20 mm diameter and the inner four joint elements were used to model the bolt whereas the outer eight elements were used to model the bolt head. This represented the bolts between the endplate and the column flange. The bolt model is shown in Figure 3-8. The properties of these elements were obtained from past FE analysis of bolts and from elastic analysis of bolts under tension. The total load was divided by twelve but the displacements were kept the same, so that it can represent the bolt load deformation behaviour.

For the first model the moment-rotation curve and moment-bolt force of the model and the test is shown in Figures 3-11 and 3-12 respectively. The moment-rotation curve appears very satisfactory but not the moment-bolt force curve. The bolt forces obtained from FE analysis are twice those of the test. Table 3-1 shows the force taken by the individual elements of the modelled bolt. Considering the deformation of the endplate, under the action of the applied load in combination with the deformation of the beam top flange and the beam web, it appears that the joint elements near the top flange and beam web i.e. elements number 7, 8, 11 and 12 will be subjected to the

highest axial load and deformation whereas elements 2, 5 and 6 will have the least deformation and axial force. From the FE results presented in Table 3-1, the same pattern can be seen. So the bolts must be represented in some other way so as to avoid compression in any spring element that is used to represent a bolt under tension.

3.3.2 Analysis ii: The bolts were modelled by using eight joint elements only to represent the bolt head, and the bolt load capacity was divided by eight to obtain the individual spring capacities. This was done to maintain the effect of the bolt head and at the same time to see if the sum of the loads taken by the eight springs matched the test load. Also those springs that gave the unwanted compressive load in the first analysis were reported. To maintain symmetry J-4, J-5, J-8 and J-9 of Figure 3-8 was removed. The resulting bolt model is shown in Figure 3-9. The connection took about 85% of the test load and then failed. The individual bolt forces are shown in Table 3-2. Compared with the previous analysis, springs J-4, J-11 and J-12 (at LF = 0.845 of Table 3-1) and J-5, J-7 and J-8 (LF = 0.845 of Table 3-2) of the current analysis took almost the same load. The moment-rotation and moment-bolt force curves are shown in Figures 3-11 and 3-12 respectively. Observing the moment-bolt force curve, it appears that the model is inferior to the previous one, and the ultimate load level was also not satisfactory.

3.3.3 Analysis iii: Considering the previous two analyses, the body of the bolt was modelled by using four joint elements and only two joint elements were used at the beam web side to represent the bolt head. The model is shown in Figure 3-10(a). This was done by keeping in mind that in a bolt-endplate-column flange interaction, the body of the bolt remains in contact with both the column flange and the endplate but the heads are either in contact with the flange or the endplate. The endplate and column flange becomes separated when the bolts elongate and there is no mechanism through which the tensile force can be transferred directly between the endplate and column flange at the bolt head region. When twelve joint elements were used it

produced a bolt of larger diameter then the one intended, since the endplate and the flanges were also tied by the joint elements in the vicinity of the head. The allowable axial loads in the springs were changed accordingly. The connection failed at almost the same load as that in the test, but as before the bolt force obtained was higher than the test. With twelve joint elements the FE bolt force was 181 kN, whereas in this case the bolt force obtained was about 162 kN. The moment-rotation and moment-bolt force curves are shown in Figures 3-11, 3-12. The individual bolt forces are shown in Table 3-3. From the tables and the moment-bolt force curve it can be seen that due to the absence of spring able to take compression the total bolt force is higher than the first case. Comparing the results of Table 3-1 (spring J-3, J-7 and J-8 at LF = 1.03) and Table 3-3 (springs J-1, J-4 and J-5 at LF = 1.03) these springs are subjected to almost twice as much force in this case with respect to the first model. Comparing the results of Table 3-2 (spring J-3 and J-5 at LF = 0.849) and Table 3-3 (springs J-1 and J-4 at LF = 0.845) these springs are also subjected to higher forces in this case as compared to the second model. The reason is the absence of the springs at the top row in this case, as compared with the other analyses.

3.3.4 Analysis iv: Only four joint elements were used to model the body of the bolt ignoring the bolt head, with appropriate axial load capacity. The bolt model is shown in Figure 3-10(b). The connection failed at 78% of the test load and the bolt force was 53 kN. The moment-rotation curve is shown in Figures 3-11, 3-12 and the individual bolt forces are shown in Table 3-4. Comparing the results of Table 3-3 (spring J-2, J-3 and J-5 at LF = 0.772) and Table 3-4 (springs J-1, J-2 and J-3 at LF = 0.778) it can be seen that due to the absence of springs J-1 and J-4 of analysis iii, in this case springs J-1 and J-3 took much more load with respect to springs J-2 and J-5 of analysis iii, whereas spring J-2 behaved similar to J-3 in analysis iii.

3.3.5 Analysis v: Results presented in Tables 3-1, 3-2, 3-3 and 3-4 show that the spring elements used in modelling the bolts, which are at the same level, did not share

equal load. The load taken by them is dependent on two factors: the amount of load allowed in each spring and the endplate deformation, i.e. as explained in the first case, the element which is closest to the top flange and beam web deforms most and takes most of the load whereas the one furthest from the top flange and beam web may even be under compression. This is a logical but unacceptable thing. This leads to the conclusion that there must be some forms of constraint imposed on the elements which will control the deformation of the bolts and not only make the sum of the spring forces equal to the bolt force in the test but also prevent any local compressive force in any spring of a tensile bolt, and if possible the spring forces should be nearer to each other although not necessarily the same. This may be obtained by specifying the displacement to be equal for the nodes of the bolt on the endplate that are on the same level.

The bolt was modelled by using four joint elements only. The graphical representation of the bolt model is similar to that in Figure 3-10(b). The displacements of the nodes which represent the bolt and are also on the endplate and on the same level were specified to have the same displacement. The model failed at about 80% of the test load. The moment-rotation and moment-bolt force curves obtained with this analysis are shown in Figures 3-11 and 3-12. Table 3-5 gives the forces in each spring element of the bolt. Comparing results of Tables 3-4 and 3-5, it appears that the improvement is not at all significant. All the analyses were conducted with the provision of bolt holes, as a check an analysis was made with out any hole for the bolts but this did not produce any hopeful results.

3.3.6 Analysis vi: From the few analyses made it was felt that the detailing of the bolts required more attention. It was felt that separate nodes were required for modelling the bolt heads, endplate and the column flange. Spring elements should be used between those nodes which were not directly on the column flange and the endplates. To model the bolt head on each side, nine stiff shell elements were used and four joint elements

were used to connect them. To establish a link between the bolt heads and endplate or column flange the displacement of the bolt head nodes at the side of the endplate were kept the same as the displacement of the nodes of the endplate and the displacement of the bolt head nodes at the side of the column flange were kept the same as the displacement of the nodes of the column flange. The bolt model are shown in Figure 3-13 Resulting moment-rotation curve and moment-bolt force curve obtained from the analysis is shown in Figures 3-15 and 3-16 and Table 3-6 gives the load in each spring of the bolt. It can be observed from the moment-rotation curve that the connection is now too stiff and can take further load if the analysis is continued. The reason is that when EQUATION is used between nodes it makes the system stiff. The greater the number of equations, the more stiffness in the system. The other reason is that a proper model should not include EQUATION between the nodes but it should have interface elements, which was not possible for practical reasons since the more interface elements used in a model the greater the number of attempts required for a successful first solution (Sometimes it may be impossible in one step to establish the contact). Also due to EQUATION the nodes of the elements on the endplate and the column flange related to the bolt heads (which are given a rigid property) behave in a rigid way. The results of Table 3-6 show clearly that at a load near the test load (LF = 1.024), the bolt force is now reduced to 128 kN, and the force in the individual springs are also close to each other. This suggests that by reducing the number of elements for bolt heads and thus reducing the number of EQUATIONS used for the bolt heads and endplate or column flange better results can be expected.

3.3.7 Analysis vii: From the previous analysis it was decided first to check the effect of the number of elements used for modelling the bolt head. To model the bolt heads; five stiff elements were used, keeping other features the same as in analysis vi. The bolt model is shown in Figure 3-14(a). Results of the analysis are shown in Table 3-7. The analysis was stopped due to time constraints. It is seen that at 93% of the test load the bolt force is 92 kN, which is quite satisfactory, yet the moment-rotation curve and the

moment-bolt force curves as shown in Figure 3-15 and 3-16 indicates that a little improvement is still necessary.

3.3.8 Analysis viii: To reduce the system stiffness, only one stiff element was used to model the bolt head and to connect the two bolt heads four spring elements were used. The displacements of the nodes on the bolt heads were equated to the displacement of the endplate or the column flange accordingly. The bolt model is shown in Figure 3-14(b). Results obtained from the analysis are shown in Table 3-8, and Figures 3-15 and 3-16. From the results presented in the table and the figures it can be seen that the bolt forces are now close to the test results. The remaining difference is due to the fact that the concrete is ignored and the initial bolt load is not included in the model. The concrete model available in ABAQUS at present does not give satisfactory results, due to the fact that after the concrete cracks the analysis fails to proceed whereas in the test the rebars take the tensile load and the ultimate load is much higher then the cracking load of the concrete. The bolt pre-loading cannot be considered at this stage as the bolts are modelled by using spring elements to transfer axial and shear load and this cannot consider the elastic property; in ABAQUS to give initial load, the elements must have an elastic property reference. But the model presented here can be considered satisfactory as it represented the test with sufficient accuracy. The difference at the ultimate load level is due to the fact that the first rebar element near the connection yielded and due to its extension the bolts are forced to extend and take more load.

3.3.9 Interim conclusion

From the above analyses it was observed from comparisons with test results that modelling the method described in analysis viii is acceptable for modelling bolts in composite connections. It can represent the bolts in a simplified but acceptable fashion.

3.4 Composite connection model verification

This section describes the extensive verification of the FE model developed, against three test results.

Figure 3-17 shows the location of different measurements made in the tests, the strain gauges on the beam web and flanges were located at 100 mm from the column face and the inclinometer on the bean web is 180 mm from the column face. The measured stress and strains will be used to compare the results obtained from the FE analysis. Results which are available from the tests and will be compared are:

1. Moment-rotation curves
2. a. Moment-beam bottom flange strain curves

   b. Moment-beam bottom flange stress curves
3. a. Moment-beam web horizontal strain curves

   b. Moment-beam web horizontal stress curves

   c. Moment-beam web von-Mises stress curves
4. a Moment-beam top flange horizontal strain curves

   b Moment-beam top flange horizontal stress curves
5. Moment-bolt force curves
6. a Moment-rebar strain curves

   b Moment-rebar stress curves
7. a Moment-column web horizontal strain curves

   b Moment-column web horizontal stress curves
8. Moment-column web von-Mises stress curves

3.4.1 Moment-rotation curves

The comparison for the moment - rotation curves is made in Figures 3-18(a), 3-18(b) and 3-18(c) for CJS-1, CJS-4 and CJS-5 respectively. CJS-1 had the lowest shear to moment ratio whereas CJS-5 had the highest. It can be seen that CJS-5 had bolt slip at a moment of about 130 kN-m. The FE analysis was performed without provision for bolt slip, although data can be easily included for bolt slip in the load-deformation data of bolts. Apart from this, the FE and the test moment-rotation curves are close to each other.

3.4.2 Moment-beam bottom flange strain and stress curves

In the test the strains were measured at a point 100 mm away from the column face and 35 mm from the beam web. Results from the FE analysis were extracted for the integration point of an element which is located at 90.2 mm from the column face and 30 mm from the centreline of the beam flange. The moment - bottom flange horizontal strain curves are compared in Figures 3-19(a), 3-19(b) and 3-19(c) for CJS-1, CJS-4 and CJS-5 respectively. The moment - bottom flange horizontal stress curves are compared in Figures 3-20(a), 3-20(b) and 3-20(c) for CJS-1, CJS-4 and CJS-5 respectively. The differences between the test and the model results are not significant. The observed difference in CJS-1 is believed to be due to the error in the strain gauge used; this decision was made after studying the equivalent curves for CJS-4 and CJS-5, also the curves presented in reference 3-1, where the curve for the equivalent bare steel connection SJS-1 is given. It is expected that when an arrangement changes from bare steel to composite, for the same moment, due to the greater lever arm in the composite connection, the force developed in the bottom flange would be smaller. So the strain and stress would also be small in the bottom flange of a composite connection. But SJS-1 (bare steel connection) and CJS-1 (composite connection) although they had the same steel detail gave the same strain for the same moment.

3.4.3 Moment-beam web horizontal strain, stress and von-Mises stress curves

In the test the strains were measured at a point along the centreline of the beam and 100 mm away from the column face. Results from the FE analysis were extracted for the integration point of an element which is located at 90.2 mm from the column face and 10.8 mm below the centreline of the beam web. The moment - beam web horizontal strain curves are compared in Figures 3-21(a), 3-21(b) and 3-21(c) for CJS-1, CJS-4 and CJS-5 respectively. The moment - beam web horizontal stress curves are compared in Figures 3-22(a), 3-22(b) and 3-22(c) for CJS-1, CJS-4 and CJS-5 respectively. The moment - beam web von-Mises stress curves are compared in Figures 3-23(a), 3-23(b) and 3-23(c) for CJS-1, CJS-4 and CJS-5 respectively. The differences between the test and the model results are not significant.

3.4.4 Moment-beam top flange strain and stress curves

The bottom flange locations for measuring points in the test and in the model were similar. The moment - beam top flange horizontal strain curves are compared in Figures 3-24(a), 3-24(b) and 3-24(c) for CJS-1, CJS-4 and CJS-5 respectively. The moment - beam top flange horizontal stress curves are compared in Figures 3-25(a), 3-25(b) and 3-25(c) for CJS-1, CJS-4 and CJS-5 respectively. The comparison shows some difference between the test and the model. The reason is that the test specimen had metal decking (CF46) over the beam top flange on which it had a cast in-situ concrete slab. Due to practical reasons the metal decking and the concrete are ignored and this caused a change in the forces along the surface of the top flange. So the variation which is observed is not unexpected.

3.4.5 Moment - bolt force curves

The comparison for the moment - bolt force curve is made in Figures 3-26(a), 3-26(b) and 3-26(c). The modelling of the bolts was not as straightforward as for the beam and the column. They were modelled using a combination of spring and shell elements and linking the shell with the endplate or column flange using EQUATION. The input properties for the spring elements were obtained from elastic analysis and FE analysis of bolts. No test was made to determine these properties. The response of the bolts was also largely influenced by the absence of the concrete and the material properties of the reinforcement. In the test it is observed that the bolts had a initial load of 30 kN; it was not possible to model this, since the spring elements have no elastic properties which are essential for specifying the initial conditions in ABAQUS. It can be seen that in the test at the initial phase of loading the bolts are below the neutral axis so the force in the bolts decreases, unfortunately this cannot be observed in the FE analysis as the concrete was neglected. Also from some preliminary studies it was observed that the bolt forces are also dependent on the reinforcement properties. When the rebar yields it extends and the bolts in turn are subjected to higher deformations and forces. The properties in the model for the reinforcement were taken from reference 3-5, as the stress-strain curve for the connection tests were not available. The variation in the bolt forces in the initial region is thus largely due to the absence of the concrete and the initial load. Considering the above facts the results can be considered reasonable.

3.4.6 Moment-rebar strain and stress curves

The comparison for the moment - rebar strain curve is made in Figures 3-27(a), 3-27(b) and 3-27(c) and the comparison for the moment - rebar stress curve is made in Figures 3-28(a), 3-28(b) and 3-28(c). The slight discrepancies observed are due to the points mentioned in sections 3.4.4 and 3.4.5.

3.4.7 Moment-column web horizontal strain and stress curves

In the test the strains were measured at the intersecting point of the centreline of the column web and beam bottom flange centreline. Results from the FE analysis were extracted for the integration point of an element which is located at 11.85 mm upwards vertically and 12.01 mm away horizontally from the point of measurement in the test. The moment - column web horizontal strain curves are compared in Figures 3-29(a), 3-29(b) and 3-29(c) for CJS-1, CJS-4 and CJS-5 respectively. The moment - column web horizontal stress curves are compared in Figures 3-30(a), 3-30(b) and 3-30(c) for CJS-1, CJS-4 and CJS-5 respectively. In the test the strains were obtained from the strain gauges and the stresses by multiplying the strain by another constant. Observing the test result of CJS-4 in the non-linear part, it appears that the FE results are more accurate, at least in this case as the stress corresponding to an 82 kN•m - moment is certainly not a true stress. The gauge probably yielded at this point.

3.4.8 Moment-column web von-Mises stress curves

The moment - column web von-Mises stress curves are compared in Figures 3-31(a), 3-31(b) and 3-31(c) for CJS-1, CJS-4 and CJS-5 respectively. The same dislocation for test and FE measuring points exists as in the previous case. Considering this the curves are reasonable.

3.5 Numerical modelling of some other connections

Tests SCJ3, SCJ4, SCJ10, SCJ11, SCJ12 reported in ref. 3-4 were modelled using the approach described above. SCJ3 and SCJ4 were flush endplate connections. SCJ10 was a partial depth endplate (bottom) connection. SCJ11 was an angle cleated connection (web cleat with seat cleat) and SCJ12 was a finplate connection.

Since SCJ3, SCJ4 were endplate connections their modelling approach was similar to CJS-1, CJS-4 and CJS-5. Comparisons of the moment rotation curves for SCJ3 and SCJ4 are made in Figure 3-32. Figure 3-33 show the comparisons of moment - rotation curves for SCJ10.

The key components that are required to numerically represent the angle cleated connection are: steel beam, column, the seat cleat, the web cleat, bolts connecting the different members, the shear studs and the rebar. Besides these to model the interaction of the seat cleat with the bottom flange of the beam and column flange and the interaction of the web cleats with the beam web and column flange interface elements were used. This represents an assembly of elements in a way that is more complicated than the endplate connections. The problem is further complicated by the bolt slip that occurs in this type of connection. It is impossible to predict in advance whether the slip will occur gradually or instantaneously and also the range or level of load for the gradual or sudden slip. This problem with the bolt shear load and slip indicate that it may not be possible to develop a finite element model that can successfully trace the moment rotation curve throughout, unless the bolt load slip behaviour is varied in every case to fit the moment rotation curves. But although the exact moment-rotation curve can not be traced, it should be possible to predict the ultimate connection moment capacity. Reference 3-4 describes the test of two composite connections with seat cleat and double web cleat (SCJ1 and SCJ11). Finite element method was applied to model these two connections which are identical in detail except for the reinforcement area. A detailed description of the modelling approach is not made as this is similar to the flush endplate connections, but with the key components stated above can be modified for the angle cleated connections. Figure 3-34 shows the comparison of moment rotation curves for SCJ11. It can be seen from this the mentioned bolt slip caused a discrepancy in tracing the moment-rotation curve but the connection moment capacity is well predicted. Similar result was obtained for SCJ1. Hence instead of going to extensive finite element analysis, the design procedures

described in chapter 8 is based on the EC3 equations and its modifications obtained from the FE analyses of composite flush endplate connections as described in chapters 5, 6 and 7 of this thesis.

Simulation procedure for SCJ12 was also similar to the other cases, only the finplate connected to the beam was to be modelled instead of the endplate or web cleat. Figure 3-35 shows the comparison of moment rotation curves. The reason for the large variation of moment-rotation values for SCJ12 is that in the test gradual slip of bolts occurred. It is almost impossible to predict in advance whether a particular bolt in a connection will undergo gradual slip, sudden slip or show no slip for fin plate and web cleat with seat cleat connections. For all these models exact material properties were not known for all the elements, only a few coupon test results giving the yield and ultimate strength were available. These tests were carried out in three phase, when a particular property was not available in a phase, it was taken from another one.

3.6 Conclusions

It is possible to model the semi-rigid composite connections in a simplified way. In sections 3.2, 3.3, 3.4 and 3.5 the modelling and verification of the composite connection was described. The results obtained from the model were compared against the available test results which showed that the model is suitable for the analysis purpose. It was observed that if the objective is to obtain a reliable moment-rotation curve only, then simplified bolt models are acceptable. But for a more accurate model, the bolts must be modelled in detail. In section 3.3 the modelling of bolts was described. In section 3.4 the verification of the composite connection FE model against three available test results was made. The comparison showed that the developed model can predict the internal forces closely to those obtained in test. It can be concluded that the developed model is suitable for the analysis of semi-rigid composite connections in a simplified but accurate way. The numerical analysis of different types

of connection shows that it is possible to model almost all type of connections, but the load slip behaviour of the individual bolts in a given test may prevent the tracing of exact moment rotation curves (and hence the initial stiffness of the connections) for finplate and angle cleated connections, although an accurate ultimate moment can be determined. This model will be used in chapter 4 to carry out parametric studies on composite flush endplate connections, which will provide an understanding of the internal force transfer mechanism.

3.7 References

3-1 Li, T. Q. (1994) *The Analysis and Ductility Requirements of Semi-Rigid Composite Frames,* Ph.D. thesis, University of Nottingham, UK.

3-2 Li, T. Q., Nethercot, D. A. and Choo, B. S. (1996) *Behaviour of flush end plate composite connections with unbalanced moment and variable shear/moment ratios: part 1: experimental behaviour*, Journal of Constructional Steel Research Vol. 38, No. 2, pp. 125-164.

3-3 Li, T. Q., Nethercot, D. A. and Choo, B. S. (1991) *Continuity Effects in Composite Frames*, Progress report No. 2 to SERC, SR92006, University of Nottingham, UK.

3-4 Xiao, Y. (1994) *Behaviour of Composite connections in steel and concrete.* Ph.D. thesis, Department of Civil Engineering, University of Nottingham, UK.

3-5 Li, T. Q., Moore, D. B., Choo, B. S. and Nethercot, D. A. *The Experimental Behaviour of a Full-scale Semi-rigidly Connected Composite Frame: Overall Considerations*, Journal of Constructional Steel Research (under review).

Table 3-1 Load taken by individual joint elements of the bolt in analysis i.

LF	J-1	J-2	J-3	J-4	J-5	J-6	J-7	J-8	J-9	J-10	J-11	J-12	Bolt Force (kN)	Moment (kN-m)
0	0	0	0	0	0	0	0	0	0	0	0	0	0	0
0.044	438.1	52.37	931.2	0.013	0.059	0.006	1213	219	0.000	251	1210	885	5	7
0.155	1534	183.1	3260	0158	0.072	0.068	4248	768	0.005	878	4235	3099	18	26
0.255	2519	300.7	5356	0425	0.195	0183	6980	1261	0.013	1442	6958	5092	30	42
0.401	3932	453	8408	1.086	0.490	0.467	11000	1996	0.035	2280	11000	8046	47	66
0.56	5283	511.6	11600	2.328	1.016	1.009	15300	2824	0.098	3240	15400	11400	66	92
0.763	6118	394.8	15000	702.7	2.315	2.416	15700	6298	0199	4572	15700	15500	80	125
0.774	6127	385 9	15200	737.3	2.406	2.529	15700	6522	0.209	4710	15700	15500	81	127
0.789	6110	364.6	15300	773.7	2.541	2.704	15700	6835	0.231	4909	15700	15500	81	130
0.813	6121	336.3	15500	868.8	273	2.965	15700	7342	0.255	5206	15700	15500	82	134
0.835	6166	308.6	15500	971 7	2.905	3.204	15700	7818	0.274	5470	15700	15600	83	137
0.84	6453	339.5	15500	1187	3.006	3.307	15700	8306	0.244	5676	15700	15600	85	138
0.845	7074	418 7	15500	1626	3153	3.434	15800	9172	0.167	6027	15800	15600	87	139
0.852	7979	540 9	15600	2248	3.429	3.624	15800	10400	0.052	6529	15800	15600	91	140
0.863	9434	734 1	15600	3172	3914	3.890	15900	12300	-0.093	7282	15900	15600	96	142
0.878	11600	1027	15700	4428	4.652	4.323	16000	14800	-0.181	8371	16000	15700	104	144
0.913	15600	1911	15900	9356	6.883	5.593	16400	15700	1827	12200	16500	15900	121	150
0.922	15600	2390	16000	11100	8.085	6.283	16600	15800	2418	13600	16700	16000	126	152
0.951	15800	3725	16400	15000	12.21	8712	17100	16000	4175	15500	17100	16300	137	156
0.995	16000	5622	16700	15600	17.2	11.200	17600	16300	7687	15700	17700	16700	146	164
1.02	16200	6678	17000	15700	1817	11.220	18100	16600	10500	15800	18300	17100	152	169
1.03	16200	6688	17000	15700	1816	11.130	18100	16600	10600	15900	18300	17100	152	169
1.032	16200	6674	17000	15700	1813	11.000	18200	16600	10800	15900	18300	17100	152	170
1.044	16200	6737	17100	15700	17.93	10.020	18300	16700	11800	15900	18500	17300	154	172
1.058	16400	9212	17500	15800	15.42	2.589	19000	17000	14500	16100	19200	17700	163	174
1.059	16500	9995	17600	15900	14.3	-0.631	19200	17100	15300	16200	19500	17900	165	174
1.061	16600	10700	17700	15900	13.31	-4.009	19500	17200	15500	16200	19700	18000	167	174
1.063	16700	11700	17900	16000	12.75	-8.841	19800	17400	15600	16300	20000	18300	170	175
1.064	16700	12200	18000	16000	12.4	-11.690	19900	17500	15600	16400	20200	18400	171	175
1.064	16800	12600	18100	16100	12.1	-14.590	20100	17600	15700	16500	20400	18500	172	175
1.066	16900	14000	18500	16200	8 902	-29 170	20900	18100	15900	16700	21200	19100	178	175
1.060	17000	13700	18800	16300	-2 95	-49.010	21700	18600	16100	17100	22200	19800	181	174

Note:

LF is the load factor corresponding to the applied load

Bolt force is obtained by summing the forces in all the joint elements

Allowed axial load in each spring is: 1.55E+04 N at a displacement of 0.0587 mm

3.00E+04 N at a displacement of 5.0000 mm

The loads shown in Tables 3-1 to 3-8 are in N

Table 3-2 Load taken by individual joint elements of the bolt in analysis ii

LF	J-1 (N)	J-2 (N)	J-3 (N)	J-4 (N)	J-5 (N)	J-6 (N)	J-7 (N)	J-8 (N)	Bolt Force (kN)	Moment (kN-m)
0	0	0	0	0.00	0	0	0	0	0	0
0.044	439	46	989	0.01	1254	249	1253	941	5	7
0.089	878	92	1979	0.03	2508	497	2506	1882	10	15
0.156	1536	161	3463	0.10	4389	870	4386	3293	18	26
0.255	2523	265	5690	0.28	7212	1429	7206	5411	30	42
0.402	3939	396	8937	0.71	11400	2260	11400	8551	47	66
0.502	4831	437	11100	1.18	14200	2855	14300	10800	59	83
0.706	6532	622	15500	2 83	15700	4150	15700	15500	74	116
0.804	7555	735	15600	4.28	15800	5575	15800	15600	77	132
0.810	7610	742	15600	4.37	15800	5660	15800	15600	77	133
0.820	7690	752	15600	4.52	15800	5787	15800	15600	77	135
0 833	7786	759	15600	4 74	15800	5972	15800	15600	77	137
0 835	8181	859	15600	4 83	15800	6147	15800	15600	78	137
0 838	8797	995	15600	4 91	15800	6620	15800	15700	79	138
0.842	9777	1229	15700	5.04	15900	7388	15900	15700	82	138
0 849	11200	1594	15700	5 26	16000	8485	16000	15700	85	139
0 845	11100	1572	15700	5 24	16000	8403	16000	15700	84	139

Note:

Allowed axial load in each spring is: 1.55E+04 N at a displacement of 0.0587 mm

3.00E+04 N at a displacement of 5.0000 mm

Table 3-3 Load taken by individual joint elements of the bolt in analysis iii

LF	J-1 (N)	J-2 (N)	J-3 (N)	J-4 (N)	J-5 (N)	J-6 (N)	Bolt force (kN)	Moment (kN-m)
0	0	0	0	0	0	0	0	0
0.044	1577	0	0	2223	536	421	5	7
0.089	3154	0	0	4446	1073	842	10	15
0.155	5521	0	0	7782	1878	1474	17	25
0.254	9072	1	0	12800	3086	2423	27	42
0.378	13500	2	1	19000	4608	3615	41	62
0.584	20400	5	2	29300	7266	5776	63	96
0.772	25000	11	5	37500	10000	7932	80	127
0.783	25100	12	6	37500	10300	8090	81	129
0.798	25300	12	6	37500	10700	8324	82	131
0.824	25700	13	6	37500	11400	8701	83	135
0.845	27100	15	7	37500	12600	9595	87	139
0.860	30300	19	9	37600	14700	11300	94	141
0.877	34100	24	11	37600	17100	13000	102	144
0.905	37500	34	17	37700	21200	16300	113	149
0.922	37600	40	23	37800	24600	17900	118	152
0.966	37700	48	31	38000	30100	20200	126	159
1.008	37800	51	36	38200	34400	22400	133	166
1.03	37800	49	39	38300	37100	23300	137	169
1.053	37900	41	39	38600	37600	26600	141	173
1.06	38100	3220	39	38900	37700	30800	149	174
1.062	38200	5602	45	39200	37800	34600	156	175
1.061	38300	6492	45	39500	37900	37200	159	174
1.056	38300	6405	35	39600	38000	37600	160	174
1.052	38400	7508	30	39800	38200	37600	162	173
1.051	38400	7506	27	39900	38200	37700	162	173

Note:

Allowed axial load in each spring is: 3.75E+04 N at a displacement of 0.0587 mm

4.50E+04 N at a displacement of 5.0000 mm

Table 3-4 Load taken by individual joint elements of the bolt in analysis iv

LF	J-1 (N)	J-2 (N)	J-3 (N)	J-4 (N)	Bolt force (kN)	Moment (kN-m)
0	0	0	0	0	0	0
0.043	901	0	1780	559	3	7
0.086	1802	0	3560	1118	6	14
0.151	3153	0	6231	1957	11	25
0.248	5182	1	10200	3215	19	41
0.391	8132	2	16100	5091	29	64
0.571	11300	4	23200	7463	42	94
0.665	12400	6	26600	8665	48	109
0.778	12800	9	30300	10100	53	128
0.778	12800	9	30300	10100	53	128
0.778	12800	9	30300	10100	53	128
0.779	12800	9	30300	10100	53	128
0.779	12800	9	30300	10100	53	128
0.779	12800	9	30300	10100	53	128

Note:

Allowed axial load in each spring is: 3.75E+04 N at a displacement of 0.0587 mm

4.50E+04 N at a displacement of 5.0000 mm

Table 3-5 Load taken by individual joint elements of the bolt in analysis v

LF	J-1	J-2	J-3	J-4	Bolt force (kN)	Moment (kN-m)
0	0	0	0	0	0	0
0.043	911	0	1774	561	3	7
0.086	1821	0	3549	1121	6	14
0.151	3188	0	6212	1963	11	25
0.248	5239	1	10200	3225	19	41
0.390	8217	2	16100	5106	29	64
0.520	10600	3	21200	6828	39	85
0.724	13200	8	28600	9473	51	119
0.724	13200	8	28600	9476	51	119
0.725	13200	8	28600	9481	51	119
0.725	13200	8	28600	9489	51	119
0.726	13200	8	28600	9501	51	119
0.727	13200	8	28700	9519	51	120
0.729	13200	8	28700	9545	52	120
0.732	13200	8	28800	9586	52	120
0.737	13200	8	29000	9645	52	121
0.744	13300	8	29200	9734	52	122
0.7534	13300	9	29500	9866	53	124
0.7679	13300	9	29900	10100	53	126
0.7893	13400	10	30600	10300	54	130
0.8012	13400	10	30900	10400	55	132
0.7985	13300	10	30800	10400	55	131

Note:

Allowed axial load in each spring is: 3.75E+04 N at a displacement of 0.0587 mm

4.50E+04 N at a displacement of 5.0000 mm

Table 3-6 Load taken by individual joint elements of the bolt in analysis vi

LF	J-1	J-2	J-3	J-4	Bolt force (kN)	Moment (kN-m)
0	0	0	0	0	0	0
0.046	1140	1209	1533	1068	5	7
0.091	2279	2419	3067	2135	10	15
0.160	3989	4233	5368	3737	17	26
0.262	6554	6956	8820	6141	28	43
0.416	10400	11000	14000	9747	45	68
0.567	14100	15000	19000	13200	61	93
0.805	18500	20500	25900	17400	82	132
0.881	19200	21700	27400	18100	86	145
0.936	19400	22500	28400	18400	89	154
0.939	19600	22700	28700	18600	90	154
0.941	19900	23000	29000	18800	91	155
0.944	20400	23300	29400	19200	92	155
0.949	21000	23900	30100	19800	95	156
0.956	21900	24600	31000	20600	98	157
0.967	23300	25800	32400	21900	103	159
0.980	25100	27200	34200	23500	110	161
0.9979	27200	29000	36300	25500	118	164
1.024	30300	31300	38900	28300	129	168
1.055	33300	33600	41400	31100	139	173
1.108	36600	36800	45000	34300	153	182
1.132	38100	38700	45000	35800	158	186
1.168	39900	41500	45000	37800	164	192
1.185	41100	43200	45000	38900	168	195

Note:

Allowed axial load in each spring is: 4.50E+04 N at a displacement of 0.0587 mm

4.80E+04 N at a displacement of 5.0000 mm

Table 3-7 Load taken by individual joint elements of the bolt in analysis vii

LF	J-1	J-2	J-3	J-4	Bolt force (kN)	Moment (kN-m)
0	0	0	0	0	0	0
0.045	1008	1109	1024	1411	5	7
0.090	2016	2218	2049	2823	9	15
0.158	3529	3883	3586	4941	16	26
0.259	5798	6380	5893	8118	26	42
0.410	9203	10100	9354	12900	42	67
0.546	12200	13400	12400	17100	55	90
0.769	16300	17700	16300	23000	73	126
0.863	17300	19000	17500	24700	78	142
0.868	17300	19000	17600	24800	79	143
0 876	17400	19100	17700	24900	79	144
0.888	17500	19200	17800	25000	80	146
0.905	17600	19400	18000	25300	80	149
0.916	17800	19700	18200	25600	81	151
0.922	18200	20400	18900	26200	84	152
0.930	18800	21500	19800	27100	87	153
0.940	19700	22900	21100	28400	92	154

Note:

Allowed axial load in each spring is: 4.50E+04 N at a displacement of 0.0587 mm

4.80E+04 N at a displacement of 5.0000 mm

Table 3-8 Load taken by individual joint elements of the bolt in analysis viii

LF	J-1	J-2	J-3	J-4	Bolt force (kN)	Moment (kN-m)
0	0	0	0	0	0	0
0.043	688	742	655	1073	3	7
0.086	1376	1485	1311	2146	6	14
0.151	2409	2599	2294	3756	11	25
0.248	3957	4270	3770	6172	18	41
0.392	6249	6749	5953	9741	29	64
0.579	8953	9616	8492	14000	41	95
0.674	10200	10700	9454	15800	46	111
0.789	11500	11300	10100	17800	51	130
0.795	11500	11300	10100	17900	51	131
0.805	11600	11300	10100	18000	51	132
0.818	11700	11400	10100	18200	51	134
0.824	11800	11300	10100	18300	52	135
0.833	12400	12300	10800	19200	55	137
0.846	13200	13600	11800	20600	59	139
0.861	14200	15100	12800	22300	64	142
0.885	15500	17400	14200	24800	72	145
0.9038	16300	19300	15200	26700	78	149
0.9162	17000	20800	16100	28100	82	151
0.9411	17800	22400	17200	29600	87	155
0.9754	18800	23900	18500	31400	93	160
1.017	20100	25600	20000	33900	100	167
1.041	20800	26400	20700	35100	103	171
1.053	21100	26700	20900	35700	104	173
1.06	21300	26800	21100	35900	105	174
1.067	21500	27100	21300	36300	106	175
1.071	21800	27800	21800	36900	108	176
1.076	22300	28500	22400	37800	111	177
1.081	22900	29400	23300	38900	115	178
1.085	23500	30100	24000	40000	118	178
1.088	23800	30500	24500	40700	120	179
1.090	24100	31200	25100	41400	122	179

Note:

Allowed axial load in each spring is: 4.50E+04 N at a displacement of 0.0587 mm

4.80E+04 N at a displacement of 5.0000 mm

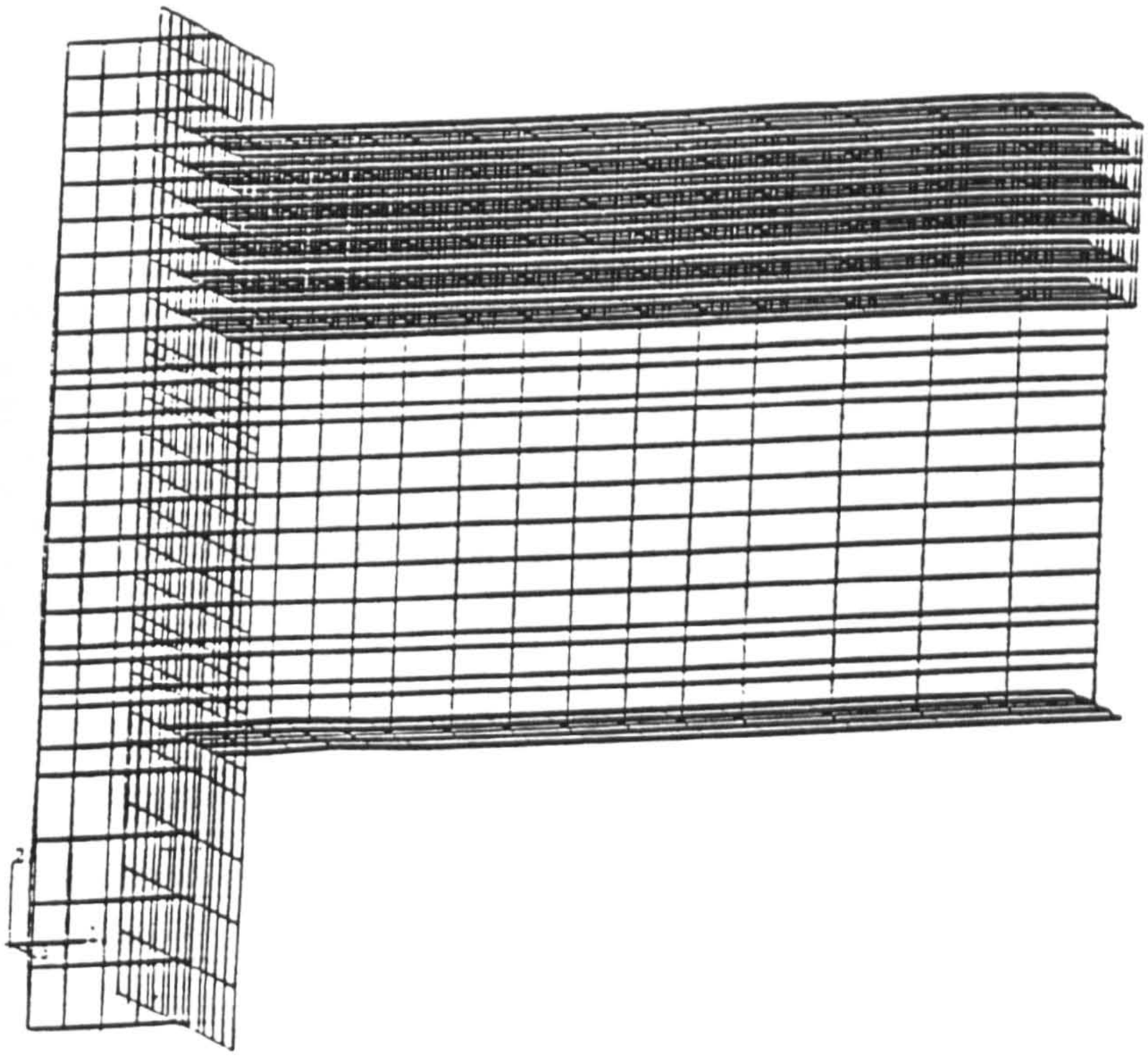

Figure 3-1 FE mesh for CJS-1, with concrete

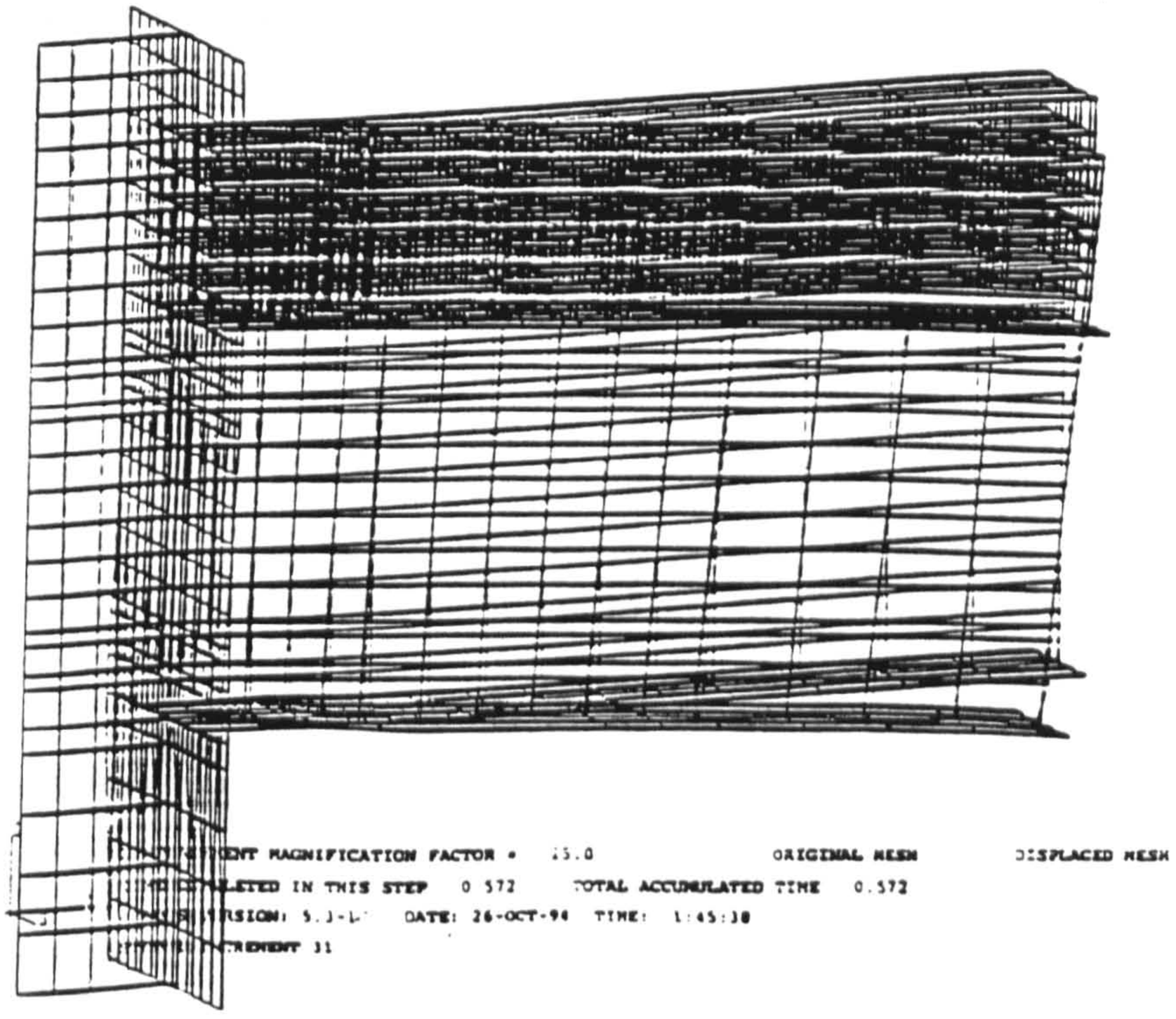

Figure 3-2 Displaced shape of FE model of CJS-1, with concrete

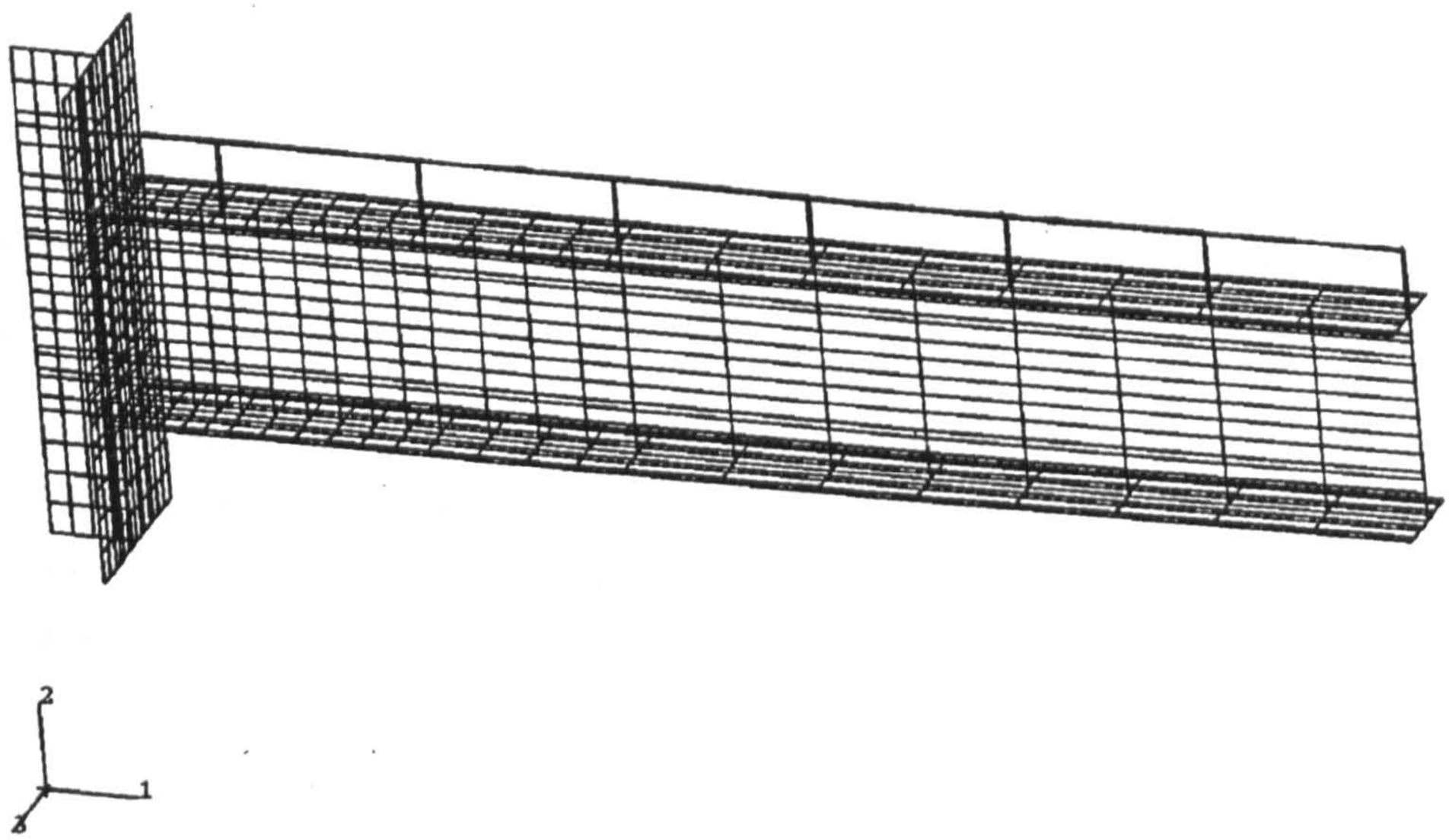

Figure 3-3 FE mesh for CJS-1, neglecting concrete

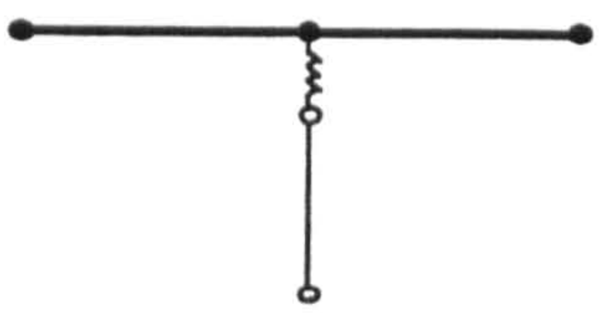

Reinforcement and shear stud model

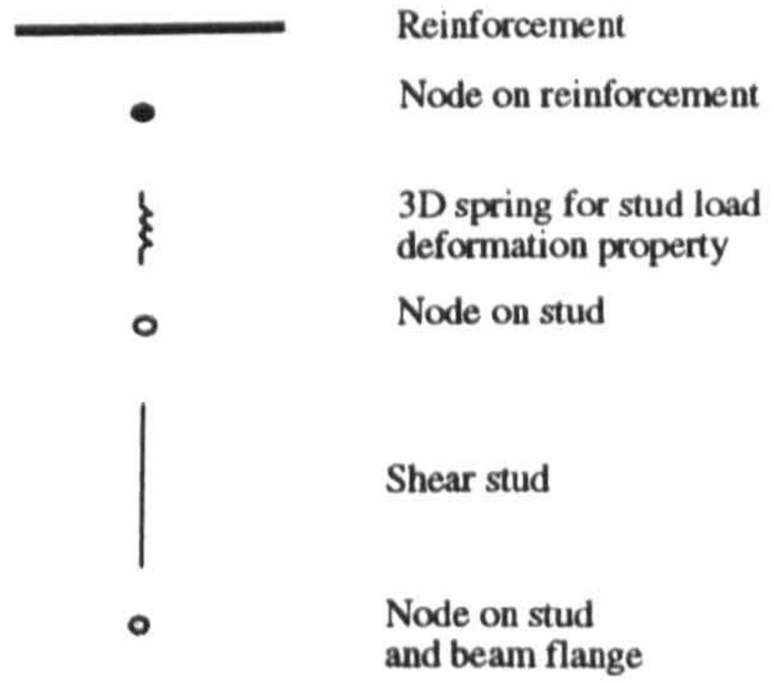

Figure 3-4 Modelling reinforcement and shear stud in composite connection

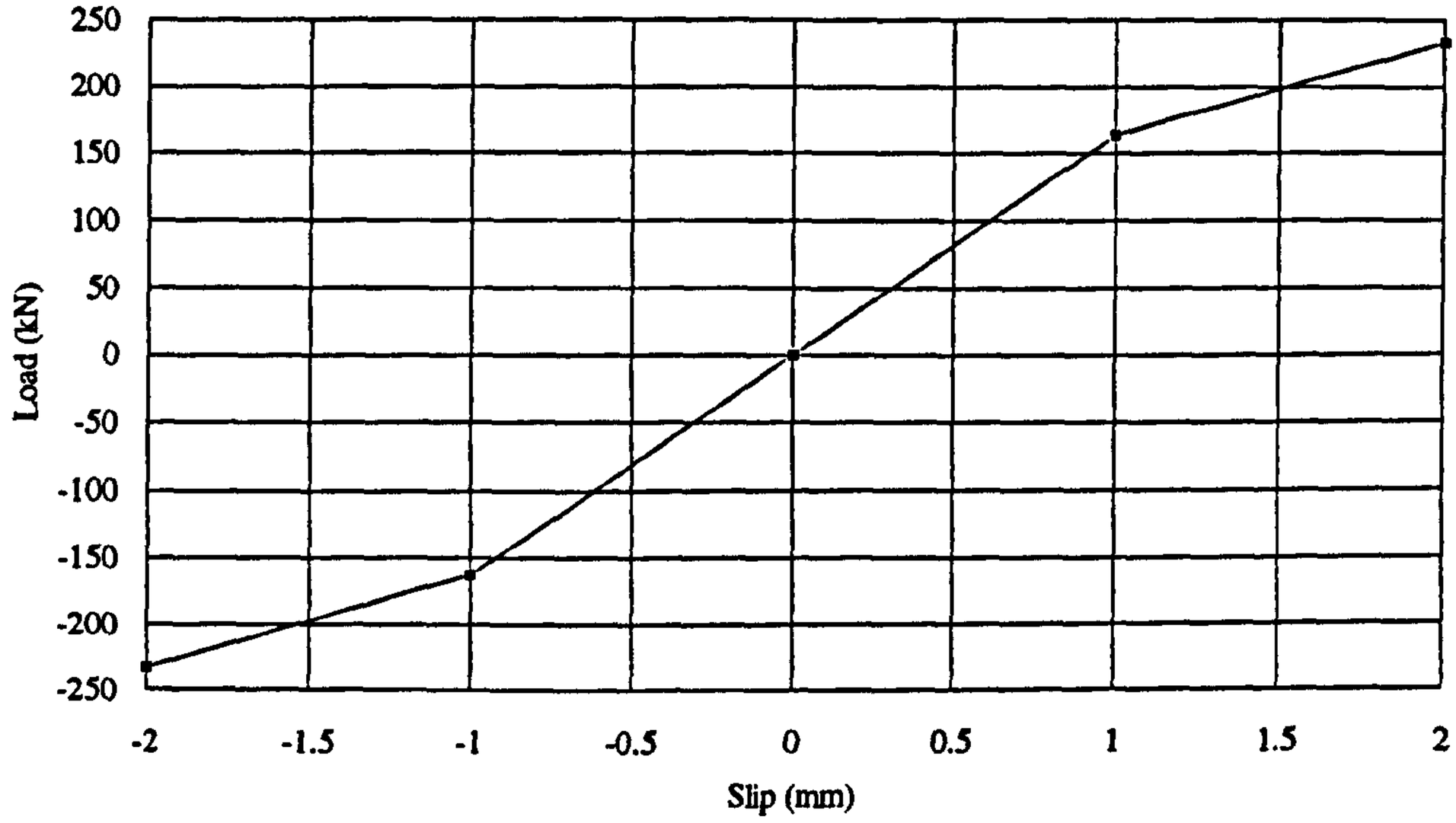

Figure 3-5 Load-slip curve used for shear studs

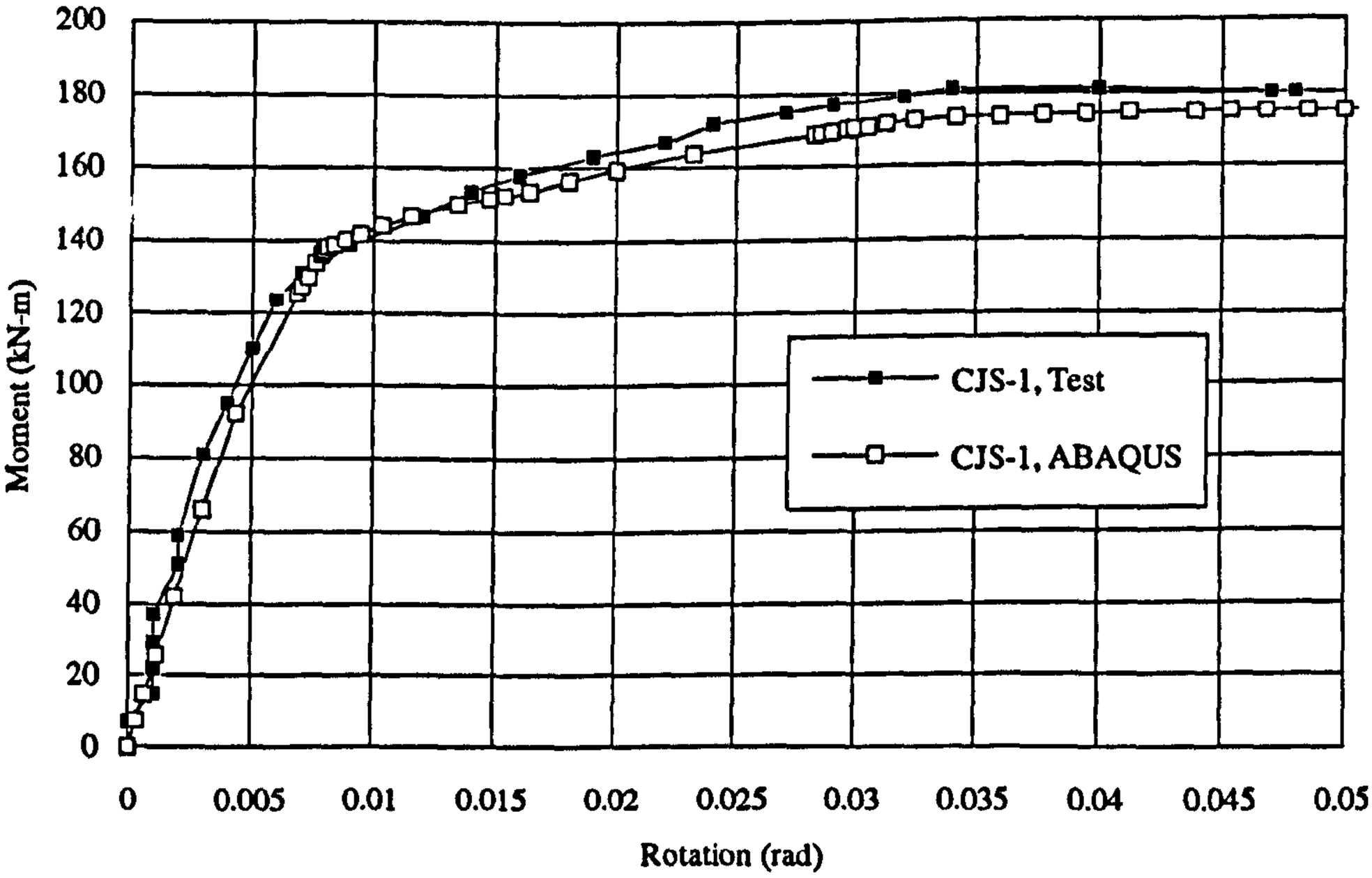

Figure 3-6 Comparison of moment rotation curves for test CJS-1

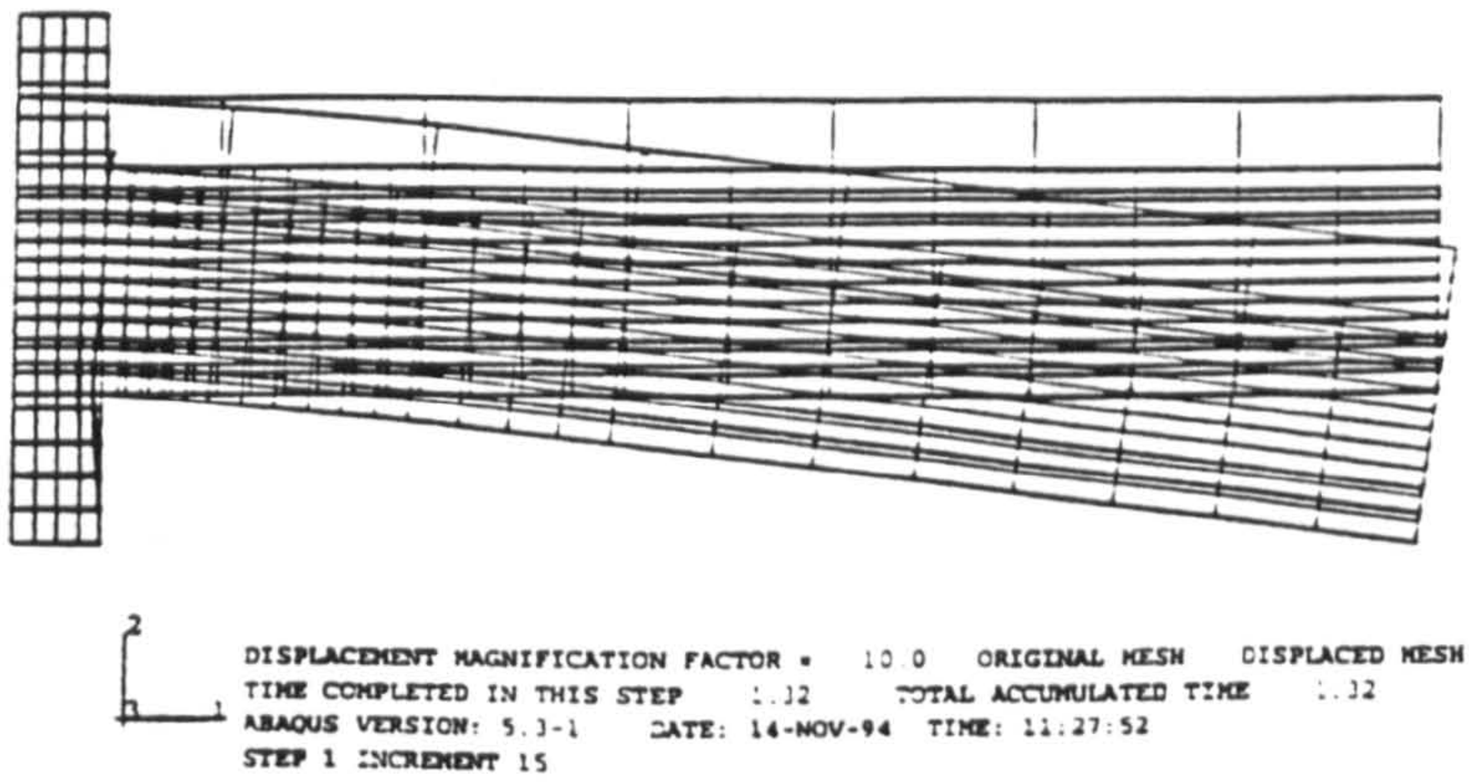

Figure 3-7 Displaced shape from the FE analysis

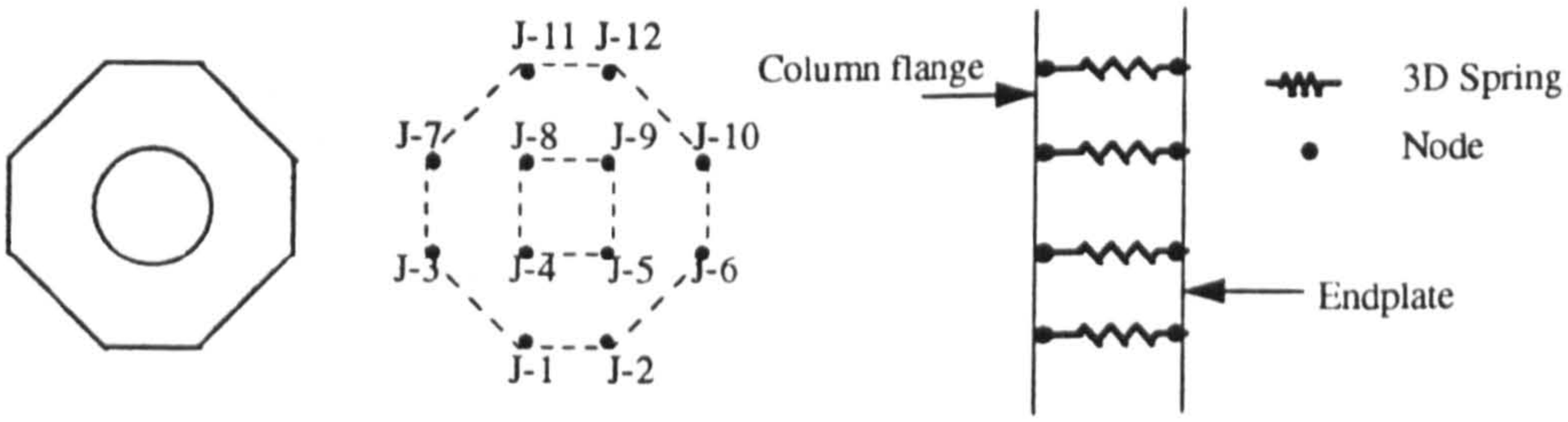

(a) The bolt head

(b) FE simulation of bolt (front view)

(c) FE simulation of bolt (side view)

Figure 3-8 FE representation of bolt for analysis i

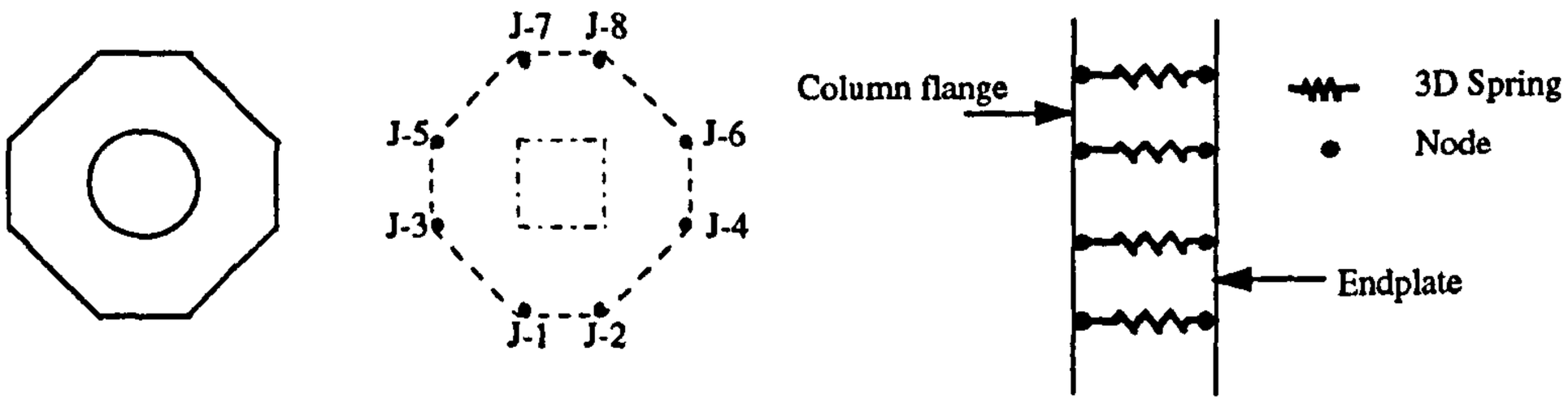

(a) The bolt head

(b) FE simulation of bolt (front view)

(c) FE simulation of bolt (side view)

Figure 3-9 FE representation of bolt for analysis ii

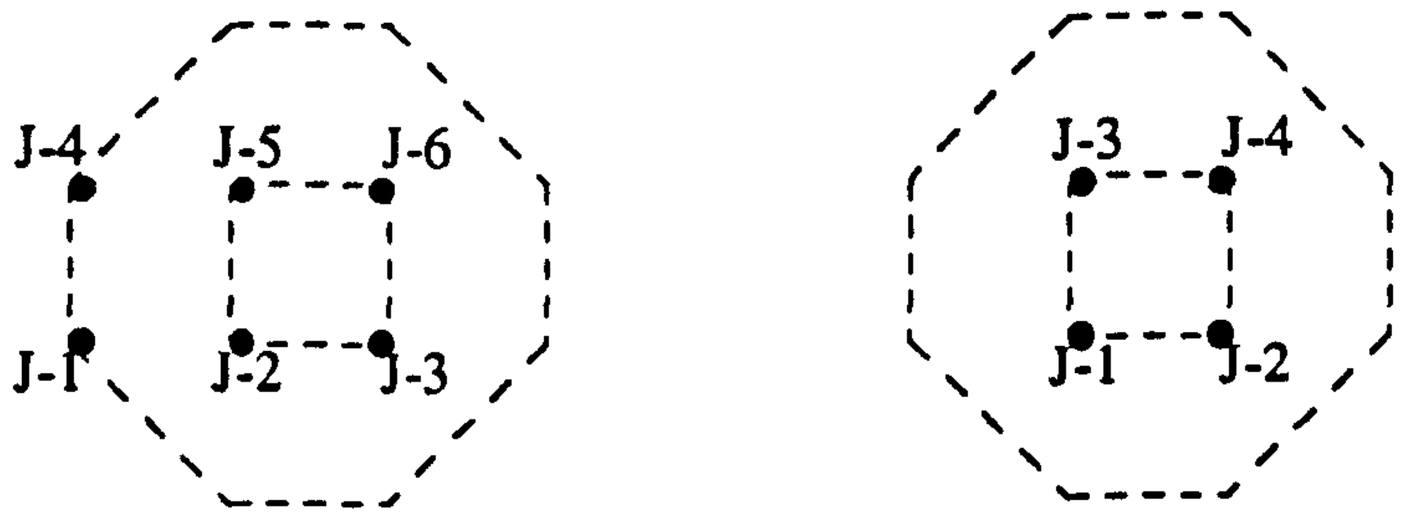

(a) FE simulation of bolt, with six spring (front view)

(b) FE simulation of bolt, with four spring (front view)

Figure 3-10 FE representation of bolt for analyses iii and iv

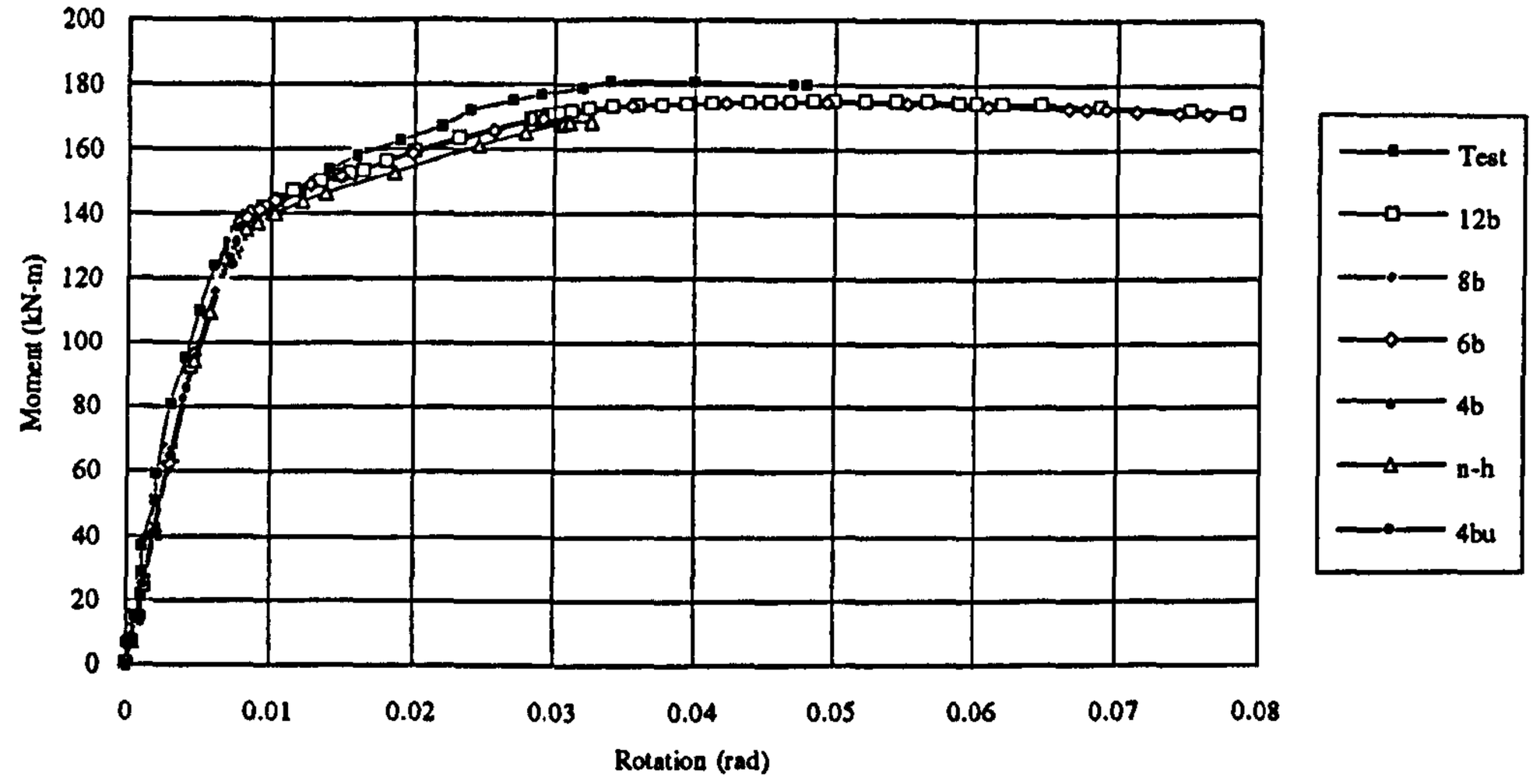

Note: 12b is 12 spring elements for bolt, 8b is 8 spring elements, 6b is 6 spring elements, 4b is 4 spring elements, 4bu is 4 spring elements with displacement restraint, n-h is no hole for bolts.

Figure 3-11 Moment-rotation curves for bolt modelling (analyses i-v)

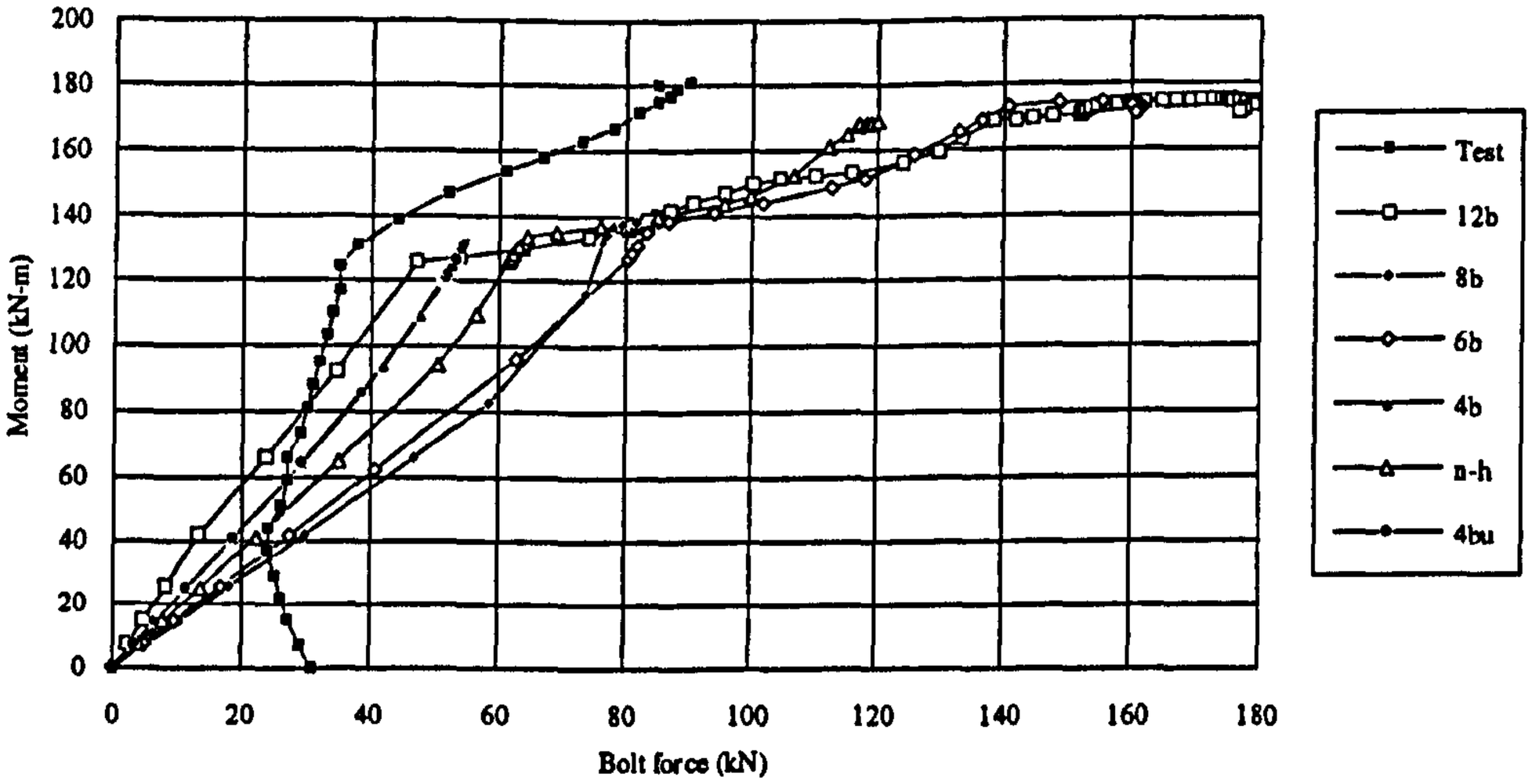

Note: 12b is 12 spring elements for bolt, 8b is 8 spring elements, 6b is 6 spring elements, 4b is 4 spring elements, 4bu is 4 spring elements with displacement restraint, n-h is no hole for bolts.

Figure 3-12 Moment-bolt force curve for bolt modelling (analyses i-v)

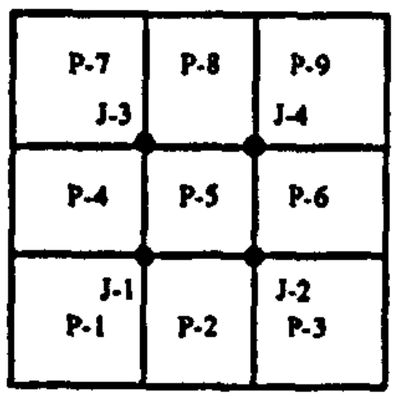

(a) FE simulation of bolt head, with nine shell elements (front view)

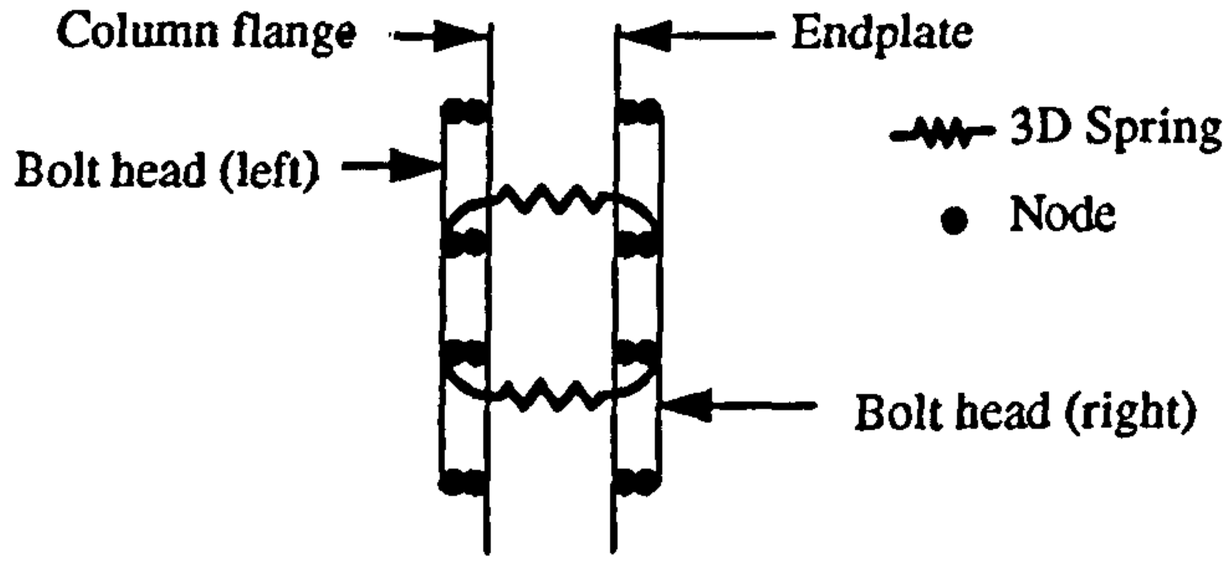

(b) FE simulation of bolt (side view)

Figure 3-13 Bolt model in analysis vi

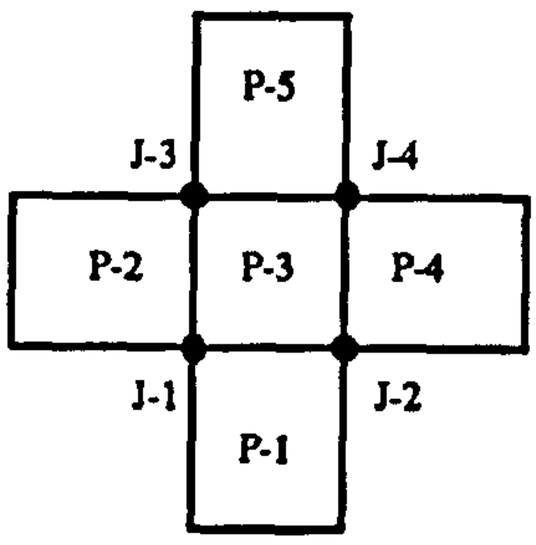

(a) FE simulation of bolt head with five shell element (front view)

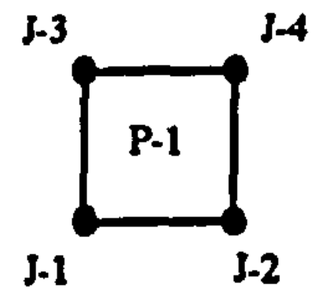

(b) FE simulation of bolt head with one shell element (front view)

Figure 3-14 Bolt head models with five and one shell element

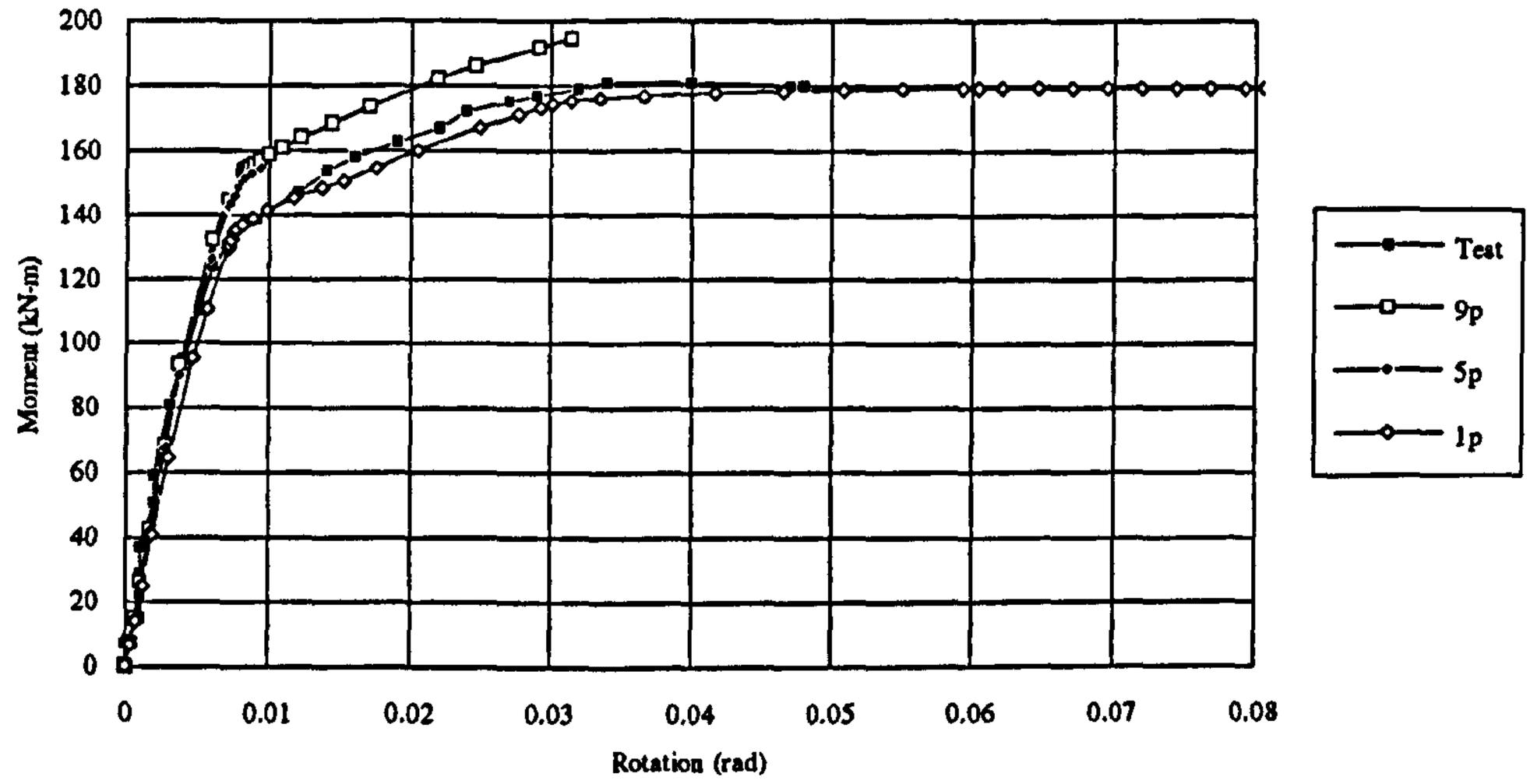

Note: 9p is 9 stiff plate elements for bolt head, 5p is 5 stiff plate for bolt head, 1p is 1 stiff plate for bolt head.

Figure 3-15 Moment-rotation curves for bolt modelling (analyses v-viii)

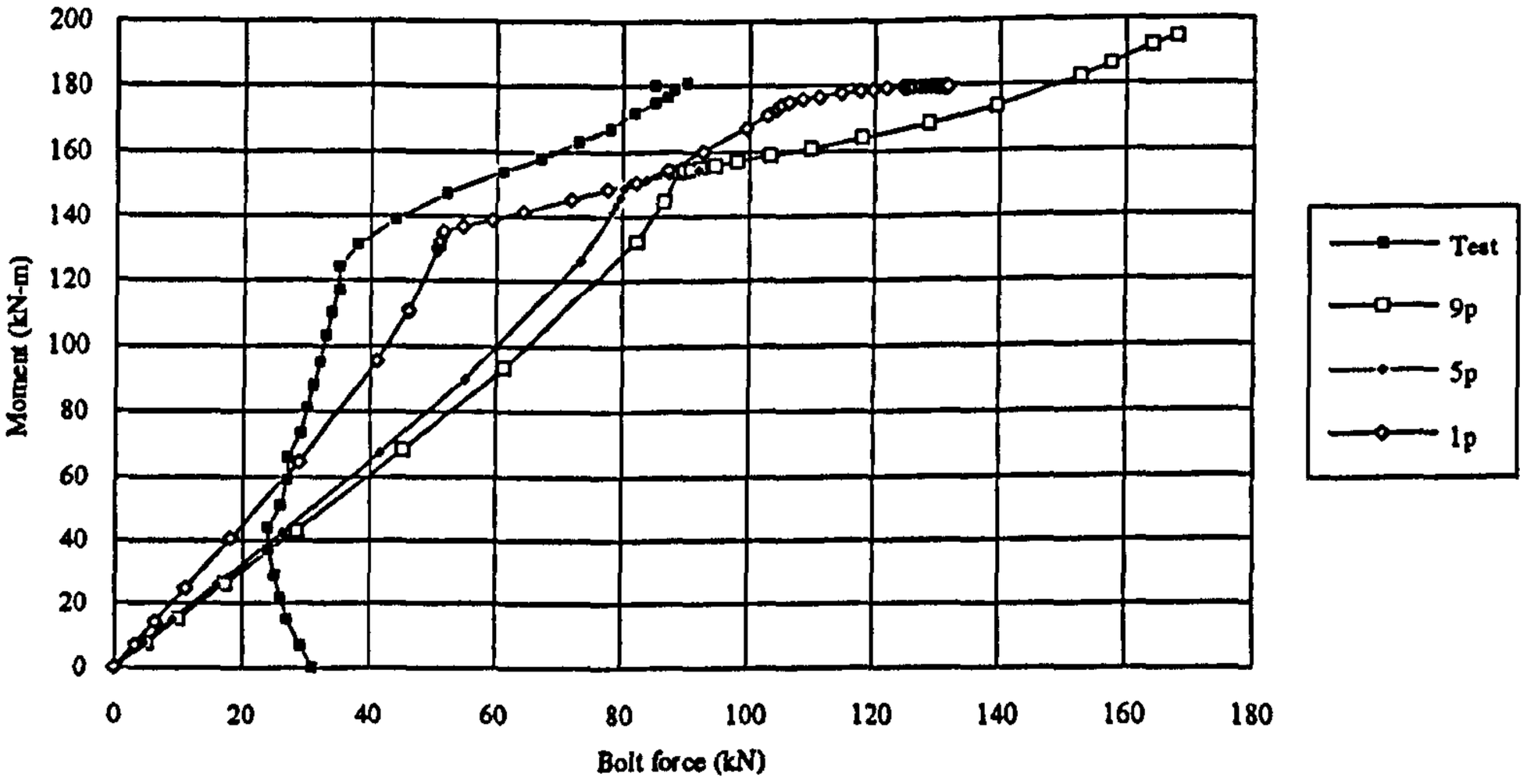

Note: 9p is 9 stiff plate elements for bolt head, 5p is 5 stiff plate for bolt head, 1p is 1 stiff plate for bolt head.

Figure 3-16 Moment-rotation curves for bolt modelling (analyses v-viii)

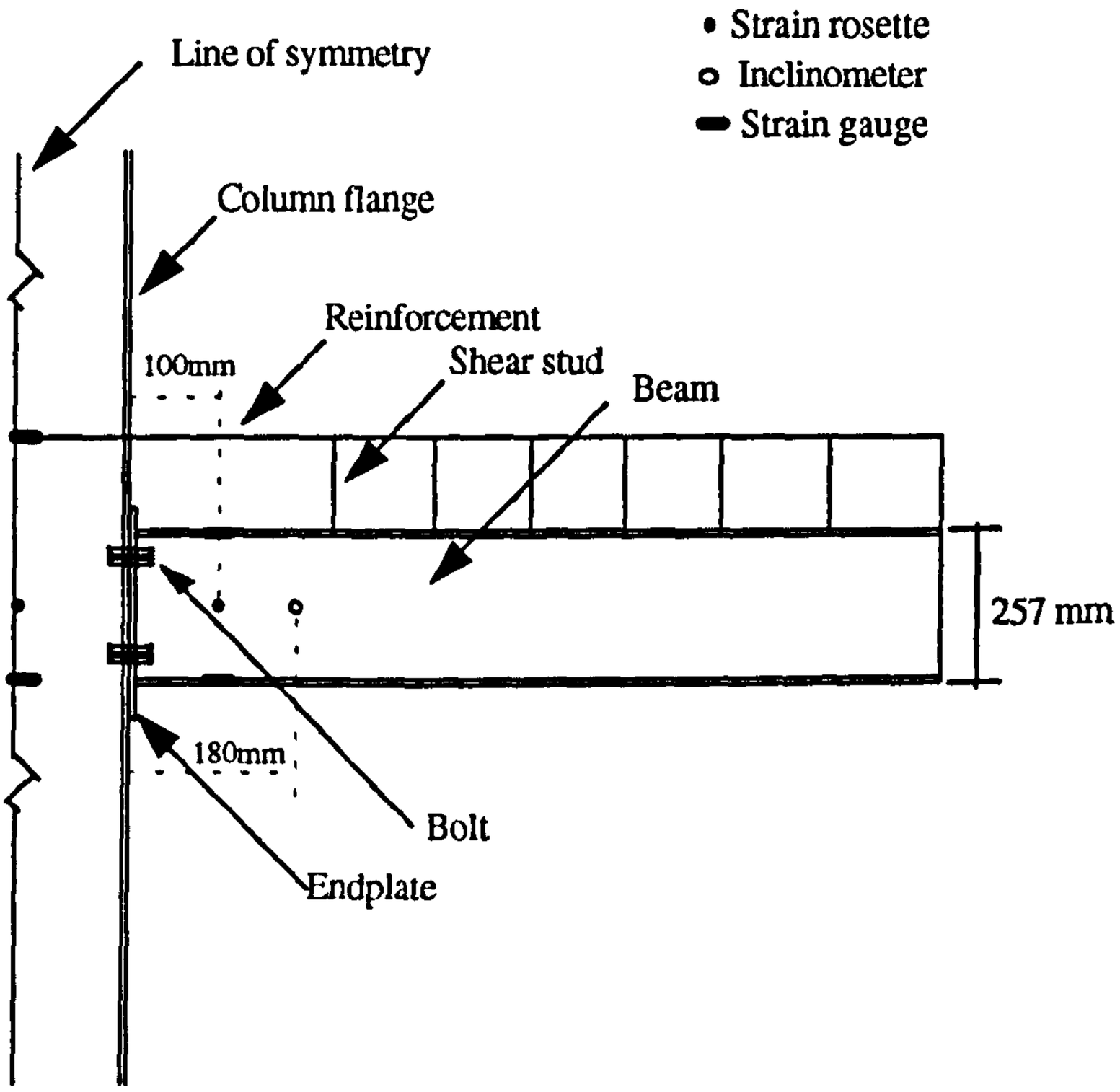

Figure 3-17 Location of strain and rotation measurements

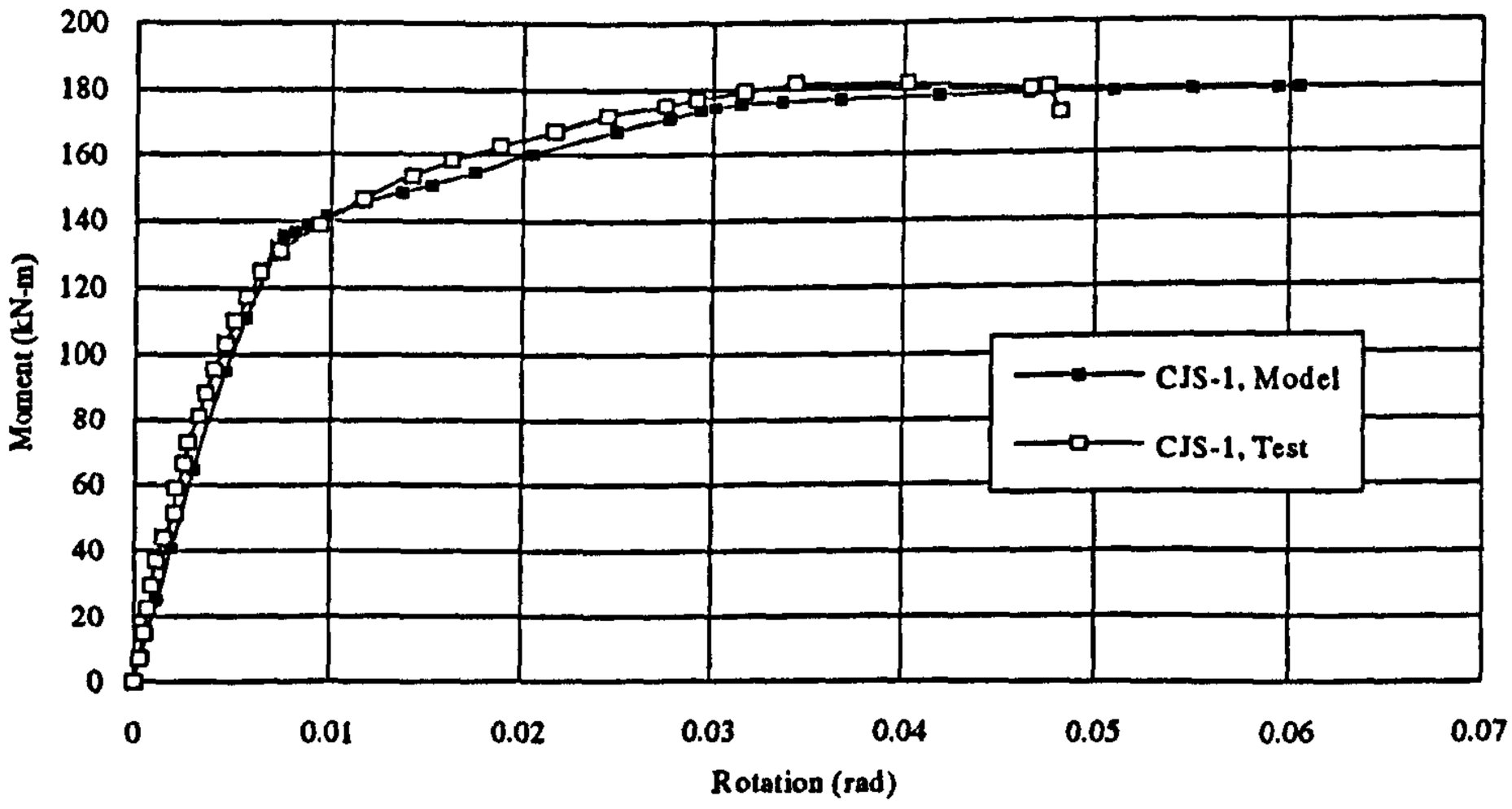

3-18 (a) Comparison of M-ϕ curves for CJS-1

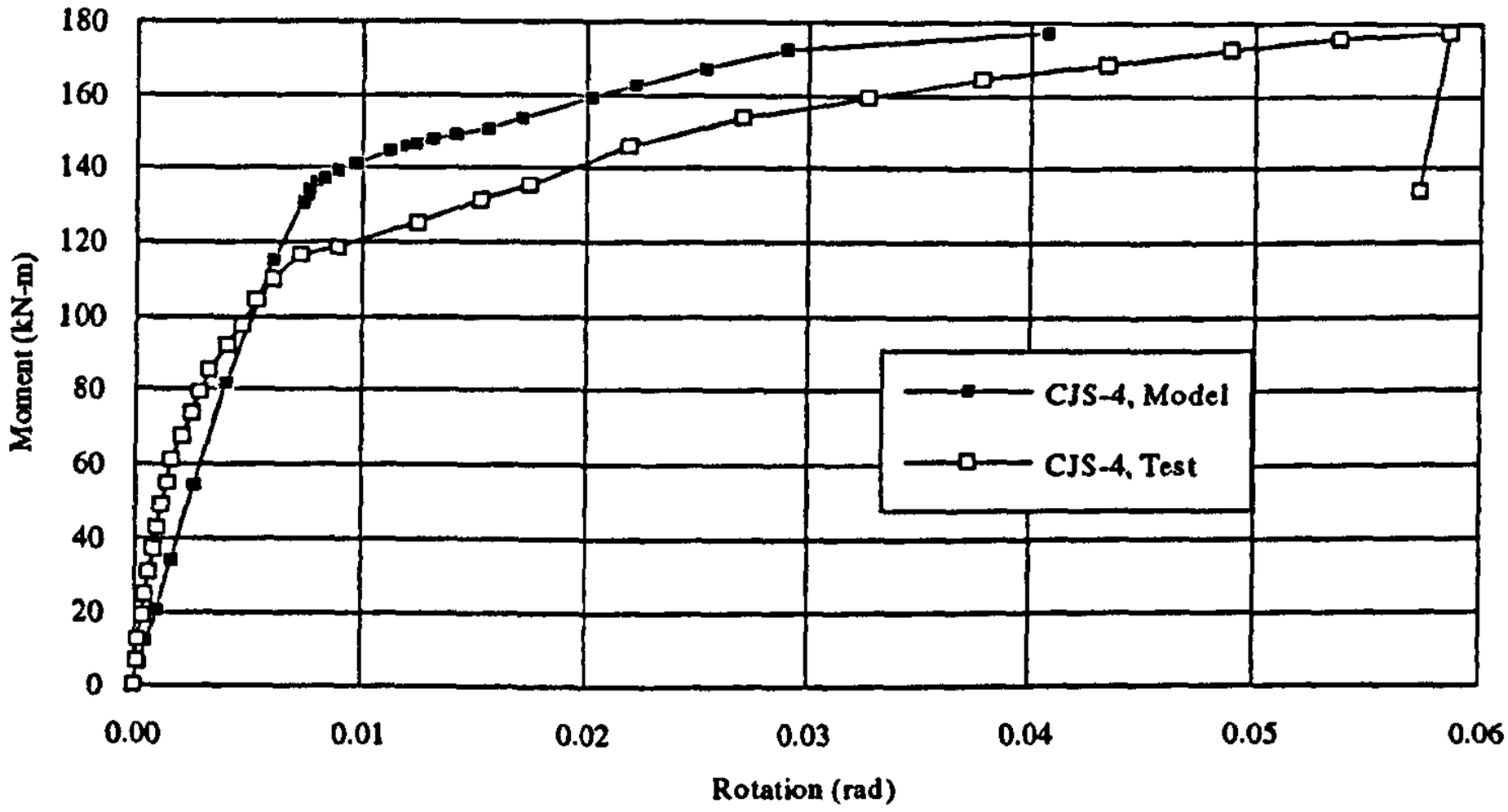

3-18 (b) Comparison of M-ϕ curves for CJS-4

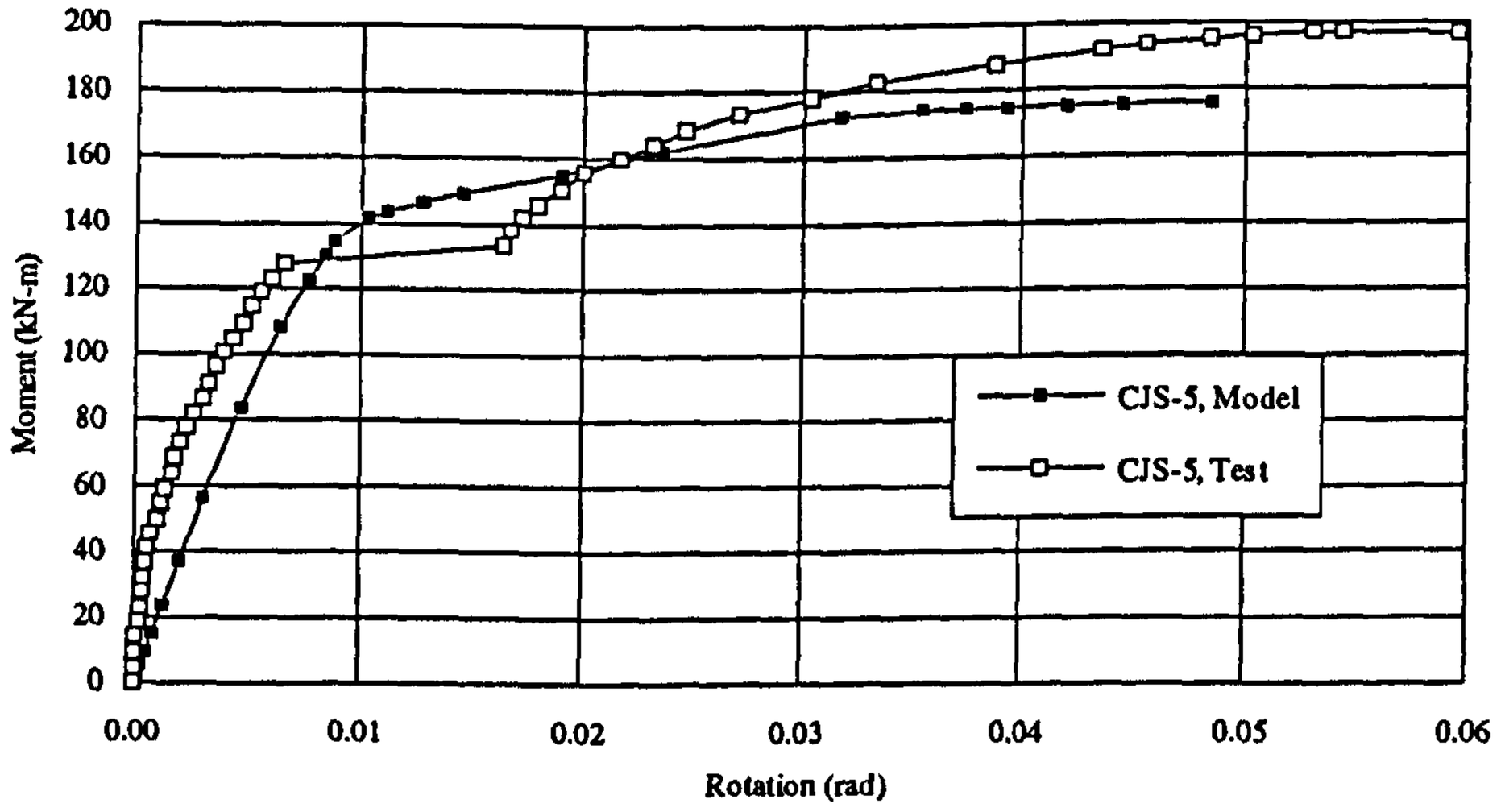

3-18 (c) Comparison of M-ϕ curves for CJS-5

Figure 3-18 Comparison of M-ϕ curves for model and test results

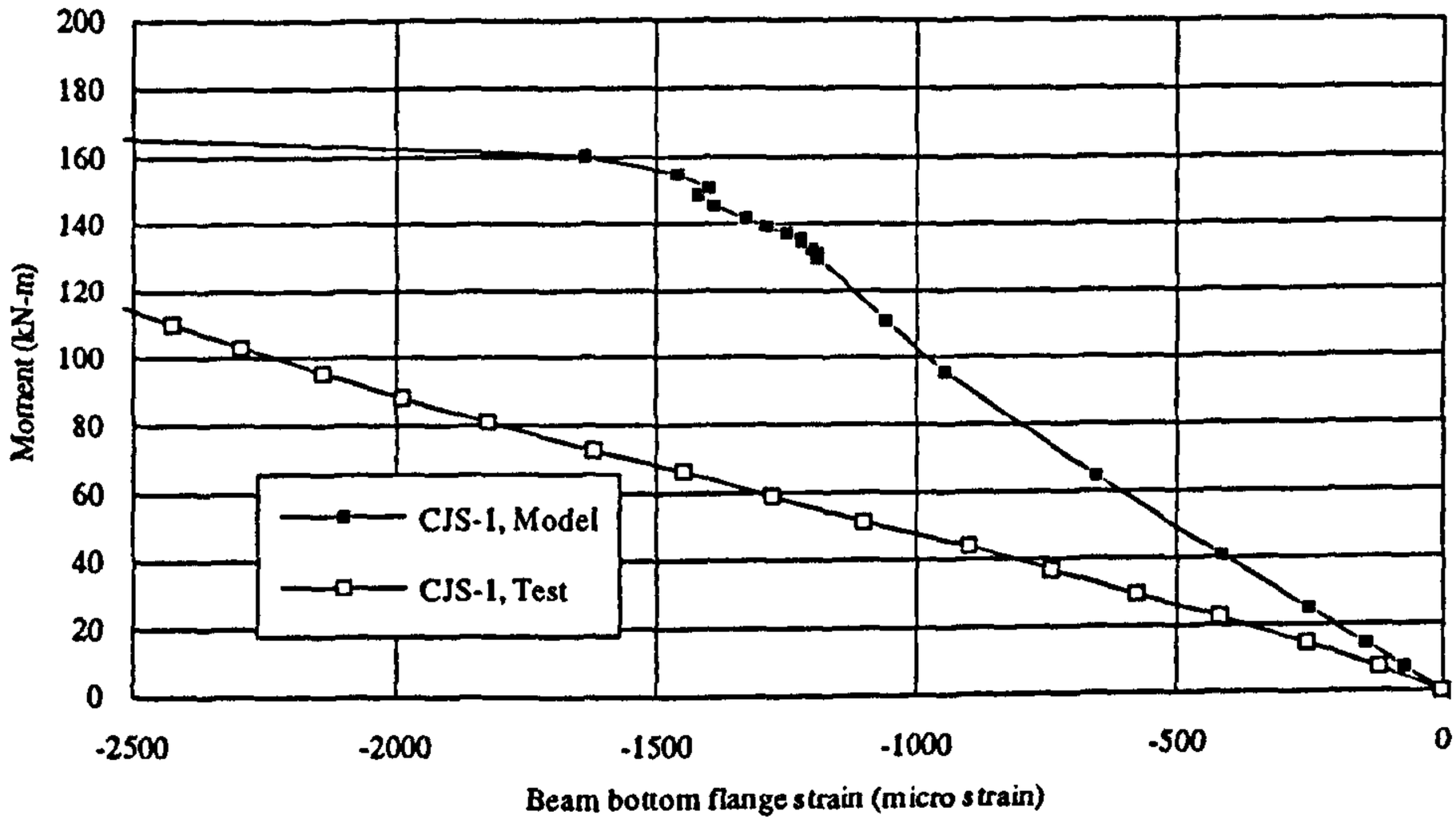

3-19 (a) Comparison of moment-bottom flange strain curves for CJS-1

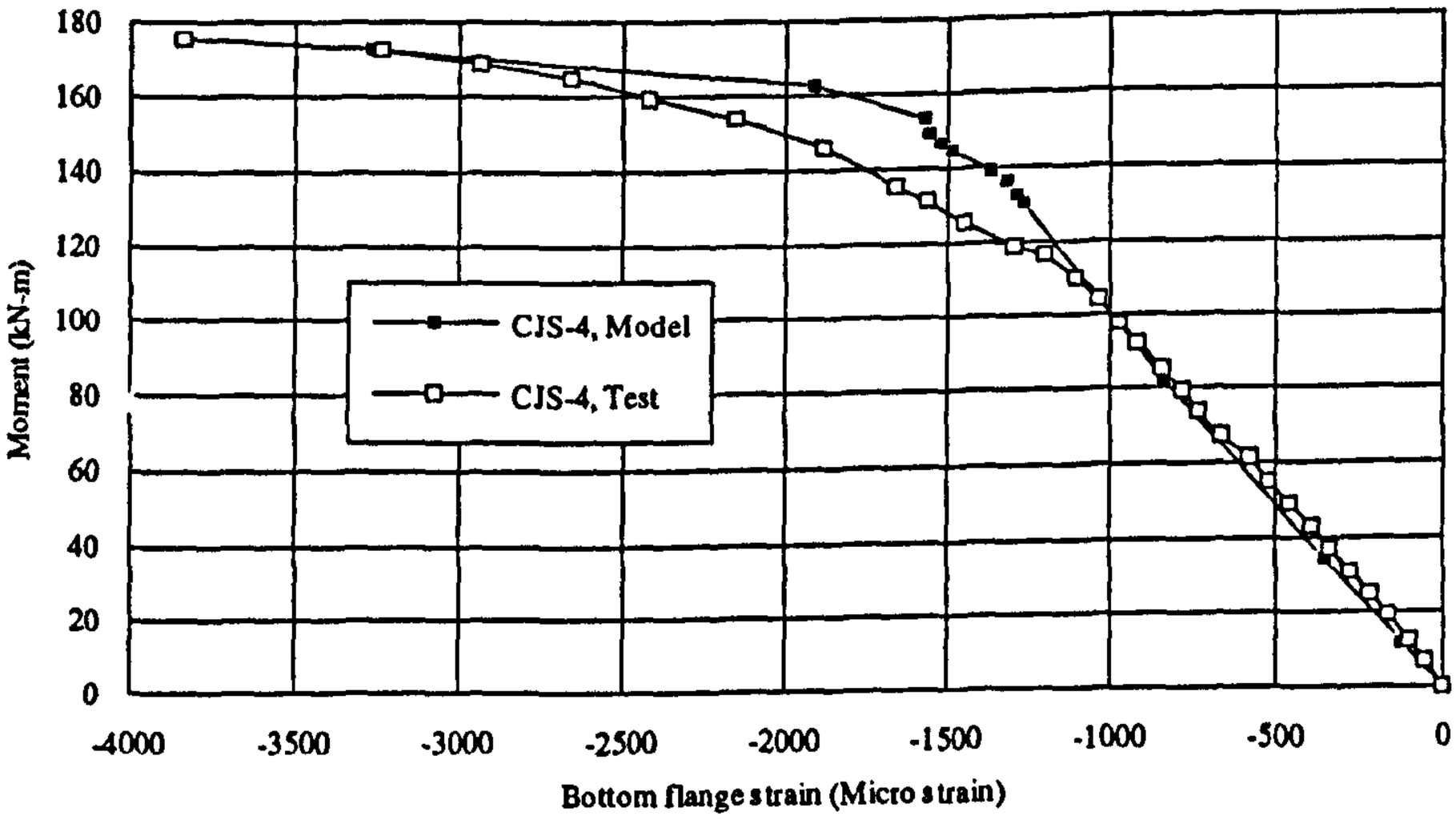

3-19 (b) Comparison of moment-bottom flange strain curves for CJS-4

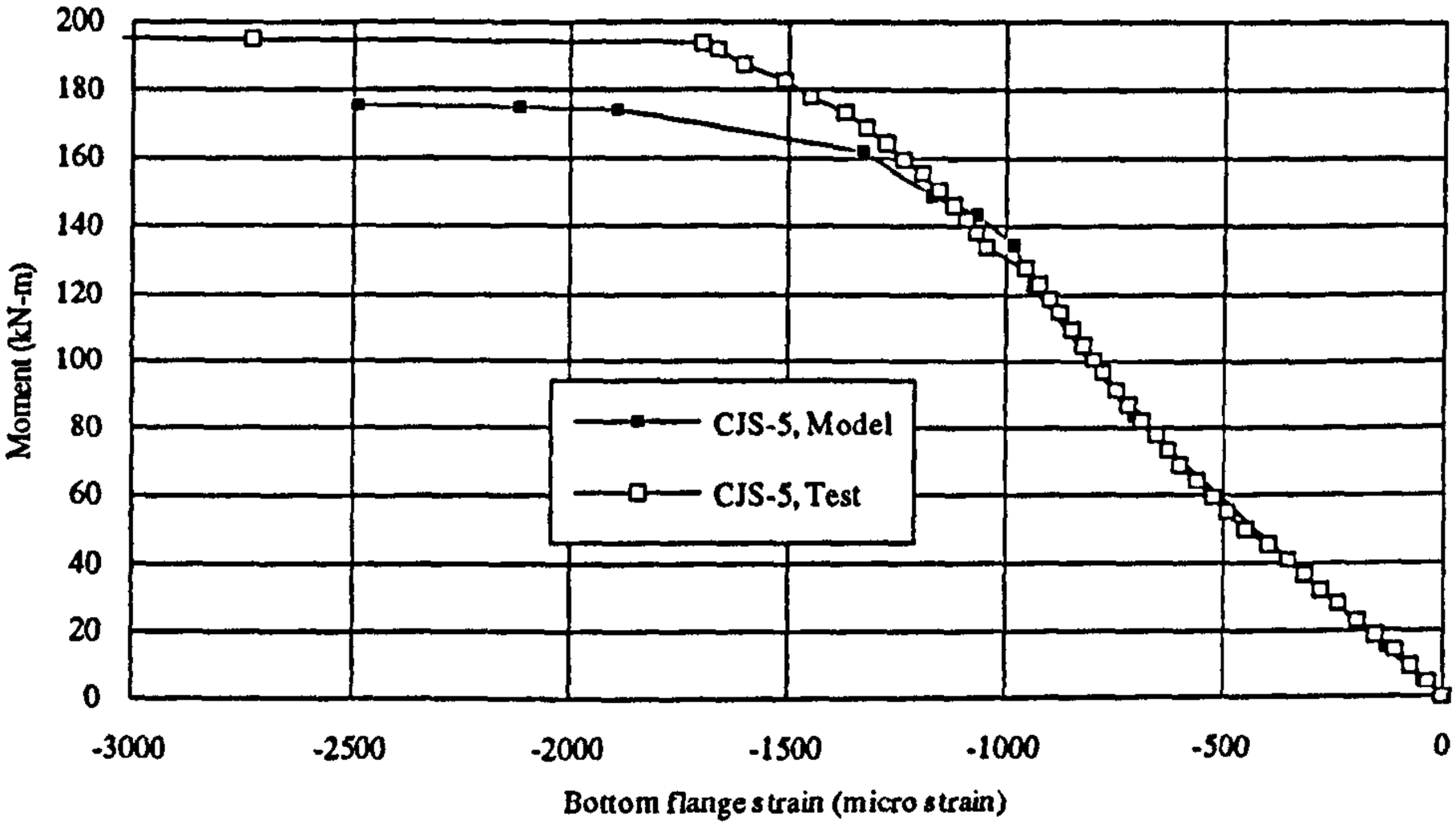

3-19 (c) Comparison of moment-bottom flange strain curves for CJS-5

Figure 3-19 Comparison of moment-bottom flange strain curves for test and model

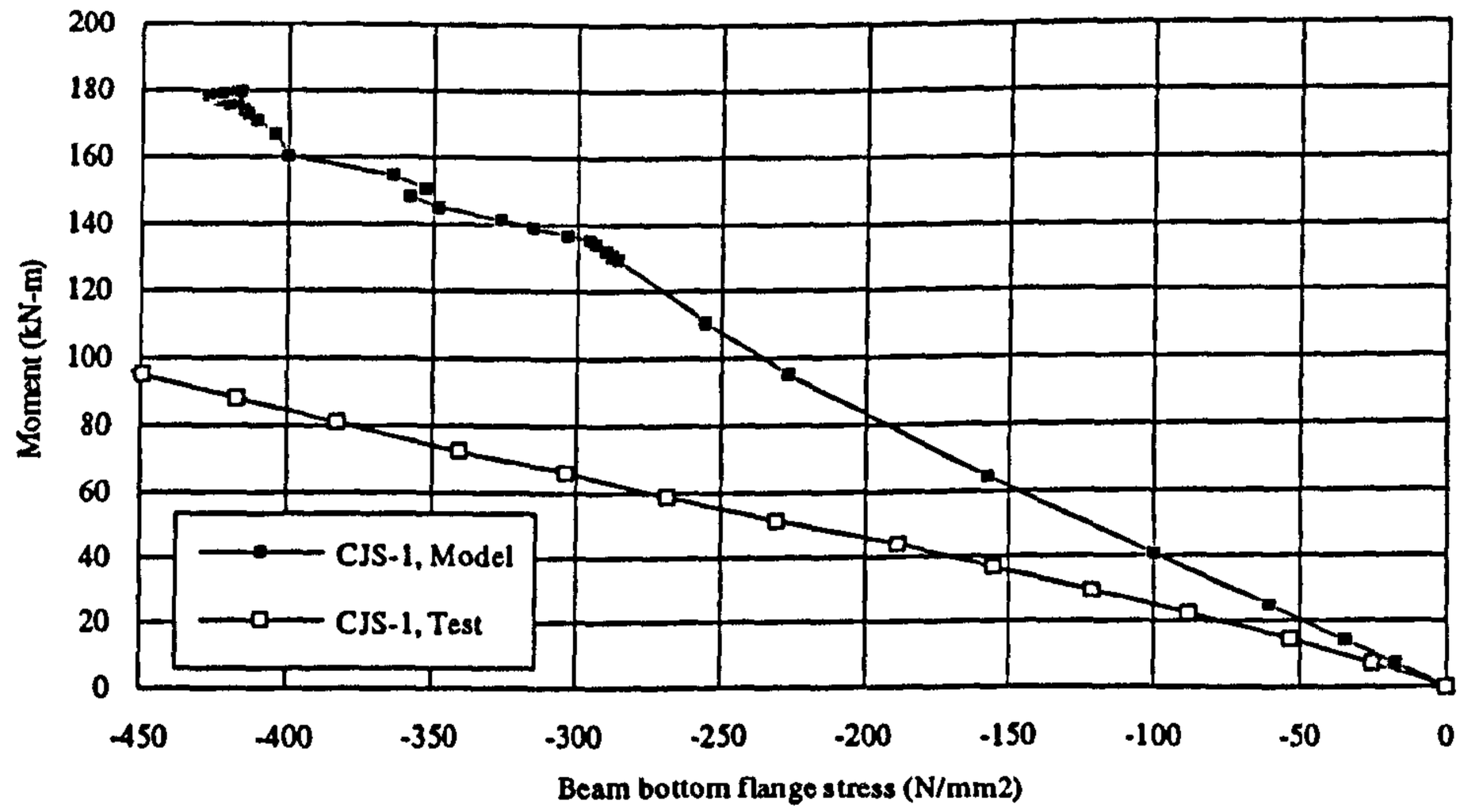

3-20 (a) Comparison of moment-bottom flange stress curves for CJS-1

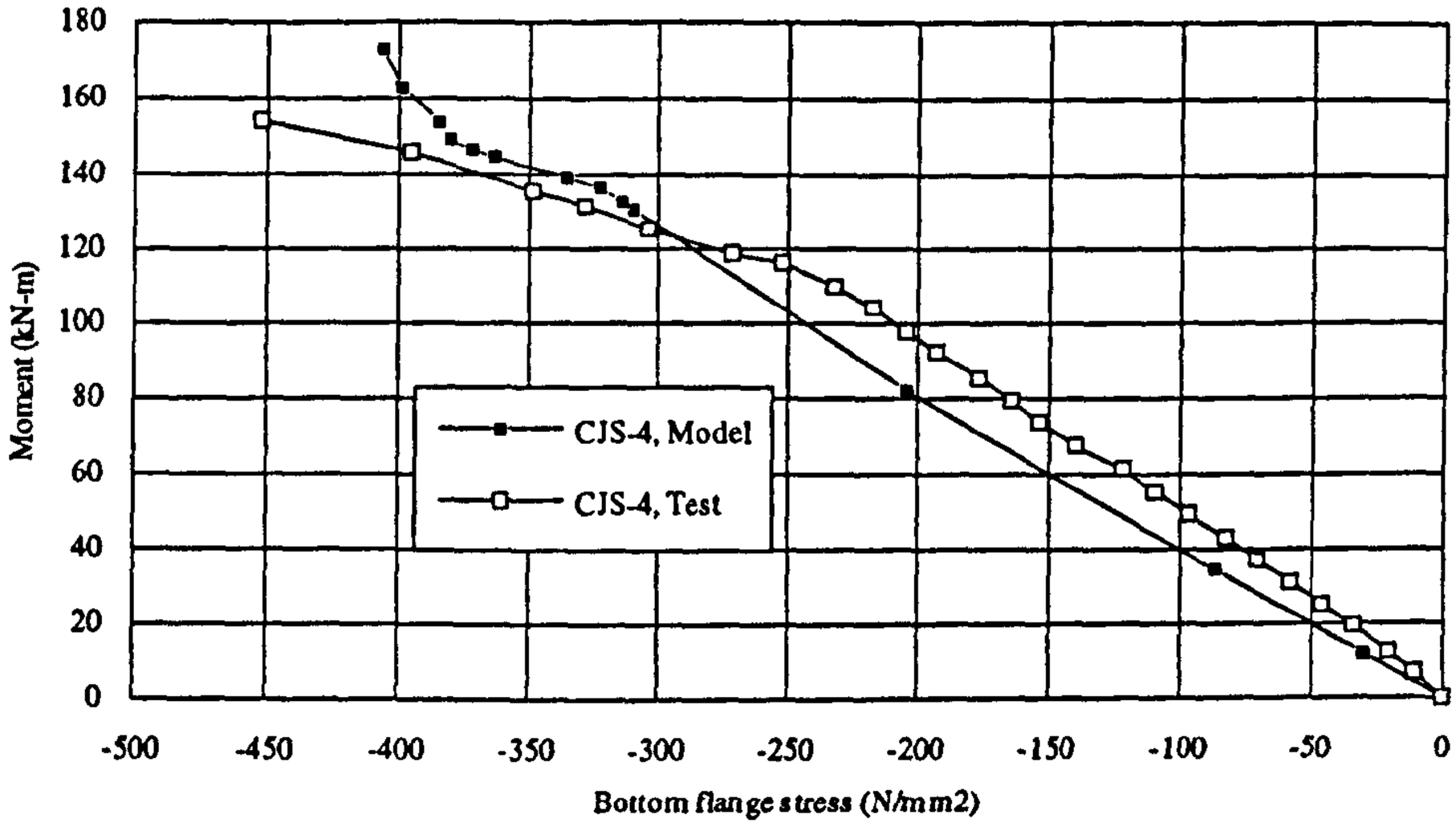

3-20 (b) Comparison of moment-bottom flange stress curves for CJS-4

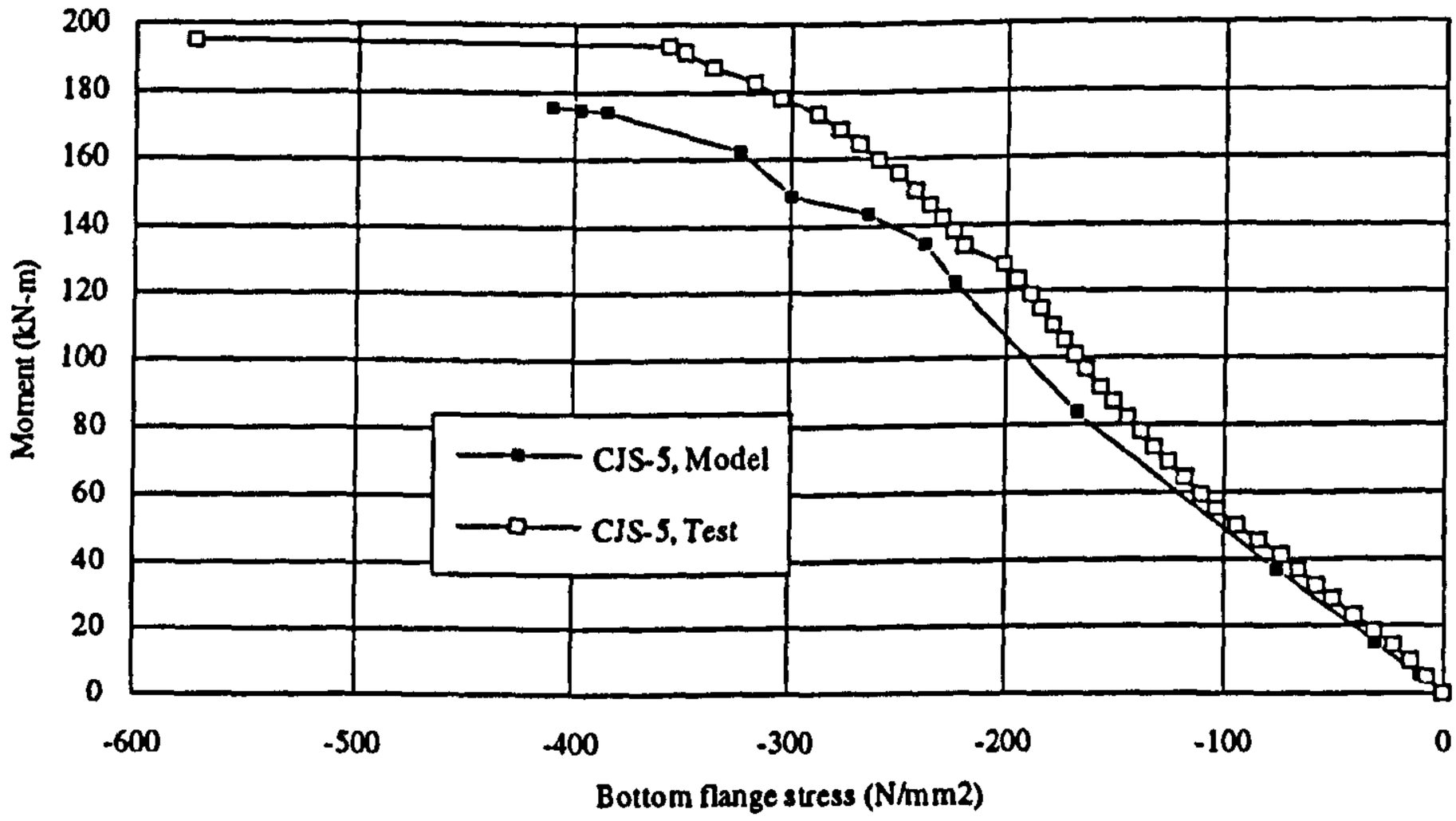

3-20 (c) Comparison of moment-bottom flange stress curves for CJS-5

Figure 3-20 Comparison of moment-bottom flange stress curves for test and model

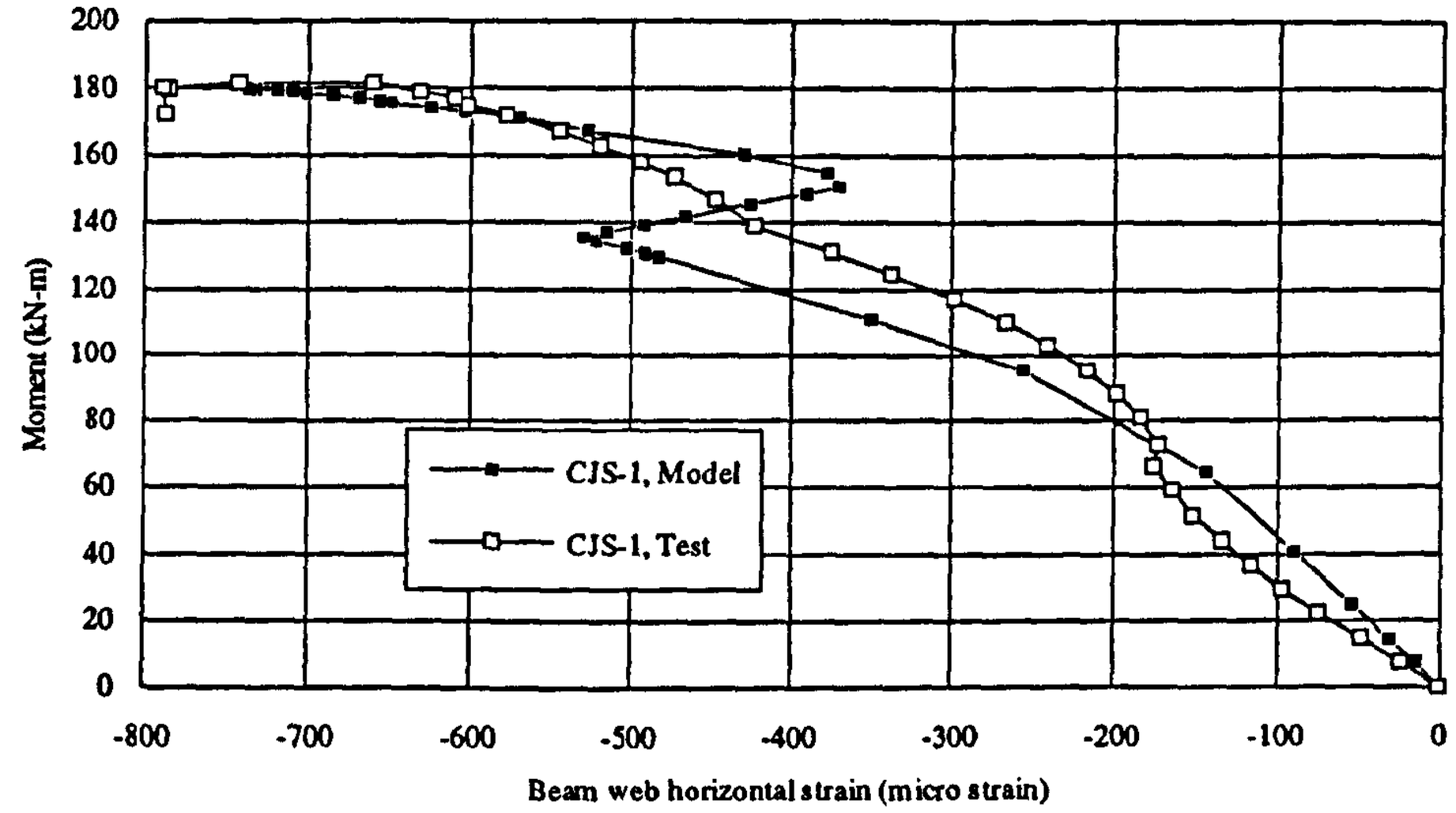

3-21 (a) Comparison of moment-beam web horizontal strain curves for CJS-1

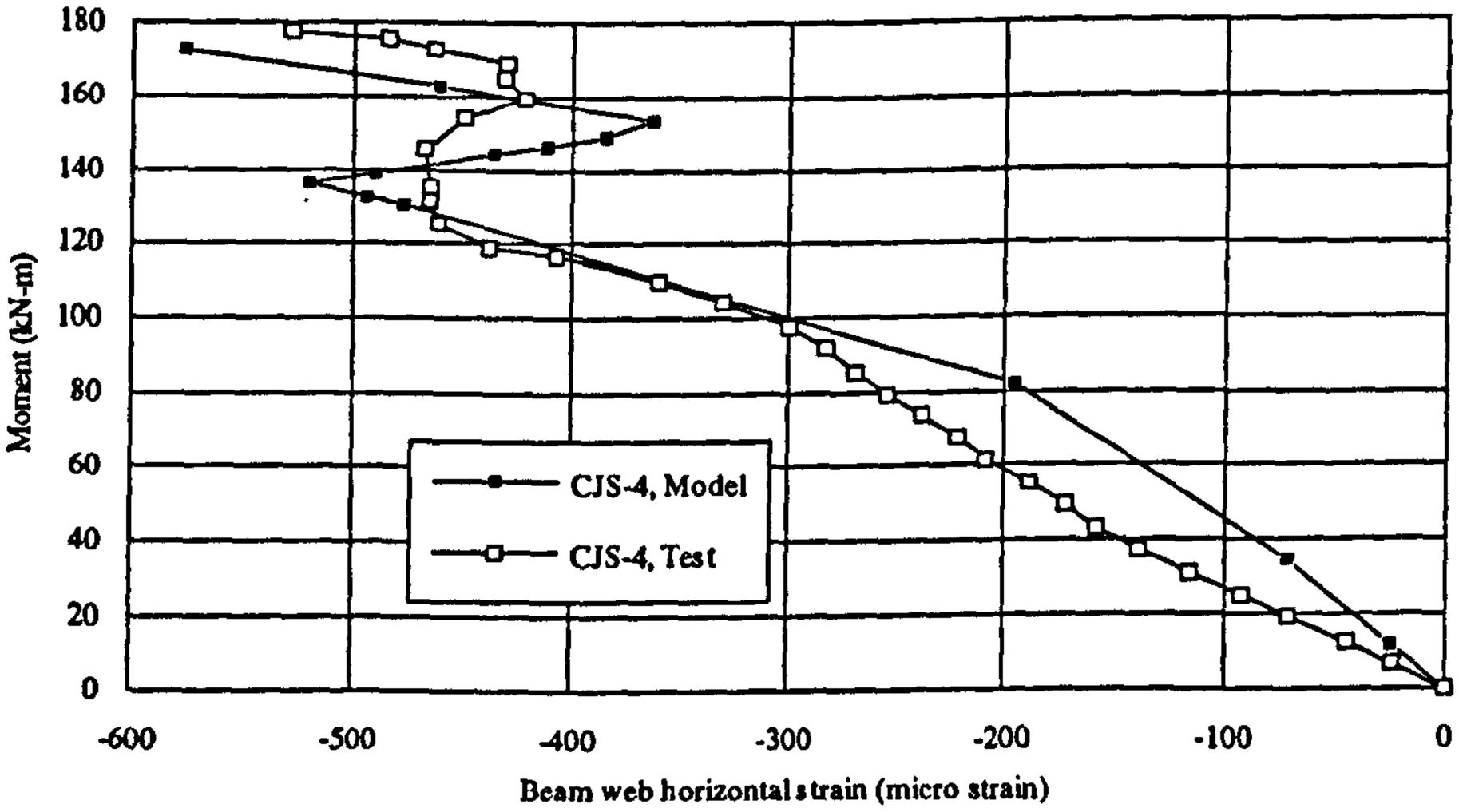

3-21 (b) Comparison of moment-beam web horizontal strain curves for CJS-4

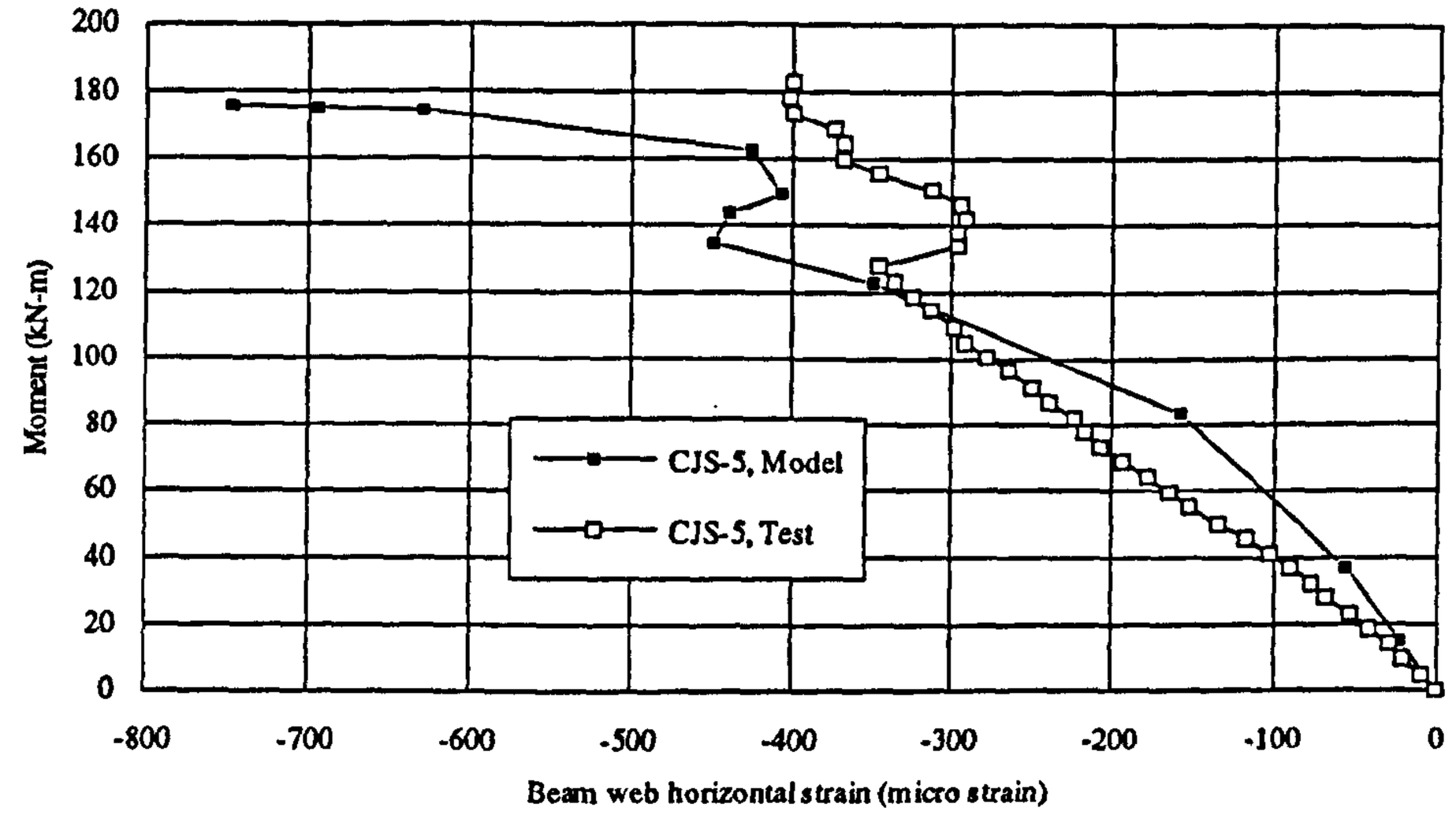

3-21 (c) Comparison of moment-beam web horizontal strain curves for CJS-5

Figure 3-21 Comparison of moment-beam web horizontal strain curves for test and model

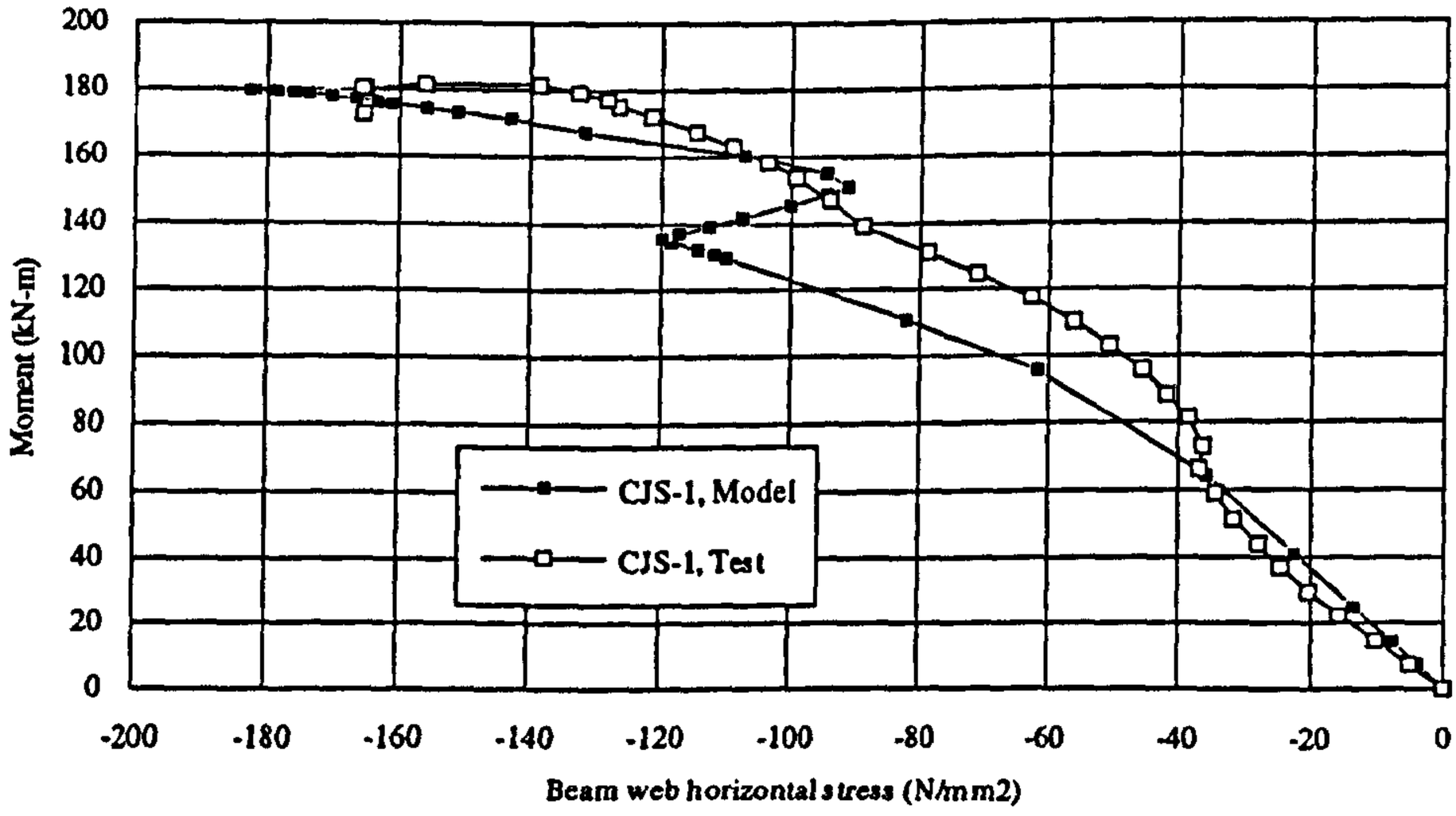

3-22 (a) Comparison of moment-beam web horizontal stress curves for CJS-1

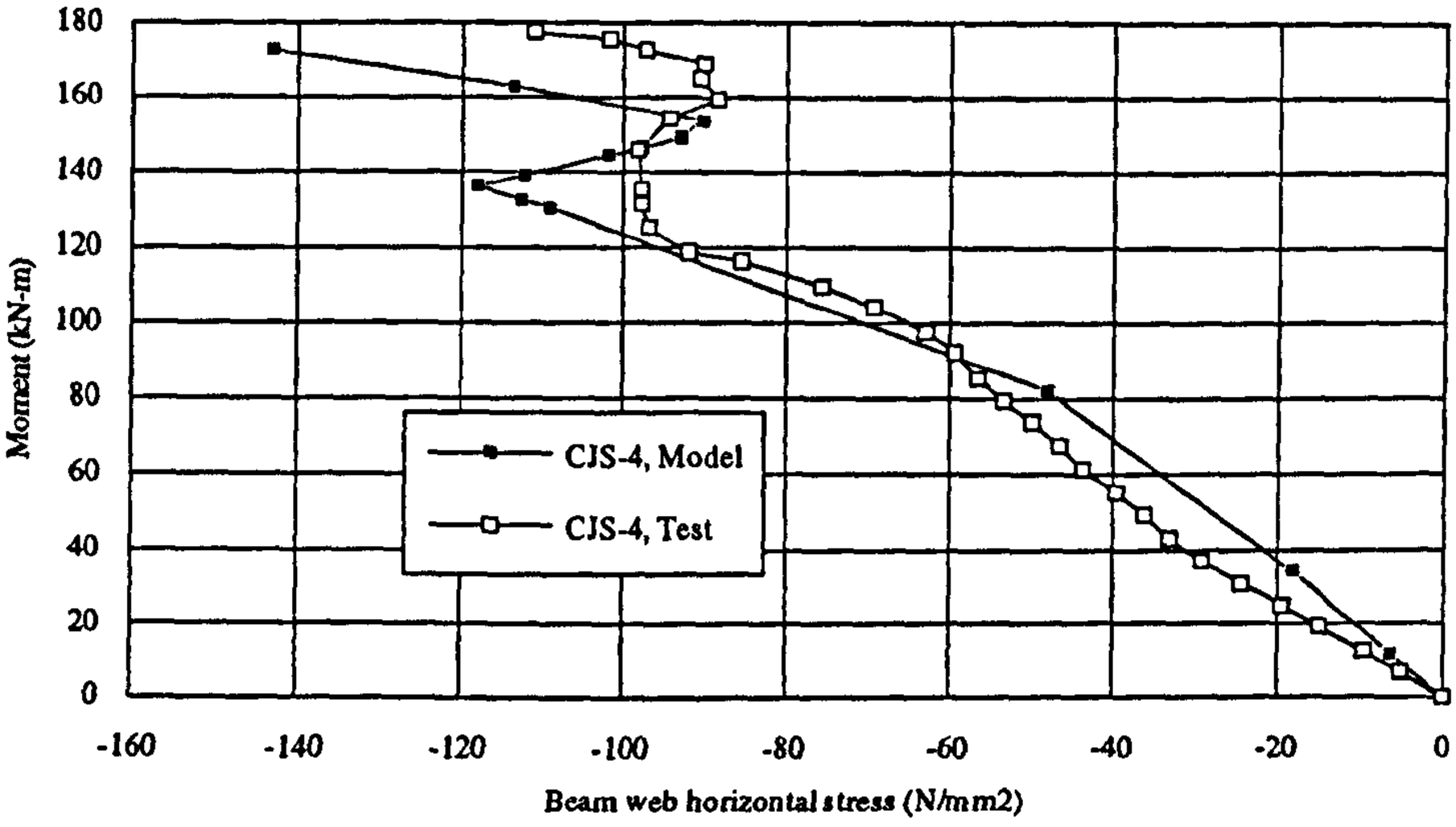

3-22 (b) Comparison of moment-beam web horizontal stress curves for CJS-4

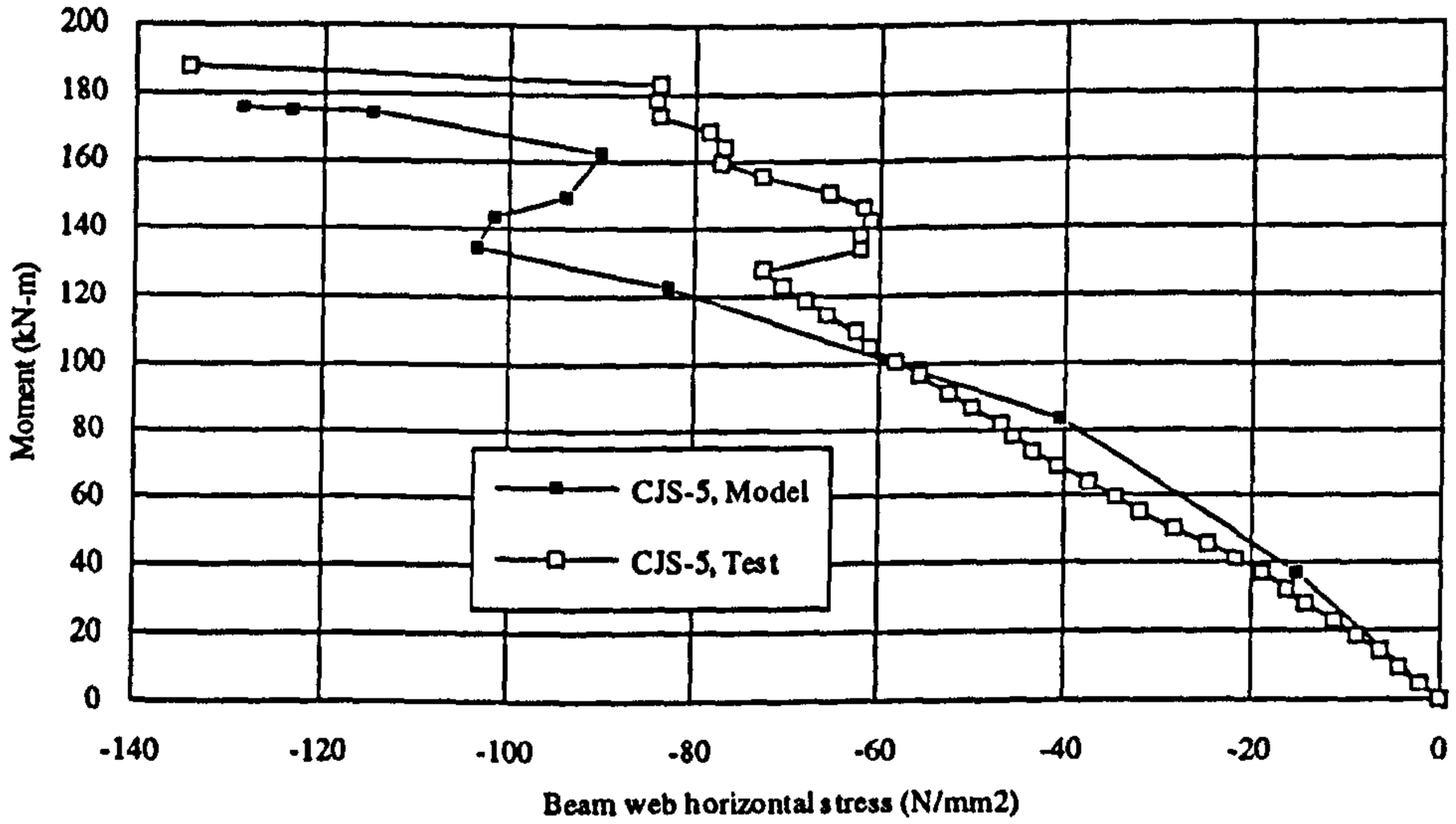

3-22 (c) Comparison of moment-beam web horizontal stress curves for CJS-5

Figure 3-22 Comparison of moment-beam web horizontal stress curves for test and model

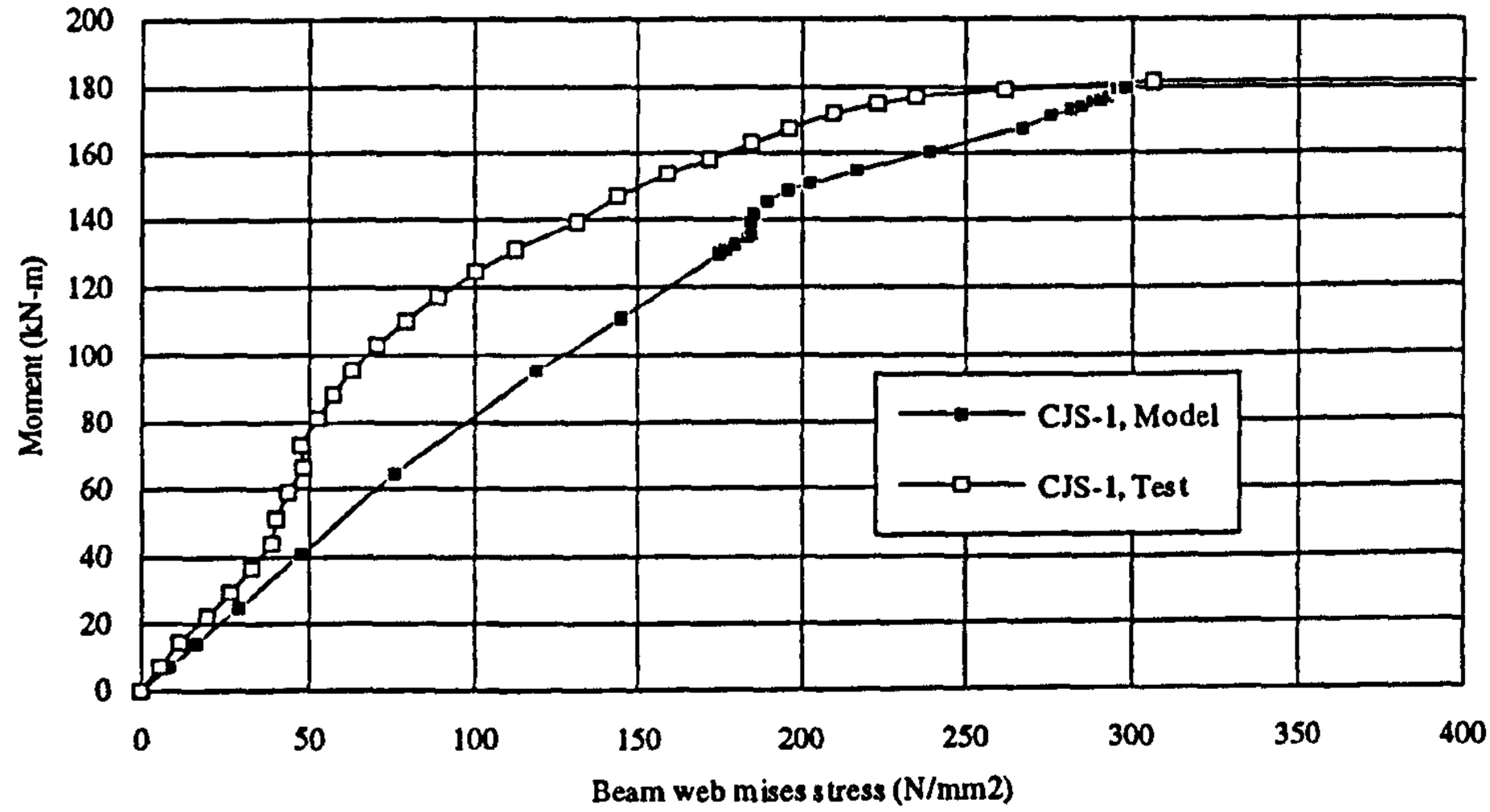

3-23 (a) Comparison of moment-beam web von-Mises stress curves for CJS-1

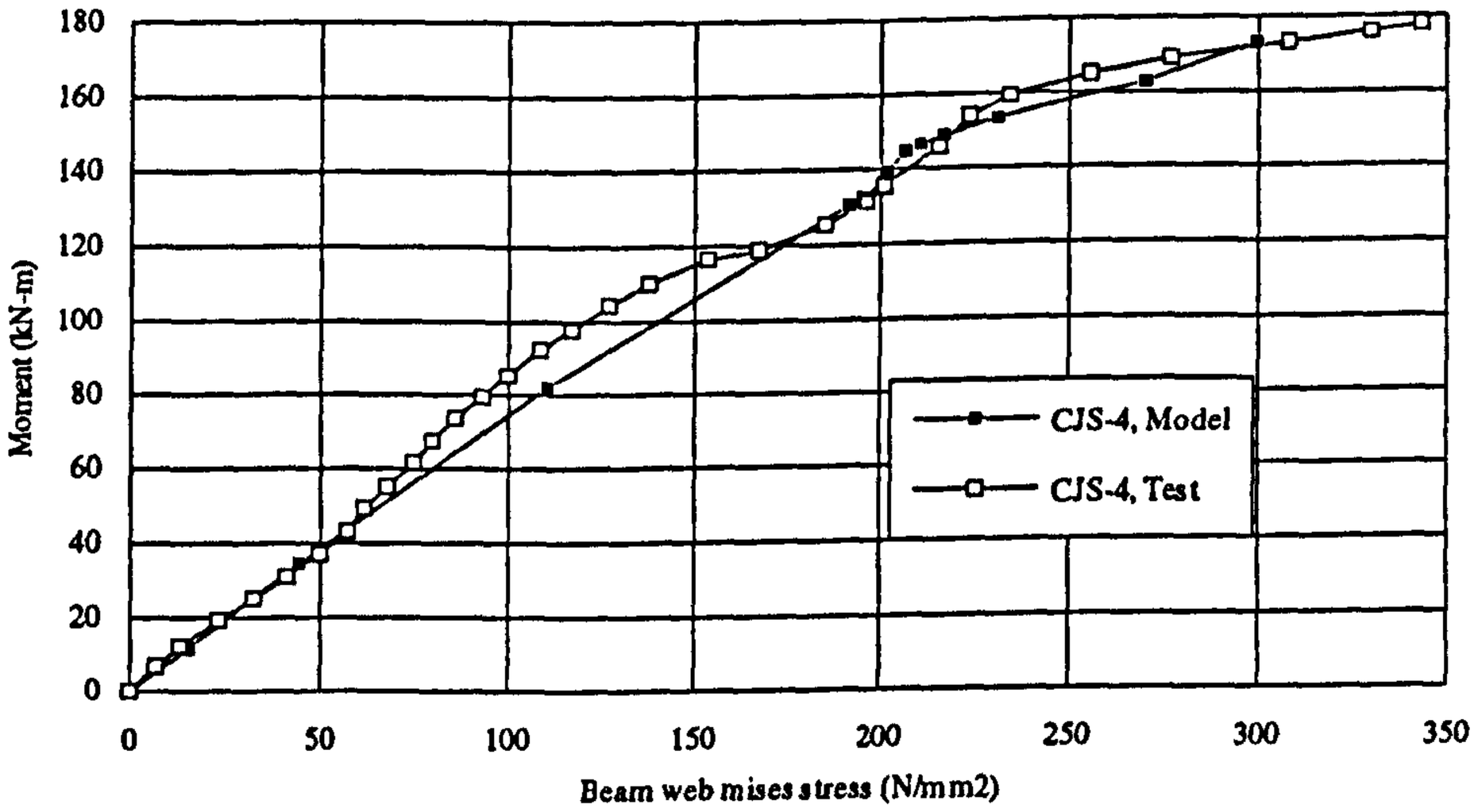

3-23 (b) Comparison of moment-beam web von-Mises stress curves for CJS-4

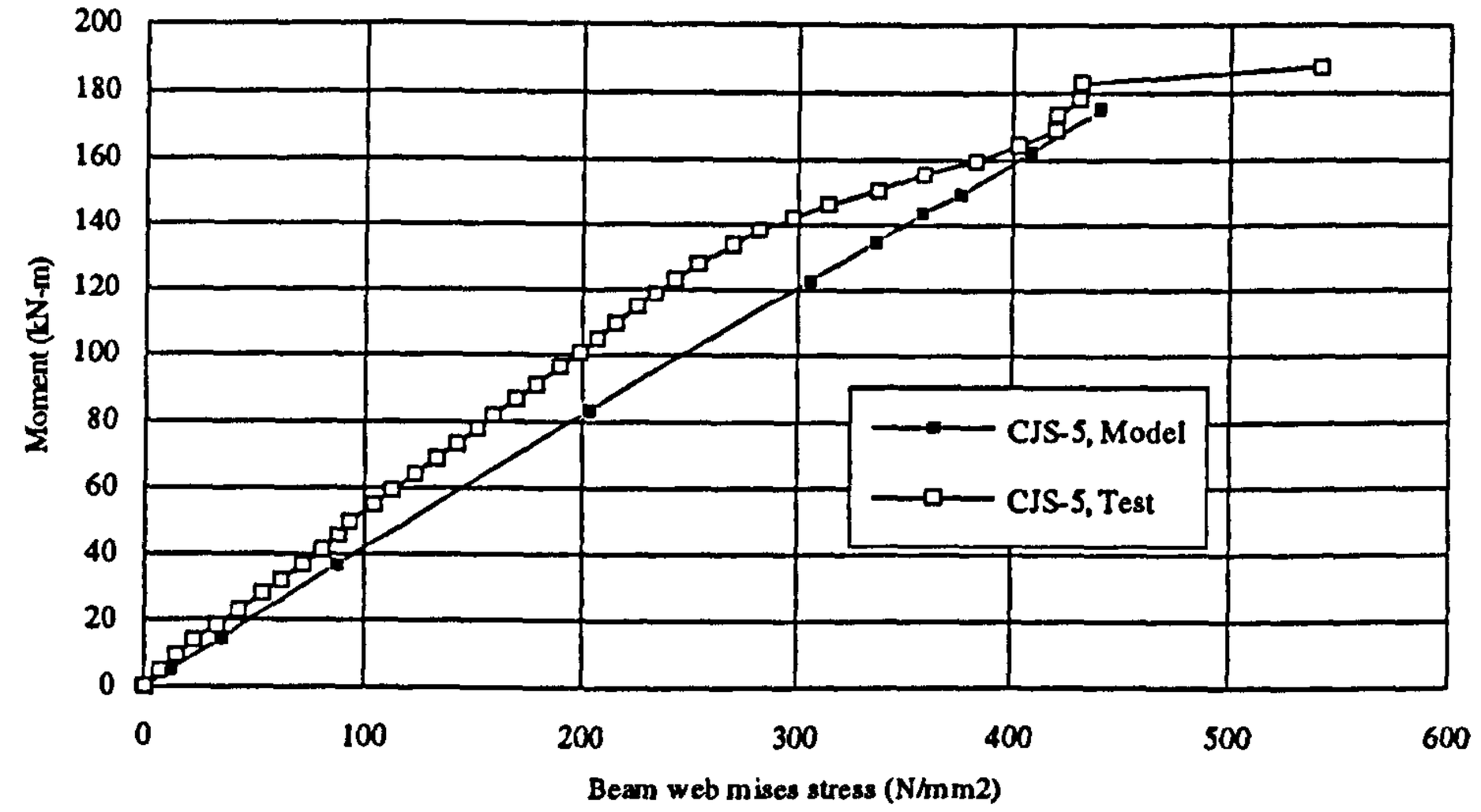

3-23 (c) Comparison of moment-beam web von-Mises stress curves for CJS-5

Figure 3-23 Comparison of moment-beam web von-Mises stress curves for test and model

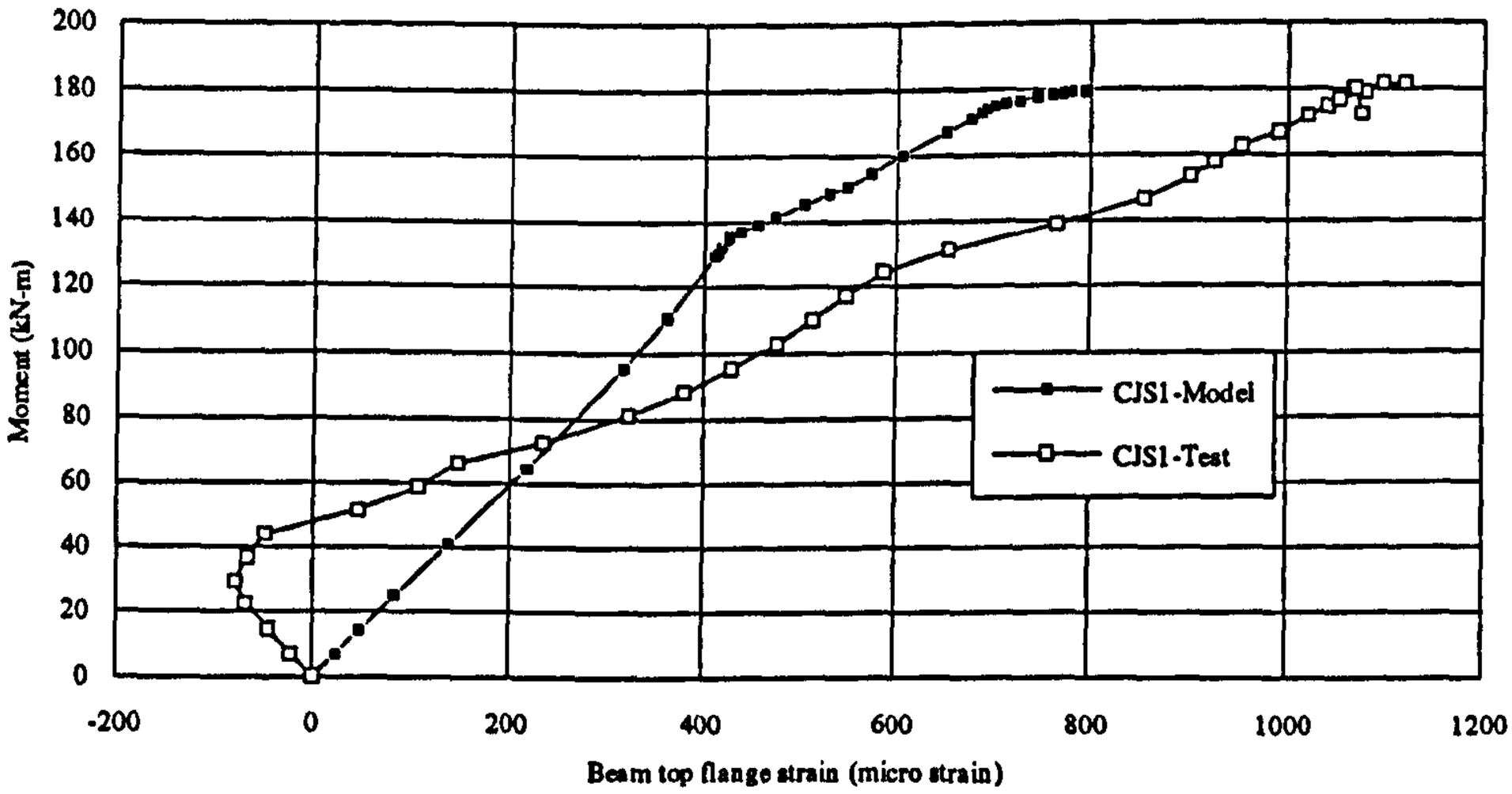

3-24 (a) Comparison of moment-beam top flange horizontal strain curves for CJS-1

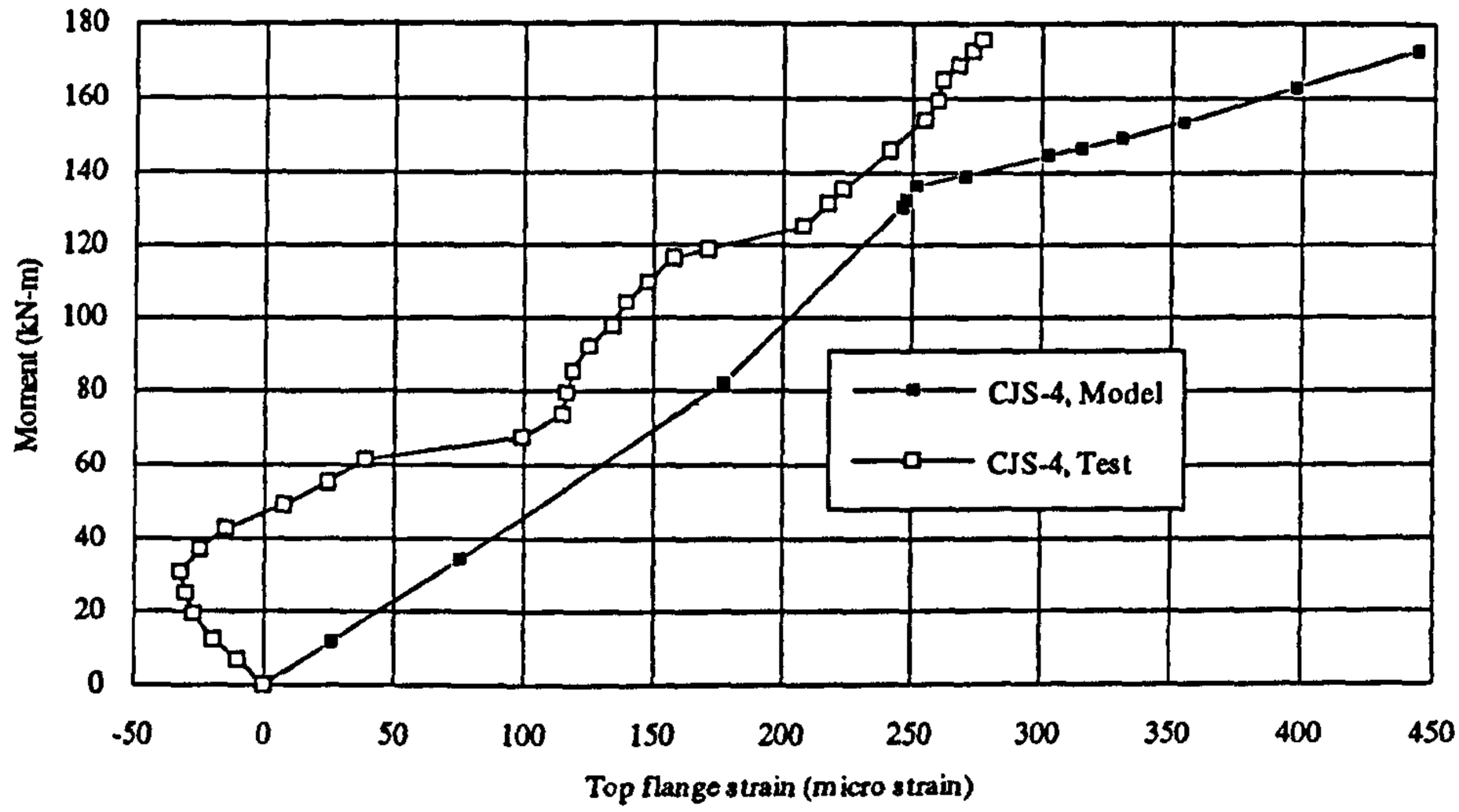

3-24 (b) Comparison of moment-beam top flange horizontal strain curves for CJS-4

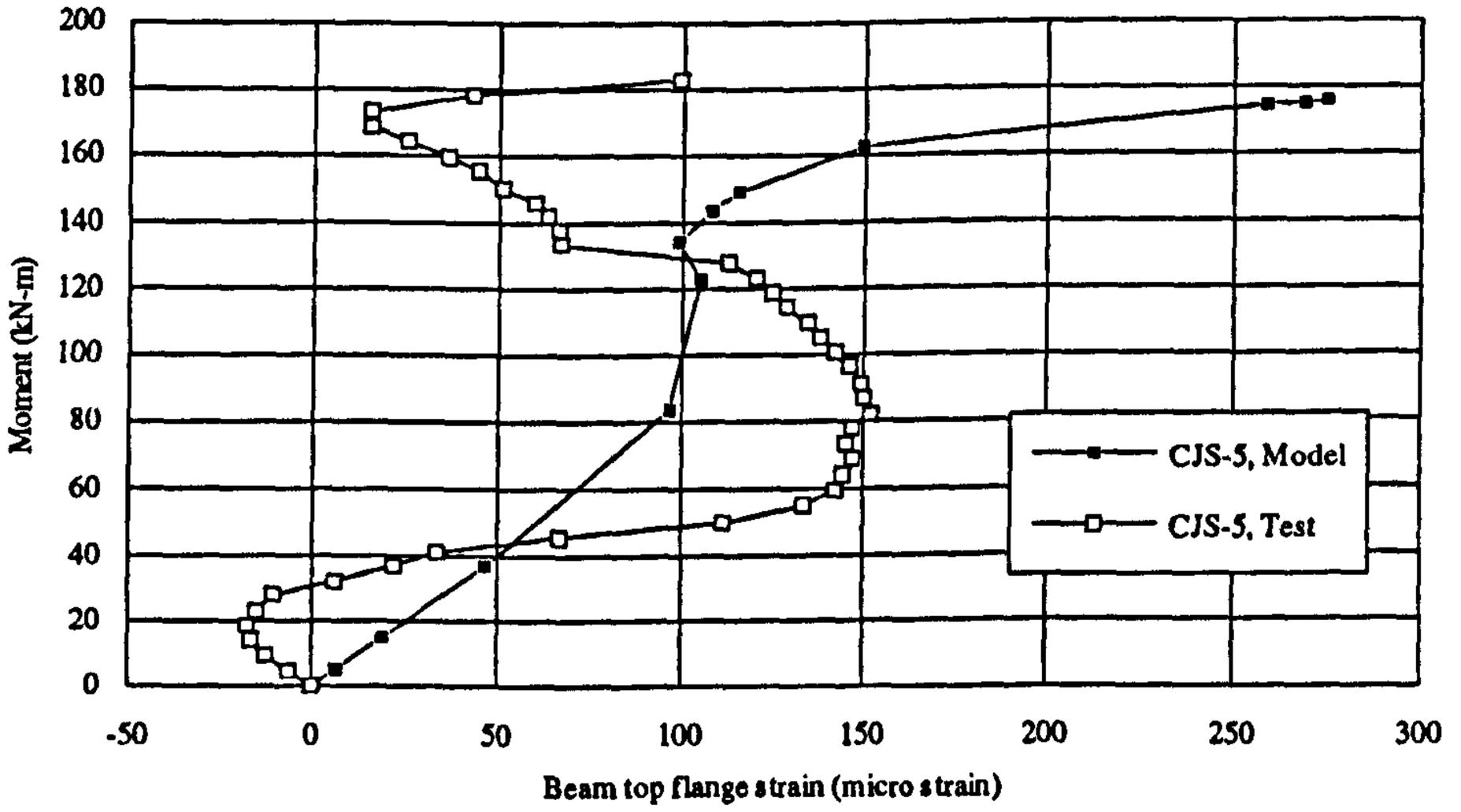

3-24 (c) Comparison of moment-beam top flange horizontal strain curves for CJS-5

Figure 3-24 Comparison of moment-top flange strain curves for test and model

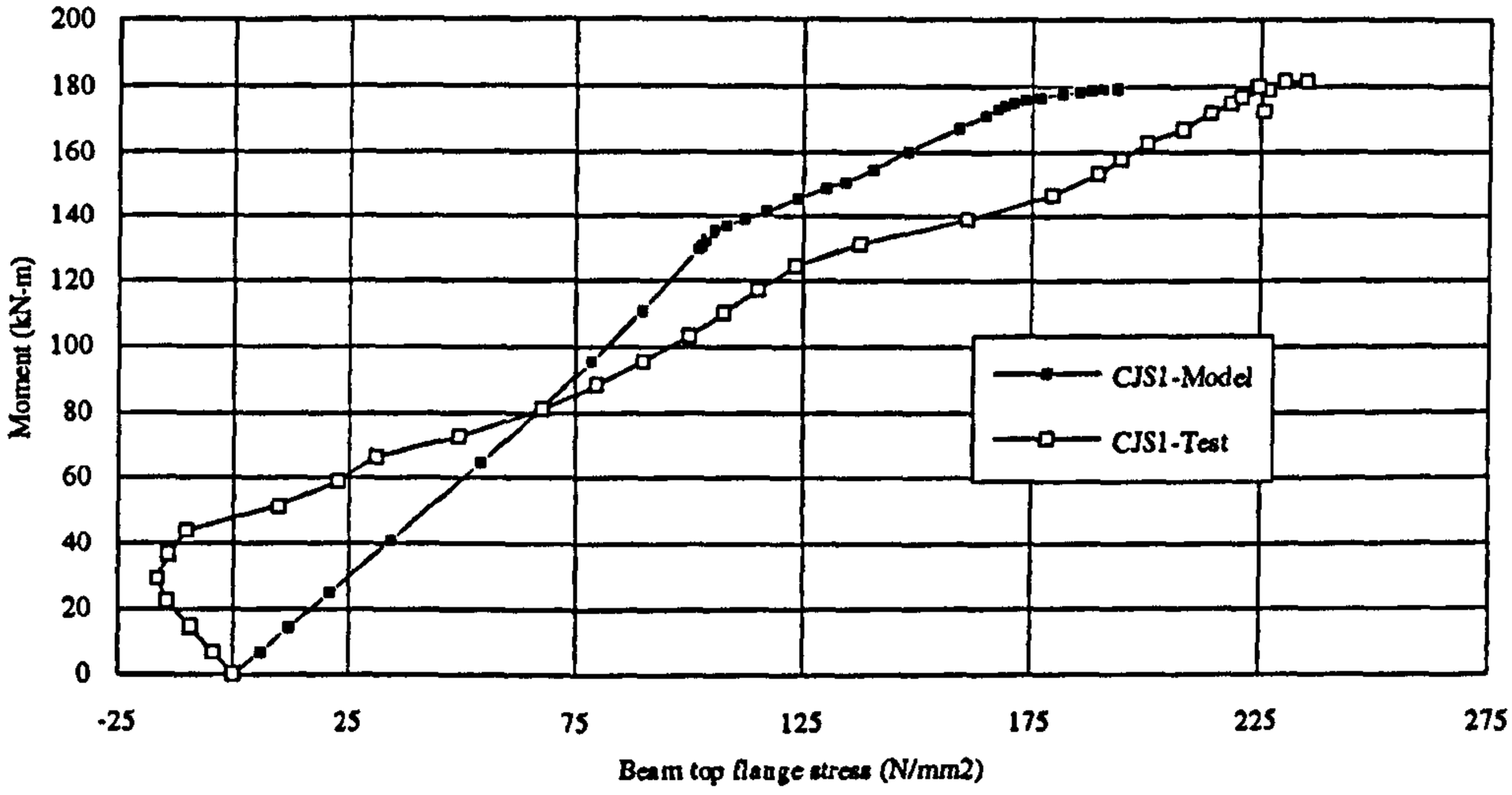

3-25 (a) Comparison of moment-beam top flange horizontal stress curves for CJS-1

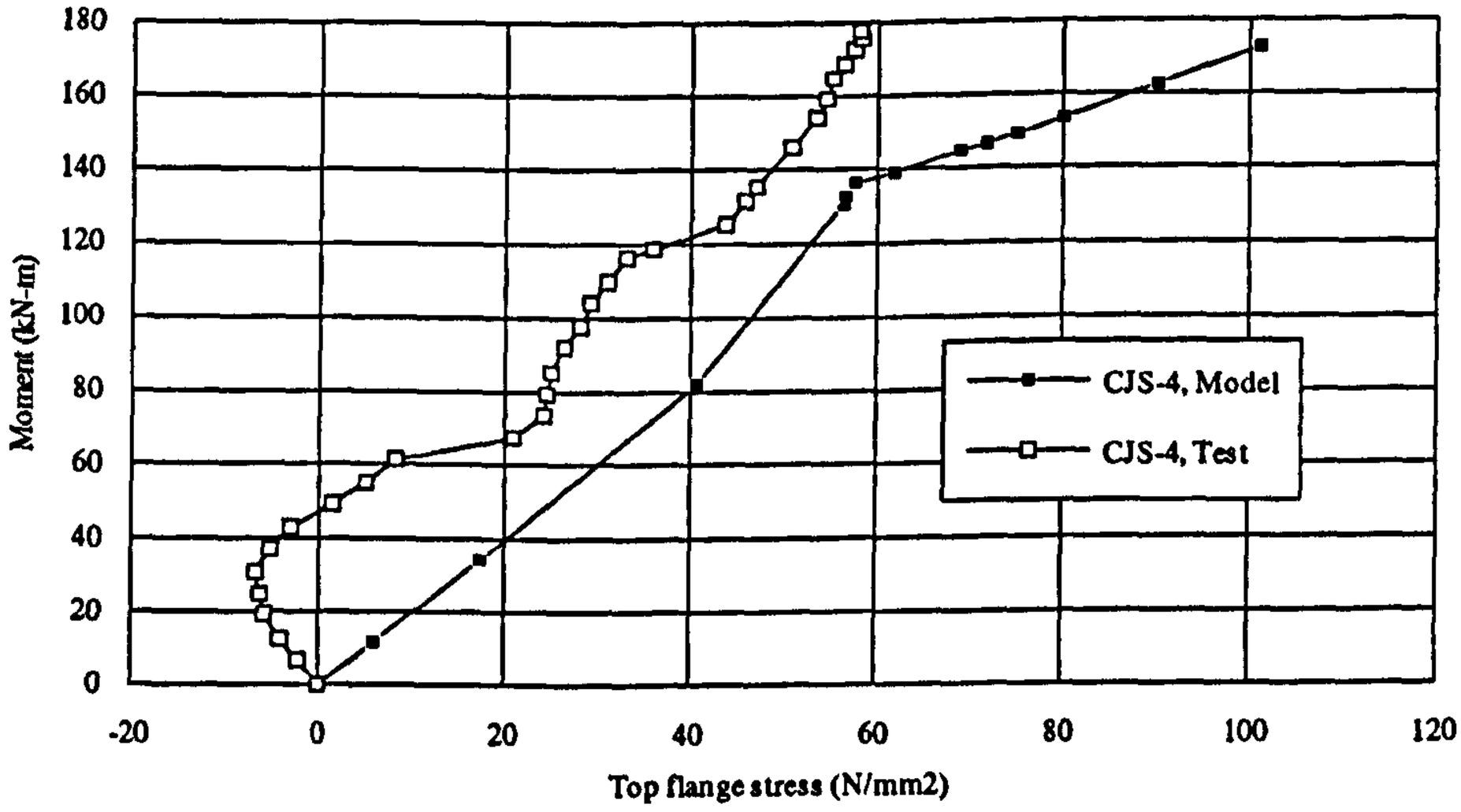

3-25 (b) Comparison of moment-beam top flange horizontal stress curves for CJS-4

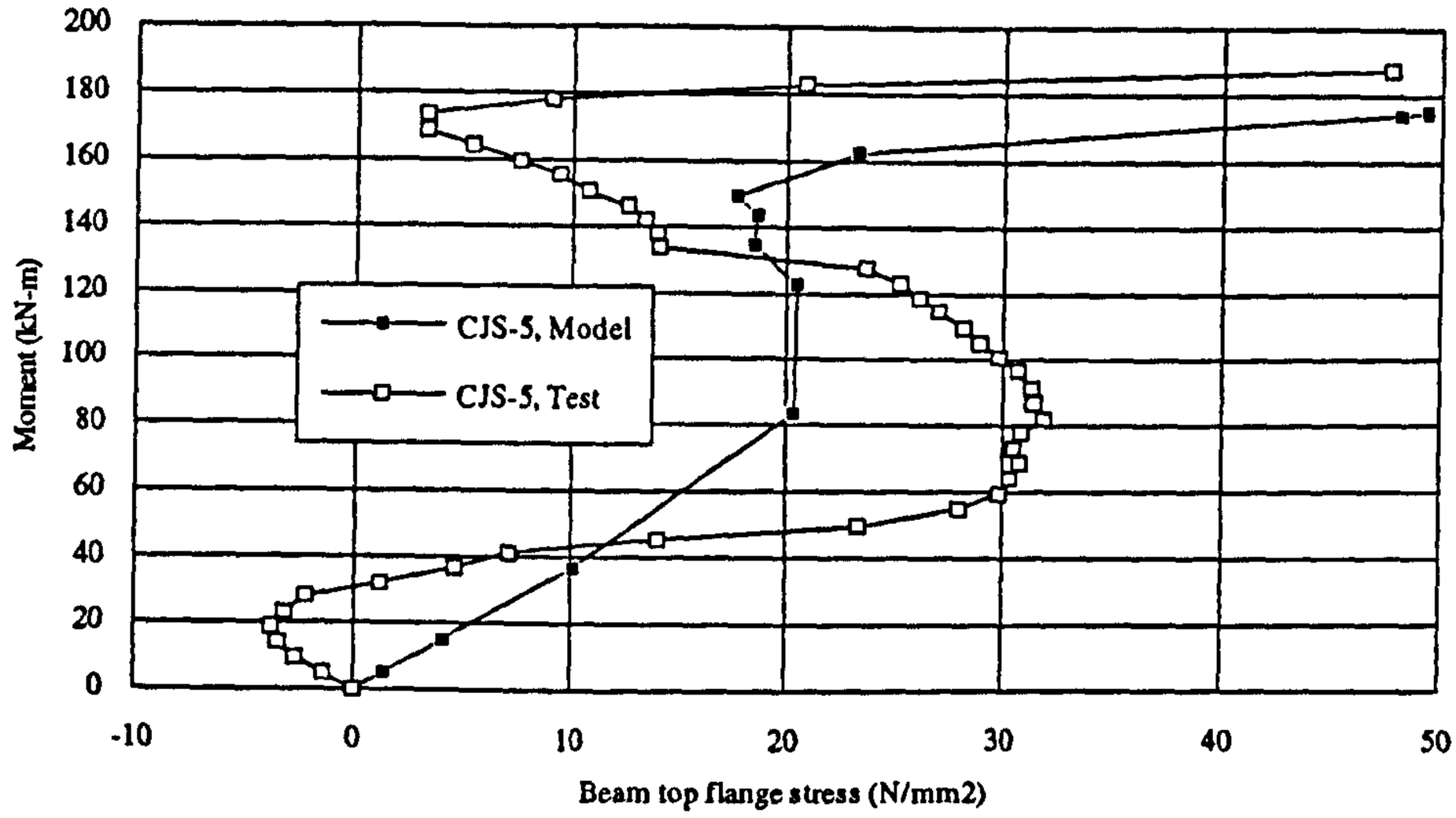

3-25 (c) Comparison of moment-beam top flange horizontal stress curves for CJS-5

Figure 3-25 Comparison of moment-top flange stress curves for test and model

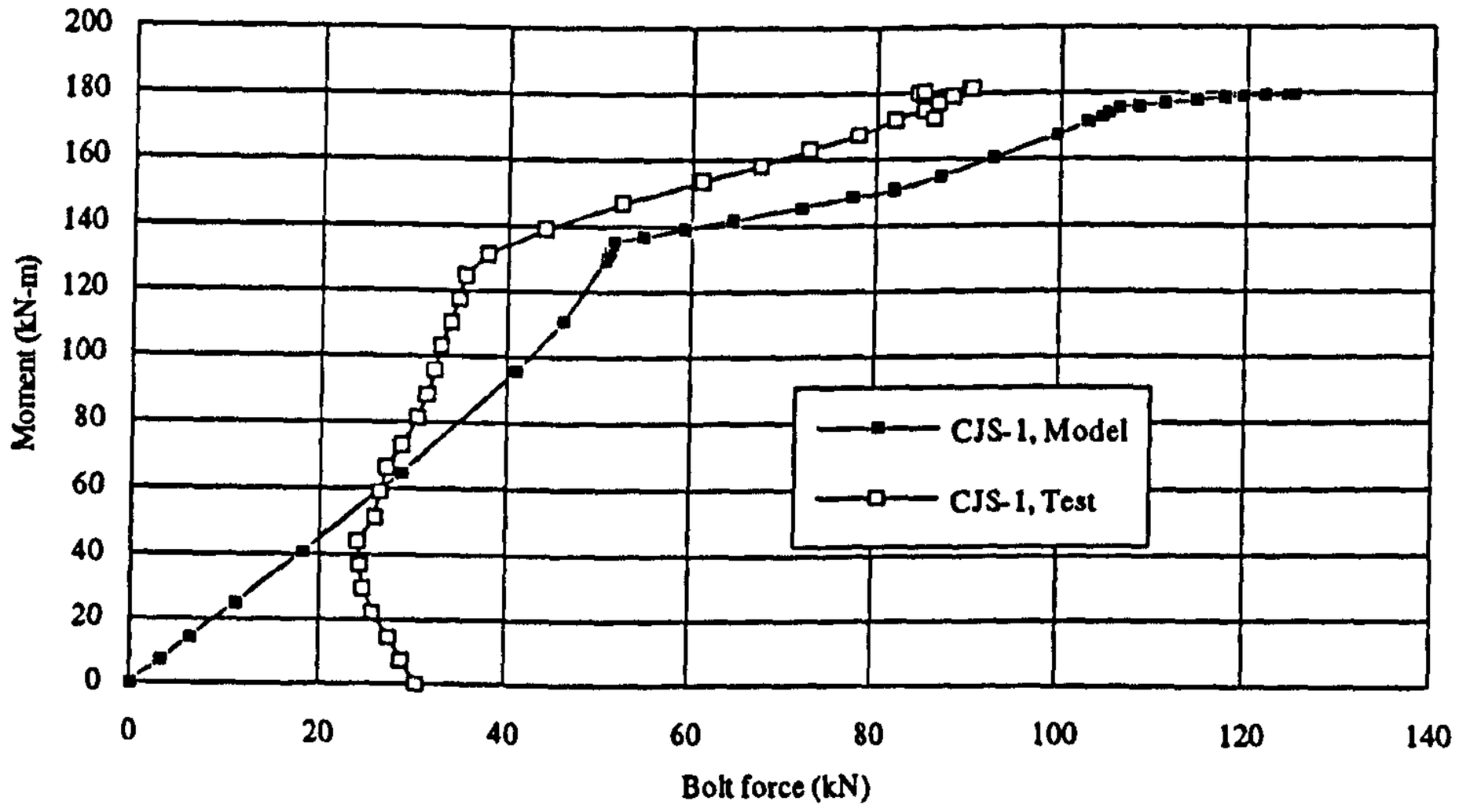

3-26 (a) Comparison of moment-bolt force curves for CJS-1

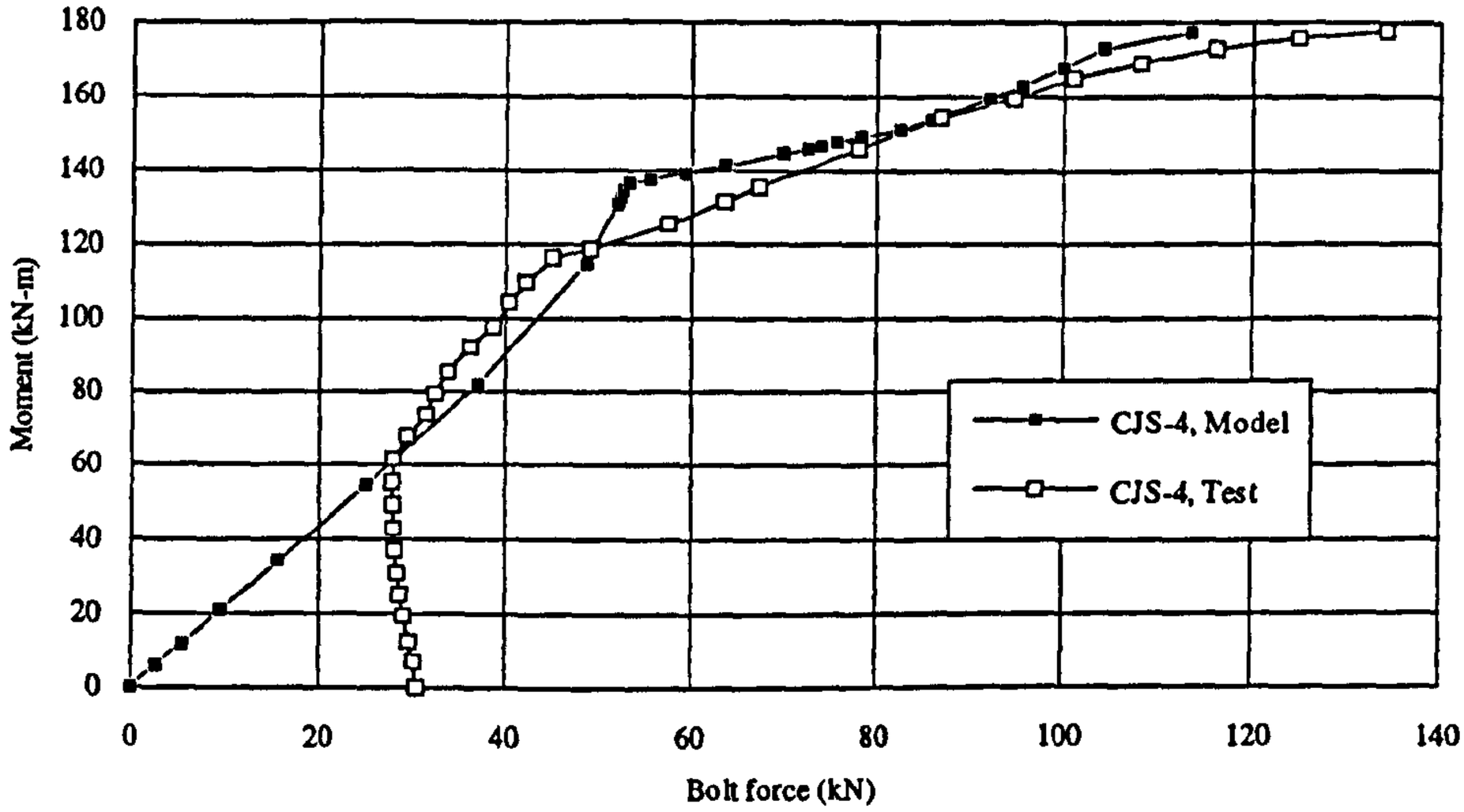

3-26 (b) Comparison of moment-bolt force curves for CJS-4

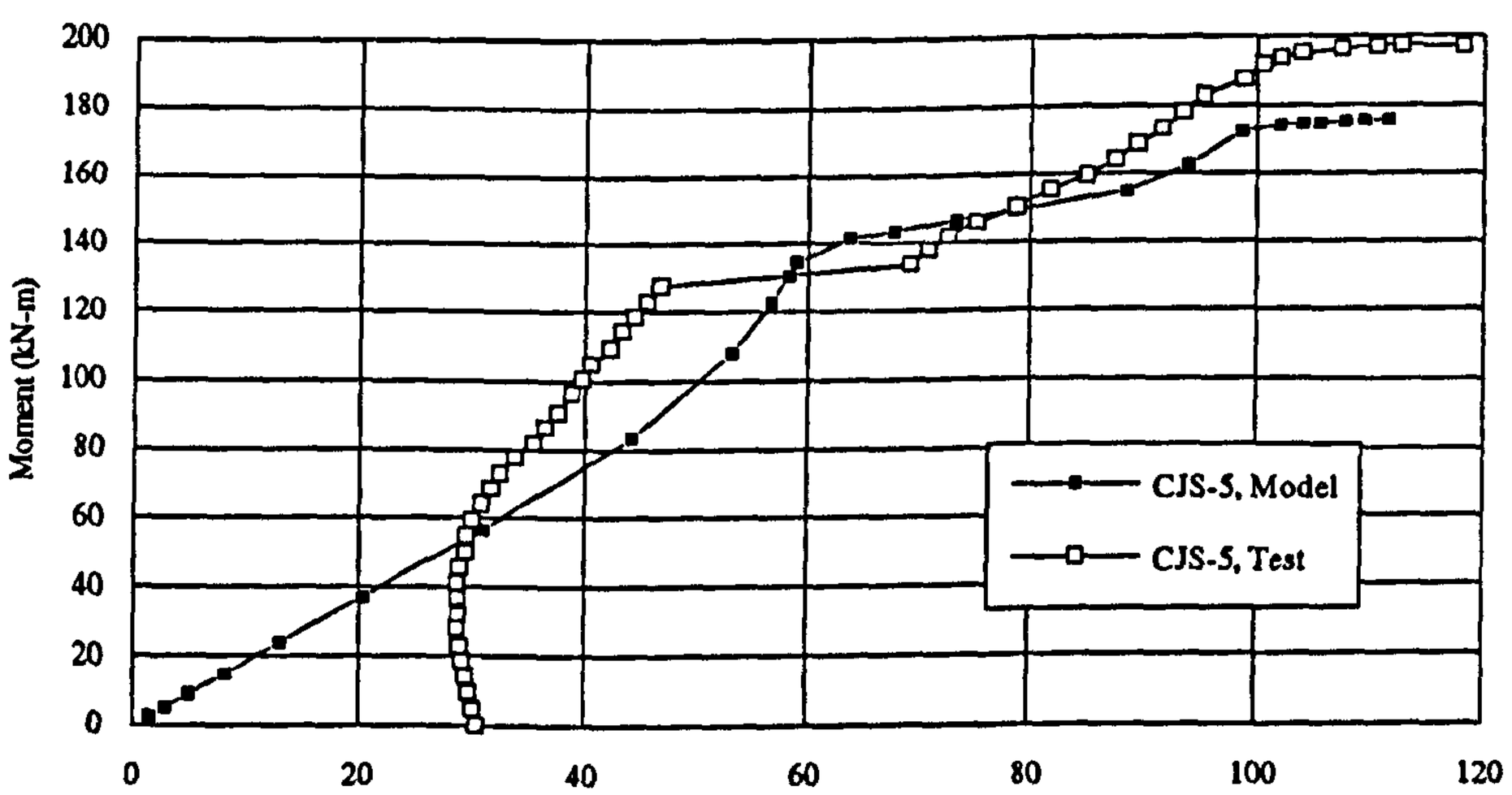

3-26 (c) Comparison of moment-bolt force curves for CJS-5

Figure 3-26 Comparison of moment-bolt force curves for test and model

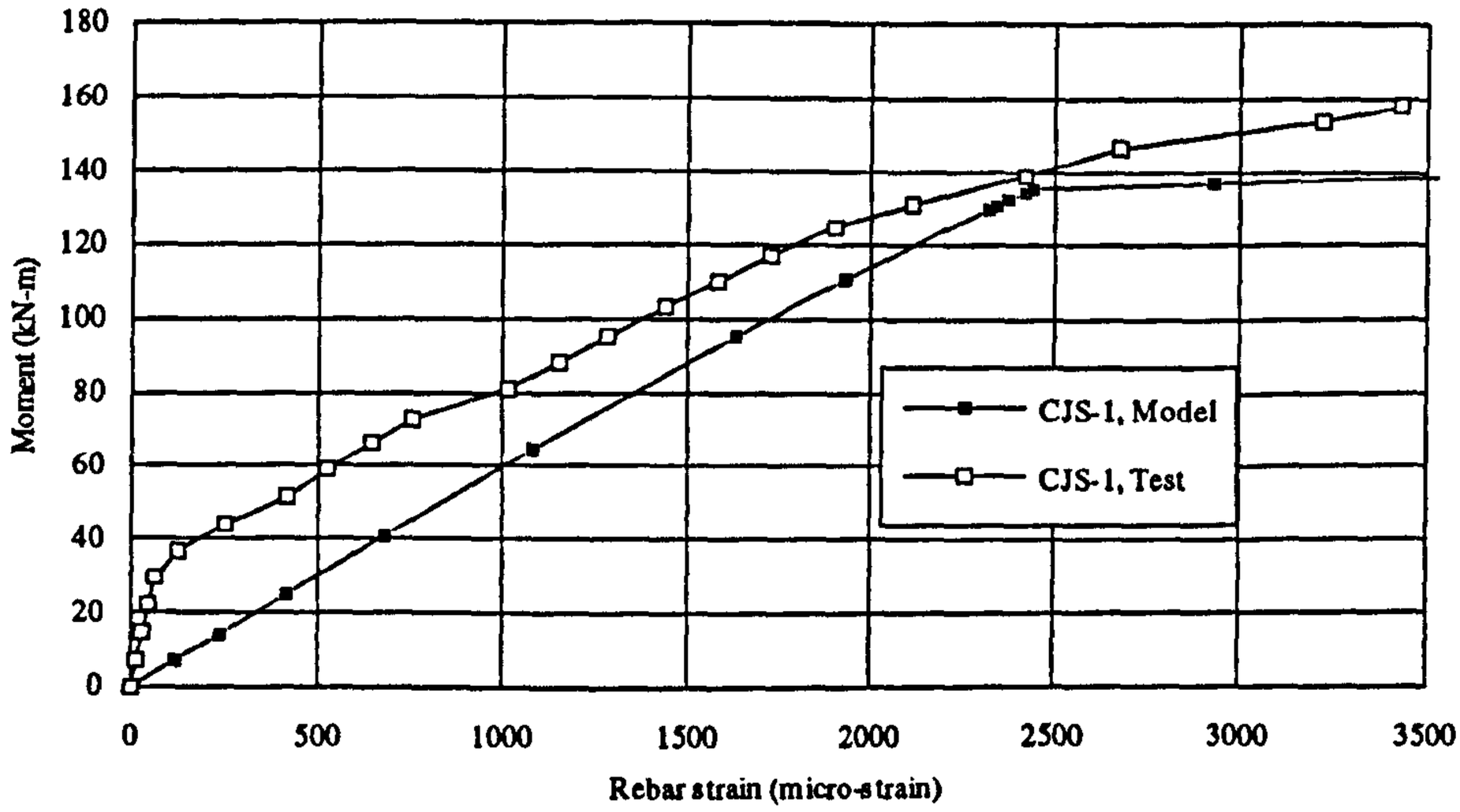

3-27 (a) Comparison of moment-rebar strain curves for CJS-1

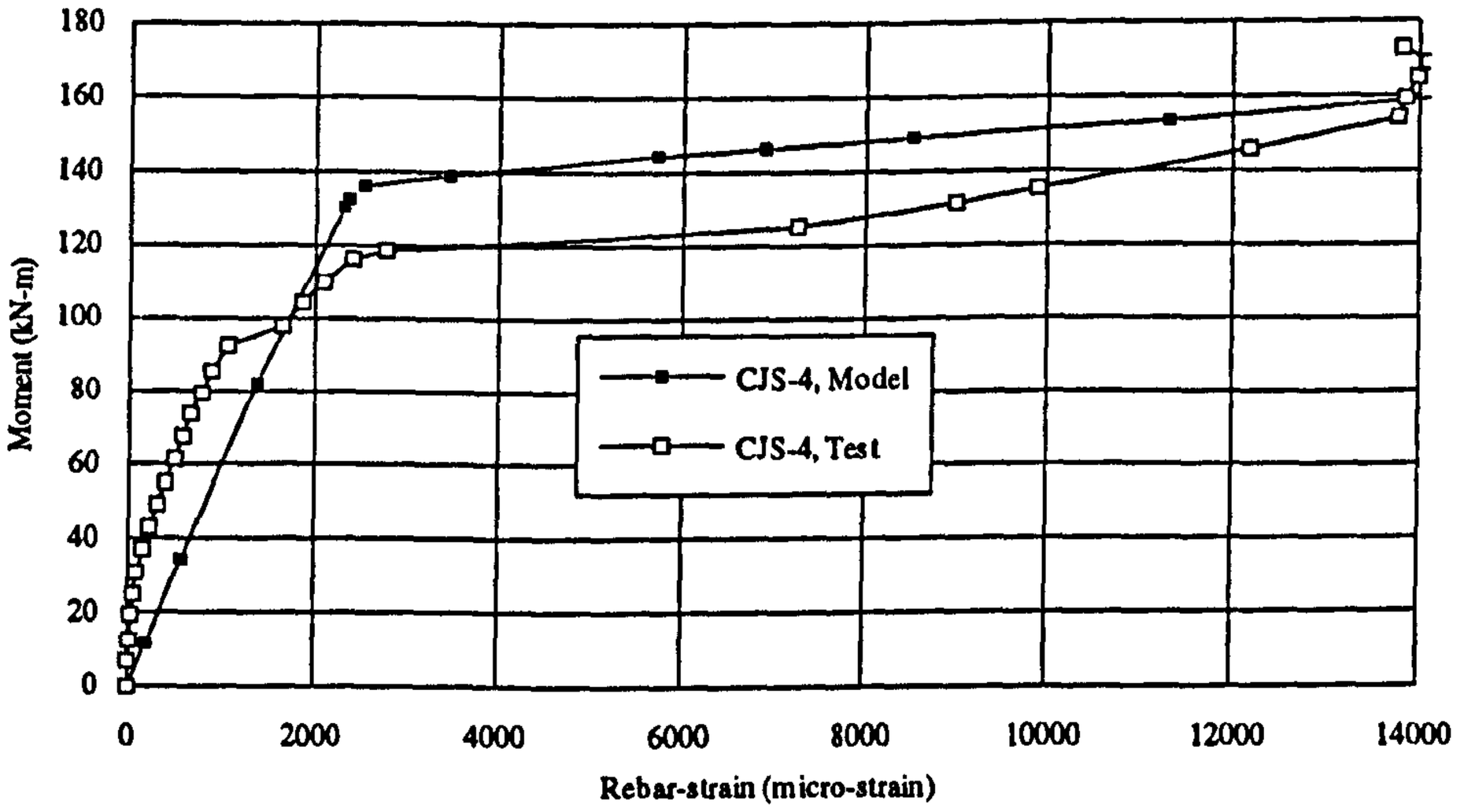

3-27 (b) Comparison of moment-rebar strain curves for CJS-4

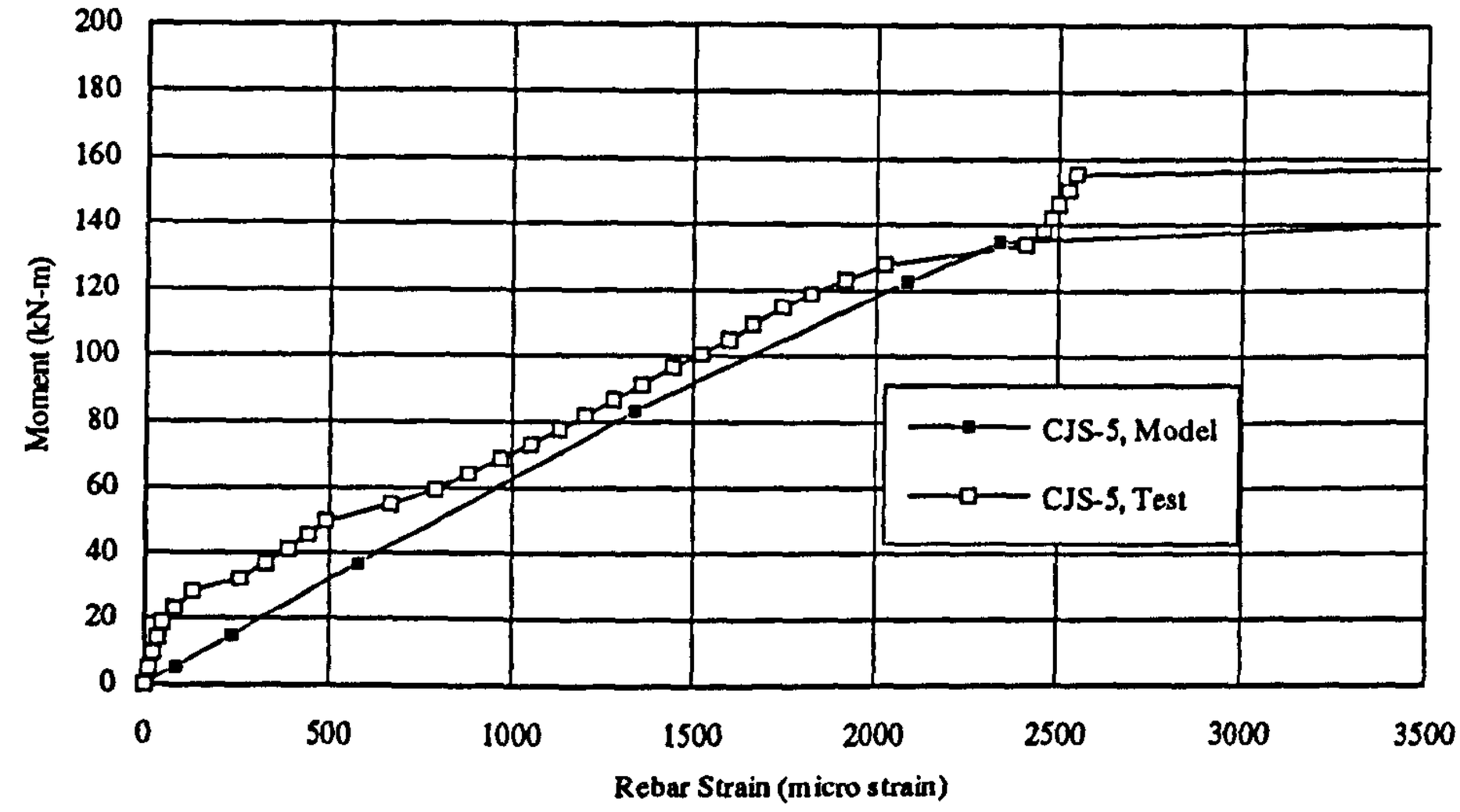

3-27 (c) Comparison of moment-rebar strain curves for CJS-5

Figure 3-27 Comparison of moment-rebar strain curves for test and model

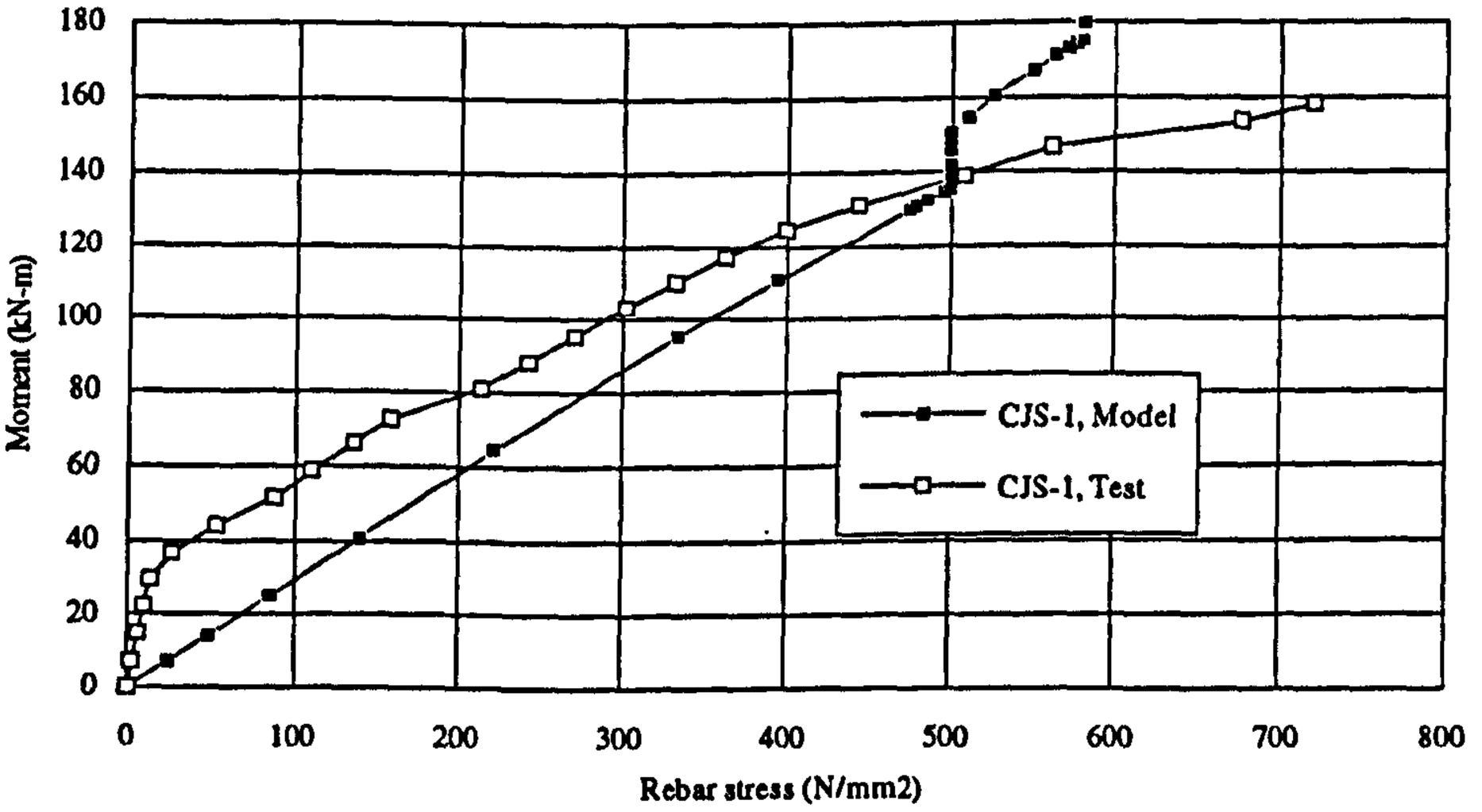

3-28 (a) Comparison of moment-rebar stress curves for CJS-1

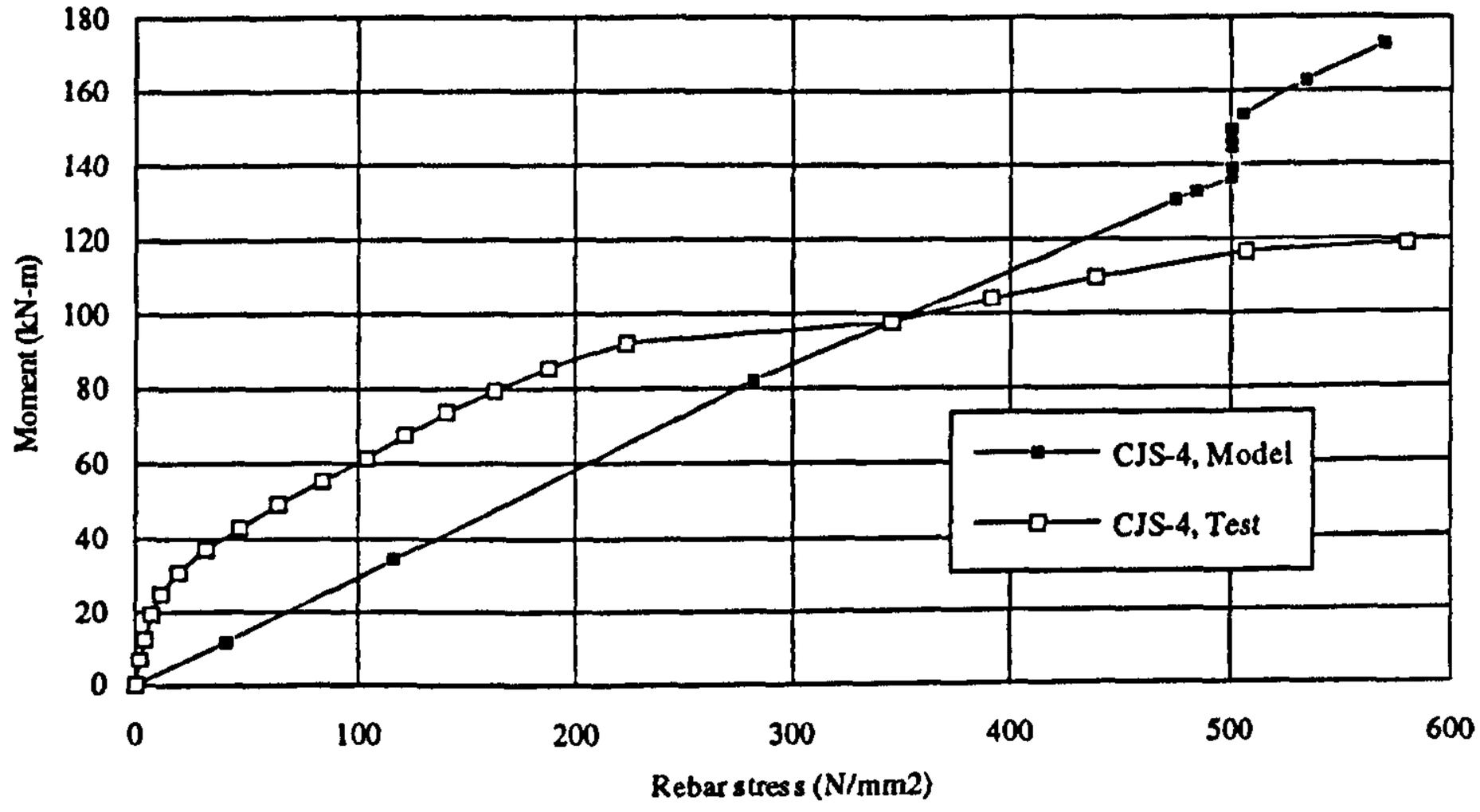

3-28 (b) Comparison of moment-rebar stress curves for CJS-4

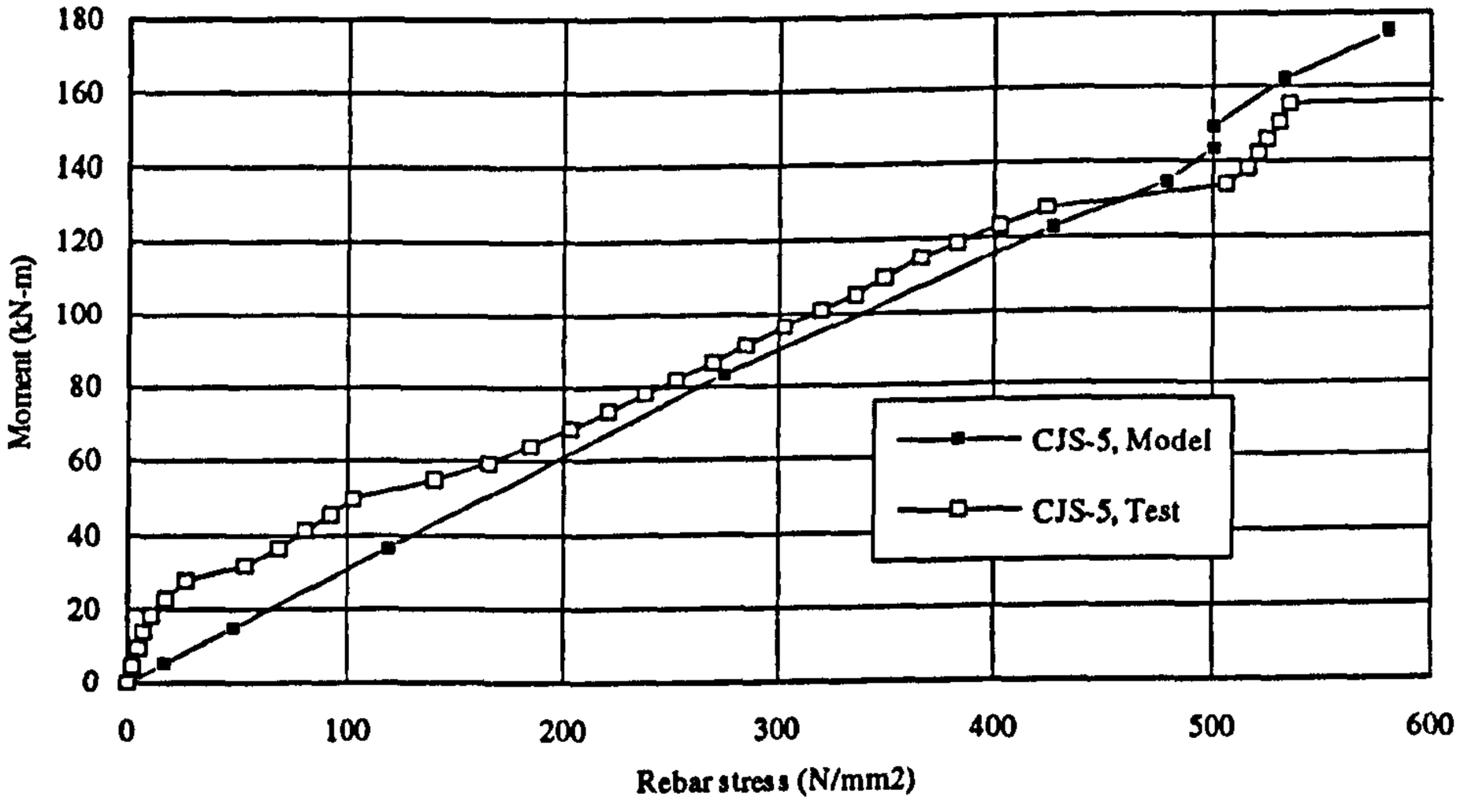

3-28 (c) Comparison of moment-rebar stress curves for CJS-5

Figure 3-28 Comparison of moment-rebar stress curves for test and model

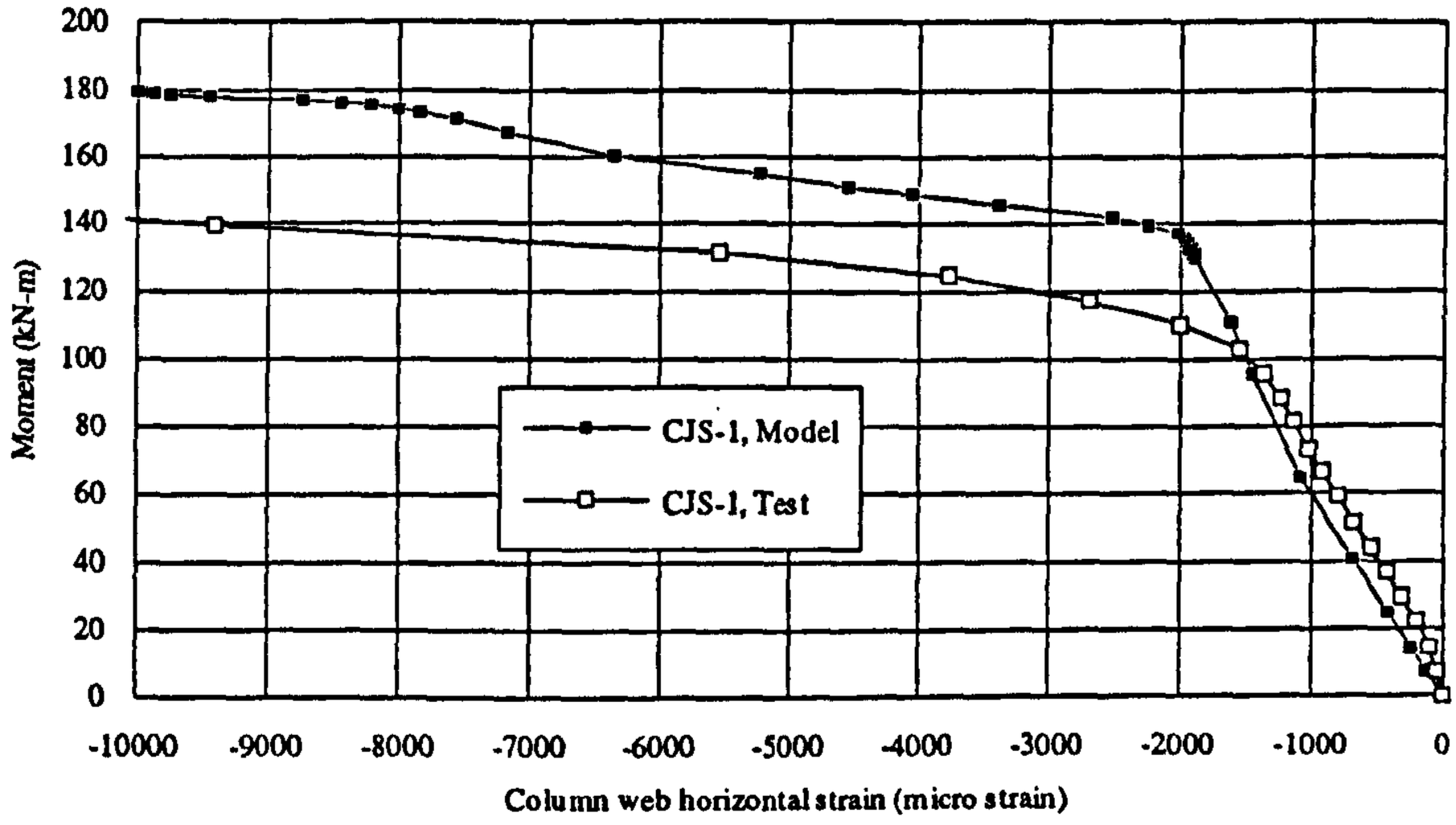

3-29 (a) Comparison of moment-column web horizontal strain curves for CJS-1

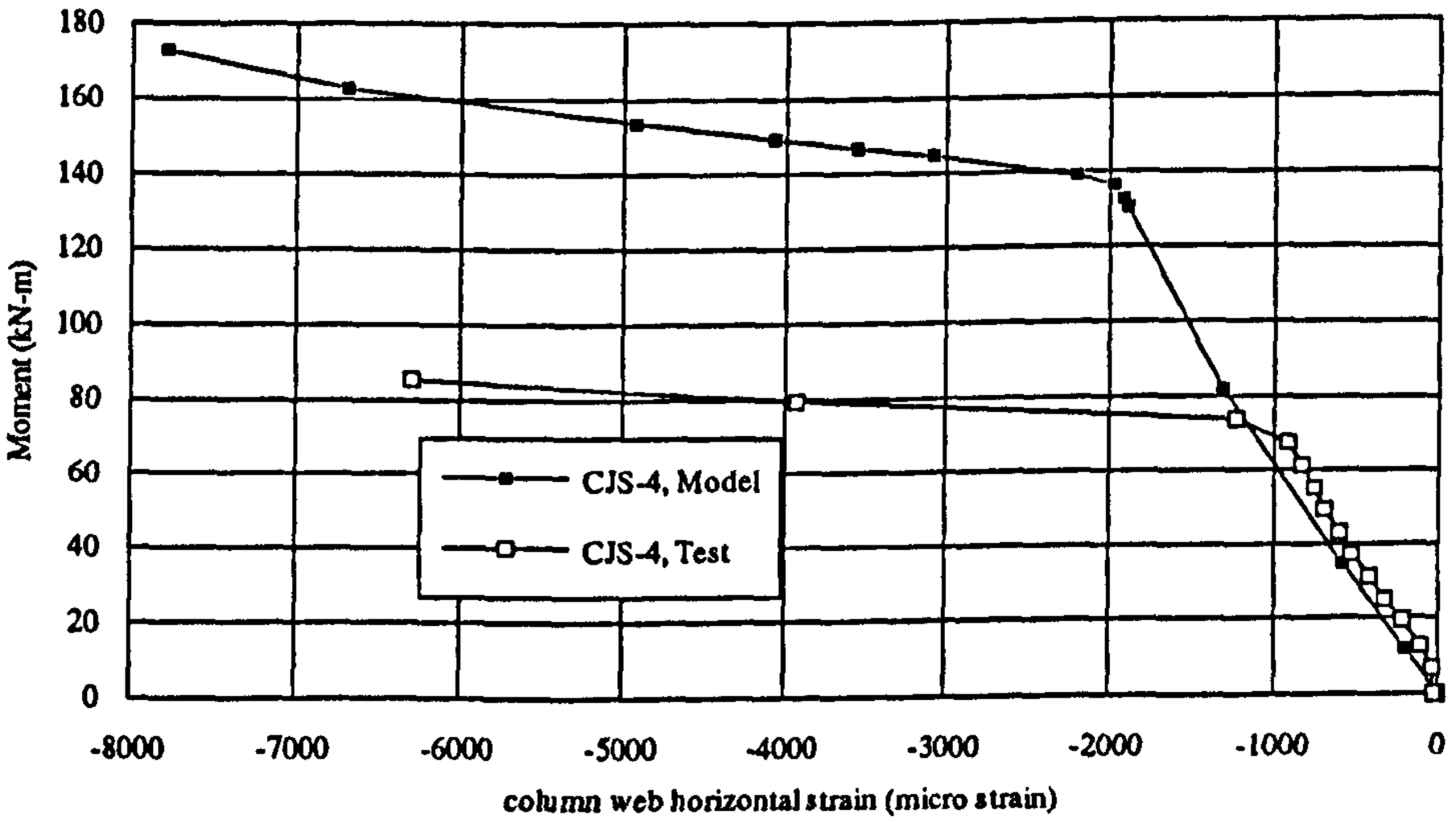

3-29 (b) Comparison of moment-column web horizontal strain curves for CJS-4

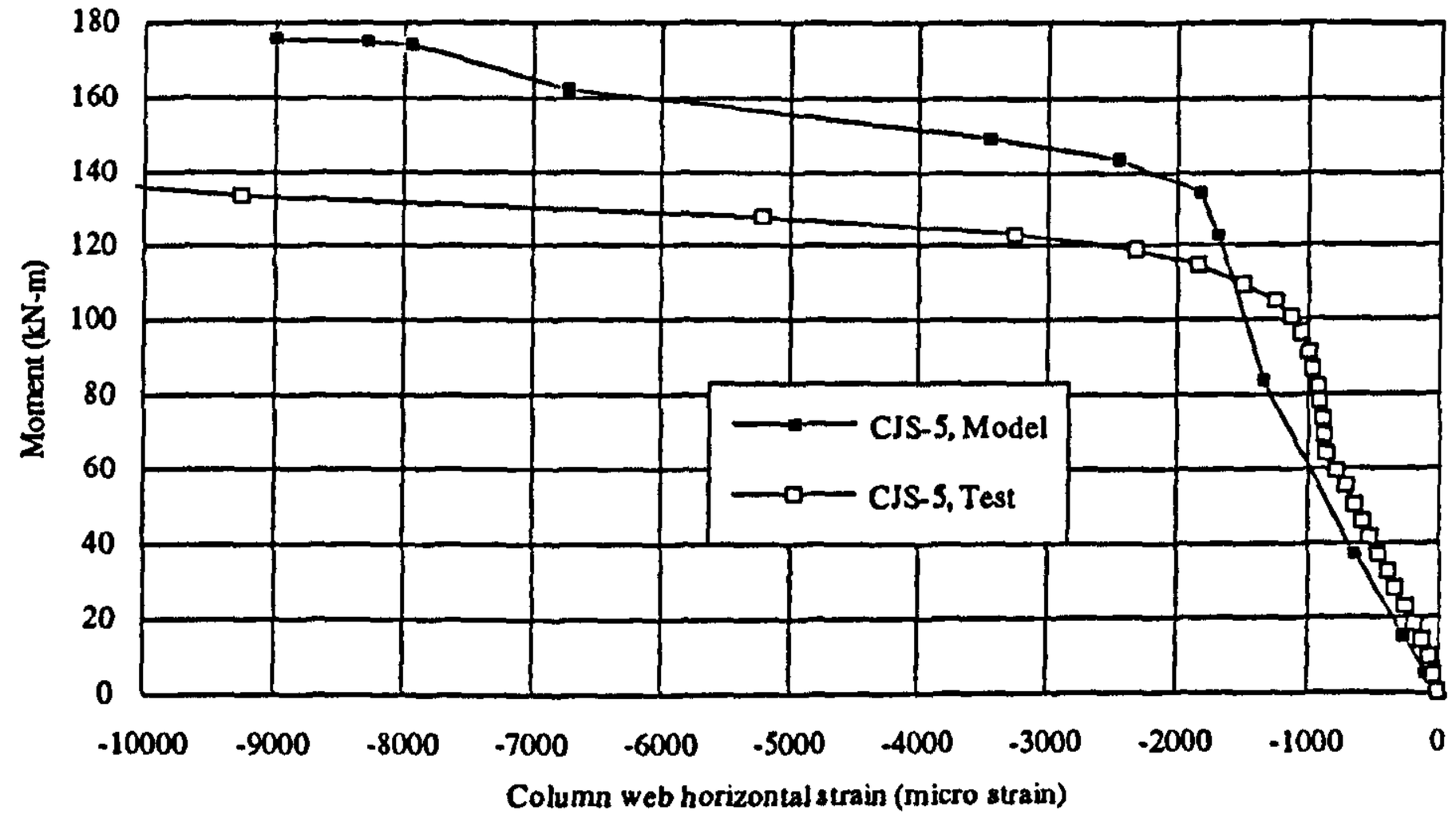

3-29 (c) Comparison of moment-column web horizontal strain curves for CJS-5

Figure 3-29 Comparison of moment-column web horizontal strain curves for test and model

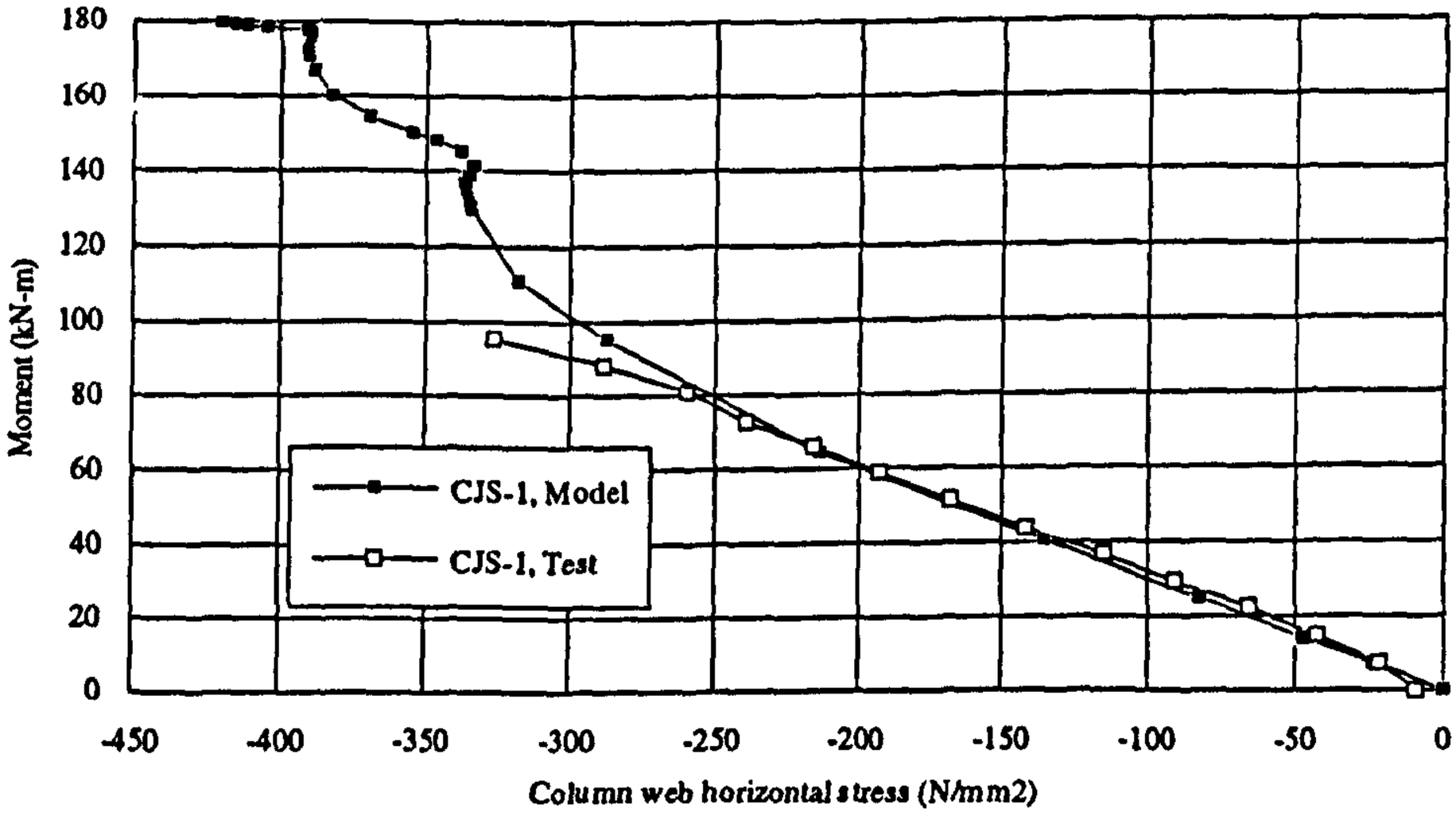

3-30 (a) Comparison of moment-column web horizontal stress curves for CJS-1

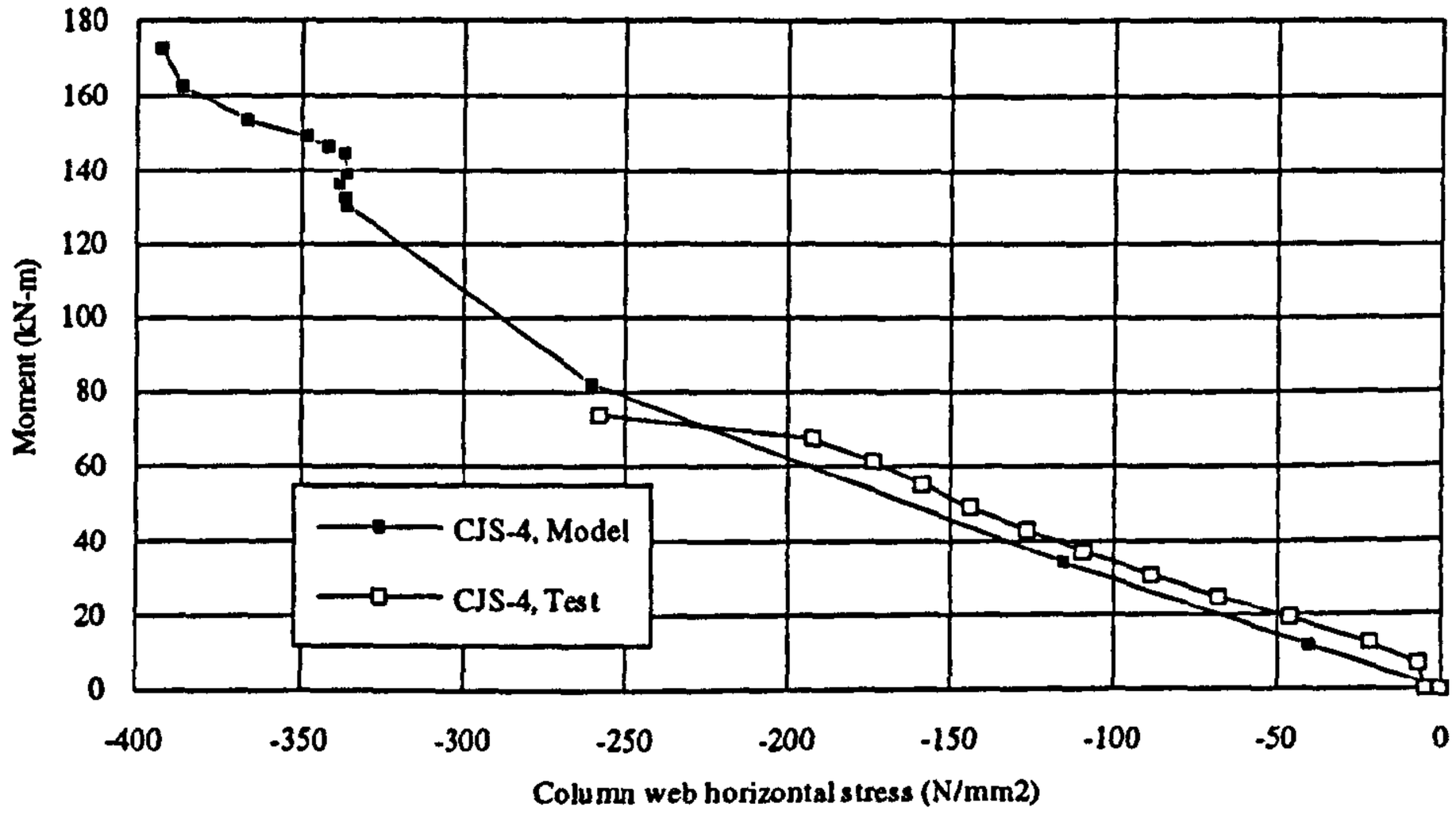

3-30 (b) Comparison of moment-column web horizontal stress curves for CJS-4

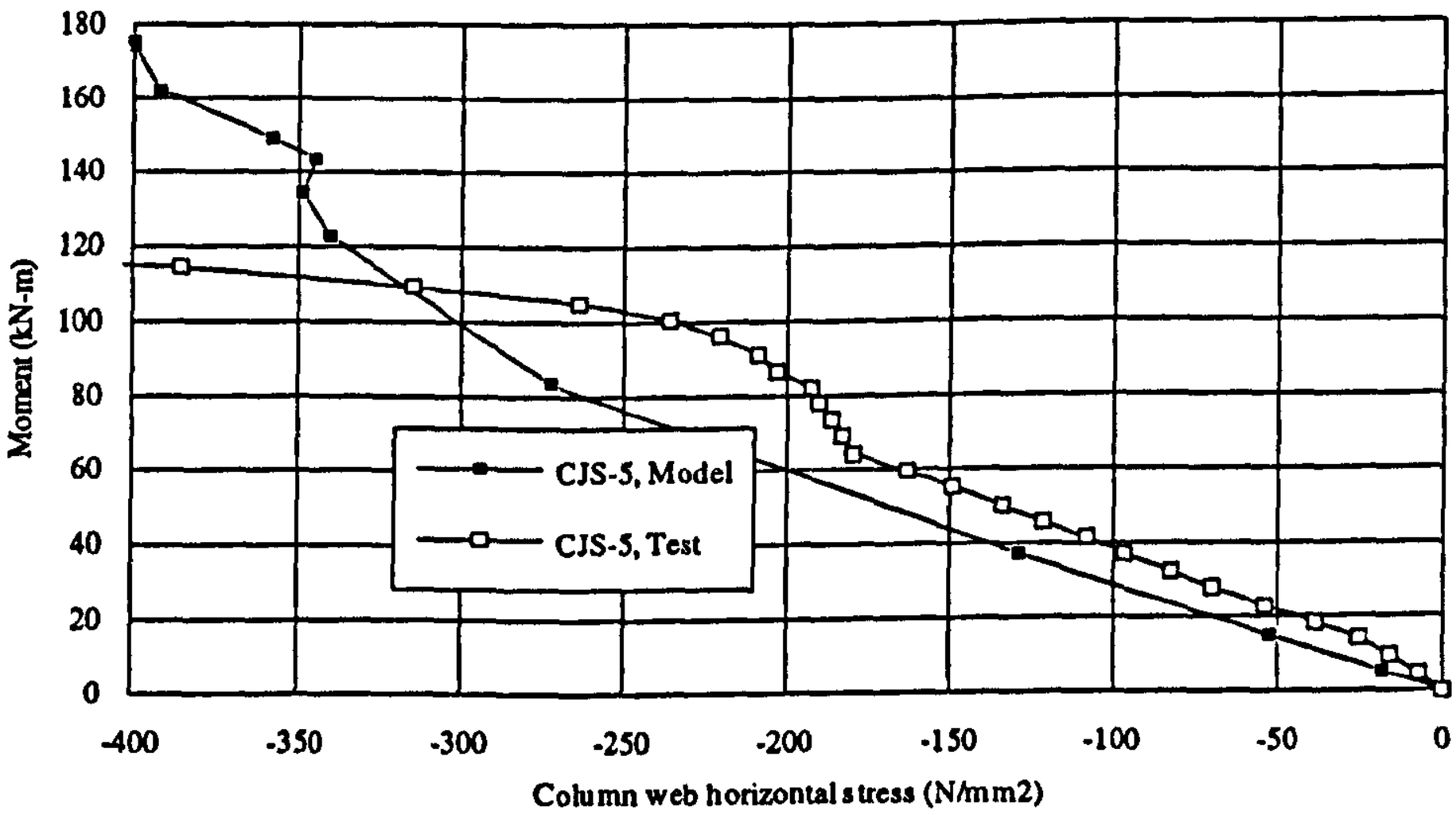

3-30 (c) Comparison of moment-column web horizontal stress curves for CJS-5

Figure 3-30 Comparison of moment-column web horizontal stress curves for test and model

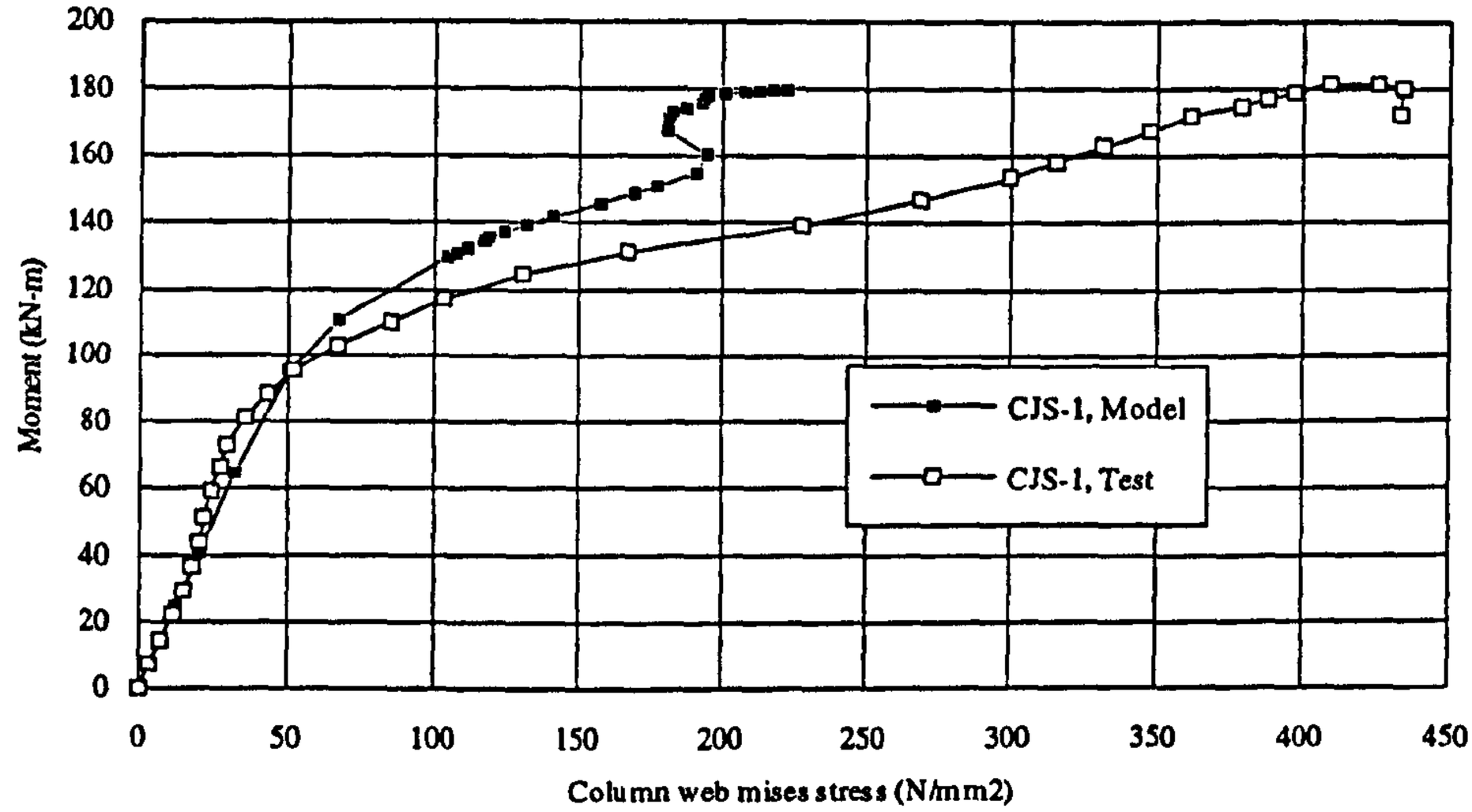

3-31 (a) Comparison of moment-column web von-Mises stress curves for CJS-1

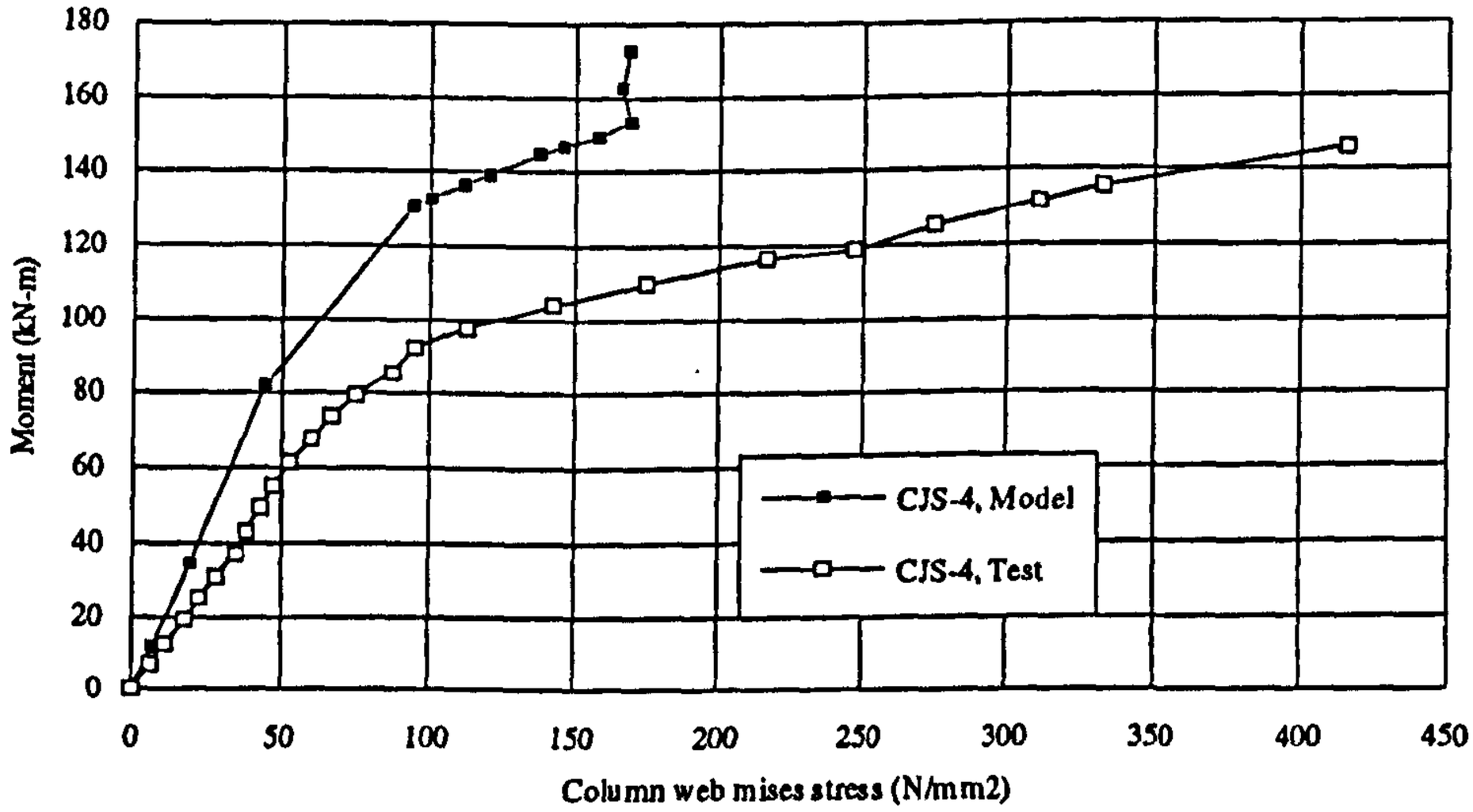

3-31 (b) Comparison of moment-column web von-Mises stress curves for CJS-4

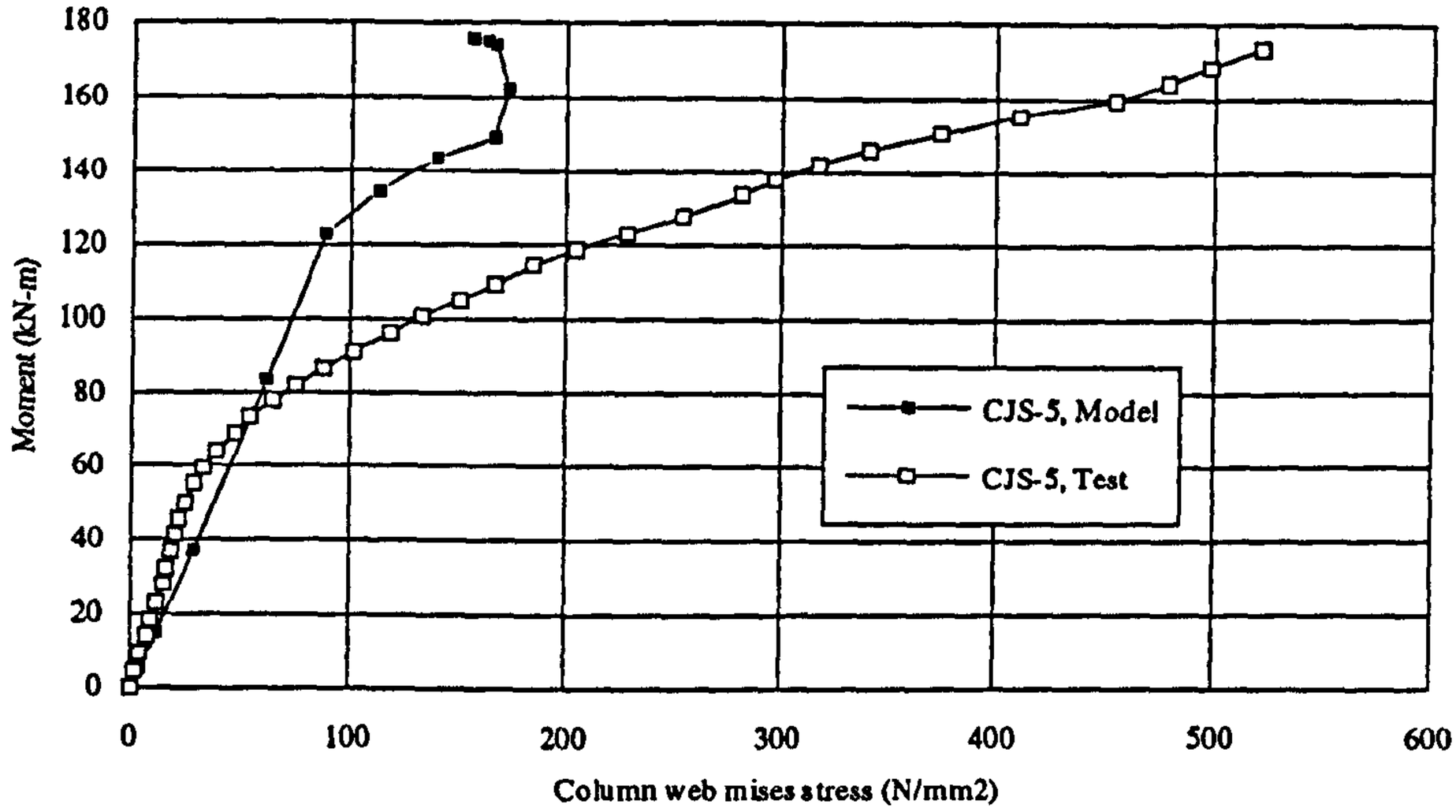

3-31 (c) Comparison of moment-column web von-Mises stress curves for CJS-5

Figure 3-31 Comparison of moment-column web von-Mises stress curves for test and model

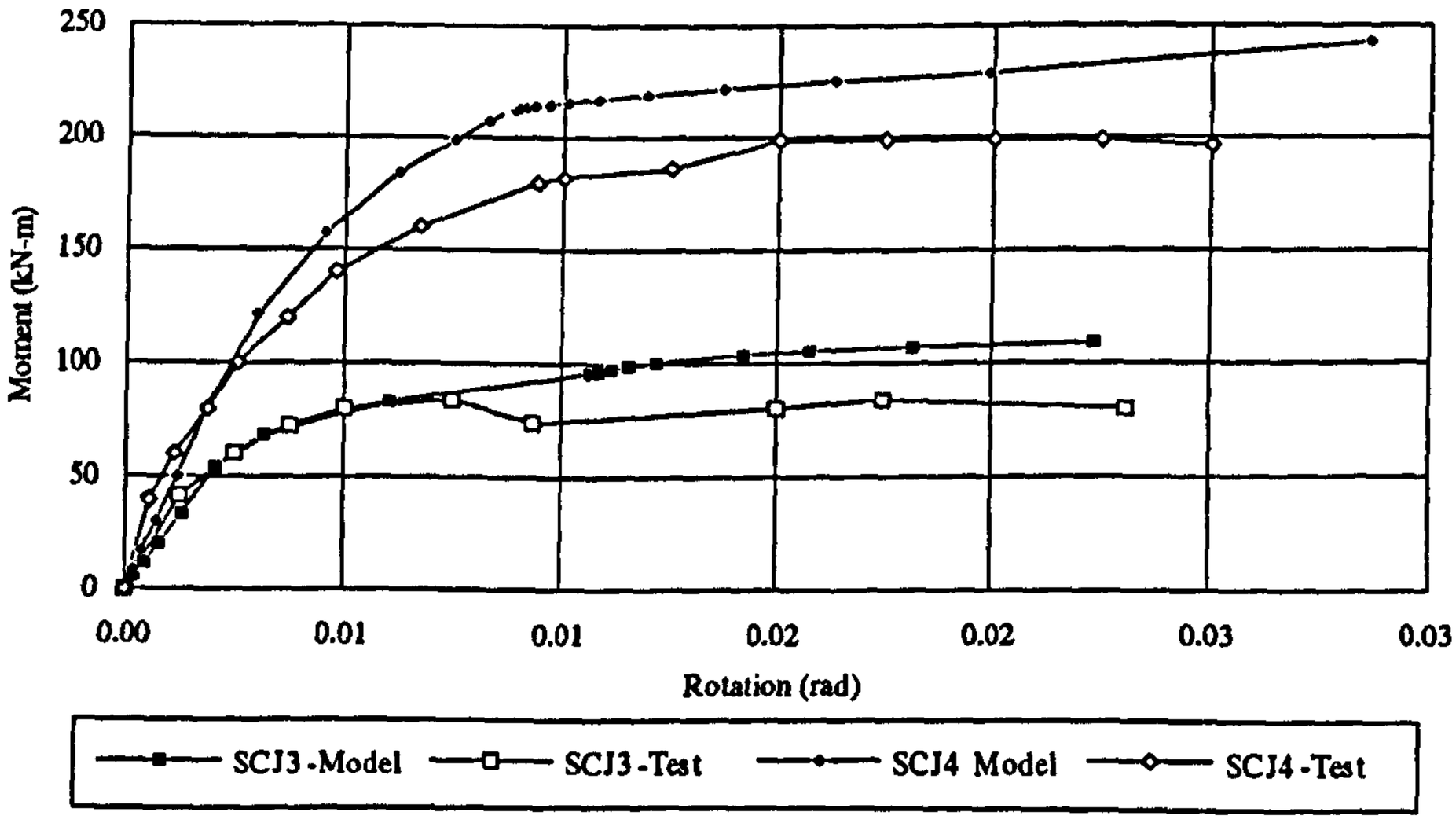

Figure 3-32 Comparison of moment rotation curves for SCJ3 and SCJ4

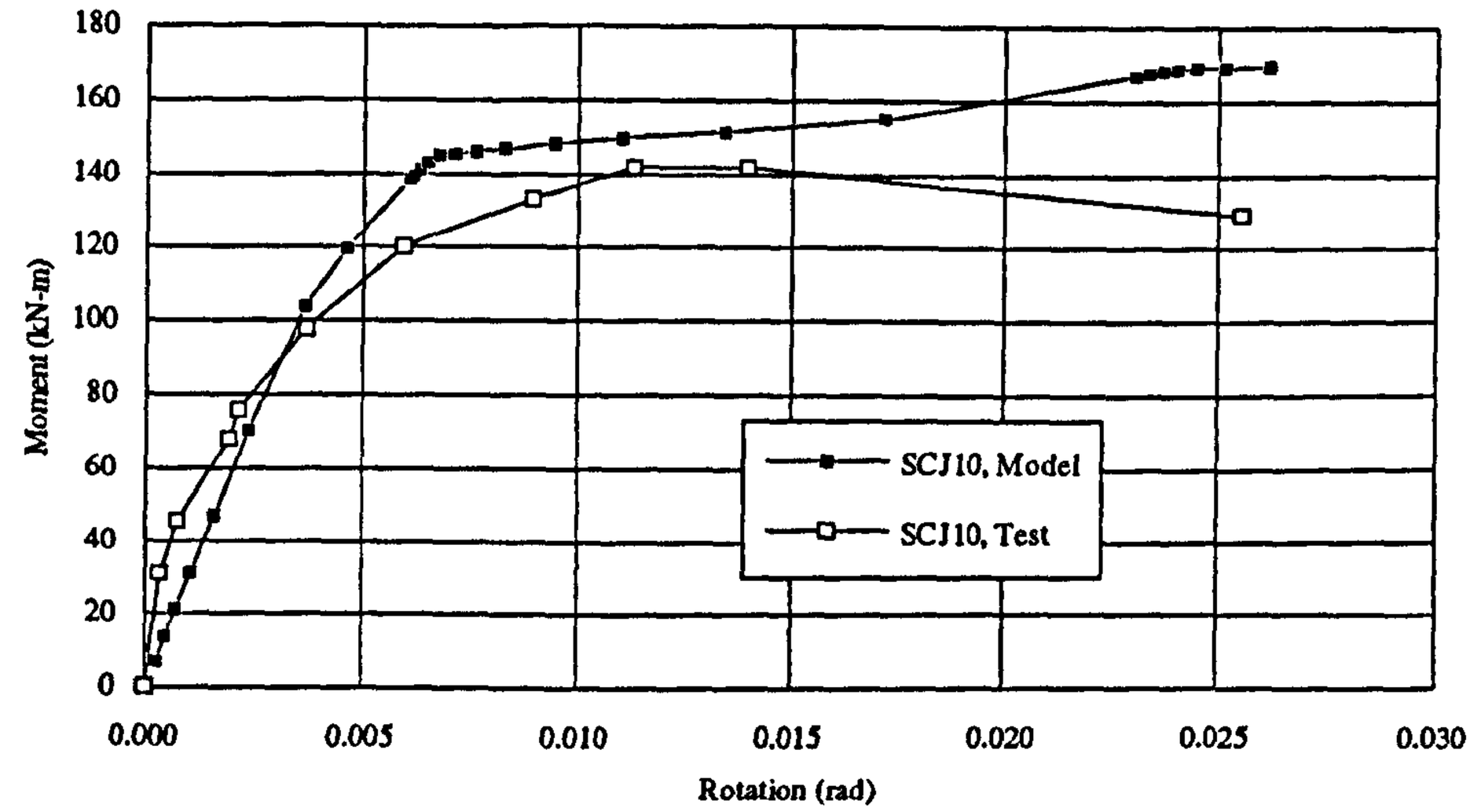

Figure 3-33 Comparison of moment rotation curves for SCJ10

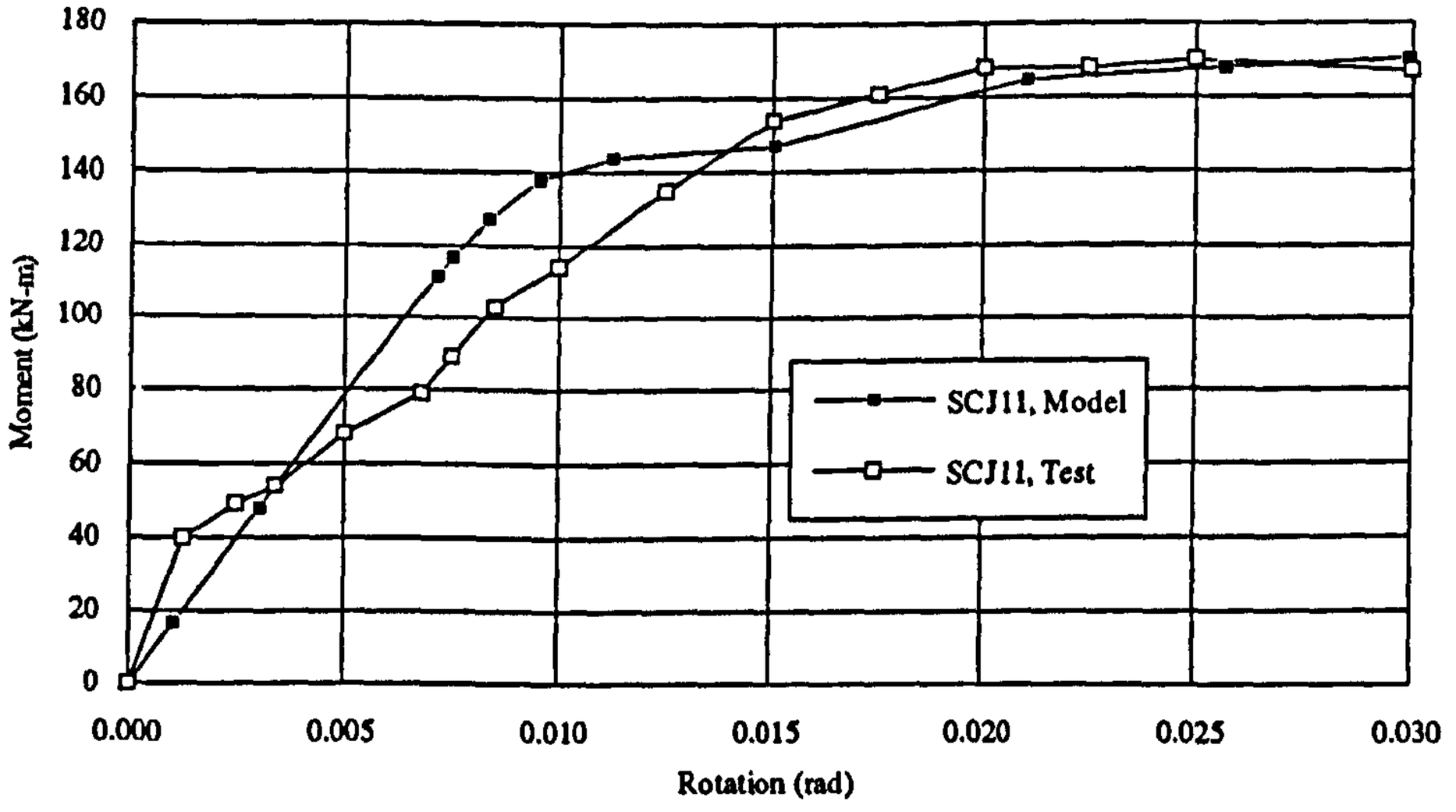

Figure 3-34 Comparison of moment rotation curves for SCJ11

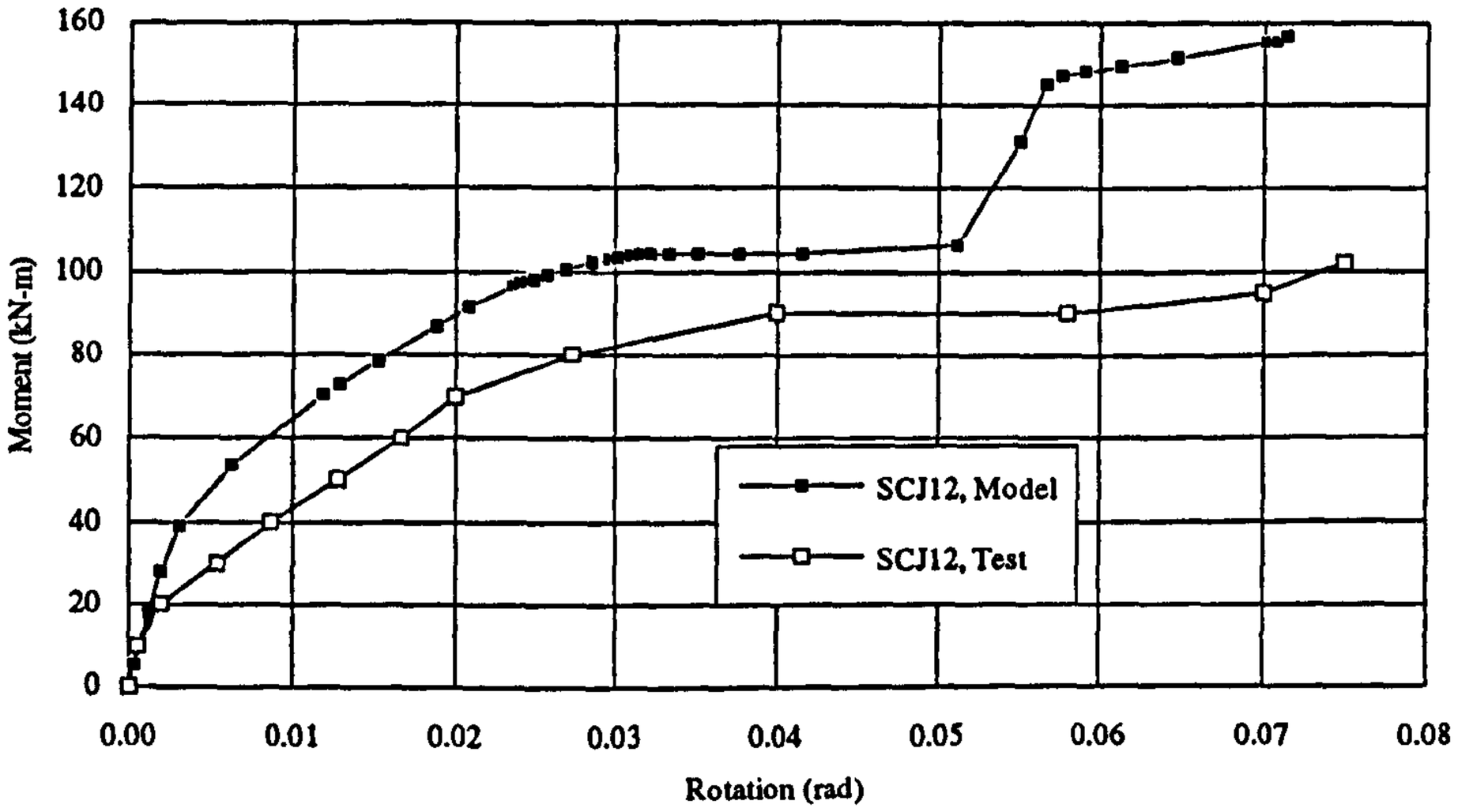

Figure 3-35 Comparison of moment rotation curves for SCJ12

Chapter 4

Parametric study for composite connections

4.1 Introduction

Understanding the detailed aspects of the connection behaviour has, thus far, largely relied on test evidence and the subsequent development of behavioural models. Because of the large number of variables and potential failure modes associated with composite connections, such an approach is unlikely ever to be able to thoroughly examine all aspects of the problem. A finite element model to simulate the structural behaviour of composite flush endplate beam to column connections was described in chapter 3. This model will now be utilised to study the behaviour of semi-rigid composite connections under various conditions to gain an insight into the load transfer mechanism. Parametric studies using the model to investigate variations in: reinforcement ratio, degree of shear connection, thickness of endplate, thickness of beam flange and thickness of column web are presented in this chapter. Few results were compared with results from a component based design method to decide the material properties to be used in a design method.

4.2 Parametric study

To understand in detail of how composite connections behave it is essential to conduct systematic parametric studies; realistically this is only possible using numerical methods. The parameters selected were: reinforcement ratio, degree of shear interaction, beam flange width to thickness ratio, endplate thickness and column web thickness. The basic connection set-up comprises a 254x102UB25 steel beam, 203x203UC46 steel column, 280x130x10 mm endplate and four M20 bolts (bolt hole

diameter 22 mm). The bolt holes are positioned 157 mm centre to centre vertically and 70 mm centre to centre horizontally. The column length is 1800 mm, and it is restrained at the top and bottom. The reinforcement area is 766 mm^2. With a total of fourteen shear studs 100 mm high and 19 mm in diameter at seven sections, each pair of shear studs was capable of transmitting 160 kN shear force. This capacity of the shear studs is equivalent to 300% shear interaction for a reinforcement area of 766 mm^2 and produces no difference in behaviour with respect to 100% shear interaction as discussed later. The reason for having such a high shear interaction is to reduce the number of variables during the parametric study for the reinforcement. The connection is a cruciform arrangement. The load is applied 1473 mm away from the column face. This basic connection set-up represents test CJS-1 as described in chapter 3 (see Figure 3-3 for the FE mesh). Only one variable was changed at a time so as to asses its effect clearly. Table 4-1 gives the set of parameters considered. The analyses were conducted for each set of parameters, by varying only that parameter over the range shown in Table 4-1, from the basic problem set-up. The values selected for reinforcement ratio were designed to show what happens if excess reinforcement is provided, the expectation being that it will not affect the moment capacity after the resistance in compression is exceeded by the tensile resistance of the reinforcement. Low shear interaction was expected to reduce the effective area of reinforcement that can carry tension, whereas more than 100% interaction should not produce any changes in behaviour. By increasing the value of beam B/T the probability of flange buckling increases. Increasing D/t for the column web should reduce the tensile and compressive resistance of the web and hence reduce the connection moment capacity. Endplate thickness was expected to affect the bolt force. Shear span was reported to have negligible effect (Ahmed *et al* [4-1], Li [4-2]) on cruciform connections, but may become significant under very high shear forces. The findings from a study of the effects of shear to moment ratio will be reported separately in chapter 5.

Table 4-1 Values of parameters selected for finite element analysis

Variable	Range of variable selected				
Reinforcement area	200 mm^2	500 mm^2	766 mm^2	1500 mm^2	2000 mm^2
Degree of shear interaction	40%	60%	100%	300%	
Beam flange width to thickness ratio	7	12	21		
Column web depth to thickness ratio	21	28	40		
Endplate thickness	8 mm	10 mm	20 mm		

4.2.1 Study for reinforcement ratio

It has been observed from tests that the addition of reinforcement to the bare steel connection can increase the stiffness and moment capacity of the connection significantly. But it is also obvious that there must be certain limit after which this increase will not alter the capacity of the connection as other mode of failure will govern the ultimate capacity of the connection. Hence studies were carried out to check the effect of varying the reinforcement ratio. These also served as a check on whether the reinforcement had been correctly introduced. If so, then reinforcement areas between a bare steel connection i.e. 0 mm^2 and the maximum of 766 mm^2 should produce load carrying capacities and moment-rotation curves which would lie between the two already obtained. Reinforcement areas of 2000, 1500, 766, 500 and 200 mm^2 (the percentages of reinforcement being 3.13, 2.34, 1.19, 0.78 and 0.31) were used for the analyses, with other parameters kept constant. The ultimate moment capacities changed to 260 kN•m, 240 kN•m, 180 kN•m, 145 kN•m and 110 kN•m respectively from 63 kN•m, which is the capacity of the bare steel connection. The moment-rotation curves are shown in Figure 4-1. Both the load carrying capacities and the

moment-rotation curves are as expected. It was observed that the variation of initial stiffness is not linear with changes to the reinforcement area. Using an experimentally based design model (ref. 4-3) the moment capacities for these reinforcement areas were calculated by taking the material strength as either the yield strength (calculated result-A in Table 4-2) or the ultimate strength (calculated result-B in Table 4-2) as obtained from ref. 4-4 supplementary tests. The results of the design calculation and the FE analyses are shown in Table 4-2, from which it appears that the design model is most appropriately used with the ultimate material strengths. The design model overestimates slightly for very high reinforcement ratios (2%), and underestimates for very low reinforcement ratios (0.31%), but for moderate reinforcement ratios the prediction of the design model is very close.

In a composite connection with a low or moderate reinforcement ratio the tensile force is developed by the reinforcement acting in combination with at least some of the bolts, whereas the compressive force is transferred through the compression in the beam's bottom flange. As the reinforcement area increases, the magnitude of tensile force that can develop exceeds the compressive force that can develop solely in the bottom flange, so to balance this part of the beam web goes into compression, and the neutral axis moves up. For low reinforcement ratios the compression capacity may be large enough that the beam web is in tension over the whole of its depth, but this changes with increasing reinforcement ratio. Figure 4-2 shows the variation of moment-beam web horizontal stress with varying reinforcement ratios. The location of the point for which the stress is plotted is the same as that in the verification section. It can be seen that points which were in tension become subject to progressively larger compressive stresses with higher reinforcement ratios. Figure 4-3 shows the variation in the von-Mises stress in the beam web with the variation of the reinforcement area. As the neutral axis (NA) moves up the amount of tensile force transferred to the bolts through the beam web decreases. When the NA moves above the centreline of the top bolt row the bolt force becomes negligible. The reduction in bolt force through the gradual

movement of the NA can be observed from Figure 4-4 for connections with 2000 and 1500 mm^2 reinforcement area. The increase in depth of the compressive zone in the beam web also causes the horizontal stress in the top flange to decrease with increasing reinforcement ratio as shown in Figure 4-5.

For low reinforcement ratios, failure is governed by the reinforcement, whereas for a high reinforcement area the failure mode shifts to the steel beam or column, depending on their relative strengths. In these analyses the increased reinforcement ratio caused the column web stress to be higher. For lower reinforcement ratios the rebar strain was high, whereas higher reinforcement ratios gave very low strains in the reinforcement. The variation of moment - reinforcement strain is shown in Figure 4-6. Variation of horizontal stress over the depth of the beam at a distance of 120 mm from the column face is shown in Figure 4-7 for various reinforcement areas. This illustrates movement of the neutral axis with changes to the reinforcement area. From the figure it is evident that for reinforcement areas of 200 mm^2, 500 mm^2 and 766 mm^2 the stress in the beam web was linear but it changed to a parabolic stress distribution for 1500 mm^2 reinforcement area and a rectangular stress block for 2000 $mm.^2$ The reason behind this was the increased force developed in the reinforcement. Table 4-3 compares the developed internal forces with different reinforcement areas. FE analysis shows that the rebar can always yield as long as the developed force can be balanced by the compressive force. From the results of the FE analyses the following conclusions can be drawn:

a) Rebar force can be calculated using the rebar ultimate strength

b) Bottom flange compressive force can be calculated from the ultimate strength

c) Initially the web compressive stresses will be linear, but to balance the rebar force, web force can be calculated by using a rectangular stress block

d) Bolts will contribute to the tensile force as long as they are above the neutral axis, after that they can be excluded from the calculation of tensile resistance

e) If the compression capacity of the connection is less then the tensile capacity of the rebar than the rebar forces should be reduced to the compression capacity of the connection

Table 4-2 Comparison of calculated moments for variation of reinforcement ratio

Reinforcement area mm^2	Calculated moment-A kN•m	Calculated moment-B kN•m	FE moment kN•m (maximum)	Test moment kN•m (ref. 4-2)
2000	223	289	259	--------
1500	201	256	238	--------
766	146	183	180	181.5
500	109	142	152	--------
200	70	90	112	--------
0	30	59	74	62.8

Note: Material properties used for calculations

1)Calculation-A (material strength is taken as the yield strength obtained from the tests)

Column: 350 N/mm^2, Beam: 420 N/mm^2, Endplate: 350 N/mm^2, reinforcement: 450 N/mm^2

2)Calculation-B (material strength is taken as the ultimate strength obtained from the tests)

Column: 480N/mm^2, Beam: 530N/mm^2, Endplate: 450N/mm^2, reinforcement: 600N/mm^2

Table 4-3 Comparison of internal forces for variation of reinforcement ratio

Reinforcement area mm^2	Rebar tensile force kN	Tensile force in upper row of Bolts kN	Bottom flange compressive force kN	Beam web compressive force kN	Depth of web under compression mm
200	116	344	348	109	98
500	290	316	382	204	135
766	444	240	384	300	165
1500	870	64	323	611	225
2000	1000	16	297	719	230

4.2.2 Study on shear interaction

To study the effect of changes in the level of shear interaction, FE analyses with 40%, 60%, 100% and 300% were conducted. 100% and 300% shear interaction gave almost identical results, so only the result for 300 % is presented here, whilst an additional analysis with 4% (not presented here) shear interaction behaved almost as for the bare steel connection, thus confirming that the shear studs were modelled properly. The moment capacities of the connection at a rotation of 0.06 rad were 127 kN•m, 148 kN•m and 179 kN•m for 40%, 60% and 300% (100% as well) interaction respectively. The initial stiffness of the connection was also affected by the degree of shear interaction.

The moment - rotation curves obtained from the FE analyses are shown in Figure 4-8. It can be seen that the effect is similar to changing the percentage of reinforcement area. It was observed in the analyses for the reinforcement ratio that the beam web can be either in tension or in compression depending on the value of reinforcement ratio. Also the strain in the beam web is tensile if the degree of interaction is low (for a constant reinforcement area, here 766 mm^2) and if the degree of interaction is high the beam web is in compression. Figure 4-9 shows the moment - strain variation in the beam web at a point 180 mm away from the column face and at the mid height of the web for different degrees of shear interaction.

The moment - bolt force relationship is also affected similarly to the case of reinforcement ratio; for low degrees of interaction the bolts are subjected to higher loads and for a high degree of shear interaction the bolt force is low. Each top bolt was subjected to 152 kN, 147 kN and 125 kN tensile force for the three cases, at the ultimate state. Although the effect of degree of shear interaction is similar to that of reinforcement ratio on overall behaviour of the connection and the stresses and strains of the different components, an essential difference between the two cases is that for

low reinforcement ratios the rebar is subjected to tensile load which causes yielding but for low degrees of shear interaction the force transmitted to the rebar is low and so the developed stress and strain is also low. For 300% and 100% shear interaction the rebar stress is 580 N/mm^2 so for 40% and 60% interaction the stress should be about 580x0.4=232 N/mm^2 and 580x0.6=350 N/mm^2. The FE result was 240 N/mm^2 and 360 N/mm^2. Figure 4-10 shows the moment - rebar strain curves for various degrees of shear interaction.

To make a comparison between the reinforcement ratio and degree of shear interaction two extra FE analyses were made with reinforcement areas of 306 mm^2 and 460 mm^2 which will be compared with the 40% and 60% interaction having a reinforcement area of 767 mm^2. The moment - rotation curves are compared in Figure 4-11, moment - beam web horizontal stress curves are shown in Figure 4-12 and moment - bolt force curves are shown in Figure 4-13.

From the presented results it can be concluded that changes to the degree of shear interaction or the reinforcement ratio produces very similar effects, with the only differences being the level of stress and strain in the reinforcement itself, which can be observed from Figures 4-6 and 4-10.

4.2.3 Variation of beam flange width to thickness ratio

The main function of the beam's bottom flange is to transfer the compressive load to the column, so there is a possibility for the beam flange to buckle. The standard beam sections generally have B/T ratios in the range of 8 to 18. To study the effect of this ratio three analyses were made with ratios of 7, 12 and 21. To initiate beam flange buckling, a very small amount of initial flange imperfection was introduced.

Results for a B/T ratio of 7 show no distortion of the bottom flange at its ultimate load. B/T of 12 shows an insignificant amount of distortion but for B/T of 21 the flange started to buckle at about 75 % of its ultimate load. The deformed shape of the bottom flange in this last case at its maximum load is shown in Figure 4-14.

For the first two cases the ultimate moment capacity was almost the same but for B/T of 21 the moment capacity was reduced by about 9 percent. The moment - rotation curves are shown in Figure 4-15.

The column web stress and strain variations with the moment were almost the same for all three cases.

Variation of the beam web horizontal stress was, however, significant. As the thickness of the flange is reduced so the ability of the bottom flange to transfer the compressive load is decreased due to the smaller available compressive area. This causes the beam web to be subjected to higher compressive stresses, and also the depth of compression in the beam web increases. When the ratio of B/T was changed from 12 to 21 the compressive stress at the middle of the beam and 180 mm away from the column flange altered to 430 N/mm^2 from 180 N/mm^2 at the ultimate load level (the yield and the ultimate material strengths being 440 and 540 N/mm^2, as shown in Figure 2-26 of chapter 2). The variation of moment-beam web horizontal stress and moment - beam web von-Mises stress are shown in Figures 4-16 and 4-17 respectively.

A B/T of 7 gave a bottom flange compressive stress of 280 N/mm^2 at the ultimate load; by changing the ratio to 12 and 21 the stress was increased to 428 N/mm^2 and 464 N/mm^2 respectively The moment - bottom flange stress curves are shown in Figure 4-18.

The bolt force and the rebar stress were almost unaffected by changes to the ratio of bottom flange width to thickness ratio. This demonstrates the ability of such connections to balance the force transfer required through changes to the exact pattern i.e. the extent to which the beam web is required to transmit compression depends upon the extent to which the tensile force component exceeds the compressive resistance available in the flange.

4.2.4 Effect of endplate thickness

To study the effect of endplate thickness three analyses were made with endplate thicknesses of 8 mm, 10 mm and 20 mm. The column flange thickness of 11 mm for a 203x203UC46 column was used in all the three cases. Results from the analyses are described below.

Increasing the thickness of the endplate increases the moment capacity of the composite connection, but the initial stiffness is not affected so much. The stiffness is, however, changed in the elastic-plastic phase of the loading response. The ultimate capacities of the connections were 171 kN•m, 180 kN•m and 203 kN•m respectively for the connections with endplate thicknesses of 8 mm, 10 mm and 20 mm respectively. The variation of the moment - rotation curves is shown in Figure 4-19.

The increased thickness of the endplate permits higher tensile forces in the bolts and as a result more compressive force is developed which must be sustained by the column web. The results of FE analyses show that the column web horizontal strain and stress increases with increasing thickness of the endplate. Figure 4-20 shows the moment - column web horizontal strain curves with varying endplate thickness.

Due to the greater tensile force, the beam web is subjected to a higher compressive force and as the endplate thickness is increased so the neutral axis moves up the beam

web, and the same point in the web is subjected to a progressively higher compressive force. Figure 4-21 shows the results of the moment - beam web horizontal strain curves obtained from FE analyses.

Thickness of the endplate is one of the important factors which controls how much force can be developed in the bolts. The results of FE analyses show that for 8 mm, 10 mm and 20 mm endplate thicknesses (column flange thickness being 11 mm) the bolt force is 95 kN, 125 kN and 161 kN respectively. FE results are shown in Figure 4-22. The increase of bolt force with increasing endplate thickness in the above three cases is reproduced by the EC3 rules which have been found to be in satisfactory agreement with the present study.

4.2.5 Effect of column web thickness on composite connections

To study the effect of column web thickness on the behaviour of composite connections the column web width/thickness was selected to be 21, 28 and 40, where 28 (203/7.3 ≈ 28) is the ratio for the standard 203x203UC46 section. To alter the ratio the only change that was made was to change the thickness of the column web; other properties such as flange width, beam size or reinforcement ratio were kept constant.

The ultimate moment capacities from the three analyses were 187 kN•m, 180 kN•m and 131 kN•m respectively for width to thickness ratios of 21, 28 and 40. The ratio of 21 caused the ultimate strength of the rebars to be achieved, whereas with ratio 40 the column web von-Mises stress reached its limit. Ratios 21 and 28 produced a rotation capacity of more than 20 mrad but 40 did not. Since symmetry was used for the FE model, buckling of the column web could not be included.

The moment - rotation curve is shown in Figure 4-23. The moment - column web von-Mises stress curves are shown in Figure 4-24. The moment - beam web horizontal

stress curves are shown in Figure 4-25. From these curves it appears that the reduction in thickness of the web reduced the compression capacity of the column web so the developed compressive force at the interface of the beam and column was also reduced. This caused the stresses in the beam to be low and stresses in the column to be higher with the increase of column web width/thickness ratio.

4.3 Conclusions

The numerical model described in chapter 3 was used to study the effects of reinforcement ratio, degree of shear interaction, thickness of column web, beam flange, endplate.

FE analyses have shown that the introduction of reinforcement to the bare steel connection significantly increases both the initial stiffness and the moment capacity of the connection. But it is also observed that beyond certain limits imposed by the compression capacity of the beam flange and beam web and column web, further increases are not possible. It is also evident that the higher the reinforcement area the lower the bolt forces. But at the same time it is observed that although the beam web is in compression the top bolts at the same level may be in tension due to the deformation of the endplate. A very high reinforcement ratio can lead to a low rotation capacity. The problem of partial shear interaction can be represented by simply reducing the reinforcement area, by keeping in mind that the reinforcement will not yield but the studs may fail at higher loads. Reduced thickness of beam flange leads to the buckling of the bottom flange, and higher web compression, but has no significant effect on the bolt forces or the rebar stresses. Increased thickness of the endplate allows more tensile force in the bolts, which increases compression in the beam web and increases the moment capacity, but the increase in capacity is not very significant.

The general conclusion to be drawn from all of these studies reported herein is that since FE modelling can accurately represent all the main features of the behaviour of composite endplate connections, it offers a reliable and very cost-effective alternative to laboratory testing as a way of generating results. Also comparison of FE results with an available design method indicated that accurate prediction can be made with ultimate strengths of the components to predict the moment capacity.

4.4 References

4-1 Ahmed, B., Nethercot, D. A. and Li, T. Q. (1996) *Modelling Composite Connection Response*, Connections in Steel Structures III: Behaviour, Strength and Design, Edited by Reidar Bjorhovde, Andre Colson, Riccardo Zandonini, Proceedings of the Third International Workshop, Trento University, 29-31 May 1995, pp. 259-268.

4-2 Li, T. Q., Nethercot, D. A. and Choo, B. S. (1996) *Behaviour of flush end plate composite connections with unbalanced moment and variable shear/moment ratios: part 1: experimental behaviour*, Journal of Constructional Steel Research, Vol. 38, No. 2, pp. 125-164.

4-3 Li, T. Q., Nethercot, D. A. and Choo, B. S. (1996) *Behaviour of flush end plate composite connections with unbalanced moment and variable shear/moment ratios: part 2: prediction of moment capacity*, Journal of Constructional Steel Research, Vol. 38, No. 2, pp. 165-198.

4-4 Li, T. Q., Moore, D. B., Choo, B. S. and Nethercot, D. A. *The experimental behaviour of a full-scale, semi-rigidly connected composite frame: Overall consideration*, Journal of Constructional Steel Research (under review).

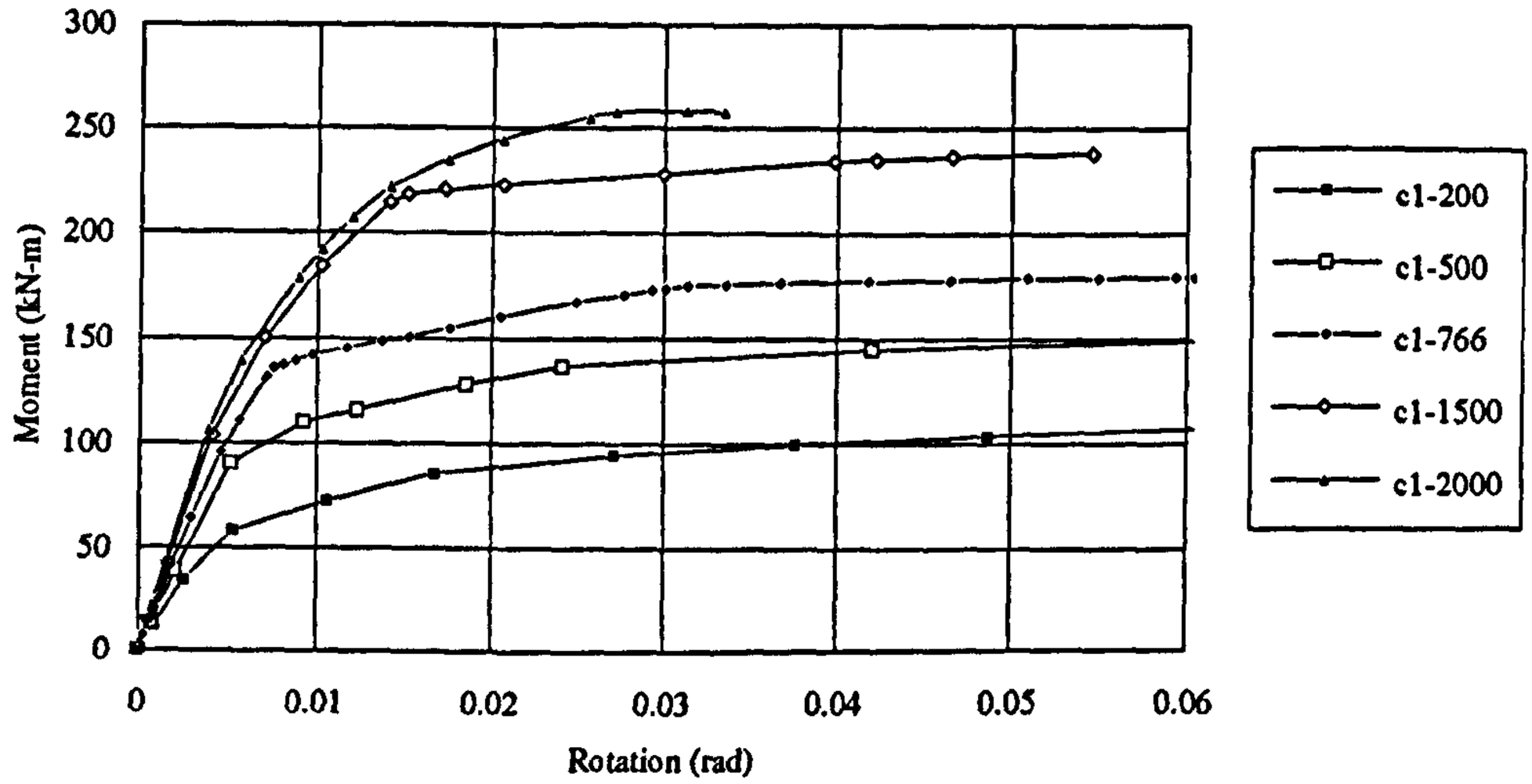

Figure 4-1 Moment-rotation curves for varying reinforcement ratio

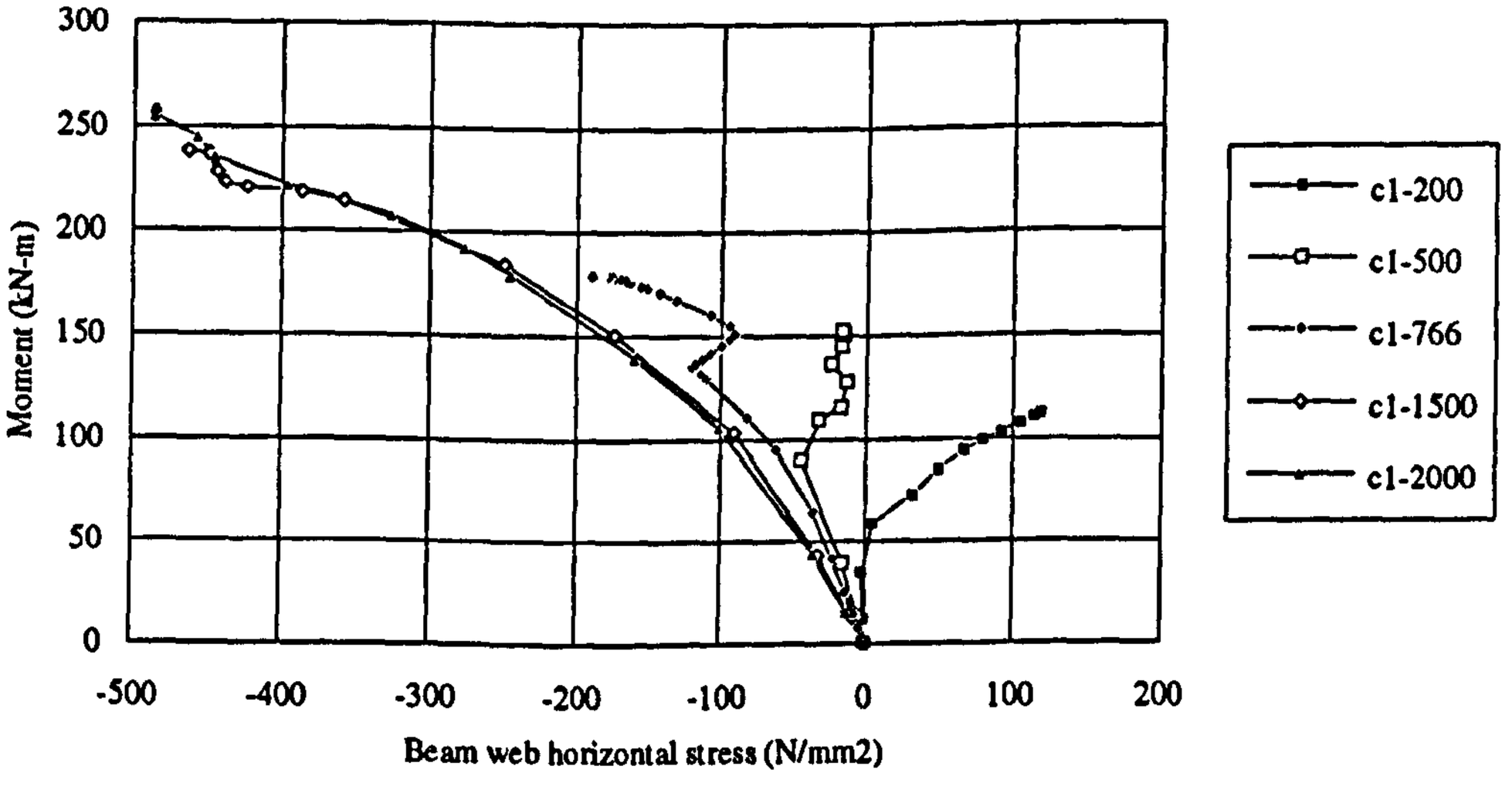

Figure 4-2 Moment-beam web horizontal stress curves for varying reinforcement ratio

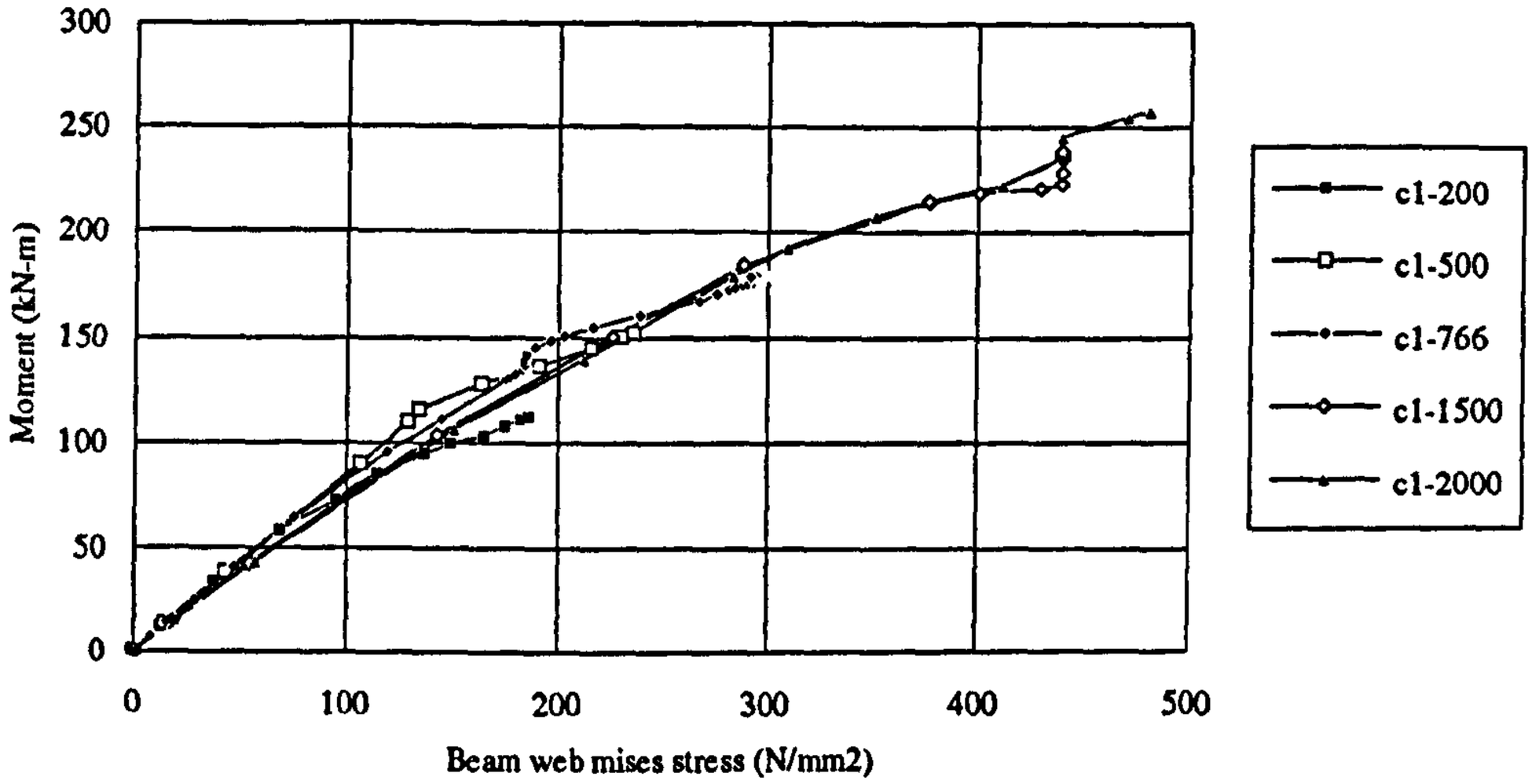

Figure 4-3 Moment-beam web von-Mises stress curves for varying reinforcement ratio

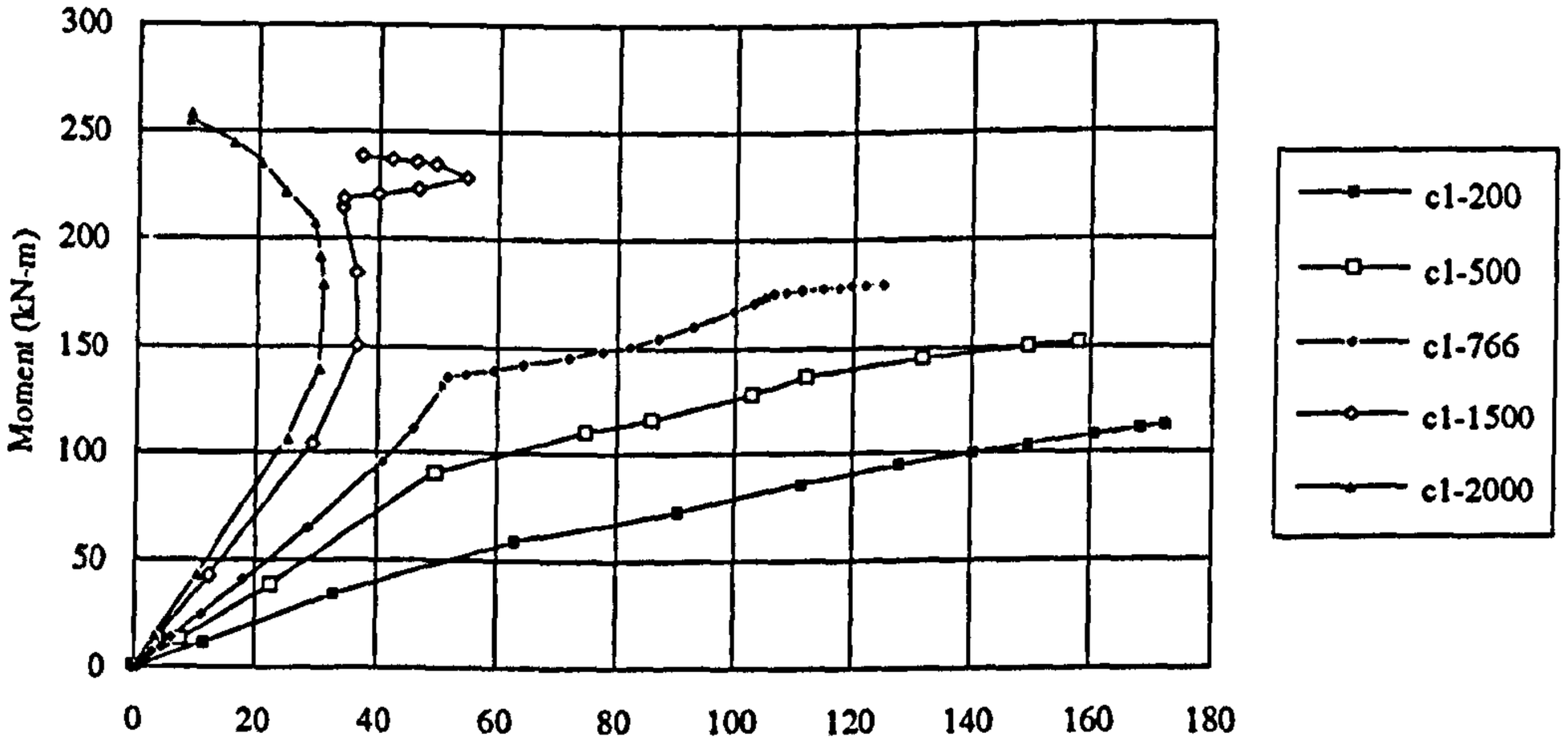

Figure 4-4 Moment-bolt force curves for varying reinforcement ratio

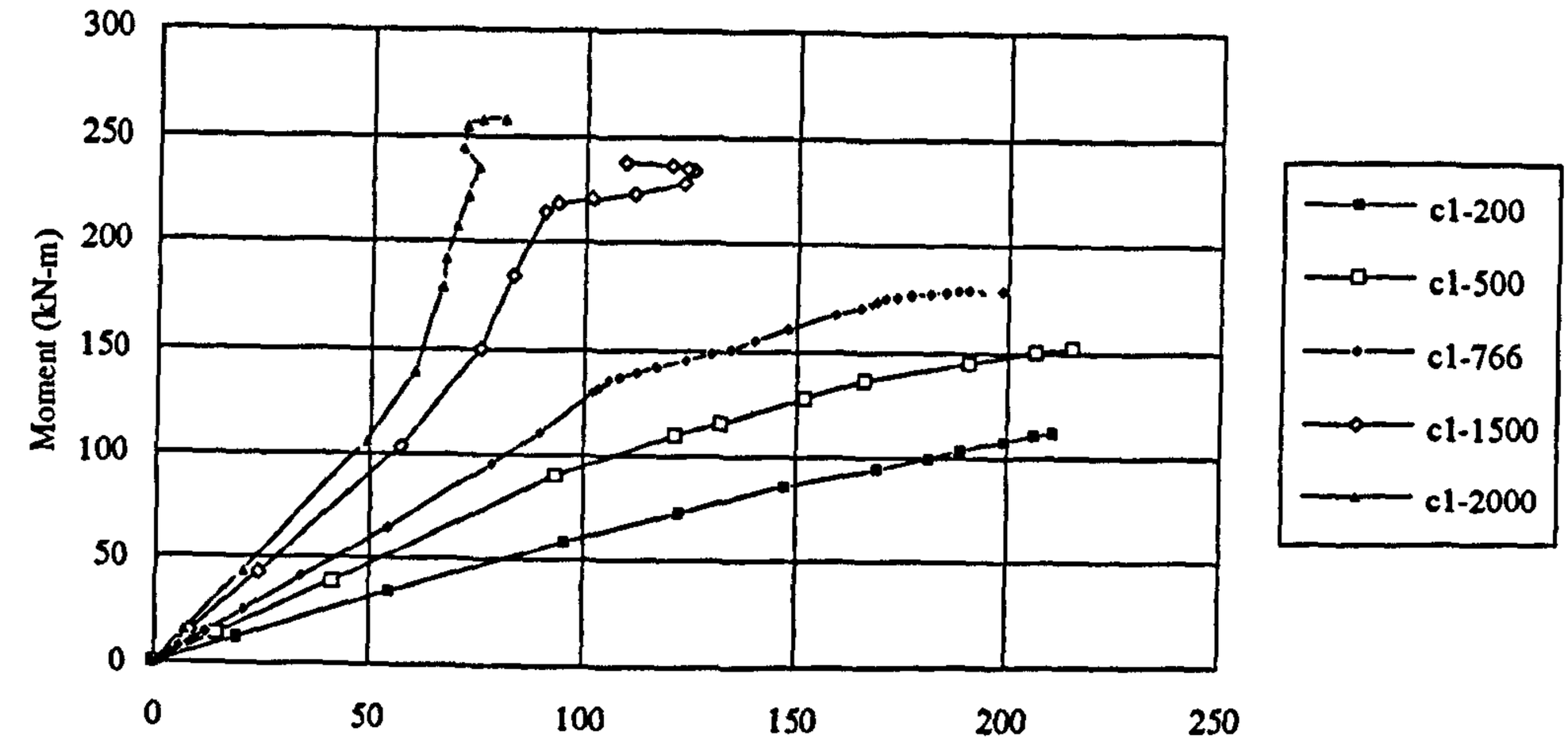

Figure 4-5 Moment-top flange horizontal stress curves for varying reinforcement ratio

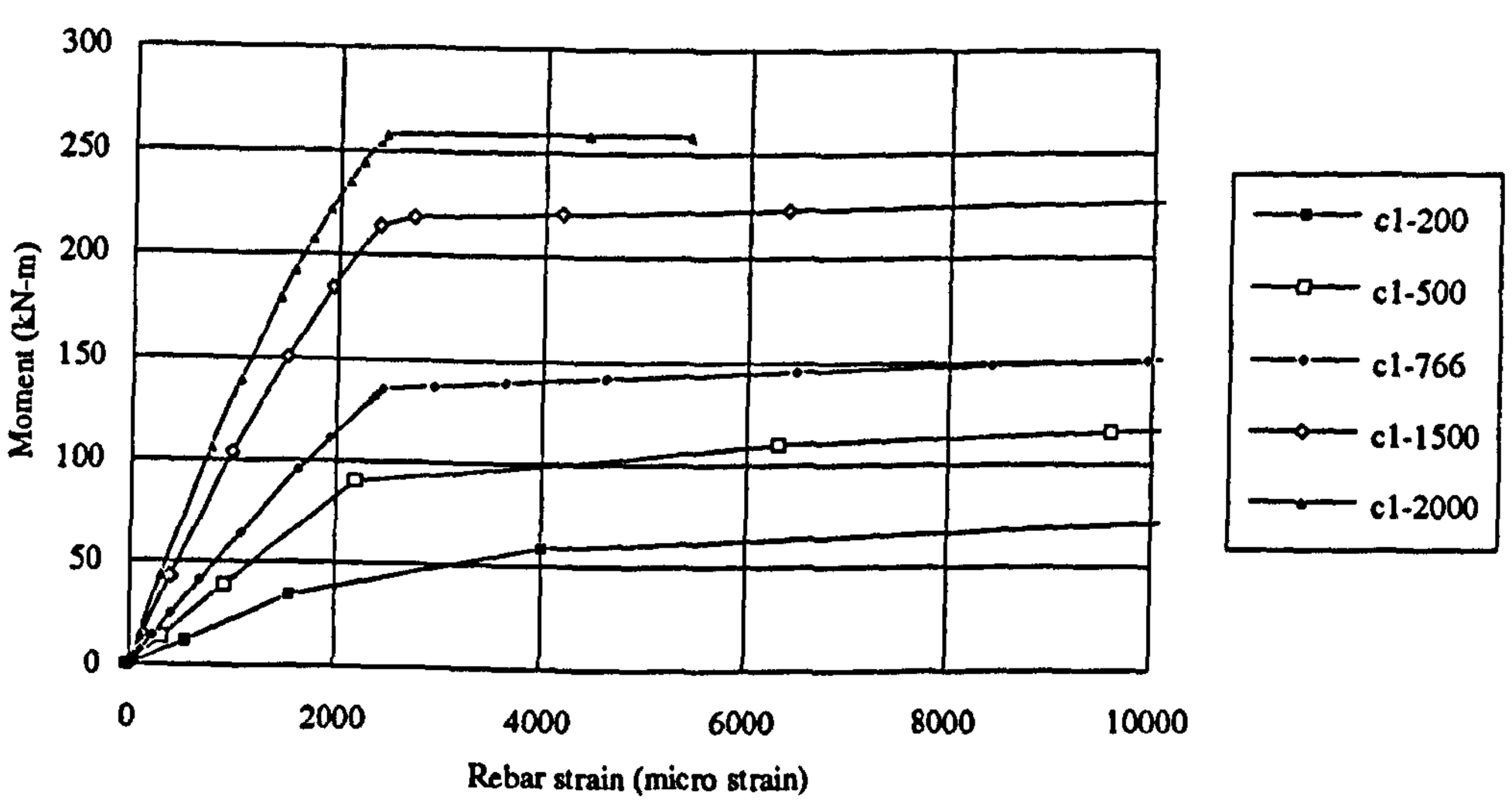

Figure 4-6 Moment-rebar strain curves for varying reinforcement ratio

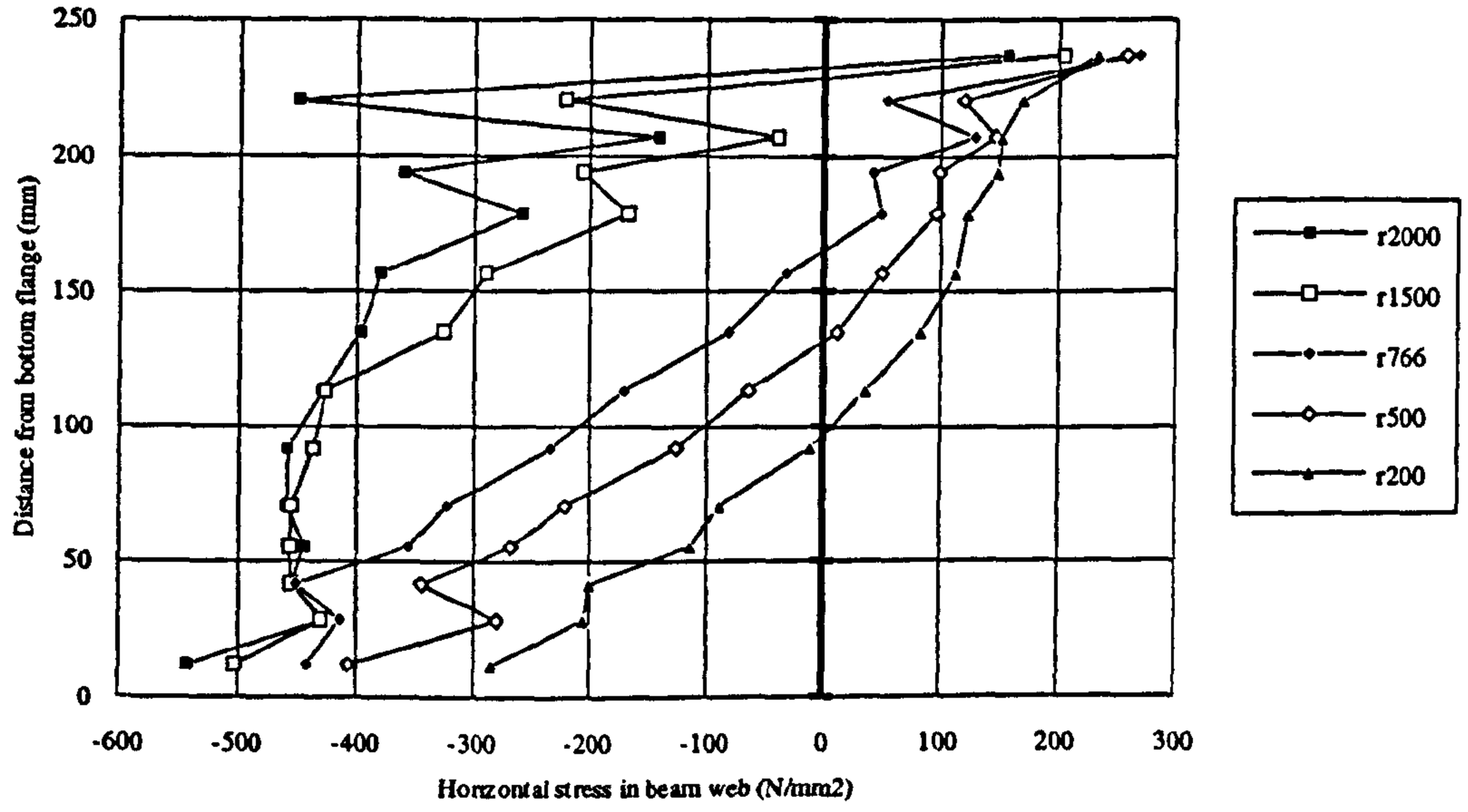

Figure 4-7 Variation of beam web horizontal stress over the depth with variable reinforcement area

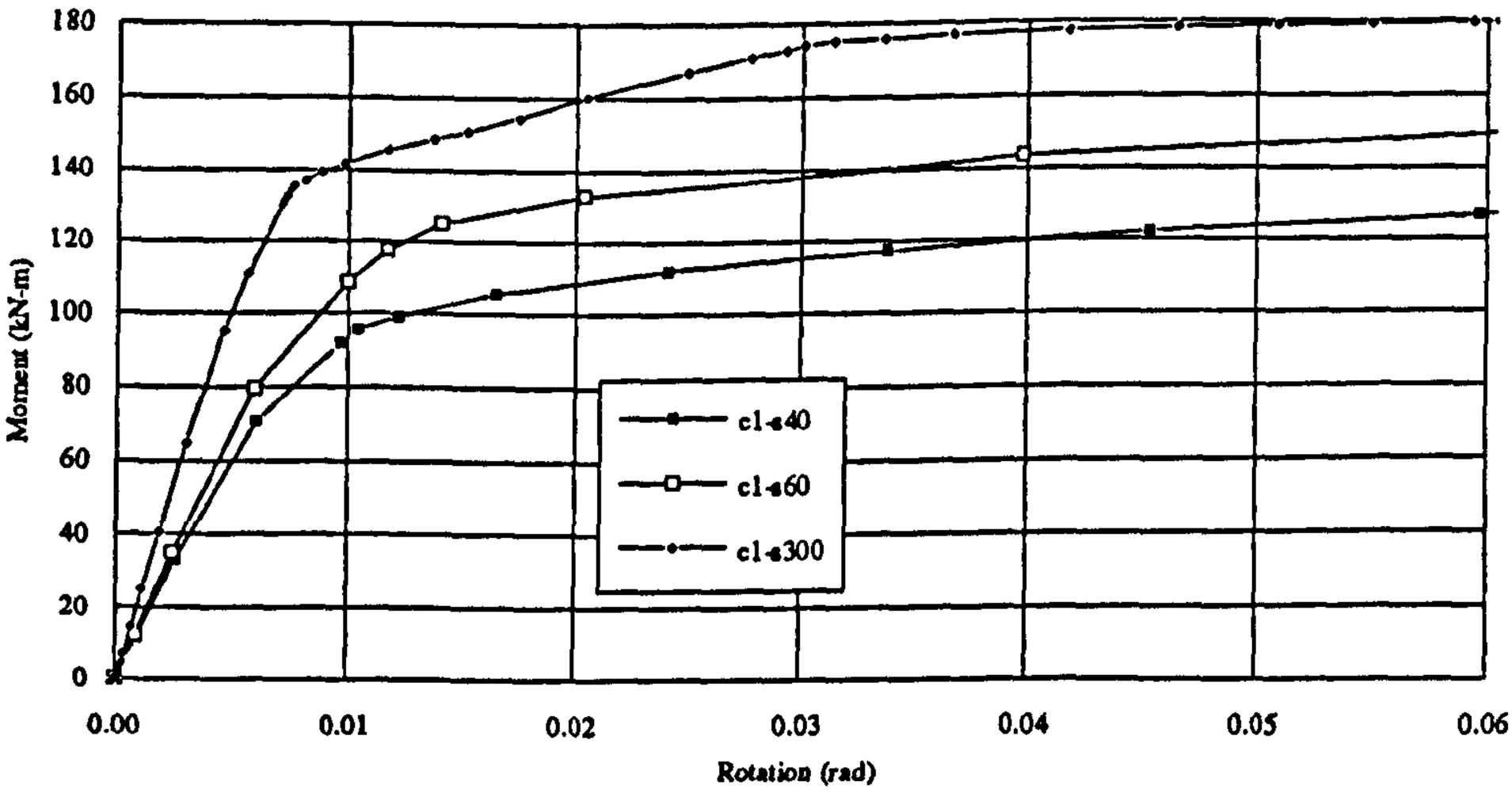

Figure 4-8 Variation of moment-rotation curves with degree of shear interaction

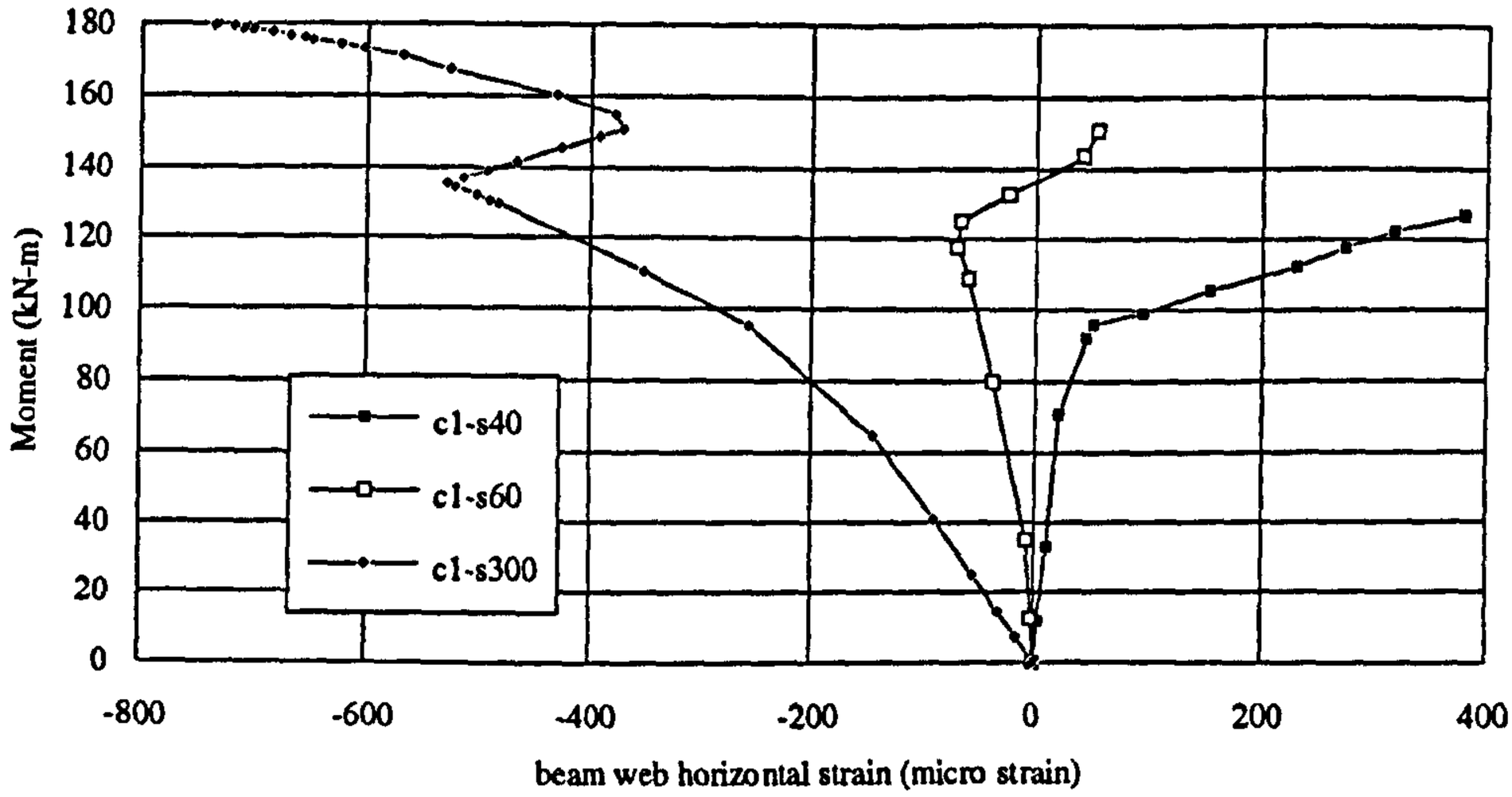

Figure 4-9 Variation of moment-beam web horizontal strain curves with degree of shear interaction

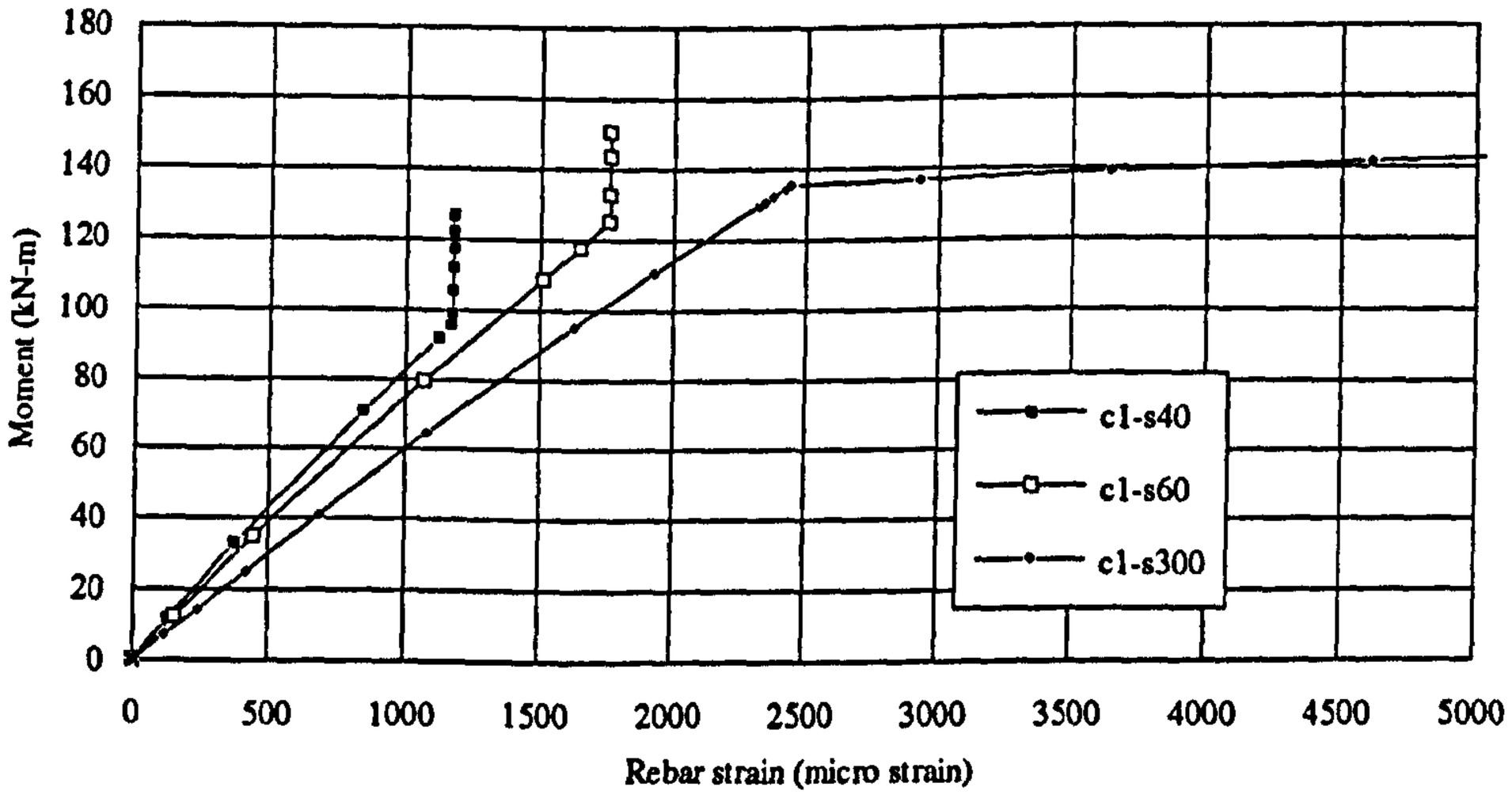

Figure 4-10 Variation of moment-rebar strain curves with degree of shear interaction

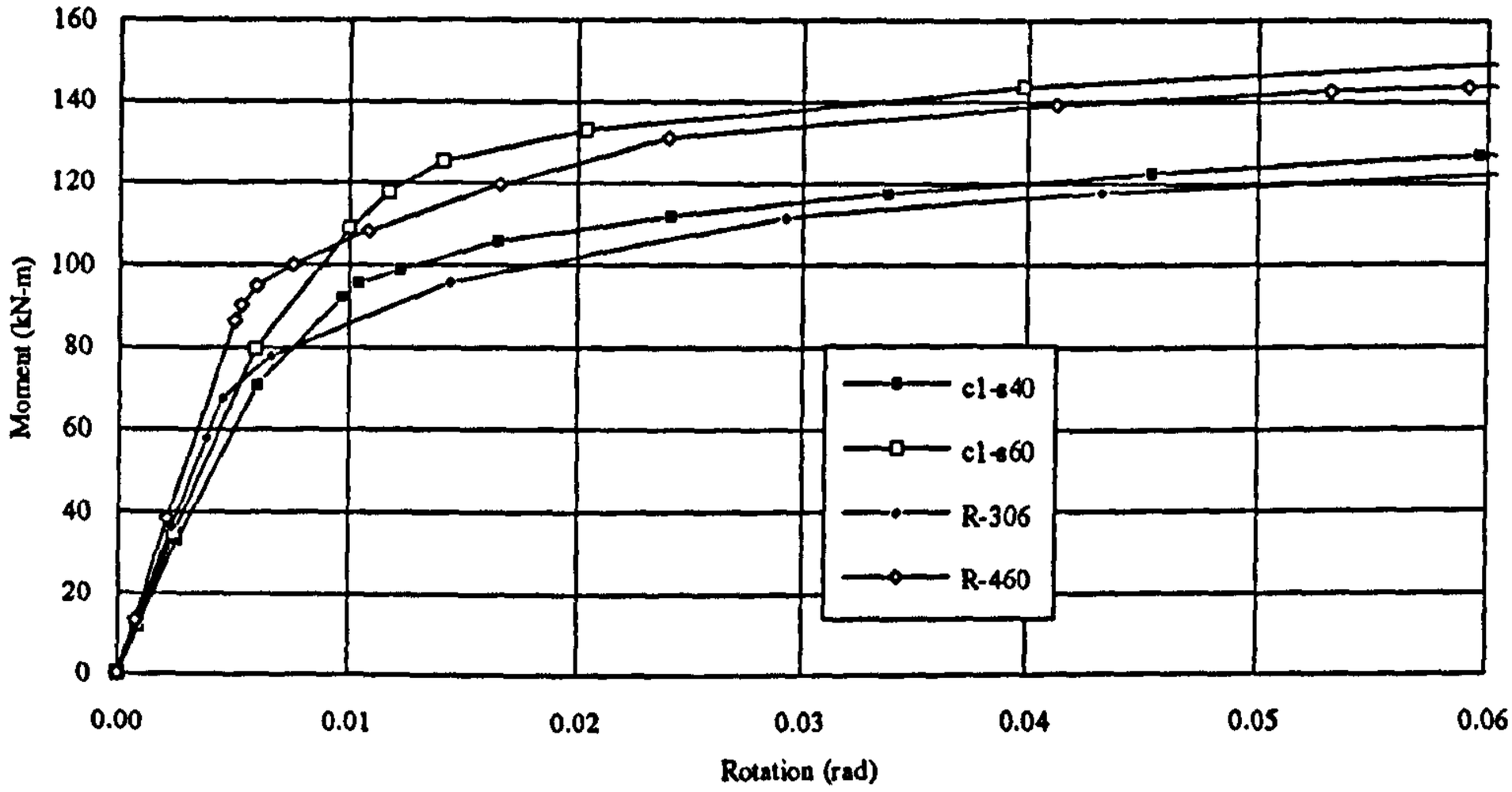

Figure 4-11 Variation of moment-rotation curves with degree of shear interaction

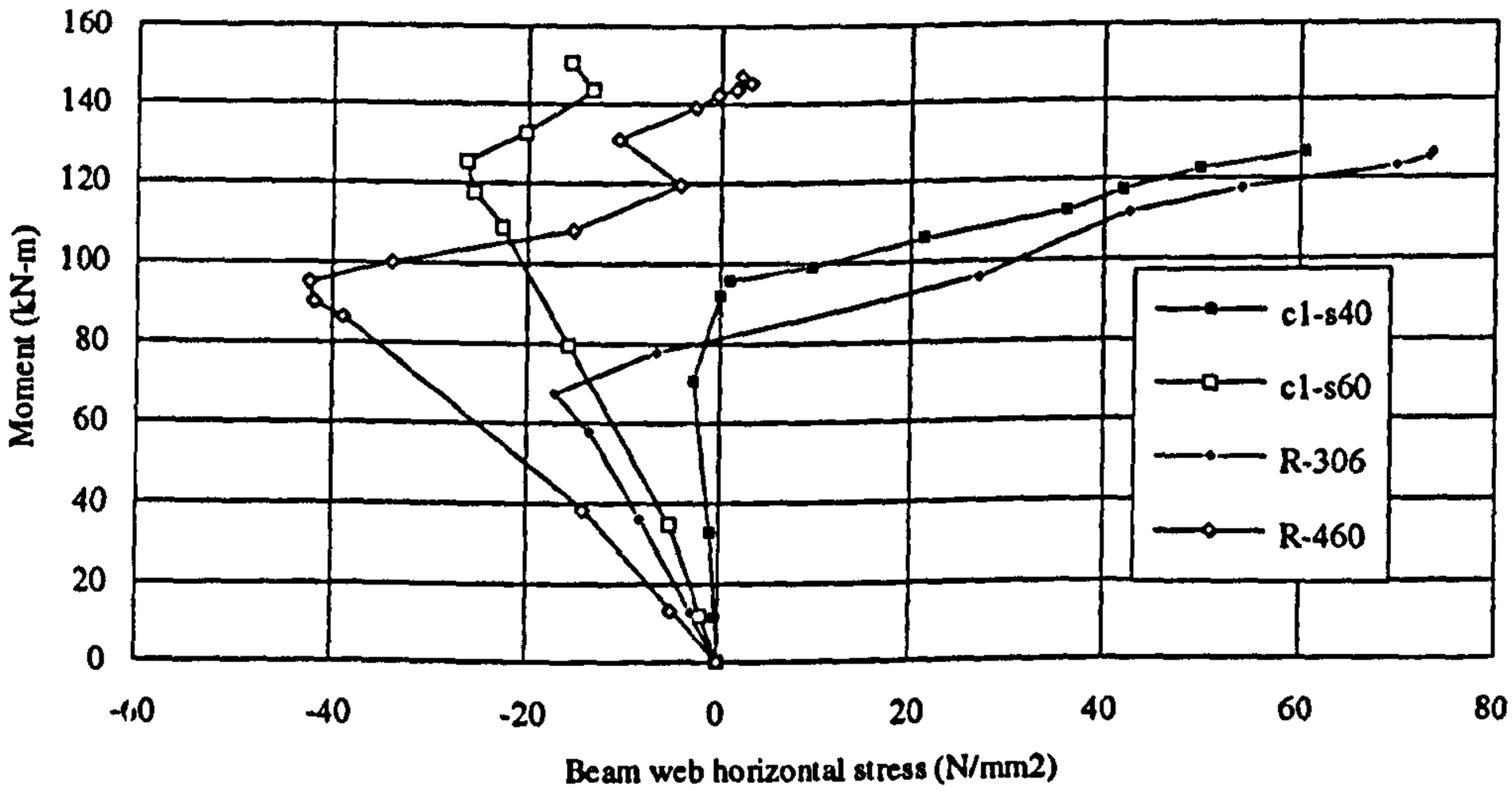

Figure 4-12 Variation of moment-beam web horizontal stress curves with degree of shear interaction and reinforcement area

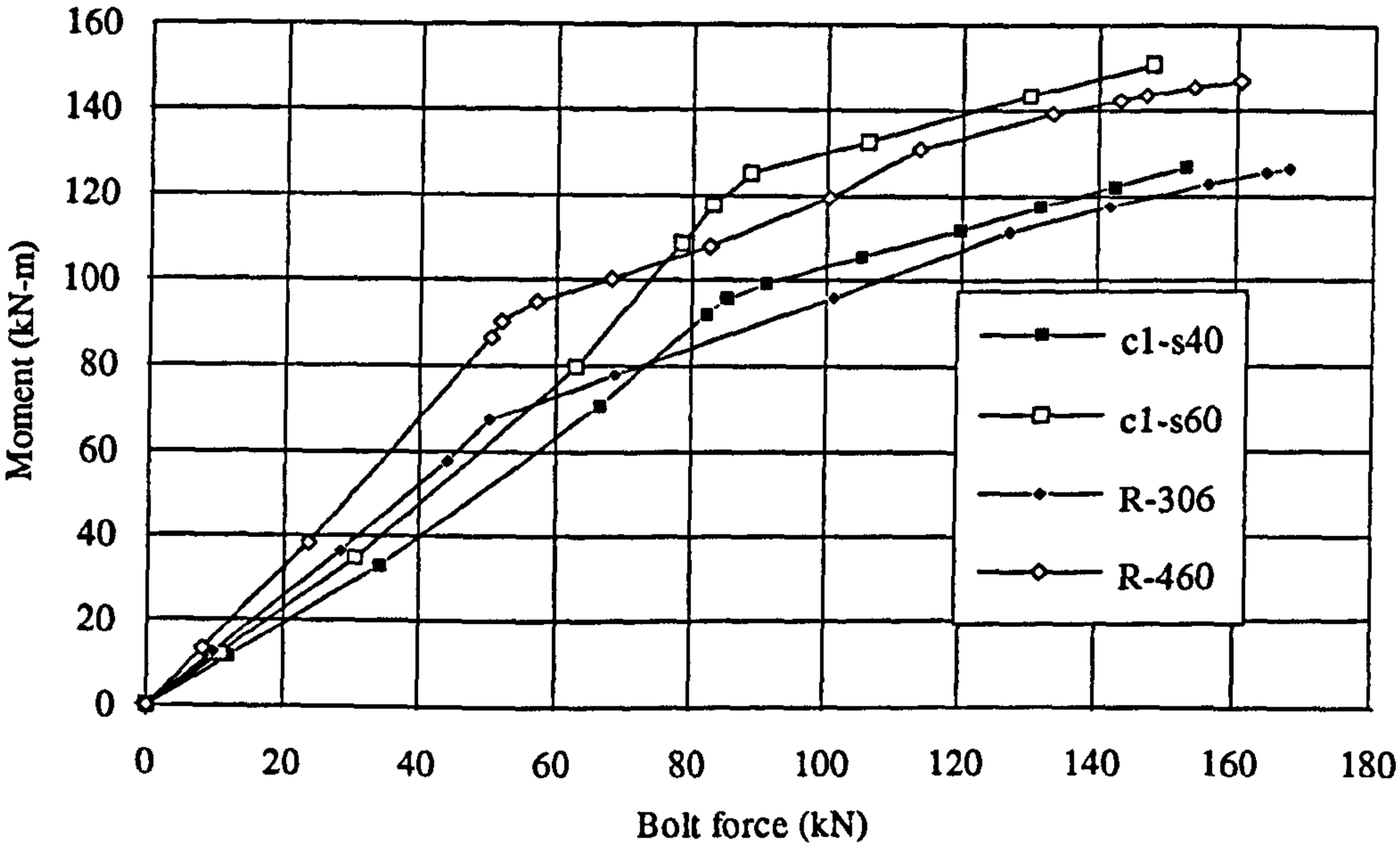

Figure 4-13 Variation of moment-bolt force curves with degree of shear interaction and reinforcement area

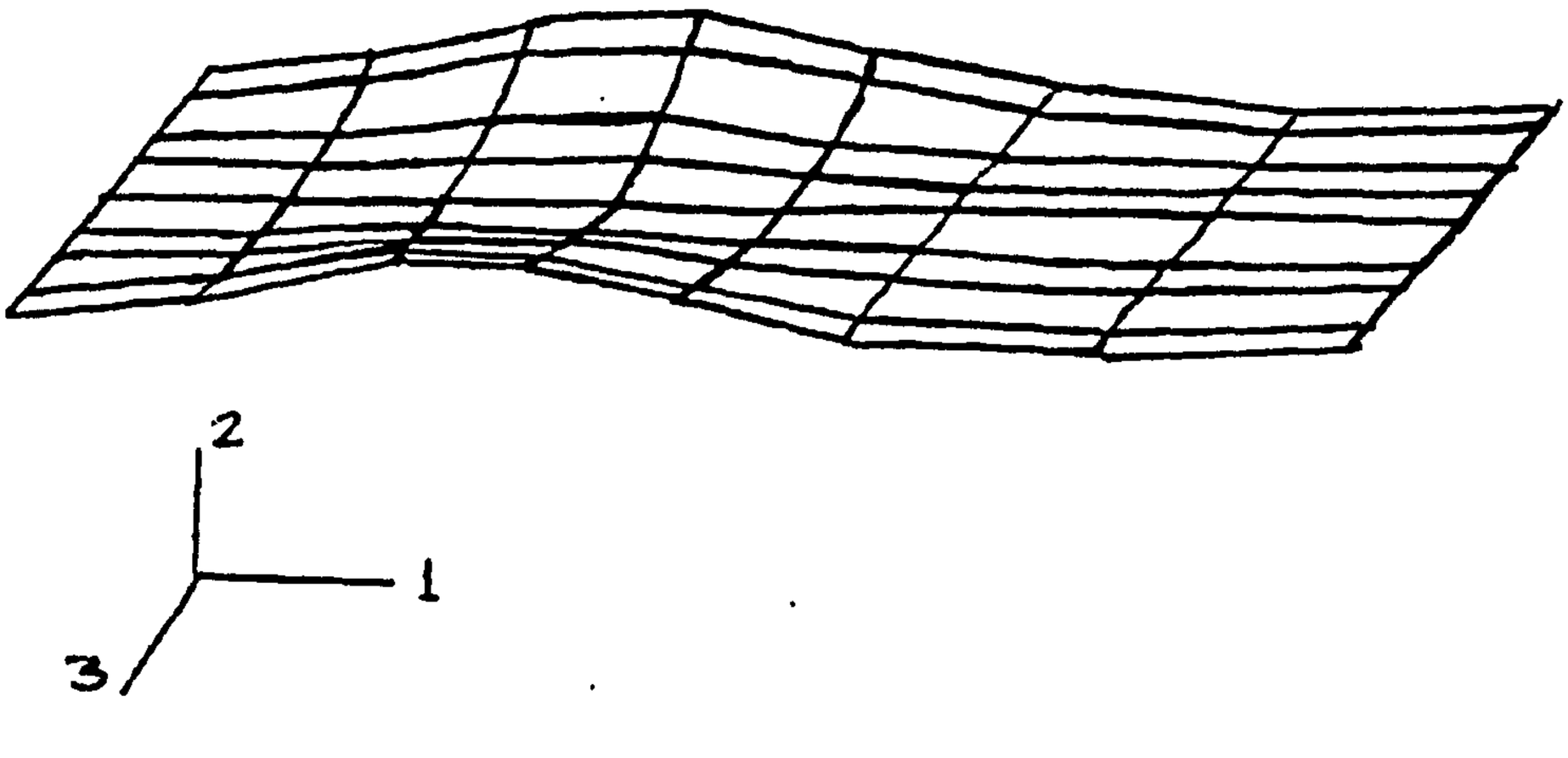

Figure 4-14 Deformed shape of the bottom flange at ultimate load (magnified three times)

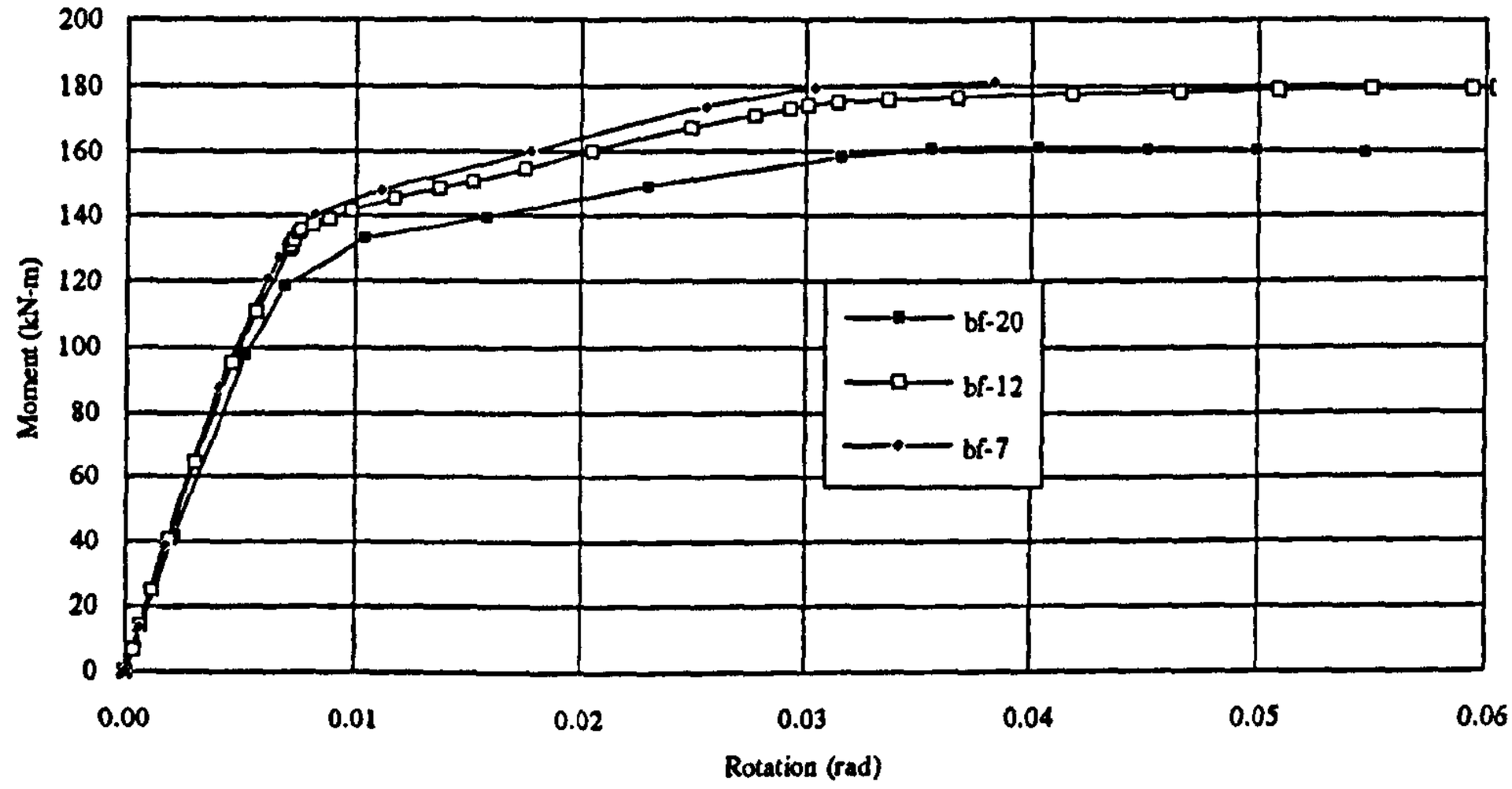

Figure 4-15 Moment-rotation curve for various B/T ratios

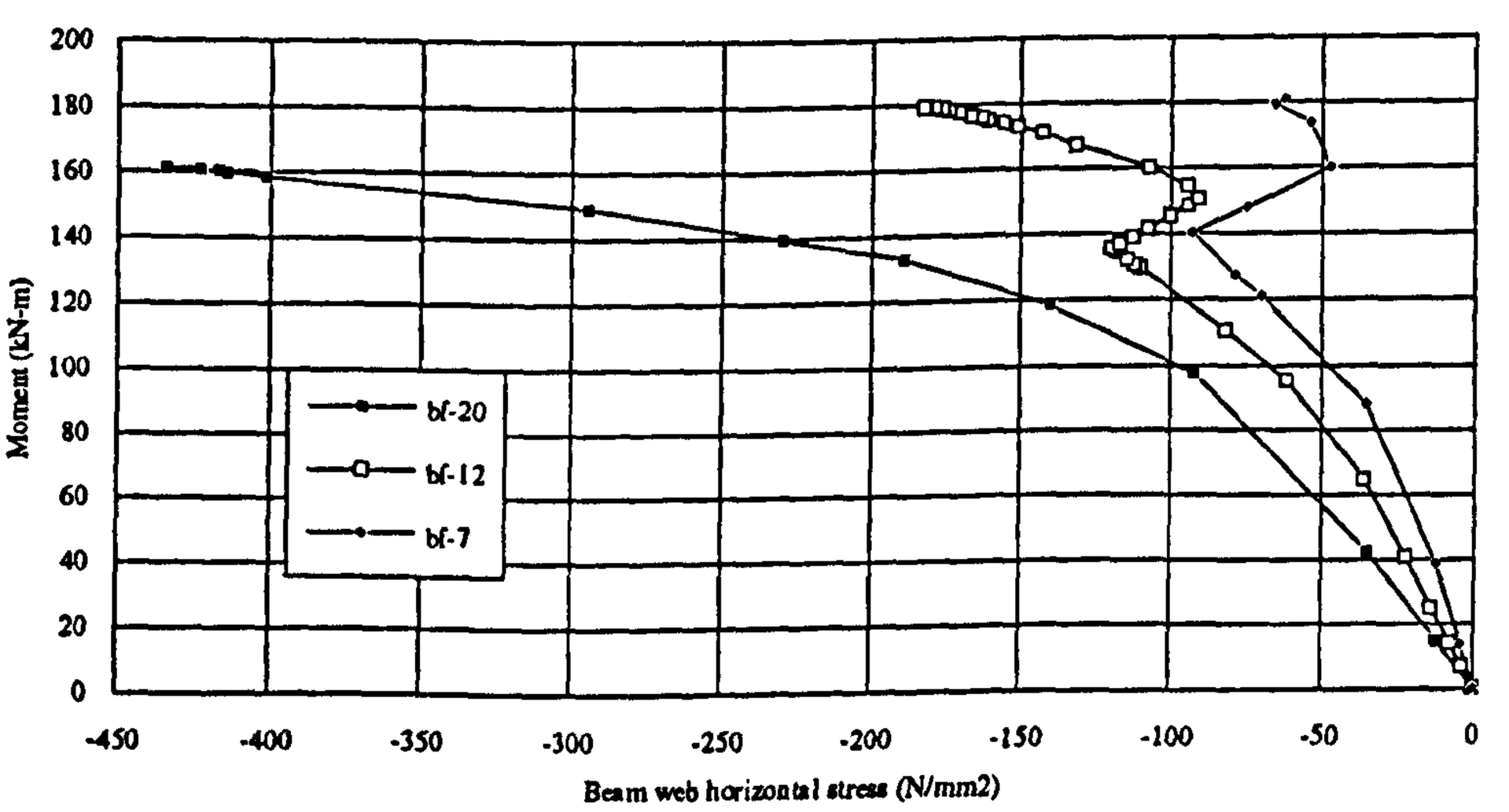

Figure 4-16 Moment-beam web horizontal stress curves for various B/T ratios

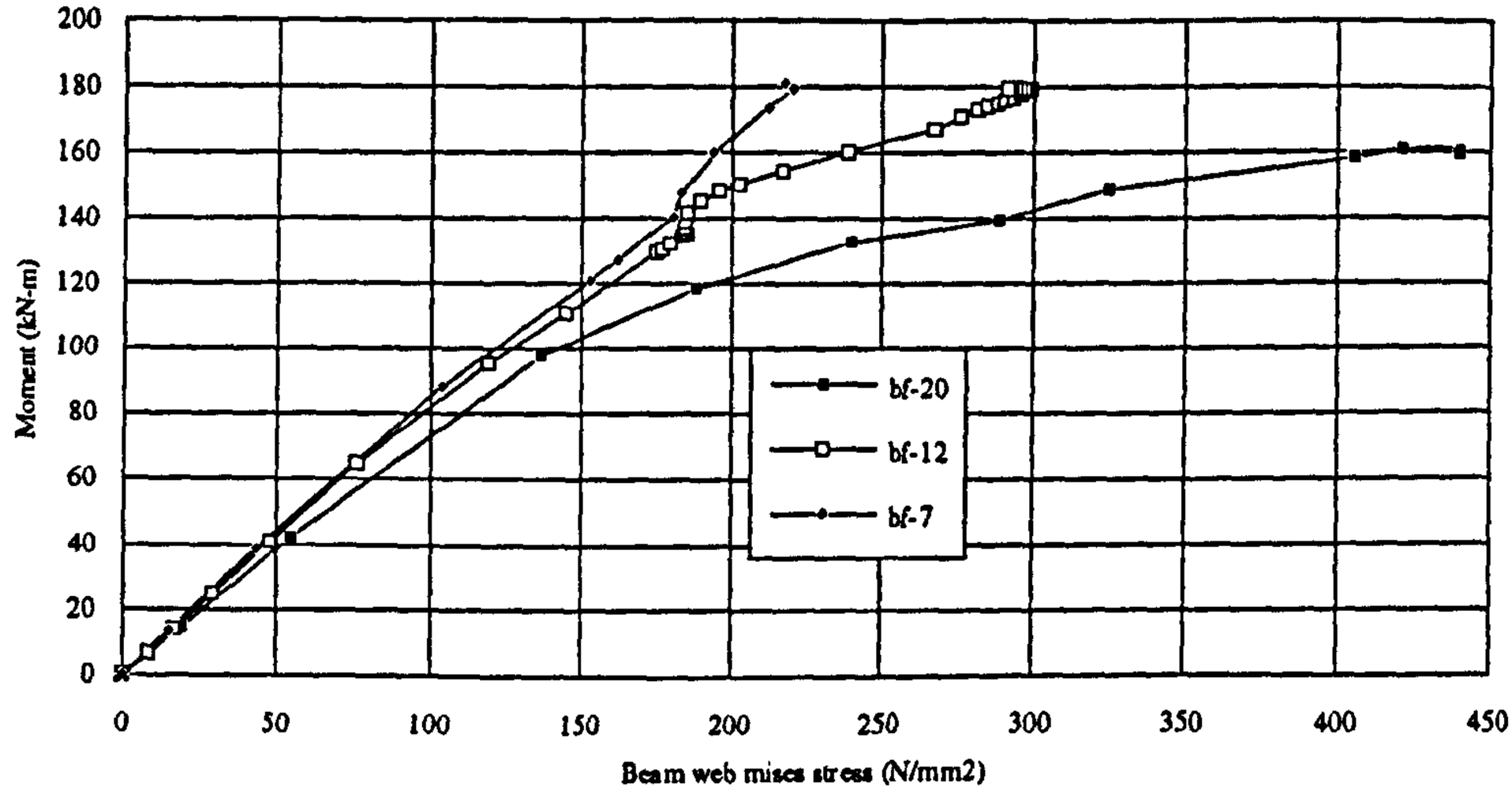

Figure 4-17 Moment-beam web von-Mises stress curves for various B/T ratios

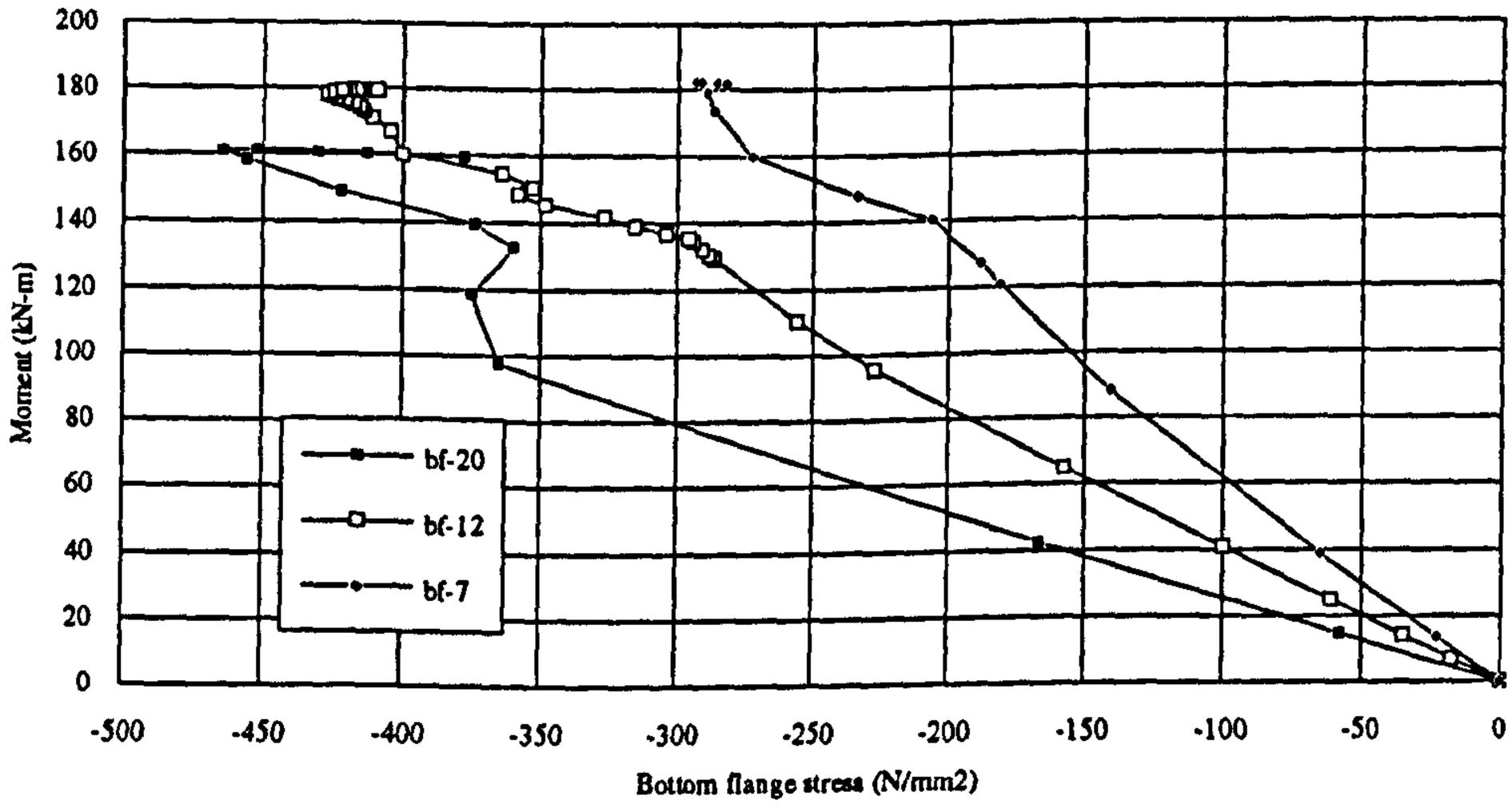

Figure 4-18 Moment-bottom flange stress curves for various B/T ratios

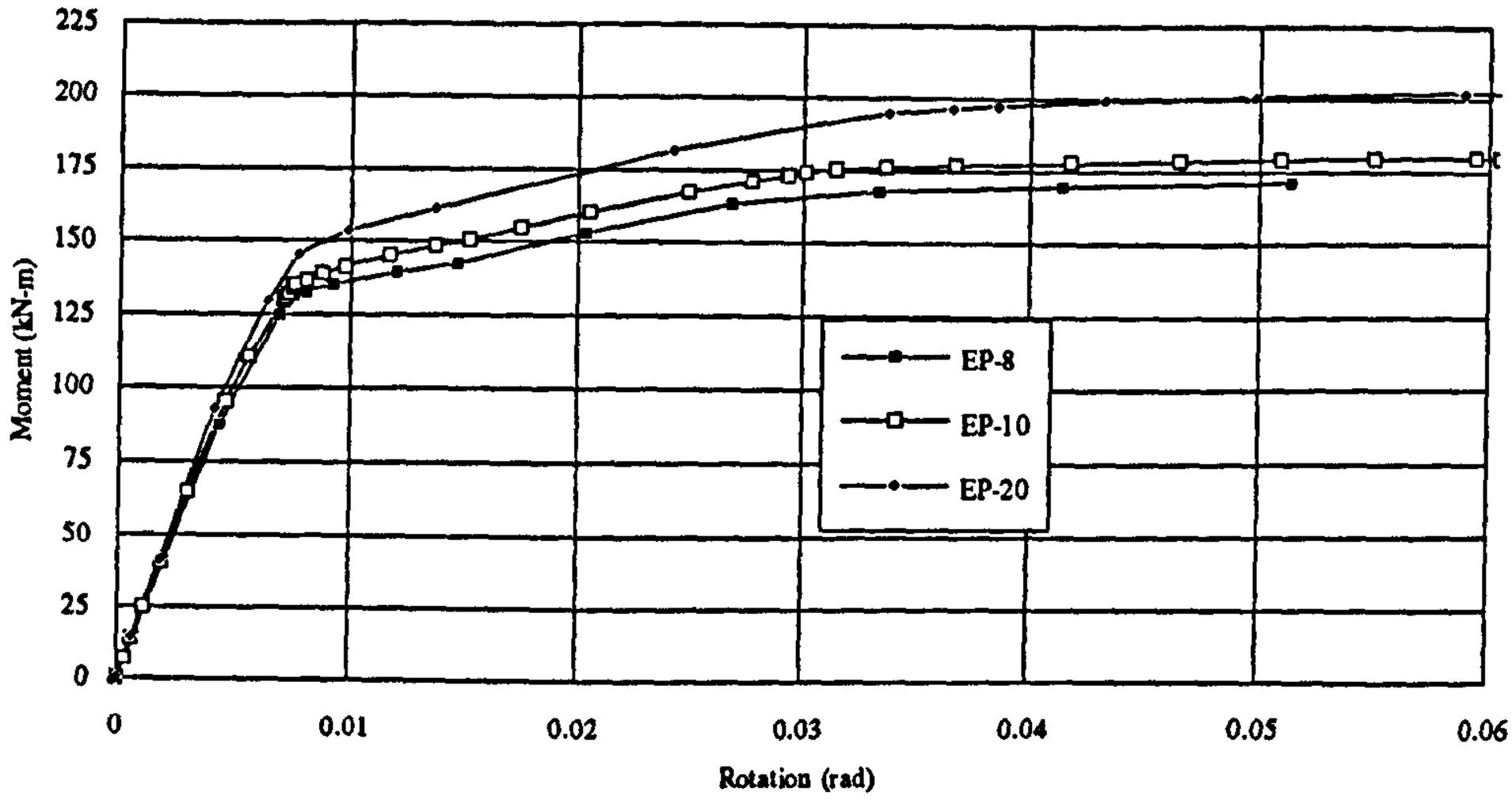

Figure 4-19 Moment-rotation curves for varying endplate thickness

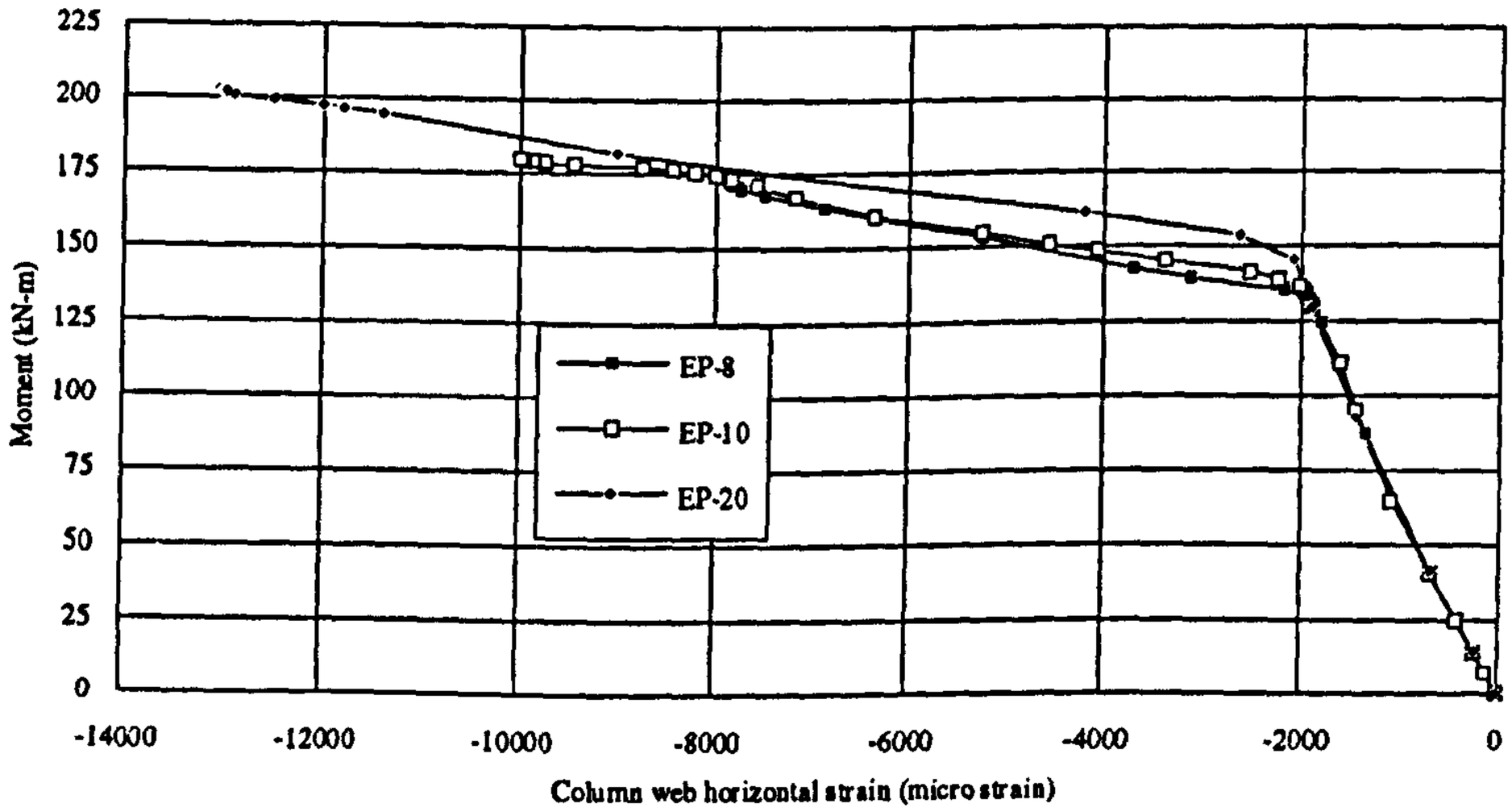

Figure 4-20 Moment-column web horizontal strain curves for varying endplate thickness

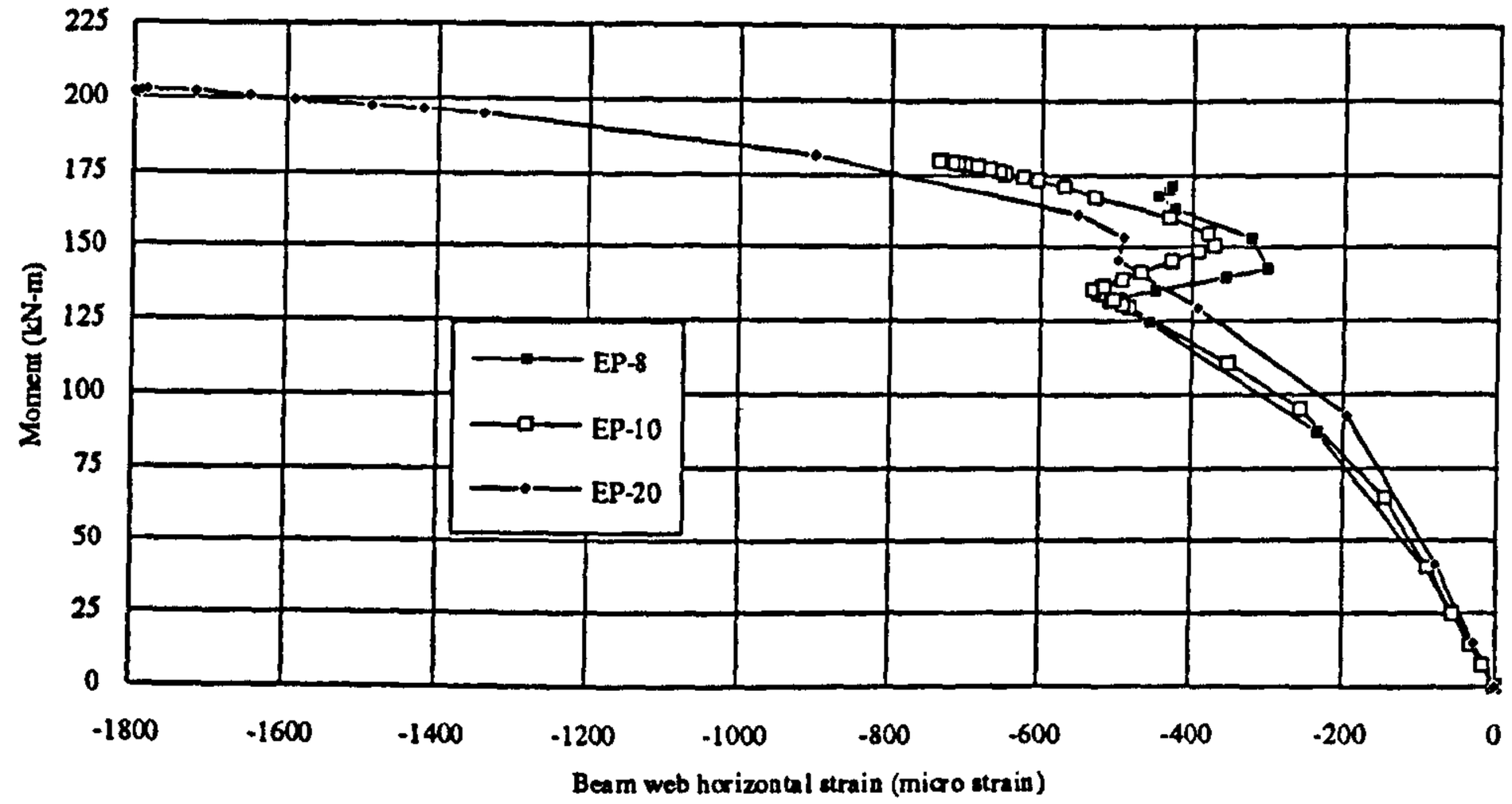

Figure 4-21 Moment-beam web horizontal strain curves for varying endplate thickness

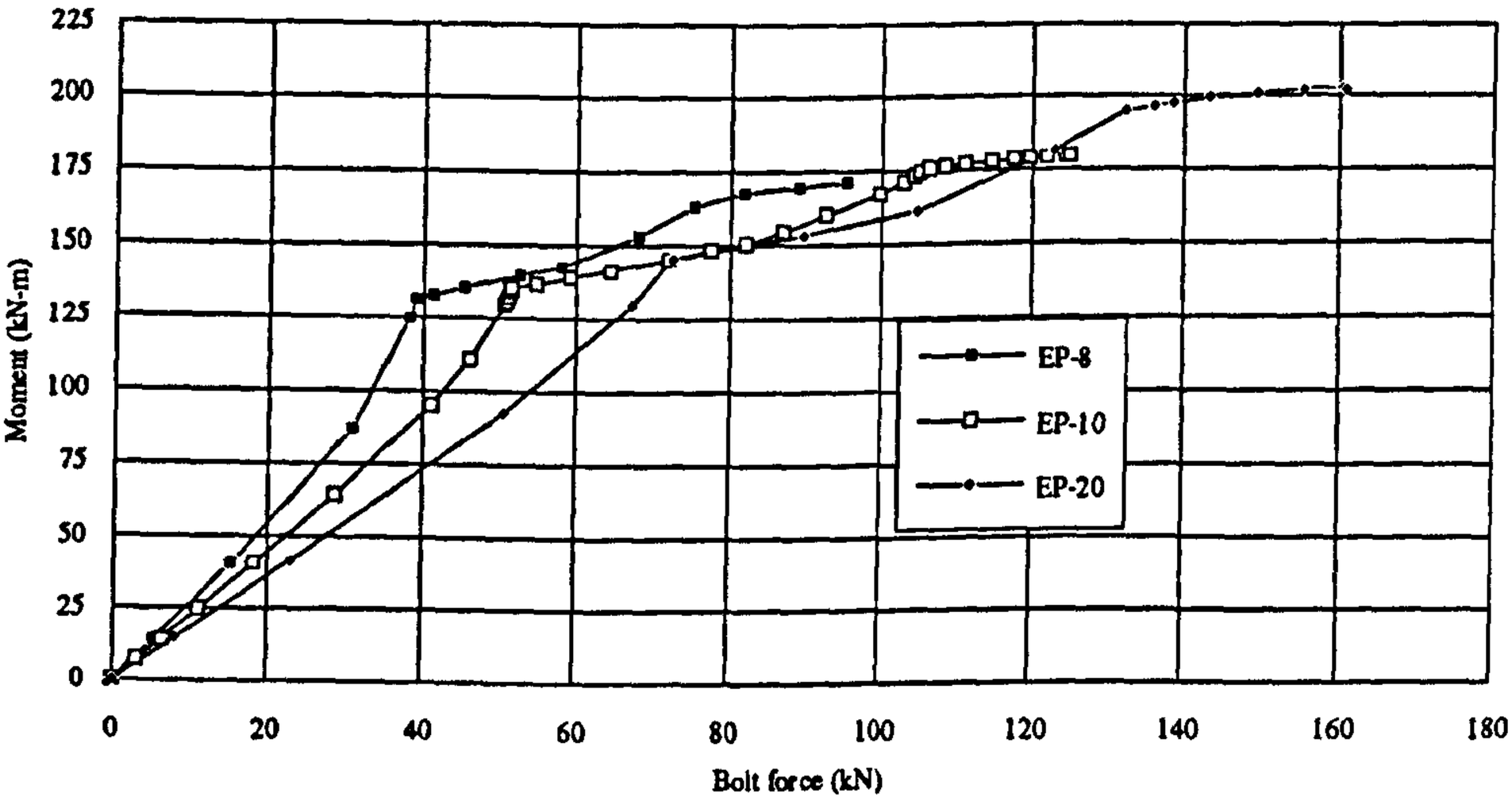

Figure 4-22 Moment-bolt force curves for varying endplate thickness

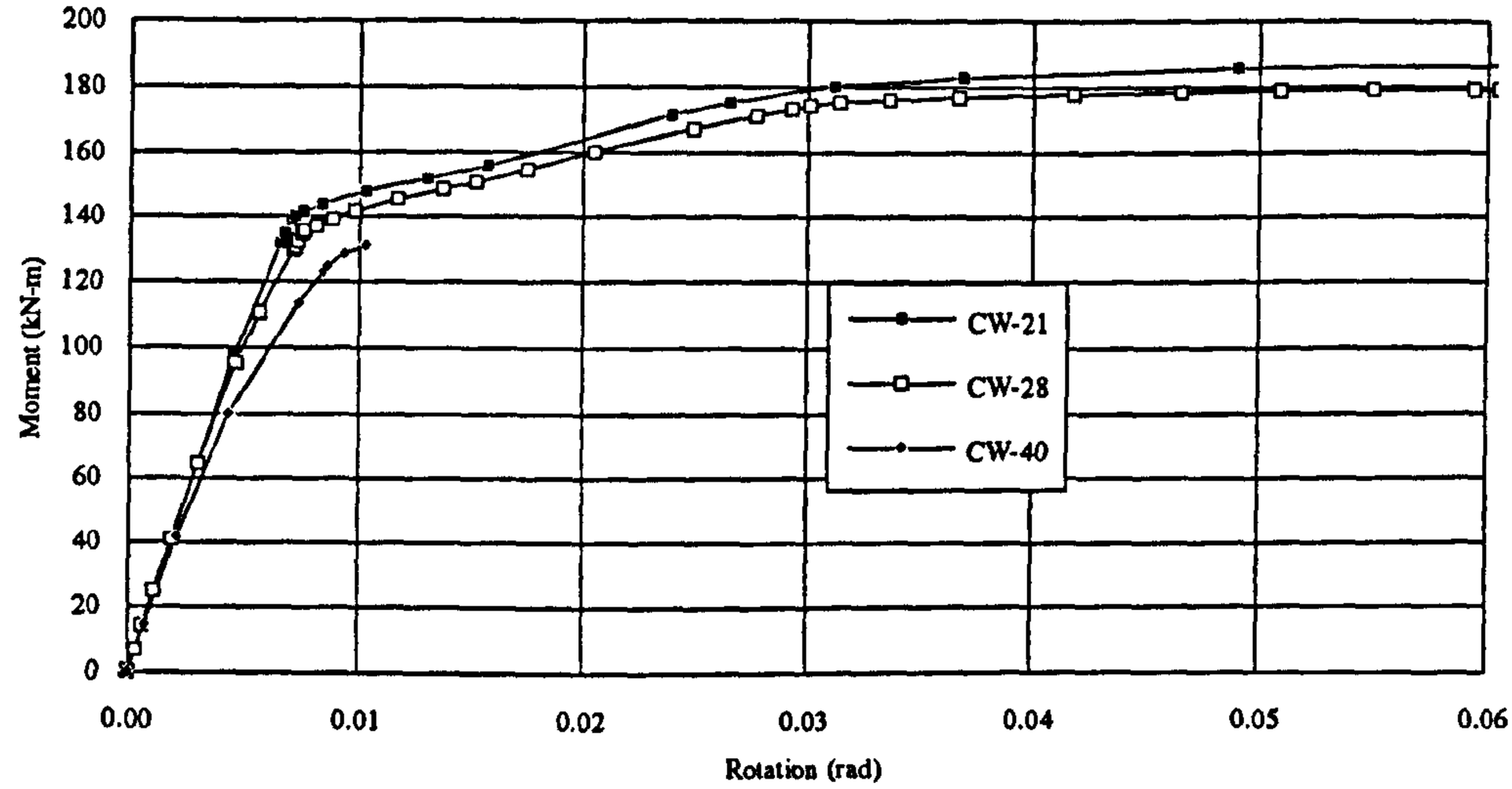

Figure 4-23 Moment-rotation curves for different column web width to thickness ratio

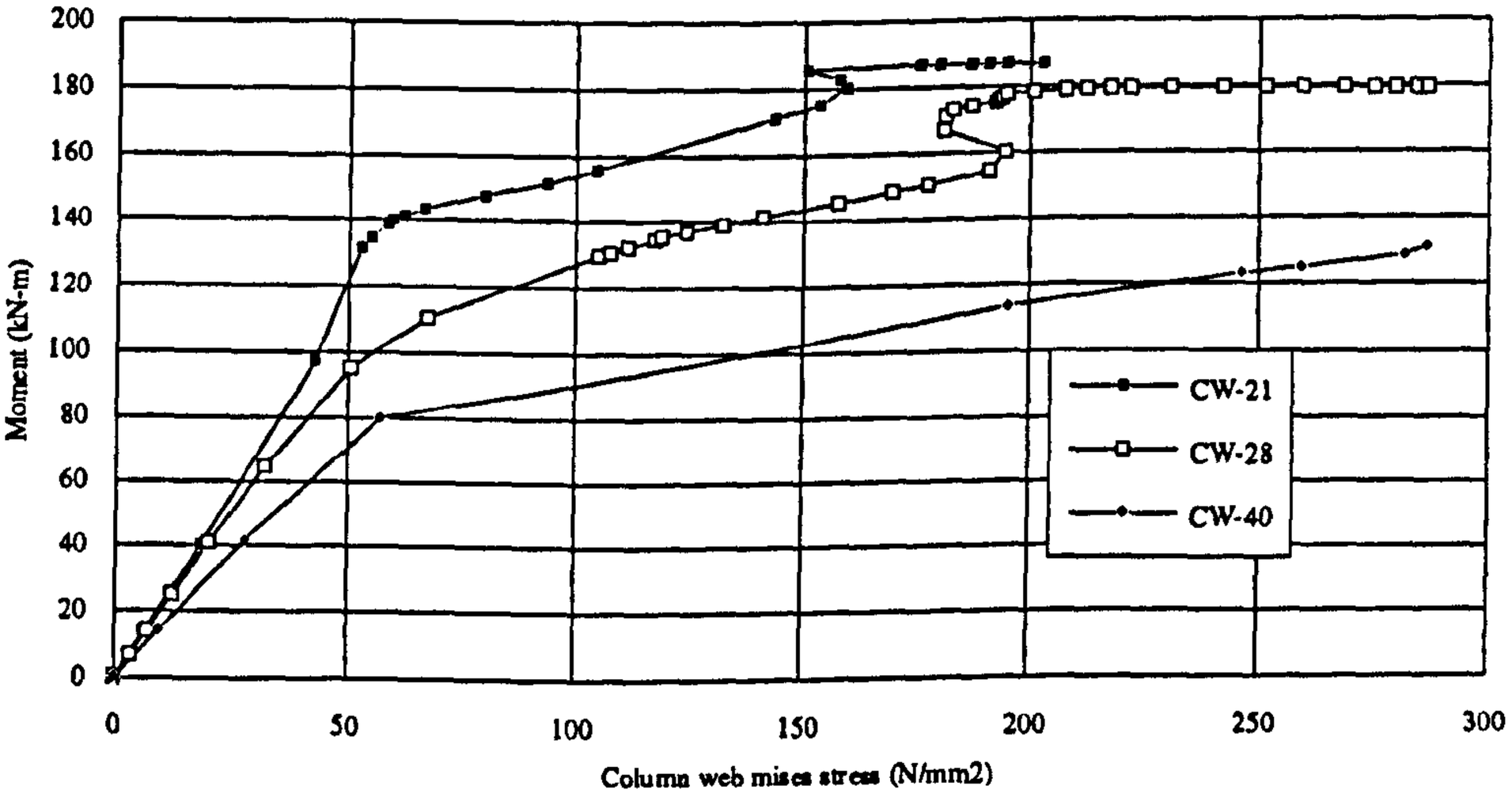

Figure 4-24 Moment- column web von-Mises stress curves for different column web width to thickness ratio

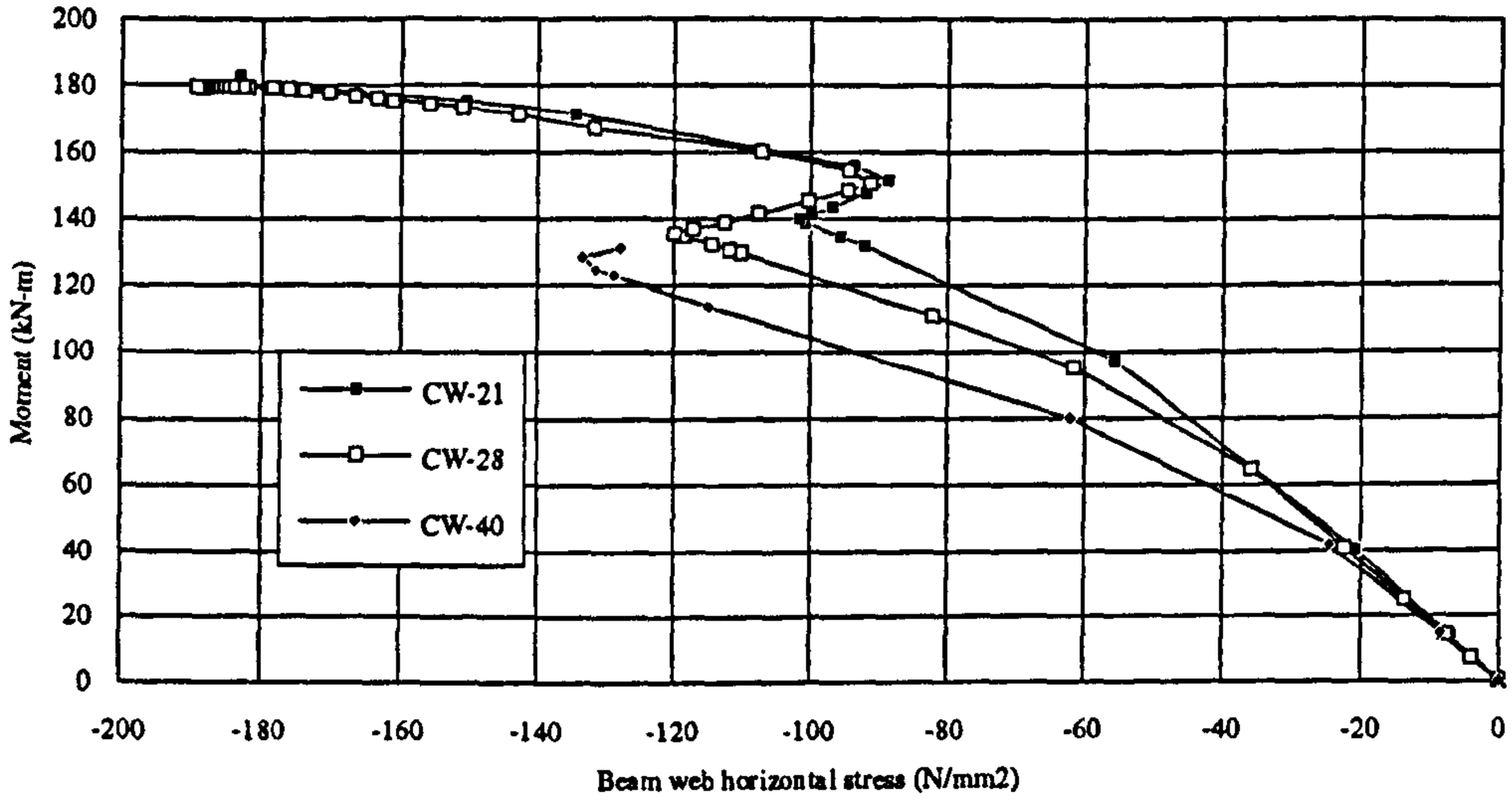

Figure 4-25 Moment- beam web horizontal stress curves for different column web width to thickness ratio

Chapter 5

Effect of high shear on the moment capacity of composite cruciform endplate connections

5.1 Introduction

It was observed in chapter 1 that examination of isolated connection tests in which the shear to moment ratio has been a controlled variable has revealed somewhat contradictory findings. Due to this the present design approaches for determining the moment capacity of composite connections cannot properly consider the influence of changes in the shear to moment ratio.

The finite element model that was fully described in chapter 3 has been used, in conjunction with some rather basic mechanics, to investigate the effects of different levels of coincident shear on the moment capacity of composite endplate connections. Because the approach permits the controlled variation of individual parameters, it has been possible to study in detail the effects of shear on a range of connections when their behaviour is controlled by different forms of failure. This has provided the key to explaining the apparently contradictory behaviour observed in the connection tests referred to above. The importance of high shears in influencing moment capacity has been found to be dependant on the mode of failure that controls the connection's strength. Six different cases have been identified: beam web overstress, reinforcement yield, failure in the shear studs, column web overstress, column web buckling and compression capacity of beam. Only in the case of the first and fourth of these does the presence of a high coincident shear reduce the connection's moment capacity. Expressions for checking all six cases are provided.

Finally, a design method to predict the actual effect - in particular the calculation of connection moment capacity in those situations for which changes to the shear to moment ratio become important - is presented in this chapter. Use of the design method is illustrated by means of a worked example.

5.2 Experimental results on shear to moment ratio

As mentioned before five test results are available in which different shear to moment ratios were employed. For tests CJS-1, CJS-4 and CJS-5 [5-1] the shear spans were 1473 mm, 1023 mm and 573 mm. So the ratios of shear to moment were 0.679, 0.978 and 1.745 m^{-1} for the three cases. The corresponding moment capacities were 181.5 kN•m, 177.5 kN•m and 197.2 kN•m respectively. CJS-4 had a decreased moment of 2.2% but CJS-5 had an increase of 8.65% in moment capacity. From the test results alone it was not possible to properly identify the cause of these changes. The reason that CJS-5 had a high moment capacity was explained as: "*Shear span for specimen CJS-5 was very small and some part of the applied load could be directly transferred to the column through the diagonal compression path crossing the concrete slab and the steel beam web. Owing to this short cut load transfer mechanism, the connection load could be increased since some part of the applied load will not generate connection moment.*"

Xiao's tests SCJ4 and SCJ6 [5-2] had shear spans of 1500 mm and 800 mm respectively. This gave shear to moment ratios of 0.667 m^{-1} and 1.25 m^{-1}, i.e. an increase of 0.583 from SCJ4 to SCJ6. For SCJ4 the ultimate moment was 202.9 kN•m, ultimate rotation was 23.4 mrad and maximum rotation was 41.1 mrad. For SCJ6 the ultimate moment was 157.6 kN•m, ultimate rotation was 11.5 mrad and maximum rotation was 23 mrad. These test results therefore show that the moment capacity was reduced by 22%, initial stiffness was unchanged and rotation capacity was decreased

by 51%. The failure mode for both connections was buckling of the column web, coupled with excessive deformation of the column flange.

From the test results it was observed that in all the three tests of Li the rebars actually yielded and reached their ultimate strength at the connection ultimate capacity, but the failure mode of Xiao's tests indicated that buckling of the column web was the factor determining the connection vertical load capacity. All the three specimens of Li had transverse beams connected into the column web, which played some role in preventing buckling of the column web. In Xiao's tests there were no such beams; this allowed the column web to buckle. This therefore suggests that it is the type of failure which controls the ultimate vertical load capacity of the connection that will determine whether there will be any effect due to changes in the shear to moment ratio.

5.3 Theoretical investigation

Using basic mechanics the attainable resistance of the connection against vertical shear P_v may be investigated. Attainable resistance is defined as the value that could be achieved if actual failure were controlled by the mode under consideration; in reality another mode of failure associated with a lower load may actually govern. Connection load capacity can be controlled by either of the following six cases studied:

- Beam stress reaching the von-Mises limit
- Reinforcement yielding
- Shear stud capacity
- Column web stresses reaching von-Mises limit
- Column web buckling
- Capacity of beam to transfer compressive force

The analyses are presented in sections 5.3.1 to 5.3.6 and in section 5.3.7 the resulting equations are used to examine the test results from Li [5-1] and Xiao [5-2].

5.3.1 Case 1 Maximum vertical force controlled by beam stresses

From the von-Mises condition:

$$\sigma^2_m = \sigma^2_x + \sigma^2_y - \sigma_x.\sigma_y + 3\tau^2_{xy} \qquad (5\text{-}1)$$

Where:

σ_x is the bending stress in the direction of the beam axis

σ_y is the bending stress in the direction normal to the beam axis

τ_{xy} is the shear stress

Finite element analysis has shown that the vertical component of the direct stress is much smaller than the other two components in the beam web. It has been observed from finite element analysis that when the shear to moment ratio is high the connection attains its maximum load by having its beam web overstressed. The von-Mises stress reaches its limit due to the action of both large shear and horizontal stresses. It was observed that at this stage the lower part of the beam web attains a plastic stress distribution for a depth of $2.0t_{bf}$ from the centreline of the bottom flange i.e. a rectangular stress block over this depth. A reasonable estimate of this load can be obtained by calculating the von-Mises stress from the horizontal stress at a point $2.0t_{bf}$ above the centreline of the bottom flange (using the simple bending theory and using the value of second moment of area from equation 5-4) and shear stress assuming a uniform distribution then equating it to the strength of the beam web. This allows the consideration of the plastic state of the beam web in a very simple way. Neglecting the stress in the y direction, the von-Mises equation reduces to:

$$\sigma^2_m = \sigma^2_x + 3\tau^2_{xy} \qquad (5\text{-}2)$$

From Figure 5-1 the beam properties are:

$$\bar{y} = \frac{A_r D_r + t_{bw}\left(H_b - 2t_{bf}\right)\frac{\left(H_b - t_{bf}\right)}{2} + b_{bf}\, t_{bf}\left(H_b - t_{bf}\right)}{\left[\left(H_b - 2t_{bf}\right)t_{bw} + 2t_{bf}\, b_{bf} + A_r\right]} \tag{5-3}$$

$$I = A_r\left(D_r - \bar{y}\right)^2 + b_{bf}\, t_{bf}\left[\bar{y}^2 + \left(H_b - t_{bf} - \bar{y}\right)^2\right] + \frac{t_{bw}\left(H_b - 2t_{bf}\right)^3}{12} + t_{bw}\left(H_b - 2t_{bf}\right)\left(\frac{\left(H_b - t_{bf}\right)}{2} - \bar{y}\right)^2 \tag{5-4}$$

Which gives:

$$\sigma_x = \frac{P_v . x . \left(\bar{y} - 2t_{bf}\right)}{I} \tag{5-5}$$

$$\tau_{xy} = \frac{P_v}{H_b . t_{bw}} \tag{5-6}$$

Combining equations 5-2, 5-5 and 5-6, the capacity of a beam under the combined action of shear and bending is:

$$P_v = \frac{\sigma_m}{\sqrt{\frac{x^2 . \left(\bar{y} - 2t_{bf}\right)^2}{I^2} + \frac{3}{H_b{}^2 . t^2{}_{bw}}}} \tag{5-7}$$

Equation 5-7 is not intended for determining the actual capacity of a composite beam section but to indicate the level of load which is controlled by the beam web attaining the von-Mises stress limit.

For this mode to govern, the slab must be over reinforced, and for the reinforcement to be fully effective shear failure of the concrete must be prevented. This will require the

number of shear studs to be high and this may well not be possible when using metal decking. Steel beam depth will also need to be small.

5.3.2 Case 2 Maximum vertical force controlled by reinforcement

If the reinforcement area is low, the maximum possible vertical load will be controlled by the force that can be developed by the reinforcement. As the rebar area is low in this case the compressive force developed in the bottom flange alone will be sufficient to balance the tensile force in the rebar and the top row of bolts. Also for an under reinforced connection the failure is governed by the fracture of the rebar which does not allow tensile force to develop in the lower row of bolts. Figure 5-2 illustrates the free body diagram for the connection. Taking moments about the centreline of the bottom flange:

$$P_v.x = F_r.D_r + F_b.d_b$$

$$P_v = \frac{[F_r D_r + F_b d_b]}{x}$$

$$P_v = \frac{[A_r f_{ur} D_r + F_b d_b]}{x} \qquad (5\text{-}8)$$

Where F_b is the force in the top row of bolt, to be determined by the equations from EC3 (J.3.5.5.2, J3.5.7 and Clause 6.5.5) or their simplifications proposed in reference 5-3 (see equation in step-1 of design proposal).

Equation 5-8 indicates the level of load when this is controlled by the reinforcement attaining yield.

5.3.3 Case 3 Maximum vertical force controlled by shear stud capacity

The maximum vertical force for a connection may also be controlled by the capacity of the shear studs. Figures 5-3 and 5-4 show the force developed in the shear studs of the connections CJS-1 and CJS-5 as obtained from FE analysis. CJS-1 and CJS-5 have the same connection configuration, the only difference is in the position of the applied load and thus the shear to moment ratio. So from the FE analyses it is clear that for the same connection detail, if the beam is loaded close to the connection, the shear studs between the column flange and the load are subjected to a much higher shear force than the shear studs beyond this region - providing they have sufficient shear transfer capacity. Thus if the combined capacity of the shear studs is much higher than the force that can develop, then the force developed in the shear studs in a connection decreases linearly away from the column flange when the beam is loaded at the end. According to the plastic design theory all shear studs should be able to take the same load if required. To check this, FE analysis was conducted for 40% shear interaction, as the tested connections had 300% interaction which is too high to verify the criterion. The resulting shear stud forces are shown in Figure 5-5. This confirms that the plastic design assumption of all studs reaching their ultimate capacity is correct, even when load is applied far from the connection. For connections with low shear interaction the distribution of load in the shear studs beyond the load is shown in Figure 5-6; this is quite similar to the previous case.

This indicates that when the beam is not loaded at the end, although the direct shear in the beam outside the loading point is zero, due to the presence of the metal decking and the reinforced concrete the shear studs outside the loading point are subjected to horizontal shear due to the interface slip. The tension in the reinforcement must be balanced by the shear force in the studs, and when the individual shear capacity is low for the studs, the shear studs not within the loaded length must resist a considerable

part of this shear. At the ultimate state they can carry horizontal forces as high as those in the inner shear studs, if they are not within hogging moment region.

So the possible maximum stud force should always be determined by multiplying the number of studs in a connection by the capacity of a single stud. Figure 5-7 shows the free body diagram for the connection used to determine the vertical load capacity of the connection. Taking moments and assuming that the moment of the beam web compressive force balances the moment of the lower bolt row forces gives:

$$P_v = \frac{[F_s D_r + F_b d_b]}{x} \tag{5-9}$$

Where:

F_S is the maximum possible shear stud force, to be calculated by multiplying the capacity of a single shear stud or a pair of shear studs by the number of rows

F_b is the force in a row of bolt, to be determined by the equations given in EC3 and reference 5-3

D_r, d_b and x are obtained from the geometry of the connection and the position of the load

The magnitude of P_v obtained from equation 5-9 will give the load level that can be supported by the shear studs.

Figures 5-3 and 5-4 suggest that the type of stud to be used needs careful consideration. If the concrete is weak and the stud is too stiff for the concrete, it might lead to concrete failure. Figures 5-5 and 5-6 indicate that soft shear studs can develop the required shear force if their number is increased sufficiently, without causing failure of the concrete. From the FE results it is observed that with 300% interaction the stud at the beam end developed 8 kN shear force, whereas with 40% shear interaction the same stud developed 26.3 kN force which is the same as the maximum value, when the

load was applied at 579 mm from the column flange. This indicates that it is preferable to use shear studs each capable of transferring a smaller shear force but with their number increased to provide the necessary amount of shear interaction.

5.3.4 Case 4 Maximum shear force governed by column web compression capacity

For a cruciform connection the main active components of stress are the horizontal and vertical stresses. The von-Mises stress equation therefore takes the following form:

$$\sigma^2{}_m = \sigma^2{}_x + \sigma^2{}_y - \sigma_x.\sigma_y$$

For a cruciform connection the normal stress in the column web due to a load P_v on each side of the connection is:

$$\sigma_y = \frac{2.P_v}{t_{cw}.D_c}$$

Using a simplified approach to calculate the horizontal compressive force on the column web (i.e. $F_c = M/D_r$) the horizontal stress is:

$$\sigma_x = \frac{P_v.x}{D_r t_{cw} b_{eff}}$$

Where :

t_{cw} is the thickness of the column web

$$b_{eff} = t_{bf} + 2\sqrt{2}a_b + 2t_p + 5\left(t_{cf} + r_c\right)$$

a_b is the throat thickness of the weld

r_c is the root radius

t_{cf} is the thickness of the column flange

t_{bf} is the thickness of the beam flange

The von-Mises stress condition gives:

$$P_v = \frac{\sigma_m . D_c . t_{cw} D_r b_{eff}}{\sqrt{4 D_r^2 b_{eff}^2 + D_c^2 x^2 - 2 x D_r b_{eff} D_c}} \qquad (5\text{-}10)$$

Where:

D_C is the depth of the column web

The load predicted by equation 5-10 is the level which can be supported by the column web based on reaching the von-Mises limit. This equation will give slightly conservative results as it disregards the contribution of the column flanges to the resistance of the force. It is to be noted that during the stress calculation the effect of the column axial load is neglected as studies (presented in chapter 6) have shown that for composite flush endplate cruciform connections, this is insignificant. The reason was found that for symmetrically loaded connections the column web compression strength was not affected by column loading and for non-symmetrically loaded connection the of column web shear strength (with column loading) and the maximum developable tensile force in the rebars makes the connection shear capacity lower than that predicted from the consideration of shear to moment ratio. It may appear that equation 5-10 is based on a localised stress condition in the column web. But as the stress to be used in this equation is the column web ultimate strength (i.e. strain hardening is considered) this will actually represent a situation where a larger part of the column web has yielded.

5.3.5 Case 5 Maximum shear force governed by column web buckling for columns without transverse beams

Another important factor that may govern the capacity of the connection is the buckling resistance of the column web in compression, for which EC3 provides a design formula. This has been simplified for ease of calculation in reference 5-3 to give:

$$F_{c,buckle} = 8.4 b_{eff}^{0.017} D_c^{0.600} t_{cw}^{1.430} f_{cw}^{0.760} \quad (5\text{-}11)$$

Where:

f_{cw} is the column web strength

The above is an empirical equation for which all the units of dimension are mm, stress is N/mm^2 and the force is N.

However, in practical situations column web buckling will be critically influenced by a number of factors not explicitly included in equation 5-11 or the original studies on which it is based. One particularly important factor is the degree of restraint against the development of out of plane deformation provided by any beams (and their connections) framing into the column web. Thus tests in which column web buckling was observed exhibit considerable scatter [5-4]. An improved method for treating this phenomenon that is capable of more correctly representing the true situation is therefore needed. In the absence of a completely satisfactory approach, equation 5-11 will be used to illustrate the way in which column web buckling should be included in the overall approach presented herein.

Assuming that the buckling force is equal to this developed bottom flange compressive force (so that the web compression force is small and can be neglected, for simplified

calculation), the same approach is used for determining the shear capacity of the connection, i.e., taking moments from the free body diagram as shown in Figure 5-2:

$$P_v = \frac{\left[F_{c,buckle} \cdot D_r - F_b(D_r - d_b)\right]}{x} \qquad (5\text{-}12)$$

5.3.6 Case 6 Maximum shear force governed by ability of beam to transfer the compressive force

It is also essential to check that the beam is capable of transferring the necessary compressive force. This is related to the compression capacity of the bottom flange of the beam and the amount of compressive force that can be developed in the beam web. The attainable shear force as governed by the other considerations should be determined first, with the lowest being taken to calculate this compression capacity. The free body diagram for the connection forces (since part of the beam web is in compression the force in the bottom row of bolts is zero) is shown in Figure 5-8. This method, is different to that described in reference 5-3 by relating the actual shear span to the connection moment capacity. It is summarised in Table 5-6.

5.3.7 Calculation of moment capacity and effect of the shear to moment ratio

Equations 5-7, 5-8, 5-9, 5-10 and 5-12 have been used to calculate the maximum possible vertical load for connections CJS-1, CJS-4, CJS-5 [5-1], SCJ4 and SCJ6 [5-2]. The von-Mises stresses used for CJS-1, CJS-4 and CJS-5 were 553 N/mm^2 for the beam web and column web and for SCJ4 and SCJ6 the values were 400 N/mm^2 and 350 N/mm^2 respectively. A rebar stress of 550 N/mm^2 was used for both cases. The former were obtained from the coupon tests of Li. Xiao's tests were conducted in three phases and the two tests of interest were conducted in the first phase for which no coupon test results are available for the columns. Therefore the values used were from

other samples in the same test series. Results of the calculations, which are presented in Table 5-1, confirm the test observations concerning the governing mode of failure.

Table 5-1 Calculation of attainable load and possible moment

Test	Reinf area A_v mm^2	P from Beam stress kN	P from Rebar stress kN	P from Shear stud kN	P from Column stress kN	P column web buckling kN	P Governed by	P selected kN	P Applied in test kN	M due to selected P kN•m	M from test kN•m [ref.]
CJS-1	767	*150*	*124*	*352*	*168*	*Not active*	*Rebar*	*124*	*123*	183	181.5 [5-1]
CJS-4	767	*206*	*179*	*507*	*245*	*Not active*	*Rebar*	*179*	*173*	183	177.5 [5-1]
CJS-5	767	*314*	*320*	*905*	*393*	*Not active*	*Beam*	*314*	*344*	180	197.2 [5-1]
SCJ4	1130	*185*	*187*	*181*	*170*	*101*	*Column-buckling*	*101*	*135*	151	203 [5-1]
SCJ6	1130	*268*	*350*	*340*	*301*	*189*	*Column-buckling*	*189*	*197*	151	158 [5-1]

For tests CJS-1 and CJS-4 there is a small reduction of less than 3% in the moment capacity; the proposed model does not predict any reduction as the load is governed by the rebars in both cases. The proposed method does not consider the possibility of some load transfer to the column through the diagonal compression path crossing the concrete and the steel beam web, so the calculated moment value for CJS-5 shows a reduction of 1.6%. The reduction observed in the proposed model is due to the change in the controlling parameter for the attainable shear force.

For SCJ4 and SCJ6 equation 5-12 governed and the failure mode is also the same as in the tests. It can be seen that in the test the column web buckling load was different for the two cases (approximately 517 kN and 402 kN for SCJ4 and SCJ6 respectively), although the same column and beam sections were used. But it should also be kept in mind that it is not possible to predict the exact buckling load and that for a given column section the predicted buckling load will be the same. So although the exact failure mode can be identified for SCJ4 and SCJ6 the magnitude of the moments did

not exactly match. It is suspected that what Xiao observed in his tests was the effect of shear to moment ratio on column web buckling capacity of unstiffened column web.

5.4 Finite element analysis

In the previous section the effect of the shear to moment ratio was investigated theoretically and the resulting simplified equations were compared against the available test data. It was observed that the simplified equations were able to predict the results, especially the controlling mode of failure with good accuracy. The developed equations suggest that only when the ultimate capacity of the connection is controlled by the beam or column stresses, the shear to moment ratio have an effect on the connection moment capacity. If at the ultimate capacity of the connection the studs or the rebars reach their limit then the shear to moment ratio should have no influence. Since only a few relevant test results are available, some further studies have been carried out using a numerical model which has already been described and validated in chapter 3 and also in references 5-5 and 5-6. The FE mesh used is shown in Figure 3-3 of chapter 3 and the assumed material properties are given in Figure 2-26 of chapter 2. The stud load-slip property and the assumed material properties are given in Figure 3-6 of chapter 3. To achieve the different degree of shear interaction the stud load values were changed without changing the slip i.e. both capacity and stiffness were changed. Using this model the following cases have been investigated:

- Tests CJS-1, CJS-4 and CJS-5 to check that equation 5-8 governs
- Same FE mesh with 1500 mm^2 reinforcement area, which should produce a higher moment and hence a higher vertical force; this may be used to validate equation 5-7
- Same FE mesh with low shear interaction to check the validity of equation 5-9
- Same FE mesh with reduced column web thickness to check the validity of equation 5-10

Since the FE analyses were conducted specifically to check certain forms of failure, care was needed to separate the cases so as to avoid unwanted features. For example, the rebar stresses should govern the first set of analyses, and all other stresses and forces should be checked to see that they do not control. For the second set of FE analyses the deciding factor should be the beam web von-Mises stress. In the third set it was necessary to check that the shear stud force controlled, whilst for the final analyses the column web stresses should govern the connection ultimate load.

From the simplified equations it appears that the presence of a large amount of reinforcement will have a significant influence on the importance of the shear to moment ratio, as the vertical load will be governed by the beam web von-Mises stress in that case. Also if the stud capacity is low the shear to moment ratio should not affect the moment capacity as the reinforcement will not yield and since the vertical force in the beam is low column stresses should also be low. The FE analyses were therefore divided into four groups:

- Case-1 Low reinforcement area (insufficient to produce beam web overstress)
- Case-2 High reinforcement area (sufficient to produce beam web overstress)
- Case-3 low capacity of shear studs (to trigger shear stud failure)
- Case-4 reduced thickness of column web (to produce column web overstress)

Case-1 and case-2 have similar details for the connection and load position except for the reinforcement area. The third group has a low capacity of shear studs but the same reinforcement area as in case-1. The fourth group has load at the same position but with reduced thickness of column web to investigate the effect of column web stress on the shear capacity.

Results obtained from the finite element analysis are described below separately for each case.

5.4.1 Case-1 Low reinforcement area

The M-ϕ curves given in Figure 5-9 are almost identical for the three models. Thus the FE models of CJS-1, CJS-4 and CJS-5 supported both the test results and the results of the earlier calculations. Figure 5-10 shows the moment-rebar stress curves for the three analyses; as in the tests the rebars yielded, thus indicating that equation 8 should govern in this case, i.e. no effect of shear to moment should be observed. This confirms the finding of Li [5-1] that there is no significant effect of shear to moment ratio on the connection moment capacity for the cruciform flush endplate connection with the condition that equation 5-8 governs.

5.4.2 Case-2 High reinforcement area

The same connection was analysed with 1500 mm^2 reinforcement area and load applied at 166.4 mm, 353.9 mm, 578.9 mm, 802.4 mm and 1473 mm from the column face. The ultimate moment values were significantly affected by the shear to span for the first two cases, whereas the other cases were not much influenced. The connection attained its ultimate capacity due to the fact that the beam web von-Mises stress reached its limit of 553 N/mm^2 throughout the region between the endplate and the loading point for the first two cases. Figure 5-11 shows the moment-rotation curves for the five analyses. Figure 5-12 shows the moment-beam web von-Mises stress curves, whilst Figure 5-13 shows the moment-rebar stress for the five analyses. Figure 5-14 shows the deformed shape for the second analysis. It is clear from this figure that the connection reached its ultimate capacity due to the high shear in the beam web. Finally the FE analyses are compared against the results obtained from the proposed equations in Table 5-2. The maximum possible loads obtained from the proposed equations and the FE results are very close, thus confirming the accuracy of the proposed equations. Also from Figure 5-12 it can be seen that the beam web von-Mises stress reached the ultimate strength of the beam for the first three cases but not

for the last two cases. The results of Table 5-2 also reflect this. The interaction of the bending moment and vertical shear is shown in Figure 5-15. From the figure it is observed that up to 75% of the design plastic shear resistance of the beam the moment capacity is almost unchanged but after this the reduction in the moment capacity is very sharp.

Table 5-2 Calculation of applicable load and possible moment for high reinforcement ratio (column web buckling not active)

Shear span mm	A_r mm^2	P Beam stress kN	P Rebar stress kN	P Shear stud kN	P Column stress kN	P Governed by	P selected kN	P from FE analysis kN	M due to selected P kN•m	M from FE analysis kN•m
166	1500	*463*	*1932*	*3116*	*467*	*Beam*	*463*	487	77	81
354	1500	*408*	*908*	*1465*	*465*	*Beam*	*408*	463	144	164
579	1500	*330*	*555*	*896*	*391*	*Beam*	*330*	*388*	191	224
802	1500	*268*	*401*	*646*	*307*	*Beam*	*268*	*284*	215	228
1473	1500	*164*	*218*	*352*	*168*	*Beam*	*164*	*174*	241	238

5.4.3 Case-3 Low shear interaction

FE analyses were made for connections with the load at 1473 mm from the column flange with 300% and 40% shear interaction and at 579 mm from the column flange with 40% shear interaction. It is known from analyses in chapter 4 that 300% and 100% interaction produce the same effect. Equations 5-7, 5-8, 5-9 and 5-10 were used to calculate the connection load capacity for these cases. The moment-stud forces for the three cases are those already shown in Figures 5-2, 5-4 and 5-6 respectively. From these Figures it is clear that the second and third connections reached their ultimate capacity due to failure of the shear studs. Results of the FE analyses and results from the proposed equations are shown in Table 5-3. It is observed that the FE analysis and the equations predicted the same determining factor for the connection load capacity and that in the second and third case there was no effect of the shear span. These

results confirm the view that if the connection reaches its ultimate capacity due to shear stud failure then it will not be affected by the shear to moment ratio. On the other hand with the same shear span the moment capacity may be affected if the failure mode is different. It should be noted that for an isolated connection test, shear studs out side the loading region (Figure 5-6) may transfer horizontal shear due to the shear slip but in a frame only those studs inside the hogging moment region will be active to transmit the tensile force to the reinforcements due to the presence of sagging moment.

Table 5-3 Calculation of applicable load and possible moment for different shear interaction (column web buckling not active)

Shear span mm	% of shear interaction	P (Beam stress) kN	P (Rebar stress) kN	P (Shear stud) kN	P (Column stress) kN	P Governed by	P selected kN	P from FE analysis kN	M due to selected P kN•m	M from FE analysis kN•m
1473	300	*150*	*124*	*352*	*173*	*Rebar*	*124*	123	183	180
1473	40	*150*	*124*	*69*	*173*	*Stud*	*69*	86	102	127
579	40	*312*	*316*	*176*	*403*	*Stud*	*176*	*219*	102	127

5.4.4 Case-4 Reduced thickness of column web

The main purpose of the FE analysis with reduced thickness of column web was to verify equation 5-10. Using the FE model, load was applied at 1473 mm from the column face and the only variable was the thickness of the column web. Results of the FE analysis are compared with results from equations 5-7, 5-8, 5-9 and 5-10 in Table 5-4. It is clear that equation 5-10 was able to predict that column web stress will govern the connection load capacity for the last case.

Table 5-4 Calculation of applicable load and possible moment for different column web thickness (column web buckling not active)

Thickness of column web mm	P Beam stress kN	P Rebar stress kN	P Shear stud kN	P Column stress kN	P Governed by	P selected kN	P from FE analysis kN	M due to selected P kN•m	M from FE analysis kN•m
9.3	*150*	***124***	*352*	*221*	*Rebar*	*124*	127	183	187
7.3	*150*	***124***	*352*	*173*	*Rebar*	*124*	122	183	180
5.0	*150*	*124*	*352*	***119***	*column*	*119*	*89*	175	131

5.5 Design proposal

Using the simplified calculations supported by the findings from the FE analyses, a new method is proposed to calculate the moment capacity of flush endplate connections, which includes the effect of the shear to moment ratio in a simple yet reliable way. The method gives very good results for the connection moment capacity when the *ultimate strengths of the materials* are used. Thus it is recommended to calculate the connection moment capacity accordingly, ignoring the material safety factor and to impose a global factor of safety on the calculated moment capacity. But if there is doubt about the accuracy of data during the calculation (such as the diameter of the reinforcing bars, position of the reinforcing bars) these should be allowed for in a safety factor associated with the material.

- ***Step-1 Determine the tensile force in the bolts using the following equations***

$$F_b = min\begin{cases} K_r(4.32 - 0.039m + 0.0116e + 0.009p)t_{cf}{}^2 f_{cf} & \textit{ref 5-3} \\ (5.5 - 0.021m + 0.017e)t_p{}^2 f_p & \textit{ref 5-3} \\ 1.8A_b f_b & \textit{EC3, clause 6.5.5} \end{cases}$$

- ***Step-2a Determine the attainable shear force***

Use Table 5-5 to calculate the attainable connection load capacity and to identify the component that governs this capacity:

Table 5-5 Equations for determining the attainable load

	Beam web overstress	Yield of reinforcement	Failure of shear studs	Column web overstress
Equation for attainable load	$P_r = \frac{f_{bw}}{\sqrt{\frac{x^2.(\bar{y}-2t_{bf})^2}{l^2} + \frac{3}{H_b^2.t^2_{bw}}}}$	$P_v = \frac{[A_r f_{ur} D_r + F_b d_b]}{x}$	$P_v = \frac{[F_s D_r + F_b d_b]}{x}$	$P_v = \frac{f_{cw}.D_c.t_{cw}D_r b_{eff}}{\sqrt{4D_r^2 b_{eff}^2 + D_c^2 x^2 - 2xD_r b_{eff} D_c}}$
		These two are properly covered in Table 5-6. This is to estimating the shear force to be considered during use of Table 5-6.		
Comments	Associated with weak beam web and high reinforcement ratio with proper shear connection	Usual case	Associated with low shear interaction	Associated with strong beam, moderate to high reinforcement area.
For columns without any transverse beams connected to the web also check the maximum shear force as controlled by buckling of the column web using the formula: $F_{c,buckle} = 8.4 b_{eff}^{0.017} D_c^{0.600} t_{cw}^{1.430} f_{cw}^{0.760}$ $P_v = \frac{[F_{c,buckle}.D_r - F_b(D_r - d_b)]}{x}$				

- ***Step-2b Connection load controlled by the ability of the beam to transfer compression***

The effective tensile force developed in the rebars should be calculated as:

$$F_r = min \begin{cases} A_r f_u \\ nkR_{Rd} \end{cases}$$

According to Clause 6.3.2 of EC4, the shear resistance of a single shear connector is:

$$R_{Rd} = min \begin{cases} 0.9 f_u \left(\frac{\pi d^2_{st}}{4} \right) \\ 0.29 \alpha d^2_{st} \sqrt{f_{ck} E_{cm}} \end{cases}$$

Where:

n is the number of shear studs in the hogging moment region

R_{Rd} is the shear resistance of a single shear stud

d_{st} is the diameter of the shank of the shear stud

h_{st} is the overall height of the shear stud

f_{us} is the ultimate strength of the stud material (maximum 500 N/mm^2)

E_{cm} is the mean value of the secant modulus of the concrete (section 3.1.4.1 of EC4)

f_{ck} is the characteristic cylinder compressive strength of concrete:

$$\alpha = 0.2 \left(\frac{h_{st}}{d_{st}} + 1 \right) \qquad for\ 3 \le \frac{h_{st}}{d_{st}} \le 4$$

$$\alpha = 1.0 \qquad for\ \frac{h_{st}}{d_{st}} > 4$$

If a composite slab with metal decking is used, the shear resistance is to be modified by the reduction factor k according to clause 6.3.3 of EC4; depending on the orientation of the metal decking with the supporting beam. Following equations can be used:

(a) Metal decking transverse to supporting beam

$$k = k_1 = \frac{0.7}{\sqrt{N_r}} \frac{b_o}{h_a} \left(\frac{h_s}{h_a} - 1 \right) \le 1.0$$

where h_s is the depth of slab but not greater than (decking depth + 75) mm

(b) Metal decking parallel to supporting beam:

$$k = k_2 = 0.6 \frac{b_o}{h_a} \left(\frac{h_s}{h_a} - 1 \right) \le 1.0$$

(c) Ribs of metal decking making an angle with the beam (between 0 and 90)

$$k = k_1 sin^2\theta + k_2 cos^2\theta$$

where k_1 and k_2 is to be taken from above equations

Note: for a solid slab $k = 1.0$

Hence the total resistance of the studs in the hogging moment region is nkR_{Rd}

Calculate the bottom flange compression force using the following equations:

$$F_{c,bf} = min\begin{cases} t_{cw} b_{eff} f_{cw}\left(1.25 - 0.5\frac{\sigma_n}{f_{yc}}\right) \le t_{cw} b_{eff} f_{cw} & EC3,\ J.3.5.3 \\ 8.4\ b_{eff}^{0.017}\ D_c^{0.60}\ t_{cw}^{1.43}\ f_{cw}^{0.76} & Ref\ 5-3 \\ t_{bf} b_{bf} f_{bf} \quad when \frac{b_{bf}}{t_{bf}} < 22\sqrt{\frac{235}{f_{yb}}} & BF\ compression, Table\ 5.3.1,\ EC3 \\ 22 t_{bf}^2 f_{bf}\sqrt{\frac{235}{f_{yb}}} \quad when \frac{b_{bf}}{t_{bf}} \ge 22\sqrt{\frac{235}{f_{yb}}} & BF\ Buckling, Table\ 5.3.1,\ EC3 \end{cases}$$

Determine the minimum shear force from Table 5-5; use this to calculate the shear force controlled by the ability of the beam to transfer the compression using Table 5-6.

Table 5-6 Attainable shear force controlled by the ability of beam to transfer the compression to the column

<table>
<tr><th>$F_r + F_b < F_{c.bf}$</th><th colspan="3">$F_r + F_b > F_{c.bf}$</th></tr>
<tr><td rowspan="2">The beam web will not take any compression. The shear capacity of the joint is:

$P_v = \frac{[F_r . D_r + F_b d_b]}{x}$</td><td colspan="3">The beam web will be under compression. The available horizontal compressive stress for the beam web is calculated as:
$\tau_{xy} = \frac{minimum\ P_v}{(H_b - 2t_{bf})t_{bw}}$
$f_{a.bw} = \sqrt{f_{bw}^2 - 3\tau_{xy}^2}$
The depth of beam web in compression is:
$d_{c.bw} = \frac{F_r + F_b - F_{c.bf}}{f_{a.bw} \cdot t_{bw}}$</td></tr>
<tr><td>$d_{c.bw} < d_b$

$F_{c.bw} = F_r + F_b - F_{c.bf}$
The centre of compression is given by
$d_{c1} = \frac{F_{c.bw}\frac{d_{c.bw} + t_{bf}}{2}}{F_{c.bw} + F_{c.bf}}$

The shear capacity of the joint is:
$P_v = \frac{[(F_{c.bf} + F_{c.bw})(D_r - d_{c1}) - F_b(D_r - d_b)]}{x}$</td><td>$d_b \le d_{c.bw} < H_b$
For bolts below the compression zone the bolt force should be taken as zero, the compression on the web and the depth of compression should be recalculated as:
$F_{c.bw} = F_r - F_{c.bf}$
$d'_{c.bw} = \frac{F_r - F_{c.bf}}{f_{a.bw} \cdot t_{bw}}$
$d'_{c.bw} < H_b - t_{bf}$
The centre of compression is given by
$d_{c2} = \frac{F_{c.bw}\frac{d'_{c.bw} + t_{bf}}{2}}{F_{c.bw} + F_{c.bf}}$
It should be noted that when recalculated with out bolt force, the depth of compression may go below the cg of the top row of bolts, even in that case the bolt force should be taken to be zero (as the force in reality will be very small). Hence the shear capacity of the joint is:
$P_v = \frac{(F_{c.bf} + F_{c.bw})(D_r - d_{c2})}{x}$</td><td>$H_b \le d_{c.bw}$
The web compression should be calculated as:
$F_{c.bw} = f_{a.bw}(H_b - t_{bf})$
The bolt force is to be taken as zero, and the rebar force to be recalculated as:
$F_r = F_{c.bw} + F_{c.bf}$
The possibility that compression extends into the top flange is extremely unlikely, so it is neglected
The centre of compression is given by:
$d_{c3} = \frac{F_{c.bw}\left(\frac{H_b - t_{bf}}{2} + \frac{t_{bf}}{2}\right)}{F_{c.bw} + F_{c.bf}} = \frac{F_{c.bw}\frac{H_b}{2}}{F_{c.bw} + F_{c.bf}}$
The shear capacity of the joint is:
$P_v = \frac{(F_{c.bf} + F_{c.bw})(D_r - d_{c3})}{x}$</td></tr>
</table>

- ***Step-2c Attainable connection load capacity***

The attainable connection load capacity is the minimum of the P_v values determined from steps 2a and 2b.

- ***Step-3 Connection moment capacity***

Connection moment capacity is determined by using the following simple equation:

$M = P_v x$

5.6 Worked example to consider shear to moment ratio

Consider a connection with a 254x102UB25 beam, 203x203UC45 column, 280x130x10mm endplate, with seven rows of 100x19 mm shear studs, each row having two studs with CF46 transverse decking. The depth of the solid concrete slab is 120 mm. Cross section of the beam is shown in Figure 5-16. All examples assume that the presence of a stub beams connected to the column web prevents column web buckling in compression. The first example illustrates the case when the full bolt force cannot actually be developed. In the second example the bolt force can reach its full capacity.

Ultimate strengths for the members are:

Concrete (cylinder):	33 N/mm^2
Beam web:	553 N/mm^2
Beam flange:	490 N/mm^2
Column web:	553 N/mm^2
Column flange:	500 N/mm^2
Endplate:	350 N/mm^2
Reinforcement:	600N/mm^2
Bolt:	600N/mm^2

The example assumes either 1500 mm^2 or 500 mm^2 reinforcement area and load at either 350 mm or 1500 mm from the column flange. Table 5-7 summarises the main differences between the four examples.

Table 5-7 Main difference between the examples

Example no	Case	Distance of load from column flange	reinforcement area mm^2
1	1	350	1500
1	2	1500	1500
2	1	350	500
2	2	1500	500

Pre calculations

For shear studs the basic shear capacity of each stud is 86 kN reduction factors the reduction factor is 1.0 so total capacity of the shear studs is:(7×2)x1.0× 86kN=1204kN.

For this arrangement the effective width: beff=[8.4+2√2×8+2×10+5(11+10.2)] =157mm.

a Bolt force

$$F_b = min\begin{cases} 1(4.32-0.039x23.2+0.0116x66.5+0.009x157)11^2\,x500\ N = 339\ kN \\ (5.5-0.021x25+0.017x30)10^2\,x.350\ N = 192\ kN \\ 2x0.9xA_b f_{\ b} = 2x0.9x314x640\ N = 362\ kN \end{cases} = 192\ kN$$

So the bolt force is 192 kN for two bolts in the top row, i.e., 96 kN per bolt.

b Determination of effective tensile force in the rebar, to be used when assessing the ability of the beam to transfer compression

Force in the reinforcement

$F_r = A_r f_y$ = 1500×600 N=900 kN and 500×600 = 300 kN

nR_{Rd} = (7×2)×1.0×86 kN= 1204 kN

Hence the reinforcement force is 900 kN, for 1500 mm^2 reinforcement area and 300 kN for 500 mm^2 reinforcement area.

c Possible compressive force developed at the bottom flange, to be used when assessing the ability of the beam to transfer compression

$$F_{c,bf} = min\begin{cases} 7.3 \times 157 \times 570\ N = 654\ kN \\ Not\ active \\ 8.4 \times 102 \times 490\ N = 420\ kN \\ Not\ active \end{cases} = 420\ kN$$

The governing magnitude of horizontal compressive force is 420 kN

Example 1

Case-1 Load at 350 mm from the column flange

For load applied at 350 mm from the column flange

$$P_v = min\begin{cases} \dfrac{553}{\sqrt{\dfrac{350^2 \times (194.4 - 2x8.4)^2}{(8.21x10^7)^2} + \dfrac{3}{257^2 \times 6.1^2}}} N & = 410\ kN \\ \dfrac{1500x600x342.8 + 192{,}000x214.5}{350} N & = 999\ kN \\ \dfrac{1204000x342.8 + 192{,}000x214.5}{350} N & = 1296\ kN \\ \dfrac{553x203.2x7.3x342.8x157}{\sqrt{4x342.8^2 x157^2 + 203.2^2 x350^2 - 2x350x342.8x157x203.2}} N & = 466\ kN \end{cases}$$

So the attainable maximum shear is 410 kN controlled by beam web overstress.

Check for compression capacity of the beam

Since the combined rebar and bolt tensile force exceeds the compressive capacity of the bottom flange it has to be supported by part of the beam web acting in compression. Using the attainable shear calculated from the above four considerations, the compressive stress that can be sustained by the beam web can be calculated as:

$$\tau_{xy} = \frac{V}{(H_b - 2t_{bf})t_{bw}} = \frac{410 \times 10^3}{(257 - 2x8.4)x6.1} = 280\ N/mm^2$$

$$f_{a,bw} = \sqrt{f_{b\omega}^2 - 3\tau_{xy}^2} = \sqrt{553^2 - 3x280^2} = 266\ N/mm^2$$

Depth of compression required to support the tensile force is

$$d_{c,bw} = \frac{F_r + F_b - F_c}{f_{a,bw} \cdot t_{bw}} = \frac{(900 + 192 - 420)x10^3}{266x6.1} = 414\ mm > H_b$$

Since the required depth of compression is above the level of the cg of the top row of bolts, these bolts cannot contribute towards the development of tensile force, i.e. $F_b = 0$. Hence the web compression depth is recalculated as:

$$d_{c,bw} = \frac{F_r - F_c}{f_{a,bw} \cdot t_{bw}} = \frac{(900 - 420)x10^3}{266x6.1} = 296\ mm > H_b$$

Hence the rebar force is *420+6.1x(257-8.4)x266/1000 = 823 kN*

The centre of compressive force is:

$$d_{c,cg} = \frac{F_{c,bw} x\left(\frac{d_{c,bw}}{2} + \frac{t_{bf}}{2}\right)}{F_{c,bw} + F_{c,bf}} = \frac{(823 - 420)x10^3\, x\left(\frac{248.6}{2} + \frac{8.4}{2}\right)}{823x10^3} = 62.9mm$$

The attainable shear force from this consideration:

$$P_v = \frac{\left[\left(823x10^3\right)\left(342.8-62.9\right)\right]}{350} N = 658\ kN$$

Hence the attainable shear is 410 kN, controlled by beam web overstress. And the moment is:

M = 410 kN x 0.35 m = 144 kN•m

Case-2 Load at 1500 mm from the column flange

For load at 1500 mm from the column flange the attainable maximum shear is 161 kN controlled by beam web overstress. Considering the beam's capacity to transfer compression, the shear is 176 kN, which is greater than 161 kN. Hence the moment is:

M = 161 kN x 1.5 m = 242 kN•m

It can be observed that for this case the moment is reduced by 40% due to the increase in shear to moment ratio by 2.19 (from 0.667 to 2.857), the governing mode being beam web overstress in both cases.

Example 2

The same problem is considered but with 500 mm^2 reinforcement area

Case-1 Load at 350 mm from the column flange

The vertical shear force is controlled by the beam web overstress and is 390 kN. Using this value of shear and considering the beam's capacity to transfer compression, the shear is 407 kN. Hence the moment is:

M = 390 kN x 0.35 m = 137 kN•m

Case-2 Load at 1500 mm from the column flange

This time for load at 1500 mm from the column flange the vertical shear force is controlled by the rebar stress and is 96 kN. The shear is 96 kN as governed by the beam's capacity to transfer compressive force, which is equal to the previously calculated value. Hence the moment is:

M = 96 kN x 1.5 m = 144 kN•m

It is clear from the second example that for this case moment capacity is not significantly affected.

These four results are compared against other design models in Table 5-8. It can be seen that the Li model predicts a slight reduction (which is basically similar to the ability of the beam to transfer the compressive force to the column, of the proposed design model) in the moment capacity. But even in that case the attainable shear force should be calculated from the proposed model so as to predict the effect of the shear to moment ratio.

Table 5- 8 Comparisons of moment values from the model with available methods

Ar	Shear	Ping Ren (ref. 5-7)	Xiao et al (ref. 5-8)	Li et al (ref. 5-3)	FE model in this thesis		Proposed method		
mm^2	span mm	(Moment) kN•m	(Moment) kN•m	(Moment)* kN•m	Shear kN	Moment kN•m	Shear kN	Moment kN•m	governed by
1500	350	272	222	244	468	164	400	140	beam stress
1500	1500	272	222	272	159	238	149	223	beam stress
500	350	143	189	133	434	152	407	137	beam stress
500	1500	143	189	134	101	152	96	144	rebar stress

* For this the shear force was calculated from the proposed model, otherwise it is not possible to relate the shear span to the attainable shear force

5.7 Conclusions

The factors governing the importance of changes to the shear to moment ratio on the moment capacity of composite endplate connections have been investigated. Equations have been proposed to determine the shear capacity of any connection using a number of criteria. The results from the equations have been verified against both test results and FE analyses. Both checks have demonstrated the accuracy of the equations. Using the developed equations it is possible to ascertain whether there is any effect of the shear to moment ratio for a particular connection. A design method to determine the moment capacity of semi-rigid composite flush endplate connections is proposed on the basis of the developed equations. The method has been illustrated with a few examples which clearly demonstrate its ability to determine the moment capacity of such connections.

5.8 References

5-1 Li, T. Q., Nethercot, D. A. and Choo, B. S. (1996) *Behaviour of flush end plate composite connections with unbalanced moment and variable shear/moment ratios: part 1: experimental behaviour*, Journal of Constructional Steel Research, Vol. 38, No. 2, pp. 125-164.

5-2 Xiao, Y., Choo, B. S. and Nethercot, D. A. (1994) *Composite connections in steel and concrete. I. experimental behaviour of composite beam-column connections*, Journal of Constructional Steel Research, Vol. 31, pp. 3-30.

5-3 Li, T. Q., Nethercot, D. A. and Choo, B. S. (1996) *Behaviour of flush end plate composite connections with unbalanced moment and variable shear/moment ratios: part 2: prediction of moment capacity*, Journal of Constructional Steel Research, Vol. 38, No. 2, pp. 165-198.

5-4 Nethercot, D. A. and Zandonini, R. (1994) *Recent Studies of the Behaviour of Semi-rigid Composite Connections*, American Society of Civil Engineers Structural Conference, Atlanta, April.

5-5 Ahmed, B., Nethercot, D. A. and Li, T. Q. (1996) *Modelling Composite Connection Response*, Connections in Steel Structures III: Behaviour, Strength and Design, Edited by Reidar Bjorhovde, Andre Colson, Riccardo Zandonini, Proceedings of the Third International Workshop, Trento University, 29-31 May 1995, pp. 259-268.

5-6 Ahmed, B., and Nethercot, D. A. (1995) *Numerical Modelling of Composite Flush endplate Connections*, Steel Structures, Journal of Singapore Structural Steel Society, Vol. 6, No.1, pp. 87-102.

5-7 Ren, P. and Crisinel, M. (1996) *Prediction method for moment-rotation behaviour of composite beam to steel column connections*, Connections in Steel Structures III: Behaviour, Strength and Design, Edited by Reidar Bjorhovde, Andre Colson, Riccardo Zandonini, Proceedings of the Third International Workshop, Trento University, 29-31 May 1995, pp. 33-46.

5-8 Xiao, Y., Nethercot, D. A. and Choo, B. S. (1992) *Moment resistance of composite connections in steel and concrete*, Proceedings of the first world conference on constructional steel design, Acapulco, Mexico, November, pp. 331-343.

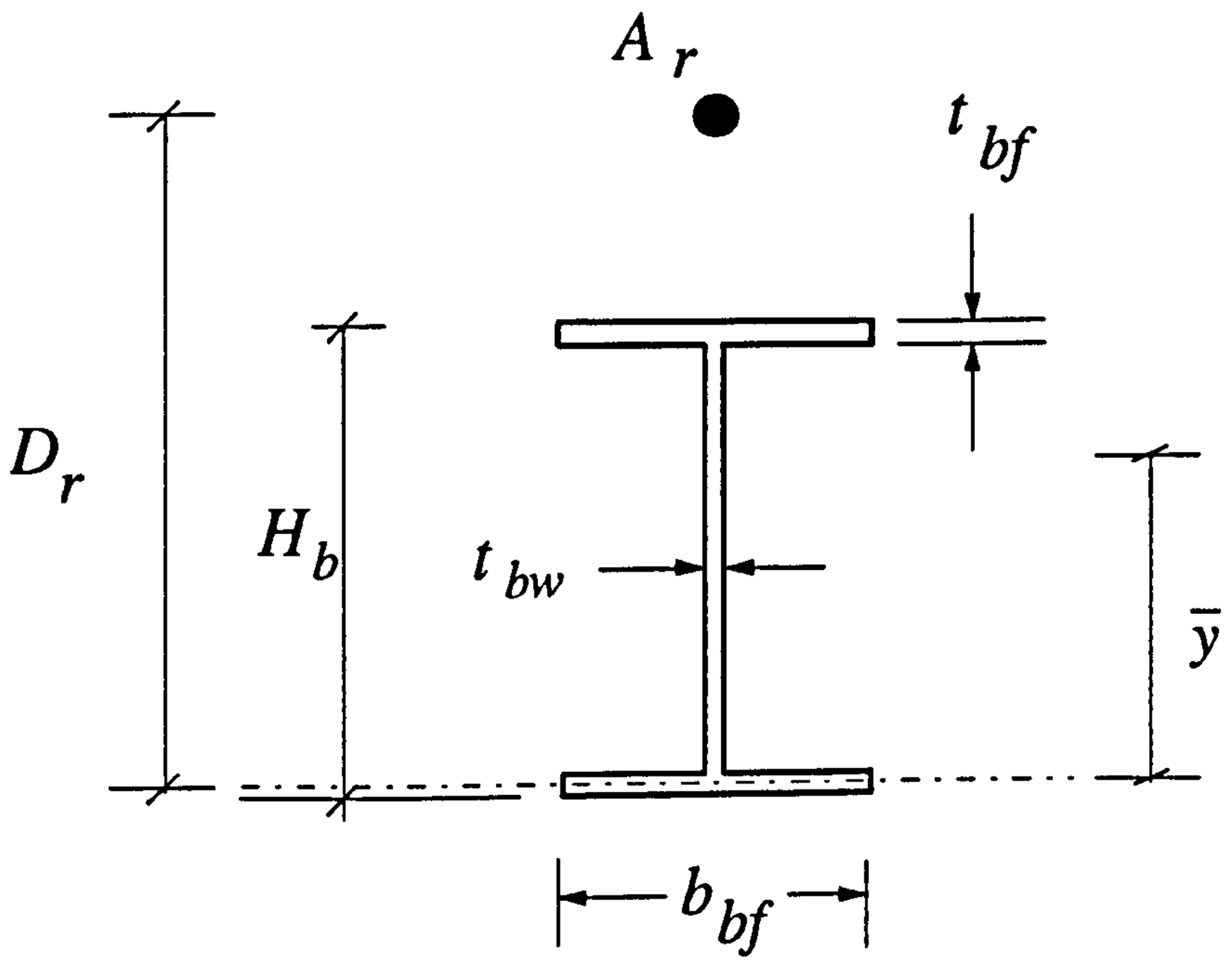

Figure 5-1 Definition of symbols used for equations in case-1

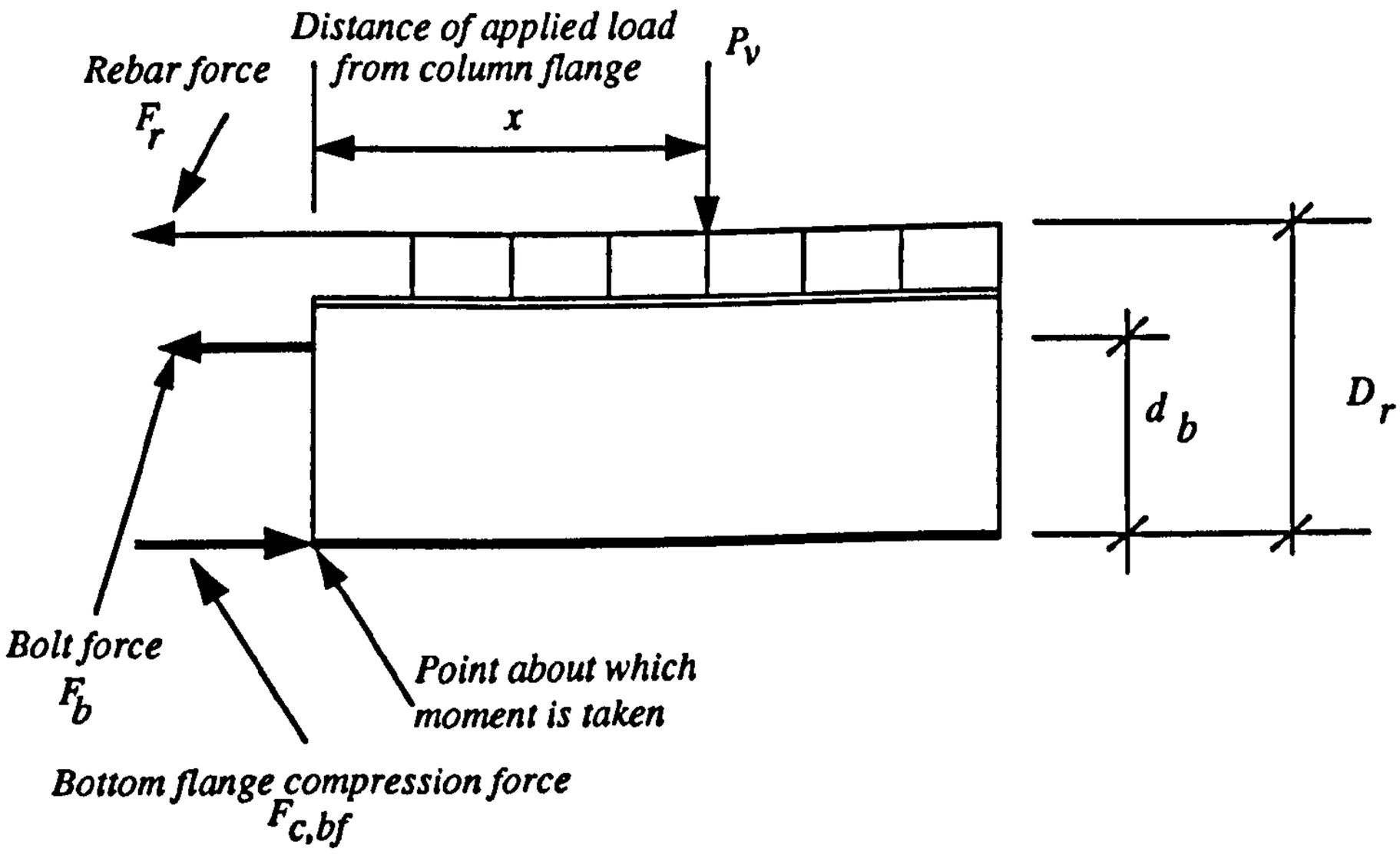

Figure 5-2 Free body diagram of the connection for case-2

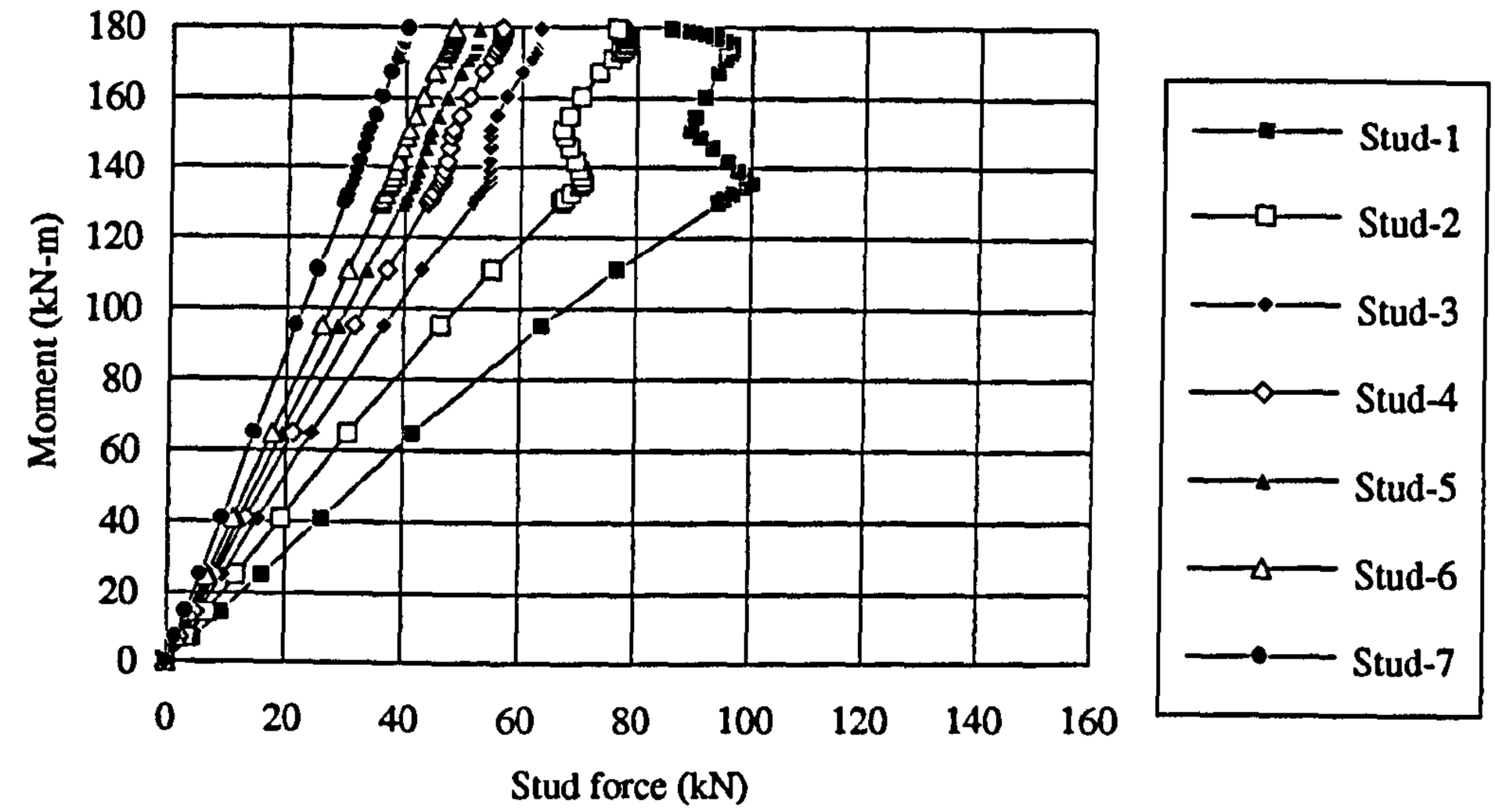

Figure 5-3 Stud forces developed in CJS-1

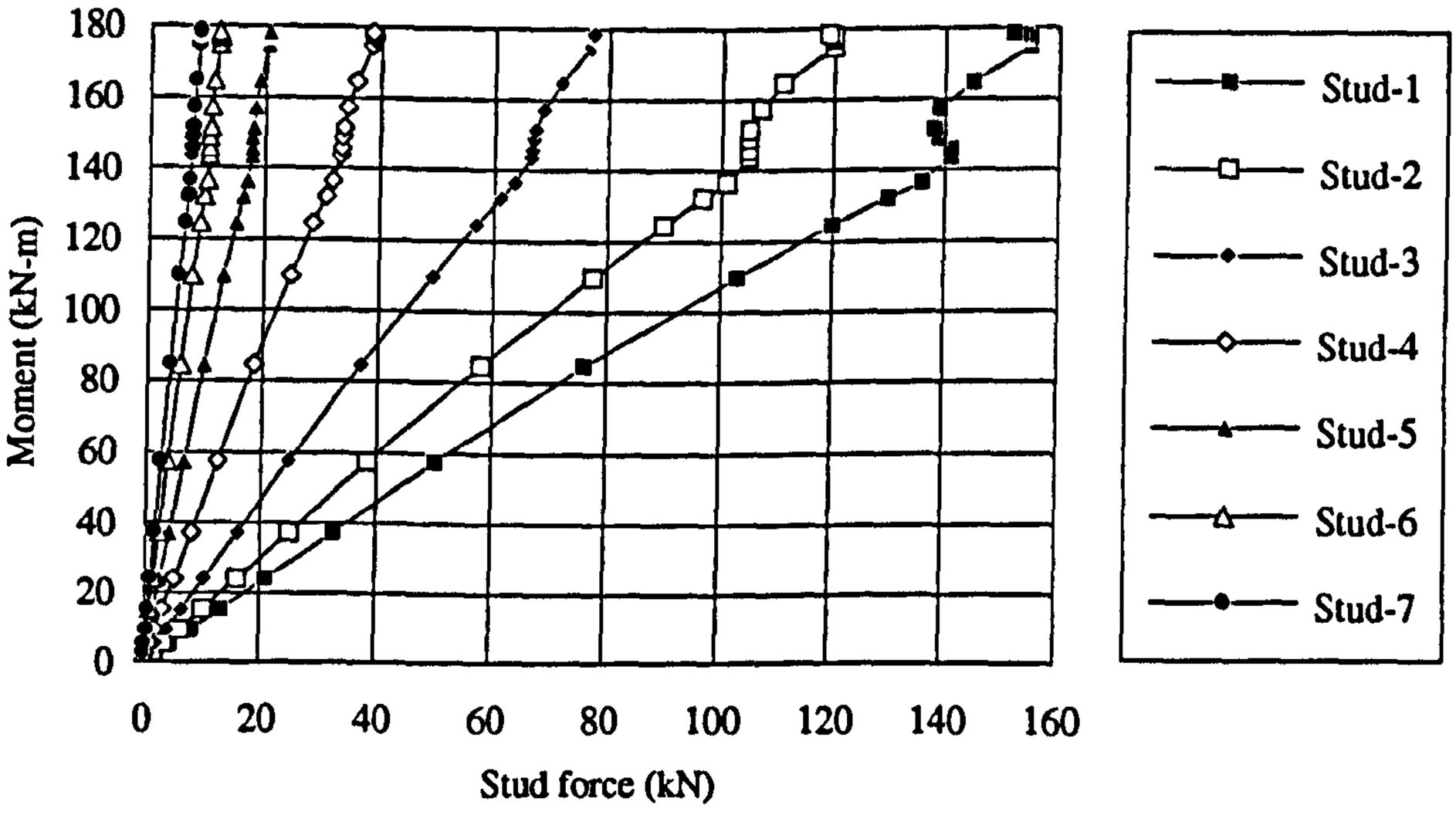

Figure 5-4 Stud forces developed in CJS-5

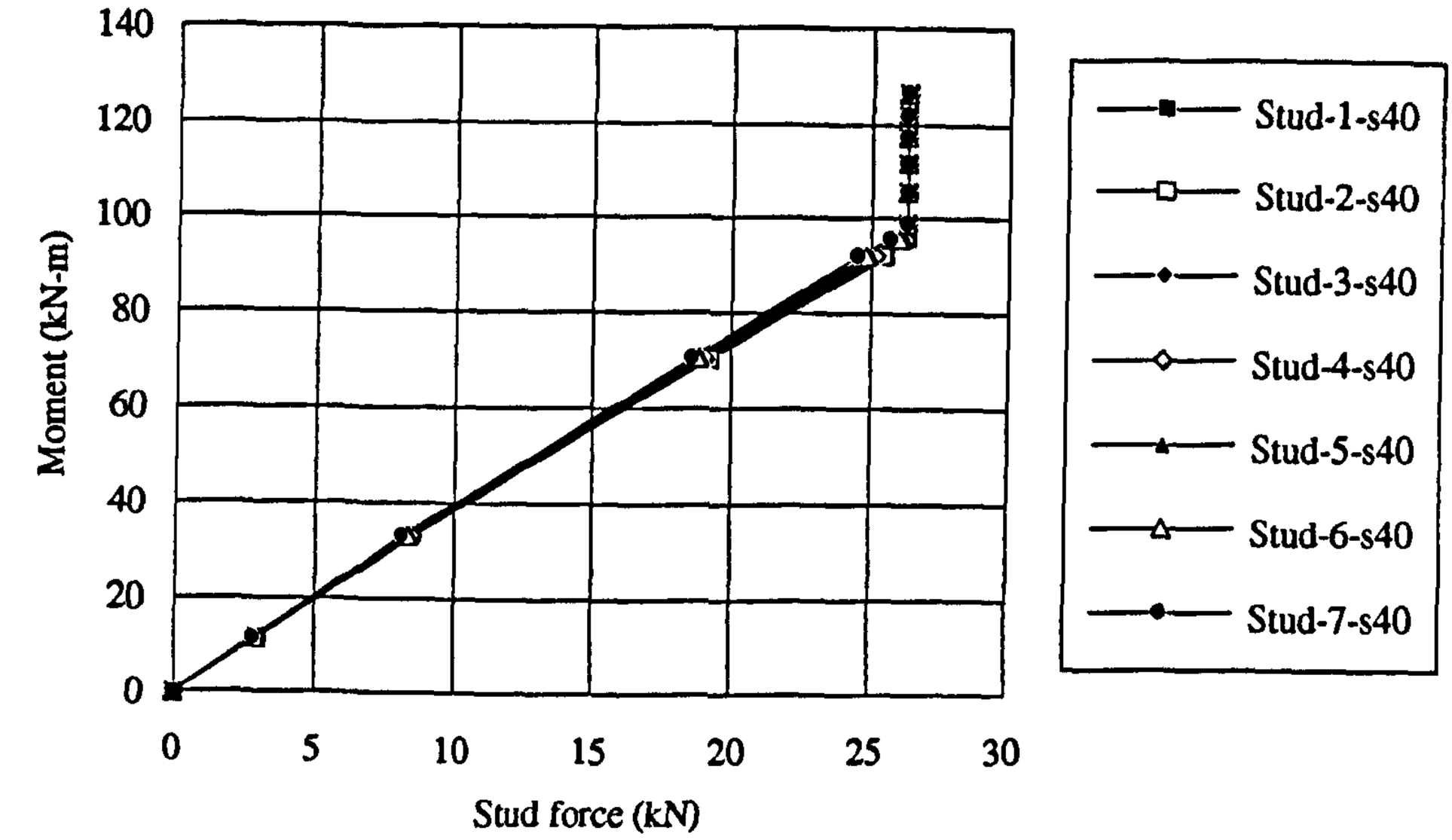

Figure 5-5 Stud forces developed with 40% shear interaction and load at 1473 mm

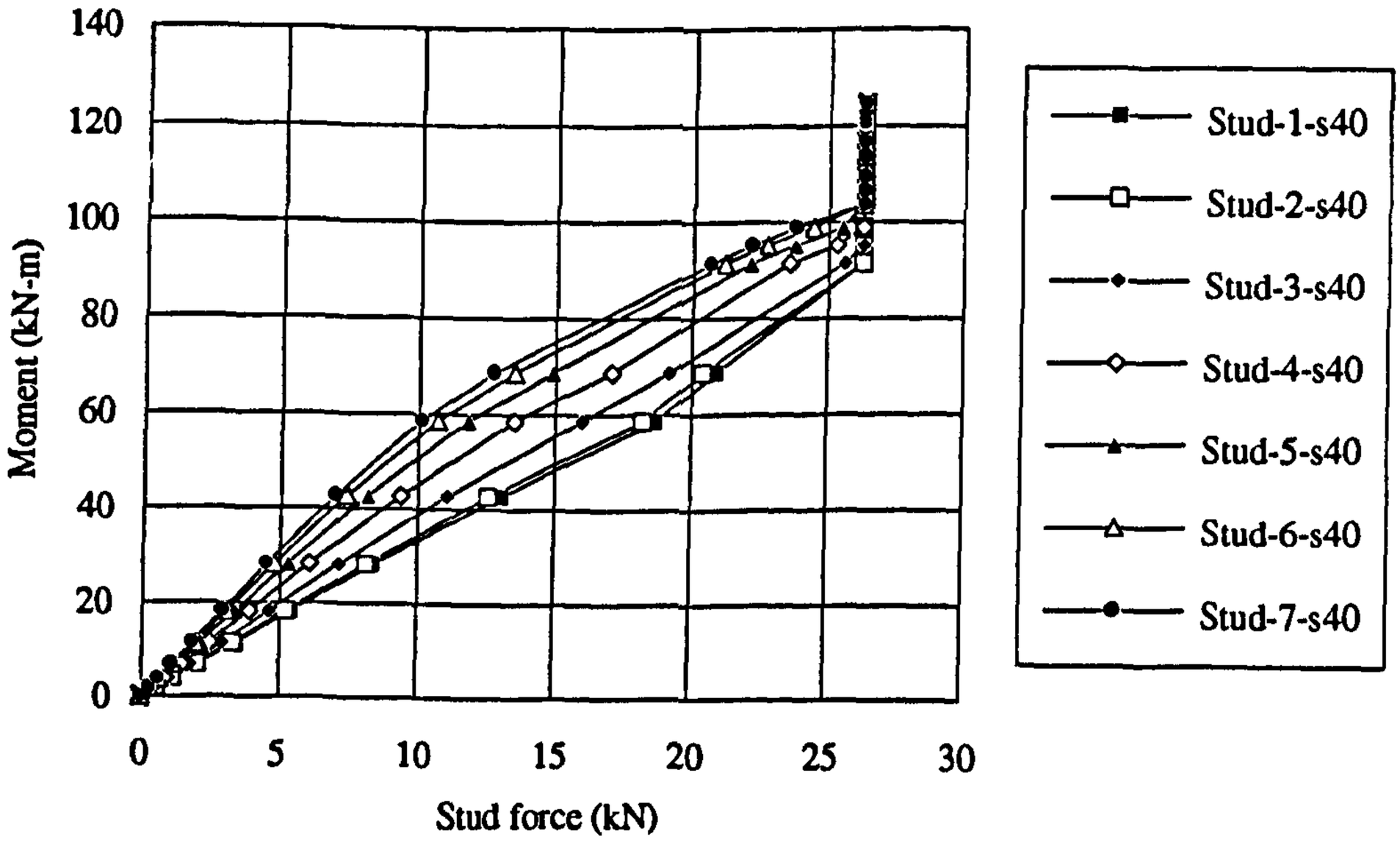

Figure 5-6 Stud forces developed with 40% shear interaction and load at 578.9 mm

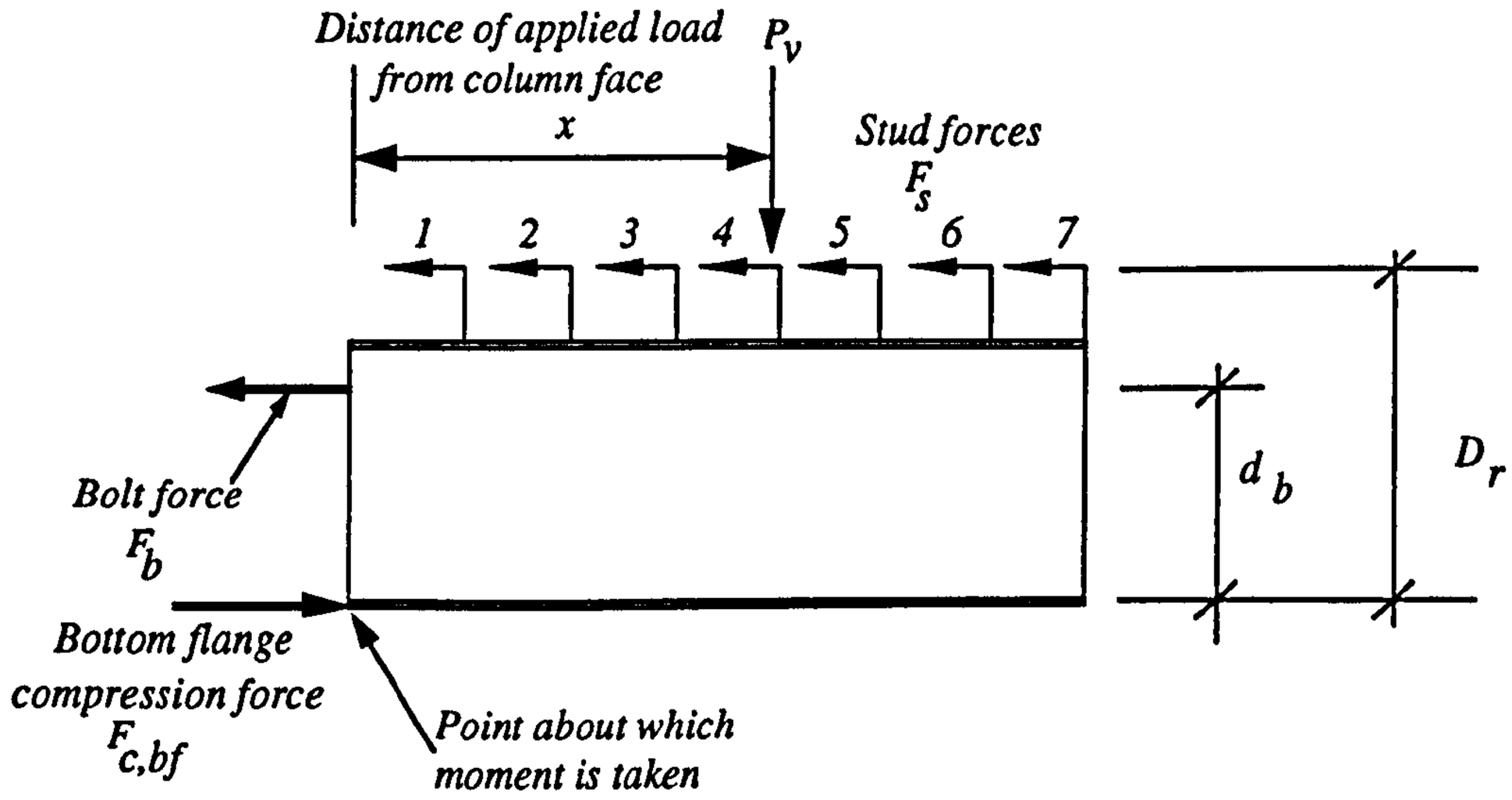

Figure 5-7 Free body diagram of the connection for case-3

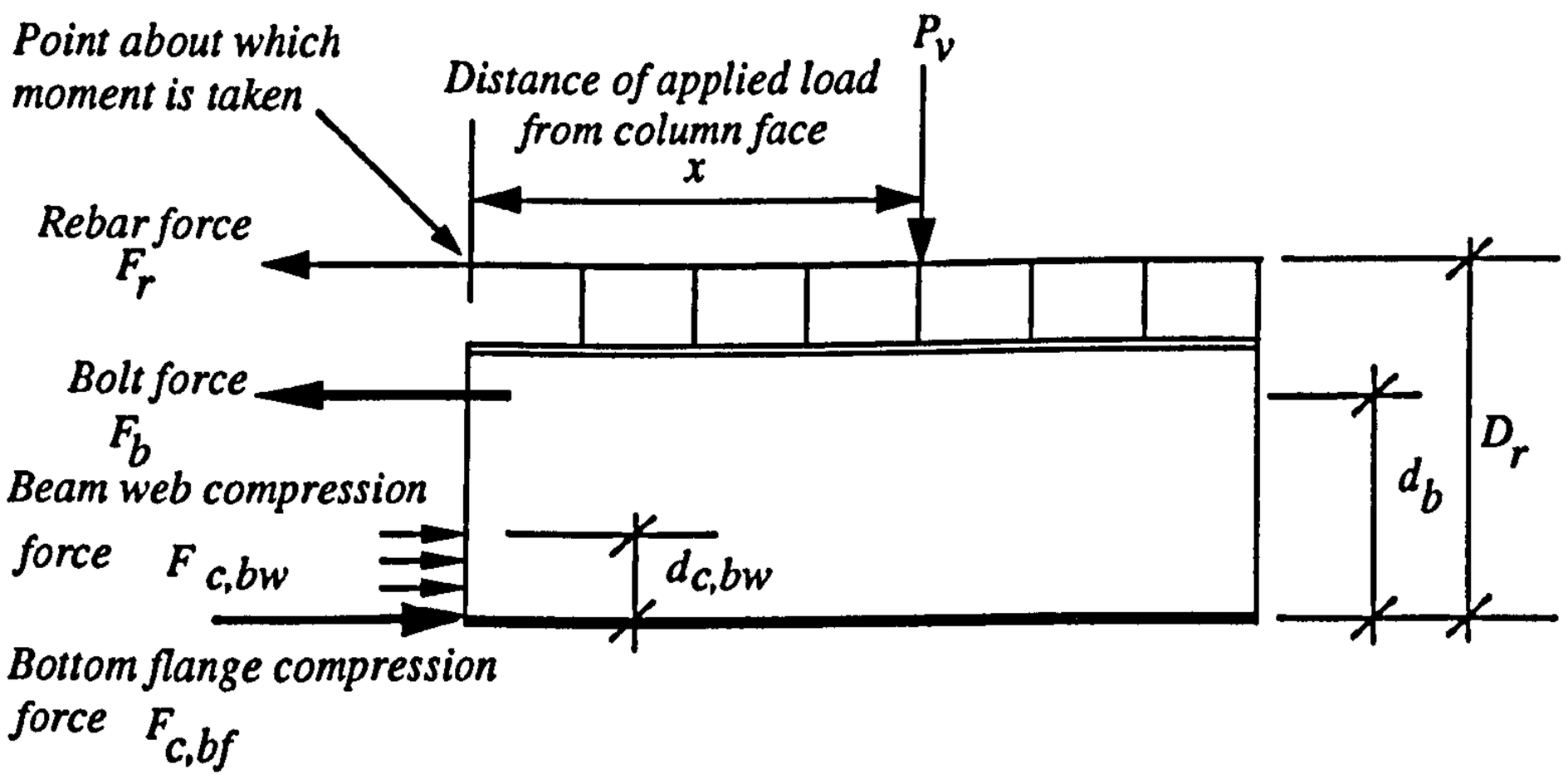

Figure 5-8 Free body diagram of the connection for case-6

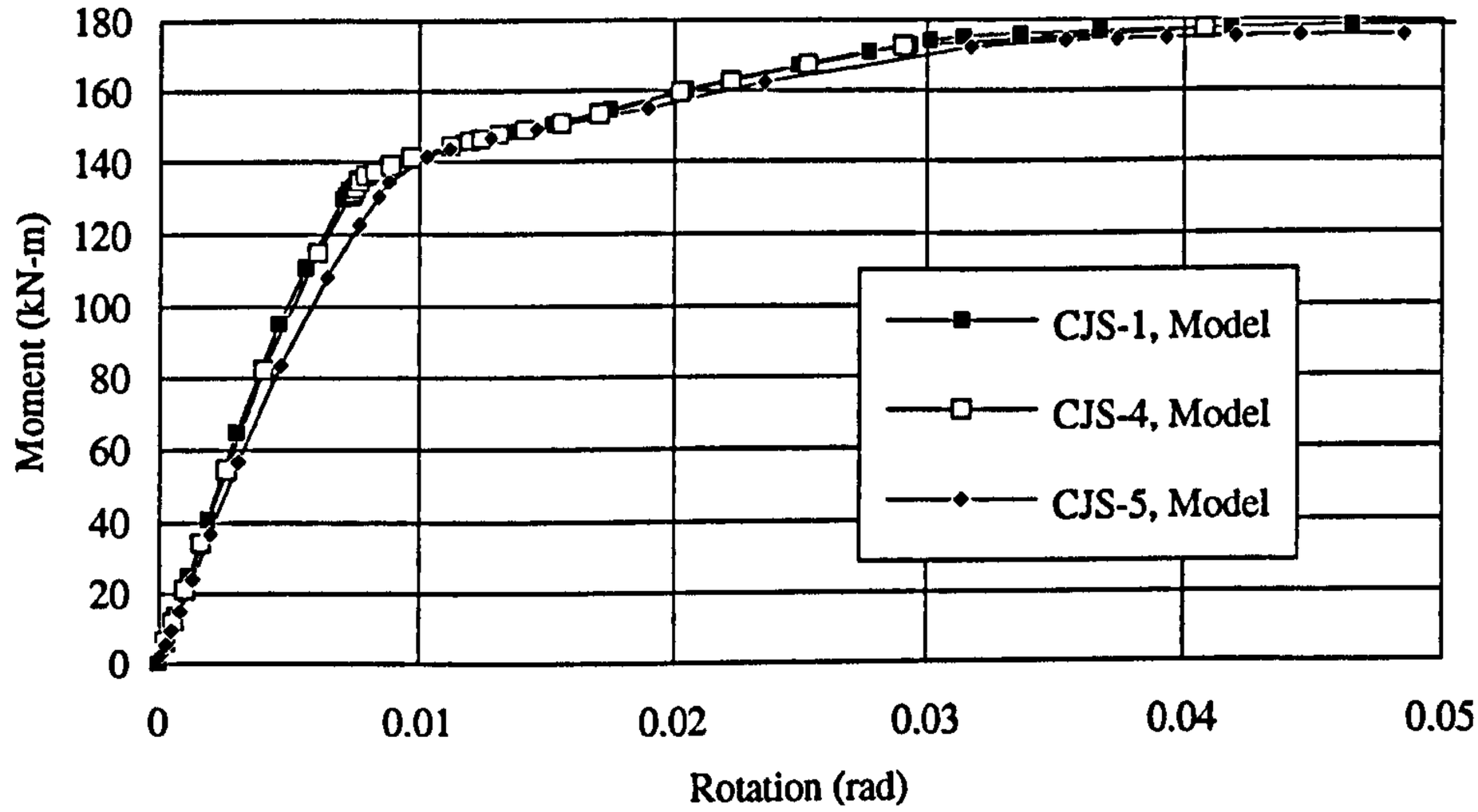

Figure 5-9 Comparison of moment rotation curves for different shear to moment ratio with 767 mm^2 reinforcement area

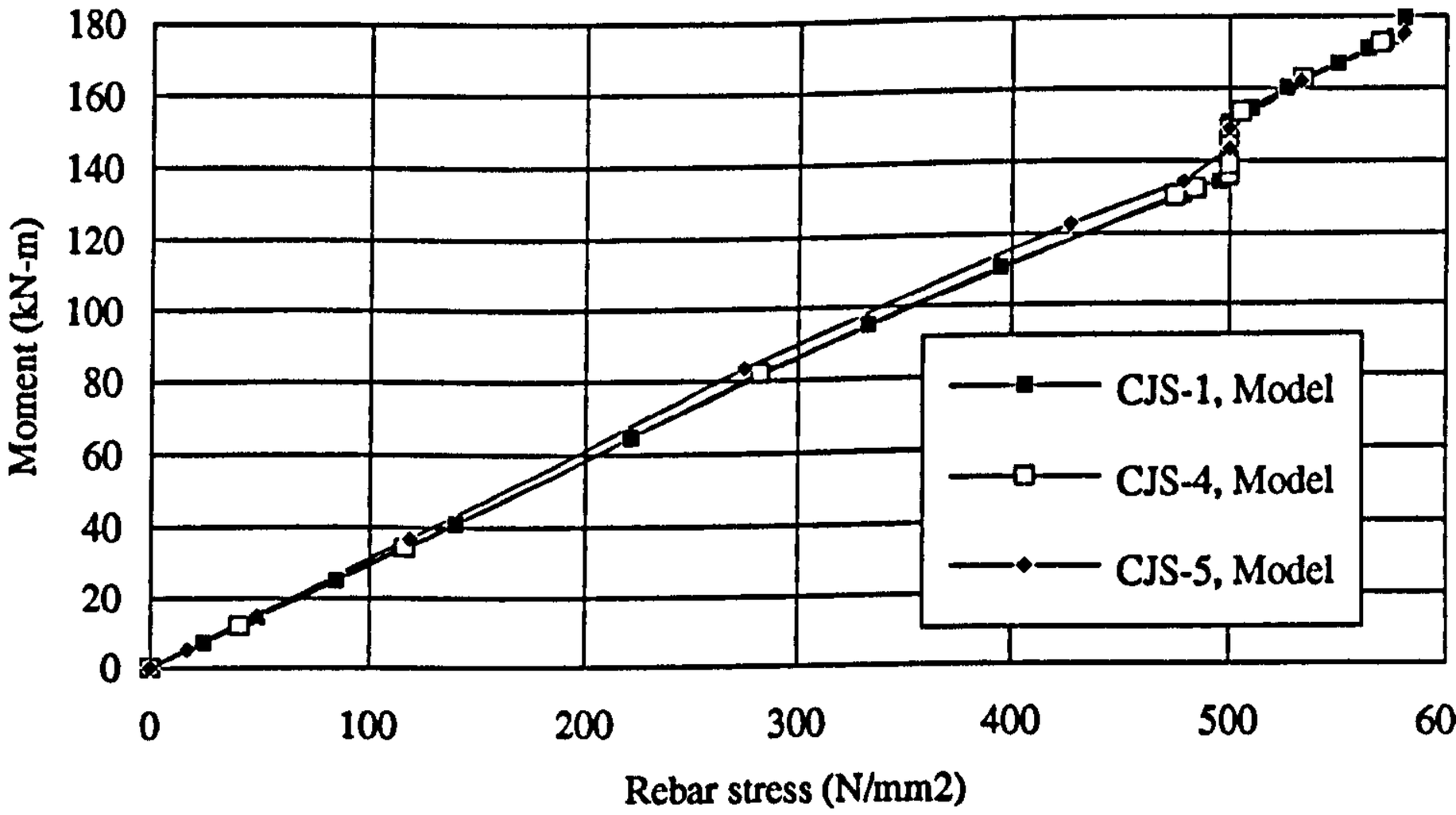

Figure 5-10 Comparison of moment rebar stress curves for different shear to moment ratio with 767 mm^2 reinforcement area

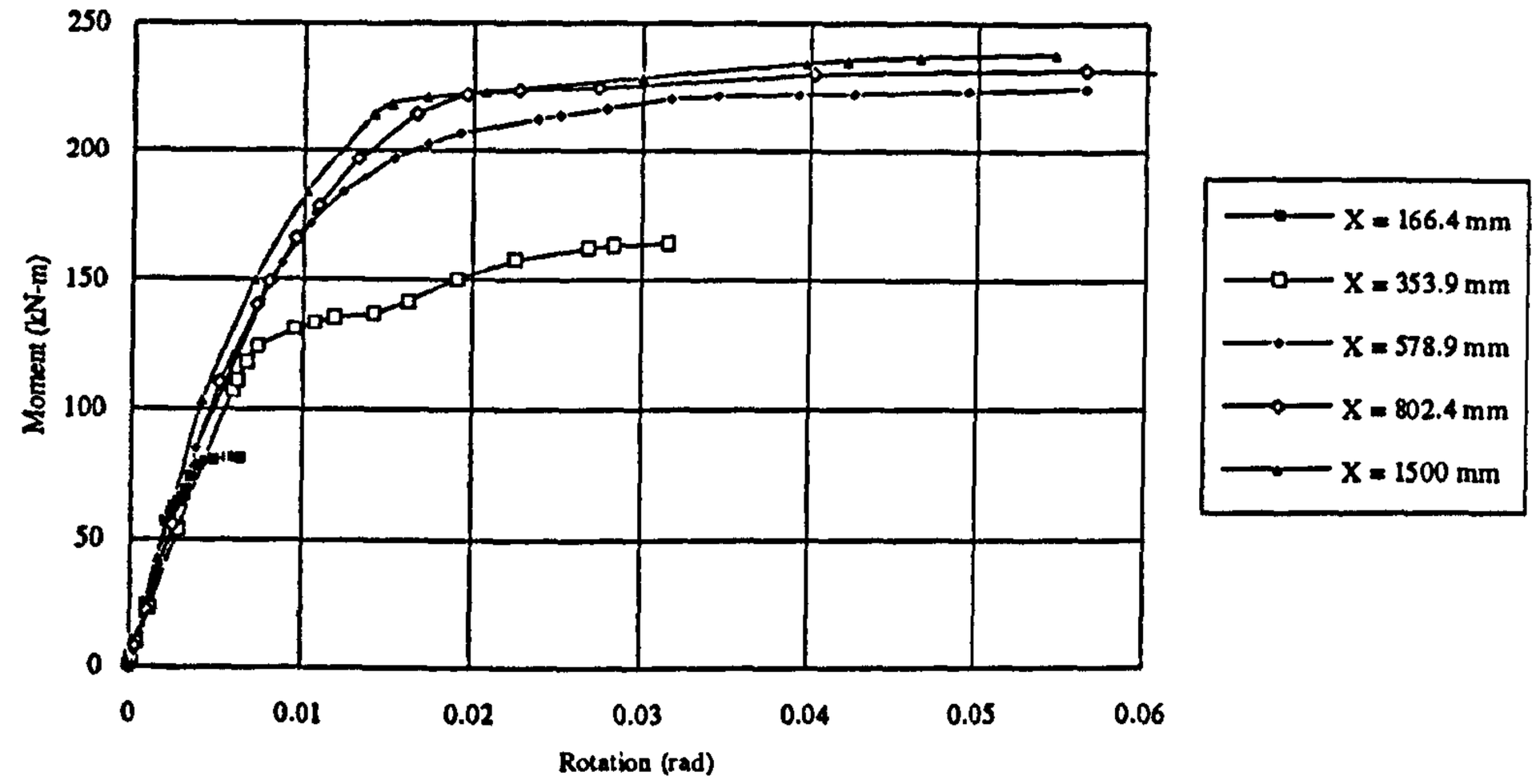

Figure 5-11 Comparison of moment rotation curves for different shear to moment ratios with 1150 mm^2 reinforcement area

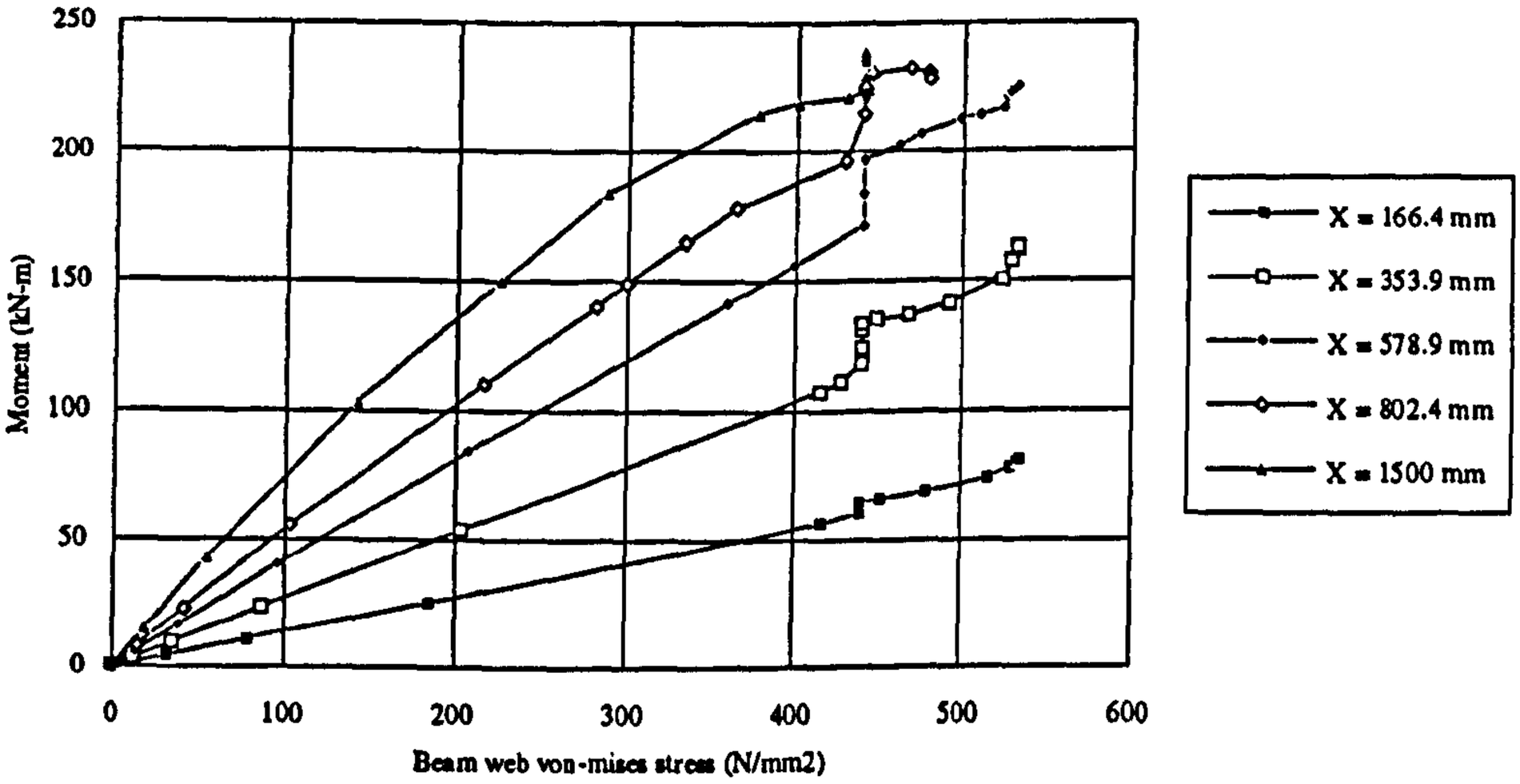

Figure 5-12 Comparison of moment beam web von-Mises stress curves for different shear to moment ratios with 1150 mm^2 reinforcement area

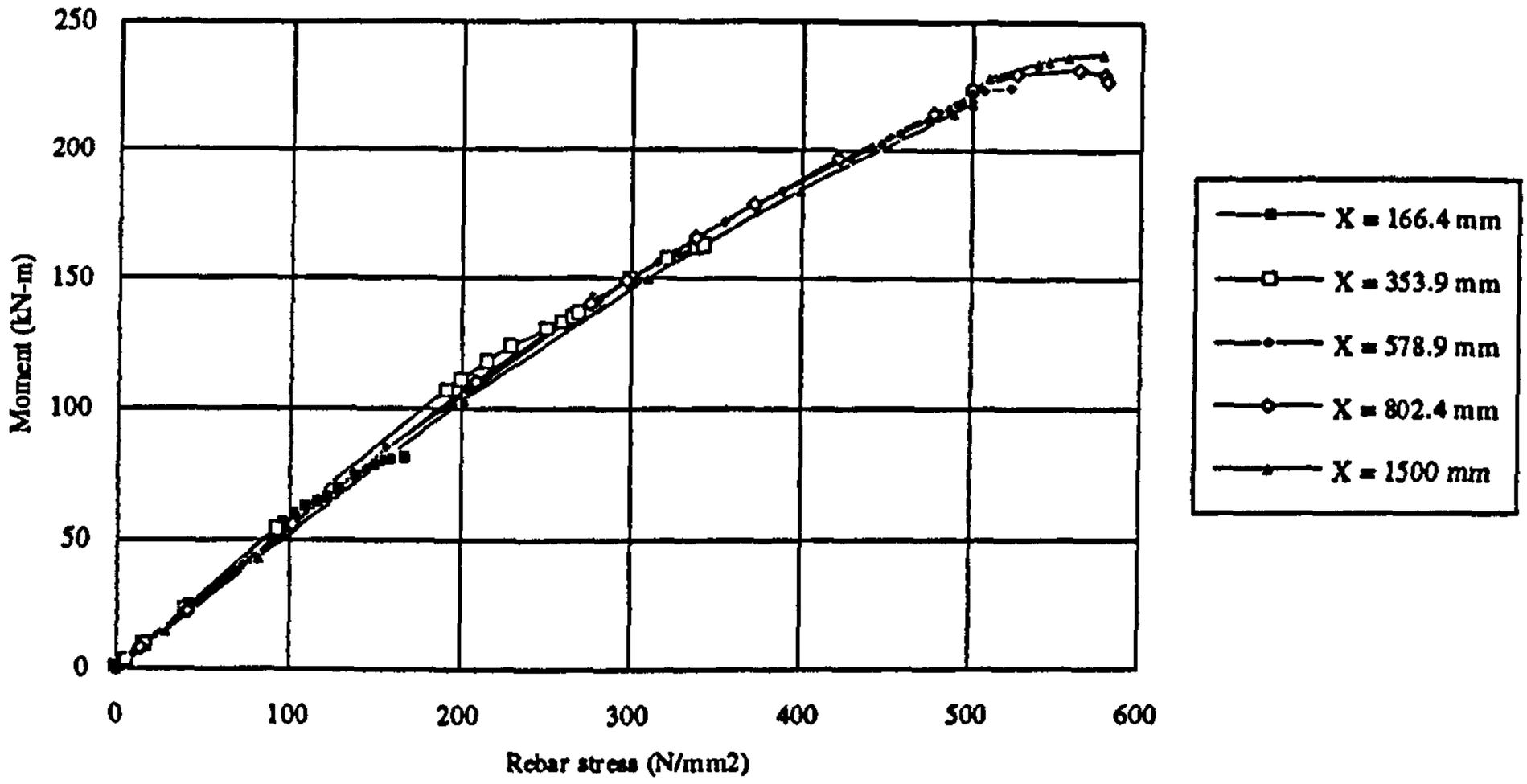

Figure 5-13 Comparison of moment rebar curves for different shear to moment ratios with 1150 mm^2 reinforcement area

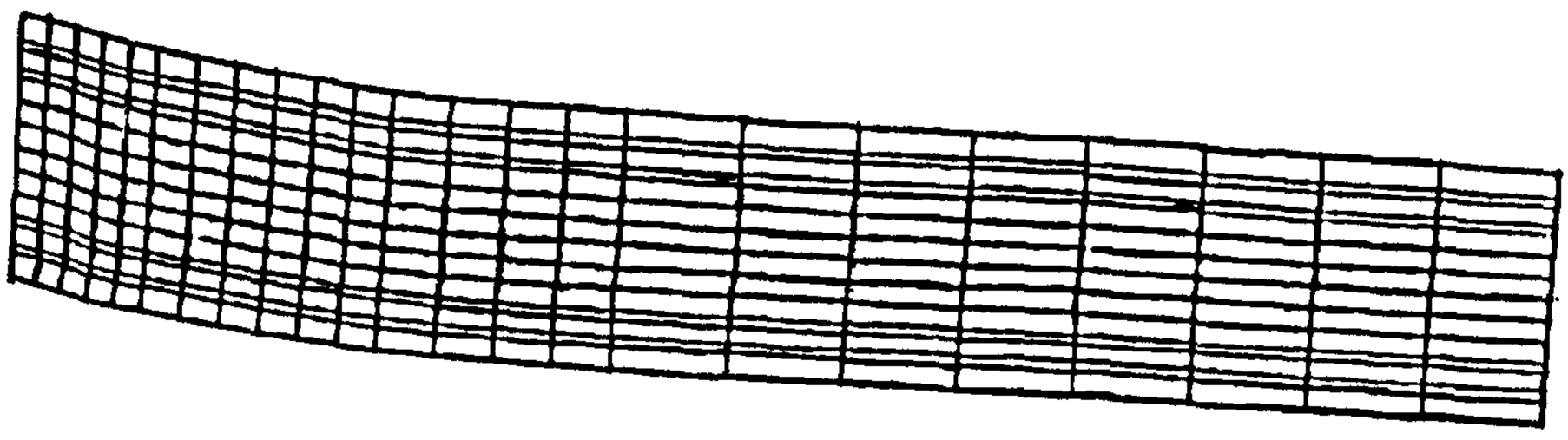

Figure 5-14 Deformed shape of the beam web at the ultimate load of the connection

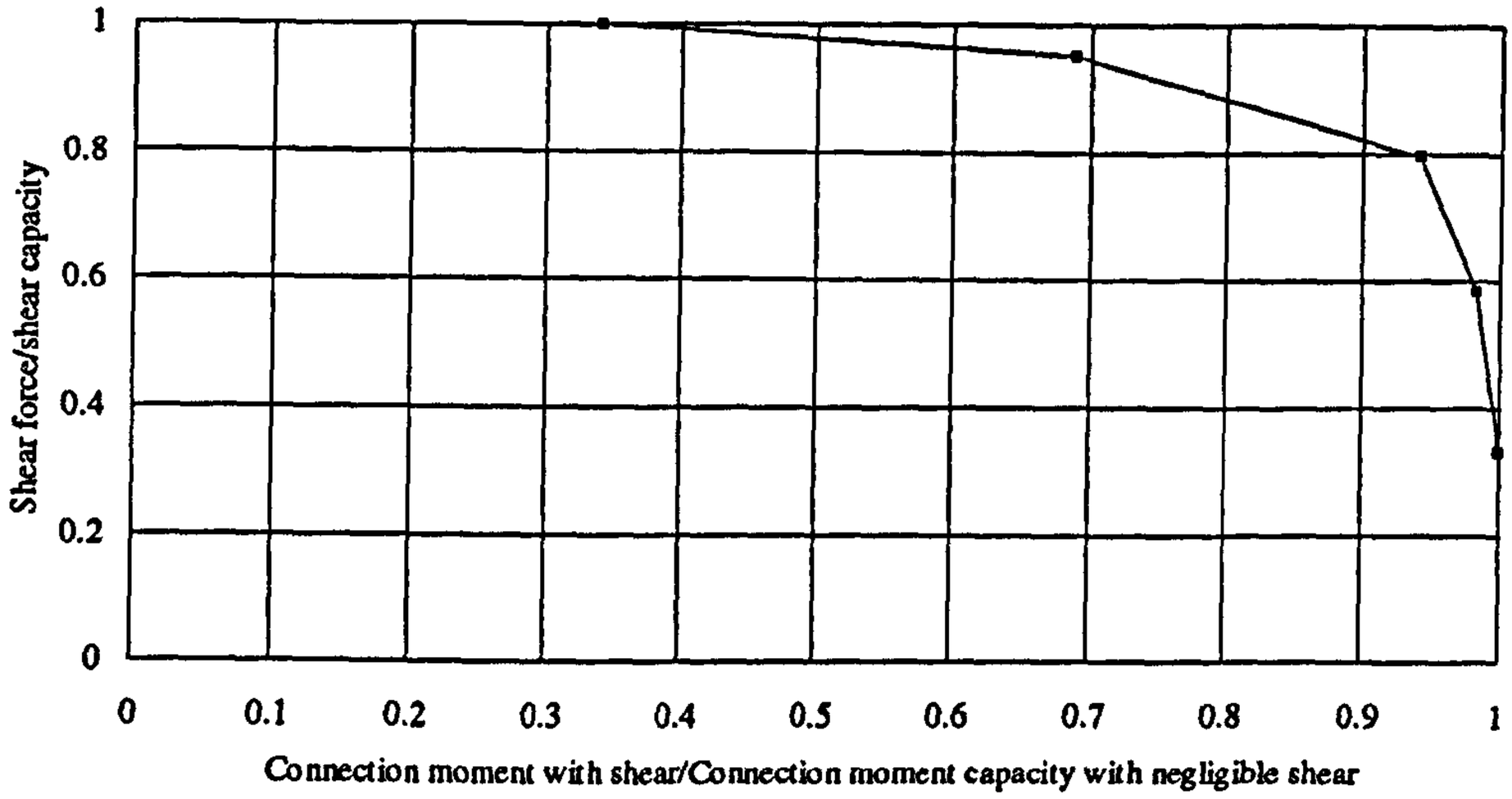

Figure 5-15 Interaction of bending moment and vertical shear

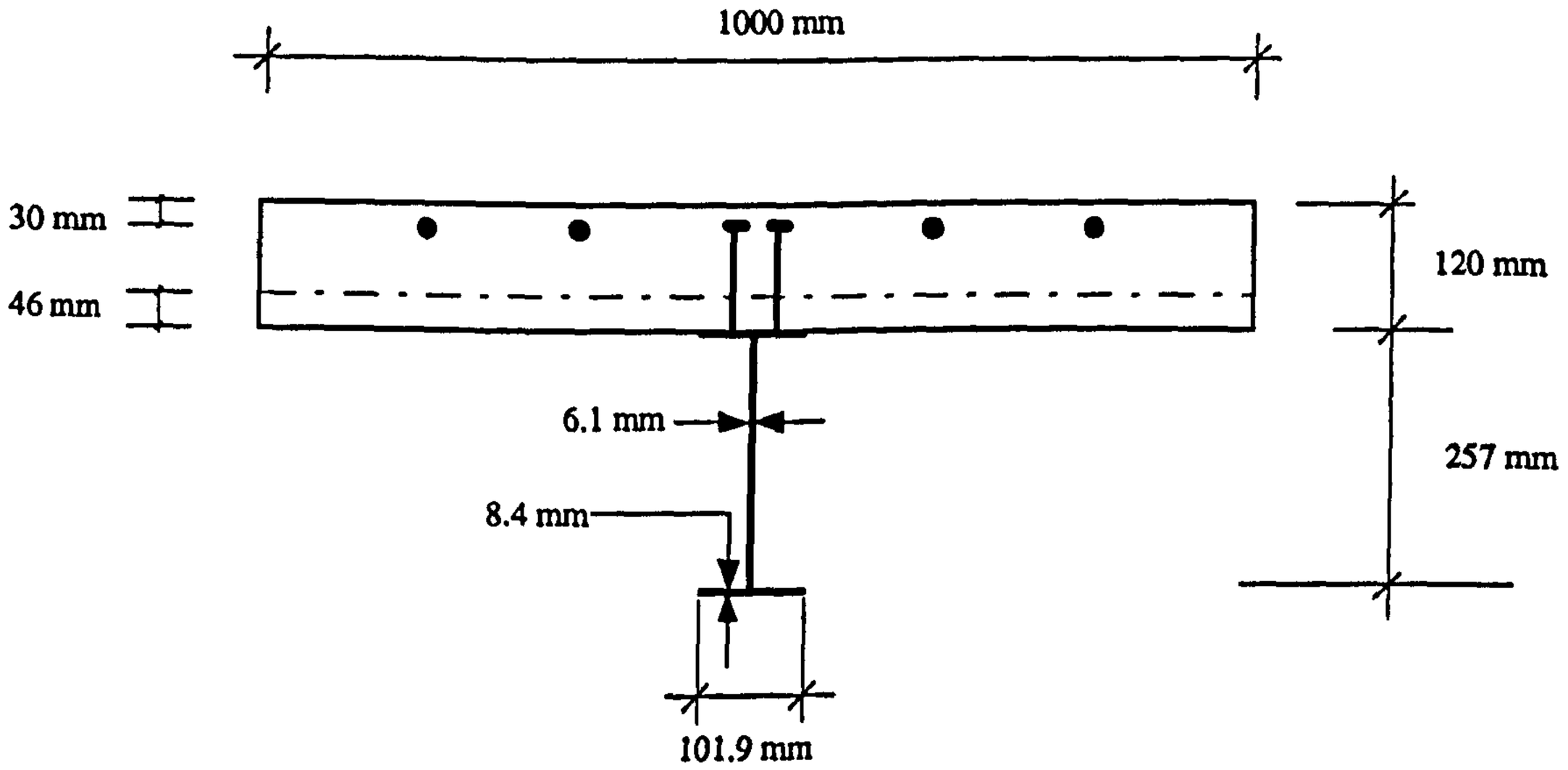

Figure 5-16 Cross section of the joint considered

Chapter 6

Effect of column axial load on composite connection behaviour

6.1 Introduction

In this chapter the numerical model described and validated in chapter 3 has been used to investigate the influence of increasing levels of axial compression in the column on the performance of the composite connection. This problem had not previously been studied, laboratory tests having utilised either zero or low column loads. However, whilst results for tests on bare steel connections [6-1] had shown an interaction, and this had formed the basis for the design rule of EC3 [6-2], more recent numerical studies of bare steel connections supplemented with further testing [6-3] have suggested that this rule might be too severe.

The studies reported herein consider the possibility of reduction in either or both of column web shear capacity and column web compression resistance, when the column web is subjected to both vertical and horizontal load. The equation presently given in EC3 for calculating shear resistance of the column web does not consider the effect of axial column loading. To investigate this factor, theoretical and numerical analyses have been made. The numerical analyses first dealt with webs subjected to horizontal compressive force only, after which vertical and then horizontal loading was applied to model the column web conditions. The findings were compared with the theoretical studies and the concept of effective shear in the column web was developed. These led to a relation between the shear strength of the column web and the loads on the two sides of the column web. Analyses were then made for composite connections. Using the findings of the study of this chapter a component based design method was

developed for non-symmetric connections allowing for the presence of varying levels of column axial load. The proposed approach first calculates the maximum achievable capacity of each component, although this may subsequently be reduced in the later phase of the calculations. The approach uses ultimate material strengths since the method is intended for the calculation of the connection's actual ultimate moment capacity. It is evident from the moment - stress curves of the different components as observed in tests [6-4] and FE studies reported in chapter 4 that when the connection reaches its ultimate capacity one or more component will exceed the yield and that stresses equal to or approaching material ultimate strengths will be attained. Predictions from the model are compared against the results of FE analysis and an existing design method based mainly on the EC3 rules. The comparison of the FE results and the proposed method are in good agreement, indicating the suitability of the proposed method. In the absence of reliable values of ultimate strengths of materials, the yield strengths may be used but this will always underestimate the connection moment capacity (especially the symmetrically loaded connections).

6.2 EC3 rules for component resistances

Three components within the connection are liable to have their resistances affected by the presence of axial load in the column. They are: column web shear capacity, column flange moment resistance in tension and column web compression capacity.

6.2.1 Calculation of column web shear capacity

The shear resistance of an unstiffened column web according to EC3 [6-2] Annex J.3.5.1 (Nov., 1990) is

$$V_{Rd} = A_v \frac{f_{y,cw}}{\sqrt{3}} \frac{1}{\gamma_{Mo}}$$

The shear strength is taken as:

$$\tau = \frac{f_{y,cw}}{\sqrt{3}} \qquad (6\text{-}1a)$$

The above equation can be obtained from the von-Mises equation simply by replacing the direct stresses σ_x and σ_y by zero. The revised [6-5] equation (Aug. 1994, clause J.3.5.2[1]), resulting from Jaspart's proposals [6-6] including the effect of the longitudinal stress σ_n is obtained by simply introducing a constant reduction factor equal to 0.9. The modified equation is:

$$V_{Rd} = \frac{0.9\, f_{y,cw}\, A_v}{\sqrt{3}\, \gamma_{Mo}}$$

The shear strength is therefore reduced to:

$$\tau = 0.9 \frac{f_{y,cw}}{\sqrt{3}} \qquad (6\text{-}1b)$$

6.2.2 Calculation of column flange resisting moment in tension allowing for column axial loading

The column flange is subjected to transverse force from the bolts, in addition to the longitudinal stress that may occur from the vertical load. For calculating the resisting moment of the column flange (which is used to calculate the developable bolt force) the EC3 Annex J.3.4.3 (Nov, 1990) reduction factor [6-2] is:

$$K_r = \frac{2 f_{y,cf} - 180 - \sigma_n}{2 f_{y,cf} - 360} \leq 1 \qquad (6\text{-}2)$$

This equation becomes effective only when the direct flange stress σ_n is greater than 180 N/mm^2.

6.2.3 Calculation of column web compression capacity under column axial loading

In EC3 Annex J.3.5.1 (Nov, 1990), the effect of the longitudinal stress σ_n is taken into account by a simple reduction factor [6-2]. The design crushing resistance of an unstiffened column web subjected to transverse compressive force is given by:

$$F_{c.Rd} = f_{y,cw} \cdot t_{cw} \left[1.25 - 0.5 \frac{\sigma_n}{f_{y,cw}} \right] \frac{b_{eff}}{\gamma_{Mo}} \qquad (6\text{-}3)$$

but, $F_{c.Rd} \leq f_{y,cw} \cdot t_{cw} \cdot \frac{b_{eff}}{\gamma_{Mo}}$

From the above two equations the reduction in horizontal compression capacity due to vertical loading can be expressed in a simplified way as:

reduction factor = $1, \quad if \quad \sigma_n \leq 0.5\, f_{y,cw}$

reduction factor = $1.25 - 0.5 \frac{\sigma_n}{f_{y,cw}}, \quad if \quad \sigma_n > 0.5 f_{y,cw}$

6.3 Theoretical investigations

6.3.1 Shear resistance

The failure criterion is used to relate the point at which failure will occur when the material is subjected to a combined stress system with the behaviour of the material as measured in a simple tension or compression test. Among the several theories i.e. the maximum principal stress theory (Rankine), the maximum principal strain theory (Saint Venant), the maximum shear stress theory (Tresca), the von-Mises yield theory, that correlate the yielding in uniaxial tests with that in a more complex state of loading, von-Mises yield theory was chosen as the failure criterion. The von-Mises yield theory generally gives results that are in good agreement with test data for ductile materials.

From the von-Mises stress equation it is known that:

$$\sigma_m^2=\sigma_x^2+\sigma_y^2-\sigma_x\sigma_y^2+3\tau_{xy}^2$$

Where:

σ_m is the material strength obtained from a uniaxial tension test

σ_x and σ_y are the stresses in the two orthogonal directions due to the applied load

When the column axial load is present, σ_y is not zero and its effect should be considered. With only (vertical) axial and shear stress present the von-Mises equation reduces to:

$$\sigma_m^2=\sigma_y^2+3\tau_{xy}^2$$

And in general the shear resistance should be calculated using:

$$\tau=\frac{\sigma_m}{\sqrt{3}}\cdot\sqrt{1-\left(\frac{\sigma_n}{\sigma_m}\right)^2} \qquad (6\text{-}4)$$

So the reduction factor to be introduced into the expression for horizontal shear stress capacity allowing for the presence of the normal stress, for unbalanced loading is:

$$F_R=\frac{\tau_{\sigma,=\sigma_n}}{\tau_{\sigma,=0}}$$

$$F_R=\sqrt{1-\left(\frac{\sigma_n}{\sigma_m}\right)^2} \qquad (6\text{-}5)$$

The above reduction factor should be used with equation 6-1a to determine the effective shear strength of the column web. Figure 6-1 shows the reduction in shear strength for various normal to von-Mises stress ratios; it is clear from this that the pattern of reduction is very different to that currently proposed for EC3 and given by equation 6-1.

6.3.2 Compressive resistance

When the connection is symmetrically loaded, in place of shear stress the horizontal compression stress governs and the von-Mises stress equation now takes the following form:

$$\sigma_x = 0.5\sigma_y \pm \sqrt{\sigma_m{}^2 - 0.75\sigma_y{}^2}$$

The reduction factor in this case is obtained in the same way as before and is:

$$F_R = 0.5\frac{\sigma_n}{\sigma_m} \pm \sqrt{1 - 0.75\left(\frac{\sigma_n}{\sigma_m}\right)^2} \qquad (6\text{-}6)$$

The above equation and the current EC3 reduction factor are plotted in Figure 6-2. It is observed that the equation resulting from the theory of elasticity (using von-Mises equation) does not suggest that any reduction is required.

6.3.3 Inferences

From the above studies the following inferences may be drawn:

1 For non-symmetric connections - for which the resistance of the column web in shear governs - EC3 equation is unconservative and there is a need to introduce a reduction factor.

2 For symmetric connections - for which instead of shear resistance, the compressive resistance will govern - EC3 equation is conservative and the reduction factor should be removed.

These will now be investigated further by means of numerical studies using the general purpose finite element software ABAQUS [6-7].

6.4 Numerical investigations (bare steel)

6.4.1 Numerical investigations for column web shear capacity reduction factor

To study the behaviour due to combined shear and horizontal compression in the presence of axial compression, care is needed to separate the two cases so that the cause of reaching the ultimate capacity can be properly identified. To study the reduction in shear capacity a plate 200 mm x 700 mm x 7.3 mm is selected. The shear resistance will be:

$$200x\ 7.3x\ \frac{\sigma_m}{\sqrt{3}} = 843\,\sigma_m \qquad (6\text{-}7)$$

Load is applied over a depth of 95 mm, so the compressive force and hence the applied web shear is:

$$7.3 \times 95 \times \sigma_m = 694\,\sigma_m$$

Thus for the analysis with no axial compression the shear resistance is greater than the applied compressive force (effective web shear). After that axial compression will be applied to the plate and on the basis of equations 6-4 and 6-5 the effect should be observed in the FE results.

Material strengths (f_{cw}) of 230 N/mm^2 and 460 N/mm^2 were assumed. The material model consists of a bilinear stress strain curve for simplicity (this makes the yield and the ultimate strengths equal). The FE mesh is shown in Figure 6-3 with the loading. The results of the FE analysis, which are given in Table 6-1, were used to develop an equation for prediction of the reduction in shear capacity due to vertical loading. The resulting equation is:

$$F_R = \sqrt{1 - 1.3\left(\frac{\sigma_n}{f_{cw}}\right)^2} \qquad (6\text{-}8)$$

The limitation of equation 6-8 is that it is only valid up to a vertical stress equal to 77% of the ultimate strength (as the quantity within the square root becomes negative), but this is considered reasonable since higher loads are impractical. It should be also kept in mind that the results of any FE analysis are to some extent approximate and that a moderate variation of a few percent can always be expected, the main feature of the results being that for a reasonable mesh they demonstrate the actual trends. Comparing equations 6-5 and 6-8 it is observed that they are almost identical in nature. Thus it can be said that equation 6-8 supports the results of the theoretical study. If equation 6-5 is to be used the term for material strength should be the yield strength (as the von-Mises equation is used with the material yield strength), and if equation 6-8 is to be used the term becomes the ultimate strength. In both cases the ultimate shear resistance should be obtained using this reduction factor. Thus the following equation is proposed for calculating column web shear resistance under non-symmetric loading:

$$F_{cs} = \sqrt{1 - \left(\frac{\sigma_n}{f_{y,cw}}\right)^2} \cdot \frac{f_{cw}}{\sqrt{3}} \cdot A_v \qquad (6\text{-}9)$$

Where:

$f_{y,cw}$ is the yield strength of the column web

f_{cw} is the ultimate strength of the column web

Table 6-1 Comparison of reduction factors for shear capacity under normal compression from theory and numerical analysis

$\frac{\sigma_n}{\sigma_m}$	FE230	FE460	Equation 6-5	Equation 6-8
0.00	1.000	1.000	1.000	1.000
0.25	0.958	0.948	0.968	0.959
0.50	0.810	0.793	0.866	0.822
0.65	0.657	0.636	0.760	0.671
0.70	0.593	0.554	0.710	0.602

For cruciform connections the web is symmetrically compressed from both sides so shear stress does not play a significant role in the web behaviour - with or without column axial loading - as the effective web shear is zero. For this case equation 6-1 should be applicable without modification and this was confirmed by the FE analysis. For various levels of axial loading the web was subjected to symmetric compression and no reduction in shear strength was observed. After this a series of analyses was conducted for a material ultimate strength of 230 N/mm^2 with a variable ratio of load on the two sides of the connection (see Figure 6-4). Results of the FE analysis are given in Tables 6-2 and 6-3. In Table 6-2 the results are presented in terms of the ratio of P_r obtained from the finite element result (see Figure 6-4) and the shear resistance determined from equation 6-7. In Table 6-3 the reduction factors are calculated by dividing the ratios of Table 6-2 by the related value in row 1 i.e. for a stress ratio of zero.

Table 6-2 Ratio of attained and predicted load with zero axial load

$\frac{\sigma_n}{\sigma_m}$	$\eta = 0.00$	$\eta = 0.25$	$\eta = 0.50$	$\eta = 0.60$	$\eta = 0.80$	$\eta = 1.00$
0.00	0.965	1.140	1.150	1.150	1.150	1.160
0.25	0.924	1.110	1.150	1.150	1.150	1.160
0.50	0.782	0.991	1.140	1.148	1.149	1.159
0.65	0.633	0.828	1.080	1.130	1.148	1.159
0.70	0.577	0.749	1.030	1.110	1.140	1.158

Note: η is the ratio of applied horizontal load on the two sides.

Table 6-3 Reduction factors according to Table 6-2

$\frac{\sigma_n}{\sigma_m}$	$\eta = 0.00$	$\eta = 0.25$	$\eta = 0.50$	$\eta = 0.60$	$\eta = 0.80$	$\eta = 1.00$
0.00	1.000	1.000	1.000	1.000	1.000	1.000
0.25	0.958	0.974	1.000	1.000	1.000	1.000
0.50	0.810	0.869	0.991	0.998	0.999	0.999
0.65	0.656	0.726	0.939	0.983	0.998	0.999
0.70	0.598	0.657	0.896	0.964	0.991	0.998

Results presented in the above two tables suggest that the shear resistance of the column web does not depend directly on whether the connection is symmetrical or not (the η ratio). Rather it is dependent on the resultant shear force acting on the column web. As the η ratio increases, it is clear from Table 6-3 that the problem becomes more of a compression problem than a shear problem. This can be explained as follows: when η is zero, the horizontal force is present on one side only of the column web and this full force acts as the effective shear in the column web. As η increases the force acts on both sides of the column web, one being larger than the other, and the difference between them is the effective shear force in the column web. This can be expressed as:

$$F_{cw,shear} = P_r - P_l = P_r - \eta P_r = (1-\eta)P_r$$

Thus due to the effect of η the effective shear force on the column web decreases. However, the maximum compressive force remains equal to the applied compressive force P_r. In the FE analysis for $\eta = 0.00$, the applied shear is 167.9 kN, and from the results of Table 6-2 it can be seen that for $\eta = 0.60$ and $\frac{\sigma_n}{\sigma_m} = 0.70$, the ratio of attained and applied load is 1.11, so the shear acting in the column web is (1-0.60)*167.9 kN = 67.2 kN, whilst the maximum compressive force is 1.11*167.9 kN = 186.4 kN; the von-Mises stress limit was reached due to this high compressive force. So it can be concluded that for any connection, the reduction factor can be applied to the effective shear force on the column web. Hence the reduced shear resistance allowing for the presence of axial loading (equations 6-8 or 6-9) should be compared with the effective shear force in the column web and the η factor should not appear on the right hand side of equation 6-9. This suggests that equation 6-9 should be modified in the following way, to check the shear capacity of the column web.

$$P_r - P_l \leq \sqrt{1-\left(\frac{\sigma_n}{f_{y,cw}}\right)^2} \cdot \frac{f_{cw}}{\sqrt{3}} . A_v \qquad (6\text{-}10)$$

P_l can be readily determined by using the "other side moment" (as shown in Figure 6-16a) M_{c2} and the distance between the bottom flange centre and rebar D_r using the following simplified equation (this equation assumes that the other side horizontal compression acts through the bottom flange, thus slightly reducing its magnitude which makes the equation very slightly conservative):

$$P_l = \frac{M_{c2}}{D_r}$$

Hence equation 6-9 takes the following final form:

$$P_r \leq \frac{M_{c2}}{D_r} + \sqrt{1-\left(\frac{\sigma_n}{f_{y,cw}}\right)^2} \cdot \frac{f_{cw}}{\sqrt{3}} . A_v \qquad (6\text{-}11)$$

These findings have led on to an investigation of the equivalent problem in composite connections, with the expectation that for non-symmetric connections the effect would be much more severe then predicted by EC3 and for symmetric connections the effect would be negligible. Thus a correction to the relevant equation of EC3 may well be necessary. The analysis and the results are described in section 6.5 of this chapter.

6.4.2 Numerical investigations for column compression capacity reduction factor

The FE model developed for this study had twice the depth of column web as compared with the previous study. Thus shear resistance is doubled and any reduction due to the column axial load should not confuse the results for compression capacity reduction. The plate selected had dimensions of 400 mm x 700 mm x 7.3 mm. The shear resistance will be:

$$400\text{x } 7.3\text{x } \frac{\sigma_m}{\sqrt{3}} = 1686\ \sigma_m$$

Load was applied over a depth of 95 mm, so the compressive force and hence the applied web shear is:

$$7.3 \text{ x } 95 \text{ x } \sigma_m = 694\ \sigma_m$$

According to the previous study the average reduction factor for shear strength was 0.56 at a stress ratio of 0.7. Hence the shear resistance at a stress ratio (axial/von-Mises) of 0.7 will be:

$$0.56\text{x}1686\,\sigma_m = 944\ \sigma_m$$

which is greater than the compressive force applied (effective web shear) and so will not affect the results for compression resistance. Material properties and FE mesh were

as before. Results (averaged for material strengths of 230 N/mm^2 and 460 N/mm^2) from the FE analyses are shown in Table 6-4. It would appear from these that the equation for compressive strength in EC3 is a little conservative. Results presented in Table 6-4 suggest that the behaviour of the column web under symmetric compression is actually similar to that predicted by the Tresca equation.

Table 6-4 Reduction factor for compression capacity under normal compression from numerical analysis, and EC3 equation

$\sigma_{n}/\sigma_{m.cw}$	FE results	EC3
0.00	1.000	1.000
0.25	1.000	1.000
0.50	0.999	1.000
0.60	0.990	0.950
0.65	0.981	0.925
0.70	0.973	0.900

6.4.3 Interim conclusions

The inferences from section 6.3.3 have been substantiated in section 6.4. So for bare steel the shear strength reduction factor of EC3 is unconservative for non-symmetric connections and the compressive strength reduction factor is conservative for symmetric connections. An equivalent study will now be made to check the effects in composite connections.

6.5 Numerical modelling of non-symmetric composite connections subjected to column axial load

6.5.1 The FE mesh, material properties and the load application procedure

The model developed for investigation consisted of a beam 254x102UB25, column 230x203UC46, endplate 280x130x10 mm. The endplate was connected to the column flange by four M20 bolts (bolt hole diameter 22 mm). The bolt holes were positioned 157 mm centre to centre vertically and 70 mm centre to centre horizontally. The reinforcement area was 767 mm^2, representing a typical ratio of 1%. The FE mesh consisted of a beam only on one side. This mesh is a representative one for the corner connections. The model had a beam length of 1500 mm. The column was 2300 mm in length. The FE mesh is shown in Figure 6-5 and the material properties are shown in Figure 2-26 of chapter 2.

Loads were applied to the FE model in two steps. The first step consisted of applying the axial compressive load to the column web and to the column flange. In the second step the load at the end of the beam was applied. For calculating the load to be applied at the top of the column the compressive capacity of the column web and column flanges was calculated using yield strength and loads were applied as a percentage of that load at the nodes of the flange or the web nodes. The moment capacity was obtained by multiplying the beam load by the distance from the edge of the column flange. Rotations were extracted at 180 mm from the column flange and at the mid height of the beam web and at the centreline of column web at the same vertical location for beam web.

6.5.2 Results of FE analyses

FE analyses were conducted for the following four cases: **a)** No column axial load. **b)** 51% of column yield capacity. **c)** 65% of column yield capacity. **d)** 82% of column

yield capacity. Table 6-5 shows the results of the FE analyses. Figures 6-6 and 6-7 show the moment-rotation and moment-bolt force curves for different levels of column axial load. The bolt forces reported in Table 6-5 and that shown in Figure 6-7, represent the force in a single bolt. It can be seen from Figure 6-7 that for any amount of column axial loading, the bolt forces reduce at a certain level of loading and then tend to increase. This is due to the total deformation of the column web and flange and is similar to the situation observed in the tests CJS-3 and CJS-6 of reference 6-4 (see also Figure 6-17a). The explanation given in reference 6-4 was *"decrease in bolt force is due to the yield of the column web in shear which caused the neutral axis to move up, and the bolt force again increased as the depth of compression zone of the connection could be increased by the column web yield due to shear"*. This is verified by the FE analyses as according to the previous calculations the reduction in shear strength should depend on the magnitude of column axial load. As the axial load in the column increases the effective shear strength of the column web decreases and this allows for more shear deformation, which causes the bolt force to reduce further as shown in Figure 6-7.

A method is described in reference 6-8 for calculating the moment capacity of non-symmetric endplate connections. This follows the EC3 equations to determine the forces in the different components of the connections. Using this method the moment capacities were obtained as 150.6 kN•m for all the cases, since the compressive force was limited by the compressive capacities of the column web, bottom flange and web of the beam. Since no factor was used to reduce the column web shear capacity because it did not govern any of the cases. The bolt force and the rebar force were constant in all cases. It was observed, however, in the FE analysis that bolt force actually decreased with increased column axial load.

The results of the FE analysis support the findings of the preliminary study that the moment capacity for non-symmetric connections is significantly affected by the level of

axial load in the column. On the basis of the studies in sections 6.3 and 6.4, together with the present results, a simplified model that is capable of incorporating the effect of column axial load is presented in sections 6.8 and 6.9.

Table 6-5 Results of FE analyses

$\frac{P_{applied}}{P_{yield}}$	Moment capacity(kN•m)	Force in a single bolt(kN)
0.0%	158	86
51%	148	70
65%	140	55
82%	121	20

6.6 Numerical modelling of symmetric composite connections subjected to column axial load

6.6.1 The FE mesh and the load application procedure

The FE mesh is shown in Figure 6-8. To simplify the analysis the left beam and the transverse beam were restrained from any movement at their ends and load was first applied at the top of the column then to the end of the right beam. This was basically to simulate the effect of axial loading on the compression capacity of the column web due to loads on both beams, i.e. to check the validity of equation 6-6 (see also section 6.6.3). The reason for using this mesh was to keep the same height of column and to use a full column section so that FE results can be easily compared with the non-symmetric case. Thus although the mesh is not actually symmetric it permits different cases to be easily handled - this assumption of symmetry is verified in section 6.6.3 using a fully symmetric mesh. The material properties were as before and the analyses were divided into two sets. The first set used the standard column mentioned before, whilst the second set used a reduced thickness of column flange and an increased thickness of column web to check for any reduction in moment capacity, i.e. due to shear in the column web or compression in the column flange.

6.6.2 Results of FE analysis

Figure 6-9 shows the moment-rotation curves obtained from the FE analysis. The moment capacities of the analysed connections were 160 kN•m,157 kN•m, 155 kN•m and 149 kN•m, at a rotation of 30 mrad (not the ultimate moment capacity). The reductions in moment capacity are 1.8 %, 3.1% and 6.9 % respectively. Figure 6-10, which gives the bolt force-rotation curves, indicates some reduction in bolt force due to the column web loading. However, these reductions did not reduce the moment capacity significantly as the connection is a composite one and the majority of the tensile force is transferred by the reinforcement. The same FE model was also used with changes to the thickness of the column web and the column flange. The column web thickness was changed to 10 mm (from 7.3 mm) and the column flange to 8 mm (from 11 mm). The same percentage of web and flange compression was applied by calculating the new compression capacities. The resulting moment-rotation curves and bolt force-rotation curves are given in Figures 6-11 and 6-12. Comparing the results of Figures 6-7, 6-10 and 6-12, it can be seen that in the symmetric type of connection the reduction in bolt force is much less than for the non-symmetric connections. The reason is that the bolt force reduction is due to the deformation of the column flange and web, which increases with the amount of column axial load present more significantly for non-symmetrically loaded connections than for symmetrically loaded connections. Table 6-5 shows the reduction in the bolt forces in each case obtained from the FE analysis. The average reductions in the bolt force together with the reduction factors from EC3 (which are actually for the bare steel arrangements) are shown in Figure 6-13. The results presented in Figure 6-13 also show that the EC3 equation only considers the amount of column stress (when greater than 180 N/mm^2), whereas this should be the stress ratio. The EC3 equation indicates that for a material having a strength of 230 N/mm^2 the reduction starts beyond a stress ratio of 0.78, whereas for a material having a strength of 460 N/mm^2 the reduction starts beyond a stress ratio of 0.39. The FE analysis confirms that the effect of column axial force is

not significant for cruciform connections. Although there is some reduction in moment capacity due to the reduction in bolt force as the column axial load increases, for composite connections it is insignificant.

From the results presented in Table 6-6, it can be seen that for cruciform connections the reduction factor for bolt force due to the deformation of the column flange as a result of the presence of axial load in the column may be expressed as:

$$K_{rb} = \sqrt{1 - 0.3\left(\frac{\sigma_n}{f_{y,cf}}\right)^2}$$

But direct examination of the results from the FE analyses of non-symmetric connections, together with the levels of bolt forces observed in the examples given in sections 6.8 and 6.9, suggest that in the case of a composite connection, instead of using bolt forces given by this equation directly, the bolt forces obtained by direct considerations of the equilibrium of the connection should be used since the bolt forces provided by the EC3 equations can be too high for the composite non-symmetric connections.

Table 6-6 Reduction factors for bolt force for various stress ratios

	Analysis set 1				Analysis set 2				
	Rotation =30 mrad		Rotation =40 mrad		Rotation =30 mrad		Rotation =40 mrad		
stress ratio	Bolt force (kN)	Reduction factor	Bolt force (kN)	Reduction factor	Bolt force (kN)	Reduction factor	Bolt force (kN)	Reduction factor	Average reduction factor
0.00	96	1.00	104	1.00	82	1.00	90	1.00	1.00
0.50	93	0.97	101	0.97	80	0.96	87	0.97	0.97
0.65	87	0.91	96	0.92	77	0.94	83	0.92	0.92
0.82	77	0.80	88	0.85	70	0.85	75	0.83	0.83

But in symmetric connections to account for the buckling of the column flange, the boly borce can be neglected for connections with high levels of column loadings (say more than 50%).

6.6.3 FE analysis for a pure symmetric connection

The FE mesh described in section 6.6.1 and the results of section 6.6.2 represent a beam loading condition that is approximately symmetric. In a real structure it is highly unlikely that any connection will be loaded in a pure symmetric condition. However, it is of interest to examine behaviour under purely symmetric beam loading. To do this symmetry is used in the FE model, also the length of the column is made shorter than that of sections 6.5.1 and 6.6.1. The mesh is shown in Figure 3-3 of chapter 3. Moment - rotation curves obtained from the analyses are given in Figure 6-14. These show how the symmetric boundary condition imposed on the column web causes the moment capacity to increase for all magnitudes of applied column axial load. However, the trend for reduction of the moment capacity with increasing axial column load is similar to the previous case. This time the moment capacities were 183 kN•m, 179 kN•m, 176 kN•m and 167 kN•m (at a rotation of 40 mrad), corresponding to reductions 2.2%, 3.8% and 8.7% respectively, whereas the reductions in the case used in section 6.6.1 were 1.8%, 3.1% and 6.9% - which are very close to each other. Examination of the detailed results revealed that in the first two cases (51% and 65%) the reduction was due to yield of the column flange but for the highest column load (82%) the column web yield produced movement of the neutral axis and hence caused reduction in the bolt force and thus in the moment capacity. Thus the FE mesh used in section 6.6.1 and the results of section 6.6.2 may be regarded as representative of the symmetric case.

6.6.4 Comparison between bare steel and composite connections

It is of interest to compare the above findings for composite connections, which indicate that even quite large column loads have little effect, with the behaviour of similar bare steel connections. This is most appropriately done by considering the non-symmetric and symmetric cases separately with the aid of the force diagram of Figure 6-15.

Non-symmetric connections: Since the compressive and tensile forces must balance and in bare steel connections the tensile force is relatively low it may well not exceed the shear capacity of the column web even under high levels of column axial load. However, in composite connections the tensile force is normally far higher, so the developed compressive force is also high, and under a high column load this can easily exceed the column shear capacity. For this reason bare steel non-symmetric connections may not show very much reduction in moment capacity due to the reduction in shear strength of the column web.

Symmetric connections: In a bare steel connection all the tensile resistance is transmitted by the bolt forces. Also as the shear strength is unlikely to govern and thus compressive capacity is not reduced, there is almost no reduction in developable compressive force. However in composite connections, the majority of the tensile force passes through the reinforcement. Whilst FE analyses of composite connections show some reduction in the bolt forces due to the reduction of column flange resisting moment in tension, this has negligible effect on moment capacity. But for bare steel connections the bolt forces will be higher and thus the reductions in effective tensile force with increasing column axial load will be much greater, thereby causing a more significant reduction in the moment capacity of the cruciform bare steel connections.

6.7 Internal force distribution in a connection

Before establishing a rule to determine the effective component forces in a connection it is essential to establish the distribution of internal forces. Figure 6-16 shows the simplified free body diagram for a connection. In order to simplify the analysis it is assumed that there is no concentrated or distributed horizontal load acting externally on the column, and that the other side moment (that is the moment on the far side of the connection being considered) can be represented by the action of reinforcement and bottom flange compressive force only to give: $P_l = F_{c,bfl} = \frac{M_{c2}}{D_r}$. Using this assumption the connection and its free body diagram are drawn in Figures 6-16(a) and 6-16(b) respectively. From Figure 6-16(b), the following equations may be obtained:

6.7.1 The bolt force

From Figure 6-16(b) it can be seen that the maximum shear force in the column web is $F_r - F_h + F_b - \frac{M_{c2}}{D_r}$, so the following relationship should be used when comparing the bolt and rebar force with the column web shear strength:

$$F_r - F_h + F_b - \frac{M_{c2}}{D_r} \leq shear\ strength$$

It is evident from the test results in reference 6-4 (CJS-1 and CJS-3) that the bolt force is more prone to reductions than the rebar force due to any lack of symmetry of the applied load (see Figures 6-17a and 6-17b) between the two sides of the connection (i.e. the effect of η); this was confirmed by the FE modelling. It can be seen from Figures 6-17a and 6-17b that the final bolt forces for the two connection are different (non-symmetric one has a large reduction in bolt force), whereas in both connections

the rebars yielded at a rotation of about 12 mrad. Hence the bolt force should be calculated using:

$$F_b = \frac{M_{c2}}{D_r} + F_h + \sqrt{1 - \left(\frac{\sigma_n}{f_{y,cw}}\right)^2}\ \frac{f_{cw}}{\sqrt{3}} A_v - F_r$$

The above equation should be used with the other available equations (i.e. EC3 equations and its simplifications proposed in ref. 6-8) to determine the maximum bolt force of the bolt row.

6.7.2 Attainable connection compressive force on the connection face considered

From the free body diagram, $F_{c,cw} = F_r + F_b$. Substituting for F_b from section 6.7.1 the following relationship is obtained:

$$F_{c,cw} = \frac{M_{c2}}{D_r} + F_h + \sqrt{1 - \left(\frac{\sigma_n}{f_{y,cw}}\right)^2}\ \frac{f_{cw}}{\sqrt{3}} A_v$$

For a simpler approach the horizontal force acting at the top and bottom of the column length may under certain conditions be taken as zero. If the shear force present in the column web is due to the beam load only, than this simplification will lead to a slightly conservative result (see examples of section 6.9). However, if the shear force is developed due to the presence of moments at the top or bottom (or both) of the column length, it is essential to draw the column web shear diagram, considering these moments, before deciding that the simplification is safe.

6.8 Recommend changes to include the effect of column loading

The accurate determination of the connection moment capacity depends on the correct determination of the internal forces in the individual components. The results from the study of composite connections have shown that even in the presence of a large axial load in the column there is no significant reduction in compression capacity, but the shear resistance and the bolt force are reduced significantly. In chapter 5 of this thesis (also reference 6-9) a design method is described which can predict the attainable beam shear; this should also be used to determine the allowable beam web horizontal stress. When considering the effect of column axial loading the following are suggested to determine the resistances of the different components:

a) For calculating the column web compression resistance

The effect of column axial load can be neglected.

b) For calculating attainable connection compressive force considering the effect of shear resistance and column axial loading

$$F_{c,cw} = \frac{M_{c2}}{D_r} + F_h + \sqrt{1 - \left(\frac{\sigma_n}{f_{y,cw}}\right)^2}\,\frac{f_{cw}}{\sqrt{3}} A_v$$

Where:

F_h is the is the shear force acting on column top and bottom

M_{c2} is the moment on the other side of the connection

D_r is the distance between the centreline of bottom flange and the rebar.

A_v is the shear area of the column

σ_n is the column web normal stress

$f_{y,cw}$ is the column web yield strength

f_{cw} is the column web ultimate strength

c) Maximum developable beam web compressive force

The magnitude of the maximum developable beam web compression may be determined by subtracting the column web compressive force at the beam bottom flange level from the attainable connection compressive force. It can be calculated by using the following formula:

$$F_{c,bw} = F_{c,cw} - F_{c,bf} \geq 0$$

d) For calculating the bolt force considering the effect of shear resistance and column axial loading

The bolt force (for a row of bolts) that can develop in a connection should be calculated first with the EC3 equations together with the simplifications proposed in ref. 6-8, but at the same time the following equation is to be used. The lower of the two results should be taken as the initial tensile force in the bolts (this may subsequently be reduced as a result of establishing equilibrium):

$$F_b = \frac{M_{c2}}{D_r} + F_h + \sqrt{1 - \left(\frac{\sigma_n}{f_{y,cw}}\right)^2} \frac{f_{cw}}{\sqrt{3}} A_v - F_r \geq 0$$

6.9 Design method for non-symmetric connections considering the effects of column axial loading

A flow chart giving the steps required to calculate moment capacity is given in Figure 6-18. Table 6-7 summarises the design procedure in terms of the actual formulae to be used.

Table 6-7 Design procedure

Initial calculation for capacity of different components

Rebar force

$$F_r = min\begin{cases} A_r f_u & \\ 0.67 b_{cf} h_{cs} f_c' \beta + \dfrac{M_{c2}}{D_r} & ref\ 6-8 \\ nkR_{Rd} & EC4,\ Clause\ 6.3.2 \end{cases}$$

Bolt force

$$F_b = min\begin{cases} (4.32 - 0.039m + 0.0116e + 0.009p) t_{cf}^{\ 2} f_{cf} & ref\ 6-8 \\ (5.5 - 0.021m + 0.017e) t_p^{\ 2} f_{yp} & ref\ 6-8 \\ 1.8 A_b f_b & EC3,\ Clause\ 6.5.5 \\ \dfrac{M_{c2}}{D_r} + F_h + \sqrt{1 - \left(\dfrac{\sigma_n}{f_{y,cw}}\right)^2}\ \dfrac{f_{cw}}{\sqrt{3}} A_v - F_r \geq 0 & \end{cases}$$

Attainable joint compressive force

$$F_{c,cw} = min\begin{cases} \dfrac{M_{c2}}{D_r} + F_h + \sqrt{1 - \left(\dfrac{\sigma_n}{f_{y,cw}}\right)^2}\ \dfrac{f_{cw}}{\sqrt{3}} A_v & \\ t_{cw} b_{eff} f_{cw} & EC3,\ J.3.5.3 \\ 8.4\ \ b_{eff}^{\ 0.017}\ \ D_c^{\ 0.60}\ \ t_{cw}^{\ 1.43}\ f_{cw}^{\ 0.76} & ref\ 6-8 \end{cases}$$

Bottom flange compression force

$$F_{c,bf} = min\begin{cases} t_{bf} b_{bf} f_{bf} & when\ \dfrac{b_{bf}}{t_{bf}} < 22\sqrt{\dfrac{235}{f_{yb}}} & (BF\ compression)\ EC3,\ Table\ 5.3.1 \\ 22 t_{bf}^{\ 2} f_{bf} \sqrt{\dfrac{235}{f_{yb}}} & when\ \dfrac{b_{bf}}{t_{bf}} \geq 22\sqrt{\dfrac{235}{f_{yb}}} & (BF\ Buckling)\ EC3,\ Table\ 5.3.1 \end{cases}$$

Estimate the attainable shear force (roughly) and beam compression capacity using the following equations

$$P_v = min\begin{cases} \dfrac{(F_r D_r + F_b d_b)}{x} \\ \dfrac{[F_{c,cw} D_r - F_b (D_r - d_b)]}{x} \end{cases}$$

$$\tau_{xy} = \frac{minimum\ P_v}{(H_b - 2t_{bf}) t_{bw}}$$

$$f_{a,bw} = \sqrt{f_{bw}^{\ 2} - 3\tau_{xy}^{\ 2}}$$

Beam compression capacity is $F_{c,b} = F_{c,bf} + f_{a,bw} \cdot (H_b - t_f) t_{bw}$

Table 6-7 Design procedure (continued)

Determination of effective internal forces	
Joint compression capacity	$F_{c,j} = min\begin{cases} F_r + F_b \\ F_{c,cw} \\ F_{c,b} \end{cases}$
Rebar force	$F'_r = min\begin{cases} F_r \\ F_{c,j} \end{cases}$
Bottom flange compression force	$F'_{c,bf} = min\begin{cases} F_{c,j} \\ F_{c,bf} \end{cases}$
Beam web compression force	$F_{c,bw} = F_{c,j} - F'_{c,bf}$
Bolt force	$F'_b = min\begin{cases} F'_{c,bf} + F_{c,bw} - F'_r \geq 0 \\ F_b \end{cases}$
Depth of compression	$d_{c,bw} = min\begin{cases} 0 \quad \text{if } F_{c,bw} \text{ is zero} \\ \dfrac{F_r + F_b - F'_{c,bf}}{f_{a,bw}.t_{bw}} \quad \geq 0 \end{cases}$
Moment capacity of the joint $M = F'_r D_r + F'_b d_b - 0.5\left(d_{c,bw} + t_{bf}\right)F_{c,bw}$	

6.10 Application in frame design

The method described above may readily be applied to the design of non-symmetric connections in frames. This will require the determination of the shear force and bending moment present at the top and bottom of the connection. Once the shear forces are known, using the previously described method, it is possible to determine the attainable rebar and bolt forces (these will be lower than the actual values). After that the shear force diagram in the column can be drawn. Using the equations presented above the connection moment capacity may be determined. This is illustrated with a worked example, for which equal shears of 86 kN are assumed at the top and bottom of the column.

6.11 Example

A non-symmetric connection consisting of: 254x102UB25 beams, a 203x203UC46 column, a concrete slab having an effective breadth of 1000 mm and a total depth of 110 mm with CF46 metal decking, a reinforcement area of 767 mm^2 with seven rows of 100x19 mm headed shear studs, each row containing two studs. The connection considered is a flush endplate connection with an endplate of 280x130x10mm. Bolt diameter is 20 mm, vertically positioned 157 mm centre to centre and the bolts are M20 grade 8.8. The cross section of the beam and slab is shown in Figure 5-16 of chapter 5, except that slab depth used herein was 110 mm. All examples assume the presence of a stub beam connected to the column web, which prevents buckling of the column web. The examples show how bolt force, and thus moment capacity are affected by changes to the column axial load, presence of column web shear and the presence of any moment on the other side of the connection.

Ultimate strengths for the components are:

Beam web: 553 N/mm^2

Beam flange: 490 N/mm^2

Column web: 553 N/mm^2

Column flange: 500 N/mm^2

Endplate: 350 N/mm^2

Reinforcement: 550 N/mm^2

Bolt: 600 N/mm^2

Concrete strength: 33 N/mm^2

Column web yield strength is: 350 N/mm^2

Axial loads of 0%, 51%, 65% and 82% of column yield load will be considered. According to the proposed equations the reduction factors for shear strength are 1.00, 0.86, 0.76, 0.57 respectively. Calculations for moment capacity are shown in Tables 6-8 to 6-10.

Table 6-8 Calculation of moment capacity for connections, without considering the shear present in the column (non-symmetric connection)

Initial calculations:	The first trial attainable vertical shear is 148 kN governed by beam web overstress and the available compressive stress is 539 N/mm^2. Beam flange compression resistance is 420 kN. Compression capacity of beam is 1215 kN. Rebar force is 360 kN.			
$\frac{P_{applied}}{P_{yield}}$	0%	51%	65%	82%
Bolt force F_b (kN)	187	110	56	0
Column web compression resistance $F_{c,cw}$ (kN)	547	470	416	313
Connection Compression capacity (kN) $F_{c,j} = min \begin{cases} F_r + F_b \\ F_{c,cw} \\ F_{c,b} \end{cases}$	547 > Rebar	470 > Rebar	416 > Rebar	313 < Rebar
Rebar force (kN) $F_r' = min \begin{cases} F_r \\ F_{c,j} \end{cases}$	360	360	360	[313]
Bottom flange compression (kN) $F_{c,bf}' = min \begin{cases} F_{c,bf} \\ F_{c,j} \end{cases}$	420	420	420	[313]
Beam web compression (kN) $F_{c,bw} = F_{c,j}' - F_{c,bf}'$	127	50	0	0
Revised bolt force (kN) $F_b' = min \begin{cases} F_{c,bf}' + F_{c,bw} - F_r' \geq 0 \\ F_b \end{cases}$	187	110	56	0
Depth of beam web in compression (mm)	38.63	15.21	0	0
Moment capacity (proposed model) (kN•m)	156	143	132	104
Moment capacity ref. 6-8 (kN•m)	151	151	151	151

Note: values within square brackets indicate that the component capacity under consideration is actually controlled by another phenomenon

Table 6-9 Calculation of moment capacity for connections, including the shear present in the column (non-symmetric connection)

Initial calculations:	The first trial attainable shear is 148 kN governed by beam web overstress and the available compressive stress is 539 N/mm^2. Beam flange compression resistance is 420 kN. Compression capacity of beam is 1215 kN. The rebar force is 360 kN.			
$\frac{P_{applied}}{P_{yield}}$	0%	51%	65%	82%
Bolt force F_b (kN)	192	192	142	39
Column web compression resistance $F_{c,cw}$ (kN)	633	556	502	399
Connection Compression capacity (kN) $F_{c,j} = min \begin{cases} F_r + F_b \\ F_{c,cw} \\ F_{c,b} \end{cases}$	552 > Rebar	552 > Rebar	502 > Rebar	399 > Rebar
Rebar force (kN) $F'_r = min \begin{cases} F_r \\ F_{c,j} \end{cases}$	360	360	360	360
Bottom flange compression (kN) $F'_{c,bf} = min \begin{cases} F_{c,bf} \\ F_{c,j} \end{cases}$	420	420	420	[399]
Beam web compression $F_{c,bw} = F_{c,j} - F'_{c,bf}$ (kN)	132	132	82	0
Bolt force (two bolts) (kN) $F'_b = min \begin{cases} F'_{c,bf} + F_{c,bw} - F'_r \geq 0 \\ F_b \end{cases}$	192	192	142	39
Depth of beam web in compression (mm)	41	41	24.9	0
Moment capacity (proposed model) (kN•m)	157.3	157.3	148.5	128

Table 6-10 Calculation of moment capacity for connections, including the moment present on the other side of the connection (non-symmetric connection with M_{c2} = 80 kN•m)

Initial calculations:	The first trial attainable shear is 148 kN governed by beam web overstress and the available compressive stress is 539 N/mm^2. Beam flange compression resistance is 420 kN. Compression capacity of beam is 1215 kN. The rebar force is 422 kN.			
$\frac{P_{applied}}{P_{yield}}$	0%	51%	65%	82%
Bolt force F_b (kN)	192	192	192	131
Column web compression resistance $F_{c,cw}$ (kN)	633	633	633	553
Connection Compression capacity (kN) $F_{c,j} = min \begin{cases} F_r + F_b \\ F_{c,cw} \\ F_{c,b} \end{cases}$	614 kN > Rebar	614 kN > Rebar	614 kN > Rebar	553 kN > Rebar
Rebar force (kN) $F_r' = min \begin{cases} F_r \\ F_{c,j} \end{cases}$	422 kN	422 kN	422 kN	422 kN
Bottom flange compression (kN) $F_{c,bf}' = min \begin{cases} F_{c,bf} \\ F_{c,j} \end{cases}$	420 kN	420 kN	420 kN	420 kN
Beam web compression (kN) $F_{c,bw} = F_{c,j} - F_{c,bf}'$	194 kN	194 kN	194 kN	133 kN
Bolt force (two bolts) (kN) $F_b' = min \begin{cases} F_{c,bf}' + F_{c,bw} - F_r' \geq 0 \\ F_b \end{cases}$	192 kN	192 kN	192 kN	131 kN
Depth of beam web in compression (mm)	59	59	59	40.5
Moment capacity (proposed model) (kN.m)	174.6	174.6	174.6	164.9

Comments on the examples

In Tables 6-8, 6-9 and 6-10, the same connection is analysed under similar loading conditions but with different assumptions regarding column shear and any moment on the far side of the connection. A comparison of the final results for the different column conditions is shown in Table 6-11, together with the results of full FE analyses.

Table 6-11 Comparison of results for different column condition with axial load

$\frac{P_{applied}}{P_{yield}}$	0%	51%	65%	82%
Moment capacity (FE) (kN•m) (M_{c2} = 0 kN•m)	157	144	140	121
Moment capacity without considering the shear present in the column (kN•m) Example-1	156	143	132	104
Moment capacity considering the shear present in the column (kN•m) Example-2	157.3	157.3	157.3	128.0
Moment capacity (kN•m) (M_{c2} = 80 kN•m) Example-3	174.6	174.6	174.6	164.9
Moment capacity (FE) (kN•m) (symmetric case)	183	179	179	167

The first analysis neglects the presence of any shear force at the top and bottom of the connection, whilst the second set of analyses considers the presence of equal shear forces at the top and bottom; this is closer to the practical situation. Since it is possible to predict the shear force in the column using conventional analysis for the structural frame, the second method can be applied to determine the non-symmetric connection moment capacity in frames and will lead to higher capacities for the connections, if the considered shear at the top and the bottom of the connection reduces the effective

shear in the column web panel of the connection (as in the second example) and if the effective shear force is increased the moment capacity will be reduced.

The third example is similar to the first but assumes a moment of 80 kN•m on the other side of the connection. This is a situation that approximately represents the case η =0.45 (as can be seen from the ratio of the moments), since calculation for a cruciform connection of the same configuration gave a moment capacity of about 180 kN•m. The third example shows clearly how the column web shear resistance and hence the moment resistance of the connection improves due to the presence of moment on the other side of the connection. This improvement in behaviour of the connection with increasing η value can also be seen from the results of finite element analysis for a symmetric connection (η = 1) with column load, where the reduction is only due to the reduction in the bolt force and there is no loss of column web shear strength.

The results predicted by numerical analysis of the non-symmetric connections using the composite connection FE model fall somewhere between the first two examples (when the axial load is sufficiently high to significantly affect the shear capacity of the connection), as the top and the bottom of the column were restrained from horizontal movements in the FE model - which caused the development of the shear force in the column from the reaction force, which is represented by the example-2. This can also be seen from the results presented in Table 6-11. When the column load is zero or very low results for the two examples and the FE result are very close. As the column load increases due to the change in connection compression capacity the first method gives a lower result than the second one - due to the greater reduction in the bolt force resulting from the reduction in shear strength of the column web. The FE results fall between the two examples but are closer to the second example. At this point it of interest to look back at the bolt forces from FE analyses and example-2. Figure 6-7 gives the force in each bolt and the second row of Table 6-9 gives the bolt force in the

bolt row (two bolts); the results are close to each other. Thus it can be said that if properly used example-2 will give more representative results.

6.12 Conclusions

The effect of column axial load on the moment capacity of bare steel and composite symmetric and non-symmetric connections has been investigated. Initial theoretical and FE studies on a single plate representing the column web suggested that when the column web is subjected to non-symmetric horizontal compression then the effect of column axial load would be significant, but for symmetrical horizontal web compression there should be no effect. This is due to the fact that for non-symmetric connections the shear capacity is reduced with increasing column axial load, but for symmetric connections the compression resistance of the column web is unaffected by the column axial loading. Further investigation of the problem showed that the effective shear resistance of the column web is also dependent on both the level of moment on the other side of the column and the axial load in the column. The analyses of twelve representative connections using a previously validated FE model supported the findings of this study. It is therefore suggested that the EC3 equation for shear resistance of the column web be modified for non-symmetric connections. At the same time the reduction in compression strength given by the design rule of EC3 was found to be over conservative. An equation has been proposed that can be used when determining the shear capacity of the column section. Instead of using a reduction factor to reduce the bolt force, an equation that can predict the actual bolt force from consideration of the basic mechanics of the problem has been developed. At the same time the bolt force is also related to the overall equilibrium of the connection. It was observed that the presence of shear at the top and bottom of the column influences the internal forces and hence the moment capacity. Based on the FE studies a new design procedure for non-symmetric connections is proposed. This allow for the level of column axial load and the probable shear force present in the column as well as the

presence of any moment on the other side of the connection. The FE studies also show that the initial stiffness of a connection is not affected by the presence of the column axial load. The findings of chapter 5 and this chapter can be combined to develop a design method for the composite flush endplate connections. In the next chapter a design method that can treat both symmetrical and non symmetrically loaded connection with shear to moment ratio effect and column loading will be described.

6.13 References

6-1 Zoetemeijer (1975) *Influence of normal-,bending - and shear stresses in the web of European rolled sections*, Report N° 6-75-18, Stevin Laboratory, Delft University of Technology, The Netherlands.

6-2 Eurocode No 3 (1992) *Design of Steel Structures, Part 1.1: General Rules for Buildings*, DD ENV 1993-1-1, April 1992, European Committee for Standardisation (CEN).

6-3 Stephen, G. and Jaspart, J. P. (1996) *Influence of Structural Frame Behaviour on Joint Design*, Connections in Steel Structures III: Behaviour, Strength and Design, Edited by Reidar Bjorhovde, Andre Colson, Riccardo Zandonini, Proceedings of the Third International Workshop, 29-31 May 1995, pp. 321-330.

6-4 Li, T. Q., Nethercot, D. A. and Choo, B. S. (1996) *Behaviour of flush end plate composite connections with unbalanced moment and variable shear/moment ratios: part 1:Experimental Behaviour*, Journal of Constructional Steel Research, Vol. 38, No. 2, pp. 125-164.

6-5 CEN/TC 250 (1994) New Revised Annex J of Eurocode 3: Part 1.1, CEN document N419E.

6-6 Jaspart, J. P. (1991) *Etude de la semi-rigidite' des noeuds poutre-colonne et son influence sur la re' sistance et la stabilite' des ossatures en acier*, Ph.D. Thesis, Department MSM, University of Lie'ge, Belgium.

6-7 *ABAQUS user manual*, Version 5.3.1 (1994), Hibbitt, Karlsson & Sorensen, inc., 1080 Main Street, Pawtucket, RI 02860-4847, USA.

6-8 Li, T. Q., Nethercot, D. A. and Choo, B. S. (1996) *Behaviour of flush end plate composite connections with unbalanced moment and variable shear/moment ratios: part 2: prediction of moment capacity*, Journal of Constructional Steel Research, Vol. 38, No. 2, pp. 165-198.

6-9 Ahmed, B. and Nethercot, D. A. *Effect of high shear on the moment capacity of composite cruciform endplate connections*, Journal of Constructional Steel Research (in press).

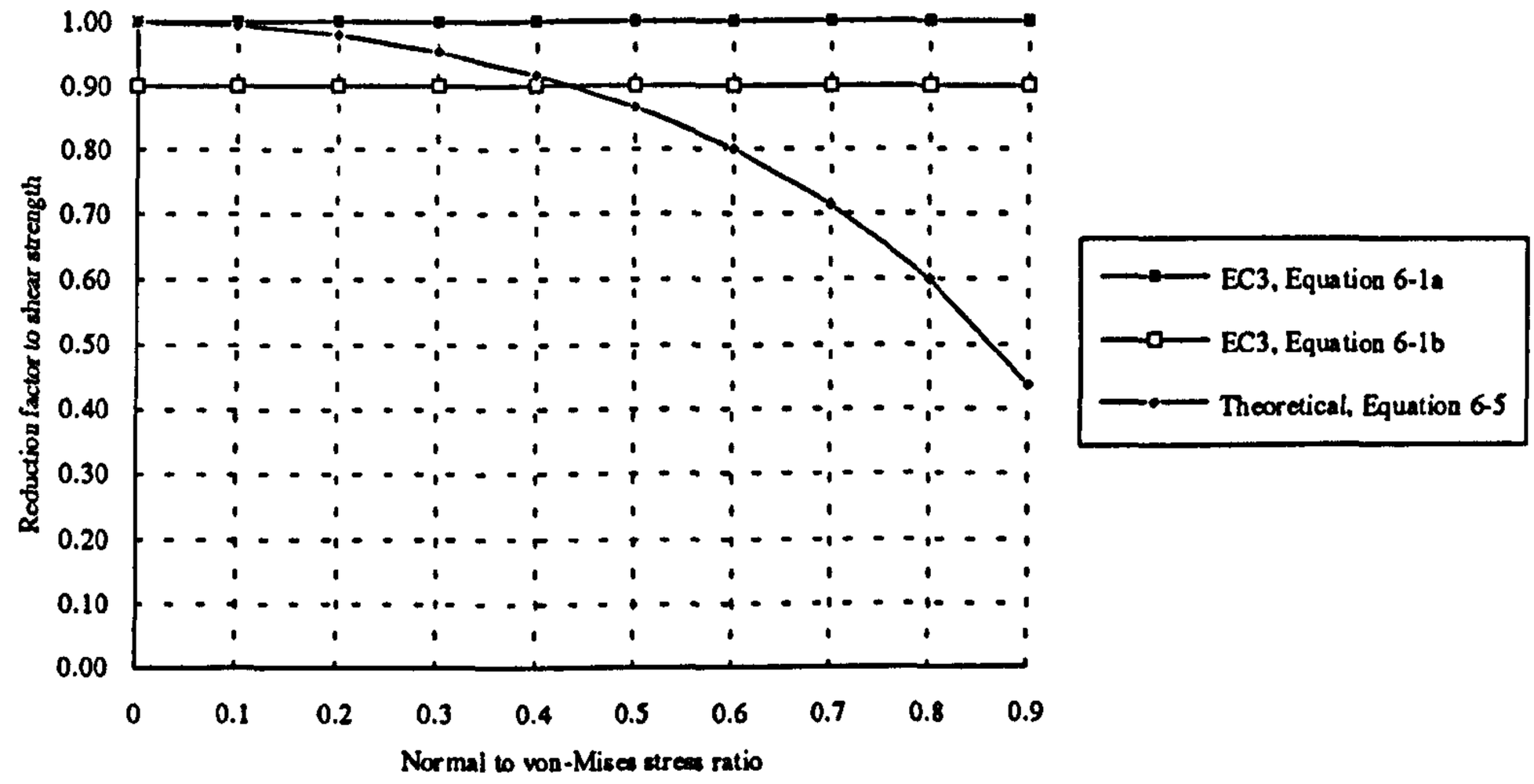

Figure 6-1 Ratio for shear strength for various normal to von-Mises stress ratios

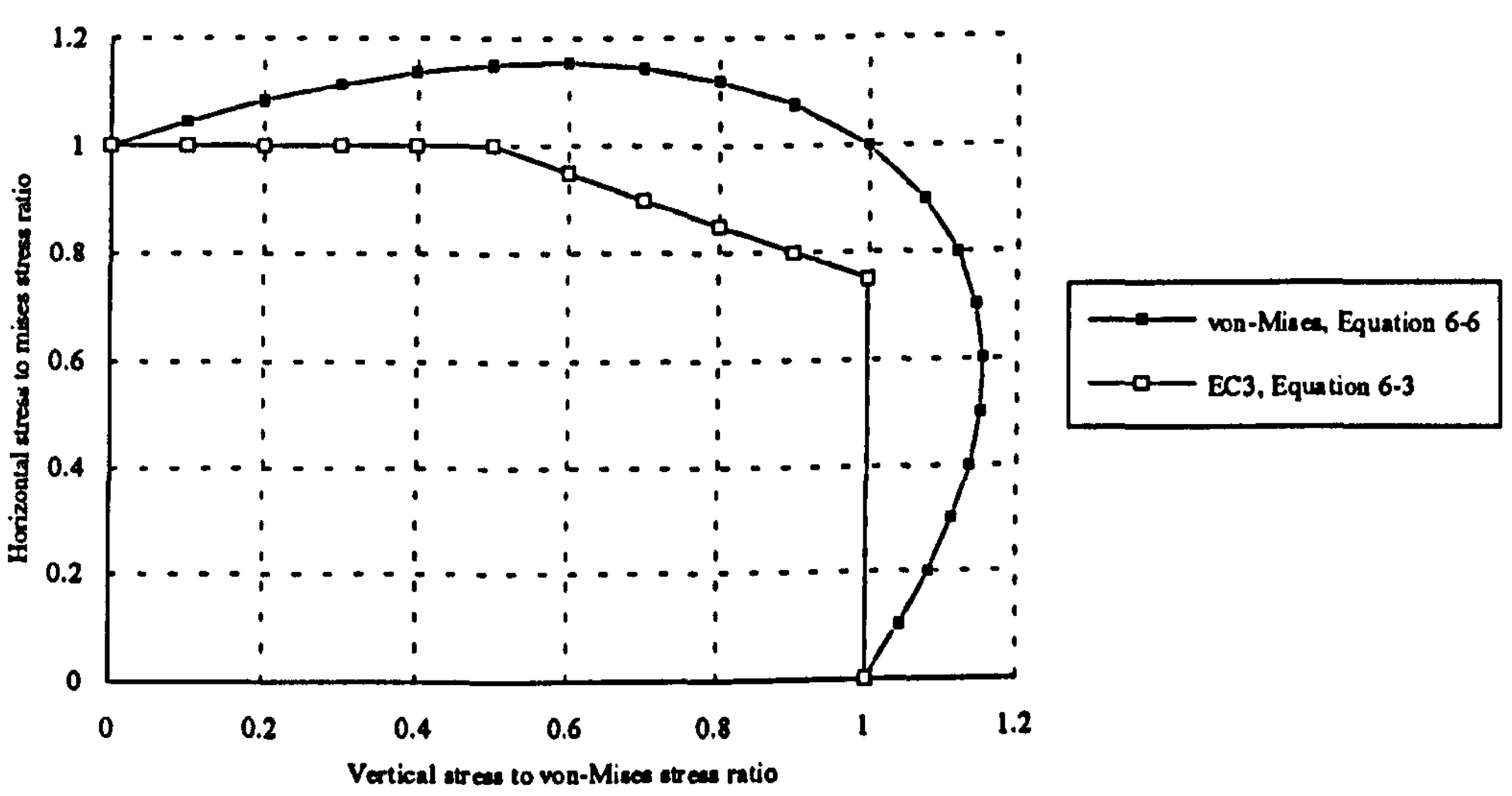

Figure 6-2 Comparison of EC3 equation and equation 6-6

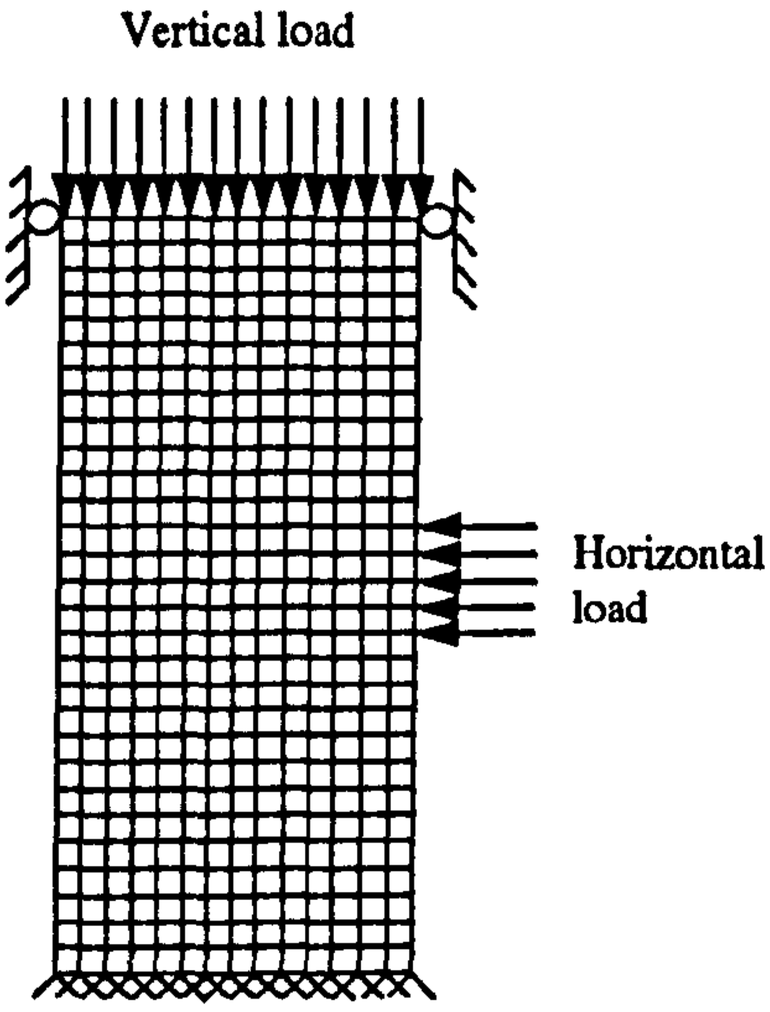

Figure 6-3 FE mesh with loading for non-symmetrical case

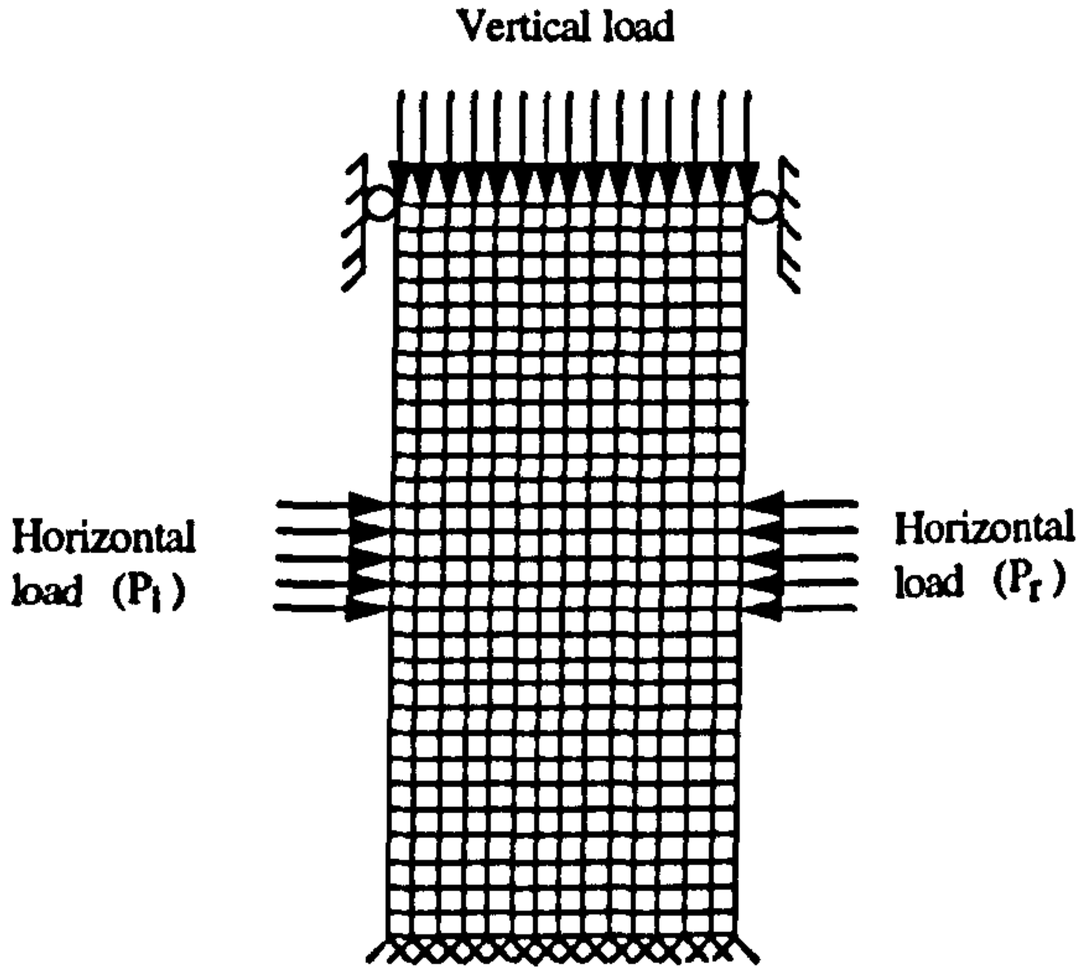

Note: $\eta = \frac{P_r}{P_l}$

Figure 6-4 FE mesh with loading for symmetrical case

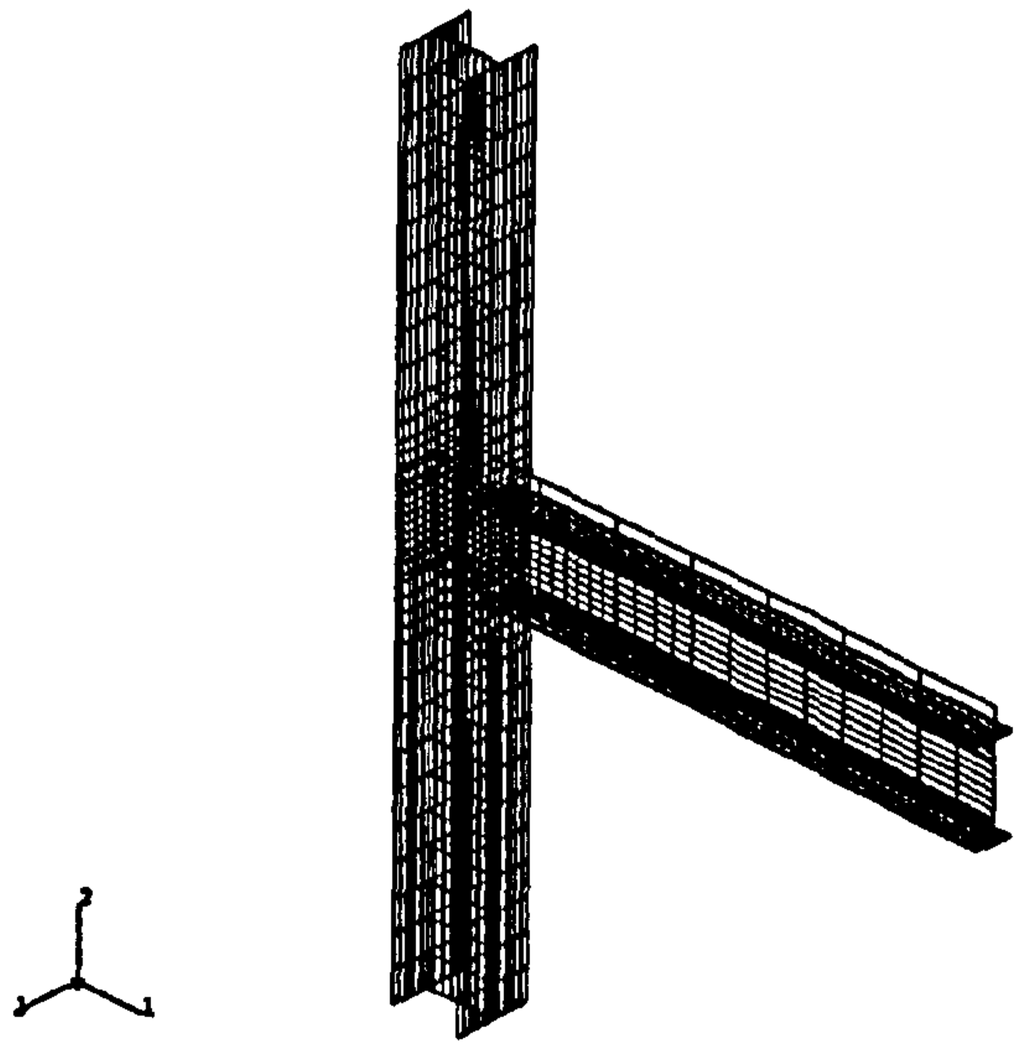

Figure 6-5 FE mesh adopted for non-symmetric composite connection analysis

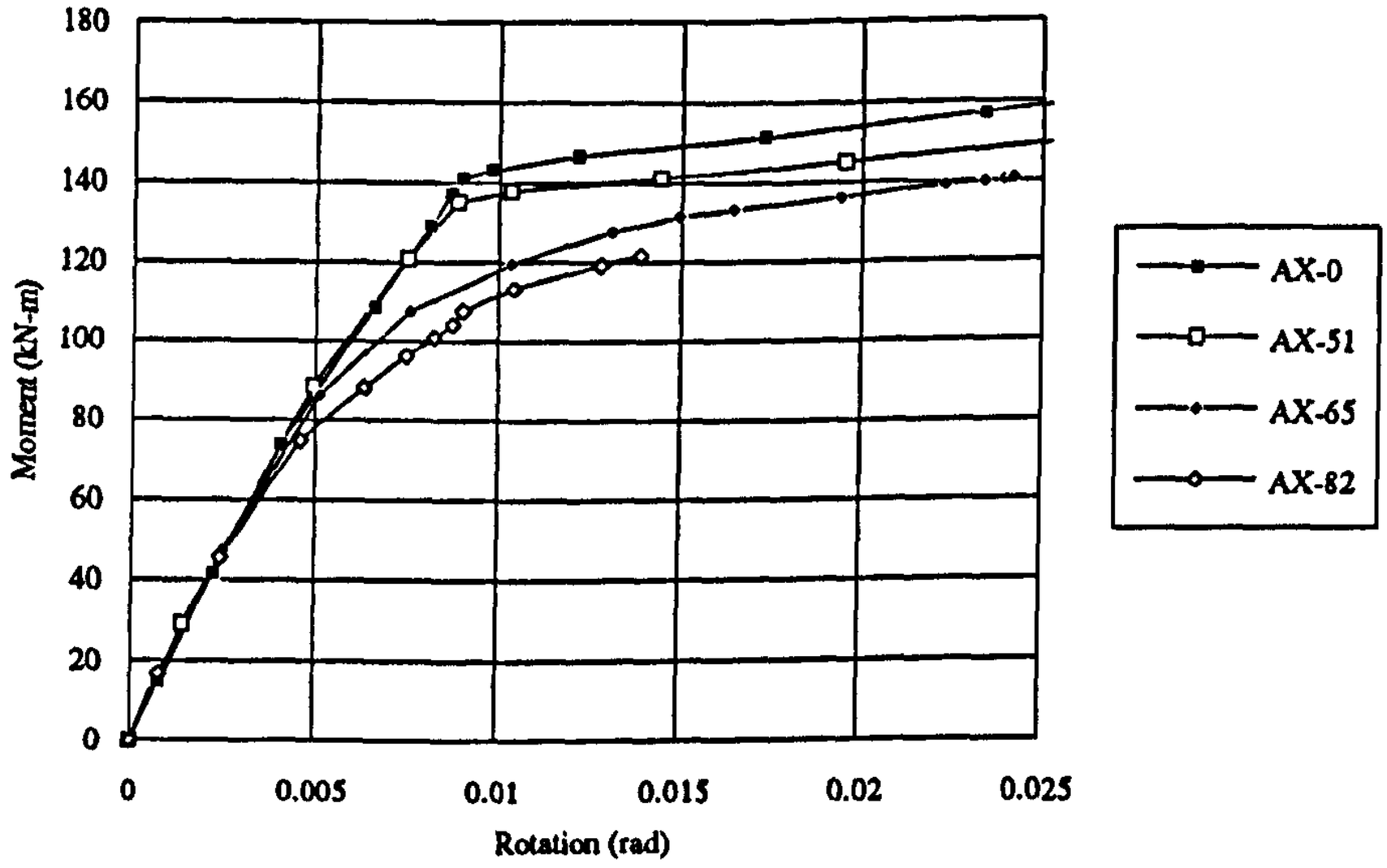

Figure 6-6 Moment - rotation curves for non-symmetric connections with column axial load

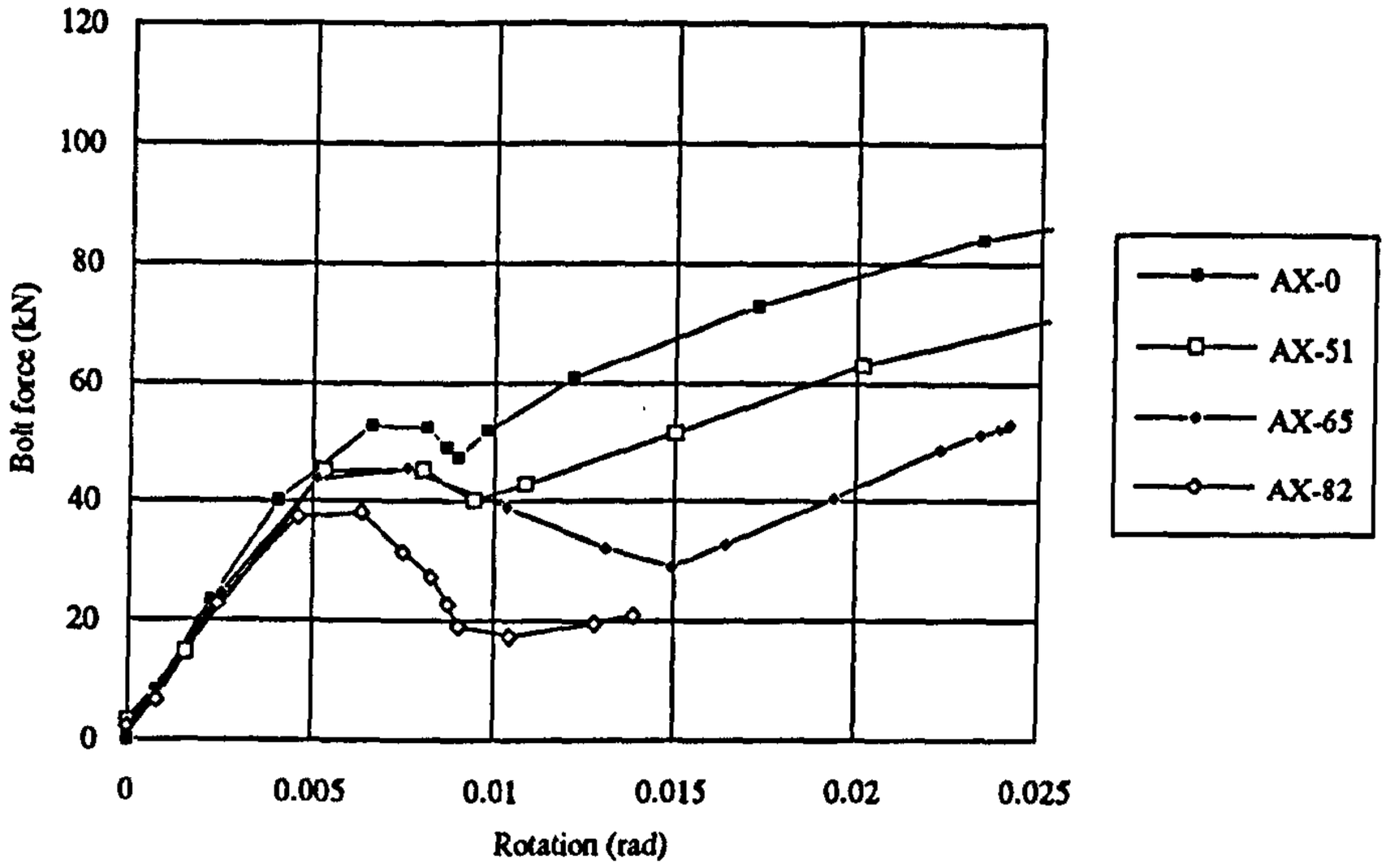

Note: AX mean that column axial load is applied and the digit before the % indicate the magnitude of column axial loading as a percentage of column yield load.

Figure 6-7 Bolt force-rotation curves for non symmetric connections

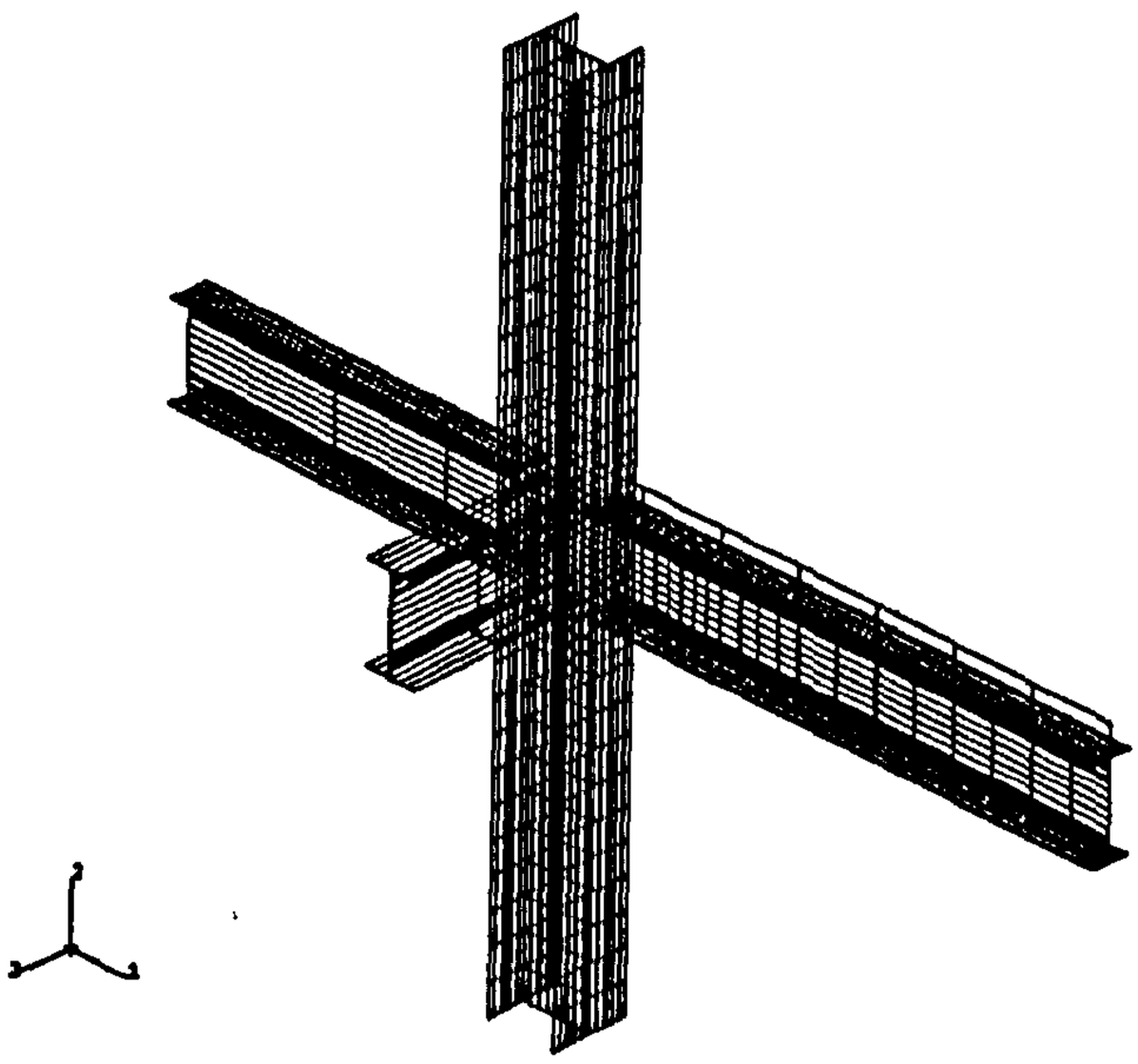

Figure 6-8 FE mesh for connection to simulate the symmetric composite connection with column axial load

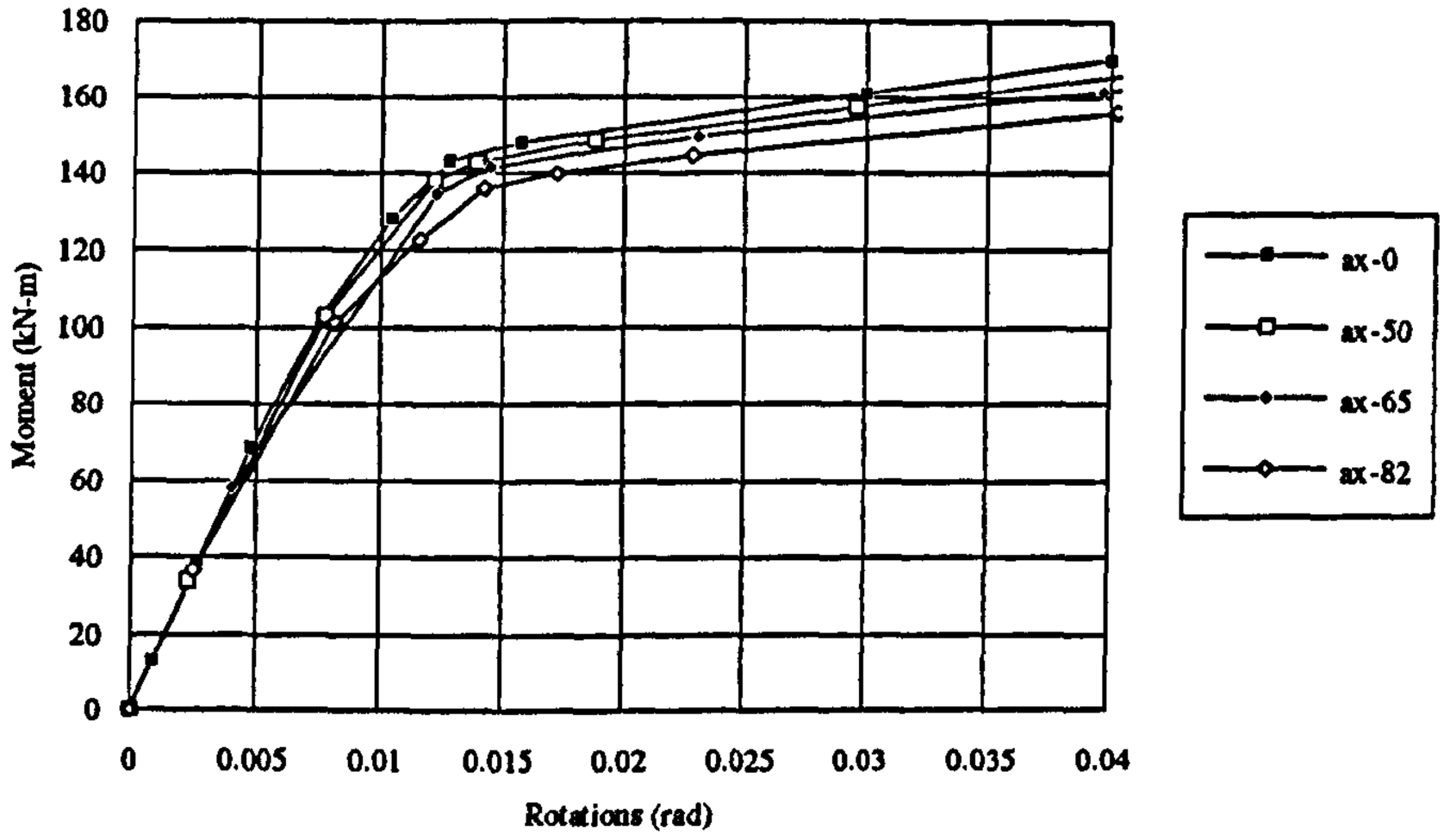

Figure 6-9 Moment - rotation curves for symmetric connections with column axial load (standard column section)

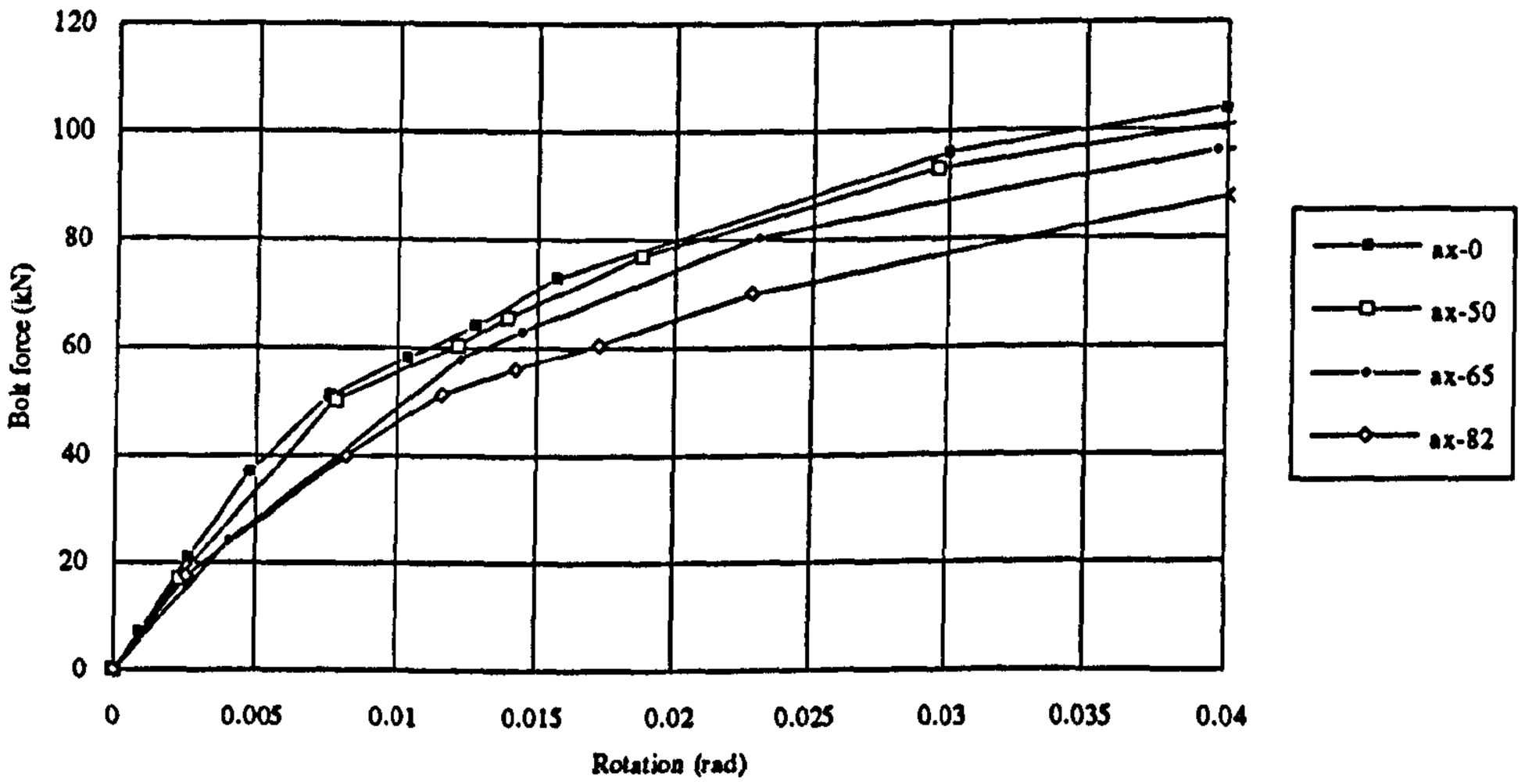

Figure 6-10 Bolt force-rotation curves for symmetric connections with column axial load (standard column section)

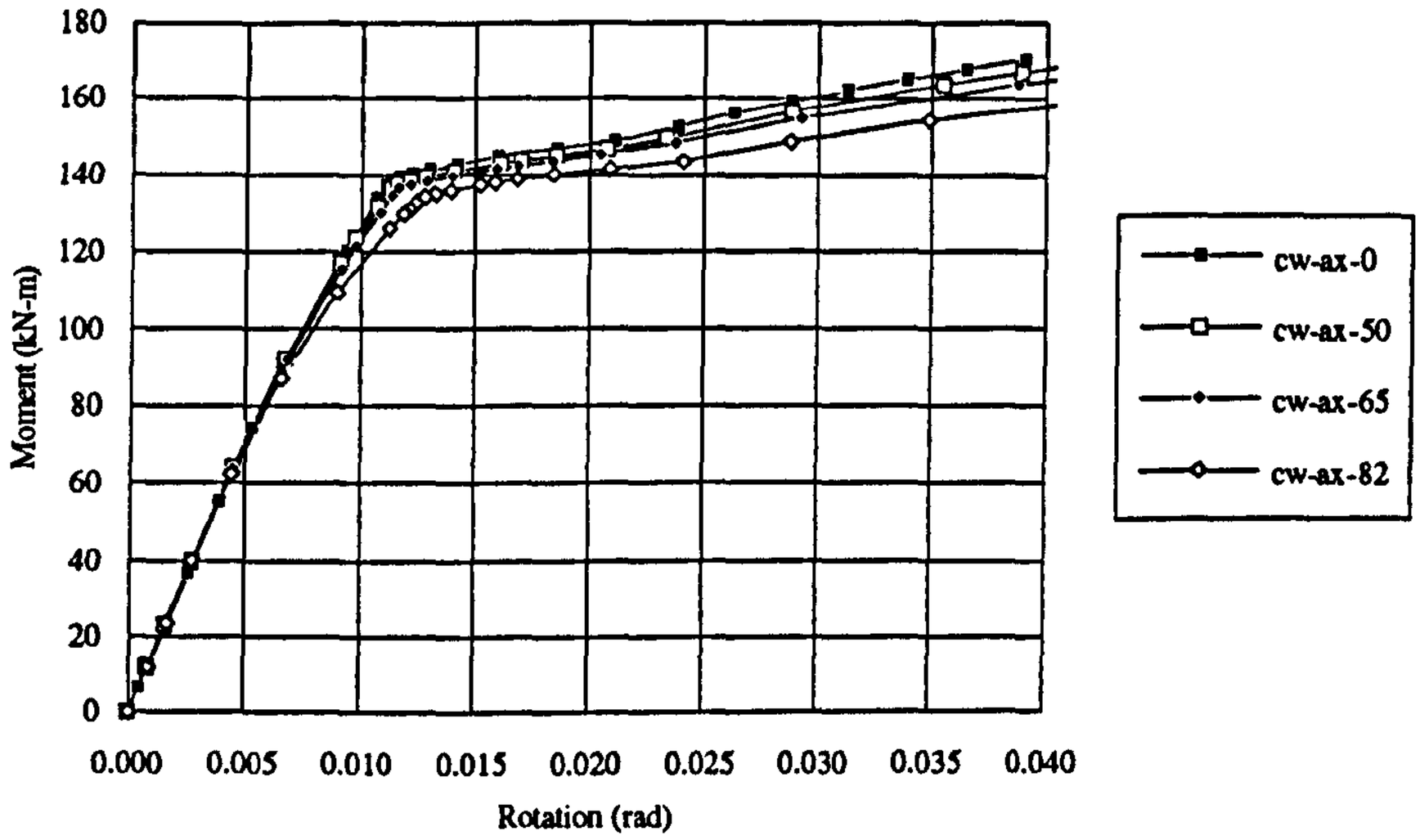

Figure 6-11 Moment - rotation curves for symmetric connections with column axial load (revised column section)

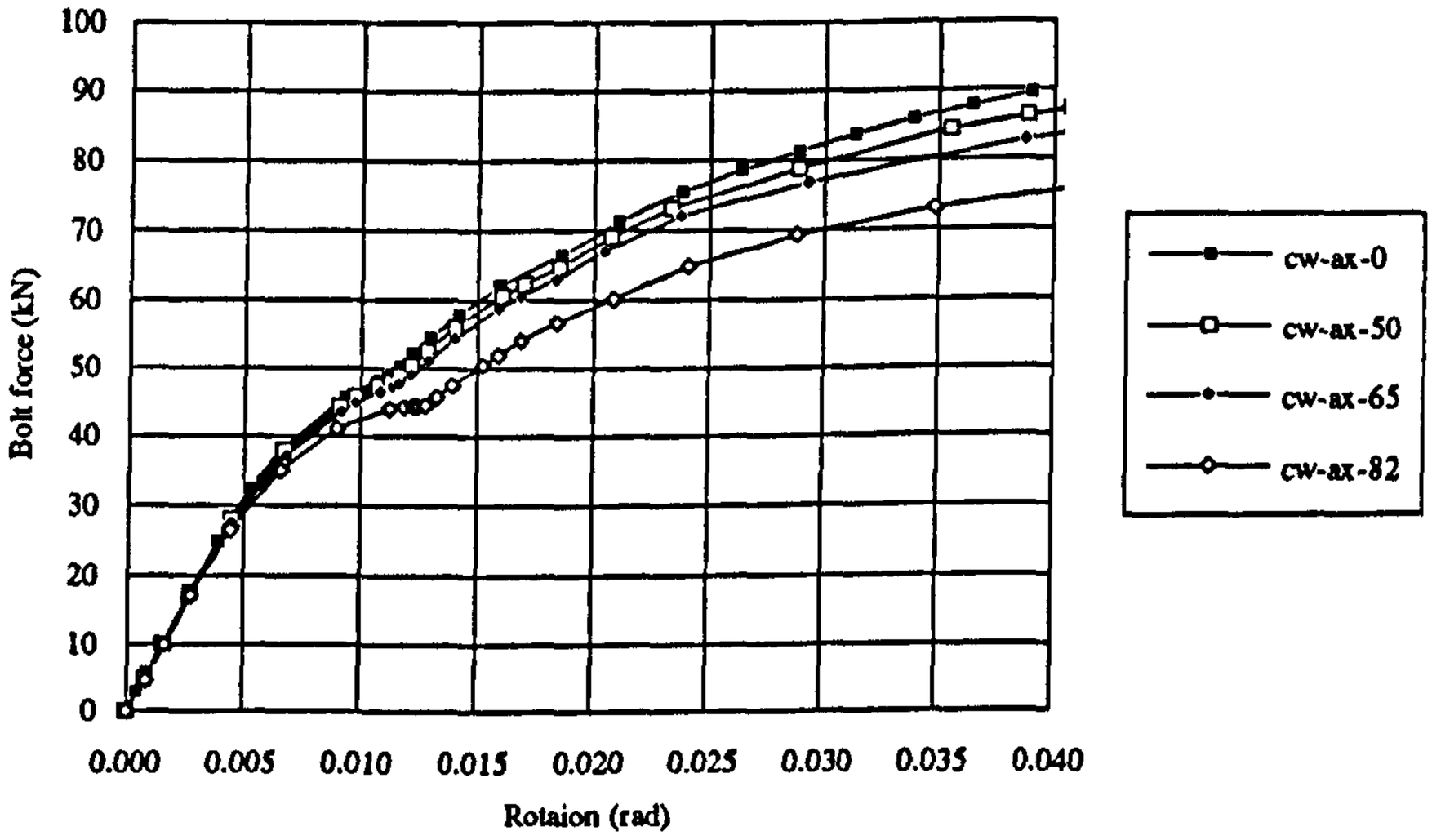

Figure 6-12 Bolt force-rotation curves for symmetric connections with column axial load (revised column section)

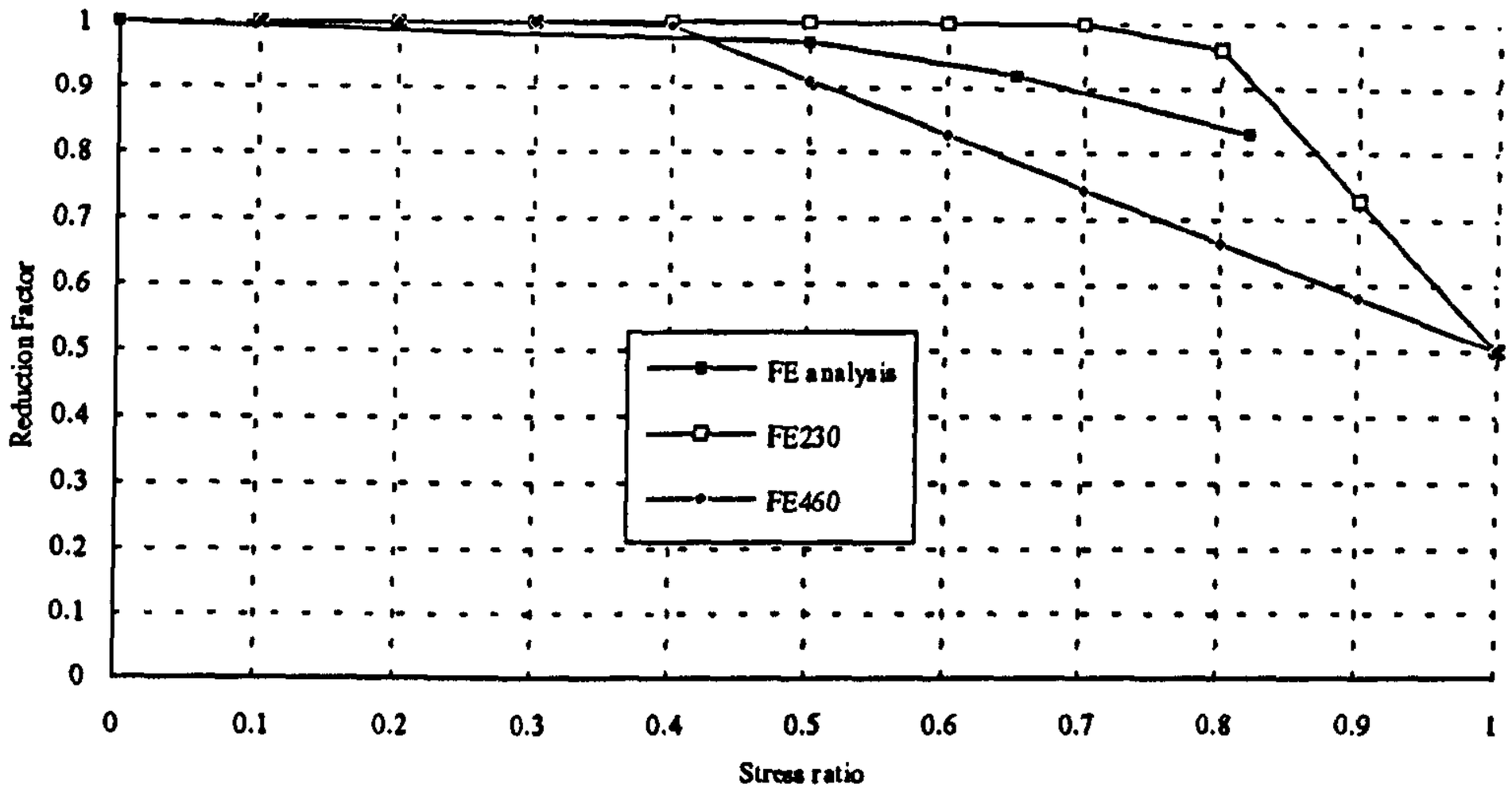

Note: Where ever stress ratio is mentioned it is calculated as a ratio of applied and yield stress ratio

Figure 6-13 Average reduction in bolt force from FE analysis compared with EC3 rules

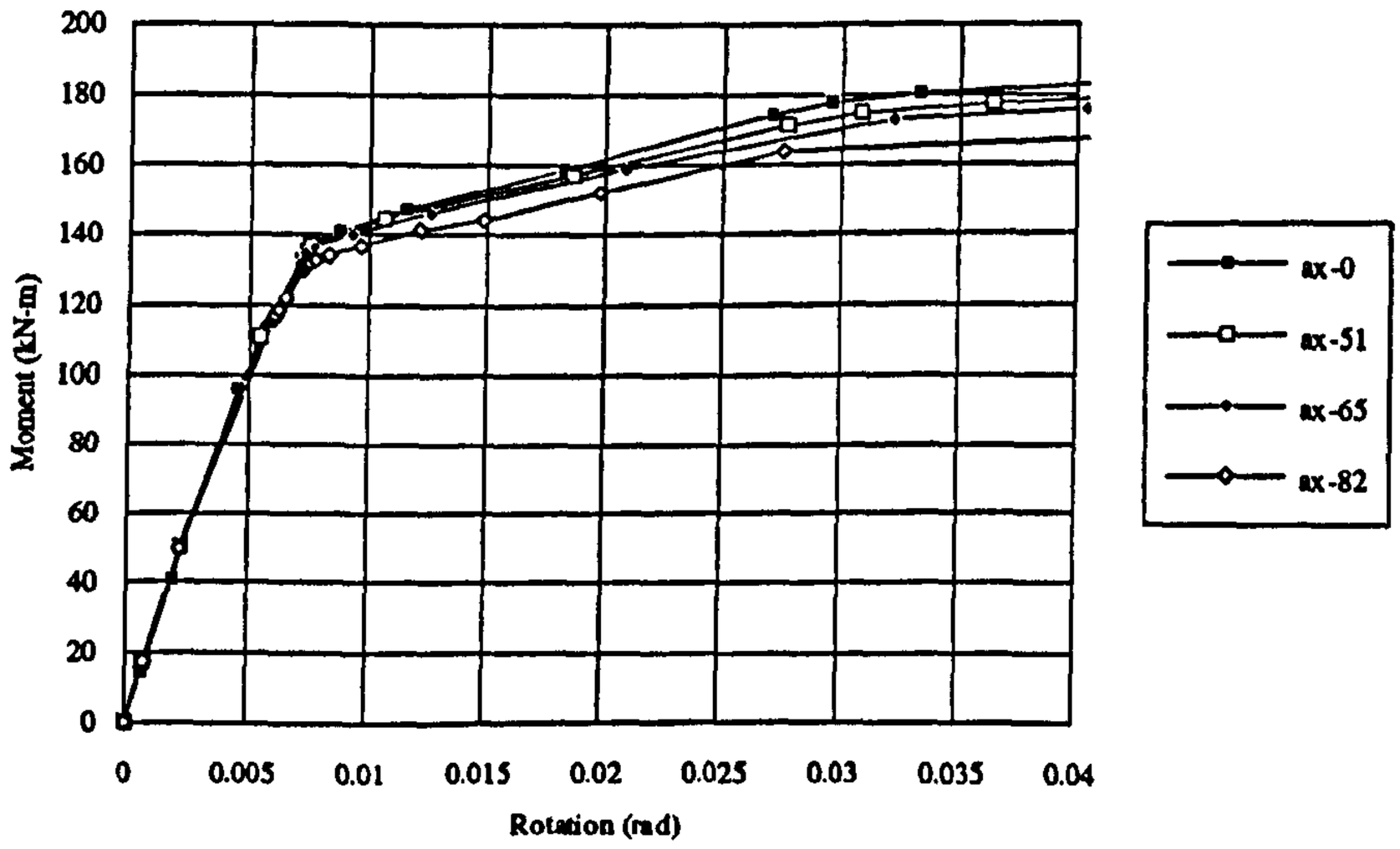

Figure 6-14 Moment-rotation curve obtained from the analysis of purely symmetric connections

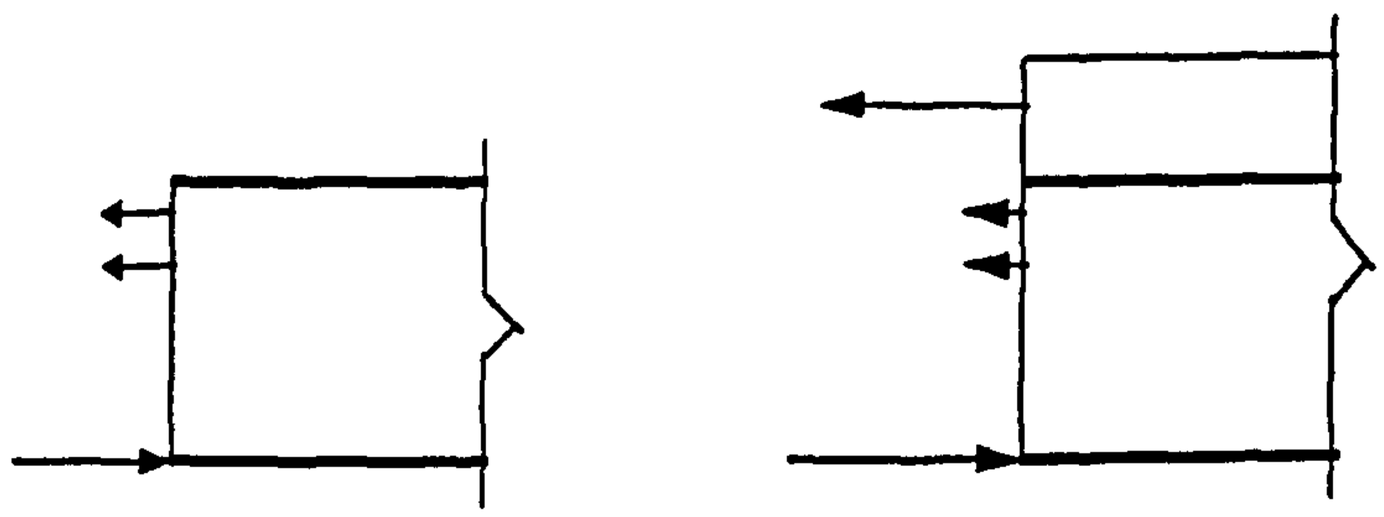

(a) Bare steel connection (b) Composite connection

Figure 6-15 Comparison of bolt forces in bare steel and composite connections

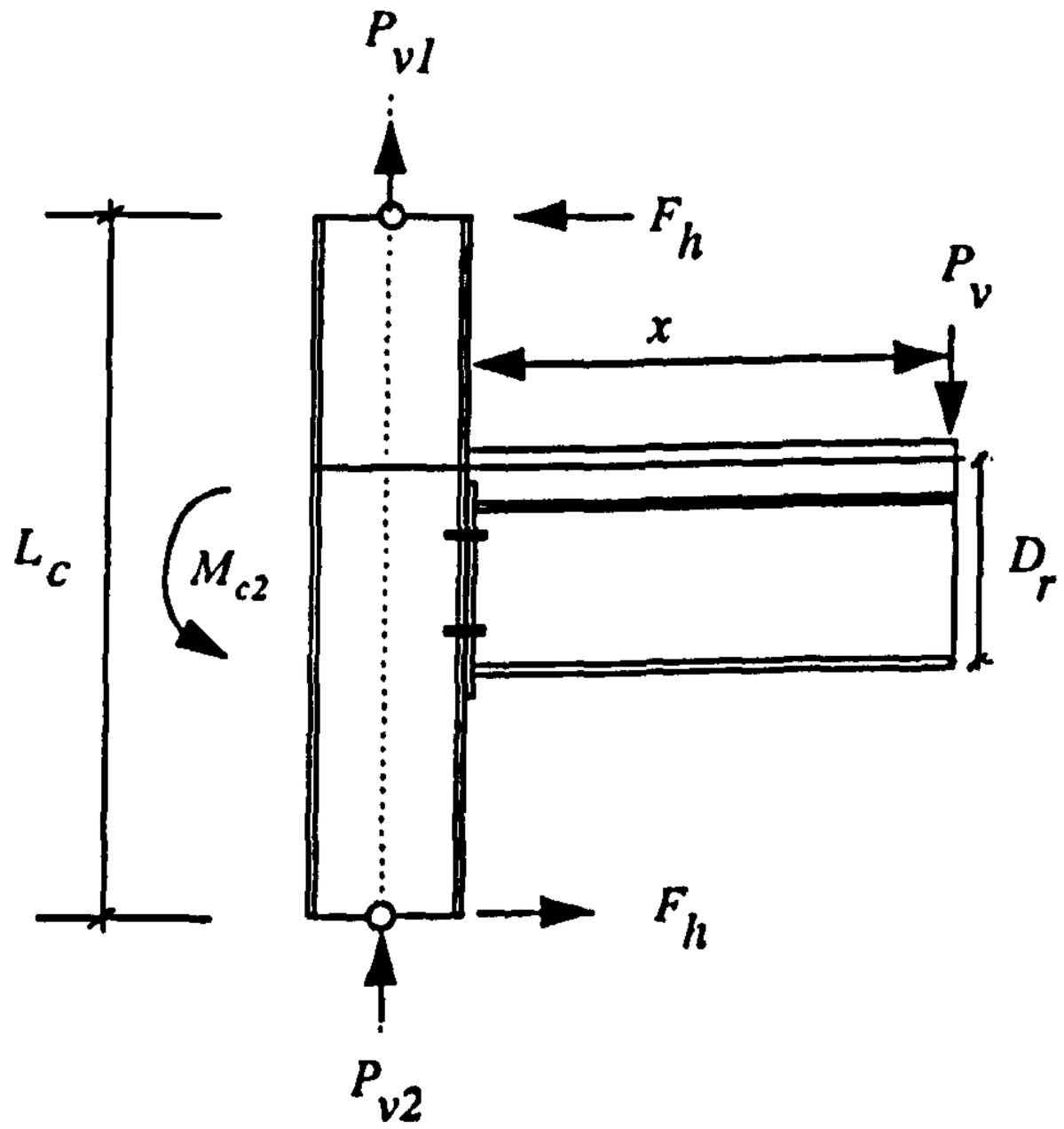

6-16(a) Connection considered to establish internal force distribution

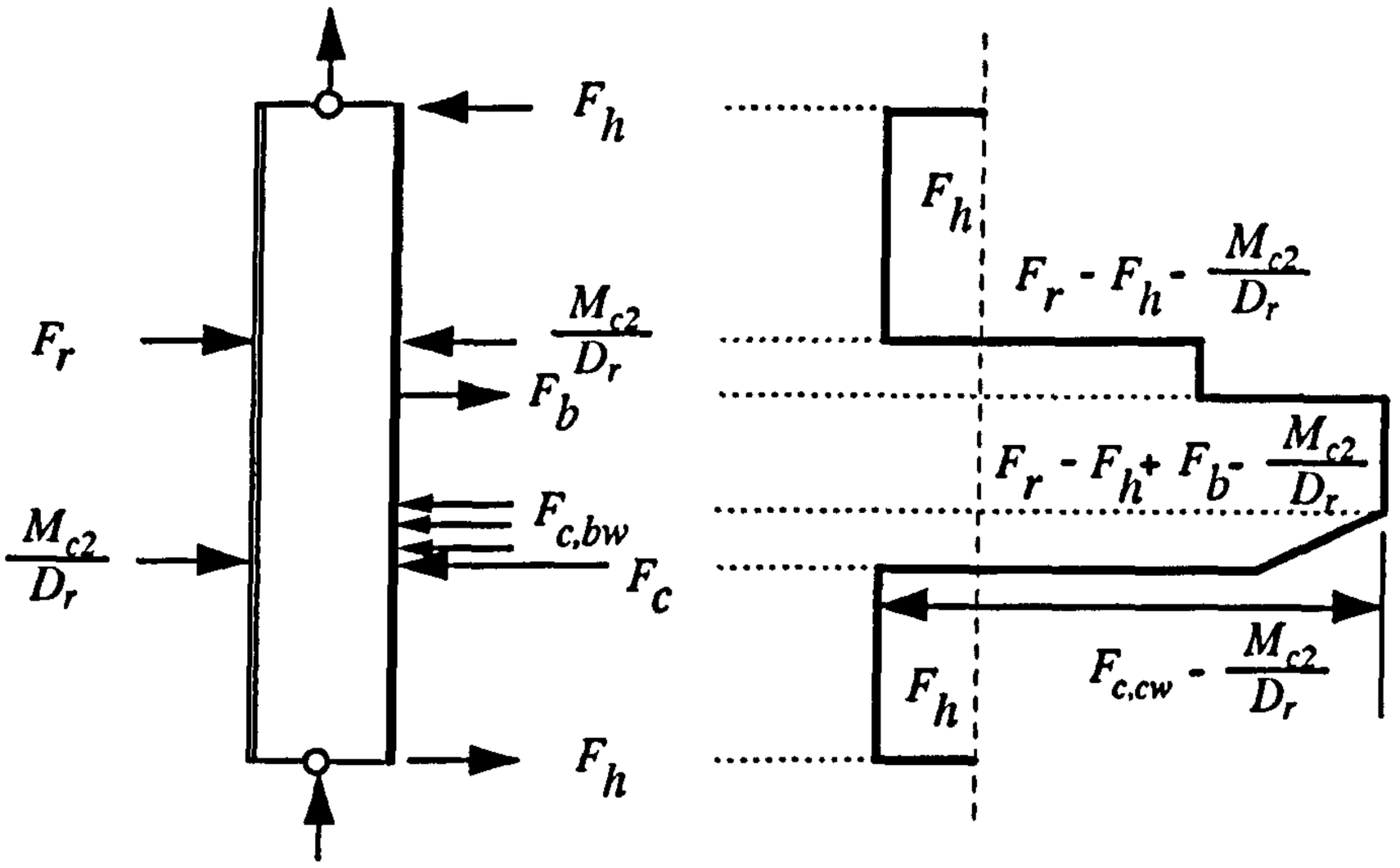

6-16(b) Distribution of internal forces of the connection shown in Figure 16(a)

Figure 6-16 Column web internal forces

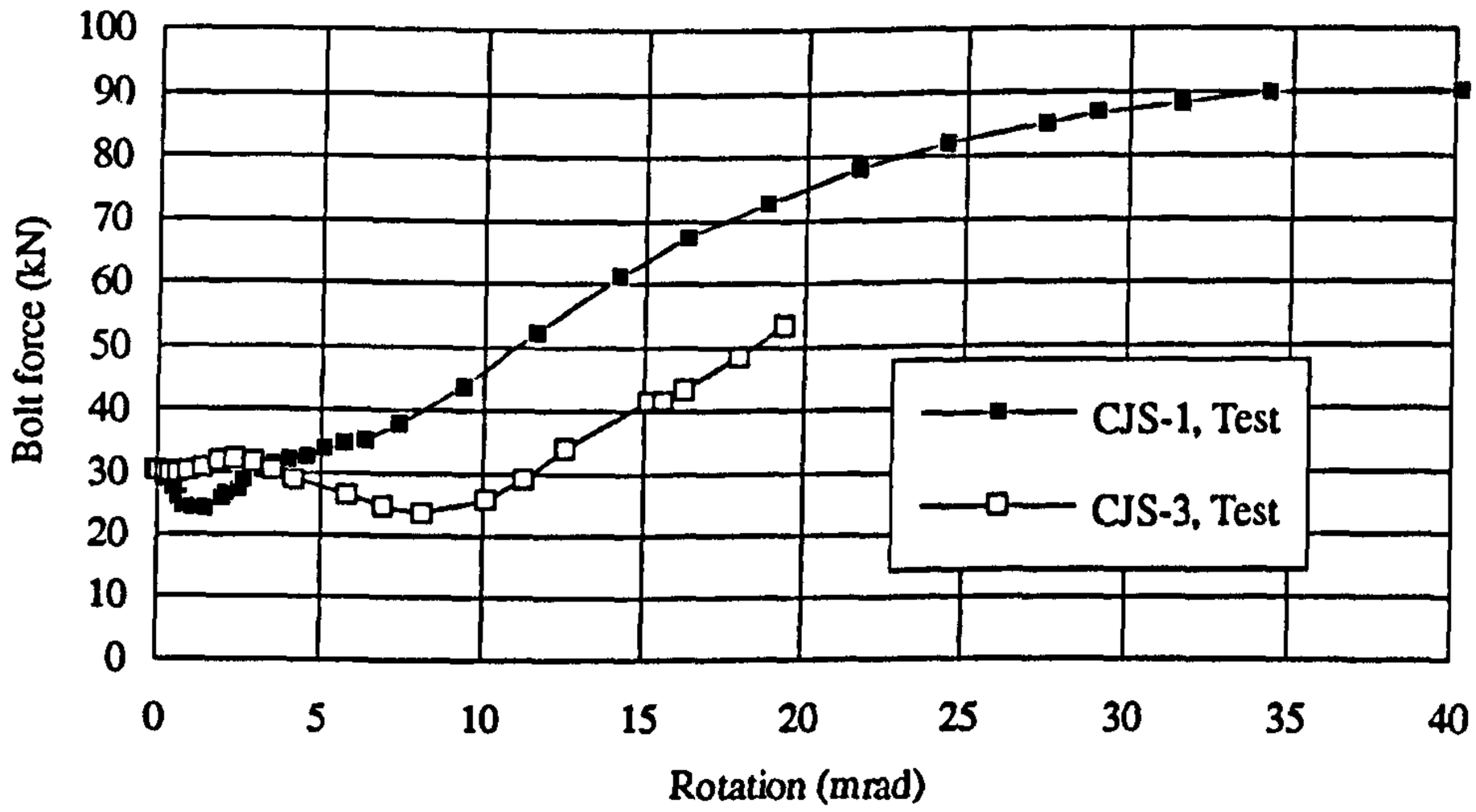

6-17(a) Bolt force (single bolt of top row)-rotation curve for CJS-1 and CJS-3

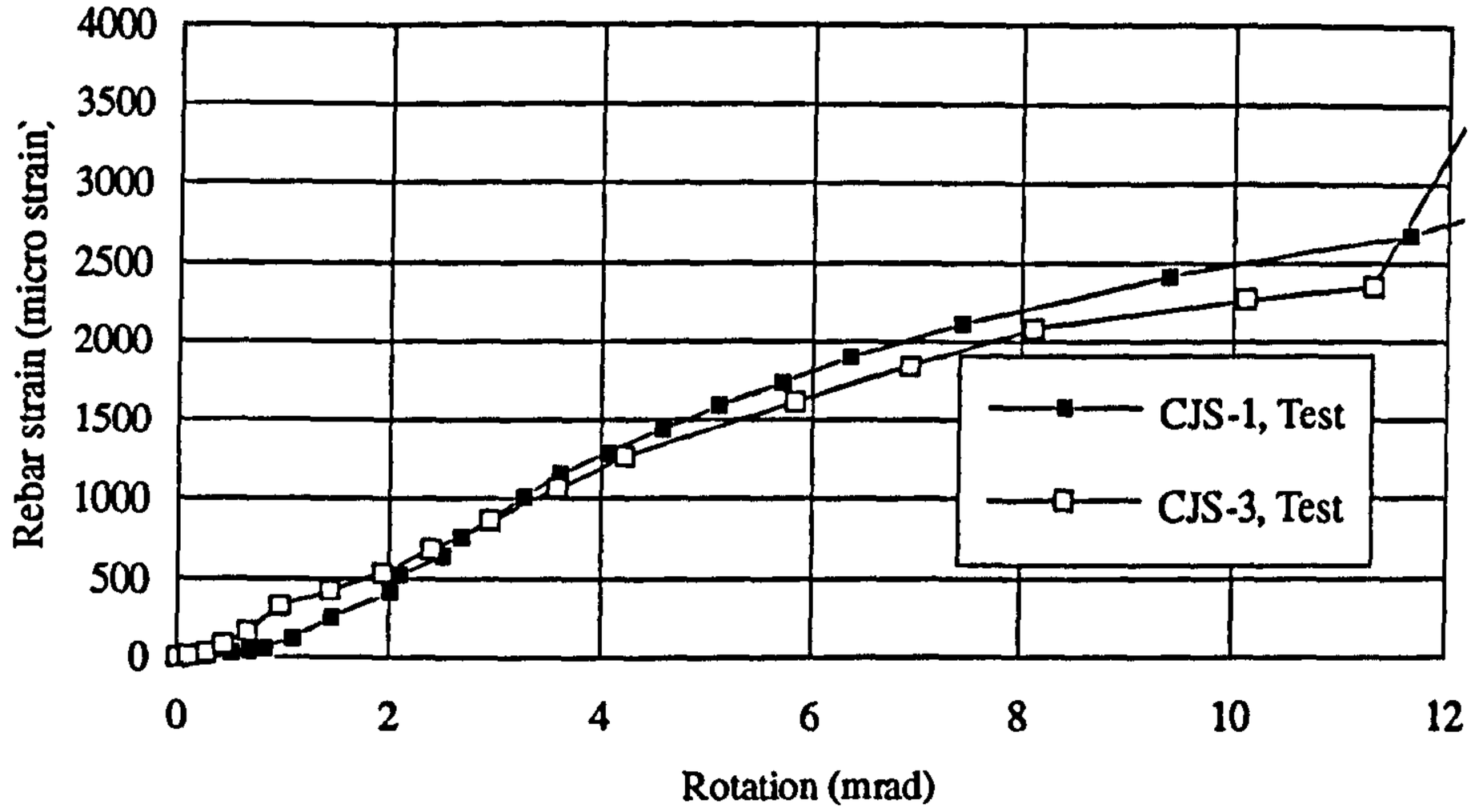

6-17(b) Rebar strain-rotation curve for CJS-1 and CJS-3

Figure 6-17 Test results for CJS-1 and CJS-3

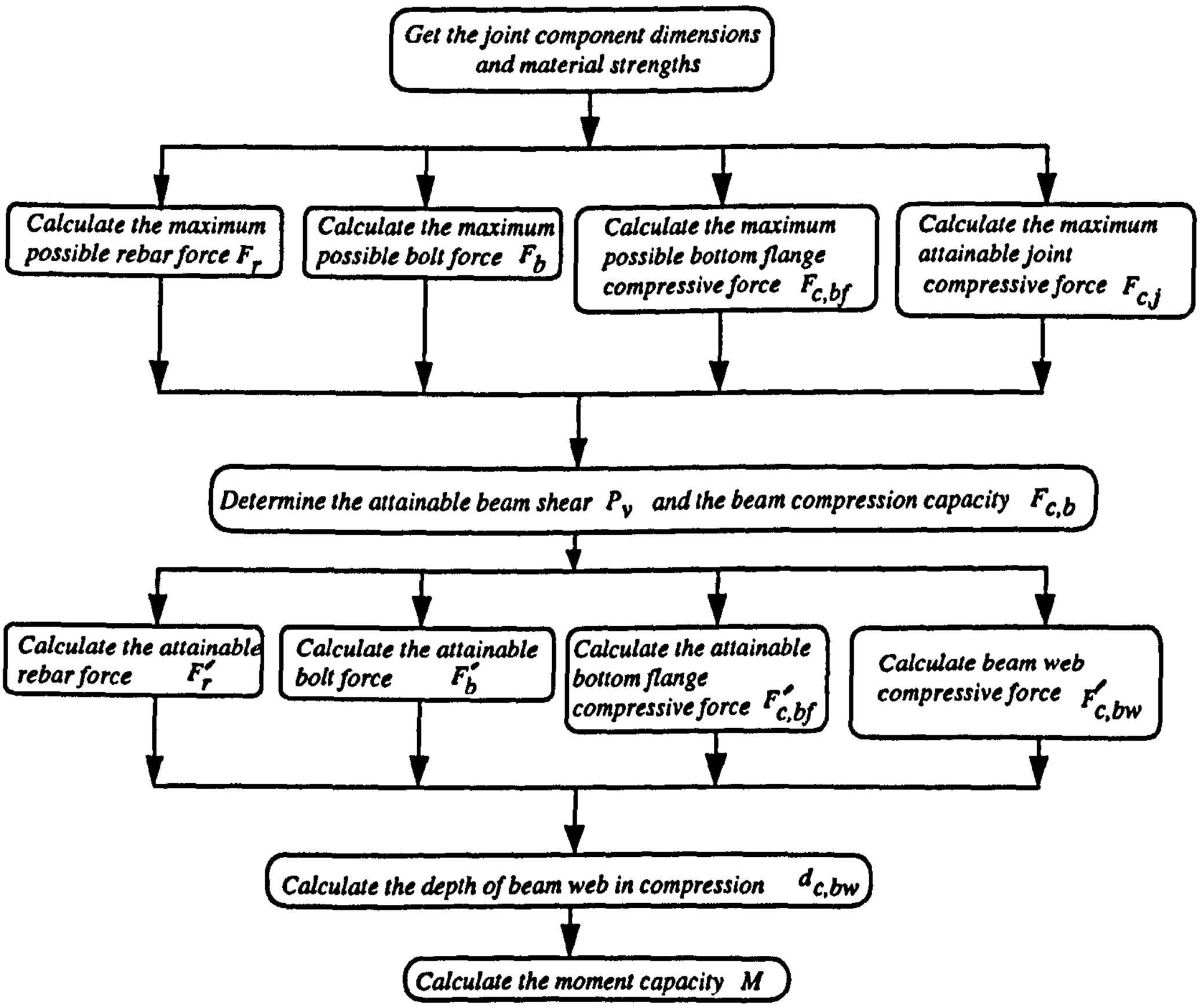

Figure 6-18 Flow chart to predict the moment capacity of the composite connection

Chapter 7

Design of composite flush endplate connections

7.1 Introduction

In order to take advantage of the more advanced and more realistic design methods that treat the structure as semi-continuous according to the principles of EC4, it is necessary for the designer to have a knowledge of the connection properties. Specifically, for ultimate strength design, both moment capacity and rotation capacity are required. Chapter 5 and chapter 6 of this thesis described methods to include the effect of shear to moment ratio and column axial loading on composite connection moment capacity. This chapter unifies previous work on the prediction of the moment capacity of composite endplate connections into a single method that allows for one or both of the effects of high coincident shear or axial compression in the column. The approach is based on considerations of the load transfers and load paths between the various components present in a composite connection and is presented as a series of explicit expressions. In order to maintain a clear picture of the proposed design method instead of referring back to the equations in the last two chapters a few equations are repeated. Validation against all relevant physical tests, supplemented so as to cover the full range of parameters by comparisons against finite element results, demonstrates the accuracy of the method. Some idea of the way in which a prediction method of this type permits design trends to be explored is provided by examining the influence of certain key parameters on both moment capacity and the physical features that control this.

Knowledge of the initial rotational stiffness of a connection is important for the global elastic analysis of frame structures. Based on a simple force transfer mechanism and consideration of the behaviour of individual components, a method has been developed to predict the initial stiffness of composite flush endplate connections. The approach is compatible with that proposed to predict moment capacity of composite connection. In order to apply plastic analysis to frame structures a knowledge of the available and the required rotation capacities is necessary. A simple technique to determine the available rotation capacity of composite flush endplates is described in this chapter. Taken together, the two methods represent key steps in the development of an approach to predict the main measures of the behaviour of composite endplate connections. Used in conjunction with the moment capacity and failure mode prediction method developed in this chapter, they provide a complete representation of the design properties of composite flush endplate connections.

7.2 Basic concept of design approach

The essence of the approach is that the maximum achievable resistances of the individual load transferring components in the connection - rebars, shear studs, bolts, beam web etc. - are determined first. Equilibrium is ensured by some redistribution of forces between components, the set of lowest key resistances (on which moment capacity depends directly) are identified and the moment capacity is obtained as the product of the connection's shear resistance times the shear span.

The procedure starts from an identification of component parts and then utilises the free body diagram of force transfer illustrated in Figure 7-1. The ratio of loading between the two sides is expressed in terms of η; when $\eta = 1$ the connection is loaded symmetrically and for $\eta < 1$ the loading is non-symmetric. Loading on the right side is assumed to be higher, so M is the larger moment (in practice either can be the more heavily loaded side providing calculations are performed for that side). The

determination of the moment capacity first requires the calculation of the internal forces on face 1. The individual component forces are listed in Table 7-1.

Table 7-1 Component internal forces in a composite connection (also see Figure 7-1)

1	Rebar force F_r
2	Bolt force F_b
3	Beam bottom flange compressive capacity $F_{c,bf}$
4	Column web compression capacity $F_{c,cw}$
5	Connection compression capacity $F_{c,j}$
6	Beam web compression force $F_{c,bw}$
7	Possible top flange compression force $F_{c,bft}$

Figure 7-2 lists all the steps in the calculation of the moment capacity of flush endplate connections in flowchart form. These steps are of 5 types as distinguished by the use of different shaped boxes. The first step calculates the maximum possible force that can develop in any component (see sections 7.2.1 - 7.2.8), allowing for the presence of the column loading. These forces are shown in square boxes without any prime. They are then used to check the equilibrium of the free body of the connection, adjusting the forces to maintain equilibrium of internal forces (see sections 7.3.1 - 7.3.5). The results are shown in circular boxes with a prime. Once these forces have been adjusted, the attainable beam shear force can be determined (see section 7.4, Table 7-2) from the possible governing values i.e. beam web overstress, column web overstress and rebar stress, of P_v shown in hexagonal boxes. Using the lowest of these P_v values, the available compressive stress in the beam web ($f''_{a,bw}$) is determined. In the determination of attainable shear from the consideration of rebar capacity, the ultimate stress of beam web was used to determine the depth of web compression, this

underestimates depth of compression in beam web and may result in higher bolt force. This can be now corrected using the available compressive stress in the beam web ($f''_{a,bw}$) determined from this step. This allows for the readjustment of various previously determined internal forces (see section 7.4, Table 7-3) to give the results of the elliptical box with double primes. From these adjusted forces the attainable shear capacity of the connection (termed shear governed by connection equilibrium) is obtained and this is also shown in the hexagonal box. The actual governing shear capacity of the connection (termed as the attainable connection shear) is the minimum P_v obtained by considering beam web overstress, column web overstress and connection equilibrium. The shear capacity as determined by rebar stress is not used at this stage as the shear governed by connection equilibrium is now known from the refined rebar and bolt forces, which is a corrected form of the attainable shear from rebar capacity. The use of shear considering the rebar capacity is to reasonably estimate the connection shear for the determination of available beam web compressive stress (Table 7-3). The available beam web compressive stress is used in the determination of connection shear capacity by considering overall connection equilibrium (see Figure 7-2). The moment capacity of the connection M is obtained by multiplying the attainable beam shear by the shear span (see section 7.5). The actual formulae needed to execute the steps of Figure 7-1 are given in sections 7.2.1-7.5, with the terms used being defined in Figure 7-3. Details of the sources of the formulae are also provided.

7.2.1 Rebar force

$$F_r = min\begin{cases} A_r f_u \\ 0.67 b_{cf} h_{cs} f_c' \beta + \dfrac{M_{c2}}{D_r} \quad when\ \eta < 1,\ ref\ 7-1 \\ nkR_{Rd} \qquad\qquad EC4,\ clause\ 6.3.2\ and\ 6.3.3,\ ref\ 7-2 \end{cases} \tag{7-1}$$

7.2.2 Bolt force

$$F_b = min\begin{cases} (4.32 - 0.039m + 0.0116e + 0.009p)t_{cf}^{\,2} f_{cf} & ref\ 7-1 \\ (5.5 - 0.021m + 0.017e)t_p^{\,2} f_p & ref\ 7-1 \\ 1.8A_b f_b & EC3:\ Part\ 1.1,\ Section\ 6.5.5,\ ref\ 7-3 \\ \dfrac{M_{c2}}{D_r} + F_h + \sqrt{1-\left(\dfrac{\sigma_n}{f_{y,cw}}\right)^2}\ \dfrac{f_{cw}}{\sqrt{3}} A_v - F_r \geq 0 & ref\ 7-4 \end{cases} \quad (7-2)$$

Where:

$$A_v = A_{sc} - 2t_{cf} b_{cf} + (t_{cw} + 2r_c)t_{cf} \qquad EC3:\ Part\ 1.1,\ Clause\ 5.4.6(2)$$

A_{sc} is the cross-sectional area of the column

A_b is the cross-sectional area of a single bolt

F_h is the column web shear due to the structural loading; this should usually be taken as zero

It is assumed that each bolt row consists of two bolts only.

7.2.3 Column web compression capacity

$$F_{c,cw} = min\begin{cases} \dfrac{M_{c2}}{D_r} + \sqrt{1-\left(\dfrac{\sigma_n}{f_{y,cw}}\right)^2}\ \dfrac{f_{cw}}{\sqrt{3}} A_v + F_h & CW\ shear\ if\ \eta < 1 \quad ref\ 7-4 \\ t_{cw} b_{eff} f_{cw} & CW\ compression \quad EC3:\ Part\ 1.1,\ J3.5.1 \\ 8.4\, b_{eff}^{\,0.017}\ D_c^{\,0.60}\ t_{cw}^{\,1.43}\ f_{cw}^{\,0.76} & CW\ buckling \quad ref\ 7-1 \end{cases} \quad (7-3)$$

7.2.4 Total developable tensile force in the bolt rows and the individual bolt row forces

The number of bolt rows in tension in a connection with K bolt rows may be calculated as:

$$N_b = min\begin{cases} \dfrac{F_{c,cw} - F_r}{F_b} \\ K \end{cases} \geq 0 \qquad (7-4)$$

The total possible force in the bolts is: $F_{BT} = N_b.F_b$

The force in each bolt row may be calculated as:

$$F_{b1} = min\begin{cases} F_b \\ F_{c,cw} - F_r \end{cases} \geq 0 \qquad (7-5)$$

For K bolt rows, the force in the i th row

$$If \quad N_b > i-1, \quad F_{bi} = min\begin{cases} F_b \\ F_{BT} - \sum_{j=1}^{i-1} F_{bj} \end{cases} \geq 0 \quad where\ i = 2\ to\ K \qquad (7-6)$$

$$if \quad N_b < i-1, \quad F_{bi} = 0$$

Applying the above technique it is possible to find the total bolt force for a connection with any number of bolt rows.

7.2.5 Connection compression capacity

$$F_{c,j} = min\begin{cases} F_r + \sum_{i=1}^{K} F_{bi} \\ F_{c,cw} \end{cases} \qquad (7-7)$$

7.2.6 Beam bottom flange compressive force

$$F_{c,bf} = min\begin{cases} t_{bf} b_{bf} f_{bf} & when \dfrac{b_{bf}}{t_{bf}} < 22\sqrt{\dfrac{235}{f_{yb}}} & BF \quad compression & EC3: Part 1.1,\ Table\ 5.3.1 \\ 22 t_{bf}{}^2 f_{bf}\sqrt{\dfrac{235}{f_{yb}}} & when \dfrac{b_{bf}}{t_{bf}} \geq 22\sqrt{\dfrac{235}{f_{yb}}} & BF \quad Buckling & EC3: Part 1.1,\ Table\ 5.3.1 \\ 8.4 b_{eff-b}{}^{0.017} D_c{}^{0.6} t_{cw}{}^{1.43} f_{cw}{}^{0.76} & & CW \quad Buckling\ if\ active & ref\ 7-1 \\ t_{cw} b_{eff} f_{cw} & & CW \quad Compression & EC3: Part 1.1,\ J3.5.1 \\ \dfrac{M_{c2}}{D_r} + \sqrt{1-\left(\dfrac{\sigma_n}{f_{y,cw}}\right)^2}\dfrac{f_{cw}}{\sqrt{3}} A_v + F_h & & CW\ shear\ if\ \eta < 1 & chapter\ 6\ and\ ref.\ 7-4 \end{cases} \qquad (7-8)$$

Note: Buckling resistance should be calculated using a different value of effective width obtained from:

$$b_{eff-b} = \sqrt{D^2 c + \left[t_{bf} + 2\sqrt{2} a_p + 2 t_p + 5\left(t_{cf} + r_c\right)\right]^2} \qquad EC3:\ Part\ 1.1,\ Clause\ 57.5 \quad (7\text{-}9)$$

7.2.7 Beam web compressive force

$$F_{c,bw} = min\begin{cases} F_{c,j} - F_{c,bf} \\ \left(H_b - 2 t_{bf}\right) t_{bw} f_{bw} \end{cases} \geq 0 \qquad (7\text{-}10)$$

7.2.8 Possible beam top flange compression force

It the top flange of the beam falls within the compression zone, the maximum force it can develop can be obtained either by subtracting the bottom flange compression and web compression from the connection compression capacity or directly by calculating the compression capacity of the flange itself.

$$F_{c,bft} = min\begin{cases} F_{c,j} - F_{c,bf} - F_{c,bw} \\ t_{bf} b_{bf} f_{bf} \end{cases} \geq 0 \qquad (7\text{-}11)$$

When the attainable beam shear is governed by the rebar capacity, this may be due to either: reinforcement yield, failure of the shear studs, or failure of the concrete. The appropriate cause can be detected readily from the expression that controls the rebar force.

7.3 Establishing connection equilibrium

It is essential that the connection remains in equilibrium when the internal forces are determined. If the forces obtained in section 7.2 do not represent a balanced condition, they must be corrected so as to ensure that the total tension capacity equates to the total compression capacity of the connection. To establish this equilibrium the following procedure is suggested:

7.3.1 Rebar force

$$F_r' = min \begin{cases} F_r \\ F_{c,j} \end{cases} \tag{7-12}$$

7.3.2 Bolt force

The maximum bolt force: In a composite connection the bolt force develops due to the extension of the bolts caused by the extension of the rebars. In a cruciform connection with a moderate (1%) amount of reinforcement usually the rebars will yield, thereby allowing for the development of the full bolt force. Problems arise when the rebar area is high (2%) or the connection is loaded non-symmetrically. In such cases the rebar may or may not yield and hence the full bolt force may or may not develop. Although the bolt force in a symmetrically loaded connection can be obtained from the equilibrium condition with sufficient accuracy, in non-symmetrically loaded connections satisfying the equilibrium condition does not properly reduce the bolt force, since the rebar force is usually controlled by the concrete strength and the width of the column flange. So when the equilibrium condition is applied the bolt force can be overestimated, as the rebars may not actually yield. Hence the maximum bolt force that may develop in the top bolt row of a connection will also be governed by rebar

strain and must be checked against that condition. The following method is suggested when the connection is loaded non-symmetrically, in which the bolt force is reduced by a factor that is the ratio of the actual rebar force developed to the value that would be developed if the rebars yielded.

$$F_{b-max} = min\begin{cases} \dfrac{F'_r}{F_{r-yield}} F_b \\ F_b \end{cases} \tag{7-13}$$

Bolt force in each row: It is essential to check whether a particular row of bolts is actually in the tensile zone before assuming that the row will take any tensile force. To do this the depth of compression in the beam web should be calculated, if this falls above the bottom row of bolts, then the depth must be recalculated assuming that the force in the bottom row of bolts is zero. This procedure must be repeated for all bolt rows. For bolt rows in the tensile zone the magnitude of the tensile force will depend on the connection properties but cannot exceed the possible maximum force for a row.

$$d_{c,bw} = min\begin{cases} \dfrac{F'_r + \sum_{i=1}^{K} F_{bi} - F_{c,bf}}{t_{bw} f_{bw}} \geq 0 \\ H_b - 2t_{bf} \end{cases} \tag{7-14}$$

The value for $d_{c,bw}$ must be calculated in a way that is similar to the DO loop statements in the FORTRAN language. Thus the calculation is to be repeated J times, where J = 1 to K. The exit condition from this loop is controlled by $d_{c,bw}$ being less than $d_{b(K+1-J)}$ $-0.5t_{bf}$, in which case the calculation is to be carried to the next step. If the exit condition cannot be satisfied, the loop continues and each time the corresponding bolt force is updated to $F_{b(K+1-J)} = 0$. At the completion of the loop

$d_{c,bw} \leq (H_b\text{-}2t_{bf})$ is to be imposed. The bolt forces established in this step are written with a single prime.

7.3.3 Bottom flange compression force

Based on considerations of equilibrium, the maximum compressive force that can develop in the bottom flange is the smaller of its compressive capacity and the tensile force developed in the connection. Hence the bottom flange compressive force is:

$$F'_{c,bf} = min \begin{cases} F_{c,bf} \\ F'_r + \sum_{i=1}^{K} F'_{bi} \end{cases} \tag{7-15}$$

7.3.4 Beam web compression force

The maximum beam web compressive force is the smaller of the previously calculated value and the difference between the total tensile force developed in the connection and the bottom flange compressive force, so

$$F'_{c,bw} = min \begin{cases} F_{c,bw} \\ F'_r + \sum_{i=1}^{K} F'_b - F'_{c,bf} \end{cases} \geq 0 \tag{7-16}$$

7.3.5 Beam top flange compression force

The magnitude of compressive force in the top flange can be obtained by subtracting the bottom flange compressive force and the beam web compressive force from the connection compression capacity, hence the top flange compressive force can be determined from:

$$F'_{c,bft} = F_{c,j} - F'_{c,bf} - F'_{c,bw} \geq 0 \tag{7-17}$$

7.4 Attainable beam shear

The attainable beam shear can be calculated once all the component forces have been determined. The following criteria must be checked:

i Beam web overstress

ii Reinforcement capacity

iii Column web overstress

iv Connection equilibrium

The full procedure is described in Tables 7-2 and 7-3 using equations 7-18 to 7-24.

The attainable beam shear is the smallest value of P_v obtained from Tables 7-2 and 7-3.

Table 7-2 Equations for determining the attainable load

Governing factor	Equation for attainable load	Comments
Beam web overstress	$$P_v = \frac{f_{bw}}{\sqrt{\frac{x^2.(\bar{y}-2t_{bf})^2}{I^2}+\frac{3}{H_b{}^2.t^2{}_{bw}}}}$$ (7-18)	Associated with weak beam web and high reinforcement ratio with adequate shear connection
Capacity of reinforcement	$$P_v = \frac{\left[F_r'D_r+\sum_{i=1}^{K}F_{bi}'d_{bi}-0.5F_{c.bw}'\left(\frac{F_{c.bw}'}{t_{bw}f_{bw}}+t_{bf}\right)\right]}{x}$$ (7-19)	Most common case
Column web overstress	$$P_v = \frac{f_{cw}.D_c.t_{cw}D_rb_{eff}}{\sqrt{4D_r{}^2b_{eff}{}^2+D_c{}^2x^2-2xD_rb_{eff}D_c}}$$ (7-20)	Associated with strong beam, moderate to high reinforcement area.

Note: F_b represents the force in a row of bolts. In the equations x represents the shear span i.e., the distance of the applied load from the column face (see Figure 7-1.a).

Table 7-3 Attainable shear force controlled by the connection compression capacity.

Part of the beam web will be in compression. The available horizontal compressive stress for the beam web is calculated as:

$$\tau_{xy} = \frac{minimum\ P_v}{\left(H_b - 2t_{bf}\right)t_{bw}}$$

$$f_{a,bw} = \sqrt{f_{bw}^{\ 2} - 3\tau_{xy}^{\ 2}} \qquad (7\text{-}21)$$

The depth of beam web in compression is:

$$d_{c,bw} = \frac{F_r' + \sum_{i=1}^{K} F_{bi}' - F_{c,bf}'}{f_{a,bw} \cdot t_{bw}} \qquad (7\text{-}22)$$

At this point the calculation process described in section 7.3.2 is repeated to establish the final bolt forces and the beam web and top flange compressive force (if any). These are shown with a double prime (i.e., $F''_{c,bw}$, F''_b and $F''_{c,bft}$)

The centroid of compression can be determined from:

$$d_c = \frac{F''_{c,bw}\left(\frac{d_{c,bw} + t_{bf}}{2}\right) + F''_{c,bft}\left(H_b - t_{bf}\right)}{F''_{c,bw} + F''_{c,bft} + F'_{c,bf}} \qquad (7\text{-}23)$$

The beam shear capacity for the connection considering connection equilibrium is:

$$P_v = \frac{\left[F_r'(D_r - d_c) + \sum_{i=1}^{K} F_{bi}''(d_{bi} - d_c)\right]}{x} \qquad (7\text{-}24)$$

7.5 Moment capacity of the connection

Moment capacity is given by:

$$M = P_v . x \tag{7-25}$$

7.6 Verification of results from the proposed model

It is essential to verify the proposed model by checking its predictions against available results. These have been selected from both laboratory tests and finite element analyses, since the available test data were not sufficient to verify the proposed model over the full range of parameters.

Verification was conducted in four separate stages. Initial comparisons were made against all available test results for composite flush endplate connections. The second set of comparisons checked the ability of the model to predict the effect of varying shear to moment ratio on moment capacity. Because comparatively little test data were available, FE results were also employed. The third set of comparisons considered variations in the degree of shear interaction in a connection and also used some FE results. The final checks investigated the influence of coincident axial column load - since no test data were available, these used only FE results.

7.6.1 Comparison of predictions against test data

The procedure of Figure 7-2 was programmed into a spreadsheet using the EXCEL package, in a way that kept a record of which physical condition governed each component force. When the equilibrium condition was applied the governing factors for component forces were updated accordingly. During the final selection of the connection shear capacity the components responsible for the rebar tensile force and bottom flange compressive force were identified and the connection was assumed to

reach its ultimate capacity as a result of one or both of the components selected. A total of 32 tests were extracted from references 7-5, 7-6, 7-7, 7-8, 7-9, 7-10 and 7-11; these represent all known major-axis composite flush endplate test results. All the connections were of cruciform type and almost all were loaded symmetrically. Test CJS-2 (reference 7-5) was a non-symmetrically loaded connection with an "other side" moment of 88 kN•m at the ultimate capacity of the connection and test CJS-3 (reference 7-5) was a non-symmetrically loaded connection with zero "other side" moment. Test CJS-6 was similar to CJS-3 but CJS-6 was designed without shear connectors on the transverse stub beams. The predicted and test moment capacities and their ratios are given in Table 7-4, whilst Table 7-5 lists the failure mode observed in the test and compares this with the components found to control the bottom flange compressive force and rebar tensile force in the model. It can be seen from Table 7-5, that in 24 cases out of 32 the proposed method picked the correct mode of failure, as shown in bold, out of this in two cases (SCJ7 & SJB14) compression failure was predicted by the model whereas in the test buckling of the associated member was observed. In some tests such as JX1, JX2 and SJB10 instead of a direct failure of any components, the tests were stopped due to the excessive deformation of the connection. It is well known that yield of the rebar generally causes a large extension of the tension zone and hence leads to excessive connection deformation. If this is taken into consideration the matching numbers increase by three and the total number of cases where the correct mode of failure is predicted, becomes 27 out of 32 tests.

As the model was developed using ultimate material strengths, it was essential to use ultimate strengths in the validation calculations. Where this information was not available from the test records the reported yield strengths have been used to estimate ultimate strengths, since in most cases yield strength and steel grade were reported. This was achieved using results from the coupon tests for the connection and frame tests given in reference 7-12, from which it was observed by regression analysis that

for a yield strength greater than 280 N/mm^2 the relation between the steel's ultimate strength and its yield strength may be written as:

$$f_{ultimate} = f_{yield}\left(2.01757549 - 0.0017102\, f_{yield}\right)$$

Table 7-6, which compares available test results with values obtained from this relationship, shows that very good agreement was obtained. It should be noted that the above equation was developed only for use in the comparisons; it is not intended for any further use.

It should be noted that Ariberts tests C1, C2 and C3 had angle shear connectors with variable degree of shear interaction. For comparing with these tests the shear connector force was made equal to the corresponding degree of interaction reported.

It can be seen from Table 7-4 that the proposed model tends to over-estimate capacity for connections containing only mesh reinforcement. The reason is that because it assumes full plasticity within the connection reinforcement yield and full bolt forces may develop as long as these can be balanced by the compression capacity of the connection. However, connections containing only mesh reinforcement fail by fracture of the mesh (e.g. SCJ3), with low levels of ductility which do not permit the development of a fully plastic force distribution and hence result in lower bolt forces. It should be noted that recommendations for the use of composite action in connections generally advise against relying on mesh only [7-13].

In some tests (SCJ4, SCJ5, SCJ6, SCJ7 and SJB14) buckling occurred. Since the actual load level at which the component will buckle depends not only on the geometry

Table 7-4 Comparison of test and predicted results for composite flush endplate major-axis connections

Author	Test	Beam	Column	ρ %	Test Moment (kN•m)	Predicted Moment (kN•m)	Ratio P/T (Ultimate)	Ratio P/T (yield)
Li, Nethercot, Choo (1994) (ref. 7-5)	CJS-1	254x102UB25	203x203UC46	1.00	181.5	174	0.96	0.74
	CJS-2	254x102UB25	203x203UC46	1.00	176	174	0.99	0.76
	CJS-3	254x102UB25	203x203UC46	1.00	148.5	153	1.03	0.79
	CJS-4	254x102UB25	203x203UC46	1.00	177.5	173	0.97	0.75
	CJS-5	254x102UB25	203x203UC46	1.00	197.2	169	0.86	0.68
	CJS-6	254x102UB25	203x203UC46	1.00	174.0	152	0.87	0.68
Xiao, Nethercot, Choo (1994) (ref. 7-6)	SCJ3	305x165UB40	203x203UC60	0.20	85.7	114	1.33	1.28
	SCJ4	305x165UB40	203x203UC60	1.00	202.9	173	0.85	0.84
	SCJ5	305x165UB40	203x203UC60	1.00	240.8	280	1.16	0.78
	SCJ6	305x165UB40	203x203UC60	1.00	157.6	173	1.10	1.08
	SCJ7	305x165UB40	203x203UC52	1.20	204.5	247	1.21	0.81
Aribert & Lachal (1992) (ref. 7-7)	A2	IPE360	HEB200	0.75	296	364	1.23	0.90
	A3	HEA200	HEB200	0.75	152	150	0.99	0.83
	A4	IPE360	HEA360	0.75	297	376	1.27	1.00
	C1	IPE360	HEB200	0.90	344	393	1.14	0.84
	C2	IPE360	HEB200	0.90	326	369	1.13	0.86
	C3	IPE360	HEB200	0.90	288	334	1.16	0.89
Anderson & Najafi (1994) (ref. 7-8)	S4F	305x165UB40	203x203UC52	0.55	179	178	1.00	0.87
	S8F	305x165UB40	203x203UC52	1.10	262	244	0.93	0.68
	S12F	305x165UB40	203x203UC52	1.65	302	254	0.84	0.59
	S8FD	457x152UB52	203x203UC52	1.10	416	343	0.82	0.59
Anderson & Najafi (1992) (ref. 7-9)	Test1	305x165UB40	203x203UC52	1.00	262	254	0.97	0.68
	Test3	305x165UB40	203x203UC52	0.50	179	226	1.26	0.87
	Test4	305x165UB40	203x203UC52	1.50	243	254	1.05	0.73
	Test 7	305x165UB40	203x203UC52	1.50	302	254	0.84	0.59
	Test 10	457x152UB52	203x203UC52	1.00	416	353	0.85	0.59
Law (1981) (ref. 7-10)	JX1	457x191UB67	203x203UC46	1.00	354	395	1.12	0.74
	JX2	457x191UB67	203x203UC46	1.00	370	395	1.07	0.70
	JC1	457x191UB67	254x254UC73	1.00	330	395	1.20	0.79
	JC2	457x191UB67	254x254UC73	0.63	530	442	0.83	0.56
Benussi, Puhali, Zandonini (1986), (ref. 7-11)	SJB10	IPE300	HEB260	0.71	208	201	0.97	0.90
	SJB14	IPE300	HEB260	1.21	261	302	1.16	1.01
Summary of results	Total no. of tests compared 32		Average P/T 1.04		Standard deviation 0.15			Avg 0.79
			Maximum 1.33		Minimum 0.82		STDV = 0.156	

Table 7-5 Comparison of test and predicted failure modes

Test	Failure mode in test	Model prediction Compression governed by	Model prediction Tension governed by
CJS-1	CH,RE,CM,BBF,BM	Bottom flange compression	Rebar
CJS-2	CM,RE,BBF	Bottom flange compression	Rebar
CJS-3	CM,CH,RE	Bottom flange compression	non-sym concrete
CJS-4	CH,RE,CM,BBF	Bottom flange compression	Rebar
CJS-5	CH,RE,CM,BM,BBF	Bottom flange compression	Rebar
CJS-6	CM,RE,BBF,CH	Bottom flange compression	non-sym concrete
SCJ3	Mesh fracture	Column web buckling	Rebar
SCJ4	Column web buckling & flange deformation	Column web buckling	Column web buckling
SCJ5	Stud, Bottom flange compression	Bottom flange compression	Stud
SCJ6	Column web buckling	Column web buckling	Column web buckling
SCJ7	Stud, column web buckling	Column web compression	Stud
A2	Rebar	Column web compression	Rebar
A3	Rebar	Bottom flange compression	Rebar
A4	Rebar	Bottom flange compression	Rebar
C1	Bolt	Web-Compression	Rebar
C2	Stud failure	Web-Compression	Stud
C3	Stud failure	Web-Compression	Stud
S4F	Rebar & mesh fracture	Column web compression	Rebar
S8F	Rebar & mesh fracture	Column web compression	Rebar
S12F	Bottom flange buckling	Column web compression	Stud
S8FD	Rebar & mesh fracture	Column web compression	Rebar
Test1	Rebar & mesh fracture	Column web compression	Stud
Test3	Rebar & mesh fracture	Column web compression	Rebar
Test4	Stud failure	Column web compression	Stud
Test7	Beam flange buckling	Column web compression	Stud
Test10	Rebar & mesh fracture	Column web compression	Stud
JX1	Joint deformation	Column web compression	Rebar
JX2	Joint deformation	Column web compression	Rebar
JC1	Rebar yield	Column web compression	Rebar
JC2	Rebar yield	Column web compression	Rebar
SJB10	Joint deformation	Bottom flange compression	Rebar
SJB14	Bottom flange buckling	Bottom flange compression	Rebar

Note:

RE means yield of rebar, CH means column web horizontal yield at beam bottom flange level, CM means column web von-Mises stress reaches yield strength, BBF means steel beam bottom flange yield, BM means steel beam von Mises stress reaches yield strength, non-sym concrete means that the tensile force is governed by the effective width of compression of concrete.

and orientation of the component but also on the initial imperfections, accurate predictions are difficult. Thus results may be expected to be both overestimated e.g. SJB14, or underestimated e.g., SCJ4.

In tests with small shear spans e.g. test CJS-5, a diagonal load path can form, which will allow the transfer of some load through diagonal compression. This transfer mechanism will allow the force to increase without a corresponding increase in the connection's internal moment. This type of load transfer is not considered in the proposed model and thus it may be expected that tests with small shear spans will be underestimated.

It was observed that if the rebar area is taken as zero for test CJS-1, the moment capacity of the connection becomes 48 kN•m and the bolt force in top row becomes 192 kN. From reference 7-5 it can be seen that the test moment for the bare steel connection SJS-1 at this level of bolt force (reported for each single bolt) was about 44 kN•m. This gives a P/T ratio of 1.09 for the bare steel connections and suggests that the model is also suitable for bare steel connections.

From Table 7-5 it can be seen that in almost all cases it is possible to identify the component actually responsible for the connection reaching its ultimate capacity. Generally this accords well with the model predictions. It should be noted that the successful tracing of the component responsible for reaching the ultimate state depends on the availability of the exact material properties; even when these are provided, buckling or shear failure of the concrete are difficult to predict accurately. When compression of the column web and beam bottom flange governs, it should be taken as an indication of possible buckling of the associated component.

The comparison with test data shows that the proposed model is capable of predicting the moment capacity of the connections and the failure mode under different types of

loading with good accuracy provided the exact material strengths are known. The average ratio of prediction to test for the 32 results was 1.04 with a standard deviation of 0.15.

Table 7-6 Relation between the yield and ultimate strengths used for model verification

Yield (Test)	Ultimate (Test)	Component tested	Test	Ultimate strength from equation	Ratio of prediction to test
N/mm^2	N/mm^2			N/mm^2	
280	450	EP	Joint	431	0.96
325	480	CF	Joint	475	0.99
300	443	CW	Frame	450	1.02
307	450	BF	Frame	457	1.02
345	495	EP	Frame	493	1.00
324	463	BW	Frame	473	1.02
355	500	CW	Joint	500	1.00
410	540	BF	Joint	541	1.00
430	540	BW	Joint	550	1.02
490	585	10mmRE	Frame	578	0.99
510	590	12mmRE	Frame	587	0.99

Note:
EP is endplate, CF is column flange, CW is column web, BF is beam flange, BW is beam web, 10mmRE is 10 mm diameter reinforcement, 12mmRE is 12 mm diameter reinforcement.

7.6.2 Comparisons for variable shear to moment ratios

The effect of the shear to moment ratio becomes important for connections with a shallow beam depth and very high reinforcement ratios. Results for an identical detail but with reinforcement ratios of 2.00% and 0.67% were available from FE studies reported in chapter 5 and in reference 7-15 for loading at a series of distances from the column face. These, together with a few additional results are compared with the proposed method in Table 7-7. In addition to using the FE results, comparisons were made for five test results (also shown in Table 7-4) in which different shear to moment ratios were used. The reason for the low P/T ratios of 0.86 and 0.85 for tests CJS-5

and SCJ4 has already been discussed in section 7.6.1. FE analyses with low rebar ratios lead to very high bolt forces reported in chapter 4 and in ref. 7-14, whereas the bolt force is limited by the EC3 rules in the proposed model. But it can be seen by examining the results of chapter 4, that at the EC3 levels of bolt force the moment capacity was about 130 kN•m, which gives a P/T ratio of 1.06. Without taking this into consideration, the average P/T value for 15 results is 0.90 with a standard deviation of 0.068.

Table 7-7 Comparison of predicted and test or FE moment capacity for various shear moment ratios

Author	Test	Shear to moment ratio m^{-1}	ρ %	Test or FE Moment (kN•m)	Predicted Moment (kN•m)	P/T
Li et al (ref. 7-5)	CJS-1	0.679	1.00	181.5	174	0.96
	CJS-4	0.978	1.00	177.5	173	0.97
	CJS-5	1.745	1.00	197.2	169	0.86
Xiao et al (ref. 7-6)	SCJ4	0.667	1.00	202.9	173	0.85
	SCJ6	1.250	1.00	157.6	173	1.10
Chapter 5 & ref. 7-15	FE Analysis high rebar ratio	0.679	1.95	238	199	0.84
		0.978	1.95	235	198	0.84
		1.247	1.95	228	197	0.86
		1.745	1.95	224	190	0.84
		2.825	1.95	164	145	0.88
Chapter 5 & ref. 7-15	FE Analysis low rebar ratio	0.679	0.65	152	138	0.91
		0.978	0.65	152	138	0.91
		1.247	0.65	152	138	0.91
		1.745	0.65	152	138	0.91
		2.825	0.65	152	138	0.91
Summary of results	Total no. of results compared 15		Average P/T 0.90, Standard deviation 0.068 Maximum 1.10, Minimum 0.84			

7.6.3 Comparisons for variable degrees of shear interaction

Table 7-8 compares the predictions from the model with results from both tests and FE analysis reported in chapter 4 and in ref. 7-14. For the model, the degree of shear interaction was allowed for by calculating the stud force directly. Comparison of seven results gave an average prediction to test or analysis ratio of 1.01 with a standard deviation of 0.142. This indicates that if the correct shear capacity of the studs is known, the method can predict the effect of partial interaction very well. It should be

noted that for low degree of shear interaction finite element method gives higher results as it allows the bolts to take high tensile force although the failure of the studs will prevent this in practice - which is accounted for in the design procedure, hence for low interaction the prediction gives lower results than the FE results.

Table 7-8 Comparison of predicted and test or FE moment capacity for various degrees of shear interaction

Author	Test	Degree of shear interaction	ρ %	Test or FE Moment (kN•m)	Predicted Moment (kN•m)	P/T
Aribert & Lachal (ref. 7-7)	C1	Full	0.90	344	393	1.14
	C2	75%	0.90	326	369	1.13
	C3	50%	0.90	288	334	1.16
Chapter 4 ref. 7-14	FE analysis	300%	1.00	180	174	0.97
		100%	1.00	180	174	0.97
		60%	1.00	148	128	0.87
		40%	1.00	127	101	0.80
Summary of results	Total no. of results compared 7		Average P/T 1.01, Standard deviation 0.142 Maximum 1.16, Minimum 0.80			

7.6.4 Comparisons for variable column loading

No test results are available for composite connections in which significant levels of axial column loading were present. Therefore, in this case the verification has used only FE results from chapter 6 (and ref. 7-4). Column loads of 0%, 51%, 65% and 82% of column yield load were considered and the predictions of the model are compared with the results in Table 7-9. FE analyses are available for both non-symmetrically loaded ($\eta = 0$) and symmetrically loaded connections ($\eta = 1$). For the $\eta = 0$ case analyses with or without considering the column shear were conducted. From Table 7-9 it can be seen that when the shear of 86 kN due to the reaction force at the column supports was included (which was precisely the condition in the FE analyses) the results predicted by the method are very close to the FE results. The average ratio

of prediction to FE results for the 12 examples considered is 0.99 with a standard deviation of 0.058.

Table 7-9 Comparison of predicted and FE moment capacity for various column loads

Author	Column load as % of yield capacity	FE Moment (kN•m)	Predicted Moment (kN•m)	P/T
Chapter 6 & ref. 7-4* non-symmetric loading	0	157	153	0.97
	51	144	142	0.98
	65	140	132	0.94
	82	121	105	0.86
Chapter 6 & ref. 7-4* non-symmetric loading, web shear = 86 kN	0	157	153	0.97
	51	144	153	1.06
	65	140	146	1.04
	82	121	128	1.06
Chapter 6 ref. 7-4 symmetric loading	0	183	174	0.95
	51	179	174	0.97
	65	179	174	0.97
	82	167	174	1.04
Summary of results	Total no. of results compared 12	Average P/T 0.99, Standard deviation 0.058		
		Maximum 1.06, Minimum 0.86		

Note: * FE results are obtained from the same set of analyses

7.6.5 Comments on the validity of the proposed method

In sections 7.6.1 - 7.6.4 predictions from the proposed method have been compared with a total of 53 test and finite element results. These comparisons gave an overall prediction to test ratio of 0.99 with a standard deviation of 0.14, thereby demonstrating that the proposed method can accurately predict the resistance of composite flush endplate connections under a variety of different connection arrangements and loading conditions. It should, however, be noted that in making the calculations for validation purposes use was made of the strain hardening properties of the materials, since the equations in the method contain terms that use ultimate material strengths. In practice, ultimate strengths may not be available and in such cases it is recommended that the yield strengths be used throughout. This will, of course, give lower connection resistances and the last column of Table 7-4 provides an

indication of this. It can be seen that in a few cases the prediction is almost as good as the result obtained using the ultimate strengths but that generally the predictions are significantly less accurate. For non-symmetrically loaded connections this conservatism is generally less than for the symmetric case since full rebar forces cannot develop, the full compression capacity may not be utilised in the test, and the connections therefore attain their ultimate capacity at a lower level of stress in the rebars.

7.6.6 Illustrations of the use of the proposed method

Availability of a comprehensive design method that makes explicit allowance for each component in the connection permits an examination of connection behaviour to be made under different conditions. Three cases have been investigated:

1 The effect of reinforcement area on bolt forces, rebar force and hence moment capacity for symmetrically and non-symmetrically loaded connections

2 The effect of axial column load on moment capacity

3 The effect of shear span on moment capacity

For both cases 2 and 3; variations in the percentage of reinforcement have also been included.

Figure 7-4 shows how rebar force and bolt force (expressed as a proportion of column web compression capacity) vary with the ratio of rebar area for a symmetrically loaded endplate connection. From the figure it can be seen that an increase of reinforcement area produces a linear increase in rebar force up to a certain limit. This occurs because the matching compression capacity is fully utilised at that limit and thus any additional tensile force cannot be balanced. At the same time it can be seen that as the rebar area is increased the bolt force decreases, eventually becoming zero. This is consistent with the FE analyses reported earlier in chapter 4 and in reference 7-14. The reason for the

decrease in the bolt force is that as the rebar area increases and carries more tensile force at a lower strain than before, less elongation takes place in the bolts and hence the developed bolt force is also lower. This can also be explained with reference to the location of the neutral axis. With low reinforcement areas the tensile force developed in the rebar area is low, so the location of the neutral axis is also lower and hence the bolts are subjected to more elongation. But as the rebar area increases, the tensile force also increases and to balance this tensile force compression develops in the beam web so the neutral axis moves upwards. Hence the distance of the bolts from the neutral axis decreases, the elongation of the bolts decreases and hence the bolt force decreases. When the rebar area is so high that the neutral axis is very close to the bolts the force in them becomes zero. Figure 7-5 shows the effect of varying reinforcement ratios on moment capacity. Due to the behaviour explained above, the moment capacity reaches a constant level once a certain amount of reinforcement is provided. From both figures it can be seen that the optimum rebar area is related to the column web compression capacity for symmetrically loaded connections. *The rebar area for which the rebar force becomes equal to the column web compression capacity is the maximum reinforcement that can be effectively utilised for any moment connection.*

Figure 7-6 illustrates the effect of changing the rebar area on the bolt and rebar force for a non-symmetric flush endplate connection, with zero "other side" moment. As the connection compression capacity is constant, the total developed tensile force is the same as in the previous case. Since the magnitude of rebar force is more dependent on the concrete strength and column width, it can be seen that the maximum developable force is limited by this criterion. Hence the developable rebar force is constant for the connection and cannot increase after a certain limit with the increase of reinforcement. As the tensile force in the rebar is fixed so the increase in rebar area causes the rebar strain to decrease, which will decrease the bolt strain. This decrease of bolt strain with increase of rebar area decreases the bolt force. As the moment capacity is the summation of the moment of all internal forces, decrease in bolt force causes a small

decrease in connection moment capacity. So beyond a certain amount of reinforcement, due to the smaller strains in the rebars, bolt force starts to decrease and this will cause a small decrease in moment capacity after the optimum reinforcement ratio for non-symmetrically loaded connections. The variation in the connection moment capacity with reinforcement area is shown in Figure 7-7. It can be seen that for the connection considered the moment capacity starts to reduce beyond a ratio of 0.8 (this is the ratio of the rebar tensile capacity to the column web compression capacity). In cruciform connections, as the rebar force is high, due to the long lever arm, the moment capacity is high, although the total tensile force may be constant (as the decrease in the bolt force increases the rebar force). For connections with low levels of reinforcement the moment capacity is equal for the symmetrical and non-symmetrical cases. *The maximum useful rebar area for non-symmetrically loaded connections (with zero other side moment) is that which can develop a force that when added to the bolt force is equal to the column web compression capacity, when there is no column load.*

Figures 7-8, 7-9 and 7-10 shows the effect of column load on the bolt force, rebar force and the moment capacity of non-symmetrically loaded (zero "other side" moment) endplate connections. As the column load increases the connection compression capacity decreases due to the decrease in shear strength of the column web. This causes the rebar force and the bolt force to decrease. From the results it can be seen that if the rebar area is high the effect of column load becomes significant at a lower column stress, whereas for low levels of reinforcement the effect may be seen only at higher column loads. The reason is that for large amounts of reinforcement the developed tensile force is also high and this permits the full shear capacity of the connection to be utilised through the balancing compressive force and as the developable compressive force decreases with increasing column load the rebar force must decrease which, in turn, causes the moment to decrease. In contrast, for low

amounts of reinforcement the connection's full tensile force will exceed the compression capacity only at a very high column load.

Figure 7-11 shows the effect of varying the shear span on moment capacity. From the results it can be seen that the shear to moment ratio affects the moment capacity when: 1) The shear span is very low, 2) The connection is highly reinforced. The reason for the reductions in moment capacity is that the reduced shear span decreases the connection's compression capacity so that the full tensile force cannot develop for the lower shear spans. The connection compression capacity will be reduced due to the high shear that develops with a low shear span or a high rebar area or both - as the developable shear force is proportional to the rebar area and inversely proportional to the shear span. The high shear stress reduces the available compressive stress in the beam web. So less compressive force can be transmitted than is required to maintain equilibrium and a constant moment capacity. Hence the moment capacity decreases. The increase in shear also increases the local horizontal stress in the column and may cause it to yield; this also causes a decrease in moment capacity.

7.6.7 Limitations in the design method

The design approach proposed herein is based on the identification and representation by means of formulae of the key aspects of load transfer within the connection. This has been derived from careful studies of test findings and numerical results. To achieve a balance between accuracy and ease of calculation certain pragmatic decisions have been taken relating to the exact nature of the treatment of certain features of the observed behaviour. These are listed below in order to assist possible further development:

1 The model assumes full plasticity within the connection and thus assumes that the reinforcement yields, which in turn allows bolt forces to fully develop as

long as they can be balanced by the compression capacity of the connection. In practice connections which contain only mesh reinforcement fail by fracture of the mesh with low ductility that does not permit a full plastic distribution to develop and hence results in lower bolt forces. This may result in over estimation of capacity for connections with very low percentages (say 0.2%) of reinforcement.

2 Bolt forces are calculated using the EC3 equations for bare steel connections. Since these assume two bolts per row, it is not possible to predict the capacity of connections having more than two bolts per row.

3 For cruciform connections any reduction in bolt force due to yield of the column flange is not included when considering the effect of column loading. This will lead to a overestimate of moment capacity for cruciform connections with high column loads.

4 For cruciform connections yield of the column web at the level of the beam bottom flange will lead to transfer load into the beam web, thereby increasing the column web compression area. This is neglected since column web compression capacity is obtained from the EC3 equation. This will cause the calculated moment capacity to be slightly low if the connection is very highly reinforced.

7.7 Proposed method to calculate the initial stiffness of composite flush endplate connections

From the review in chapter 1 it is apparent that the methods already proposed by Anderson & Najafi [7-8] and Ping Ren [7-16] would be improved if they could be modified so that the stiffnesses of the individual components could be properly

addressed. The problem with the Anderson & Najafi method is that it neglects the stiffness of the column web and also the stiffness of the shear studs is not properly represented as only the stiffness from one stud is used. In the Ping Ren method the assumption that the total moment $M = M_c + F_r Z$ is not reliable and since it uses rebar spacing to calculate the stiffness of the rebar, connections with mesh reinforcement only cannot be analysed. Improvements to the calculation of initial stiffness are suggested by including the factors that are presently neglected in the two methods.

The following assumptions are made:

i For initial stiffness the developed internal forces are low, so only the influence of the rebar, bolts and the column web at the level of beam bottom flange need be considered when calculating the initial stiffness. In other words compression in the beam web will not influence the connection initial stiffness.

ii Only the top bolts will be in tension at the load level for which initial stiffness is determined.

iii Beam web deformation at this load level is linear.

In the clause for the determination of the stiffnesses of basic components in the revised Annex J of EC3 [7-17], it is stated (J.4.4.3) that:

"The following components need not be taken into account when calculating the rotational stiffness S_j:

- beam flange and web in compression

- beam web in tension

- plate in tension or compression"

Also in this same clause for rotational stiffness, the basic model (J.4.1) assumes that [J.4.1(2)]: *"In a bolted connection with more than one bolt-row in tension, as a simplification the contribution of any bolt-row may be neglected, provided that the contributions of all other bolt-rows closer to the centre of compression are also neglected. The number of bolt-rows retained need not necessarily be the same as for the determination of the design moment resistance".* This supports the second assumption made herein.

These assumptions can be verified by the test results presented in reference 7-5. Table 7-10 shows the strain of different components at 45% of the ultimate moment capacity. The reason for checking against the level of moment is that the M-ϕ curve can be treated as linear up to this limit. It is clear from the test results that the influence of the beam web is insignificant and may be neglected. It can also be seen that at this level of load (45% of ultimate) the bottom row of bolts is below the neutral axis; hence its main function is shear transfer only. Also results presented in reference 7-5 show that the web strain is linear at this load level; hence the web deformations must be linear.

Table 7-10 Strain of various components as observed in tests (ref. 7-5) at 45% of ultimate capacity

Test	Rebar strain (με)	Top bolt strain (με)	Beam web strain (με)	Bottom flange strain (με)	Column web strain (με)
CJS-1	**1015**	**413**	-182	-2000	**-1105**
CJS-2	**1095**	**450**	-160	-920	**-953**
CJS-3	**632**	**450**	-190	-670	**-550**
CJS-4	**780**	**480**	-280	-780	**-1200**
CJS-5	**1200**	**500**	-250	-750	**-1000**
CJS-6	**770**	**410**	-160	-900	**-650**

7.7.1 Finite element analysis to identify the most important influences on connection stiffness

Chapters 3, 4, 5 and 6 described the numerical simulation and several studies on the composite connections using ABAQUS. These studies have provided a vast source of

information on detailed aspects of connection behaviour and also contains valuable information regarding the initial stiffness of connections. These results therefore provide a valuable source from which the major parameters that influence connection initial stiffness can be identified.

Chapter 4 describes the overall connection behaviour for varying reinforcement areas, degrees of shear interaction, thickness of: endplate, beam bottom flange and column web. It can be seen from the results that reinforcement area (Figure 4-1) and degree of shear interaction (Figure 4-8) have most influence. Column web thickness is less important (Figure 4-23), whilst other parameters are insignificant.

Chapter 5 explains the influence of the shear to moment ratio on connection behaviour. Results (Figures 5-9 and 5-11) from the study show that for a given connection detail the initial stiffness is not influenced by the distance of the load from the column flange. Besides these, reference 7-5 describes 3 tests on identical connections and variable shear to moment ratios. The results confirm that the initial stiffness is independent of distance of load from the column flange provided other things are constant. Hence the load position need not be considered in the equation for initial stiffness.

Chapter 6 describes the effect of axial column loading on composite connection behaviour. It is clear from the results (Figures 6-6 and 6-14) that the connection initial stiffness is independent of the level of column axial loading present. In addition, reference 7-10 describes tests (JY2P) using concrete encased columns, in which column axial loading was present; although the results were not presented for the full loading, the early part shows that column axial load does not influence connection initial stiffness. It was concluded by the author that *"The influence of column load on the stiffness of the joint was small. This was demonstrated by the test result (Figure C.18) of joint JY2P, which had a substantial amount of concrete encasement"*. This test actually failed due to local buckling of the beam bottom flange which was followed

by buckling of the steel beam. Thus the presence of column loading need not be considered when determining initial connection stiffness.

7.7.2 Equation for initial stiffness

Using the above assumptions the proposed spring model is shown in Figure 7-12.

The equilibrium condition gives:

$$F_r + F_b = F_c$$
$$F_r = F_s \qquad (7\text{-}26)$$

Where:

F_r is the tensile force in the reinforcement

F_s is the shear force transferred by the shear studs

F_b is the tensile force in the bolts

F_c is the compressive force transferred by the beam bottom flange

From the stiffness deformation relations:

$$F_r = K_r \Delta_r$$
$$F_b = K_b \Delta_b \qquad (7\text{-}27)$$
$$F_s = K_s \Delta_s$$

Where:

K and Δ are the stiffnesses and displacements of the related components

From Figure 7-12 the compatibility condition is:

$$\frac{\Delta_s + \Delta_r + \Delta_c}{H_b} = \frac{\Delta_b + \Delta_c}{d_b} = \phi \qquad (7\text{-}28)$$

Where:

H_b is the depth of beam section

d_b is the distance of the top bolt row from the bottom flange

Substituting the displacements from equation 7-27 into equation 7-28 the following equations are obtained:

$$\frac{F_s}{K_s}+\frac{F_r}{K_r}+\frac{F_c}{K_c}=H_b\phi$$
$$\frac{F_b}{K_b}+\frac{F_c}{K_c}=d_b\phi \qquad (7\text{-}29)$$

Where:

ϕ is the rotation of the connection

Substituting values for F_s and F_c from equation 7-26 into equation 7-29 gives:

$$F_r\left(\frac{1}{K_r}+\frac{1}{K_s}+\frac{1}{K_c}\right)+\frac{F_b}{K_c}-H_b\phi=0 \qquad (7\text{-}30a)$$

$$\frac{F_r}{K_c}+F_b\left(\frac{1}{K_b}+\frac{1}{K_c}\right)-d_b\phi=0 \qquad (7\text{-}30b)$$

Solving for F_r and F_b from equations 7-30a and 7-30 gives:

$$F_r=\frac{H_b\phi\left(\frac{1}{K_b}+\frac{1}{K_c}\right)-d_b\phi\frac{1}{K_c}}{\left(\frac{1}{K_r}+\frac{1}{K_s}+\frac{1}{K_c}\right)\left(\frac{1}{K_b}+\frac{1}{K_c}\right)-\frac{1}{K_c^{\,2}}} \qquad (7\text{-}31a)$$

$$F_b = \frac{d_b\phi\left(\frac{1}{K_r}+\frac{1}{K_s}+\frac{1}{K_c}\right)-H_b\phi\frac{1}{K_c}}{\left(\frac{1}{K_r}+\frac{1}{K_s}+\frac{1}{K_c}\right)\left(\frac{1}{K_b}+\frac{1}{K_c}\right)-\frac{1}{K_c^{\,2}}} \qquad (7\text{-}32b)$$

Since the interest is in initial stiffness, the internal tensile forces are low so there is no compression force developed in the beam web and hence the moment can be calculated using the rebar force and bolt force in this case. The equilibrium condition gives:

$$M = F_r D_r + F_b d_b$$

Where:

M is the connection moment

D_r is the distance of the reinforcement from the bottom flange centreline

Substituting F_r and F_b from equations 7-31a and 7-31b in the above equation and applying the condition $M=K_i\phi$ gives:

$$K_i = \frac{H_b D_r\left(\frac{1}{K_b}+\frac{1}{K_c}\right)+d_b^{\,2}\left(\frac{1}{K_r}+\frac{1}{K_s}+\frac{1}{K_c}\right)-d_b\left(H_b+D_r\right)\frac{1}{K_c}}{\left(\frac{1}{K_r}+\frac{1}{K_s}+\frac{1}{K_c}\right)\left(\frac{1}{K_b}+\frac{1}{K_c}\right)-\frac{1}{K_c^{\,2}}} \qquad (7\text{-}32)$$

Where:

K_i is the initial stiffness of the connection

It can be seen that the Anderson & Najafi [7-8] equation is a special form of the above general equation corresponding to the assumption of an infinite stiffness for the column web.

7.7.3 Selection of key parameters

An equation to represent the initial stiffness of the connection has been developed above. However, its successful use in practice depends on the accurate estimation of the individual terms i.e. the component stiffnesses of the items present in the equation. Before the formula is applied, it is essential to decide on suitable values for these key parameters. These are the length of reinforcement to be considered to calculate the rebar stiffness, the stiffness of the shear studs and the stiffness of the bolts. To investigate this; a basic value is first selected - from which the effect of variations of the parameters can be studied. The selection of the initial values is described below.

7.7.3.1 Length of reinforcement to calculate the rebar stiffness

If the first stud is very near the column flange, the distance to the next stud should be used. It was found by Benussi and Noe [7-18] and also confirmed by Anderson and Najafi [7-8] that if the length of rebar considered for calculating the rebar stiffness is equal to half the depth of column, the resulting model overestimates the stiffness of the connection due to overestimating the rebar stiffness. They concluded that this can be corrected by increasing the length of rebar considered for the elongation.

For the basic set-up the length selected is:

$$l_r = (D_c / 2 + 225)\ mm$$

Hence:

$$K_r = \frac{A_r E_r}{\frac{D_c}{2} + 225} \tag{7-33}$$

Where:

D_c is the depth of column web

7.7.3.2 Stiffness of the shear studs

This can be calculated for all the shear studs in the hogging moment region or if the connection has more studs than are required for full interaction the actual number of studs required for full interaction should be used. Assessment of push-out test results of welded studs by several researchers [7-19, 7-20 and 7-21] shows that the elastic stiffness of the shear stud can vary between 200 kN/mm and 350 kN/mm at 45% of the stud load capacity. On the other hand the finite element analyses reported by Razaqpur & Nofal [7-22], which were verified against the tests of other researchers, used a constitutive law for the force deformation response of the shear studs based on the empirical equations developed by other researchers. The stud stiffness resulting from the coefficient used by them represents a stiffness of 118 kN/mm. Also the load slip curve adopted for numerical analysis of composite beams by Mistakidis *et al* [7-23] from test results of other researchers gives a stiffness of 110 kN/mm. It can be seen that the stiffness of the shear studs can be in a range between 110 kN/mm and 350 kN/mm. As a reasonable estimate the value is taken as 200 kN/mm. Hence stiffness of a single stud is:

$$K_{s1} = 200\ kN/mm$$

But it is also acknowledged that the true stiffness of the shear connector for a specific test should provide better results, and the amount of slip that can occur in a connection can vary. If the average slip of the studs is Δ, the force transmitted by them is:

$$F_s = 200 x N_s x \Delta$$

Hence from the stiffness deformation relationship:

$$K_s = 200x\ N_s \qquad (7\text{-}34)$$

Where N_s is the smaller of either the total number of studs present in the hogging moment region or the number of studs required for full interaction.

7.7.3.3 Stiffness of the bolts

It is taken as 155 kN/mm following the Anderson method (ref. 7-8).

$$K_b = 155 \text{ kN/mm} \tag{7-35}$$

It is accepted that there will be some variation according to the equation in reference 7-8, due to the variation of the distance of the top bolt from the bottom flange centreline. This is neglected as the relative contribution of the bolts to the connection stiffness is insignificant with respect to the other associated components as indicated in Tables 7-11 to 7-13.

7.7.3.4 The stiffness of the column web

It is calculated from the basic principles (AE/L) for a compression member only, using the depth of compression from EC3 and is:

$$K_c = \frac{2E_{cw}}{D_c}\left[t_{cw}\left\{t_{bf} + 2\left(t_p + \sqrt{2}a_p\right) + 5\left(t_{cf} + r_c\right)\right\}\right] \text{ without web stiffener} \tag{7-36}$$

But when a column web stiffener is present its contribution towards resisting deformation must be included, hence the stiffness should be calculated as:

$$K_c = \frac{2E_{cw}}{D_c}\left[t_{cw}\left\{t_{bf} + 2\left(t_p + \sqrt{2}a_p\right) + 5\left(t_{cf} + r_c\right)\right\} + t_{ws}b_{cf}\right] \text{ with web stiffener} \tag{7-37}$$

And in general E is constant for all members.

References 7-5, 7-6, 7-7, 7-8, 7-9, 7-10 and 7-11 describe 32 flush endplate connection tests. These are selected to study the effect of the parameters. Calculations are performed to study the average and the standard deviations of the ratio of prediction to test initial stiffness ratio. Tables 7-11 to 7-13 show the results of the study.

From the results obtained, the values that are selected are:

l_r : $(D_c/2 + p_1 + p_2)$ *mm*

K_b : *155 kN/mm (this value has been used by other researchers, ref. 7-8)*

K_s : $200\ N_s$ *kN/mm*

Table 7-11 Effect of stiffness of the shear studs on the prediction method

K_s (kN/mm)	100	200	300
Average	0.98	1.12	1.21
Standard deviation	0.20	0.21	0.22

Table 7-12 Effect of stiffness of the bolts on the prediction method

K_b (kN/mm)	50	100	155	200
Average	1.00	1.06	1.12	1.19
Standard deviation	0.19	0.20	0.21	0.21

Table 7-13 Effect of rebar length on the prediction method

l_r (mm)	$(D_c/2 + 225)$	$(D_c/2 + p_1 + p_2)$	$(D_c/2 + p_1 + 2p_2)$
Average	1.12	0.99	0.76
Standard deviation	0.21	0.21	0.16

Note: p_1 is the distance of the first stud from the column face
p_2 is the pitch of the shear studs

7.7.4 Validation of the proposed equation

In order to validate equation 7-32, test results obtained from references 7-5, 7-6, 7-7, 7-8, 7-9, 7-10 and 7-11 have been used. When the initial stiffness was not directly reported, the slope of the line connecting the origin to 45% of the ultimate moment has been taken as the initial stiffness. Table 7-14, which presents the comparison of test and prediction, indicates that except for a few cases a very good agreement is achieved. It can be seen that if the first 4 results are ignored the average is 0.99 with a standard deviation of 0.21 for the proposed method, whereas under the same conditions, Anderson & Najafi [7-8] method gives an average prediction of 0.64 with standard deviation of 0.16, Ping Ren [7-16] method gives an average prediction of 1.41 with a standard deviation of 0.29. From these comparisons it is clear that the proposed method provides better predictions of the connection stiffness.

From Table 7-14 it can be seen that tests conducted by Law [7-10] exhibit the largest discrepancies. These had a beam depth of 453.6 mm with connection initial stiffnesses of 50, 75 and 80 kN/mm (for JX1 JX2 and JC1 respectively), while the predicted values were 134 kN/mm for all. But it can also be seen that connections with similar beam depth and reinforcement level, for example JC2, Test10 and S8FD (453.6, 449.8 and 449.8 mm depth of beam) gave an initial stiffness of 200, 154 and 141 in the test while the predicted values were 149, 115 and 115 kN/mm. These early tests by Law and Johnson had concrete encasement on the columns. While the other tests demonstrate that an increase of beam depth causes the initial stiffness to increase (with other things constant) - the reason for reduced stiffness for these particular tests is not clear.

Table 7-14 Comparison of predicted and test connection initial stiffness(see Table 7-4 for references)

Test	K_r kN/mm	K_s kN/mm	K_b kN/mm	K_c kN/mm	K_i kN• mm/mrad	K_i Test kN• mm/mrad	P/T	Anderson Najafi[7-8] method *	Anderson Najafi P/T	Ren Ping[7-16] method *	Ren Ping P/T
JX1	540	4000	155.00	8739	133.91	50	**2.68**	69.16	1.38	179.80	3.60
JX2	540	4000	155.00	8739	133.91	75	**1.79**	69.16	0.92	179.80	2.40
JC1	540	4000	155.00	8739	133.91	80	**1.67**	69.16	0.86	179.80	2.25
JC2	540	4000	155.00	8739	149.04	200	**0.75**	75.36	0.38	231.94	1.16
CJS-1	348	2800	155.00	6340	31.04	31	1.01	21.55	0.70	47.03	1.53
CJS-2	348	2800	155.00	6340	31.04	28	1.12	21.55	0.78	47.03	1.69
CJS-3	348	2800	155.00	6340	31.04	42	0.74	21.55	0.52	47.03	1.13
CJS-4	348	2000	155.00	6340	30.03	33	0.90	21.55	0.65	47.03	1.41
CJS-5	348	800	155.00	6340	25.86	36	0.71	21.55	0.59	47.03	1.29
CJS-6	348	2800	155.00	6340	31.04	32	0.98	21.55	0.68	47.03	1.48
SCJ3	115	1400	155.00	8873	20.31	29	0.70	23.88	0.82	NA	NA
SCJ4	573	1400	155.00	8873	53.54	49	1.08	29.68	0.60	87.94	1.78
SCJ5	573	1400	155.00	77271	56.45	61	0.93	29.68	0.49	87.94	1.44
SCJ6	573	800	155.00	8873	45.70	65	0.71	29.68	0.46	84.80	1.31
SCJ7	691	1400	155.00	7517	58.83	50	1.19	29.77	0.60	86.79	1.75
Test1	520	1400	155.00	68861	54.55	63	0.86	30.78	0.48	86.38	1.36
Test3	298	1400	155.00	68861	38.78	36	1.09	28.70	0.80	50.75	1.42
Test4	742	1400	155.00	68861	66.99	51	1.31	31.54	0.62	97.88	1.91
Test7	742	1400	155.00	68861	66.99	73	0.91	31.54	0.43	97.88	1.33
Test10	520	1400	155.00	68879	115.26	154	0.75	66.92	0.43	162.58	1.06
S4F	261	1400	155.00	68861	35.71	30	1.18	27.96	0.93	39.80	1.32
S8F	522	1400	155.00	68861	54.67	64	0.86	30.78	0.48	81.58	1.28
S12F	743	1400	155.00	68861	67.06	66	1.02	31.54	0.48	97.91	1.49
S8FD	522	1400	155.00	68879	115.49	141	0.82	66.98	0.47	153.41	1.09
A2	232	2789	155.00	87000	55.08	67	0.82	47.15	0.70	69.94	1.04
A3	232	2789	155.00	86917	14.85	13	1.14	12.33	0.95	27.11	2.09
A4	198	2789	155.00	85081	50.46	43	1.17	44.21	1.03	66.76	1.55
C1	324	3903	155.00	87000	68.77	73	0.94	48.46	0.66	97.11	1.33
C2	324	3903	155.00	87000	68.77	76	0.90	48.46	0.64	81.53	1.07
C3	324	3903	155.00	87000	68.77	78	0.88	48.46	0.62	61.77	0.79
SJB10	390	2901	155.00	100071	48.50	38	1.28	27.71	0.73	53.93	1.43
SJB14	765	4800	155.00	100071	84.96	51	1.67	29.45	0.58	91.51	1.79
Average prediction/test						1.08 (0.99)		0.67 (0.64)		1.53 (1.41)	
Standard deviation						0.40 (0.21)		0.21 (0.16)		0.53 (0.29)	

* Note: These were not calculated by the relevant authors. Using their proposed equations the present authors have calculated the values.

7.8 Proposed method to calculate the available rotation capacity of composite flush endplate connections

While the determination of the initial stiffness assumes low internal forces, the determination of rotation capacity requires the opposite. The forces associated with the rotation capacity are the forces in the different components at the connection's ultimate capacity. Hence to calculate the rotation capacity the possible ultimate forces are required, from which the elongation of the associated component may be determined.

7.8.1 Determination of the elongation of components and the rotation capacity

The method described to calculate the moment capacity of connections included the determination of internal forces for all the components considering the effect of loading conditions and the necessary compatibility conditions at the beam-to-column connection interface. The magnitude of the internal forces from this model are used herein to determine the deformation of the components. Whilst the model for initial stiffness dealt with the initial linear behaviour of the connection; the available rotation capacity model requires the plastic deformation of the components. The model is shown in Figure 7-13.

A process similar to that already described when selecting values for key parameters used to calculate the initial stiffness of the connection has been adopted.

It is observed in the composite connection tests that the strain of the reinforcement can vary between 3000με to 15,000με. Elongation of the rebar is calculated by considering plastic strain of the rebar as:

$$\Delta_r = 0.01\left(p_1 + p_2 + \frac{D_c}{2}\right) \tag{7-38}$$

The slip of the stud at the interface of the slab and the beam top flange can be estimated as:

$$\Delta_s = \frac{F_r}{K_{sr}} \tag{7-39}$$

Note: K_{sr} is determined with a secant stiffness of 50 kN/mm. This represents the average failure load to slip at failure observed in push out tests for shear studs.

hence $K_{sr} = 50\ N_s$

Extension of the bolts can be calculated as:

$$\Delta_b = \frac{F_b}{K_b} \tag{7-40}$$

Where K_b has already been defined through equation 7-28.

From this the rotation capacity can be calculated as:

$$\phi = \frac{\Delta_r}{D_r - d_{c,bw}} + \frac{\Delta_s}{D_r - d_{c,bw} - d'_c} + \frac{\Delta_b}{D_r - d_{c,bw} - d'_b} \tag{7-41}$$

Where:

$d_{c,bw}$ is the depth of compression in the beam web

d'_c is the distance of the top of the beam from the rebar

d'_b is the distance of the bolts from the rebar

Tables 7-15, 7-16, 7-17 and 7-18 show the effect of variations of these components on the ratio of prediction to test rotation capacity. From these the selected values are:

$\varepsilon_r = 10{,}000\ \mu\varepsilon$

$l_r = (D_c/2 + p_1 + p_2)\ mm$

$K_{sr} : 50N_s\ kN/mm$

$K_b : 155\ kN/mm$

Where N_s is the smaller of the total number of studs present in the hogging moment region or the number of studs required for full interaction as described in section 7.7.3.2.

Table 7-15 Effect of secant stiffness of the shear studs on the rotation capacity prediction method

K_s (kN/mm)	20	30	40	50
Average	0.82	0.71	0.63	0.59
Standard deviation	0.33	0.27	0.25	0.24

Table 7-16 Effect of stiffness of the bolts on the rotation capacity prediction method

K_b (kN/mm)	50	100	155	200
Average	1.15	0.82	0.72	0.66
Standard deviation	0.52	0.32	0.27	0.25

Table 7-17 Effect of rebar length on the rotation capacity prediction method

l_r (mm)	$(D_c/2 + 225)$	$(D_c/2 + p_1 + p_2)$	$(D_c/2 + p_1 + 2p_2)$
Average	0.59	0.71	0.65
Standard deviation	0.24	0.27	0.25

Note: p_1 is the distance of the first stud from the column face
p_2 is the pitch of the shear studs

Table 7-18 Effect of strain of rebar on the rotation capacity prediction method

ε_r ($\mu\varepsilon$)	3000	5000	7000	10000
Average	0.62	0.71	0.79	0.92
Standard deviation	0.24	0.27	0.30	0.36

7.8.2 Validation of the proposed method

Test results obtained from references 7-5, 7-6, 7-7, 7-8, 7-9, 7-10 and 7-11 are used for the verification of the proposed method. Predictions and test values are compared in Table 7-19. In addition to the test results, comparisons are made against the other available prediction methods. It can be seen that the proposed method predicts the rotation capacity fairly well in many cases, but that in some cases it considerably underestimates the rotation capacity. The proposed model assumes full plasticity in the connection and hence does not account for the brittle type of failure which can occur in connections with low levels of reinforcement, especially with mesh reinforcement only such as SCJ3. Recommendations for connection design [7-13] generally advise against such practice. From Table 7-19 it can be seen that the other methods give higher standard deviations and unsafe predictions of rotation capacity. For example Xiao's method gives an average of 0.95 with a standard deviation of 0.39, SCI method gives an average of 1.66 with a standard deviation of 0.97, while the proposed method gives a standard deviation of only 0.36 with an average of 0.94, making the prediction safer. If the brittle failure mode of the mesh reinforced connections is taken into consideration, i.e. the extension of the bolts and the slip of shear studs is neglected, a much better comparison is obtained. For example, with this modification for SCJ3, rotation becomes 9.27 mrad, which makes the average 0.91 with a standard deviation of 0.29. The reason for the large variations observed in a few cases can be explained from Figure 7-14. From the Figure it is clear that the rotation is very sensitive to the moment at the plastic state of the connection, especially near the ultimate moment capacity. In this region a variation of moment of 5-10% can change the rotation by more than 100%.

Table 7-19 Comparison of predicted and test rotation capacities (see Table 7-4 for references)

Test	*Najafi Anderson*[7-8] *mrad* *	*SCI*[7-24] *mrad* (1) *	*Aribert Lachal*[7-7] *mrad* *	*Xiao*[7-25] *mrad* (2)	*Proposed method* *mrad* (3)	*Test rotation* *mrad* (4)	*Ratios of prediction to test rotation* 1/4	2/4	3/4
JX1	5.30	30.6	2.09	14.1 *	11.99	13	2.36	1.09	0.92
JX2	5.54	30.6	2.09	14.1 *	11.99	10	3.06	1.41	1.20
JC1	4.94	30.6	2.09	14.1 *	11.99	10	3.06	1.41	1.20
JC2	7.26	27.0	2.09	14.1 *	10.96	18	1.50	0.77	0.61
CJS-1	8.42	36.4	2.12	33.4	28.87	35	1.04	1.04	0.82
CJS-2	8.17	36.4	2.12	33.4	28.87	42	0.87	0.87	0.69
CJS-3	6.89	36.4	2.12	33.4	24.03	18	2.02	2.02	1.34
CJS-4	8.24	36.4	2.12	33.4	30.68	58	0.63	0.63	0.53
CJS-5	9.15	36.4	2.12	33.4	41.24	60	0.61	0.61	0.69
CJS-6	8.08	36.4	2.12	33.4	24.77	22	1.65	1.65	1.13
SCJ3	3.59	8.4	1.17	8.8	15.58 (9.27)	7.2	1.16	1.22	2.16 (1.29)
SCJ4	6.84	36.4	5.83	23.5	13.41	23.4	1.55	1.00	0.57
SCJ5	8.11	36.4	5.83	23.5	20.14	26	1.40	0.90	0.77
SCJ6	5.31	36.4	5.83	20.5	16.52	11.5	3.16	1.78	1.44
SCJ7	6.87	43.3	7.00	23.5	16.11	26.5	1.63	0.89	0.61
Test1	8.51	44.6	6.75	18.7	18.09	20	2.23	0.94	0.90
Test3	6.24	27.3	3.87	12.9	21.31	15.7	1.74	0.82	1.36
Test4	7.70	61.9	9.63	9.5	18.09	12	5.15	0.79	1.51
Test7	9.57	61.9	9.63	24.5	18.09	24	2.58	1.02	0.75
Test10	6.22	32.6	6.75	14.3	12.76	14	2.33	1.02	0.91
S4F	6.40	19.3	2.53	13.5 *	20.17	15	1.29	0.90	1.34
S8F	8.51	34.5	5.07	19.9 *	19.23	30	1.15	0.66	0.64
S12F	9.57	47.4	7.22	26.2 *	18.09	25	1.90	1.05	0.72
S8FD	6.21	25.2	5.07	15.2 *	13.45	14	1.80	1.08	0.96
A2	6.82	19.9	1.01	11.8 *	17.60	26	0.77	0.45	0.68
A3	12.83	31.9	1.01	16.3 *	35.48	36	0.89	0.45	0.99
A4	7.34	23.3	1.01	11.8 *	24.17	35	0.66	0.34	0.69
C1	7.69	26.0	1.41	14.0 *	17.60	28	0.93	0.50	0.63
C2	7.29	26.0	1.88	15.5 *	17.30	29	0.90	0.54	0.60
C3	6.44	26.0	2.82	21.8 *	17.00	21	1.24	1.04	0.81
SJB10	7.51	17.5	0.87	16.8	18.43	22	0.79	0.76	0.84
SJB14	8.86	29.1	1.71	20.5	27.54	24	1.21	0.86	1.15
						Average	1.66	0.95	0.94 (0.91)
						SD	0.97	0.39	0.36 (0.29)

* Note: These were not calculated by the relevant authors. Using their proposed equations the present authors have calculated the values.

7.9 The overall behaviour

It has been observed from the test results for endplate connections that the overall behaviour can be best described by a combination of straight lines and an elliptical arc. The first part of the curve can be assumed as linear elastic (up to 0.45 M_u). Beyond this up to the point which the connection attains its ultimate moment capacity (0.45 M_u to 1.00 M_u) response can be represented by the arc of an ellipse; the final part is plastic. The relationship can be defined as:

$$M = K_i\phi \qquad 0 \le \phi \le \frac{0.45M_u}{K_i}$$

$$M = 0.45M_u + b\sqrt{1-\left[\frac{\phi_u - \phi}{a}\right]^2} \qquad \frac{0.45M_u}{K_i} \le \phi \le \phi_u$$

$$M = M_u \qquad \phi \ge \phi_u$$

Where constants a and b are defined as:

$$a = \phi_u - 0.45\frac{M_u}{K_i}$$

$$b = 0.55M_u$$

The derivation of the overall behaviour is explained in Figure 7-15. During the derivation of initial stiffness it was assumed that up to 0.45 M_u the moment rotation curve is linear, hence the equation of line OA is the equation of the line passing through the origin and having a slope equal to the initial stiffness. As soon as the connection attains its full moment capacity the moment-rotation curve will have a zero or negative slope (unloading); this is approximated as a straight line parallel to the rotation axis. The relation in between is approximated as an elliptical arc. "R" the centre of the ellipse is located by the intersection of lines AR and BR parallel to the rotation and moment axes respectively. The successful tracing of a moment-rotation curve depends on the successful determination of several items which are: moment

capacity, initial stiffness and available rotation capacity. Comparisons of test and predicted overall behaviour are shown in Figures 7-16 to 7-22 for CJS-1, CJS-6, SCJ5, SCJ6, Test4, S8F and SJB10. The results show that the proposed method can predict the overall behaviour of the endplate connections with sufficient accuracy if the geometry and exact material properties are known.

7.10 Conclusions

A unified method - based on a fundamental consideration of equilibrium of the force transfers between the individual components - for predicting the moment capacity of composite endplate connections has been presented. In addition to allowances for variations in the connection detail e.g. reinforcement ratio, member sizes, number of bolts etc., it also recognises the influence of axial column load and the ratio of shear to moment present. It can deal with symmetrical (balanced) and non-symmetrical arrangements of load. Predictions from the method have been compared with the results of 32 laboratory tests from 7 different sources and with a further 21 numerical results so as to provide validation over the full range of parameters. Because the method predicts the ultimate capacity, it employs ultimate (strain hardening) material strengths.

All checks in the method have been provided as explicit formulae. It is therefore possible to select the governing mode of failure or to optimise performance against certain fixed properties. However, due to the volume of calculations required, the procedures are best implemented via a spreadsheet. This permitted the effects of varying the connection details to be readily examined. Some illustrations of this have been presented as a way of identifying the main behavioural trends. These provide guidance on suitable levels of reinforcement.

Starting from the basic mechanism of force transfer within the components of a composite connection, a method has been proposed herein to estimate the initial stiffness and available rotation capacity of major axis flush endplate composite connections. The method is fully compatible with the method proposed for the prediction of moment capacity. Comparisons against test data have demonstrated that the method is capable of predicting the initial stiffness and rotation capacity of flush endplate connections with very good accuracy.

It can be seen from the comparison of the predicted and test results that it is more easy to predict the initial stiffness but it is difficult to predict the rotation capacity correctly. This is because of the fact that the ultimate capacity of the connection may be governed by many criteria (such as buckling of component) which cannot be predicted accurately. Also the exact determination of internal forces is essential during the rotation capacity prediction, a few percentage of variation of forces near the ultimate capacity can cause a large variation in rotation. This small variation of forces does not affect the moment capacity of the connection so much. Allowing for this the prediction gives reliable estimates of rotation capacity and initial stiffness that closely match the test values. A simplified model to represent the overall behaviour of a given connection detail has also been proposed.

7.11 References

7-1 Li, T. Q., Nethercot, D. A. and Choo, B. S. (1996) *Behaviour of flush end plate composite connections with unbalanced moment and variable shear/moment ratios: part 2: prediction of moment capacity*, Journal of Constructional Steel Research, Vol. 38, No. 2, pp. 165-198.

7-2 Eurocode No 4 (1992) *Design of Composite Steel and Concrete Structures*, March, European Committee for Standardisation (CEN).

7-3 Eurocode No 3 (1992) *Design of Steel Structures, Part 1.1: General Rules for Buildings*, DD ENV 1993-1-1, April 1992, European Committee for Standardisation (CEN).

7-4 Ahmed, B. and Nethercot, D. A. *Effect of column axial load on composite connection behaviour*, Structural Engineering Review (under review).

7-5 Li, T. Q., Nethercot, D. A. and Choo, B. S. (1996) *Behaviour of flush end plate composite connections with unbalanced moment and variable shear/moment ratios: part 1: experimental behaviour*, Journal of Constructional Steel Research, Vol. 38, No. 2, pp. 125-164.

7-6 Xiao, Y., Choo, B. S. and Nethercot, D. A. (1994) *Composite connections in steel and concrete. I. experimental behaviour of composite beam-column connections*, Journal of Constructional Steel Research, Vol. 31, pp. 3-30.

7-7 Aribert, J. M. and Lachal, A. (1992) *Experimental investigation of composite connection and global interpretation.* Proceedings of the COST C1 conference on semi-rigid joints, Strasbourg, France, pp. 158-169.

7-8 Anderson, D. and Najafi, A. A. (1994) *Performance of Composite Connections: Major Axis End Plate Joints*, Journal of Construction Steel Research, Vol. 31, No 1, pp. 31-57.

7-9 Najafi, A. A. and Anderson, D. (1992) *Composite Connections with Structural Steel Endplate*, Final report to SCI, Department of Engineering, University of Warwick, UK.

7-10 Law, C. L. C. (1981) *Planar no-sway frames with semi-rigid beam-to-column joints*, Ph.D. thesis, Department of Engineering, University of Warwick, UK.

7-11 Benussi. F., Puhali, R. and Zandonini, R. (1989) *Semi-rigid joints in steel-concrete composite frames*, Construzioni Metalliche, No. 5, pp. 1-28.

7-12 Li, T. Q. (1994) *The analysis and ductility requirements of semi-rigid composite frames*, Volume II, Ph.D. thesis, Department of Civil Engineering, University of Nottingham, UK.

7-13 SCI (1995) *Moment Connections in Composite Construction: Interim Guidance for End-Plate Connections*, Technical Report, SCI publication 143.

7-14 Ahmed, B. and Nethercot, D. A. (1995) *Numerical Modelling of Composite Flush endplate Connections*, Journal of Singapore Structural Steel Society, Vol. 6, No.1, pp. 87-102.

7-15 Ahmed, B. and Nethercot, D. A. *Effect of high shear on the moment capacity of composite cruciform endplate connections*, Journal of Constructional steel Research (in press).

7-16 Ren, P. and Crisinel, M. (1996) *Prediction method for moment-rotation behaviour of composite beam to steel column connections*, Connections in Steel Structures III: Behaviour, Strength and Design, Edited by Reidar Bjorhovde, Andre Colson, Riccardo Zandonini, Proceedings of the Third International Workshop, Trento University, 29-31 May 1995, pp.33-46.

7-17 CEN/TC 250 (1994) *New Revised Annex J of Eurocode 3*: Part 1.1, CEN document N419E.

7-18 Benussi, F. and Noe, S. *On the modelling of semi-rigid connections,* Journal of Construction Steel Research, to be published.

7-19 Chapman, J. C. (1964) *Experiments on composite beams*, The Structural Engineer, November, Volume 42, No 11, pp. 369-383.

7-20 Lloyd, R. M. and Wright, H. D. (1990) *Shear Connection between Composite Slabs and Steel Beams*, Journal of Constructional Steel Research, Vol. 15, pp. 255-285.

7-21 Lam, D., Elliot, K. S. and Nethercot, D. A. *Push off tests on studs with hollow cored floor slabs* (in preparation).

7-22 Razaqpur, A. G. and Nofal, M. (1989) *A Finite Element for Modelling the Nonlinear behaviour of Shear Connectors in Composite Structures*, Computers & Structures Vol. 32, No. 1, pp. 169-174.

7-23 Mistakidis, E. S., Thomopolos, K. T., Avdelas, A. and Panagiotopoulos, P. D. (1995) *Analysis of composite beams with shear connectors allowing for softening*, Steel Structures - Eurosteel '95, Kounadis (ed.) Balkema, Rotterdam, pp. 73-80.

7-24 SCI report (1992) *Partial strength moment resisting connections in composite frames,* Document No. SCI-RT-275, Revision 0, April.

7-25 Xiao, Y. (1994) *Behaviour of Composite Connections in Steel and Concrete*, Ph.D. thesis, University of Nottingham, UK.

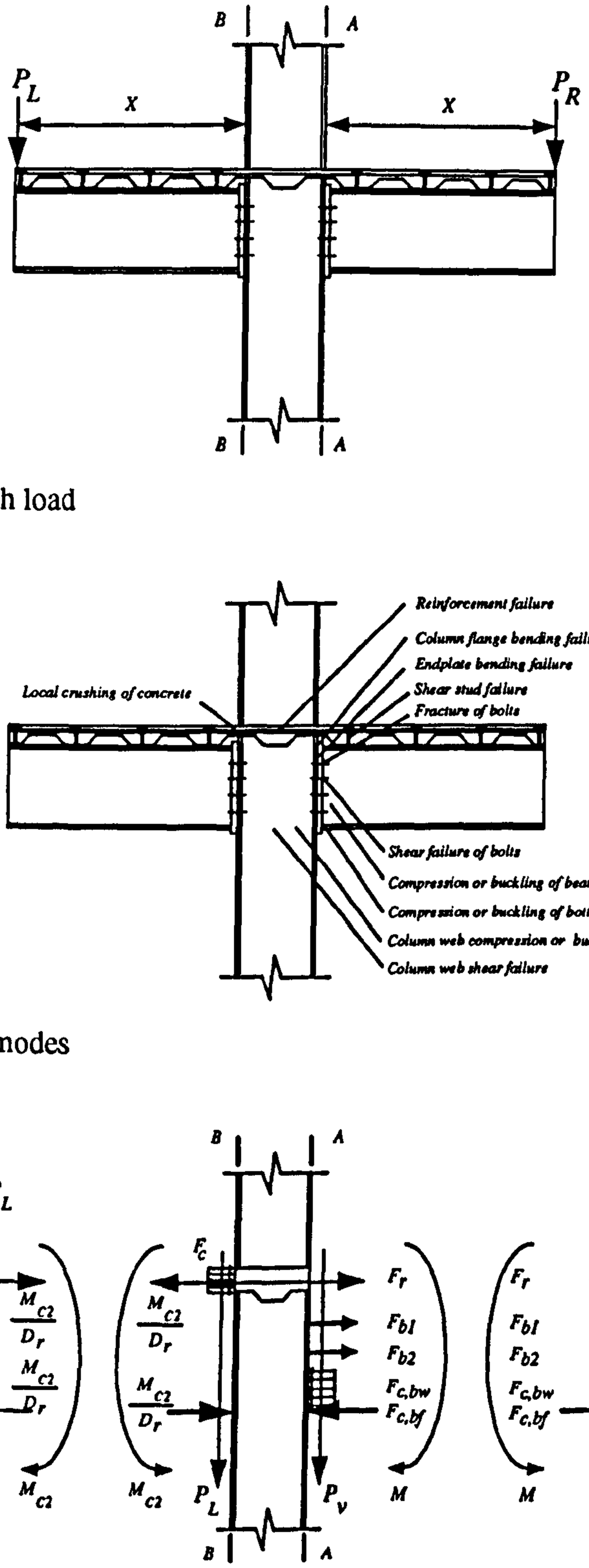

(a) Connection with load

(b) Possible failure modes

(c) Free body diagram of the connecting patrs

Note: $M_{c2} = \eta M$

Figure 7-1 Non-symmetrically loaded composite flush endplate connection with internal forces

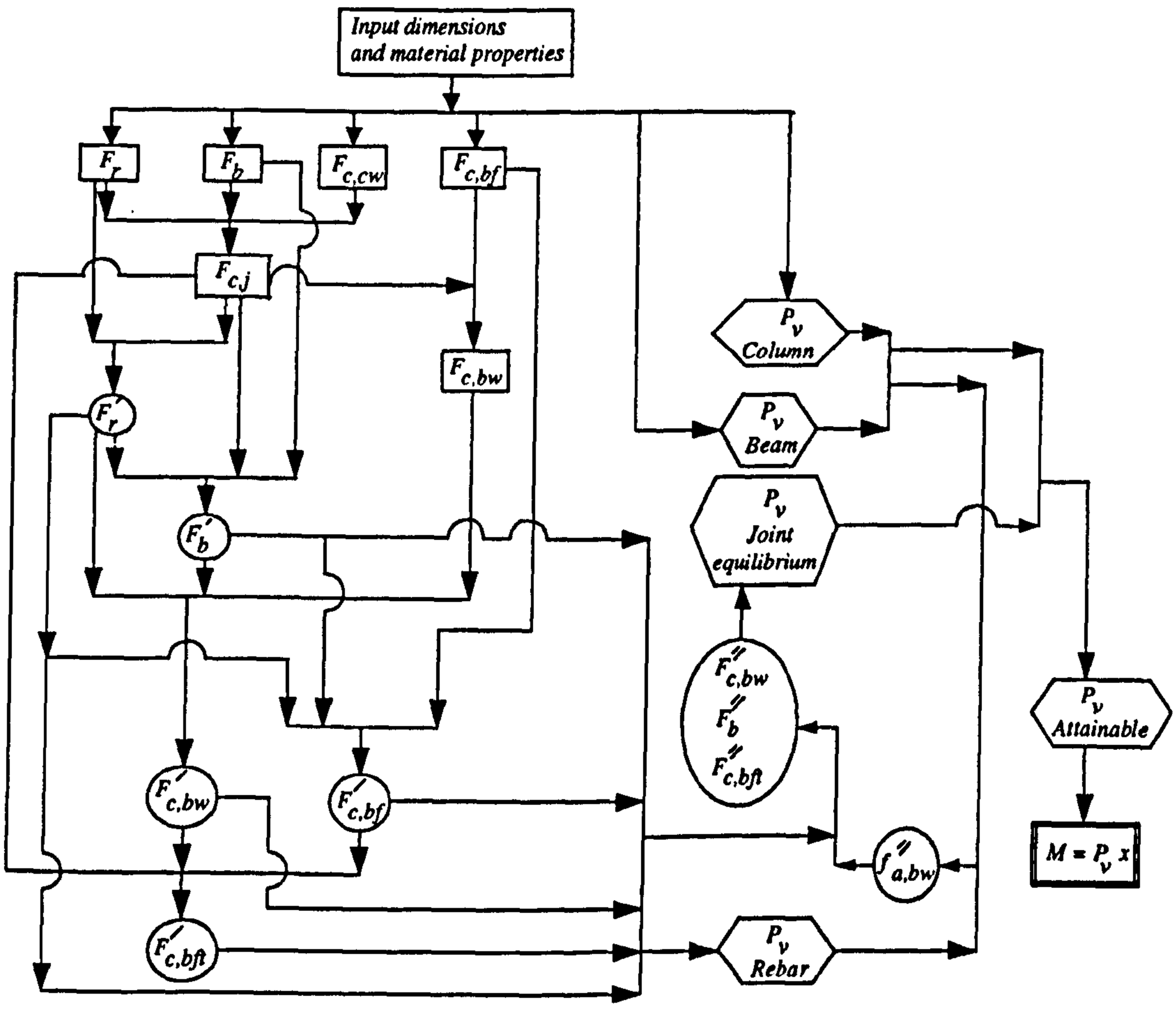

Figure 7-2 Simplified flow chart for calculating the composite connection moment capacity

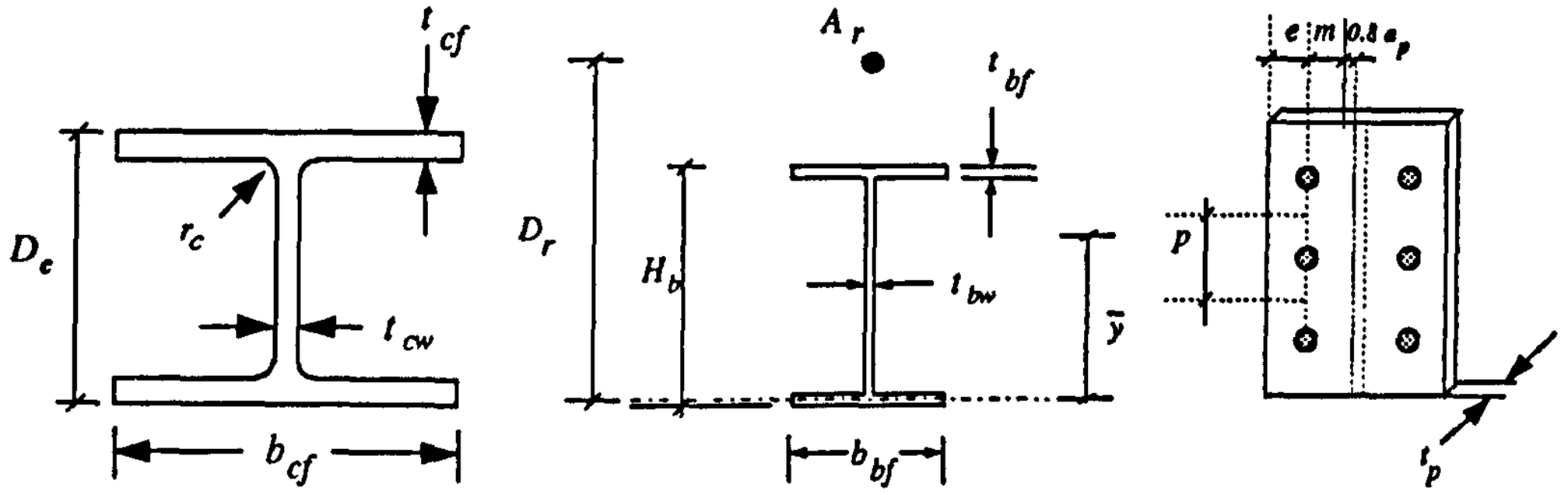

(a) Column section (b) Beam section with reinforcement (c) Endplate

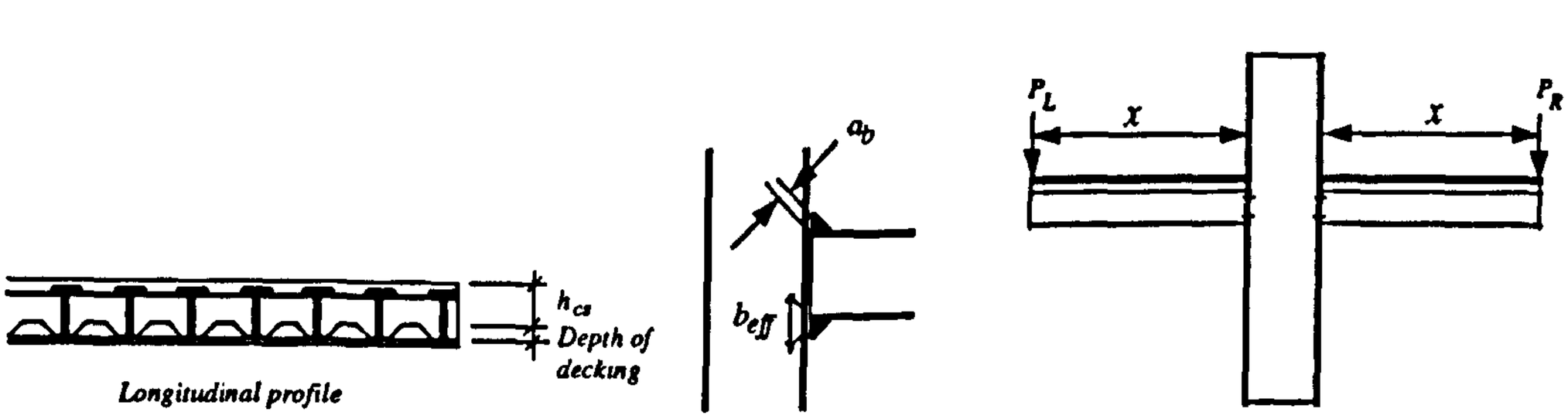

(d) Concrete slab (e) Column & weld (f) Connection and load position

Note: Similar definitions for e and m are used for both the column flange and the endplate. Both equation is to use the minimum e.

$$b_{eff} = t_{cf} + 2\sqrt{2}a_p + 2t_p + 5\left(t_{cf} + r_c\right) \quad \textit{EC3: Part 1.1, J.2.4.1}$$

Figure 7-3 Definition of terms used in the equations

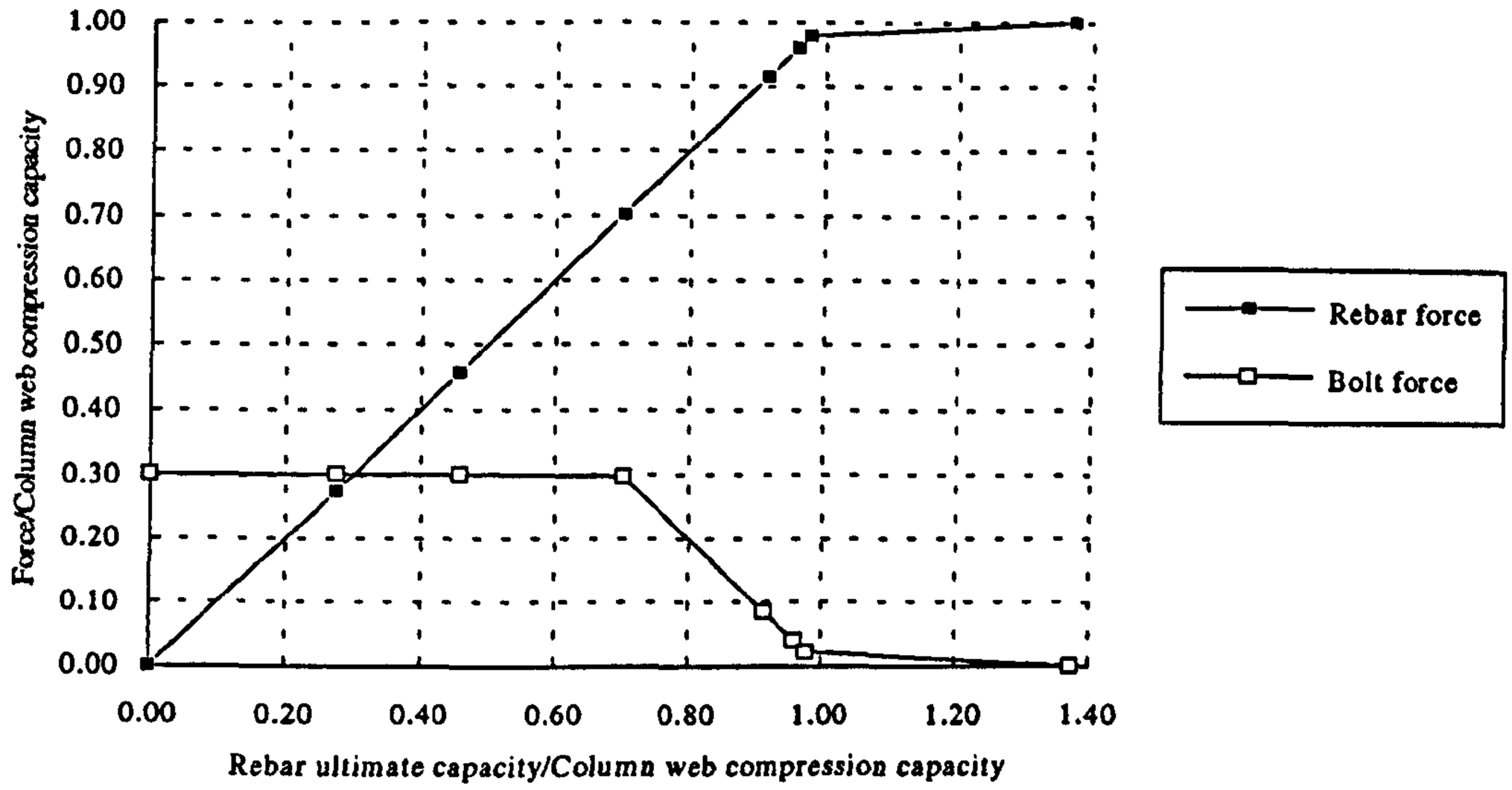

Figure 7-4 Forces in rebars and bolts for varying rebar area in a cruciform connection

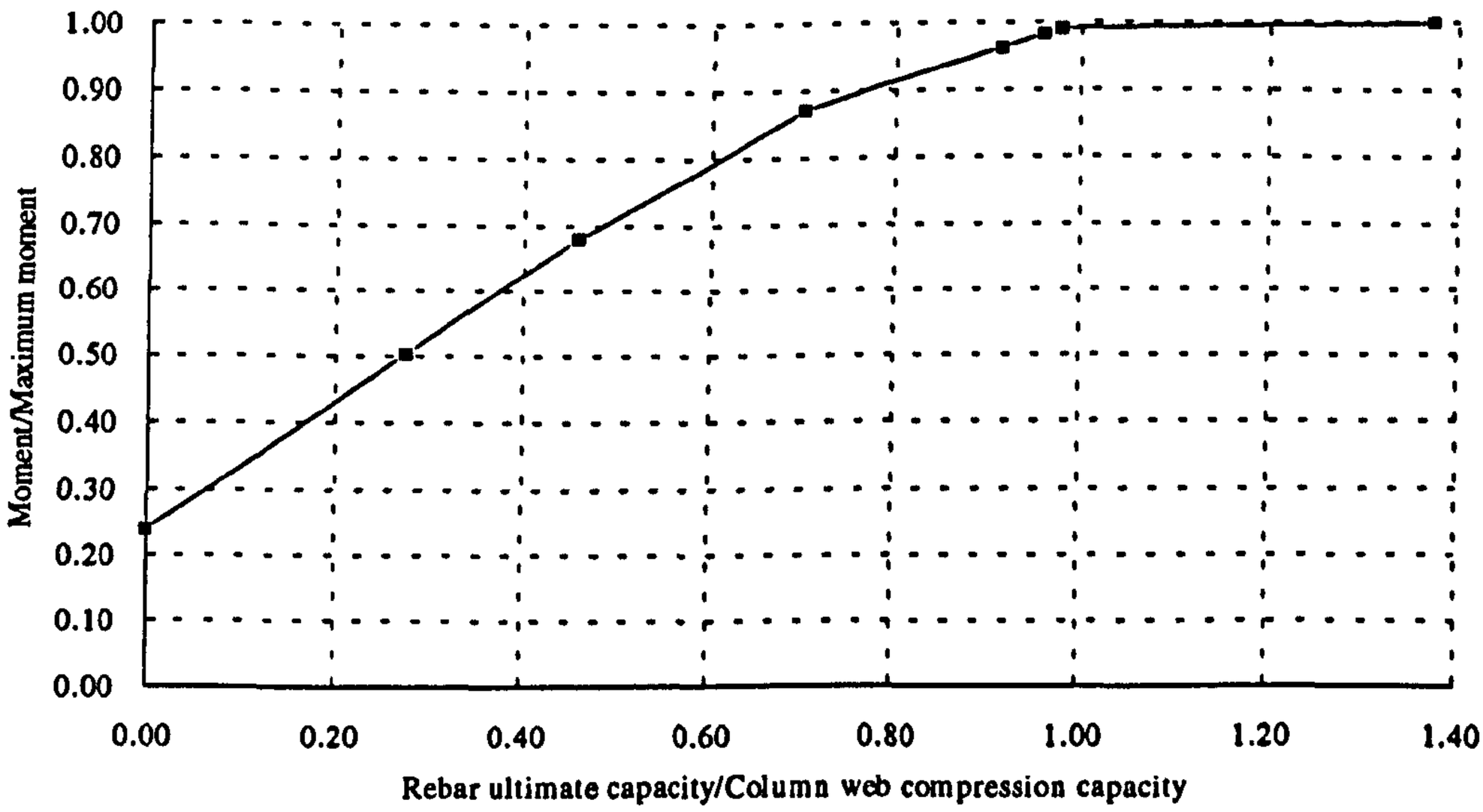

Figure 7-5 Moment capacity for varying rebar area in a cruciform connection

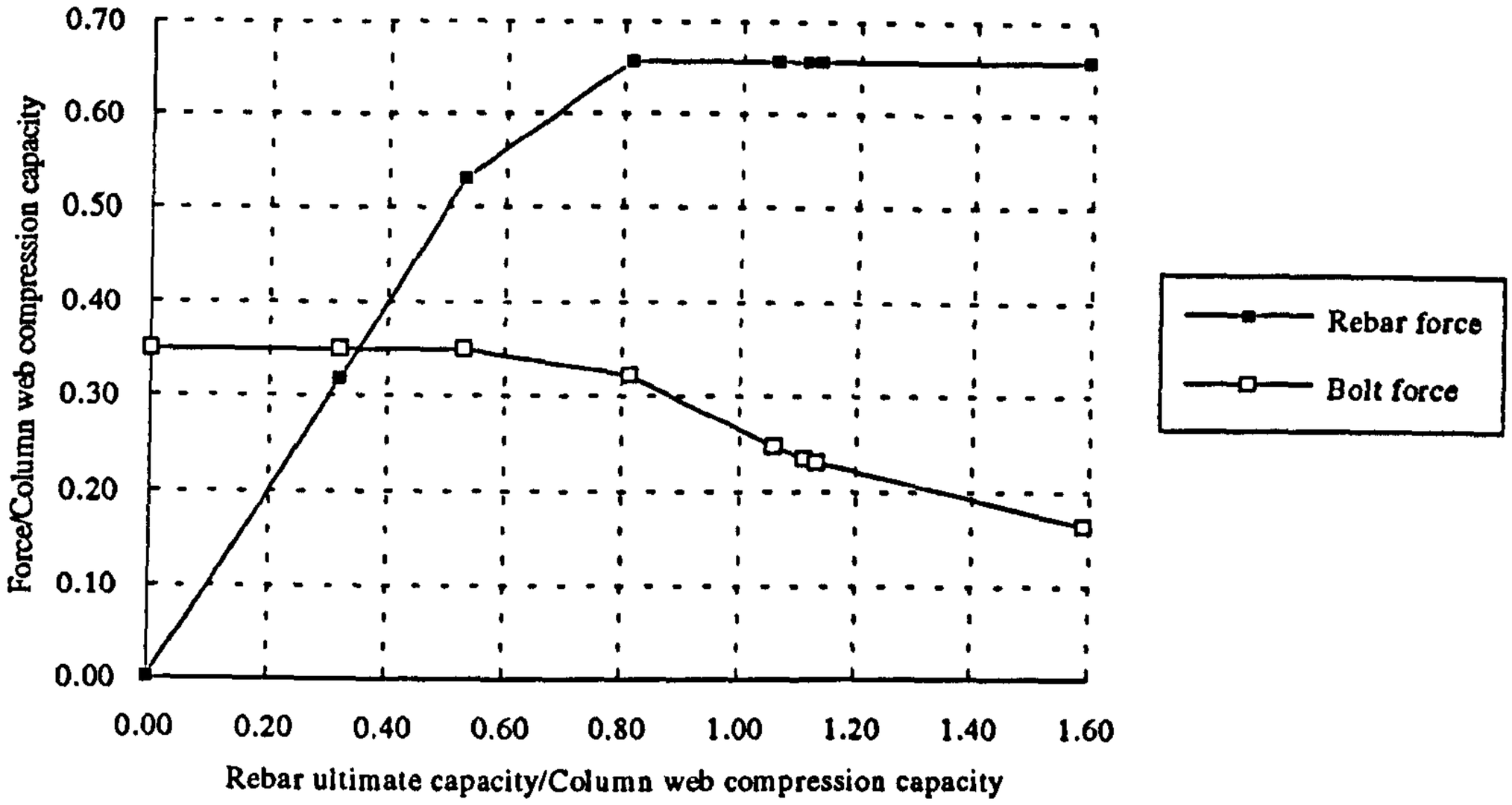

Figure 7-6 Forces in rebars and bolts for varying rebar area in a non-symmetric connection

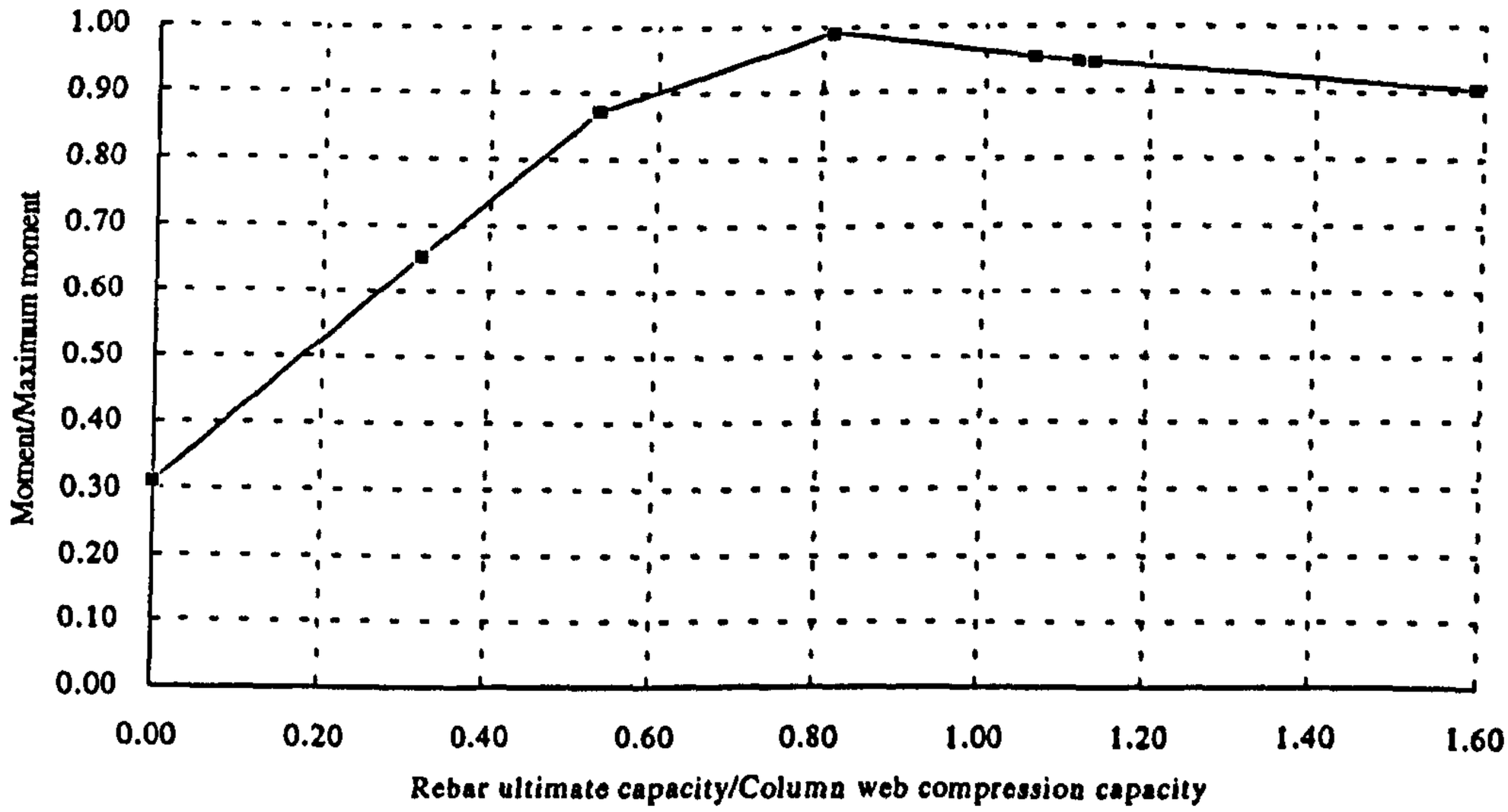

Figure 7-7 Effect of rebar area on the moment capacity of non-symmetric flush endplate connections

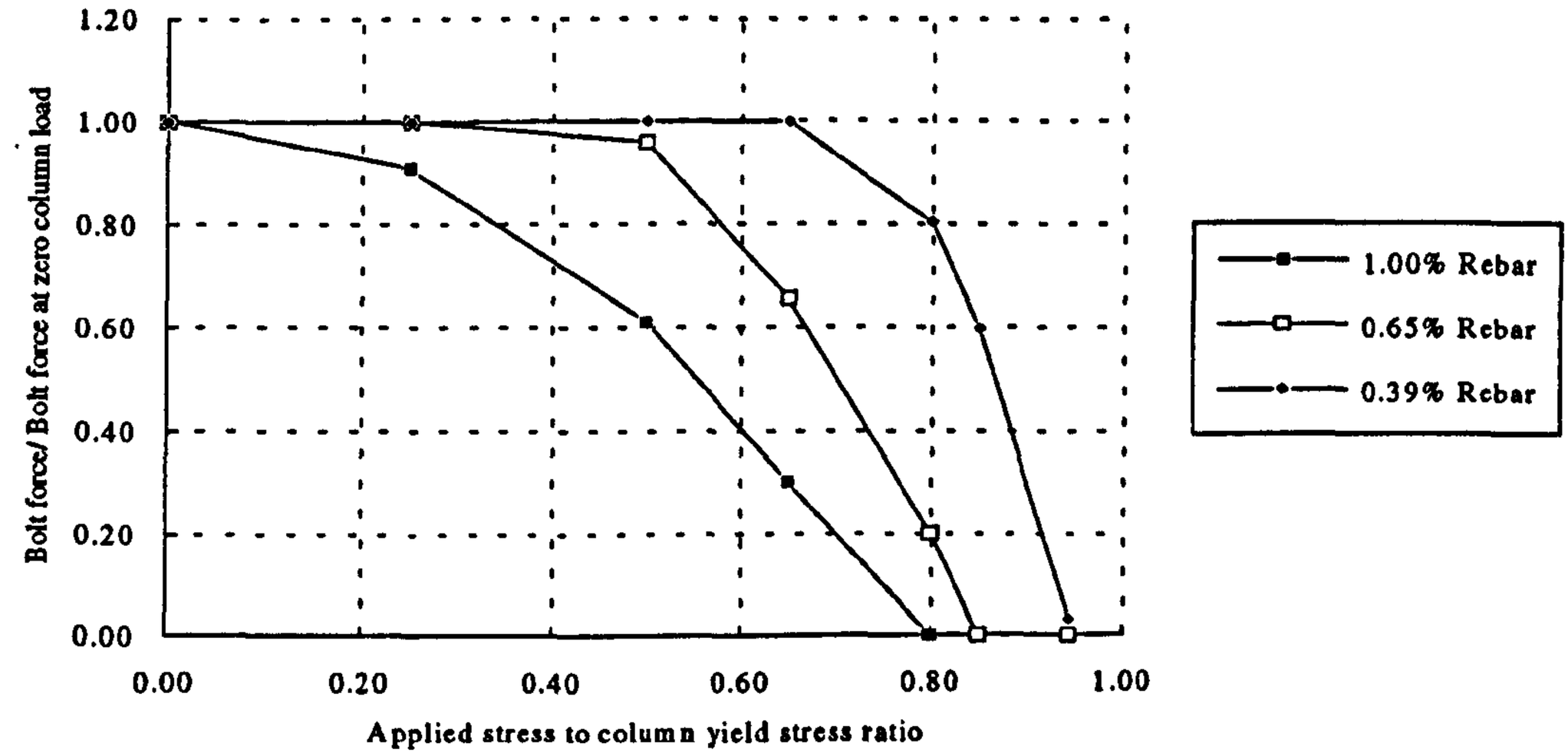

Figure 7-8 Effect of column stress on the bolt force in a non-symmetrically loaded flush endplate connections with zero "other side" moment

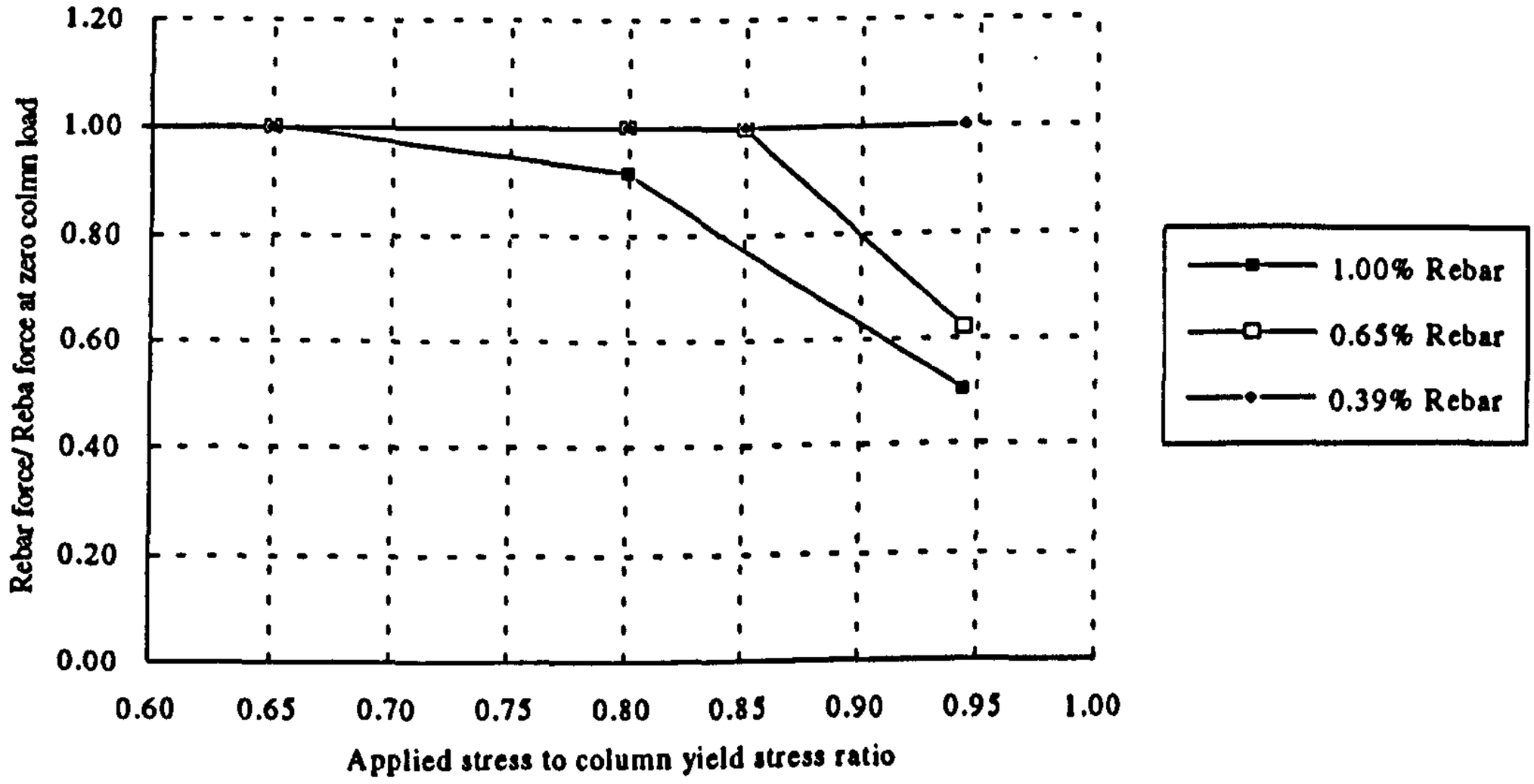

Figure 7-9 Effect of column stress on the rebar force in a non-symmetrically loaded flush endplate connections with zero "other side" moment

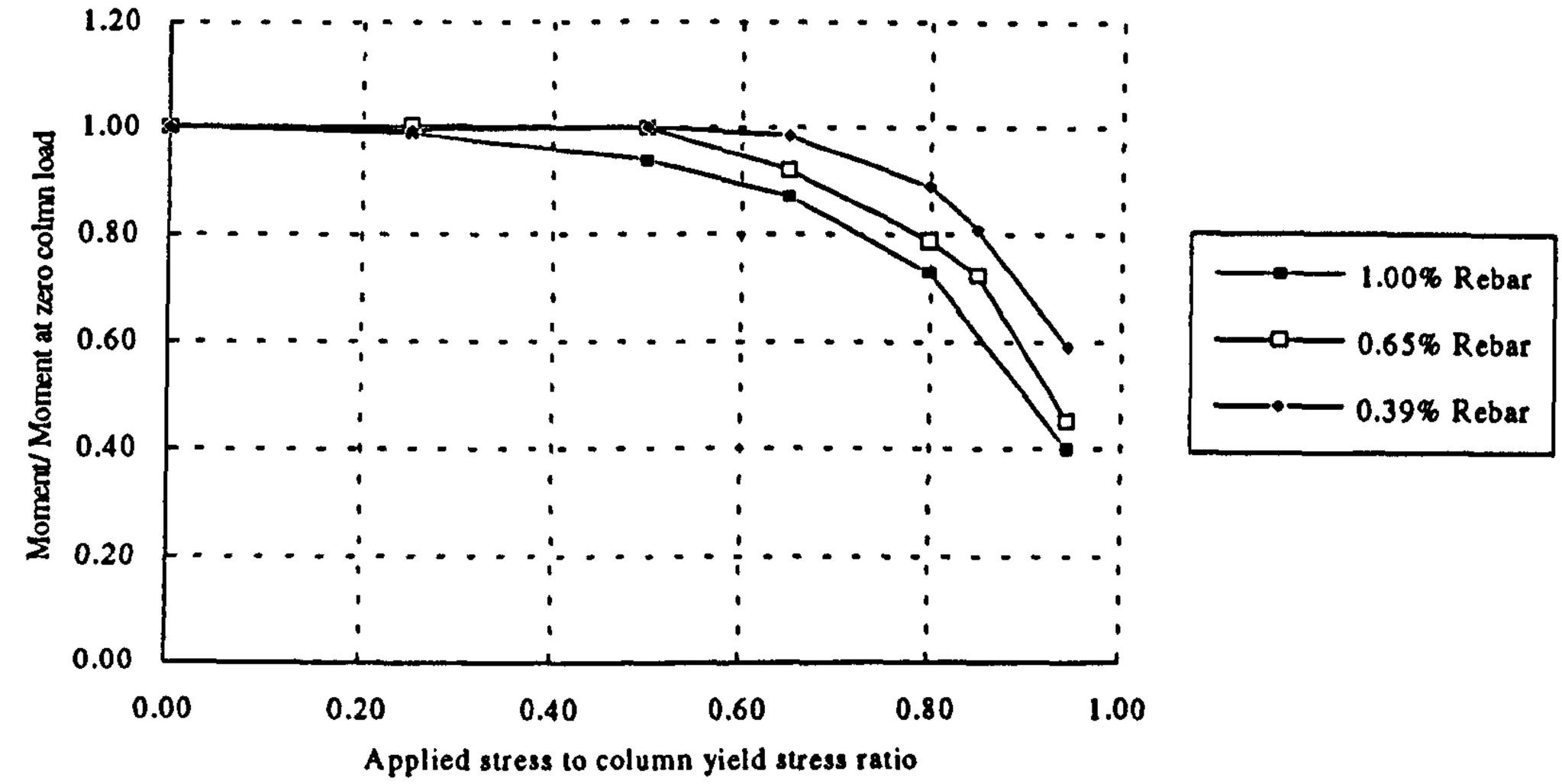

Figure 7-10 Effect of column stress on the moment capacity of non-symmetrically loaded flush endplate connections with zero "other side" moment

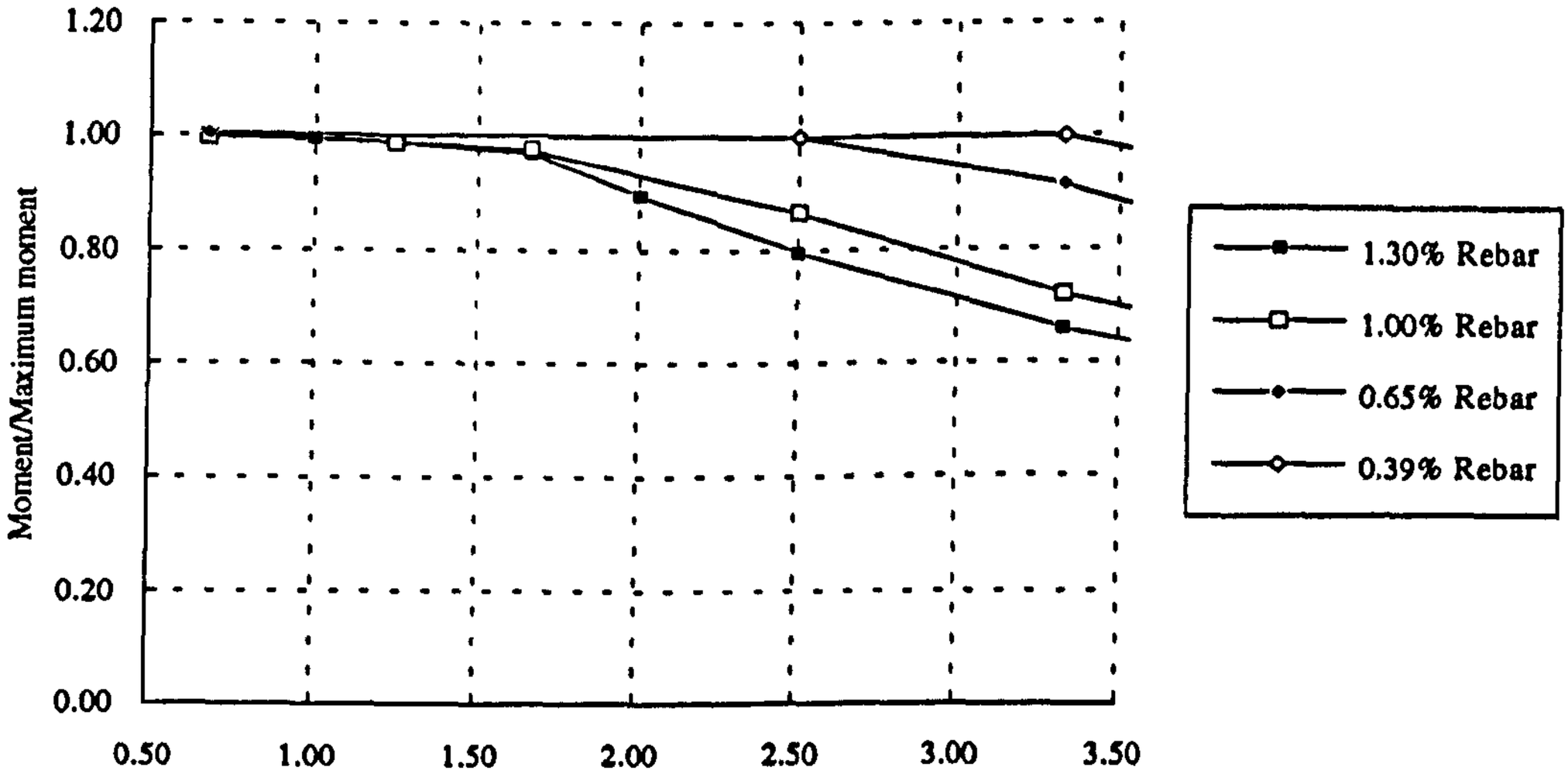

Figure 7-11 Effect of shear to moment ratio on the moment capacity of symmetrically loaded flush endplate connections

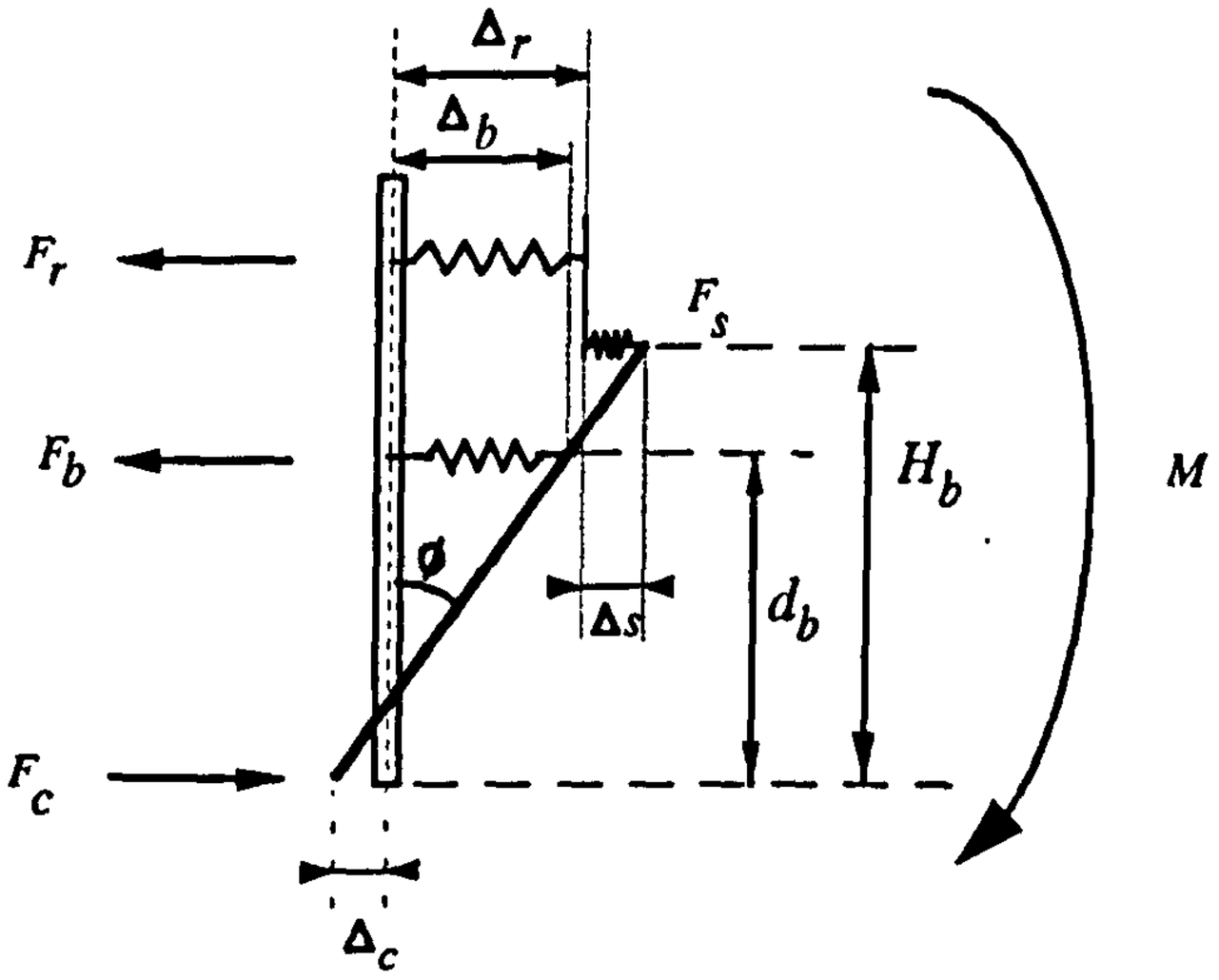

Figure 7-12 A spring model for composite cruciform flush endplate connections

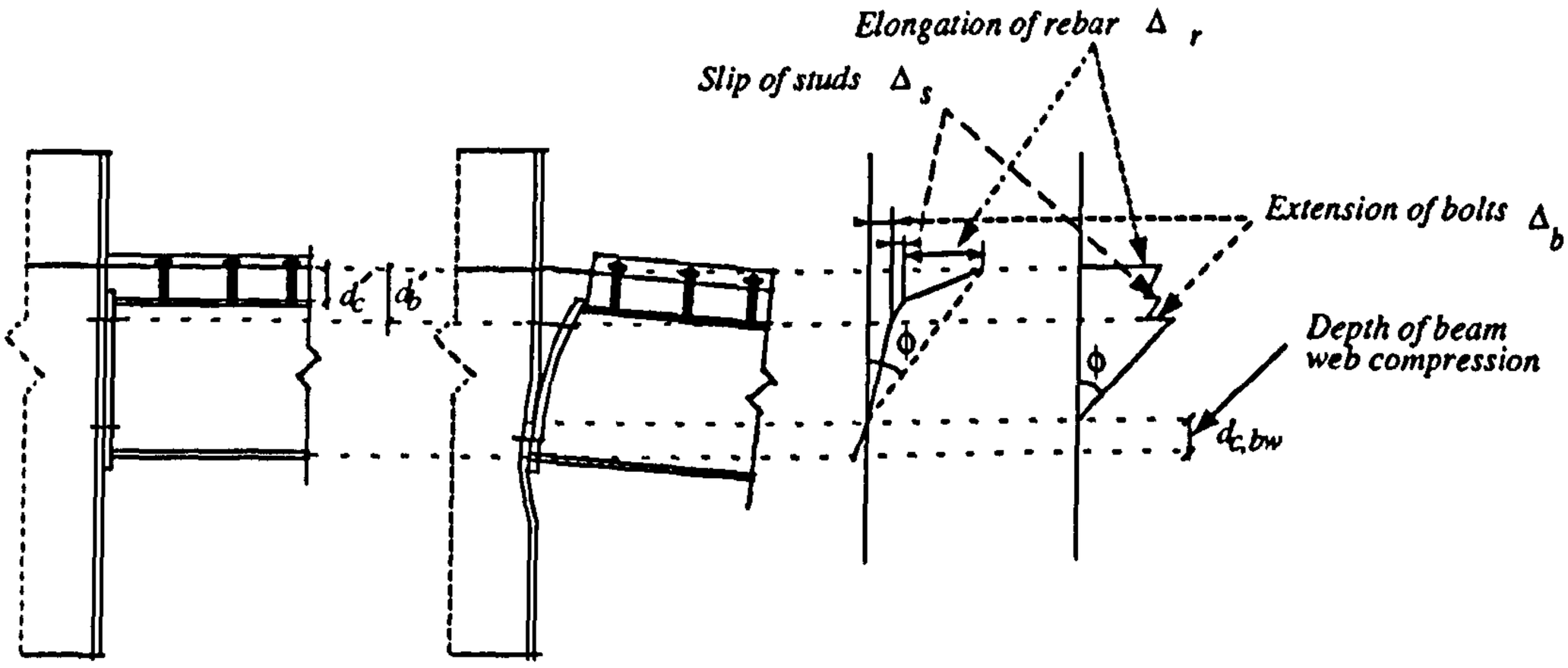

(a) Connection before deformation

(b) Connection after deformation

(c) Deformation of components at connection face

(d) Representation of deformations for rotation calculation

Figure 7-13 Beam to column connection available rotation model

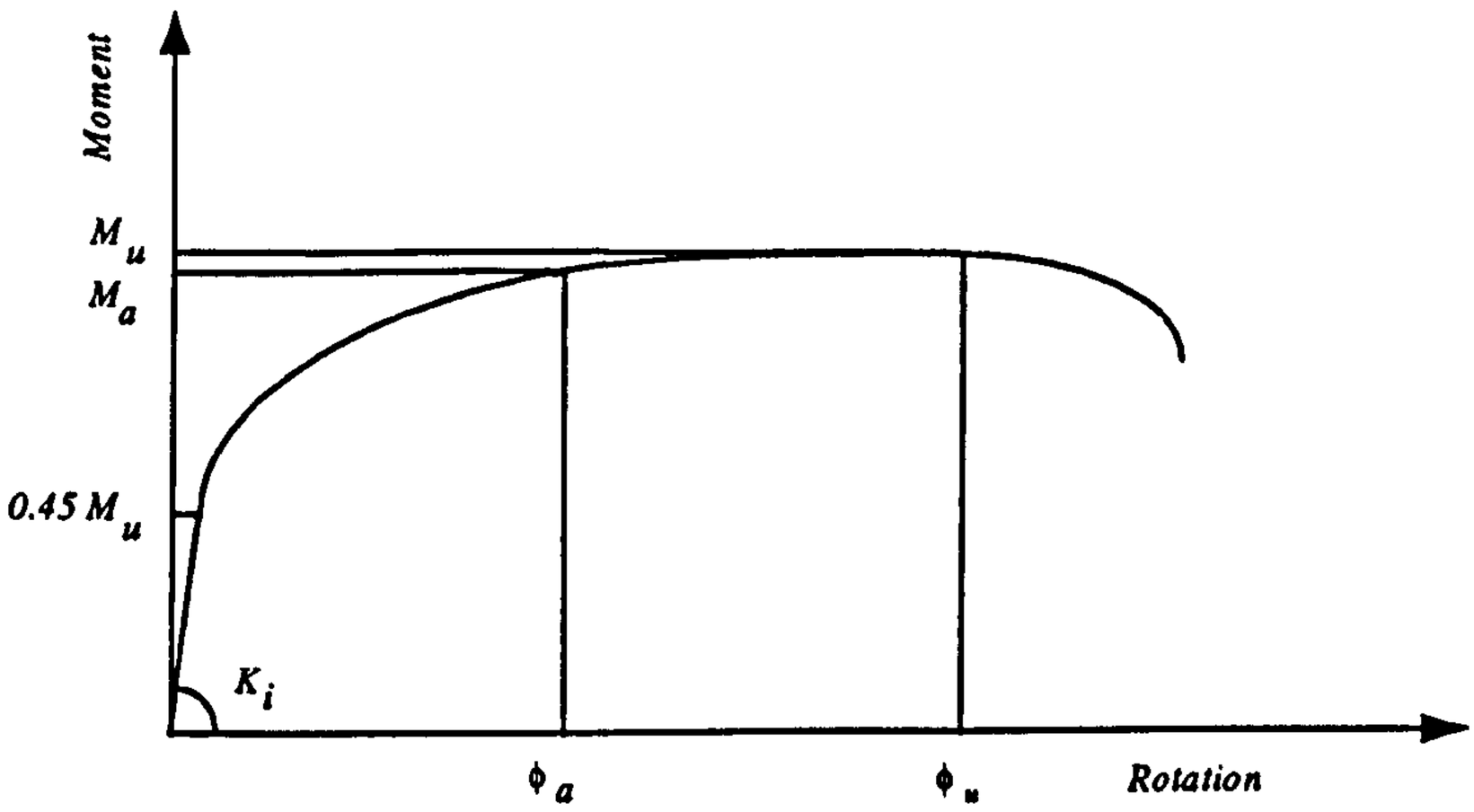

Figure 7-14 Typical moment rotation curve showing the initial stiffness and the rotation capacity

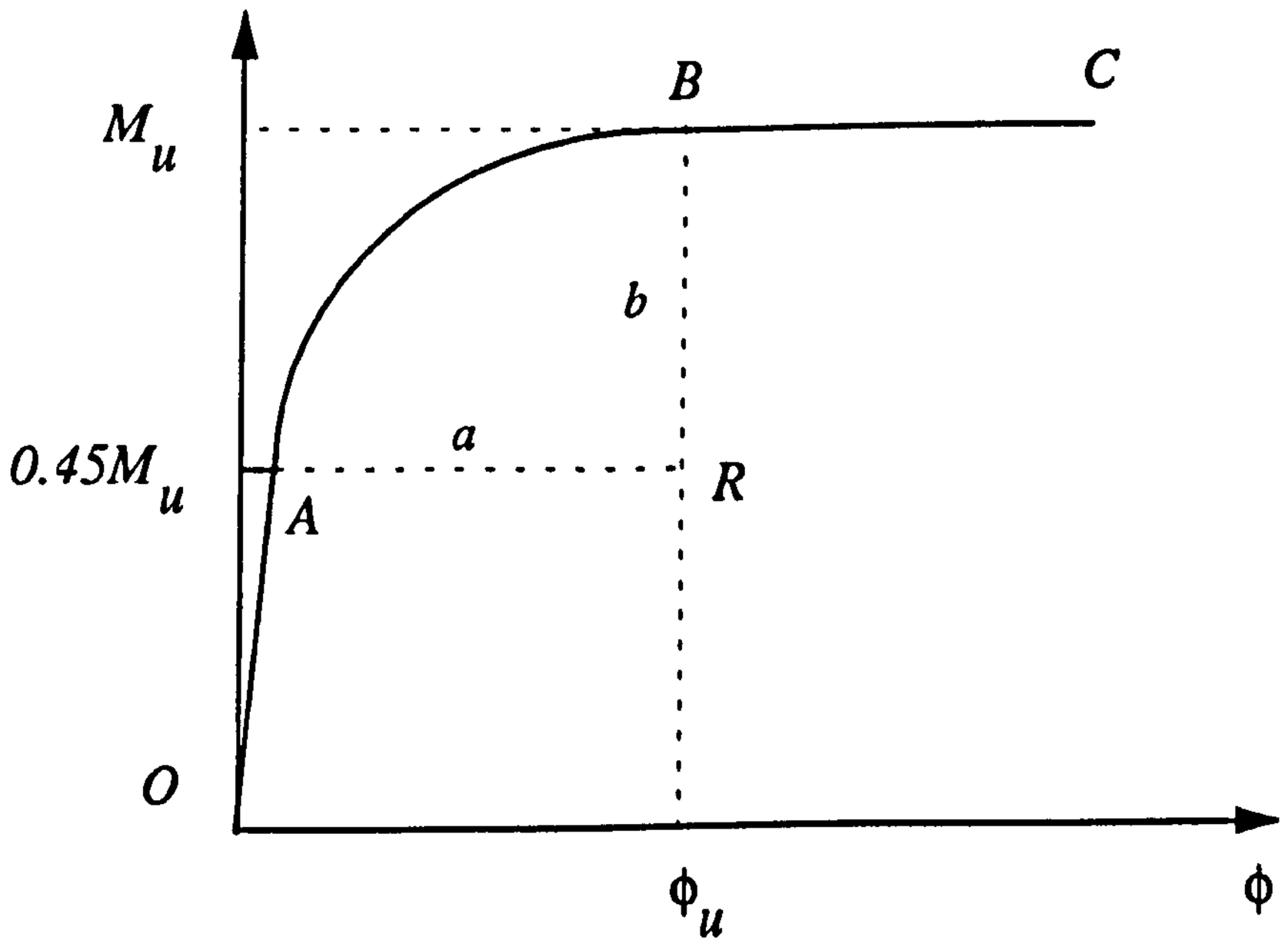

Figure 7-15 Model for overall behaviour of flush endplate connection

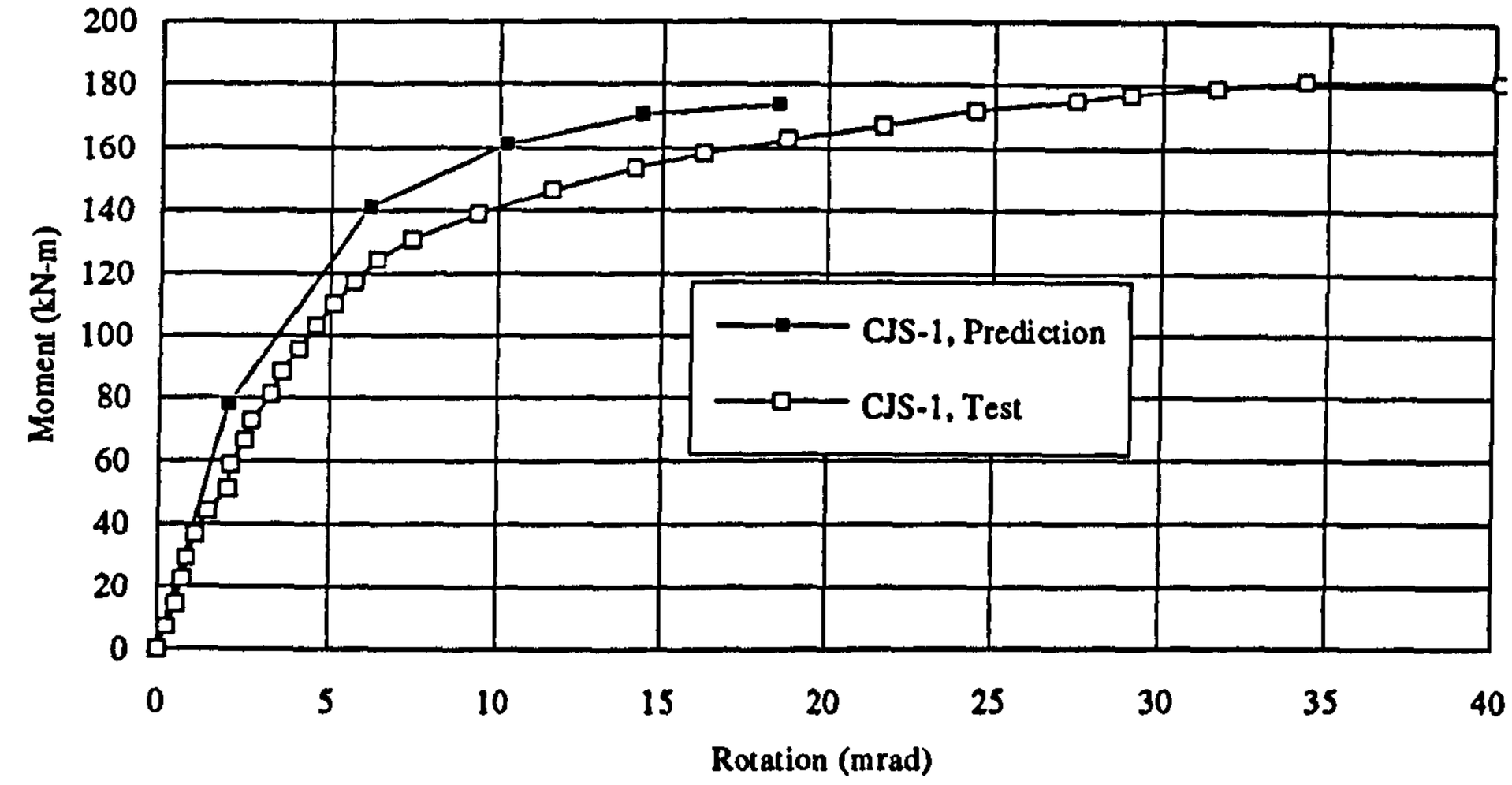

Figure 7-16 Comparison of test and predicted overall behaviour of test CJS-1

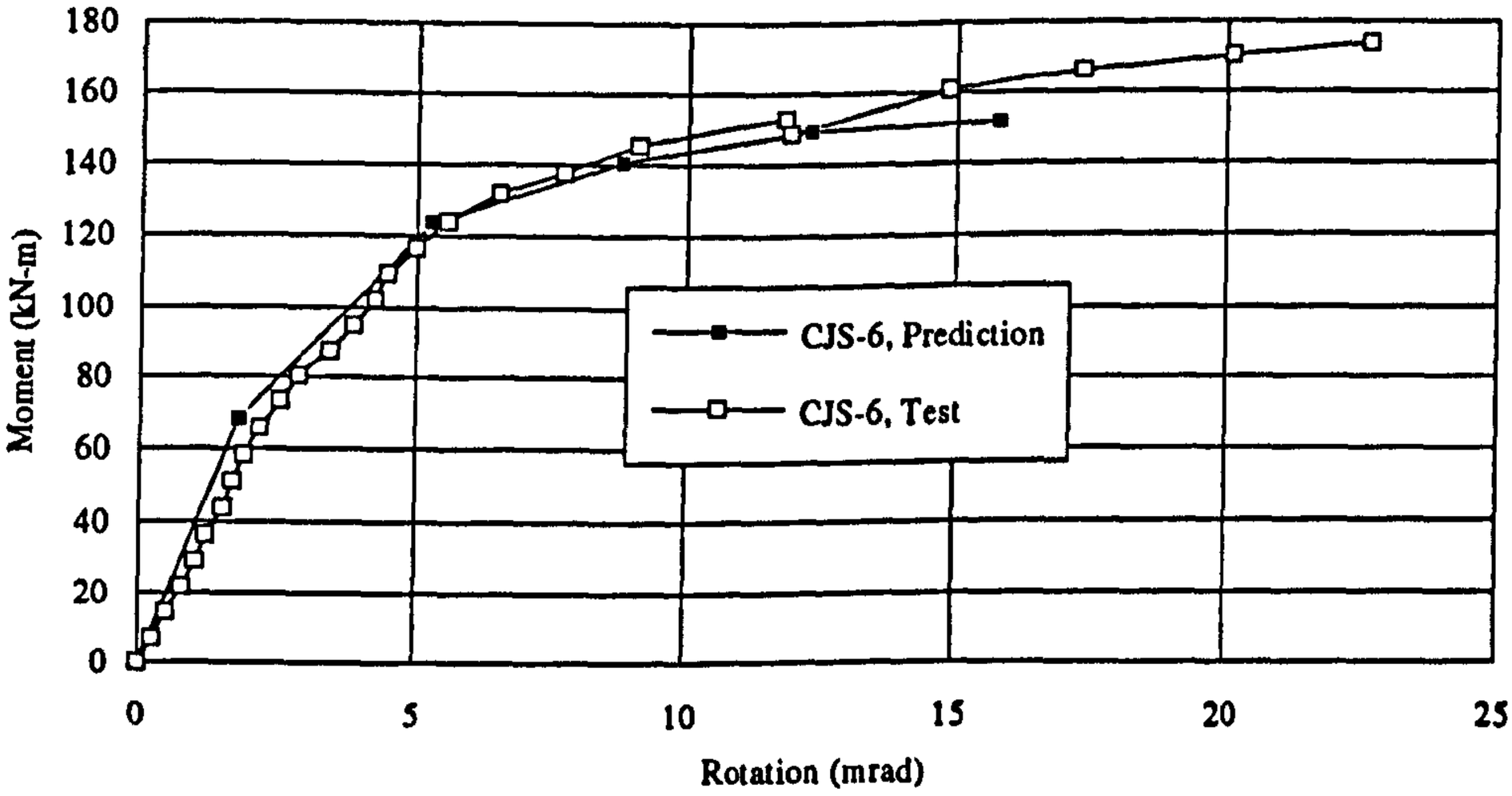

Figure 7-17 Comparison of test and predicted overall behaviour of test CJS-6

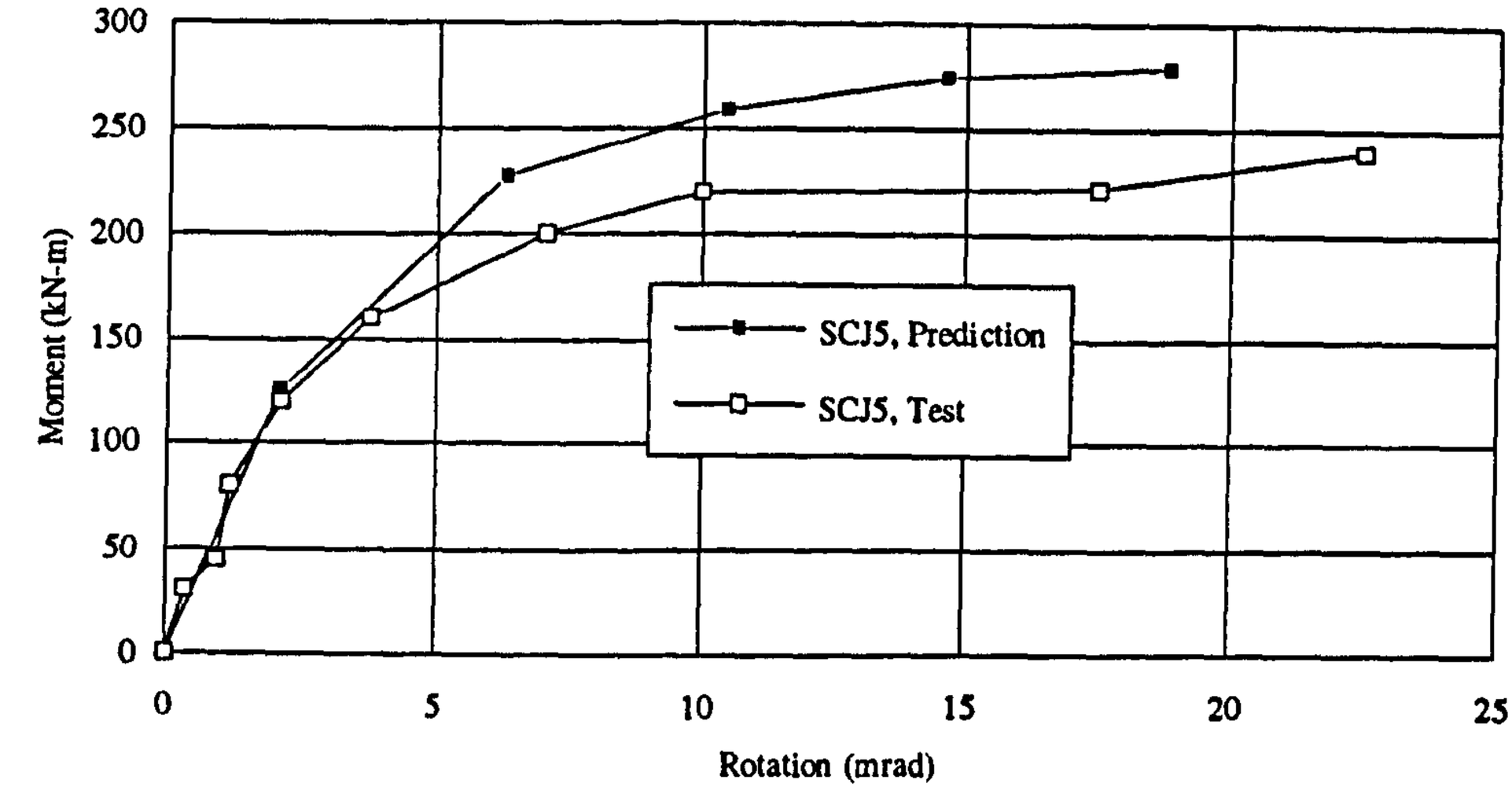

Figure 7-18 Comparison of test and predicted overall behaviour of test SCJ5

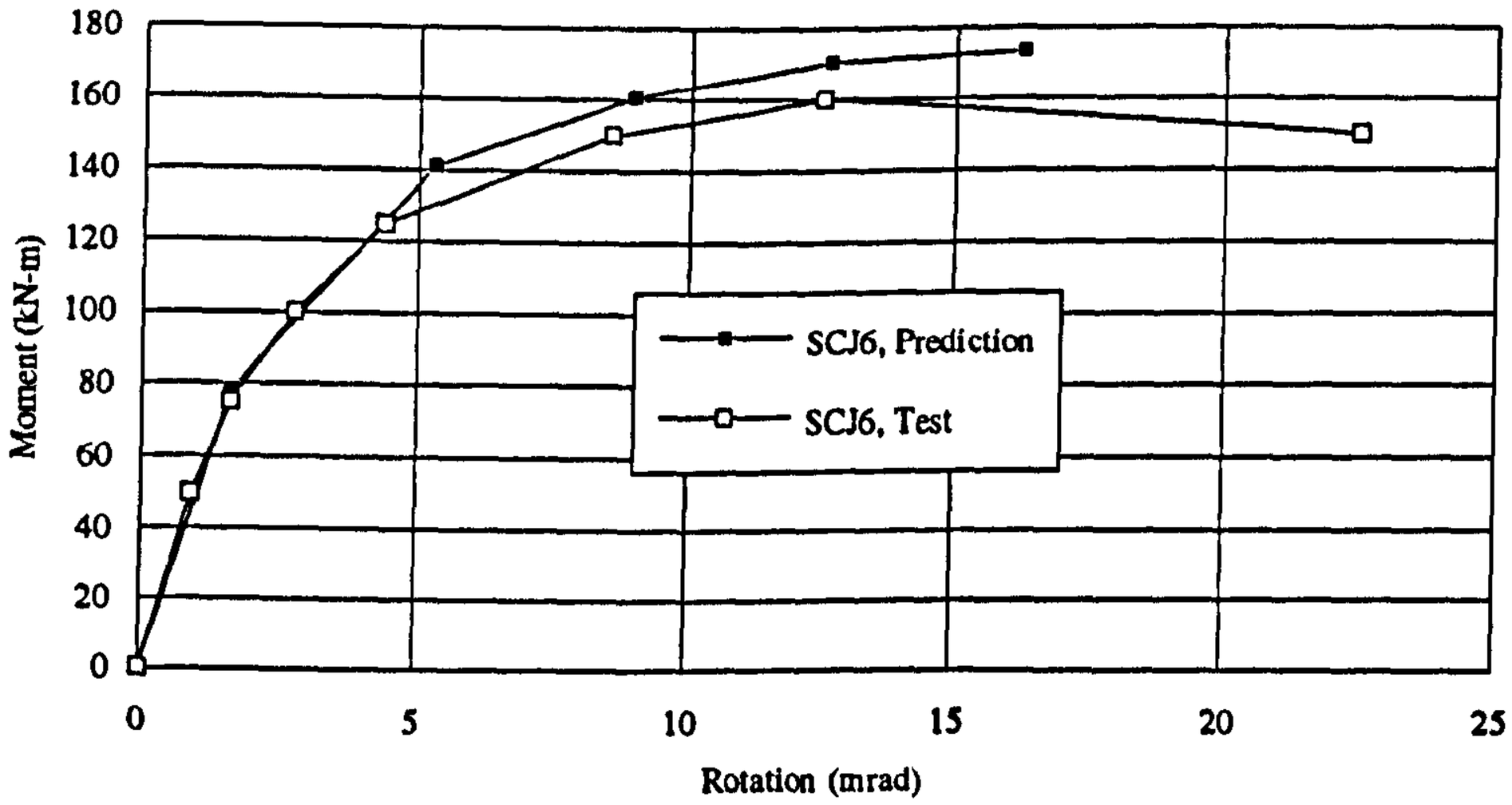

Figure 7-19 Comparison of test and predicted overall behaviour of test SCJ6

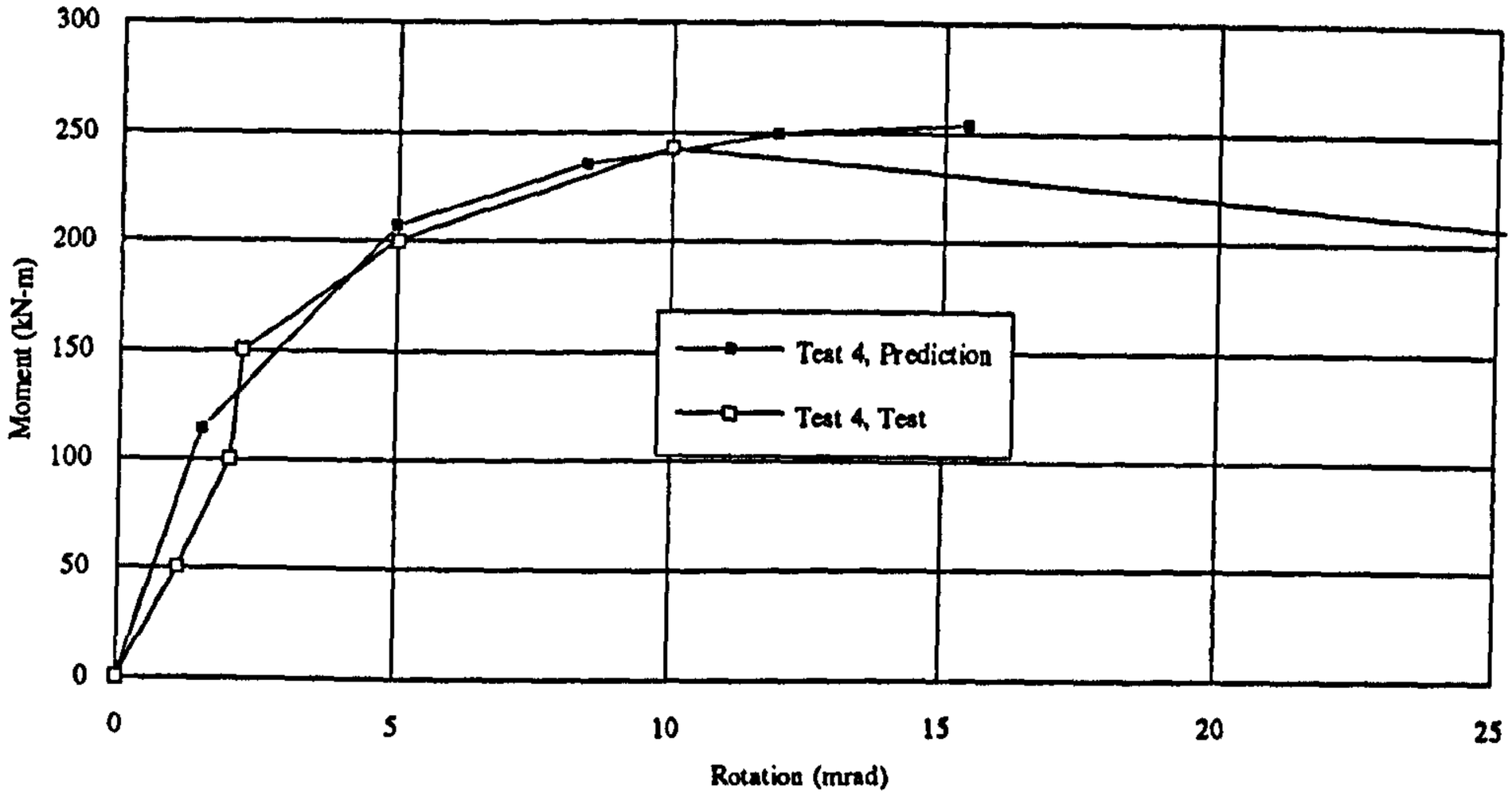

Note : Average smooth curve is drawn for test

Figure 7-20 Comparison of test and predicted overall behaviour of Test4

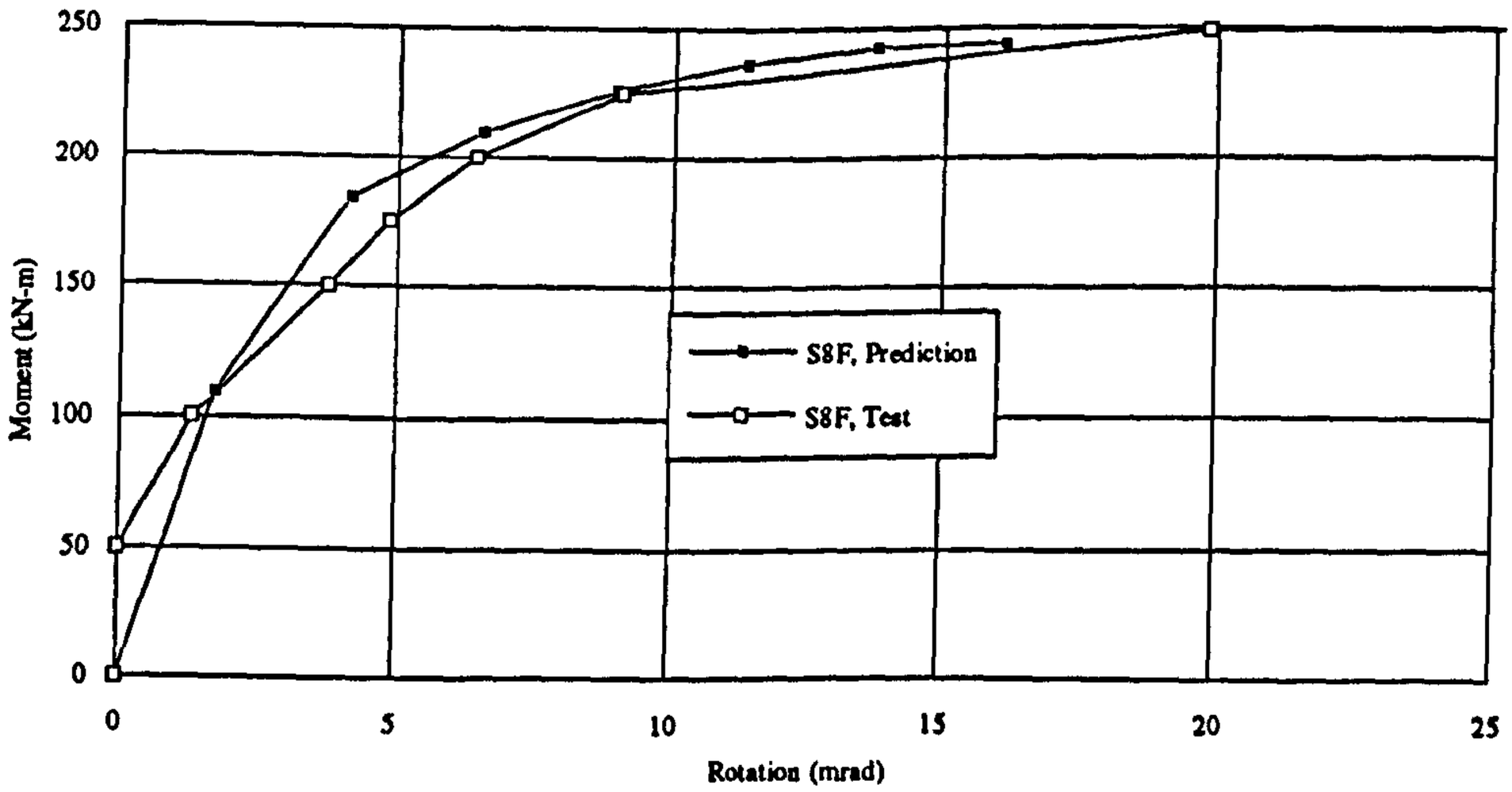

Note: The test curve is smoothened

Figure 7-21 Comparison of test and predicted overall behaviour of test S8F

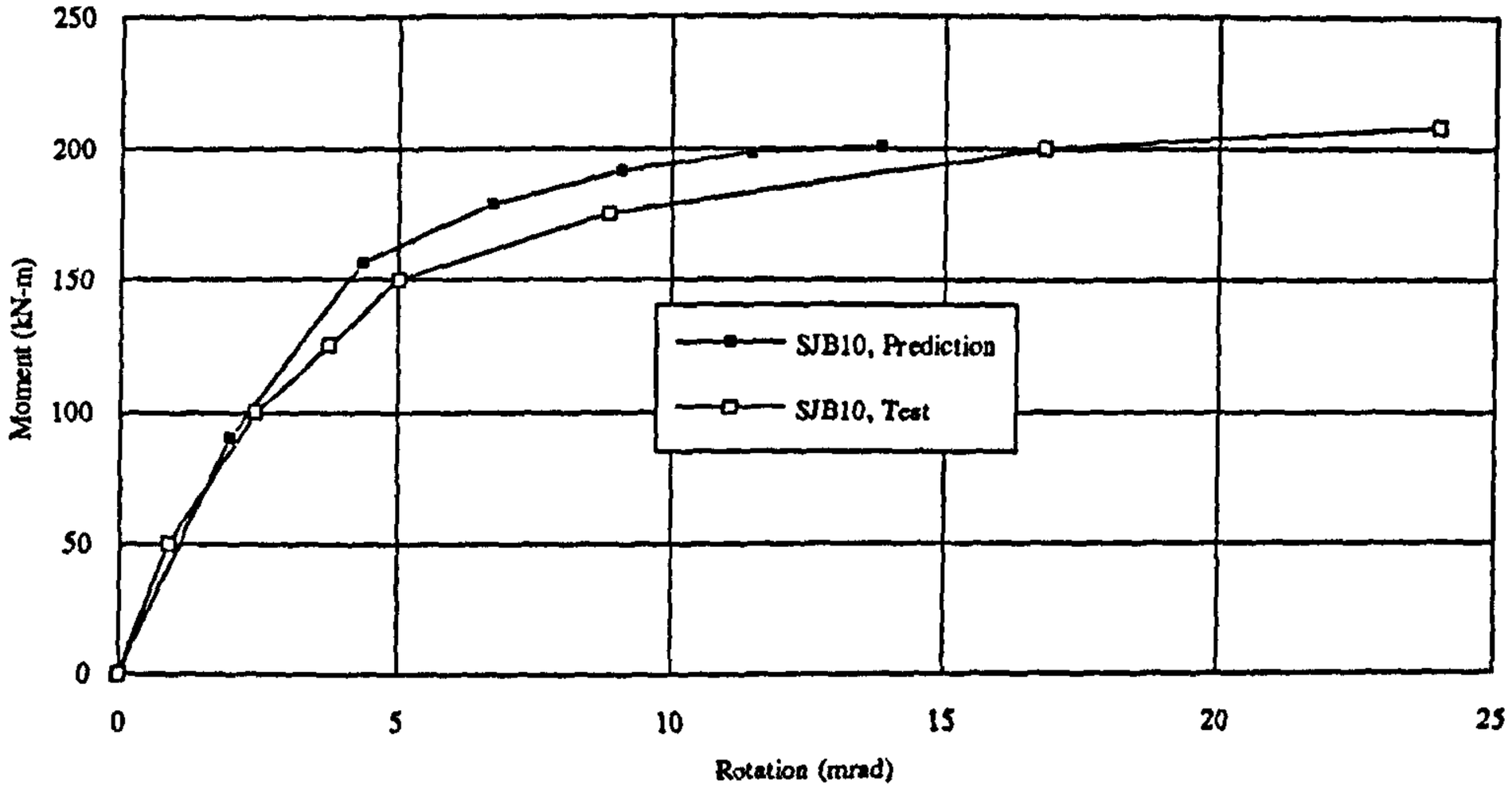

Figure 7-22 Comparison of test and predicted overall behaviour of test SJB10

Chapter 8

Design of composite finplate and angle cleated connections

8.1 Introduction

This chapter describes the design procedures for composite finplate and angle cleated connections. The methods can consider both symmetric and non-symmetric connections. The design procedure includes the use of the equations for basic component forces given in EC3 and EC4 as well as the equations derived in chapter 5 to consider the influence of shear to moment ratio and interaction of axial column loading obtained from chapter 6. The design procedures were set in a way that they were consistent with the design procedure for the flush endplate connections.

During the formulation of the equations care has been taken not only to determine the maximum resistance of each component, but also to reflect the effect of the resistance of the other components. Thus the proposed method predicts the internal forces in the connection accurately. To maintain a clear picture of the design procedures, a few equations were repeated instead of referring them to other chapters.

The basic concept is to determine the maximum attainable shear force for the connection which in turn depend on different criteria. Once the attainable shear is known for the connection the moment capacity can be obtained by multiplying it by the shear span. The design method is verified against all available test results: for angle cleated connections 16 test results taken from 4 different sources and for finplate connections 6 test results taken from 2 different sources. Comparison against the available test results shows that the method can predict the moment capacity of both

composite finplate and angle cleated connections accurately and that it is suitable for inclusion in design documents like EC4.

8.2 Finplate and cleated connections

Finplate connections (Figure 8-1a) were initially used in North America and Australia. The popularity of this type of connection is largely due to its simplicity in fabrication and erection. The use of such connections does not require holes to be drilled in the column and can lead to an increased construction speed. The lever arm between the internal forces is small in a bare steel finplate connection and this makes the moment capacity small. However, the introduction of a reinforced concrete slab over the steel beam, the use of proper shear interaction and moving the finplate towards the bottom flange of the beam combine to make it possible to increase the lever arm and hence the moment capacity of the connection.

Cleated connections (Figure 8-1b) are commonly used beam-to-column connections for frames designed according to the principles of "simple construction" [8-1]. Site welding is not required and fast erection can readily be achieved for frames with this type of connection. Since some tolerance is present in the bolt holes, a small degree of site adjustment is available during construction. Therefore, requirements for hole positions and beam length are not quite as strict as for endplate connections. Owing to the wide use of this type of connection in bare steel frames a large amount of experimental work has been conducted on bare steel connections [8-2]. Investigations of composite action in angle cleated arrangements started in the 1980's along with the introduction of composite beams [8-3, 8-4]. These have shown that strengthening the tensile zone with longitudinal reinforcement in the concrete slab near the column makes the connection act as a partial strength connection.

In this chapter a design method to predict the moment capacity of composite finplate and angle cleated connections is described; this is based on the component method of EC3 [8-5] for bare steel connections. Thus most of the basic equations are taken from EC3, while the other features of the design process are based on recent work described in chapters 5, 6 and 7 also in references 8-6, 8-7 and 8-8. The design procedure described herein is therefore similar to that already presented for endplate connections in chapter 7 and reference 8-8.

For angle cleated connections the proposed method may be used to calculate the shear and moment capacity of connections with:

i Web cleats and seating cleat

ii Web cleats only

iii Seating cleat only

8.3 The design approach

To determine the shear capacity of the connections the following items must be known:

1 Connection shear capacity from geometry of the connection

2 Connection shear capacity governed by beam web overstress, rebar stress and column web overstress

3 Connection shear capacity governed by the internal force equilibrium

The attainable shear of the connection is the minimum shear obtained from 1, 2 and 3.

Definitions of the geometric parameters for both type of connection is shown in Figure 2-3. Consideration of force transfers between the beam, finplate or cleats and column

of the type illustrated in Figures 8-3a and 8-3b suggest rather different features for the finplate, web cleat or seating cleat arrangements. It can be seen from these figures that for finplates and web cleats the depth of compression can increase as required and can be as great as the depth of finplate or the vertical leg length of the web cleats. For these arrangements the effective column web area that resists the compressive force is substantial and overstressing of the column web in compression does not occur. But in the case of a connection with a seating cleat the depth of web in compression is small and the column web can easily develop a high level of local compressive stress. Thus it must be checked in this case.

More localised stress in the beam web is associated with finplate design and for this beam web buckling in compression has been observed in some tests [8-4,8-10]; insufficient information on this is presently available to permit the development of a design procedure.

8.4 Connection shear capacity from geometry of the connection

For finplate connections shear capacity governed by the following items must be checked:

i Shear resistance of the bolt group

ii Bearing of the bolts against the finplate or beam web

iii Weld resistance in shear

iv Block shear failure of the beam web

v Block shear failure of the finplate

vi Equilibrium of the internal forces

The minimum of the above will give the actual shear capacity of the connection.

For angle cleated connections, the shear capacity at the following levels is required:

i At web cleat and beam web interface, governed by the shear resistance of the bolt group connected to the beam web and web cleats

ii At web cleat and beam web interface, governed by the bearing of the bolts against the web cleats or beam web

iii At web cleat and column flange interface, governed by the shear resistance of the bolt group connected to the column flange and web cleats

iv At web cleat and column flange interface, governed by bearing of the bolts against the column flange or web cleats

v At the seating cleat and column flange interface, governed by the shear resistance of the bolt group connected to the column flange and seating cleat

vi At the seating cleat and column flange interface, governed by bearing of the bolts against the column flange or seating cleat

Besides this the block shear resistances are required for the:

vii Web cleat legs connected to either the column flange or the beam web

viii Beam web

The minimum value from *i, ii, iii, iv, vii* and *viii* will give the shear resistance of connection with web cleat only and the minimum of *v* and *vi* will give the shear resistance of the connection with seating cleat only. The sum of these two forces gives the shear capacity of the connection from the geometric properties of the connection with both web and seating cleat.

8.4.1 Shear resistance of bolts connecting the: finplate or web cleat to the beam web, web cleat to the column flange and seating cleat to the column flange

The resistance of a bolt in shear can be calculated by multiplying the shear area by the shear strength. Hence the total resistance of a bolt group is obtained by the shear resistance times the number of bolts connecting the web cleat to the beam web or column flange.

The shear resistance of a bolt group connecting beam web and finplate or web cleat can be written according to EC3 Clause 6.5.5 as:

$$P_{v-bolt\ shear} = 0.6\ N_{bw} . f_{.b} . A_b \qquad (8\text{-}1)$$

For bolt group connected to web cleats and column flange:

$$P_{v-bolt\ shear} = 0.6\ N_{cw} . f_{.b} . A_b \qquad (8\text{-}2)$$

For bolt group connected to seating cleat and column flange:

$$P_{v-bolt\ shear} = 0.6\ N_{cs} . f_{.b} . A_b \qquad (8\text{-}3)$$

8.4.2 Bearing resistance of bolts connecting the: finplate or web cleat to the beam web, web cleat to the column flange and seating cleat to the column flange

According to clause 6.5.5 of EC3, the bearing resistance of a group of bolts connecting beam web and finplate or web cleat can be written as:

$$F_{v-bearing} = N_{bw} . \min imum \begin{cases} 2.5\alpha_i . f_{uwc} . d_o . t_{wc.b} & \textit{finplate or web cleat controls} \\ 2.5\alpha_i . f_{bw} . d_o . t_{bw} & \textit{beam web controls} \end{cases} \qquad (8\text{-}4)$$

For bolt group connected to web cleats and column flange:

$$F_{v\text{-}bearing} = N_{cw}.\min imum\begin{cases} 2.5\alpha_i.f_{uwc}.d_o.t_{wc.c} & web\ cleat\ \ controls \\ 2.5\alpha_i.f_{cf}.d_o.t_{cf} & column\ flange\ \ controls \end{cases} \quad (8\text{-}5)$$

For bolt group connected to seating cleat and column flange:

$$F_{v-bearing} = N_{cs}.minimum\begin{cases} 2.5\alpha_i.f_{usc}.d_o.t_{sc.v} & seating\ cleat\ \ controls \\ 2.5\alpha_i.f_{cf}.d_o.t_{cf} & column\ flange\ \ controls \end{cases} \quad (8\text{-}6)$$

Where:

$$\alpha_i = min\begin{cases} \dfrac{f_{.b}}{ultimate\ strength\ of\ the\ jointed\ part} \\ 1 \end{cases}$$

Note: α_i will vary in each of the expressions given above.

8.4.3 Shear capacity of the connection governed by the block shear failure of the finplate or web cleat legs connected to either the column or the beam web

According to Clause 6.5.2 of EC3, the block shear resistance of the finplate or web cleats is equal to:

$$P_{v-block} = 0.6Cf_{uwc}A_{vbc} \quad (8\text{-}7)$$

Where:

C =1 for finplate and single web cleat; 2 for double web cleats

For finplate connections:

$$A_{vbc} = t_{fp}\left(L_v + L_1 + L_2 - nd_h\right)$$

For angle cleated connections:

$$A_{vbc} = min\begin{cases} t_{wc.c}\left(L_v + L_1 + L_2 - nd_h\right) & \textit{leg connected to column} \\ t_{wc.b}\left(L_v + L_1 + L_2 - nd_h\right) & \textit{leg connected to beam} \end{cases}$$

$$L_1 = min\begin{cases} 5.0d_h \\ a_{1f} \end{cases}$$

$$L_2 = min\begin{cases} 2.5d_h \\ a_{2f} \end{cases}$$

L_v, a_{1f} and a_{2f} is defined in Figures 8-2a and 8-2b.

8.4.4 Block shear resistance of the beam web

According to Clause 6.5.2 of EC3, the block shear resistance of the beam web is equal to:

$$P_{v-block} = 0.6 f_{bw} A_{vb} \tag{8-8}$$

Where:

$$A_{vb} = t_{bw}\left(L_v + L_1 + L_2 - nd_o\right)$$

$$L_1 = min\begin{cases} 5.0d_h \\ a_{1s} \end{cases}$$

$$L_2 = min\begin{cases} 2.5d_h \\ a_{2s} \end{cases}$$

L_v, a_{1s} and a_{2s} is defined in Figures 8-2a and 8-2b.

8.4.5 Shear capacity of the finplate connection governed by the weld resistance in shear

From Clause 6.6.5 of EC3, the design resistance of the weld per unit length is:

$$F_{w.Rd} = a\frac{f_{uw}}{\sqrt{3}\beta_w}$$

Where a is the throat thickness of weld and β_w is a correlation factor as shown in Table 8-1.

Table 8-1 Weld material ultimate strength and correlation factors

EN10025 steel grade	F_{uw} N/mm^2	β_w
Fe360	360	0.80
Fe430	430	0.85
Fe510	510	0.90

Shear capacity of the connection governed by the weld resistance in shear is obtained by multiplying the above equation by the depth of the finplate times the number of sides welded.

$$P_{v-weld} = n.D_{fp}.F_{w.Rd} \qquad (8\text{-}9)$$

8.4.6 Shear capacity of the connection from geometric properties

From the above equations the connection shear capacity from the geometric properties of the connection can be determined from the summation of the minimum resistances at the levels of web cleat and seating cleat. Hence the connection shear capacity from geometric properties can be calculated by the following equations.

8.4.6.1 Angle cleated connection

Connection with seating and web cleat:

$$P_{v\text{-}cleats} = minimum\begin{cases} equation\ 8-1 \\ equation\ 8-2 \\ equation\ 8-4 + minimum\begin{cases} equation\ 8-3 \\ equation\ 8-6 \end{cases} \\ equation\ 8-5 \\ equation\ 8-7 \end{cases} \qquad (8\text{-}10a)$$

Connection with web cleat only:

$$P_{v-web} = minimum\begin{cases} equation\ 8-1 \\ equation\ 8-2 \\ equation\ 8-4 \\ equation\ 8-5 \\ equation\ 8-7 \end{cases} \qquad (8-10b)$$

Connections with seating cleat only:

$$P_{v-seat} = minimum\begin{cases} equation\ 8-3 \\ equation\ 8-6 \end{cases} \qquad (8\text{-}10c)$$

Hence connection shear capacity from geometric properties of the connection:

$$P_{v-geometry} = minimum\begin{cases} equation\ 8-8 \\ equation\ 8-10 \end{cases} \qquad (8-11a)$$

8.4.6.2 Finplate connection

For connections with a finplate the shear capacity from geometry of the connection is simply the minimum of the values determined above for it, hence:

$$P_{v-web} = minimum\begin{cases} equation\ 8-1 \\ equation\ 8-4 \\ equation\ 8-7 \\ equation\ 8-8 \\ equation\ 8-9 \end{cases} \qquad (8-11b)$$

8.5 Shear capacity of the connection governed by beam web overstress and column web overstress

In addition to considerations of the geometric properties of the connection, the attainable shear capacity of the connections is also governed by the component capacities. These are: the overstressing of the beam web and the overstressing of the column web. Table 8-2 summarises the actual formulae to be used to estimate the attainable shear capacities obtained from chapter 5 and reference 8-6.

Table 8-2 Equations for determining the attainable load (chapter 5 and ref. 8-6)

Governing factor	Equation for attainable load	Comments
Beam web overstress	$P_v = \dfrac{f_{bw}}{\sqrt{\dfrac{x^2.(\bar{y}-2t_{bf})^2}{I^2} + \dfrac{3}{H_b^2.t^2_{bw}}}}$ (8-12)	Associated with weak beam web and high reinforcement ratio with adequate shear connection
Column web overstress	$P_v = \dfrac{f_{cw}.D_c.t_{cw}D_r b_{eff}}{\sqrt{4D_r^2 b_{eff}^2 + D_c^2 x^2 - 2xD_r b_{eff} D_c}}$ (8-13)	Associated with strong beam, moderate to high reinforcement area.

Note: F_b represents the force in a row of bolts. In the equations x represents the shear span i.e. the distance of the applied load from the column face.

$b_{eff} = t_{sc.h} + t_{sc.v} + 5(t_{cf} + r_c)$

8.6 Shear capacity of the connection governed by the internal force equilibrium

The determination of the shear capacity based on equilibrium of the internal forces requires the determination of the following forces:

- Column web shear resistance for the non-symmetric connections
- Column web buckling resistance for connections without any stub beam (can be ignored for finplate connections)
- Column web compression resistance (can be ignored for finplate connections)
- Rebar force
- Bolt shear capacity
- Bolt bearing against the finplate or the web cleats and the beam web

8.6.1 Determination of internal forces

8.6.1.1 Column web shear resistance for the non-symmetric connections

If the connection is loaded non-symmetrically, the column web shear strength must be considered; this is given by:

$$F_{cw,s} = \frac{M'_{c2}}{D_r} + \sqrt{1 - \left(\frac{\sigma_n}{f_{y,cw}}\right)^2}\,\frac{f_{cw}}{\sqrt{3}} A_v \qquad if\ \eta < 1,\quad ref\ 8-7 \tag{8-14}$$

8.6.1.2 Column web buckling resistance

If there is no stub beam connected to the column web, the buckling resistance of the column web must be considered; this is given by:

$$F_{c,buckling} = 8.4\, b_{eff-b}{}^{0.017}\ D_c{}^{0.60}\ t_{cw}{}^{1.43}\ f_{cw}{}^{0.76} \qquad ref\ 8-8 \tag{8-15}$$

Where:

For cleated connections:

$$b_{eff\text{-}b} = \sqrt{D_c^{\,2} + S_s^{\,2}}$$

$$S_s = t_{sc.h} + t_{sc.v}$$

For finplate connections:

$$b_{eff-b} = \sqrt{D_c^{\,2} + D_{fp}^{\,2}}$$

8.6.1.3 Column web compression resistance

$$F_{c,compression} = b_{eff}\ t_{cw}\ f_{cw} \qquad (8\text{-}16)$$

For cleated connections:

$$b_{eff} = t_{sc.h} + t_{sc.v} + 5\left(t_{cf} + r_c\right)$$

For finplate connections:

$$b_{eff} = D_{fp} + 5\left(t_{cf} + r_c\right)$$

8.6.1.4 Maximum developable column compression

From equilibrium of internal forces the maximum developable column compression force for a given connection is the minimum of the values given by equations 8-14 to 8-16.

$$F_{c,cw} = minimum\begin{cases} equation\ 8-14 & for\ \eta < 1 \\ equation\ 8-15 & if\ no\ stub\ beam \\ equation\ 8-16 & \end{cases} \qquad (8-17)$$

8.6.1.5 Rebar force

$$F_r = min\begin{cases} A_r f_u & ref\ 8-7 \\ 0.67 b_{cf} h_{cs} f_c' \beta + \dfrac{M_{c2}}{D_r} & when\ \eta < 1,\quad ref\ 8-8 \\ nkR_{Rd} & EC4\ Clause\ 6.3.2\ and\ 6.3.3 \\ equation\ 8-17 & \end{cases} \qquad (8-18)$$

8.6.2 Seating cleat compression force (connections having a seating cleat)

The seating cleat compression force can be obtained form the shear resistance of the bolts connecting the seating cleat to the beam bottom flange or bearing of the same bolts against the beam bottom flange or the seating cleat. Also it cannot exceed the resistance provided by the column web.

$$F_{c-bolt\ shear} = 0.6\, N_{cb} . f_{.b} . A_b \qquad (8\text{-}19)$$

$$F_{c-bearing} = N_{cb} . minimum\begin{cases} 2.5\alpha_i . f_{usc} . d_o . t_{sc.h} & seating\ cleat\ controls \\ 2.5\alpha_i . f_{bf} . d_o . t_{bf} & beam\ flange\ controls \end{cases} \qquad (8\text{-}20)$$

α_i is to be determined as before.

The developable seating cleat compressive force is the minimum of the values given by equations 8-17, 8-19 and 8-20.

$$F_{sc} = minimum\begin{cases} equation\ 8-17 \\ equation\ 8-19 \\ equation\ 8-20 \end{cases} \qquad (8-21)$$

8.6.3 Finplate or web cleat bolt forces

There are three possible cases for cleated connections and one for finplate connections:

i No web cleats present

ii The rebar force > seating cleat force and connections without a seating cleat and also finplate connection

iii The rebar force < seating cleat force

Depending on which of the above cases is present, the horizontal shear force that develops in the bolts connecting the web cleats to the beam web will make a tensile or compressive force contribution towards the connection moment capacity.

8.6.3.1 No web cleat present or the rebar and seating cleat forces are equal

Web cleat horizontal bolt forces are zero and both rebar and seating cleat forces are the same in this case (equations 8-17 and 8-18). The shear capacity from internal force equilibrium is given by:

$$P_{v-equilibrium} = \frac{F_r D_r}{x - x_1} \qquad (8-22)$$

8.6.3.2 The rebar force > seating cleat force and connections without a seating cleat and also finplate connection

In this case the web cleat bolt shear (connected to the beam web) will act as a compressive force contribution to the moment capacity. The total force that can develop in the bolts can be determined using equations 8-1 and 8-4. Also it cannot exceed the difference of the rebar and seating cleat force for connections having both seating and web cleats, hence:

$$F_{b,\,total} = minimum\begin{cases} equation\ 8-1 \\ equation\ 8-4 \\ (eq\ 8-18)-(eq\ 8-21) \end{cases} \qquad (8-23a)$$

For finplate connections and cleated connections having only web cleats, the total bolt force is:

$$F_{b,\,total} = minimum\begin{cases} equation\ 8-1 \\ equation\ 8-4 \\ equation\ 8-18 \end{cases} \qquad (8-23b)$$

Once the total compressive force is calculated, it can now be distributed among the bolts *starting from the bottom.* The maximum force permitted per bolt is:

$$F_{b,\,single} = \frac{1}{N_{bw}} minimum\begin{cases} equation\ 8-1 \\ equation\ 8-4 \end{cases} \qquad (8-24)$$

Hence the bolt forces starting from the bottom are:

$$F_{b,1} = minimum\begin{cases} F_{b,\,single} \\ equation\ 8-23 \end{cases} \qquad (8-25)$$

The forces in the remaining bolts are:

$$F_{b,\,i} = minimum\begin{cases} F_{b,\,single} \\ F_{b,\,total} - \sum_{k=1}^{i-1} F_{b,\,k} \geq 0 \end{cases} \qquad (8-26)$$

Note: Bolts are numbered from the bottom.

Rebar force is:

$$F_r' = minimum\begin{cases} eq\ 8-21 + \sum_{i=1}^{N_{bw}} F_{b,\,i} \\ equation\ 8-18 \end{cases} \qquad (8-27)$$

With the bolt forces and rebar force determined as above, Figures 8-4a and 8-4b can now be used to calculate the connection shear capacity from consideration of connection internal force equilibrium. Taking moments about point O gives:

$$P_{v-equilibrium} = \frac{F_r' D_r - \sum_{i=1}^{N_{bw}} F_{b,i} D_{bi}}{x - x_1} \qquad (8-28)$$

8.6.3.3 The rebar force < seating cleat force

In this case the web cleat bolt shear (connected to the beam web) will act as a tensile contribution to the moment capacity. But it is worth mentioning that if the reinforcement is only in the form of mesh reinforcement, the contribution of bolts should be neglected, as fracture of the mesh will not allow the development of the tensile bolt forces. The total force that can develop in the web cleat bolts connected to the beam web can be determined using equations 8-1 and 8-4. Besides this, the tensile resistance of the bolts connected to the column flange and the web cleat must be taken into consideration. This will be governed by:

a) Tensile resistance of the web cleats controlled by web cleat bending

b) Tensile resistance of the web cleats controlled by column flange bending

c) Tensile resistance of the web cleats controlled by bolt tensile resistance

a) Tensile resistance of the web cleats controlled by web cleat bending

The bending resistance of the web cleat can be obtained from its equivalent T-stub. According to Table J.6 of EC3, the equivalent T-stub for the web cleats (all bolt rows included) can be obtained from:

$$l_{eff.a} = minimum\ of\ \frac{C}{2}m \bullet \begin{cases} 2pm_a \\ 4m_a + 1.25e_a \\ p \\ 0.5p + 0.5e_{1w} \end{cases} \qquad (8-29)$$

Where:

C =1 for a single web cleat and C = 2 for double web cleats

p is the pitch of the bolts (Figure 8-2)

e_a, m_a and e_{1w} defined in Figure 8-2c

The resistance of the web cleats is dependent on the failure modes of the equivalent T-stub. According to the two possible failure modes that are: i) complete T-stub yield and ii) both T-stub and bolt yield, the effective tensile resistance of the web cleats in bending is given by:

$$F_{wcb} = minimum \begin{cases} \dfrac{l_{eff.a} t_{wc.c}^{\ 2} f_{wc}}{m_a} \\ \dfrac{0.5 l_{eff.a} t_{wc.c}^{\ 2} f_{wc} + 0.9 C m A_b f_{\ b} e_a}{m_a + e_a} \end{cases} \qquad (8-30)$$

b) Tensile resistance of the web cleats controlled by column flange bending

According to Table J.6 of EC3, the effective length of the equivalent T-stub for the column flange (all bolt rows are included) is equal to:

$$l_{eff.c} = minimum\ of\ \frac{C}{2} m \bullet \begin{cases} 2pm_c \\ 4m_c + 1.25e_c \\ p \end{cases} \qquad (8-31)$$

e_c and m_c are defined in Figure 8-2c.

The resistance of the column flange in bending should also be determined by the two possible failure modes (complete T-stub yield and both T-stub and bolts yield), and the smaller resistance should be used, which is given by:

$$F_{cfb} = minimum \begin{cases} \dfrac{l_{eff.c} t_{cf}^{\ 2} f_{cf}}{m_c} \\ \dfrac{0.5 l_{eff.c} t_{cf}^{\ 2} f_{cf} + 0.9 C m A_b f_{.b} e_c}{m_c + e_c} \end{cases} \qquad (8-32)$$

c) Tensile resistance of the web cleats controlled by bolt tensile resistance

Tensile resistance of a single bolt can be calculated according to Clause 6.5.5 of EC3. The tensile resistance of the web cleats controlled by bolt resistances is equal to the sum of the tensile resistance of the bolts connected to the column flange and web cleats and is:

$$F_{b,t} = 0.9 C m f_{\ b} A_b \qquad (8\text{-}33)$$

With the above values determined, the total tensile force in the web cleat bolts connected to the beam web can be determined as:

$$F_{b,\ total} = min\begin{cases} equation\ 8-1 \\ equation\ 8-4 \\ equation\ 8-30 \\ equation\ 8-32 \\ equation\ 8-33 \\ (eq\ 8-21)-(eq\ 8-18) \end{cases} \qquad (8-34)$$

The allowable force in a single bolt connected to the beam web is given by equation 8-24.

Hence the bolt forces starting from the top are:

$$F_{b,\ 1} = minimum\begin{cases} equation\ 8-24 \\ equation\ 8-34 \end{cases} \qquad (8-35)$$

The forces in the remaining bolts are:

$$F_{b,i} = minimum\begin{cases} equation\ 8-24 \\ F_{b,total} - \sum_{k=1}^{i-1} F_{b,k} \geq 0 \end{cases} \qquad (8-36)$$

Note: Bolts are numbered from the top.

With the bolt forces and rebar force determined as above, Figure 8-4c can now be used to calculate the connection shear capacity from consideration of connection internal force equilibrium. Taking moments about point O gives:

$$P_{v-equilibrium} = \frac{F'_r D_r + \sum_{i=1}^{N_{bw}} F_{b,i} D_{bi}}{x - x_1} \qquad (8-37)$$

8.7 Attainable connection shear

For finplate connections the attainable shear force is:

$$P_v = min\begin{cases} equation\ 8-11 \\ equation\ 8-28 \end{cases} \qquad (8-38a)$$

The attainable connection shear for angle cleated connection can be obtained as follows:

$$P_v = min\begin{cases} equation\ 8-11 & \\ equation\ 8-12 & \\ equation\ 8-13 & connection\ with\ only\ seating\ cleate \\ equation\ 8-22 & if\ rebar\ force = Seating\ cleat\ force \\ & or\ connection\ with\ only\ seating\ cleate \\ equation\ 8-28 & if\ rebar\ force > Seating\ cleat\ force\ or \\ & connection\ with\ only\ web\ cleat \\ equation\ 8-37 & if\ rebar\ force < Seating\ cleat\ force \end{cases} \qquad (8-38b)$$

8.8 Connection moment capacity

The moment capacity is obtained by multiplying the attainable connection shear as obtained in section 8.7 by the shear span.

$$M = P_v x \qquad (8\text{-}39)$$

8.9 Validation of the proposed model against the test results

Until now 4 tests are known to have been conducted on composite finplate connections. These are SCJ2, SCJ12, SCJ16 and SCJ17 tested by Xiao [8-4 and 8-10] in the University of Nottingham. Besides this Jarrett [8-9] conducted tests on a composite sub-frame with long and short finplates, these are also included in the

comparison. Comparison of the model's prediction, together with the method proposed by Xiao [8-4 and 8-10] is shown in Table 8-3. Results presented in Table 8-3 show that the prediction from the Xiao method gives a standard deviation of 0.37, while the method proposed herein gives a standard deviation of 0.18 for six tests. This clearly indicates that the results are more consistent with the proposed method. It can also be seen that the average P/T ratio from the proposed method is 1.06 for six tests compared with 0.97 using the Xiao method for the four tests of reference 8-10.

It should be noted that in reference 8-10 results were presented as test to prediction ratio which were 0.65, 1.35, 1.15 and 1.29, which gives standard deviation of 0.32 instead of 0.08 as reported in reference 8-10.

Table 8-3 Comparison of results for composite finplate connections

Author	Test	Beam	Column	ρ %	Test Moment (kN•m)	Moment Xiao [ref8-10] (kN•m)	Ratio P/T Xiao	Moment Proposed (kN•m)	Ratio P/T Proposed
Xiao Choo Nethercot [ref. 8-4]	SCJ2	305x165UB40	203x203UC60	0.20	30	46	1.53	33.8	1.13
	SCJ12	305x165UB40	203x203UC52	0.70	101	75	0.74	91.8	0.91
	SCJ16	454x191UB98	203x203UC52	1.00	225	196	0.87	195.2	0.87
	SCJ17	305x165UB40	203x203UC52	0.70	97	75	0.77	91.8	0.95
Jarrett [ref. 8-9]	NR1S	305x165UB40	203x203UC60	1.00	88	x	x	114	1.29
	NR1L	305x165UB40	203x203UC60	1.00	102	x	x	127	1.25
Summary of results	Total no. of tests compared 6					Avg.0.97,SD0.37 Max.1.53,Min0.74		Avg. 1.06, SD 0.18 Max.1.29, Min0.87	

References 8-10 (SCJ1 and SCJ11), 8-11 (SRCC1C, SRCC3C), 8-12 (C1 to C11) and 8-13 (30X2C1 to 30X2C7, 36X2C1 to 36X2C7 a total of 12 tests, excluding 30X2C4 and 36X2C4) describe the testing of composite angle cleated connections. Among the available tests C1, C2, C3 and C4 attained their capacity due to rebar anchorage failure and are thus excluded. Tests 30X2C3, 30X2C6, 36X2C1 36X2C3 and 36X2C5 reached their ultimate capacity by buckling of the column web at the seating cleat level; these are also excluded. The reason for excluding the later tests is that the EC3 equation or its simplification (equation 8-15) that gives the buckling resistance of the

column web gives very low values with respect to the compressive force attained in these connections as indicated in Table 8-4.

Table 8-4 Comparison of compressive forces for tests exhibiting buckling

Test	Moment (kN•m)	Average D_r (mm)	Average compression developed (kN)	Equation -8-15 (kN)**
30X2C3	322	345	933	528
30X2C6	292	345	846	528
30X2C7	324	345	939	528
36X2C1	343	405	846	528
36X2C3	367	405	906	528
36X2C5	366	405	903	528

** Note : This is obtained by using a stress of 415 N/mm^2 for the column web

Comparison of the results is shown in Table 8-5. It can be seen that with 2 exceptions (C6 and SCJ1) very good agreement between the test and the prediction is obtained. Only where the connection was mesh reinforced was the predicted capacity significantly higher than the test result. This was due to the fact that full plasticity was assumed in the model, whereas in a connection with mesh reinforcement only the connection fails due to fracture of the mesh with no possibility for the full development of the bolt forces. Additional analysis for the mesh reinforced connections (values in brackets) shows that if the contribution of the bolts is ignored, better agreement is achieved. The results of Table 8-5 show that for 16 tests from 4 different sources the average prediction to test ratio is 1.11, with a standard deviation of 0.38. If the contribution of the bolts is ignored for the 2 mesh reinforced connections, the values improve to 0.98 and 0.13 respectively. It should be noted that in reference 8-10 test to prediction ratios of 0.43, 1.17, 1.26, 1.19, 0.67 and 1.39 for C6, C7, C8, C9, SCJ1 and SCJ11 respectively were quoted. This gives a standard deviation of 0.37 instead of 0.09 as reported in reference 8-10 and if the ratio is calculated in-terms of prediction to test moment ratio it becomes 0.63.

It should, however, be noted that for finplate connections with any type of reinforcement and cleated connections that have bar reinforcement with or without mesh reinforcement (i.e. not only mesh reinforced) the design method should give better predictions than for cleated connections with only mesh reinforcement. The design approach for the latter will essentially predict a tensile force in the bolts which cannot actually develop due to the non-ductile fracture of the mesh reinforcement. Hence it is concluded that for cleated connections with only mesh reinforcement the contribution of the bolts should be ignored.

Table 8-5 Comparison of results for composite angle cleated connections

Author	Test	Beam	Column	ρ %	Predicted Moment (Pm) (kN•m)	Test Moment (Tm) (kN•m)	Ratio Pm/Tm	Moment Xiao [8-10] (kN•m)	Ratio P/T Xiao [8-10]
Lam, Davison Nethercot [ref. 8-12]	C5	305x165UB40	203x203UC52	0.75	98	94	1.04	x	x
	C6	305x165UB40	203x203UC52	0.20	67	31.5	2.14 (1.34)	74	2.33
	C7	305x165UB40	203x203UC52	0.75	140	140	1.00	124	0.85
	C8	305x165UB40	203x203UC52	1.00	175	181	0.97	144	0.79
	C9	457x191UB92	203x203UC52	0.75	140	160	0.88	134	0.84
	C11	356X171UB67	203x203UC52	1.00	195	200	0.98	x	x
Leon [ref. 8-11]	SRCC1C	W14X38	W14X120	1.20	218	191	1.14	x	x
	SRCC3C	W14X38	W14X120	1.20	218	212	1.03	x	x
Xiao [ref. 8-10]	SCJ1	305x165UB40	203x203UC60	0.20	99	49.4	1.99 (0.85)	74	1.49
	SCJ11	305x165UB40	203x203UC52	0.70	145	169.5	0.85	122	0.72
Altmann Maquoi Jaspart [ref. 8-13]	30X2C1	IPE300	HEB200	1.3	210	263	0.80	x	x
	30X2C2	IPE300	HEB200	0.67	210	209	1.00	x	x
	30X2C5	IPE300	HEB200	0.67	210	205	1.02	x	x
	36X2C2	IPE360	HEB200	0.67	240	251	0.96	x	x
	36X2C6	IPE360	HEB200	0.67	243	253	0.96	x	x
	36X2C7	IPE360	HEB200	0.67	243	253	0.96	x	x
Summary of results	Total no. of tests compared 16		Average P/T		1.11 (0.98)				1.17
			Standard deviation		0.38 (0.13)				0.63

8.10 Worked example for a connection with a seating and double web cleats

Consider a connection with a 305x165UB40 beam, 203x203UC52 column, L150x150x10 seating cleat and two L90x90x10 web cleats. All bolts are M20 grade 8.8. The web cleats are connected to the column flange by a single bolt at their centre and to the beam web by two bolts at 60 mm centre to centre. The seating cleat is

connected to the column flange by two rows of bolts, with a spacing of 50 mm between the rows and 90 mm centre to centre in a row. This cleat is connected to the bottom flange of the beam by two rows of bolts in a similar manner. Shear connection is provided with seven rows of 100x19 mm shear studs, each row having one stud. The depth of the solid concrete slab is 120 mm, with a width of 1200 mm. A cross section of the composite beam is shown in Figure 8-5. Reinforcement is 8 T10 bars plus A142 mesh. The load is assumed to act at 1500 mm from the column face and the centreline of the beam web bolts is located at 50 mm from the column face. It is assumed that there is no stub beam connected to the column web.

Ultimate strengths for the members are:

Beam web:	490 N/mm^2
Beam flange:	490 N/mm^2
Column web:	469 N/mm^2
Column flange:	469 N/mm^2
Web and seating cleat:	350 N/mm^2
Reinforcement:	600 N/mm^2
Bolt:	600 N/mm^2
Concrete:	33 N/mm^2

Pre calculations

Single bolts

Single shear strength: 122.5 kN

Bolt bearing against beam web: 149.5 kN

Bolt bearing against web cleat: 175 kN

Bolt bearing against column flange: 293 kN

Bolt bearing against seating cleat: 262.5 kN

Contribution of web cleat

For bolts connected to the beam web and web cleat, vertical shear resistance from shear strength of bolts = 2 x 2 x 122 kN = 488 kN. Consideration of bearing strength gives 299 kN (minimum of 2x 149.5 and 2 x 2 x175).

For bolts connected to the column flange and web cleat, vertical shear resistance from shear strength of bolts = 2 x 122.5 kN = 245 kN. Consideration of bearing strength gives 350 kN (minimum of 2x 293 and 2 x175).

The block shear resistance of the web cleat is 0.6x 2 x [10 (60 + 100 + 50 -2 x 20)] x350 /1000 = 714 kN.

Hence shear capacity of the connection from contribution of web cleat = minimum of 448, 299, 245, 350 and 714 i.e., 245 kN.

Contribution of seating cleat

For bolts connected to the column flange and seating cleat, vertical shear resistance from shear strength of bolts = 2 x 2 x 122.5 kN = **490 kN**. Consideration of bearing strength gives 1050 kN (minimum of 4x 293 and 4 x262.5).

Hence shear capacity of the connection from contribution of the seating cleat = minimum of 490 and 1050 i.e., 490 kN.

Block shear resistance of beam web

The block shear resistance is 0.6 x 490 x [6.1 x (120 +100 + 50 -2 x 20)]/ 1000 kN = **412 kN.**

(a) Shear resistance of the connection from geometric properties

From geometric properties the connection shear resistance is **412 kN** [minimum of (245 kN + 490 kN) and 412 kN] (E-1)

(b) Shear resistance of the connection from beam web overstress Using equation 8-11, the force is **233 kN** (E-2)

(c) Shear resistance of the connection from geometric properties Using equation 8-12, the force is 240 kN (E-3)

(d) Shear resistance of the connection from connection equilibrium

Column web shear resistance for the non-symmetric connections: not active

Column web buckling resistance: 351 kN (as no stub beam present)

Column web compression resistance: 538 kN

Seating cleat compression force: 490 kN

Maximum developable column compression at seating cleat level: 351 kN

Rebar force: 351 kN

Rebar force = Developable seating cleat force (351 kN)

This gives an attainable shear of **96.67 kN** from connection equilibrium. (E-4)

Hence the attainable shear is **96.67 kN,** minimum of E-1, E-2, E-3 E-4.

M = 96.67 kN x 1.5 m = 145 kN-m.

8.11 Conclusions

By considering the force transfers within composite finplate and cleated connections a design method has been developed that is capable of treating symmetrically and non-symmetrically loaded connections. In addition to allowances for variations in the connection detail, e.g. reinforcement ratio, member sizes, number of bolts etc., it also recognises the effect of the shear to moment ratio and the influence of axial column load. Because the method predicts the ultimate capacity, it employs ultimate (strain hardening) material strengths. Predictions from the method have been compared with the results of 6 laboratory tests for finplate connections from 2 different sources and 16

laboratory tests for cleated connections from 4 different sources. The comparisons clearly show that the method can predict the moment capacity of the composite finplate and angle cleated connections accurately.

8.12 References

8-1 BSI, BS5950 (1990) *Structural use of steelwork in building, Part 1: Code of practice for design in simple and continuous constructions*, London.

8-2 Jones, S. W., Kirby, P. A. and Nethercot, D. A. (1983) *The analysis of frames with semi-rigid connections - A state-of-the-art report*, Journal of Constructional Steel Research, Vol. 3, No. 2, pp. 2-13.

8-3 Zandonini, R. (1989) *Semi-Rigid Composite Joints*, Chapter 3 of Stability and Strength of Connection, ed. R. Narayanan, Elsiver Applied Science Publisher.

8-4 Xiao, Y., Choo, B. S. and Nethercot, D. A. (1994) *Composite connections in steel and concrete, part:1, Experimental behaviour of composite beam - column connections*, Journal of Constructional Steel Research, Vol. 31, pp. 3-30.

8-5 Eurocode No 3 (1992) *Design of Steel Structures, Part 1.1: General Rules for Buildings*, DD ENV 1993-1-1, April 1992, European Committee for Standardisation (CEN).

8-6 Ahmed, B. and Nethercot, D. A. *Effect of high shear on the moment capacity of composite cruciform endplate connections,* Journal of Constructional Steel Research (in press).

8-7 Ahmed, B. and Nethercot, D. A. *Effect of column axial load on composite connection behaviour,* Structural Engineering Review (under review).

8-8 Ahmed, B. and Nethercot, D. A. *Design of Composite Flush Endplate Connections,* The Structural Engineer (in press).

8-9 Jarrett, N. D. (1993) *Tests on four composite steel and concrete sub-frames,* Final report to BRE.

8-10 Xiao, Y. (1994) *Behaviour of Composite connections in steel and concrete,* Ph.D. thesis, Department of Civil Engineering, University of Nottingham, UK.

8-11 Leon, R. T., Ammerman, D. J., Lin, J. and McCauley, R. D. (1987) *Semi-rigid Composite Steel Frames*, AISC Engineering Journal, fourth quarter, pp. 147-155.

8-12 Davison, J. B., Lam, D. and Nethercot, D. A. (1990) *Semi-rigid action of composite joints*, The Structural Engineer, Vol. 68, No. 24, December, pp. 489-499.

8-13 Altmann, R., Maquoi, R. and Jaspart, J. P. (1991) *Experimental Study of the Non-Linear Behaviour of Beam-to-Column Composite Joints*, Journal of Constructional Steel Research, Vol. 18, pp. 45-54.

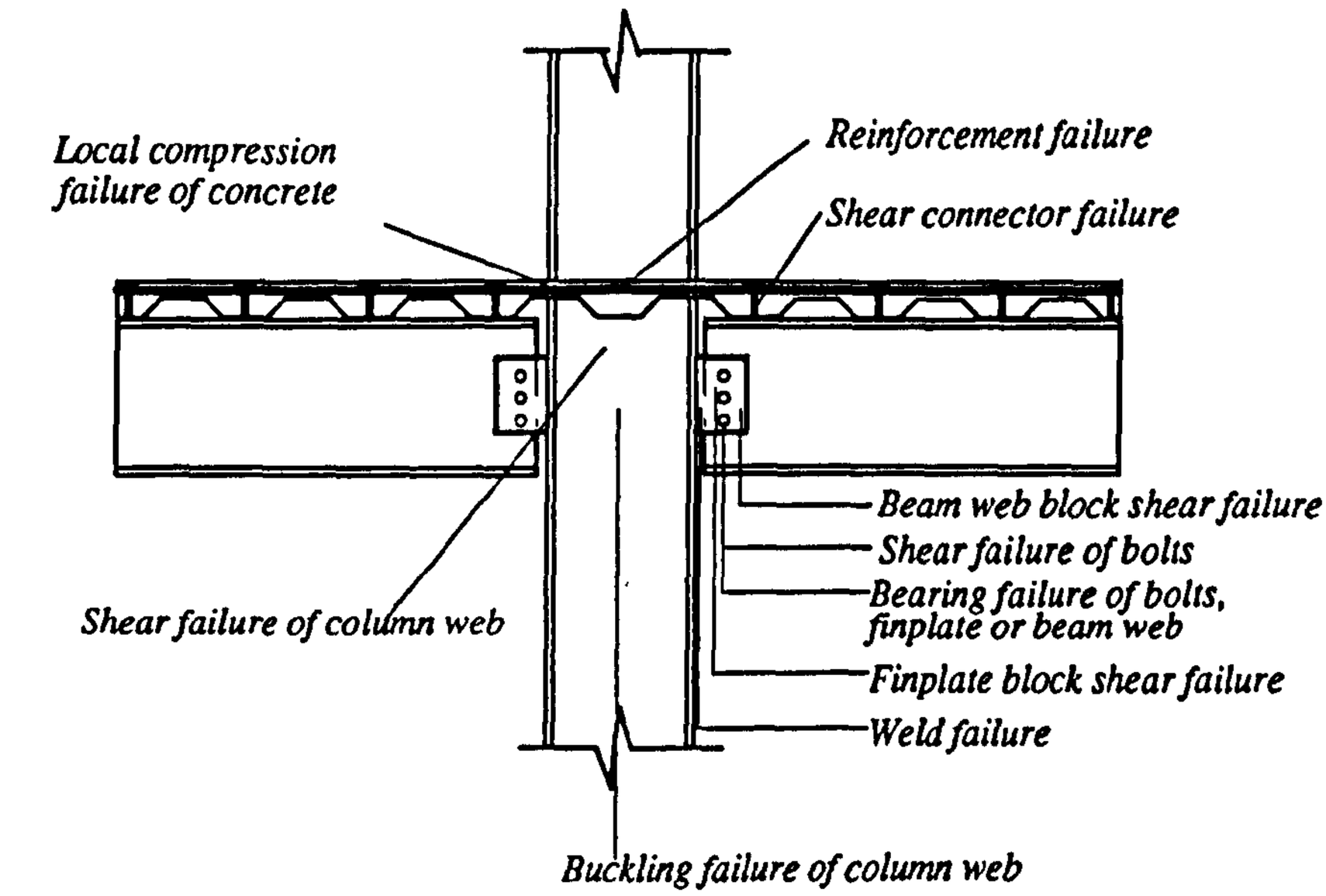

8-1(a) Composite finplate connection with possible failure modes

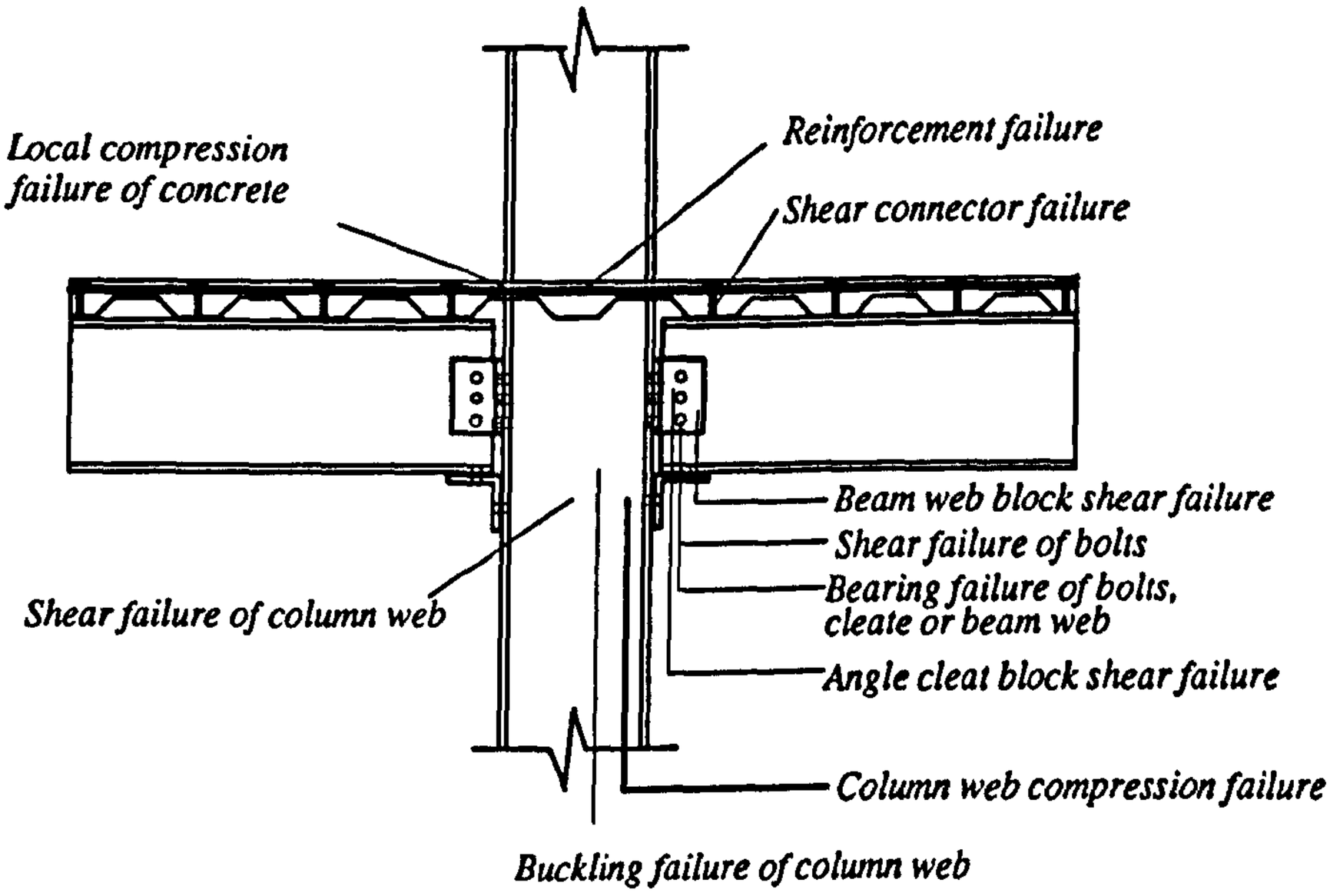

8-1(b) Composite angle cleated connection with possible failure modes

Figure 8-1 Composite finplate and angle cleatedconnections with possible failure modes

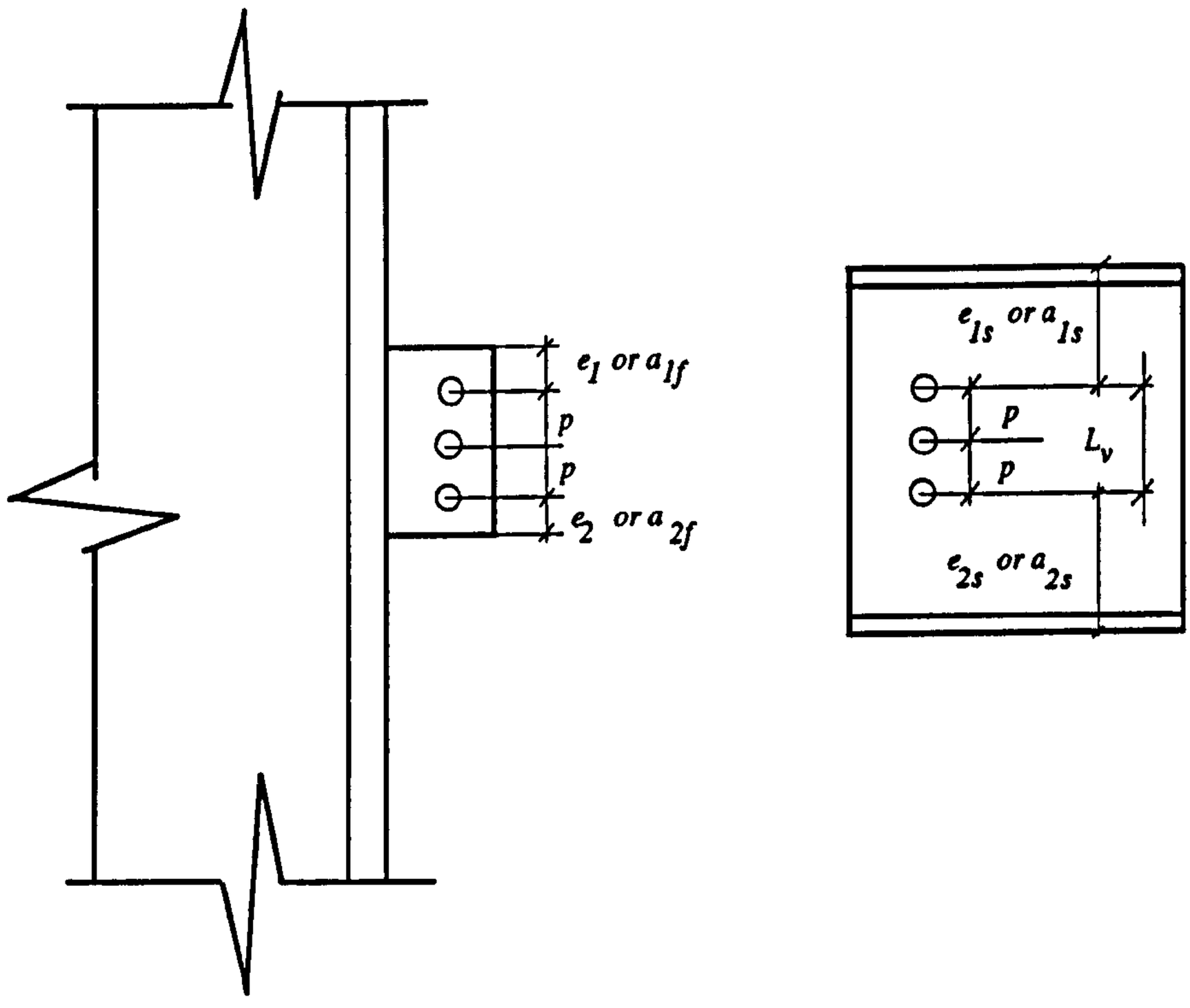

8-2(a) Side view of the finplate connection

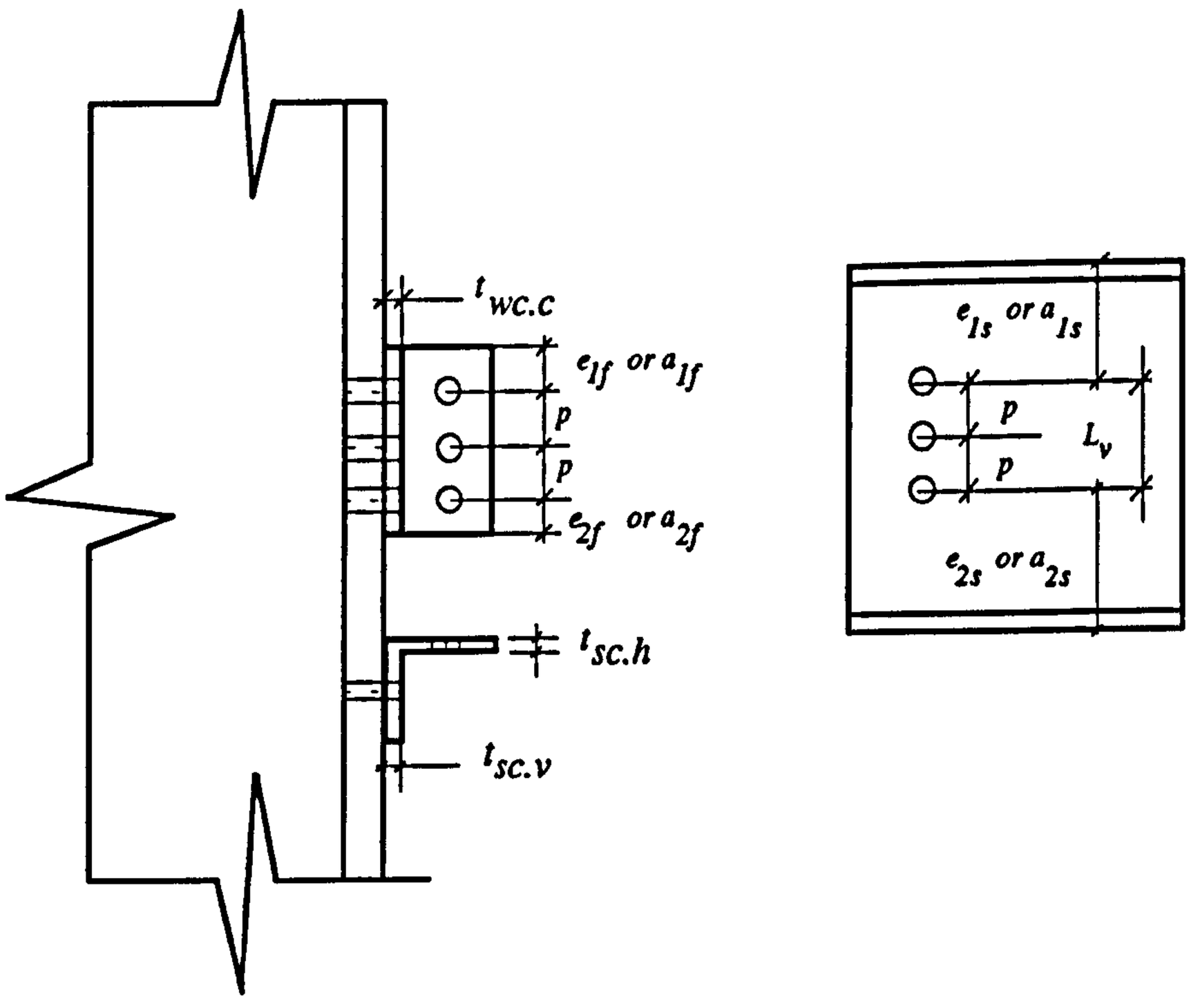

8-2(b) Side view of the cleated connection

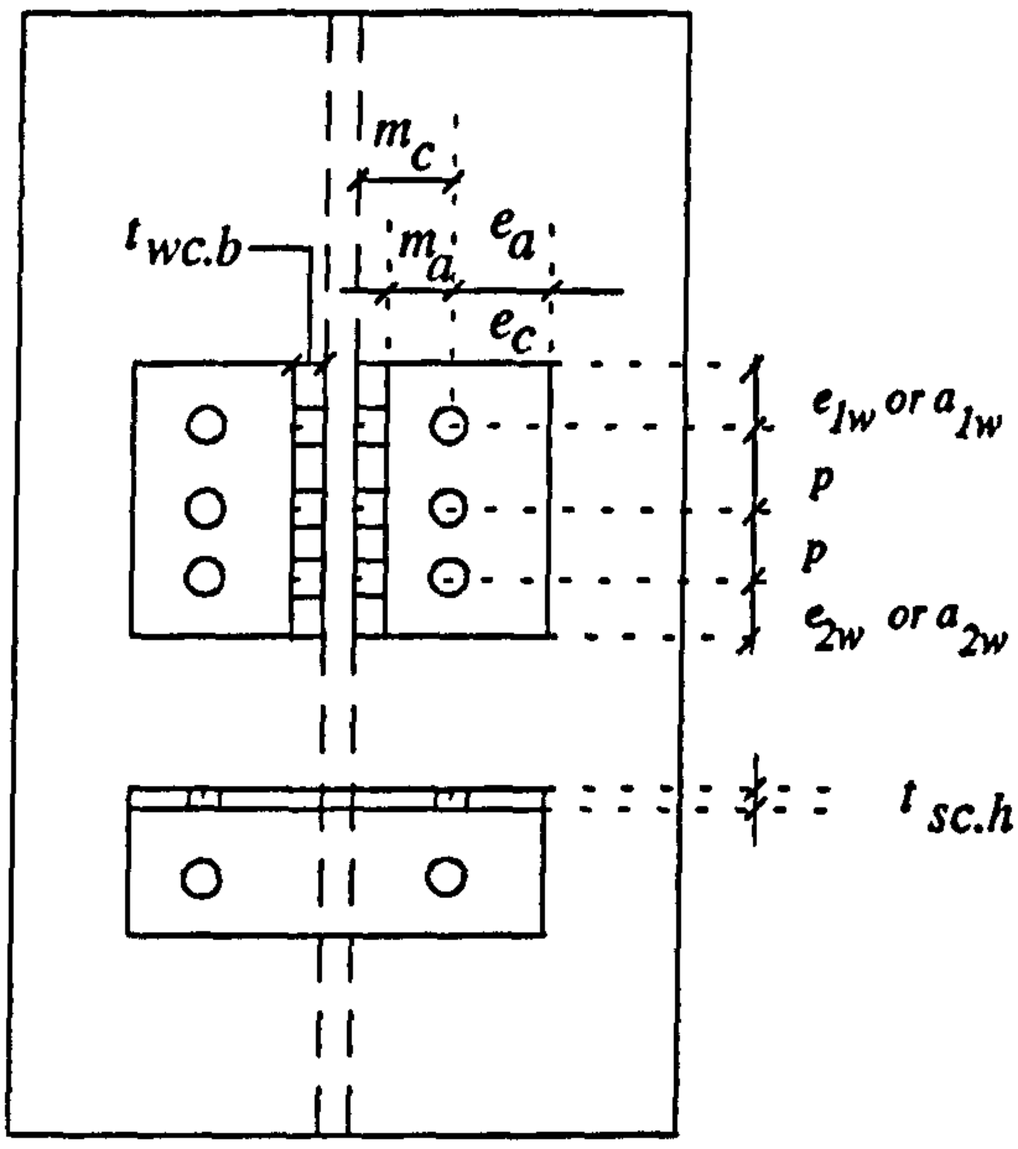

8-2(c) Front view of the cleated connection

Figure 8-2 Definition of geometrical parameters

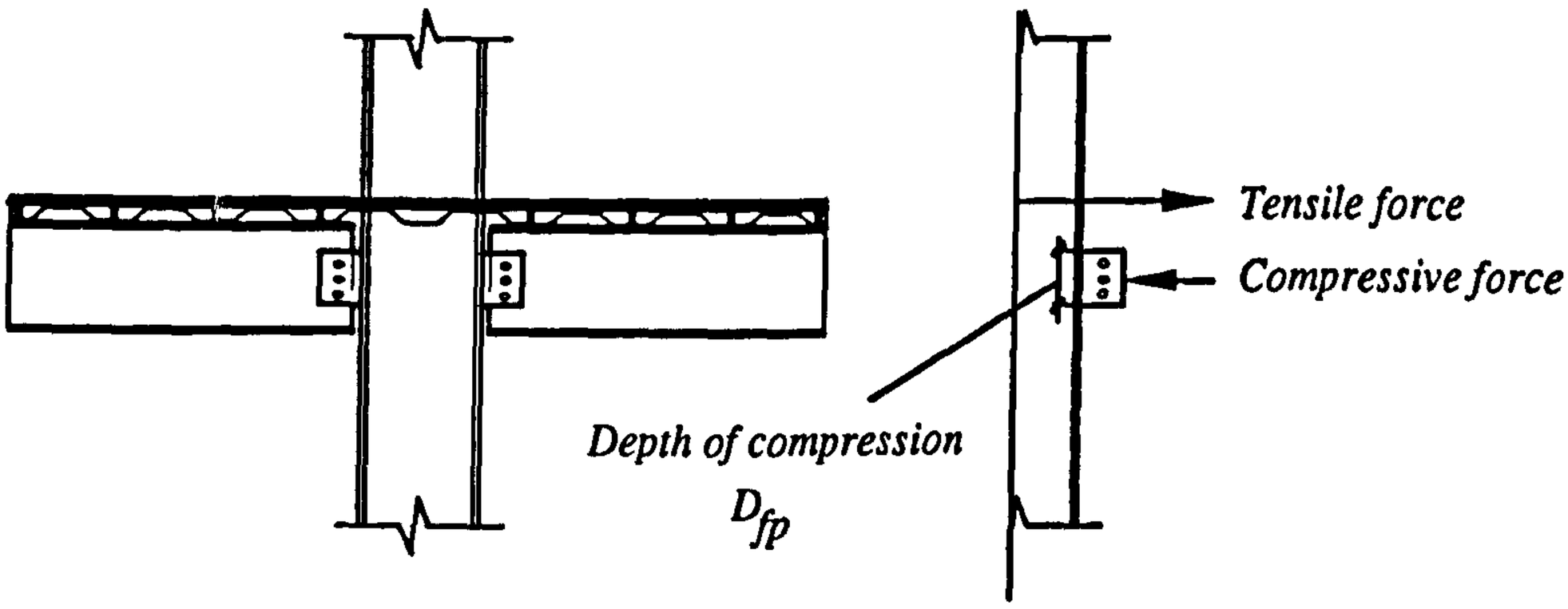

Column web compression area = $t_{cw}\ D_{fp}$

(a) Finplate and web cleat connection

8-3a Column web compression area for finplate and web cleat connections

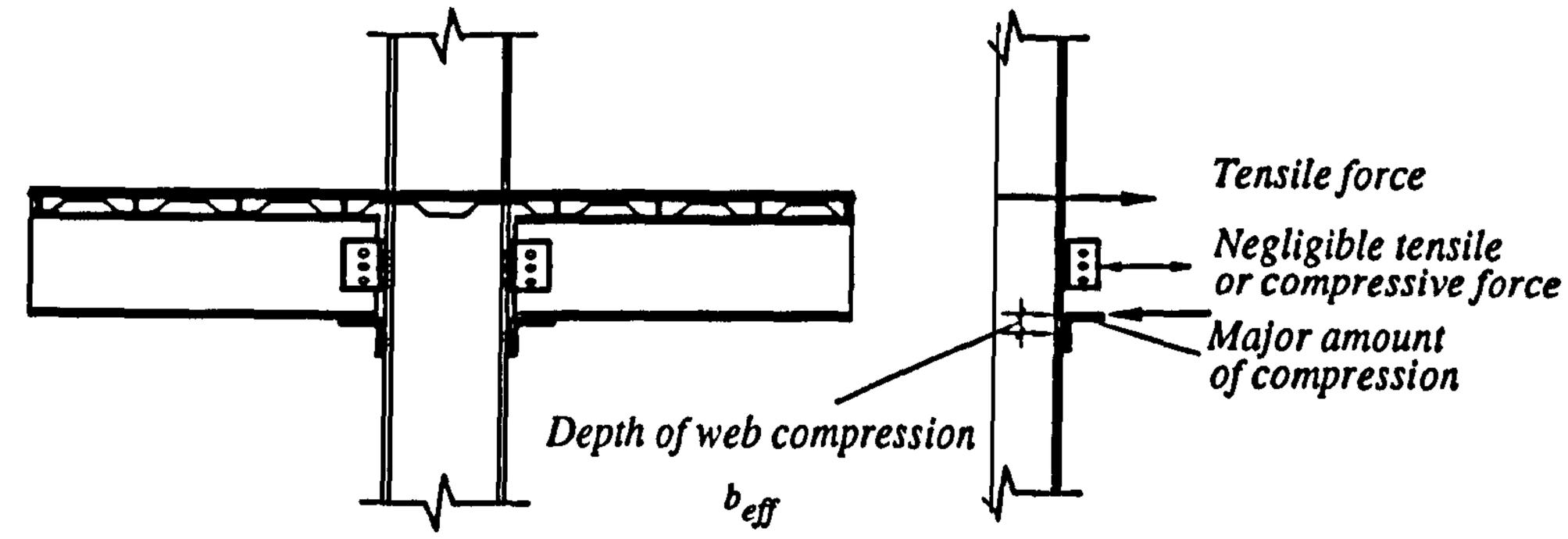

Column web compression area = b_{eff} t_{cw}

(b) Connection having a seating cleat

8-3b Column web compression area for connections having a seating cleat

Figure 8-3 Column web compression area for different conditions

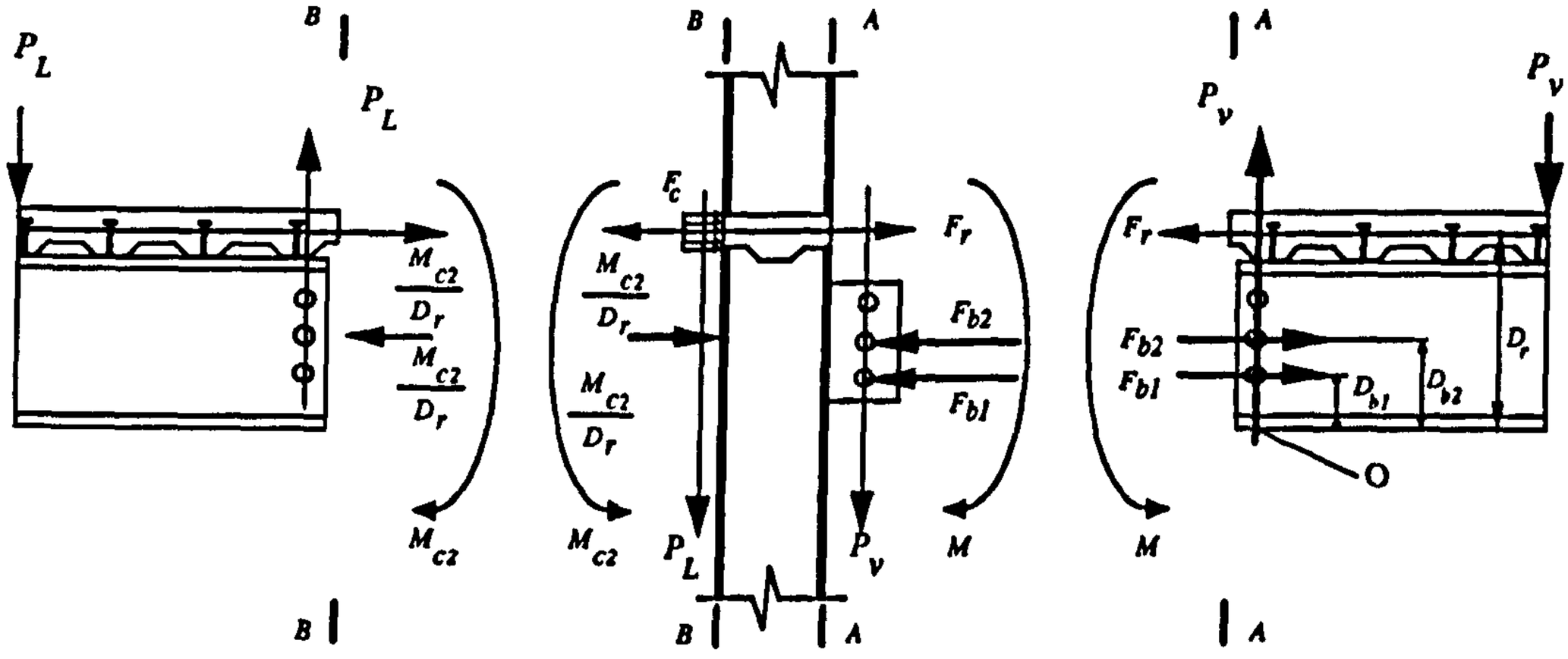

8-4(a) Free body diagram of the connecting parts showing internal forces (finplate connection and cleated connection with web cleats only)

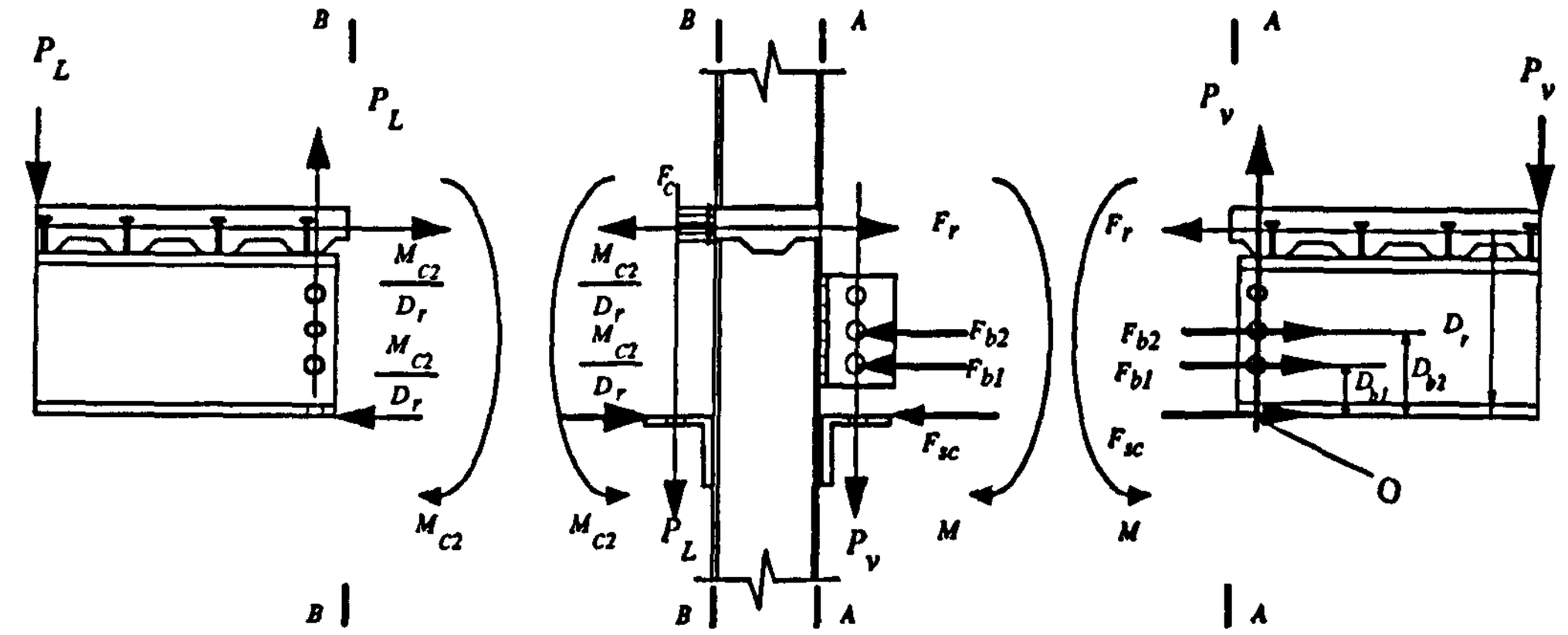

8-4(b) Free body diagram of the connecting parts showing internal forces (cleated connection with rebar force greater than seating cleat force)

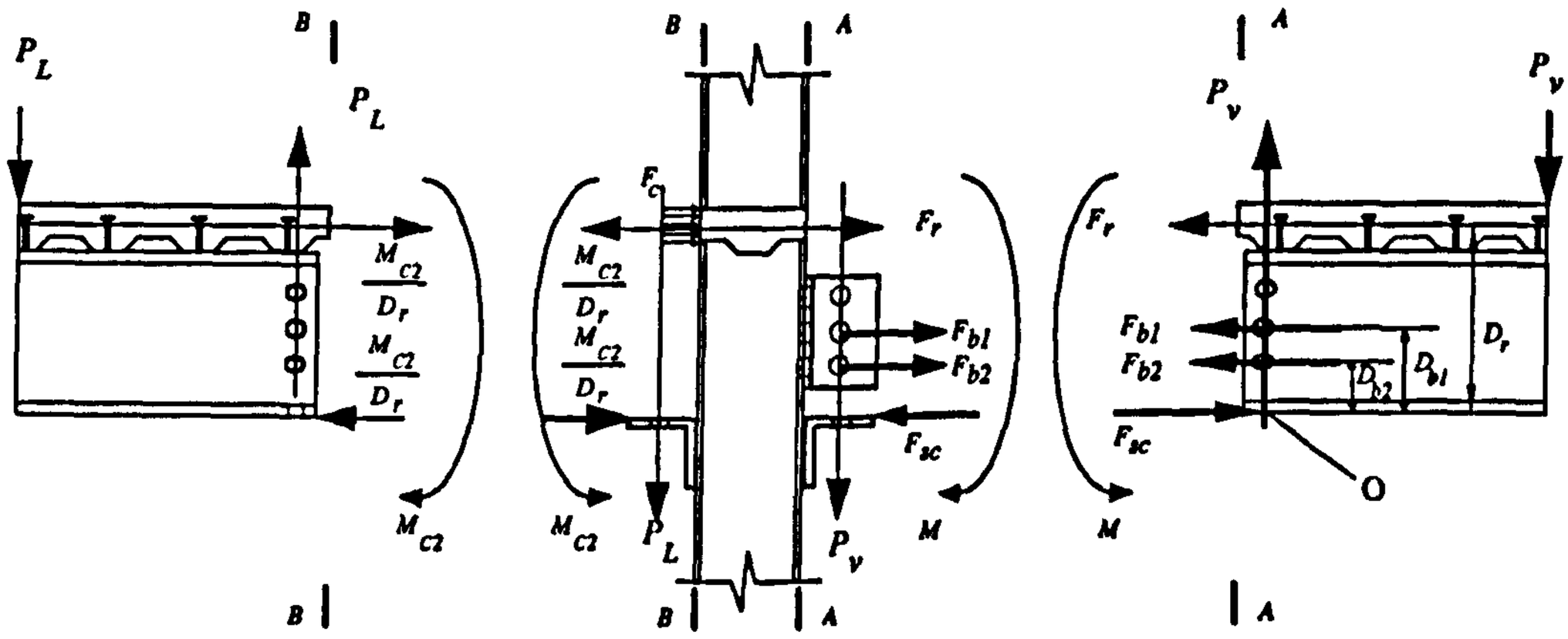

8-4(c) Free body diagram of the connecting parts showing internal forces (cleated connection with rebar force smaller than seating cleat force)

Note: $M_{c2} = \eta M$

Figure 8-4 Internal forces in composite finplate and angle cleated connection

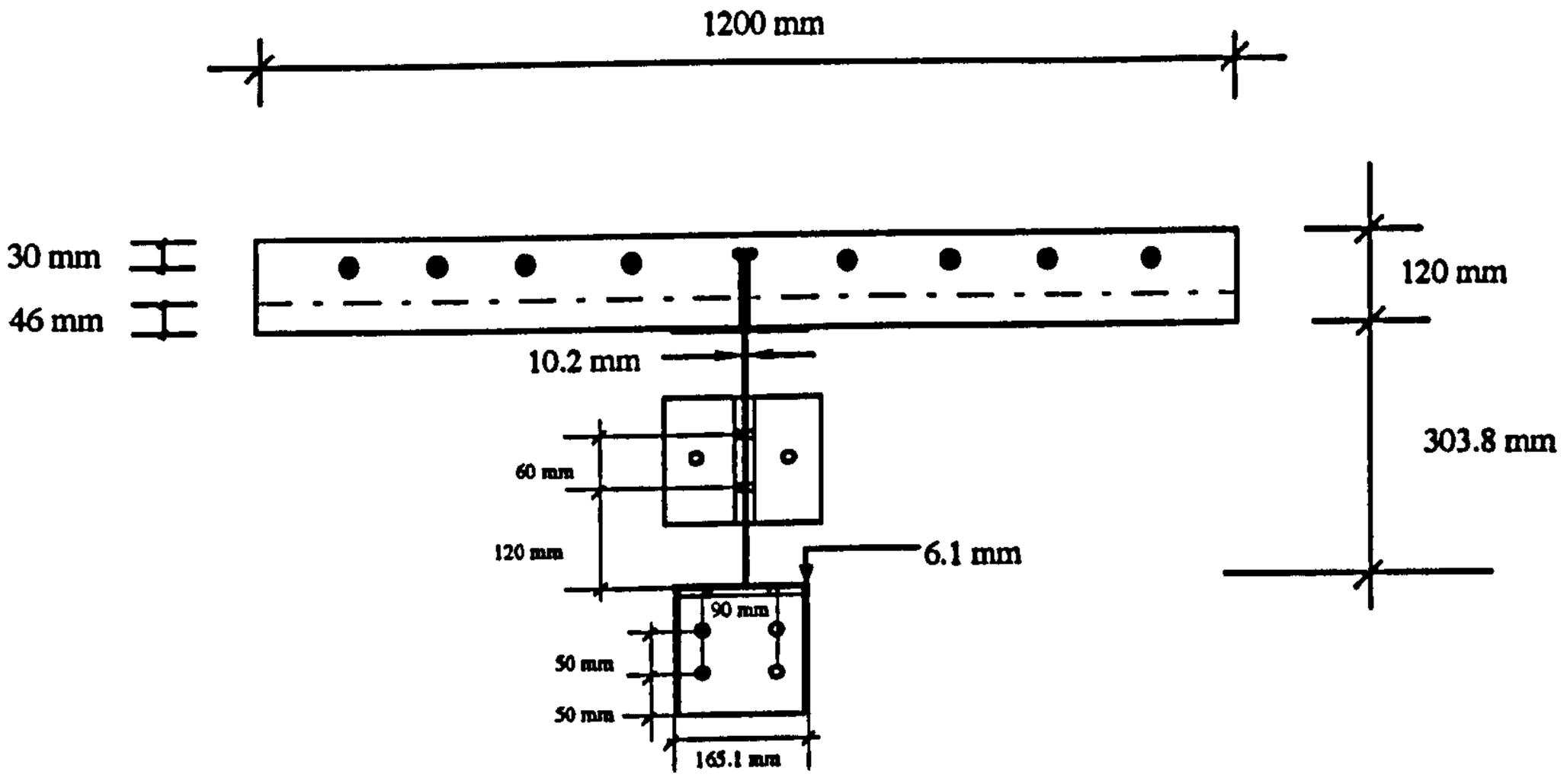

Figure 8-5 Cross section of the joint considered

Chapter 9

Numerical modelling and analysis of frames

9.1 Introduction

In chapters 3 to 8 simulation of composite connection's response, numerical techniques to investigate connection behaviour and that subsequently formed the basis for the development of design procedures for composite connections has been described. This chapter describes the numerical simulation of composite frames. The frame model is validated against test results for non-sway composite frames but due to limited availability of data, comparison was made only against bare steel results for sway frames. The results are used to develop a prediction equation for the sway of simple portal frames, which is extended to cover frames with multiple spans and multiple stories. This equation can be used either to calculate the sway deflections directly or to find the required column sections so as to limit the sway to a certain value for a given horizontal force during the design of frame structures.

9.2 Proposed FE model for the composite frame analysis

The modelling of the connections described earlier was undertaken in considerable detail as the objective was to develop a detailed understanding of connection behaviour; due to computing limitations frame analysis must employ a more economic approach that properly accounts for the essential features of frame behaviour. Since ABAQUS does not provide a composite element, three node quadratic beam elements, together with the BEAM GENERAL SECTION option to input properties, were chosen to model the composite beam; this allows for the inclusion of the moment curvature relationship for the beam, which can be obtained from the work of Li *et al*

[9-1]. The column was modelled by using BEAM section with I shape. For analysing bare steel frames the procedure is simple, both beam and the column are modelled by the BEAM section elements with I shape. The beam-to-column connections were modelled by spring elements based on the test moment rotation curve of the connections taken from reference 9-2.

The proposed model is similar to Ye Mei-xin *et al* [9-3] method for composite frames and the Li *et al* [9-4] method for steel frames with the following differences:

i) The proposed model of Ye Mei-xin made the assumption of the location of the points of contraflexure at 1/6 of span. The moment-curvature relations were imposed according to that assumption, i.e. for 1/6 of span on each side the moment-curvature for both positive and negative moment was taken as the negative moment-curvature relation. And for the inner 4/6 th of the span the moment-curvature for both positive and negative moment was taken as the positive moment-curvature relation. To eliminate this, instead of using a pre-decided location of contraflexure point the positive and negative moment-curvatures were used as input for all the beam members.

ii) The model proposed by Ye Mei-xin contains SPRING2 elements - which can take rotational properties as input but is basically a spring in two directions so it cannot give the rotations of connections as output.

iii) Ye Mei-xin's model does not consider the axial force that is transferred from the beam to the column through the connection; the proposed model is capable of doing so. The shear force that can be transferred to the column was calculated by dividing the moment capacity of the connection by the depth of the composite beam section and displacements were obtained by multiplying the rotation value of 0.06 rad by the depth of the composite section. This is done for positive and negative bending. Also the shear deformation of the bolts in the connection is introduced using spring elements.

iv) Instead of BEAM GENERAL SECTION for the columns BEAM SECTION with I shape beam elements was used.

v) Inclusion of the moment-rotation curve for beam upward loading, through the use of FE analysis of connections, which will allow the frame model to study sway frames.

9.2.1 Preparation of connection moment-rotation curve

A three step approach was taken to determine the connection moment-rotation curve which is described below:

- Step-1 Obtain the moment rotation curve of the connection for loading in the downward direction using the previously described FE model or from test results
- Step-2 Obtain the moment rotation curve of the connection for loading in the upward direction using the previously described FE model or from test results
- Step-3 Combine the moment rotation curves to obtain a moment rotation curve for loading in any direction

The above three step procedure is a generalised one; for non-sway composite frame modelling, preparation of a moment rotation curve as described in Step-1 is sufficient.

9.2.2 Preparation of composite beam moment-curvature curve

Once the connection moment - rotation data preparation is complete, the focus should be the modelling of the composite beam. Unfortunately the software in use does not provide any composite beam element. So it becomes essential to represent the composite beams in such a way that the actual behaviour of the composite beam is

modelled. To prepare the moment-curvature relation of the composite beam section the following equations proposed in ref. 9-1 were used:

In the sagging moment region the moment-curvature relation of a composite beam is:

$$\Phi = \begin{cases} \dfrac{M}{EI} & 0 \le M \le M_y \\ \dfrac{M}{EI} + \left(\Phi_u - \dfrac{M_u}{EI}\right)\left(\dfrac{M - M_y}{M_u - M_y}\right)^2 & M_y \le M \le M_u \end{cases}$$

$$\Phi_u = 5.7\left(\frac{h_s}{h_c}\right)^{0.2} \bullet \frac{M_y}{EI}$$

Where:

M_y is the first yield moment

M_u is the ultimate moment

Φ_y is curvature at first yield moment

Φ_u is curvature at ultimate moment

h_s is the depth of steel beam

h_c is the depth of concrete slab

In the hogging moment region the moment-curvature relation of a composite beam is:

$$\Phi' = \begin{cases} \dfrac{M'}{EI'} & 0 \le M' \le M'_y \\ \dfrac{M'}{EI'} + \left(\Phi'_u - \dfrac{M'_u}{EI'}\right)\left(\dfrac{M' - M'_y}{M'_u - M'_y}\right)^2 & M'_y \le M' \le M'_u \end{cases}$$

$$\Phi'_u = 5.3\frac{M'_y}{EI'} + 2.4$$

The symbols are similar to the previous ones, but $'$ stands for hogging moment region.

9.2.3 Comparison of results for non-sway composite frame

In reference 9-5 two composite frame tests are described: frame-A and frame-B. Analyses were carried out for both. The test set-up of the frame-A test is illustrated in Figure 9-1. The bases of the columns were restrained from all displacements and rotations and other restraints as mentioned in reference 9-5 were applied to maintain the non-sway behaviour. Details of the connections can be obtained from reference 9-2.

To model the frame it was essential to make a reasonable choice of the connection moment-rotation curve. From the loading shown in Figure 9-1b, it was decided that connections 1, 4, 5, 6, 7 and 8 should use the moment rotation curve for the non-symmetrically loaded connections and connections 2 and 3 should use the moment rotation curve of the symmetrically loaded connections. These curves were taken from the connection tests reported in reference 9-2 from connections CJS-2 and CJS-1 respectively. The chosen curves are shown in Figure 9-2. Following the procedure described in section 9.2.2 the moment - curvature relation was constructed for the composite beams. These are shown in Figure 9-3 (as the test sagging moment of beam-2 (252kN•m) shown in Figure 9-10 was greater than the calculated moment of resistance using the methods of BS5950 the full curve shown in Figure 9-3 was proportionately increased for beam-2).

Results of the FE analysis are compared with the experiment [9-5] in Figures 9-4 and 9-5 for the connection moment rotation curves. It can be seen that a reasonable estimate of the connection moment rotation behaviour was obtained. Figure 9-6 compares the deflection at mid-span of beams 1, 2 and 4. The comparison shows a good agreement between the test and numerical results. Table 9-1 compares the beam moment distribution. The moments at different sections agree with the results obtained from the finite element analysis. This shows clearly that with proper attention to detail

it is possible to model the behaviour of non-sway composite frames in a way that closely simulates their physical behaviour.

Table 9-1 Comparison of beam moment at final load in test [9-5] with FE results

Connection moment (kN-m)								
	J-1	J-2	J-3	J-4	J-5	J-6	J-7	J-8
Test	121.0	154.0	154.0	95.0	27.7	67.0	133.0	101.0
FE	105.4	152.3	151.3	104.7	16.7	52.9	111.3	108.7
Span moment (kN-m)								
	beam-1-L	beam-1-R	beam-2-L	beam-2-R	beam-3-L	beam-3-R		
Test	238.0	226.0	250.0	269.0	236.0	247.0		
FE	248.8	233.1	248.9	264.4	247.8	248.7		

9.2.4 Simplified approach for frame model

To obtain a good comparison between the test and the FE results, besides the moment distribution in the beam and connection, it is essential to compare the moment distribution in the columns. To compare the moments at the top and bottom of the connections two approaches may be used. One is to introduce additional spring elements at the top and the bottom of the connection, having the plastic moment capacity of the column section. The other way is to introduce additional nodes at the top and the bottom of each connection that approximately represent the location of the top and bottom of the actual connection; this will require very small elements to model the columns so as to prevent the sudden change in element size. The first possibility will be explored herein.

Figure 9-7 shows the finite element representation of the beam-to-column connection. Until now results have been compared for the beams, as the behaviour of the beams is now representative of the test, attention can be focused on the columns. From Figure 9-7b, which is a slight modification to Ye Mei-xin *et al* [9-3] model of composite

connections or Li *et al* [9-4] model for bare steel connections, it can be seen that the following discrepancies from the real behaviour are still present:

1 It does not account for the beam-to-column connection's capacity to transfer tensile force and the connection deformation

2 It does not account for the beam-to-column connection's capacity to transfer shear force and the connection deformation

3 It does not account for the presence of different shear forces at the top and bottom of the beam-to-column connection

4 It does not account for the presence of different bending moments at the top and bottom of the beam-to-column connection

To overcome these shortcomings the connection model shown in Figure 9-8 was adopted. The beam-to-column connection shown in Figure 9-8 consists of four springs, each spring property is the force-deformation in the horizontal and vertical direction, and the moment rotation property of the component which it represents. For example the maximum possible horizontal force in spring OA is the axial load capacity of the connection, the maximum possible vertical force in spring OA is the shear capacity of the connection, and the moment-rotation behaviour is the moment-rotation behaviour of the connection. For spring OD, the horizontal load is the column web shear capacity, vertical load is the column ultimate tensile load, and the moment is the plastic moment of the column section. The use of an additional two springs for the column web eliminates the problem mentioned above and makes the model sufficiently flexible to study the moment distribution in the full frame. Results for column moments are compared in Table 9-2 for frame-A.

Table 9-2 Comparison of column moment and shear force for with and without column springs

Comparison of connection moments						
	$M_{J5\text{-}a}$ (kN-m)	$M_{J5\text{-}J1}$ (kN-m)	$M_{J7\text{-}b}$ (kN-m)	$M_{J7\text{-}J3}$ (kN-m)	$M_{J5\text{-}c}$ (kN-m)	$M_{J8\text{-}J4}$ (kN-m)
No column spring	-11.39		0.52		9.85	
With column spring	1.73	-13.23	39.7	-35.09	-46.71	55.19
Comparison of connection shear force						
	$V_{J5\text{-}a}$ (kN)	$V_{J5\text{-}J1}$ (kN)	$V_{J7\text{-}b}$ (kN)	$V_{J7\text{-}J3}$ (kN)	$V_{J5\text{-}c}$ (kN)	$V_{J8\text{-}J4}$ (kN)
No column spring	7.79		7.61		-33.57	
With column spring	0.899	16.83	16.72	-11.35	19.29	-29.85

The moments in Table 9-2 for the frame model without the column web spring at first appearance may be thought misleading concerning the equilibrium due to the difference in column moment and the connection moment. The fact is, that the results are calculated for the integration point for the beam elements representing the column - which is not the point where the connection is located, but the integration point of the spring element which represents the connection of the beam and the column. So when the column moment is calculated at the nodal point (connection point as well), the two results from the two integration points which are extrapolated to the nodal point are added together, and the magnitude becomes small as they have opposite signs due to the sign convention (although acting in the same direction). It is observed that in Table 9-2, values - without column web spring elements - are the difference between the values of the two nodes. The minor difference which occurs is due to the other changes made to the model.

Figure 9-9 shows the test arrangement for frame-B. This frame was analysed by including the springs to simulate the column moment distribution. Figure 9-10 shows the moment distribution in the composite frame obtained from the test; whilst Figure 9-11 shows the FE results for frame-B. Comparison of the results shows that the

agreement between the test and the FE analysis is very good, thereby confirming that FE analysis is suitable to carry out the analysis of composite frames, including the allowance for semi-rigid connection effects. It is worth mentioning at this point that with this modified model (rather than the one shown in section 9.2.3), the beam deflection may become less accurate than the one shown in Figure 9-6. This is primarily due to the spring elements at the top and bottom of the connection that contains the moment - rotation for column. If the given rotation values are higher the deflection of the beam span will be larger and vice versa.

9.2.5 Conclusions on the FE modelling of composite non-sway frames

A numerical model using the general purpose finite element software ABAQUS to simulate the response of semi-rigid composite non-sway frames has been described. Tests carried out by the University of Nottingham in conjugation with BRE were used to verify the model. Availability of these proven numerical techniques greatly increases the range of issues that can economically be studied.

9.3 Sway of unbraced steel frames

9.3.1 Theoretical derivations for the two extreme cases for the calculation of sway

For the simple portal frame of Figure 9-12, with rigid beam-to-column connections, the lateral drift can be expressed as:

$$\Delta = \frac{PH_1^3}{6EI_{col}} \frac{2\alpha+3\beta}{2\alpha+12\beta} \qquad (9\text{-}1)$$

Where:

$$\beta = \frac{EI_2}{EI_{col}}$$

$$\alpha = \frac{L_2}{H_1}$$

H_1 is the height of the column

L_2 is the span of the beam

EI_{col} is the rigidity of the storey

EI_2 is the rigidity of the beam

If the beam is assumed to have a large stiffness compared to that of the columns i.e. β is very large compared with α in equation 9-1, for storey height H_1, column inertia I_{col}, the sway of the column top can be simplified as:

$$\Delta = \frac{PH_1^3}{24EI_{col}} \qquad (9\text{-}2)$$

The above is equivalent to the assumption of a connection element at the beam-to-column connection with infinite rotational stiffness, which is capable of transferring any magnitude of moment.

When the beam stiffness is fairly low compared to that of the column, i.e. β becomes very small compared with α in equation 9-1, the column acts as a cantilever and the beam becomes a link to transfer the force P between columns, and the sway becomes:

$$\Delta = \frac{PH_1^3}{6EI_{col}} \qquad (9\text{-}3)$$

The above is equivalent to the assumption of a connection element at the beam-to-column connection with zero rotational stiffness, which cannot transfer any level of moment.

Comments on the equations

Equation 9-1 is based on the assumption that the connection between the beam and the column is rigid and any magnitude of moment can be transferred without rotation of the beam - column connection itself. Equations 9-2 and 9-3 are special forms of equation 9-1. In practice, the beam-to-column connection may not be rigid and may have a limited moment capacity. In this case, in addition to the stiffness of the beam relative to the columns, the stiffness and the moment capacity of the connection will also affect the load - sway response of the frame. If the presence of the beam - to column connection between the columns is neglected i.e. the load is divided equally between the columns, the sway is equal to that given by equation 9-3. So it can be concluded that equation 9-2 represents a rigid connection between the beam and columns with a rigid beam, whilst equation 9-3 represents a pin connection between the beam and the column - where the beam serves only to transfer the load between columns and its bending stiffness plays no role on sway displacement.

Equations 9-2 and 9-3 define the extreme cases: if the column is much stiffer than the beam it will behave as a cantilever and the connection's rotational stiffness will not significantly affect the sway behaviour, but when the beam is stiffer than the column the sway behaviour will be dependent solely on the connection stiffness and depending on the precise value the sway may be as little as 1/4 of that of the stiffer rigid column frame. Although equation 9-1 covers the intermediate cases, it does not include connection stiffness. It is therefore necessary to expand the scope of the analysis to include the connection stiffness during the sway calculation, since equation 9-1 can only be used to calculate the sway of rigid-jointed frames. To cover the whole range three equations are needed: equation 9-1 for rigid-jointed frames, equation 9-3 for pin connected frames and an extra equation to deal with semi-rigidly connected frames.

9.3.2 Multi-storey frames

Ammerman and Leon [9-6] proposed an equation to calculate the sway of frames with multiple stories and multiple bays as:

$$\Delta = \frac{PH^3}{\alpha E \sum I_{col}} \qquad (9\text{-}4)$$

Equation 9-4 proposed by Leon [9-6] uses the total frame height to calculate the sway of multi-storey frames. Previously, the derivation of sway (equations 9-1 to 9-3) was based on a single storey, single bay frame. The difference in sway behaviour for a single storey frame and a frame with several stories is that the single storey frame moves horizontally due to the action of the applied load only (Figure 9-13a) as shown in equations 9-1 to 9-3. For the bottom storey of a frame with several stories (Figure 9-13c), horizontal movement is produced by a combination of i) the shear (Figure 9-13a) which is equal to the horizontal applied load and ii) the concentrated moments (Figure 9-13b) at the tops of the columns of that storey. Sway of the upper stories (Figure 9-13c) will be due to the combined effect of: the horizontal load, rotation of the base and sway of the base of that storey. So the sway given by equations 9-1 to 9-3 must be corrected to include these effects. When the equation proposed by Leon [9-6] is used, it does not consider the effect of the moment at the column tops for the intermediate stories for load above those (e.g. when calculating the sway of the 3 rd storey with load at the 6 th storey, only the height of storey 3 and the load is used, the induced moment is not taken into consideration). The Leon equation was discussed in detail in chapter 1. These additional effects will now be investigated.

Calculation of sway for the bottom storey

For direct load *P* the sway (Figure 9-13a) is:

$$\Delta_p = \frac{PH_1^3}{6EI_{col}} \frac{2\alpha+3\beta}{2\alpha+12\beta}$$

For the moment $M = \frac{P(H_T - H_1)}{N_b}$ (assuming that the moment is equally divided at the top of each column), where N_b is the number of columns, using simple calculations the sway (Figure 9-13b) is:

$$\Delta_m = \frac{MH_1^2}{2EI_{col}} \frac{\alpha}{\alpha+6\beta}$$

So the total sway at the top of the bottom storey is obtained by summing the above two components:

$$\Delta_1 = \left[\frac{(2\alpha+3\beta)}{6} PH_1 + M\alpha\right] \frac{1}{\alpha+6\beta} \frac{H_1^2}{2EI_{col}}$$

$$= \left[4+6\frac{\beta}{\alpha}+12\frac{H_T-H_1}{H_1N_b}\right] \frac{1}{1+6\frac{\beta}{\alpha}} \frac{PH_1^3}{24EI_{col}}$$

Where:

$$M = \frac{P(H_T - H_1)}{N_b}$$

H_T and H_1 are the total and ground floor height of the frame and the total moment is assumed to be equally shared by the columns.

Using $K_b = \frac{4EI_2}{L_2}$

$$6\frac{\beta}{\alpha} = 6\frac{EI_2}{EI_{col}}\frac{H_1}{L_2} = \frac{4EI_2}{L_2}\frac{3H_1}{2EI_{col}} = \frac{3K_bH_1}{2EI_{col}}$$

Substituting $6\frac{\beta}{\alpha} = \frac{3K_bH_1}{2EI_{col}}$, Δ_1 becomes

$$\Delta_1 = \frac{PH_1^3}{3E(2I_{col})}\frac{1+\frac{3K_bH_1}{8EI_{col}}+3\frac{H_T-H_1}{H_1N_b}}{1+\frac{3K_bH_1}{2EI_{col}}}$$

In general terms for any number of bays the equation for sway deflection can be written in a simplified form as:

$$\Delta = \frac{PH_1^3}{3E\sum I_{col}}\frac{1+\frac{3K_bH_1}{8EI_{col}}+3\frac{(H_T-H_1)}{N_bH_1}}{1+\frac{3K_bH_1}{2EI_{col}}} \qquad (9\text{-}5)$$

Calculation of sway for the upper storey of a two storey frame

The top of the lower storey rotates due to the horizontal load and the moment to give the rotation:

$$\theta = \frac{PH_1^2}{2EI_{col}}\frac{\alpha}{2(\alpha+6\beta)} + \frac{MH_1}{EI_{col}}\frac{\alpha}{\alpha+6\beta} \qquad (9\text{-}6)$$

$$= \left(\frac{PH_1}{4}+M\right)\frac{H_1}{EI_{col}}\frac{\alpha}{(\alpha+6\beta)}$$

Equation 9-6 is based on the assumption that the top of the ground floor column is not constrained against rotation by the upper floor column; this assumption leads to a higher rotation for the case of rigid connections. This is due to the fact that in a frame with rigid connections the horizontal movement will be restrained by the combined action of connections and the beams. Hence the above rotation, when used to calculate the sway of the top floors, will generally overestimate the sway of rigid-jointed frames. But for pin-connected frames this problem would not arise (as no rotational restraint is provided by the beam-to-column connections). Due to the transfer of moments to the beams in the case of rigid and semi-rigid beam-to-column connections, the moments at the top of a column and at the bottom of the column above it will not be equal and thus the rotations are overestimated by the above equation and hence the displacements will also be overestimated.

The sway of the top floor according to equations 9-5 and 9-6 is:

$$\Delta_2 = \left(\frac{PH_1}{4} + M\right)\frac{H_1^2}{EI_{col}}\frac{\alpha}{(\alpha+6\beta)} + \frac{(2\alpha+3\beta)}{2(\alpha+6\beta)}\frac{PH_1^3}{6EI_{col}} + \left[\frac{(2\alpha+3\beta)}{6}PH_1 + M\alpha\right]\frac{1}{\alpha+6\beta}\frac{H_1^2}{2EI_{col}} \qquad (9\text{-}7)$$

the first term is the sway due to rotation of the base of the upper floor

the second term is the deflection of the upper floor

and the third term is the sway of the top of the lower floor

Substituting zero for both M and β to simulate a two storey pinned frame the sway from equation 9-7 is:

$$\Delta_2 = 8\frac{PH_1^3}{6EI_{col}}$$

Which is the same as that obtained by replacing H_1 by $2H_1$ in equation 9-3 i.e. the equation gives the correct result for pin connected frames.

Since the equation becomes fairly complicated for multi-storey frames, a simpler method is required. The form of equation 9-7 will now be used to develop an empirical formula using results from finite element analysis to calibrate the equation.

Adjustments to stiffness value to account for connection stiffness

It should be noted that for rigid-jointed frames the theoretical equations contain a term that includes the stiffness of the beams; for semi-rigid frames either the stiffness of the connection or the stiffness of the beam may govern. So the equations must be modified to ensure that the smaller of these stiffnesses will govern. The simplified approach to this is to use the minimum stiffness K_e between the connection stiffness (K_i) and the beam rotational stiffness (K_b) in equation 9-5 instead of using the beam rotational stiffness. Thus:

$$\Delta = \frac{PH_1^3}{3E\sum I_{col}} \frac{1+\frac{3K_eH_1}{8EI_{col}}+3\frac{(H_T-H_1)}{N_bH_1}}{1+\frac{3K_eH_1}{2EI_{col}}} \qquad (9\text{-}8)$$

Where:

$$K_e = min\begin{cases} K_b \\ K_i \end{cases}$$

It should be noted that K_i represent the rotational stiffness of the connection obtained from the moment rotation curve and corresponding to the level of induced moment in the connection.

9.4 Verification of the FE model in sway mode

In the absence of sufficient information about the sway behaviour of composite frames, it was decided to validate the numerical model against the available results for bare steel frames. This was considered sufficient as the numerical model of the composite frame is already validated for gravity loading, which provided excellent comparisons against the test results. For bare steel frames the results presented by Lui and Chen [9-7, 9-8] were selected.

The verification of the model is made for three separate types of analyses:

1 Elastic buckling load of simple portal semi-rigid frame

2 Elastic stability limit load of two storey unbraced semi-rigid frame, with fixed and pinned support

3 Analysis of a simple sway portal frame with beam span loading

9.4.1 Elastic buckling load of simple portal semi-rigid frame

This check uses a single bay one storey portal frame with semi-rigid connections. The supports are pinned, EI and L of all members are constant. It has been shown by Lui & Chen [9-7] that under such conditions if EI/LR_k=0.1 (connection stiffness is constant), the theoretical critical load for elastic-buckling is $1.56EI/L^2$. The frame is shown in Figure 9-14(a), and the result with non-dimensional quantities is shown in Figure 9-14(b). Deflections are that of the left column top. It can be seen that the results of the FE analysis are very close to the results reported in reference 9-7, thereby demonstrating that the column behaviour is accurately modelled.

9.4.2 Elastic stability limit load of two storey unbraced semi-rigid frame, with fixed and pinned supports

The second example is also selected from Lui and Chen [9-7]. It is a single bay two storey portal frame. One of the analyses is for a rigidly jointed frame and the other assumes semi-rigid connections, for which the connection moment rotation curve is described by Lui & Chen. Figure 9-15(a) shows the frame analysed by Lui & Chen. Figure 9-15(b) shows the comparison of results between the developed FE model and results of Lui & Chen, for two types of connections, when the supports are fixed. Figure 9-15(c) shows the comparison of results between the developed FE model and results of Lui & Chen, for two types of connections, when the supports are pinned. These demonstrate that the support conditions, connection types and the influence of several stories are properly simulated in the finite element model.

9.4.3 Analysis of a simple sway portal frame with beam span loading

The third example is chosen from Lui & Chen [9-8]. The sway frame is shown in Figure 9-16(a). The moment rotation curve was described in terms of column plastic moment, assuming 50 ksi strength, the curve was generated for FE analysis using ABAQUS. First the vertical load was applied then the horizontal load was applied. Comparison of the results is shown in Figure 9-16(b). The discrepancies at the ultimate load level occurred due to the assumed connection moment rotation curve, which was reported by Lui & Chen in terms of non-dimensional moment (connection moment/column plastic moment) verses rotation. It was found that the displacement magnitudes reported by Lui & Chen were lower than those obtained at the ultimate load levels which indicate that the assumed column plastic moment was lower than that used by Lui & Chen.

9.5 FE analysis for sway of steel frames

The FE analyses can be classified into two categories. The first is the simple case of a single storey frame. This will provide an indication of the main trends in behaviour. The second covers frames with several stories, which is required for practical calibration. Within both categories, the following items have been considered:

1 Connection stiffness

2 Relative stiffness of beam and columns

3 Effect of beam to column span ratio

4 Effect of multiple bays

The frames selected for analysis consist of several combinations of beams and columns as well as connection stiffnesses. Connection stiffness 0 (pin connection), 200, 1000, 2000, 4000, 8000, 10000, 20000, 30000 kN-m/rad and infinite (rigid connection) have been used. The beam and column sections used in the analyses were the same in most cases and represent the cross section of a universal column section of 203x203UC46; where the effect of relative stiffness was studied a column section of 356x368UC202 was used. To maintain the same relative stiffness of beam and column, storey height and width is kept constant at 4.953 m (and the section for beam and column) in most of the analyses except those discussed in section 9.5.2 which had a larger column section to study the effect of greater column stiffness.

9.5.1 Results of FE analysis, effect of connection stiffness

Results of the analyses using the sections 203x203UC46 for beams and columns having lengths of 4.953m are shown in Figure 9-17. From this it can be seen that even with very large connection stiffnesses it was not possible to obtain the load-sway response of a rigidly-jointed frame. Using a very low connection stiffness produces a

load-sway response virtually identical to that of the pin connected frame. Thus any general equation relating the connection stiffness with sway should be based on the load-sway behaviour of the pin connected frame. From Figure 9-17 it can also be seen that the load sway relation is linear. So if it is possible to determine the deflection for one load level, the sway for any other load levels can be calculated. To determine the relation between sway and connection stiffness for various load levels the sway versus connection stiffness is plotted in Figure 9-18. From this it can be seen that the relation takes the form of an exponential decay. When plotted as non dimensional quantities the curves of Figure 9-18 actually merge with each other as shown in Figure 9-19. Applying regression analysis to the results, the following equation is developed to link non dimensional sway with non dimensional connection stiffness:

$$\Delta_n = 0.6057 K_n^{-\frac{1}{6}} \tag{9-9}$$

Where:

$$\Delta_n = \frac{\Delta}{\Delta_{pin}} \tag{9-10}$$

$$K_n = N_c \frac{k_i}{K_{col}} \tag{9-11}$$

N_{con} and K_{col} are the number of connections and columns stiffness respectively.

Hence the deflection for any connection stiffness K_i can be expressed as:

$$\Delta = 0.6057 \frac{PH^3 1}{3E\sum I_{col}} \left(N_c \frac{k_i}{K_{col}} \right)^{-\frac{1}{6}} \tag{9-12}$$

Results from equation 9-9 are compared in Figure 9-19 with the FE results. Results from equation 9-12 are compared against the FE results in Table 9-3. The equation is used for predicting sway of frames with intermediate connection stiffness values. Sway for the two extreme cases should be determined from equations 9-2 and 9-3.

In Figure 9-20 the results of FE analysis are compared against the results obtained from the Leon equation. It can be seen that the Leon equation overestimates the sway. This is due to the fact that it does not properly recognise the restraint provided against sway by the lower floors. At this point it is interesting to compare the sway for high connection stiffness with the theoretical equation 9-1, which is based on the rigid connection analysis. The value of both α and β is 1 in the analysis, so from equation 9-1 for 10 kips load the sway is 7.73×10^{-3} m. From the FE analysis, which considers the presence of a connection with high stiffness the sway is 9.23×10^{-3} m and assuming a rigid connection the sway is 8.08×10^{-3} m. Leon's equation gives 16×10^{-3} m. This indicates that the proposed equation gives better results for the calculation of sway.

Table 9-3 Comparison of sway from FE analysis and equation 9-12 (Beam to column span ratio 1.4)

Connection stiffness K_j	Sway from FE analyses	Non dimensional stiffness	Non-dimensional displacement	Non-dimensional displacement	Sway from Equation 9-12
(kN-m/rad)	(m)		FE	Equation 9-9 (m)	(m)
0	0.022232	0	1	-	0.0221
200	0.020677	0.027012	0.930056	0.985126	0.02177
1000	0.017043	0.135062	0.766628	0.75335	0.01665
2000	0.014916	0.270124	0.670933	0.671159	0.01483
4000	0.013031	0.540249	0.586162	0.597935	0.01321
6000	0.012168	0.810373	0.547317	0.558863	0.01235
10000	0.011351	1.350621	0.510572	0.513252	0.01134
20000	0.010645	2.701243	0.47883	0.457255	0.01011
30000	0.010389	4.051864	0.467322	0.427376	0.00945
80000	0.009832	10.80497	0.442257	0.362924	0.00802

9.5.2 Results of FE analysis, effect of relative stiffness of beam and column

The stiffness of the column is about 14.25 times that of the beam for this case. The results for this set are very close to each other. For pin connection sway is 1.55×10^{-3} m, for rigid connections it is 1.23×10^{-3} m. From equation 9-3 the calculated sway for pin connected frame is 1.56×10^{-3} m, and using equation 9-1 for the rigidly connected

frame the sway is 1.21×10^{-3} m. It can be seen that the percentage reduction in sway is 21%, as the columns behave more like individual cantilevers, (for a frame with the same beam and column stiffness reduction in sway from rigid connection to pin connection is 75% calculated with respect to the pin connection sway). Results are expressed in terms of decrease, not in terms of increase, as the situations match equation 9-3, not equation 9-2. At the same time it was found that if the beam stiffness is increased with respect to the column stiffness, the sway behaviour can be expressed by equation 9-9. In a composite frame the stiffness of the beam will be greater than the column stiffness so no further analysis is carried out for the frames with high column stiffness. But for the frame where the inertia of the column section is too high the sway should be calculated from equations 9-1 and 9-3 first and if the difference is not high, the larger of the sways can be taken as the sway - as a safe result. In most cases in practice the beam sections are deeper than the columns, hence the discrepancy given by the equations can be neglected.

9.5.3 Results of FE analysis, effect of beam and column span ratio

To study the effect of beam to column span ratio, the values selected for the ratio were 1.00, 1.40 and 2.00. The reason for selecting these span ratios was that they represent the practical range. The results of the analysis show that the form of equation 9-9 is still valid, with a the change in the first constant term by a very small amount. The variation was found to be linear. Equation 9-9 was modified as:

$$\Delta = \frac{PH^3{}_1}{3E\sum I_{col}}\left(0.5697 + 0.036\frac{L_2}{H_1}\right)\left(N_c\frac{k_i}{K_{col}}\right)^{-\bar{\sigma}} \qquad 1 \le \frac{L_2}{L_{col}} \le 2 \qquad (9\text{-}13)$$

9.5.4 Results of FE analysis, effect of multiple spans

To study the effect of multiple bays on the sway, one frame with two bays was analysed with different connection conditions. The results of these analyses matched

equation 9-9 as shown in Figure 9-21. This indicates that the equation is suitable for single storey multiple span frames.

9.5.5 Results of FE analysis, multi-storey frame

FE analyses with the same beam and column sections and connection element properties were used to investigate the pattern of sway in frames with multiple stories. The analyses were performed with frames having a single span and, 2 stories, 3 stories and 4 stories. It was found that the sway of the bottom storey is independent of the exponential variation of connection stiffness as observed for the single storied frames analysed, but dependent on the amount of moment developed at the top of the columns of that storey. It was also observed that due to the restraint provided by the connections and the beams at the lower levels the sways of the upper floors are also significantly reduced. Equation 9-9 can be used for calculating the sway for the bottom storey while the modification of equation 9-13 can be used for the top story. Since the analyses used more than one storey, its effect must be included in the sway equations. The proposed equations are:

For the 1 st floor of a multi storey frame:

$$\Delta = \frac{PH_1^3}{3E\sum I_{col}} \frac{1+\frac{3K_eH_1}{8EI_{col}}+3\frac{(H_T-H_1)}{N_bH_1}}{1+\frac{3K_eH_1}{2EI_{col}}} \qquad (9\text{-}14)$$

For the top floor:

$$\Delta = \frac{PH_T^3}{3E\sum I_{col}} \frac{1+\frac{3K_eH_T}{8EI_{col}}}{1+\frac{3K_eH_T}{2EI_{col}}} \left(0.5697+0.036\frac{L_2}{H_1}\right)\left(N_c\frac{k_i}{K_{col}}\right)^{-\frac{1}{6}} \qquad (9\text{-}15)$$

Where N_c is the number of connections in the frame under consideration. N_b is the number of spans, K_e is the minimum of the rotational stiffness as of the beam and the connection. It was observed that when equations 9-14 and 9-15 are used for the sway calculation of the lower and upper floors, the sway of the intermediate floors can be obtained from linear interpolation of the two.

Results of FE analyses for frames with 3 and 4 stories with equal beam and column sections having a single span, and the sway from and the above formulae are compared in Figures 9-22 and 9-23. From Figure 9-23 it can be seen that the proposed formula slightly overestimates the sway for rigid connections and gives more accurate results for the lower connection stiffnesses - where the sway is high. So it can be said the formula gives fairly good results in the range of stiffness where the sway is critical for a given column stiffness.

At this point it is of interest to compare the sway of frames with multiple stories and bays - which represent practical frames. A frame with two bays and four stories comprising of 16 connections was analysed by the FE model. The coefficicnt N_c is 16 and N_b is 2. Results are compared in Figure 9-24. Very good agreement was obtained with the predictions of equations 9-14 and 9-15.

9.6 Design proposal for steel frames

For steel frames the sway of the ground floor column top can be calculated by:

$$\Delta = \frac{PH_1^3}{3E\sum I_{col}} \frac{1+\frac{3K_eH_1}{8EI_{col}}+3\frac{(H_T-H_1)}{N_bH_1}}{1+\frac{3K_eH_1}{2EI_{col}}}$$

For the top floor the sway can be calculated by:

$$\Delta = \frac{PH_T^3}{3E\sum I_{col}} \frac{1+\frac{3K_eH_T}{8EI_{col}}}{1+\frac{3K_eH_T}{2EI_{col}}} \left(0.5697+0.036\frac{L_2}{H_1}\right)\left(N_c\frac{k_i}{K_{col}}\right)^{-\frac{1}{6}}$$

For the intermediate floors the sway can be obtained through linear interpolation. It should be noted that the connection rotational stiffness utilises the moment - rotation behavicur of the connection and corresponds to the moment developed in the connection.

9.7 Conclusions

The modelling of a composite non-sway frame, verified against the results of full-scale tests, has been described in this chapter. It has been demonstrated that it is possible to predict the frame moment distribution, connection moment-rotation and the beam span deflections using the numerical model. The results from the FE analyses show that the finite element formulation has now reached a state where it is possible to obtain realistic results for an equivalent physical test provided proper attention is given to the modelling. Used in this way numerical modelling represents a valuable complement and extension to large-scale physical testing. Availability of these proven numerical techniques greatly increase the range of issues that can economically be studied.

Using simplified techniques, equations were derived for the sway deflection of: single storey frame and multi-storey frames. It was observed that in a single storey frame the sway of the column tops is dependent on the connection stiffness, whilst the sway of the ground floor top is less dependent of connection stiffness but is highly dependent on the induced moment at that level. At the same time it was observed that the sway of the column top of the top storey of a multi-storey frame is dependent on the

connection stiffness. This is actually similar to the single storey frame. The reason is that in both case the tops can move without the influence of any extra constraint as there is no extension of the columns (sway will depend on the connection properties). It was observed that this fact makes the relative stiffness of the beams to the columns less important in the calculation for sway in single storey frames. The analyses conducted with the single storey frame actually provided the insight into the basic behaviour of frames in sway i.e. the effect of connection stiffness and number of spans. Finally, a simple equation is proposed to predict sway deflections for unbraced frames. The method is based on simple derivations and subsequent calibration with finite element results. The proposed method consists of calculation of the sway of the bottom storey and the top storey from two similar equations and uses linear interpolation with storey height for intermediate floors.

9.8 References

9-1 Li, T. Q., Nethercot, D. A. and Choo, B. S. (1993) *Moment Curvature Relations for Steel and Composite beams*, Steel Structures, Journal of Singapore Structural Steel Society, Vol. 4, No. 1, pp. 35-51.

9-2 Li, T. Q, Nethercot, D. A. and Choo, B. S. (1996) *Behaviour of flush end plate composite connections with unbalanced moment and variable shear/moment ratios: part 1: experimental behaviour*, Journal of Constructional Steel Research, Vol. 38, No. 2, pp. 125-164.

9-3 Ye Mei-xin, Nethercot, D. A. and Li, T. Q. (1996) *Non Linear Finite Element Analysis of Composite Frames*, Proceedings of the Instution of Civil Engineers, Structures & Buildings, Vol. 116, pp. 244-247.

9-4 Li, T. Q., Choo, B.S. and Nethercot, D. A. (1995) *Connection Element Method for the Analysis of Semi-rigid Frames,* Journal of Constructional Steel Research, Vol. 32 pp.143-171.

9-5 Li, T. Q, Moore, D. B., Choo, B.S. and Nethercot, D. A. *The Experimental Behaviour of a Full-scale Semi-rigidly Connected Composite Frame: Overall Considerations*, Journal of Constructional Steel Research (under review).

9-6 Ammerman, D. J. and Leon, R. T. (1990) *Unbraced Frames with Semi-Rigid Composite Connections,* Engineering Journal/American Institute of Steel Construction, first quarter, pp. 12-21.

9-7 Lui, E. M. and Chen, W. F. (1988) *Behaviour of braced and unbraced semi-rigid frames,* Int. J. Solids Structures Vol. 24. No. 9. pp. 893-913.

9-8 Lui, E. M. and Chen, W. F. (1987) *Steel Frame Analysis with Flexible Joints, Journal of Construction Steel Research,* Vol. 8, pp. 161-202.

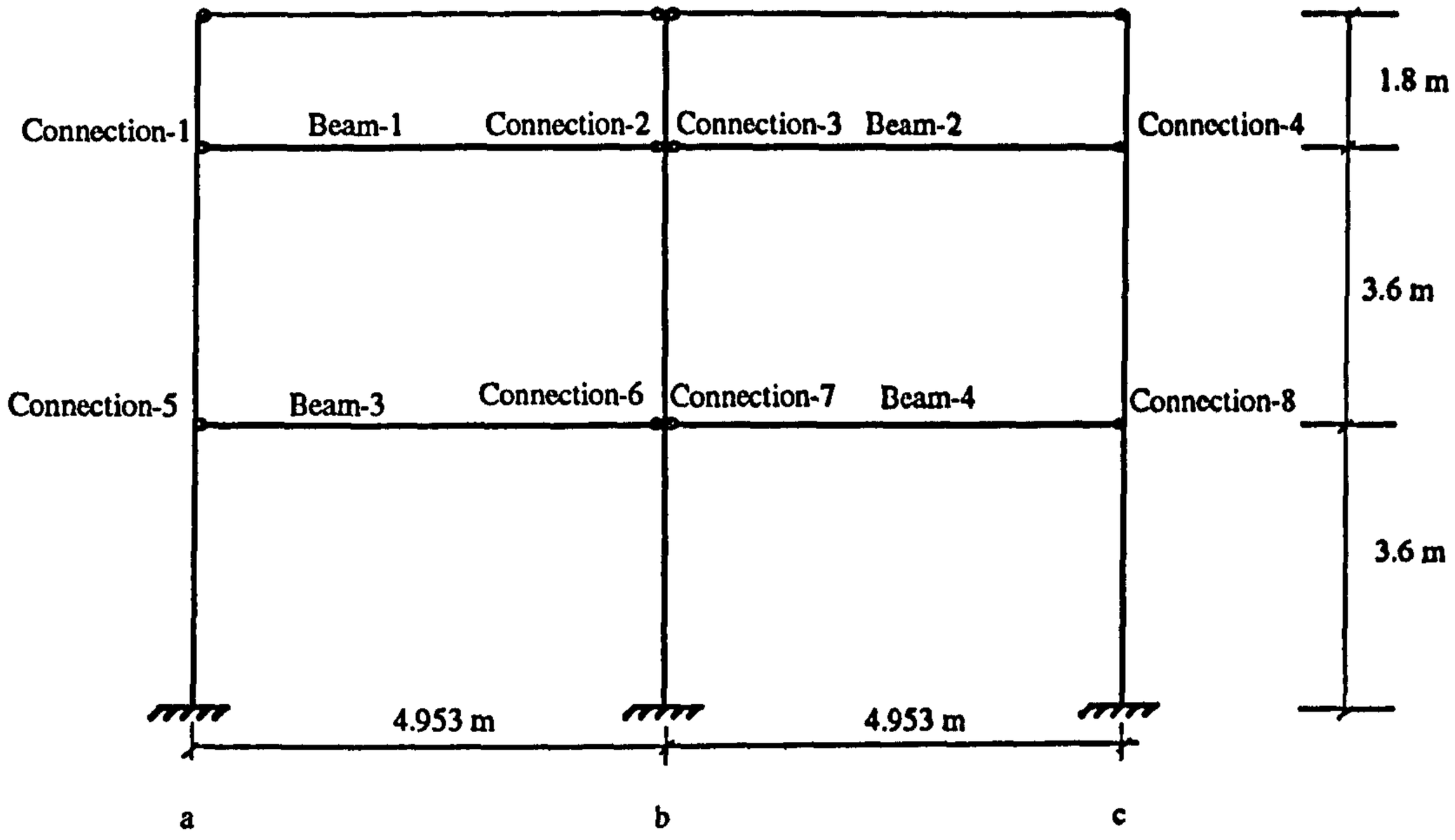

9-1a Composite frame-A tested (Li *et al* ref. 9-5) and analysed

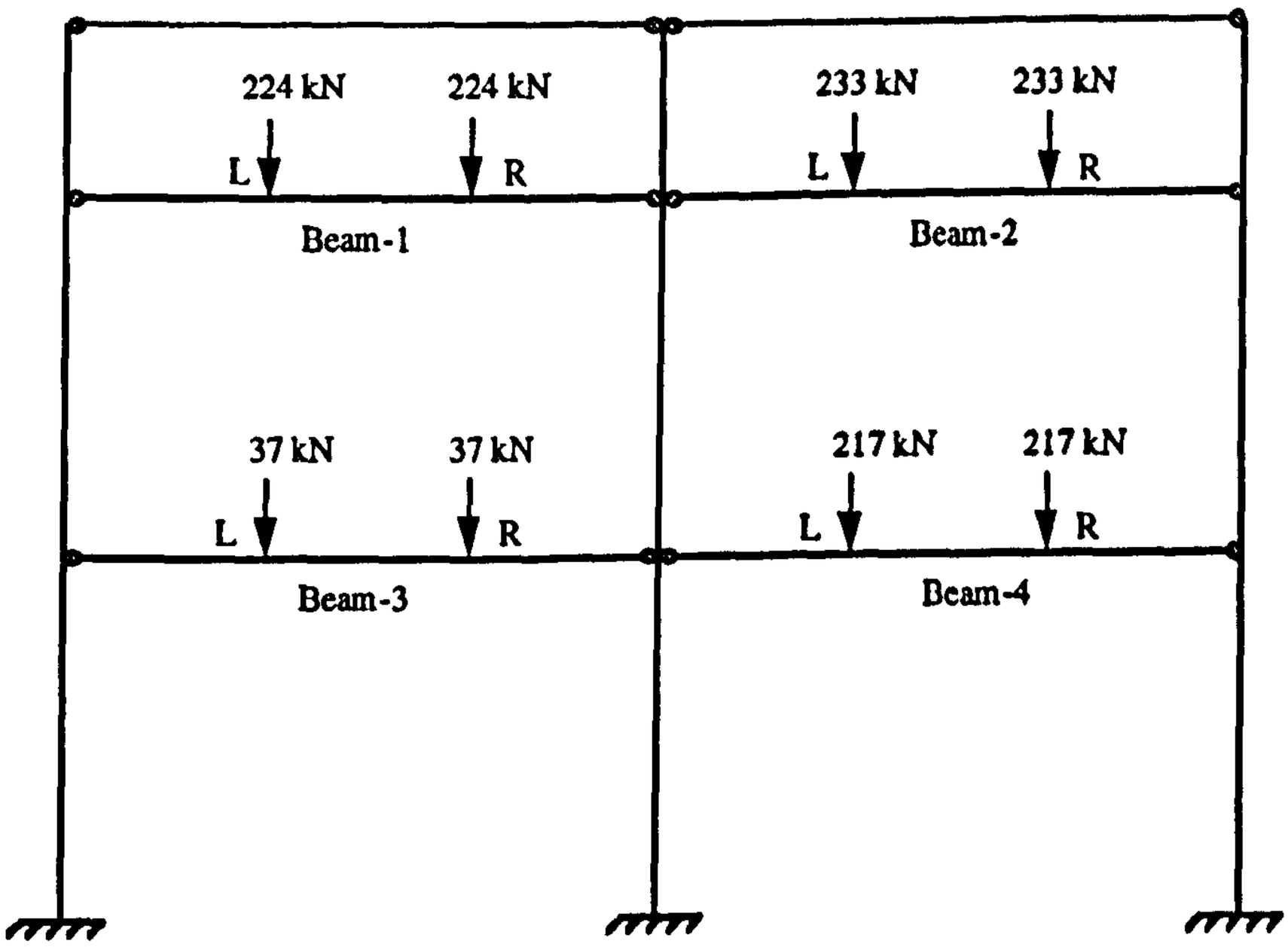

9-1b Final load of test (Li *et al* ref. 9-5) and FE analysis, frame-A

Figure 9-1 Composite Frame-A (Li *et al* ref. 9-5) and loads

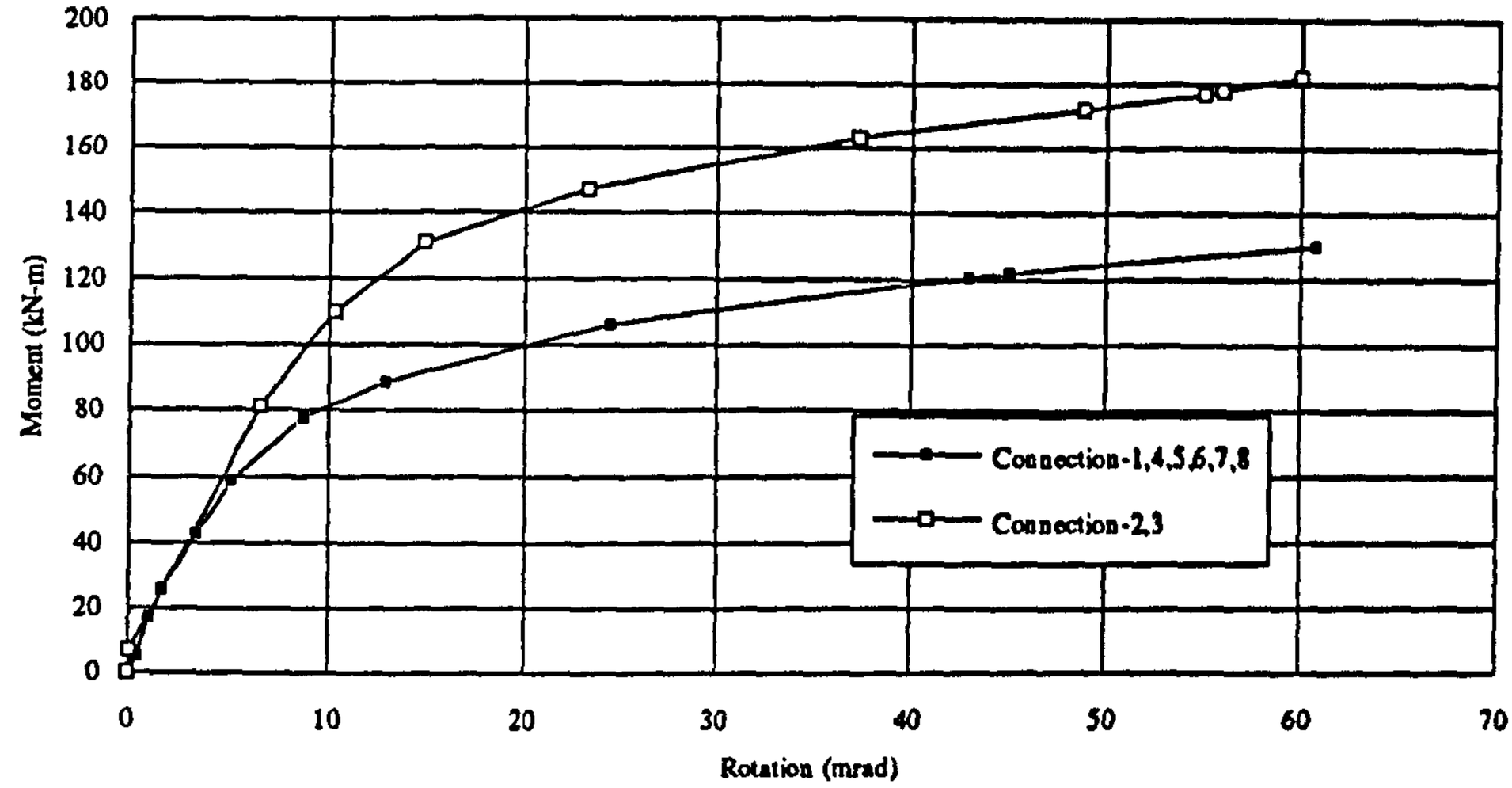

Figure 9-2 Moment rotation curves used in the FE model of the frame (Li *et al* [9-2])

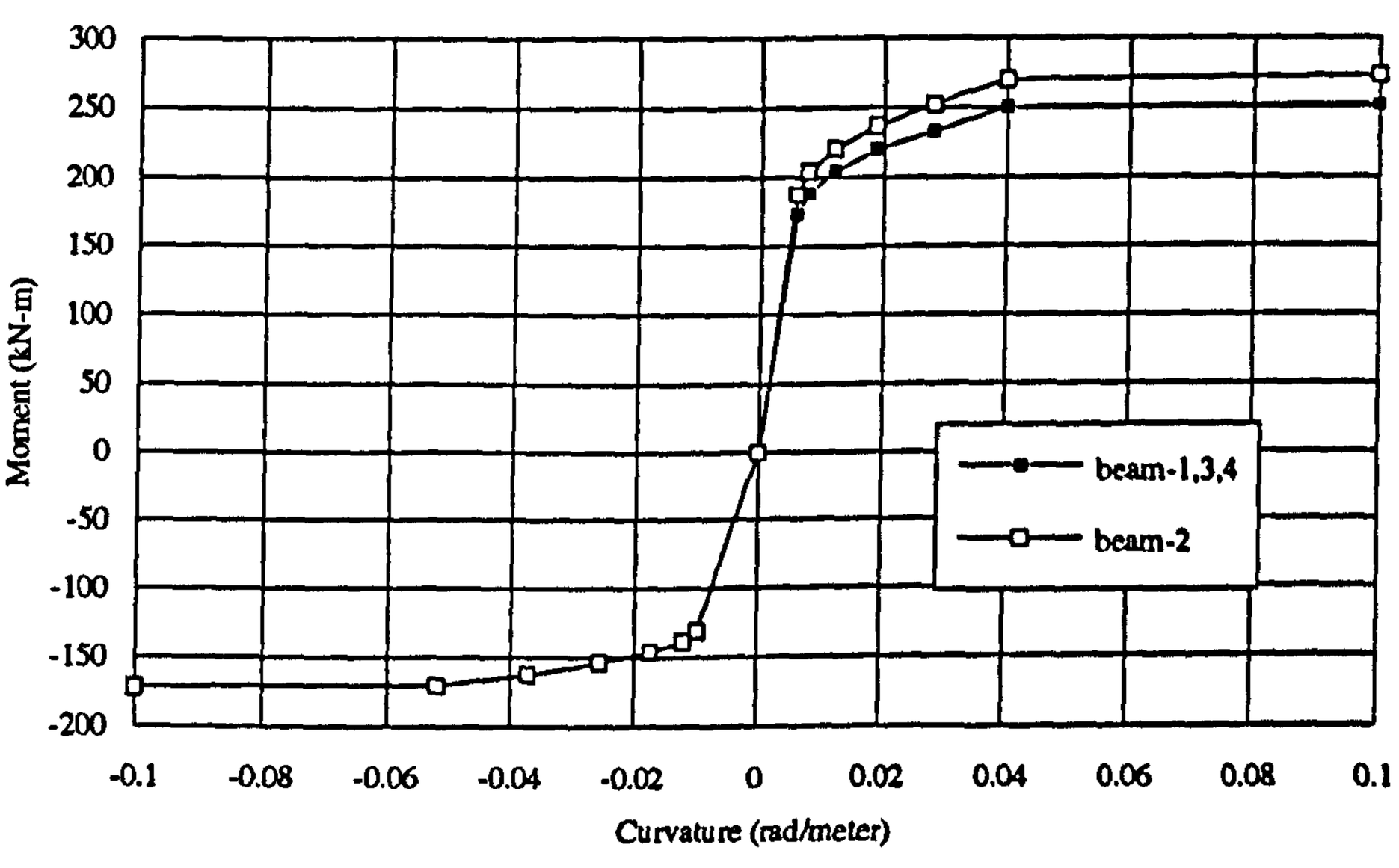

Figure 9-3 Moment - curvature relation used in the FE model of the frame

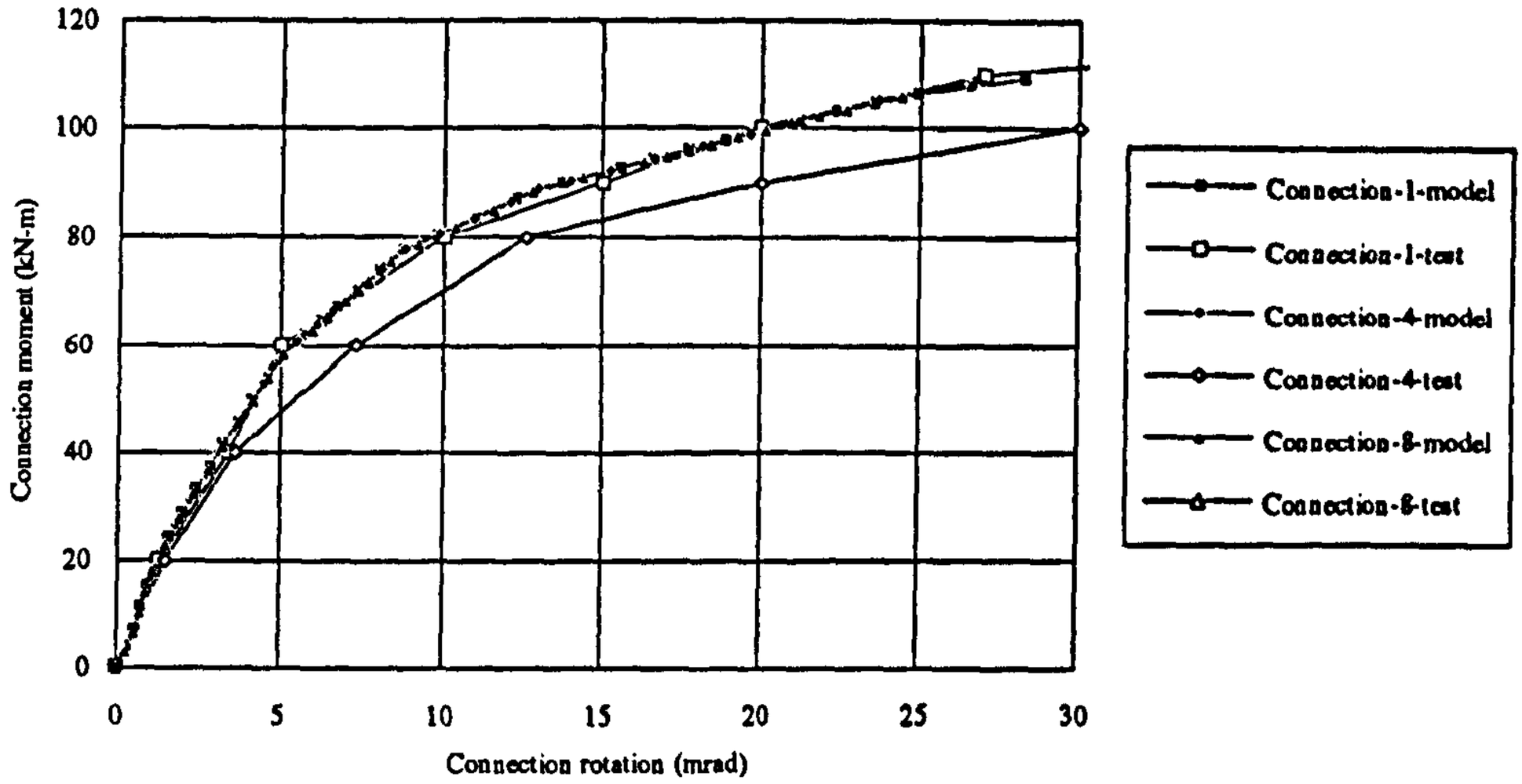

Figure 9-4 Comparison of moment rotation curves from FE analysis and test (Li *et al* ref. 9-5) forexternal connections of frame-A

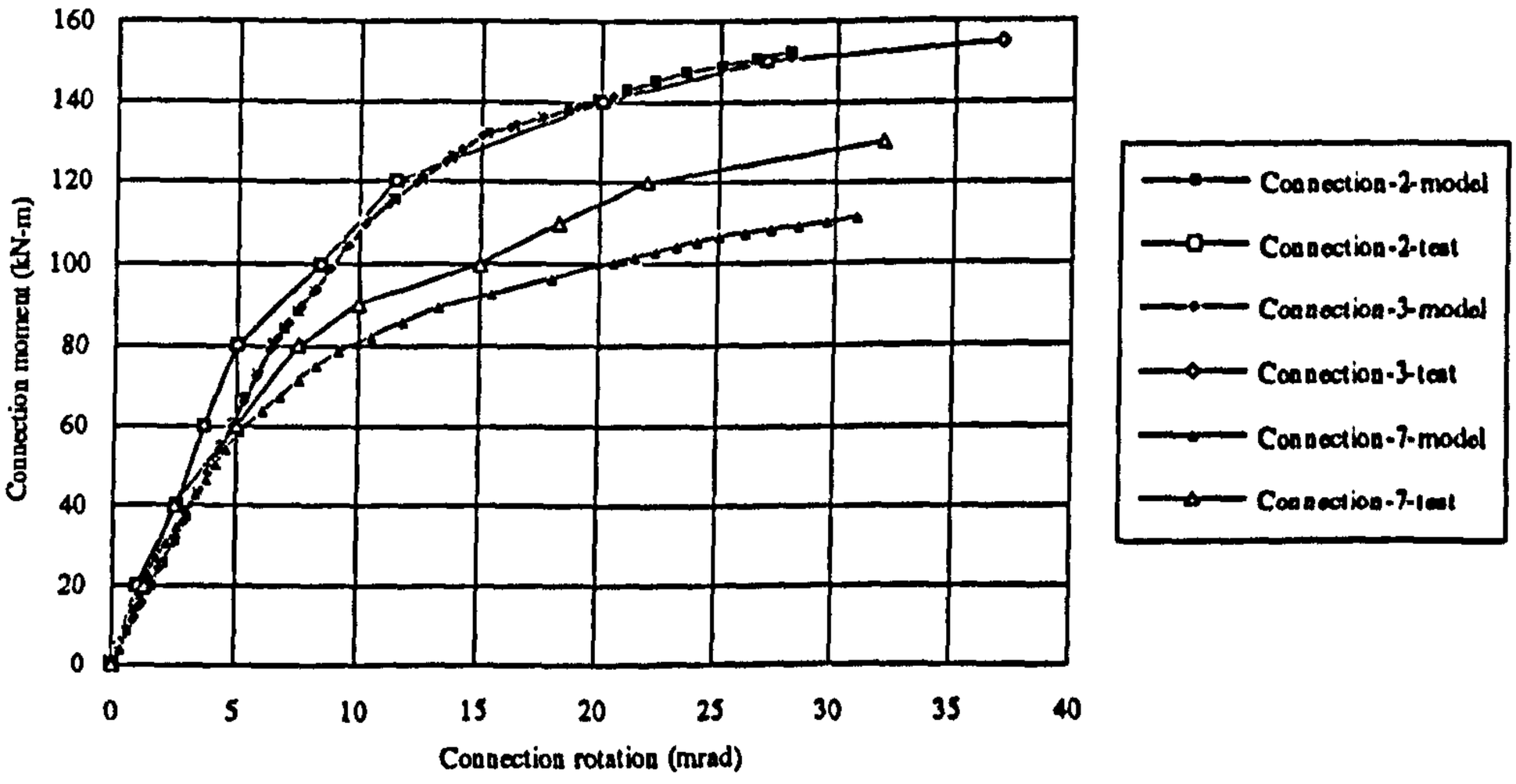

Figure 9-5 Comparison of moment rotation curves from FE analysis and test (Li *et al* ref. 9-5) for internal connections of frame-A

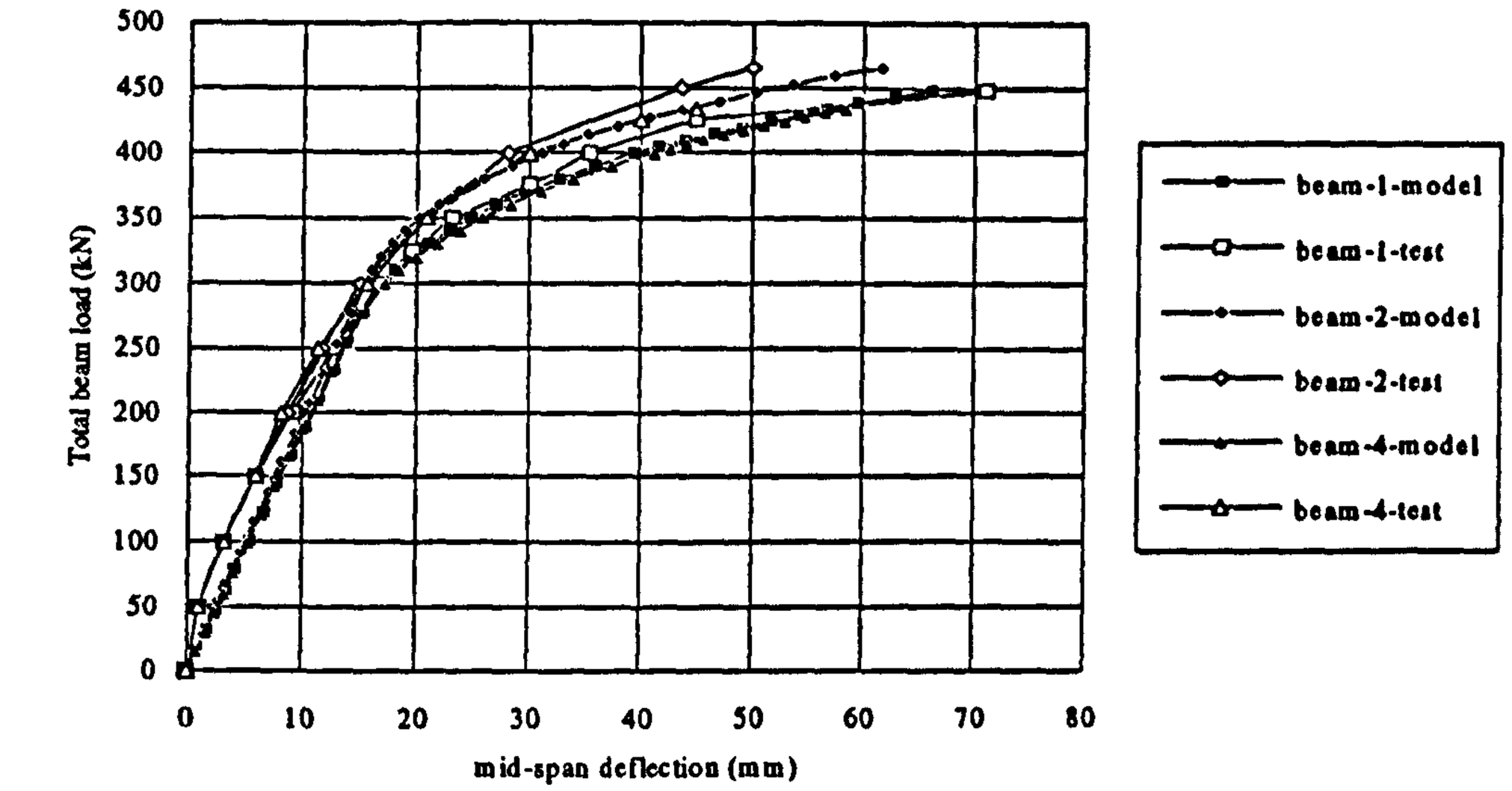

Figure 9-6 Comparison of beam load - mid span deflection curves obtained from test (Li *et al* ref. 9-5) and FE analysis, frame-A

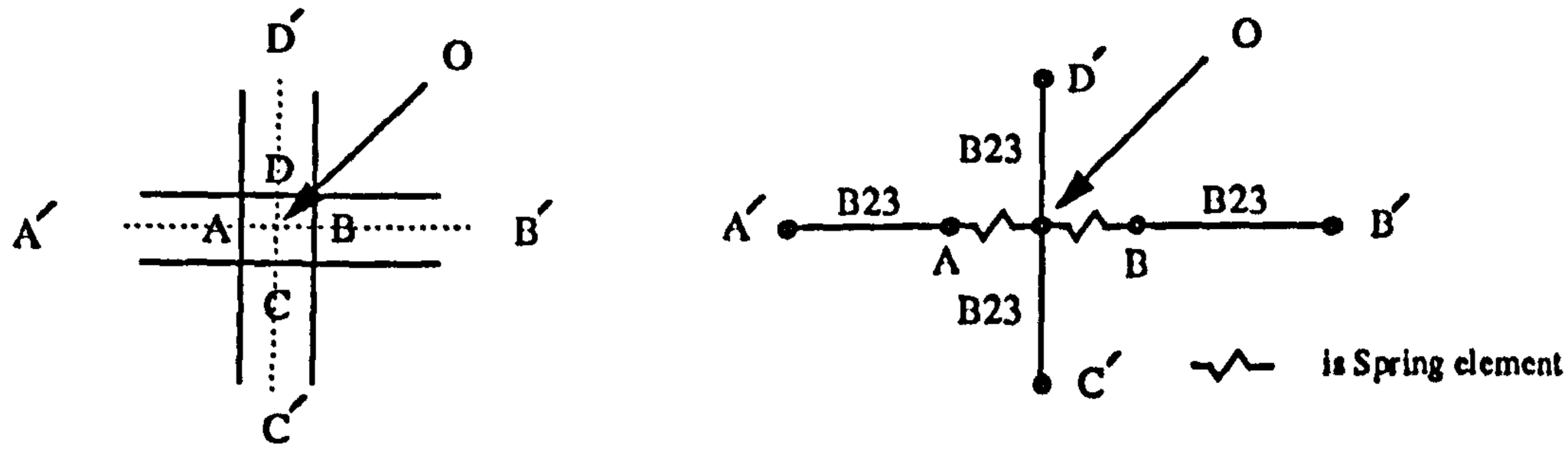

Figure 9-7 FE representation of the beam to column connection

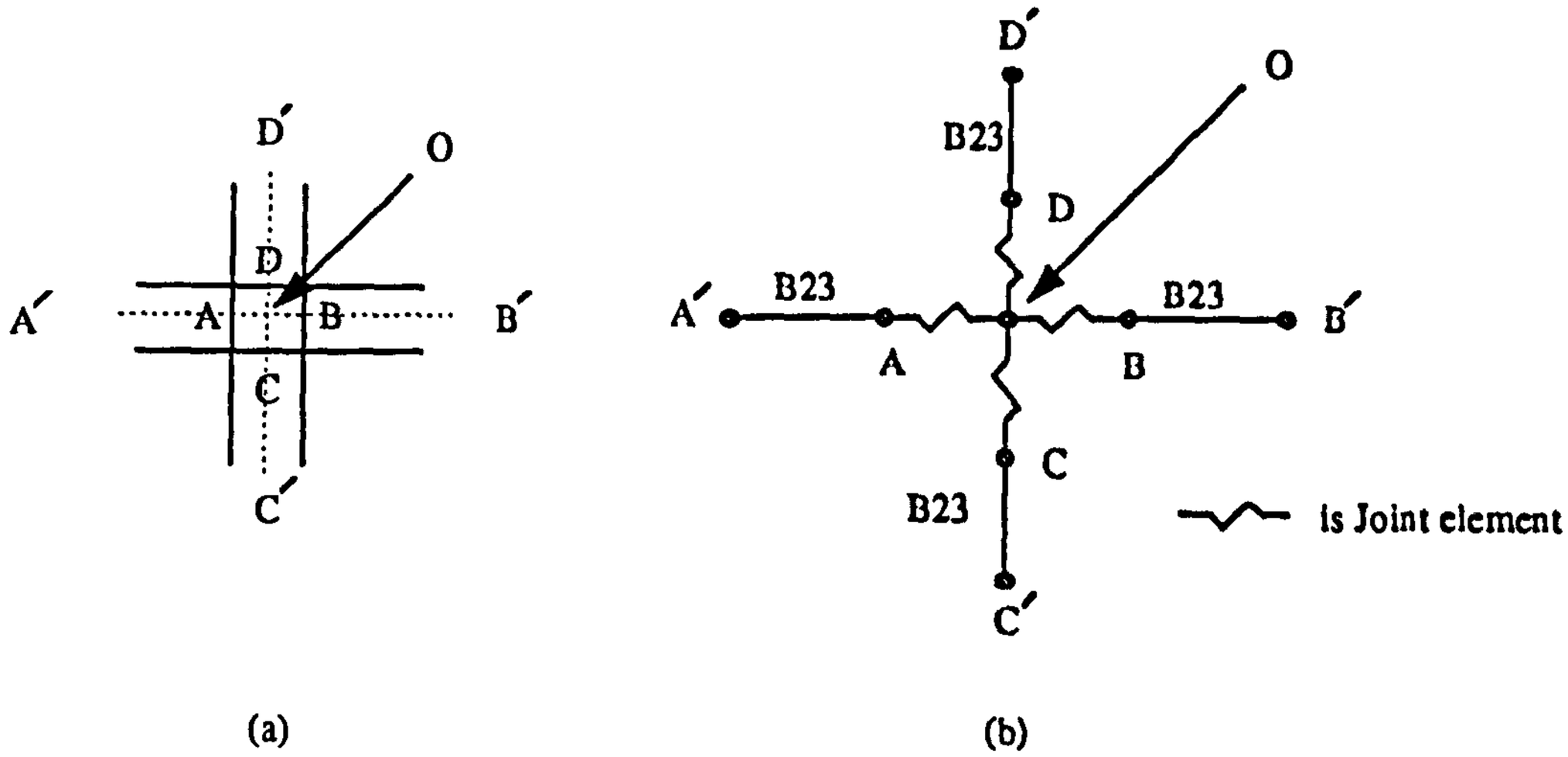

(a) (b)

Figure 9-8 Modified FE representation of the beam to column connection

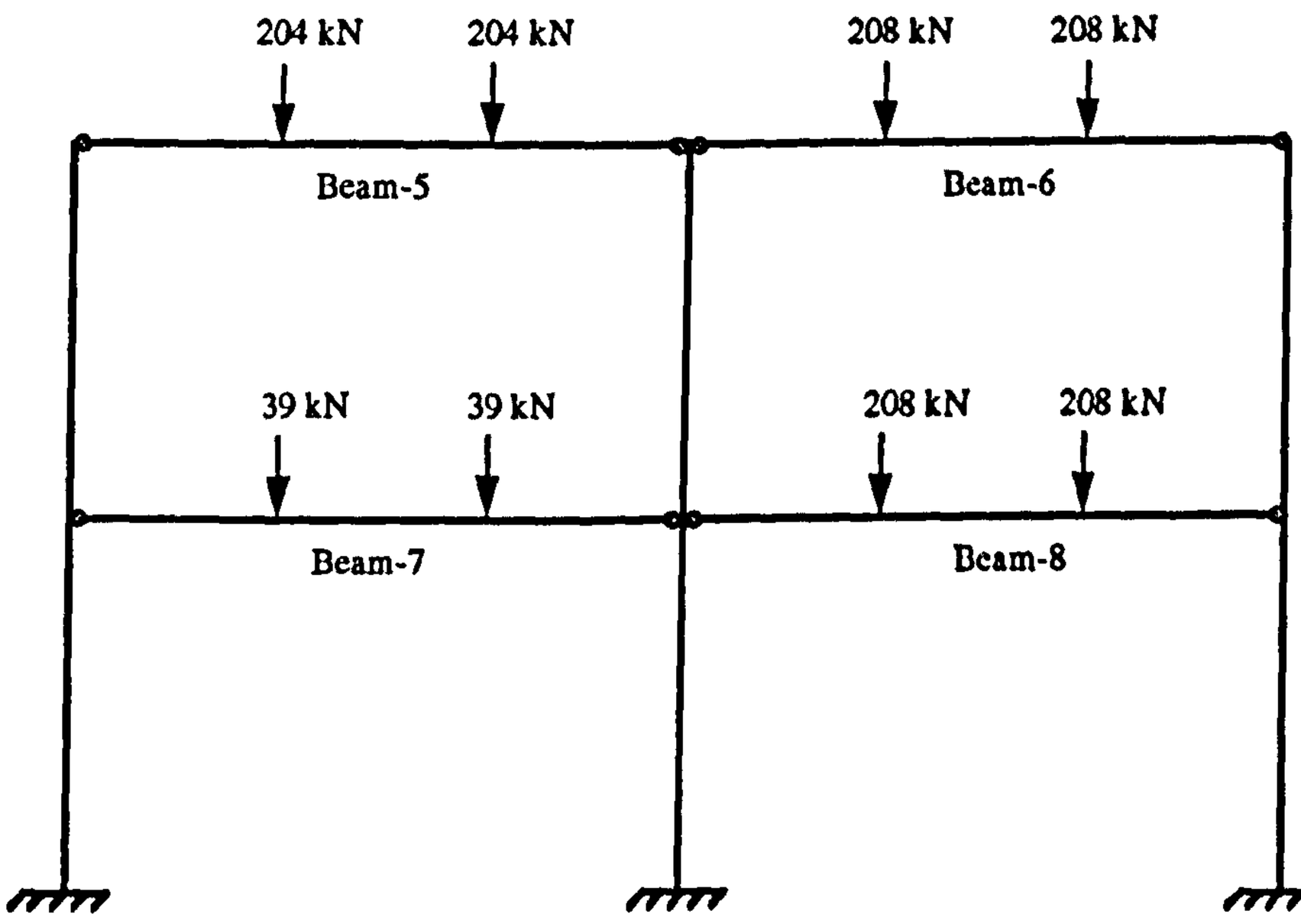

Figure 9-9 Frame-B loads (Li *et al* ref. 9-5)

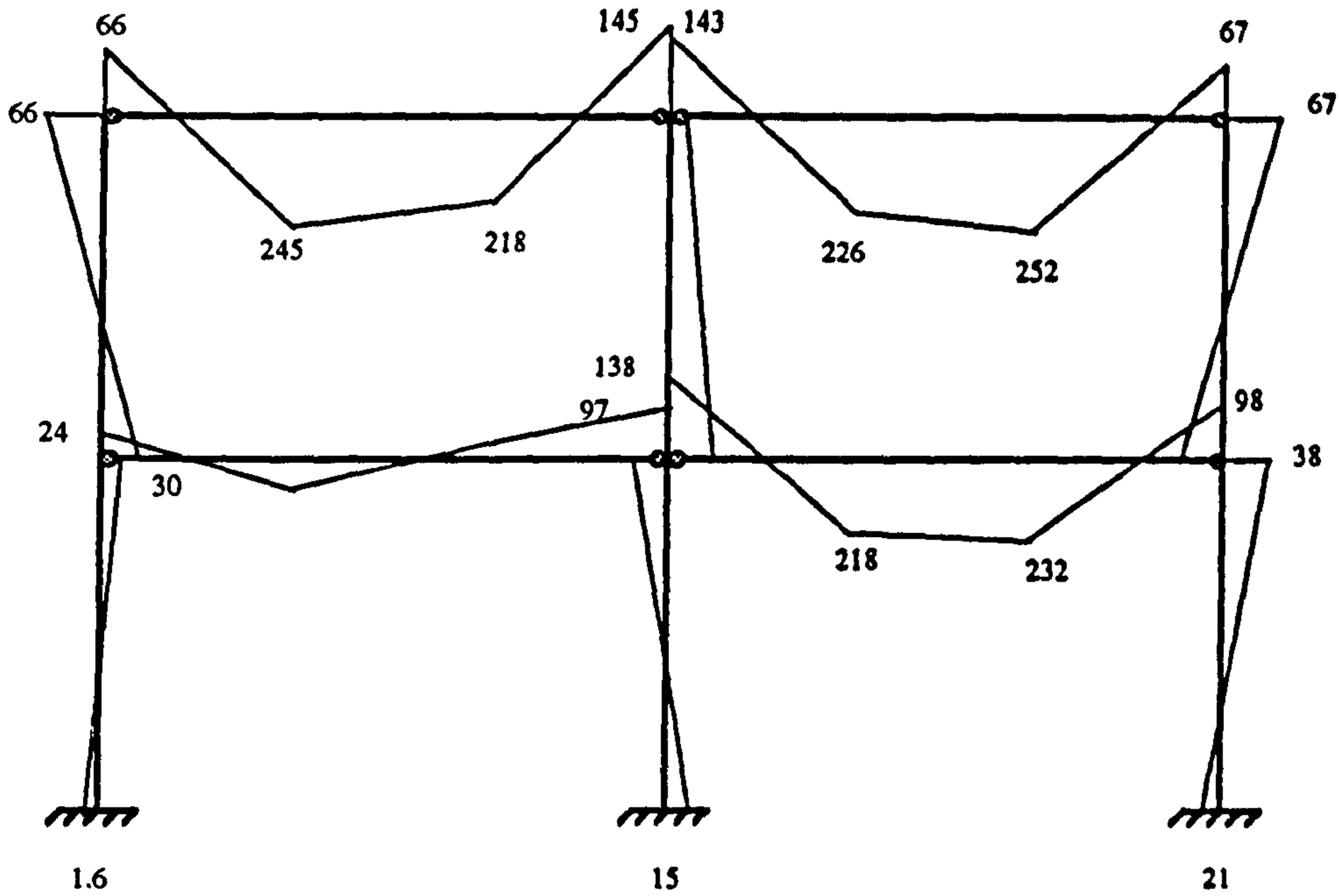

Figure 9-10 Frame-B moment distribution from test (Li *et al* ref. 9-5)

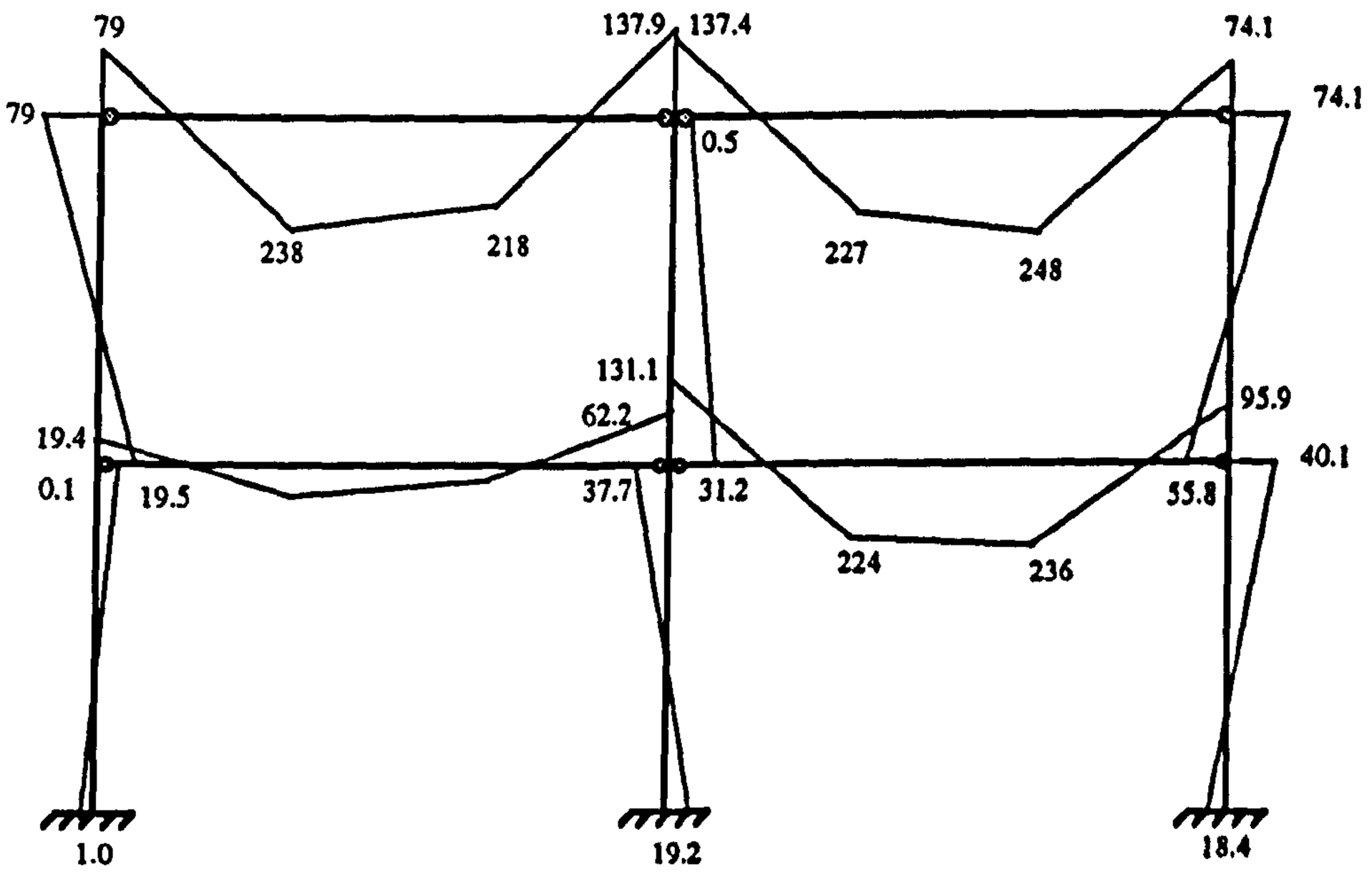

Figure 9-11 Frame-B moment distribution from FE analysis

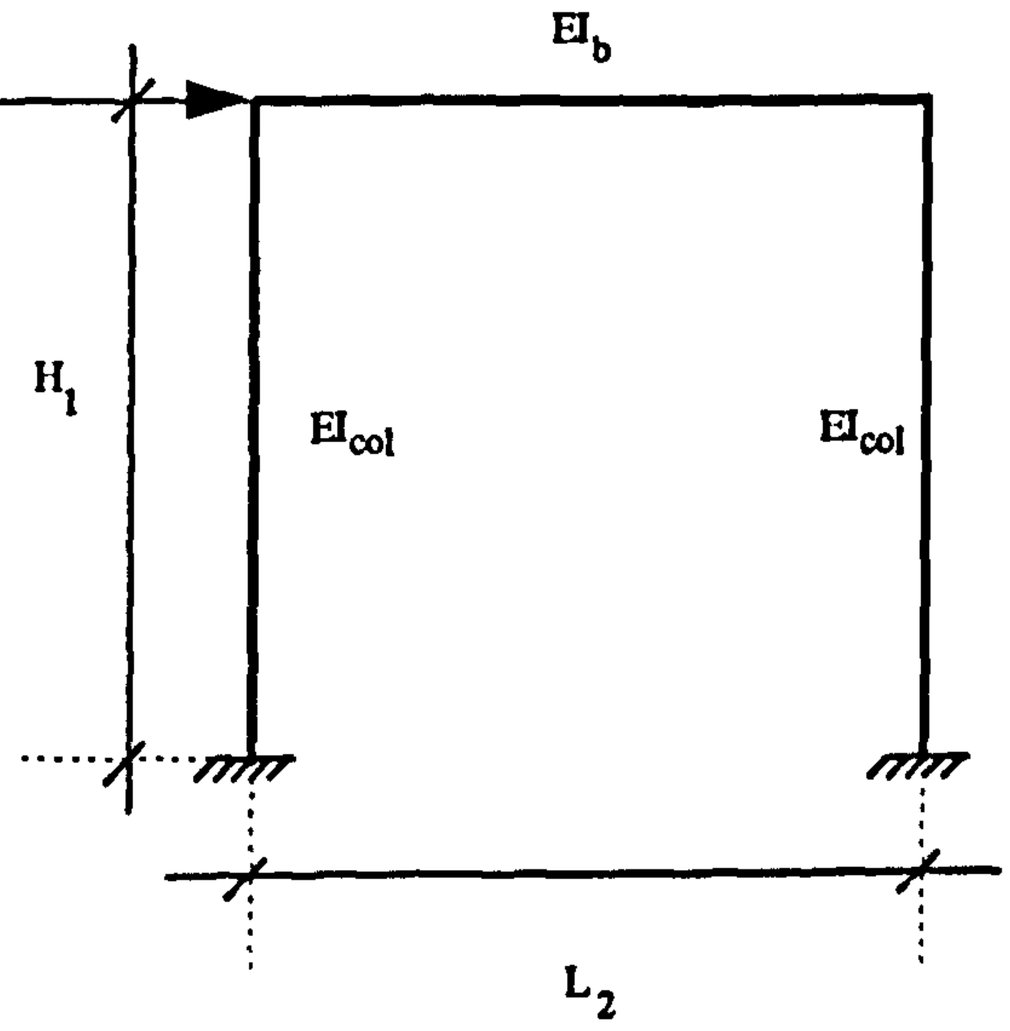

Figure 9-12 Simple portal frame for sway analysis

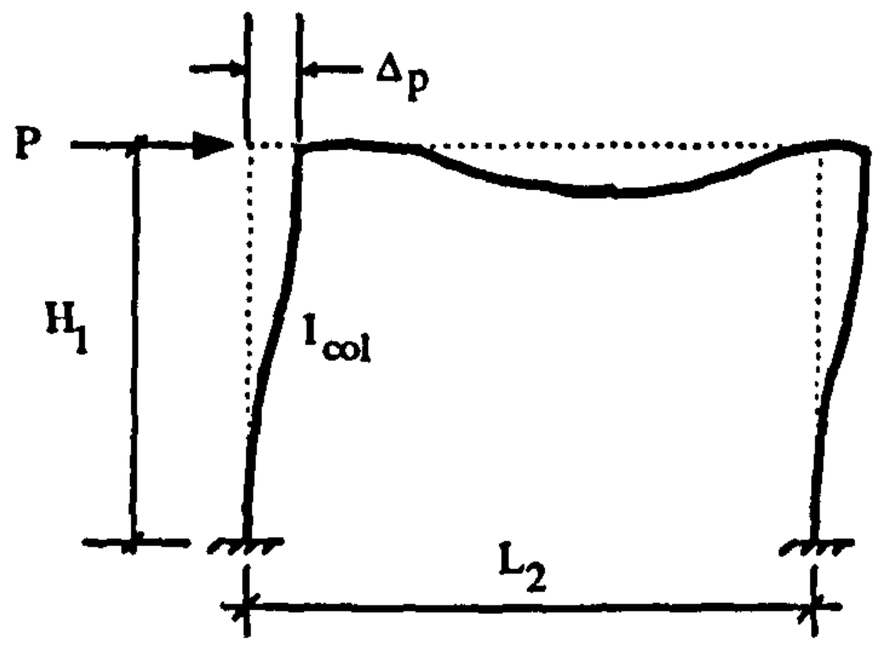

9-13(a) Sway due to horizontal load

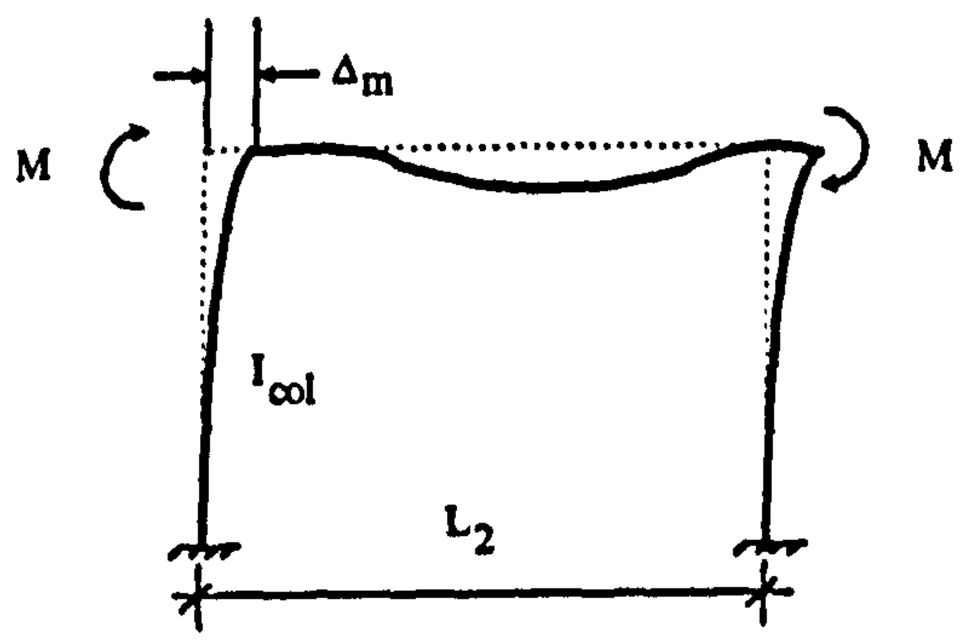

9-13(b) Sway due to moment at column top

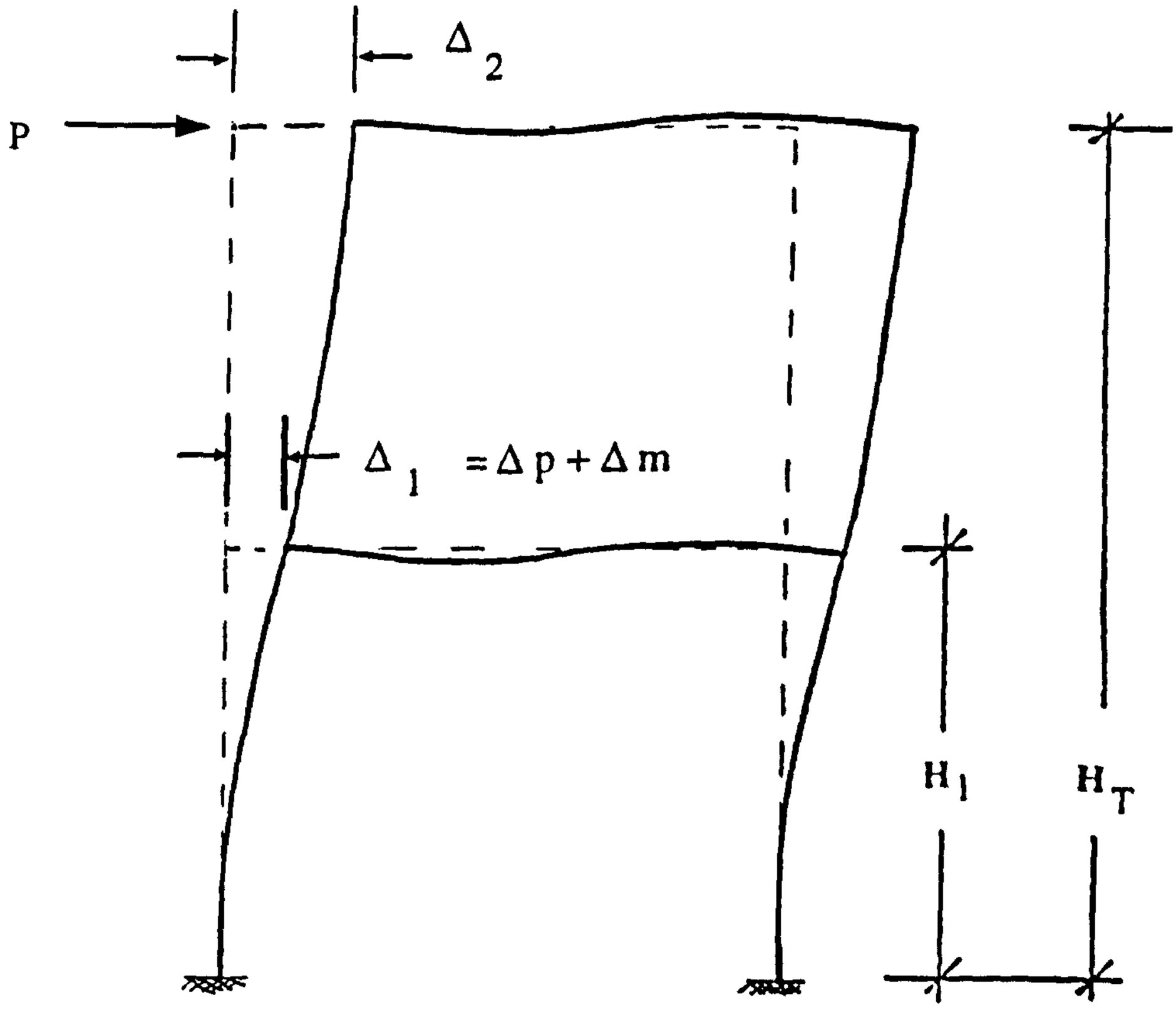

9-13(c) Sway of a two storied frame with semi-rigid connections

Figure 9-13 Sway of single and two storied frame with semi-rigid connection

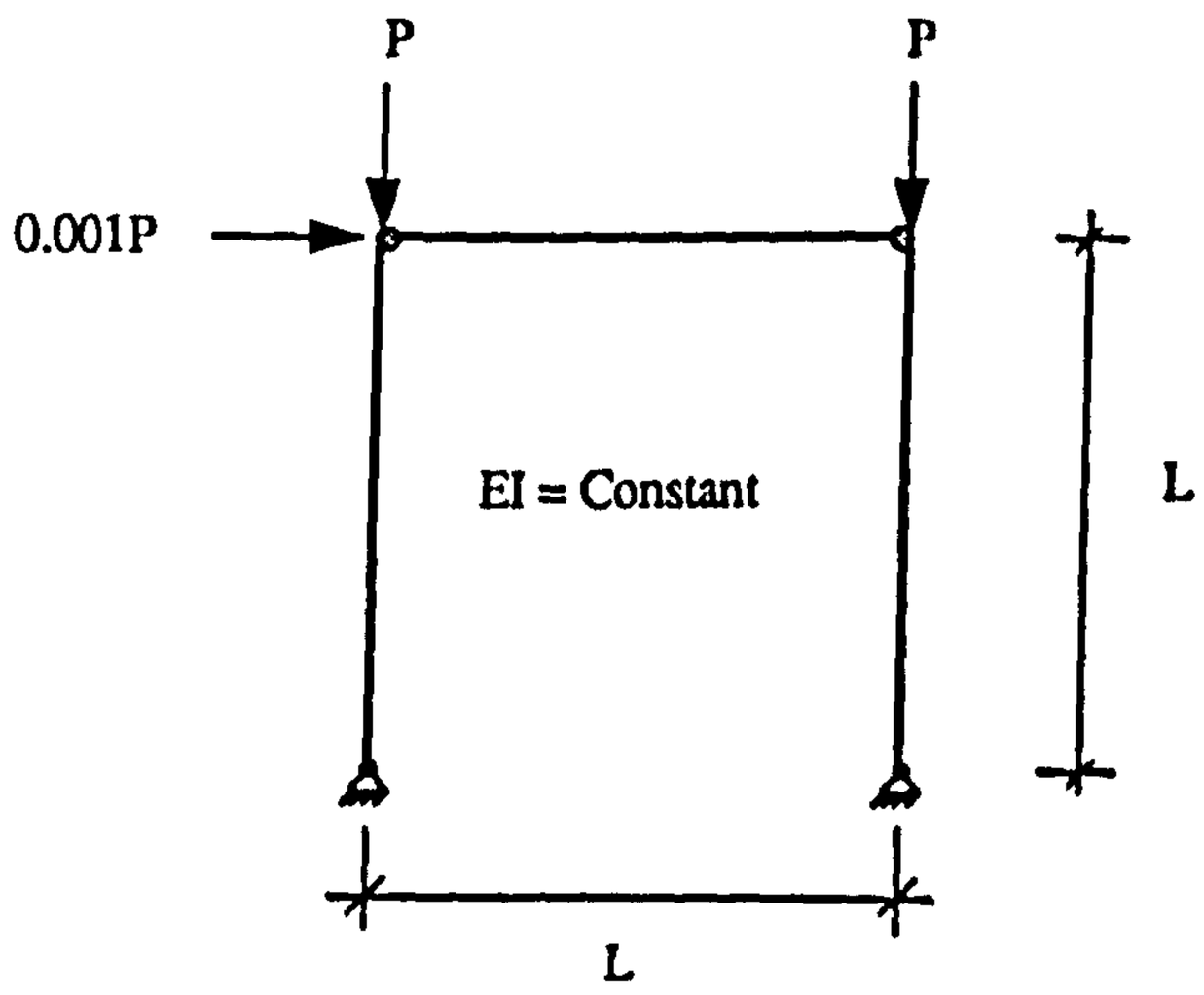

Figure 9-14(a) Simple portal frame analysed by Lui & Chen (ref. 9-7)

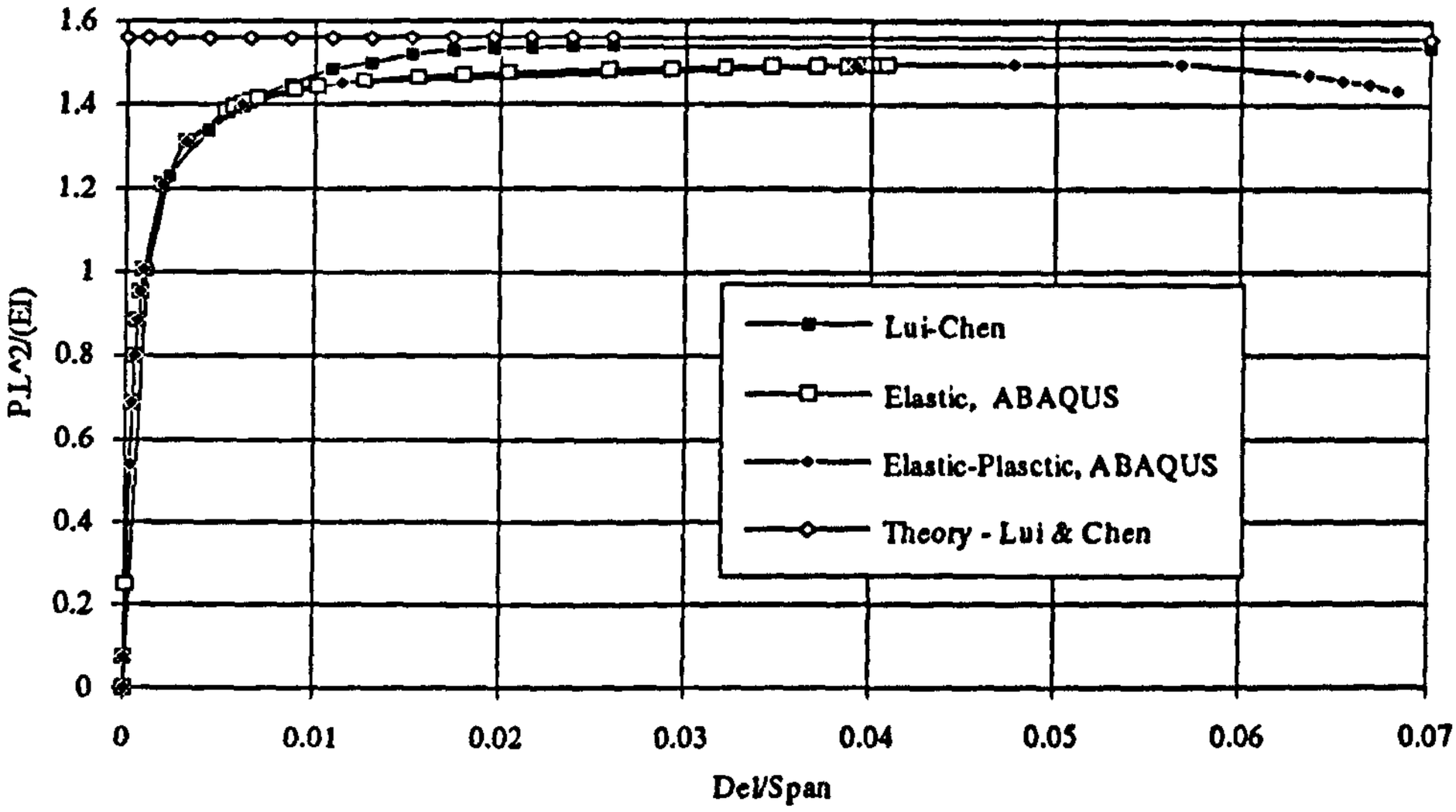

Figure 9-14(b) Comparison of ABAQUS-result with Lui & Chen's results for sway buckling

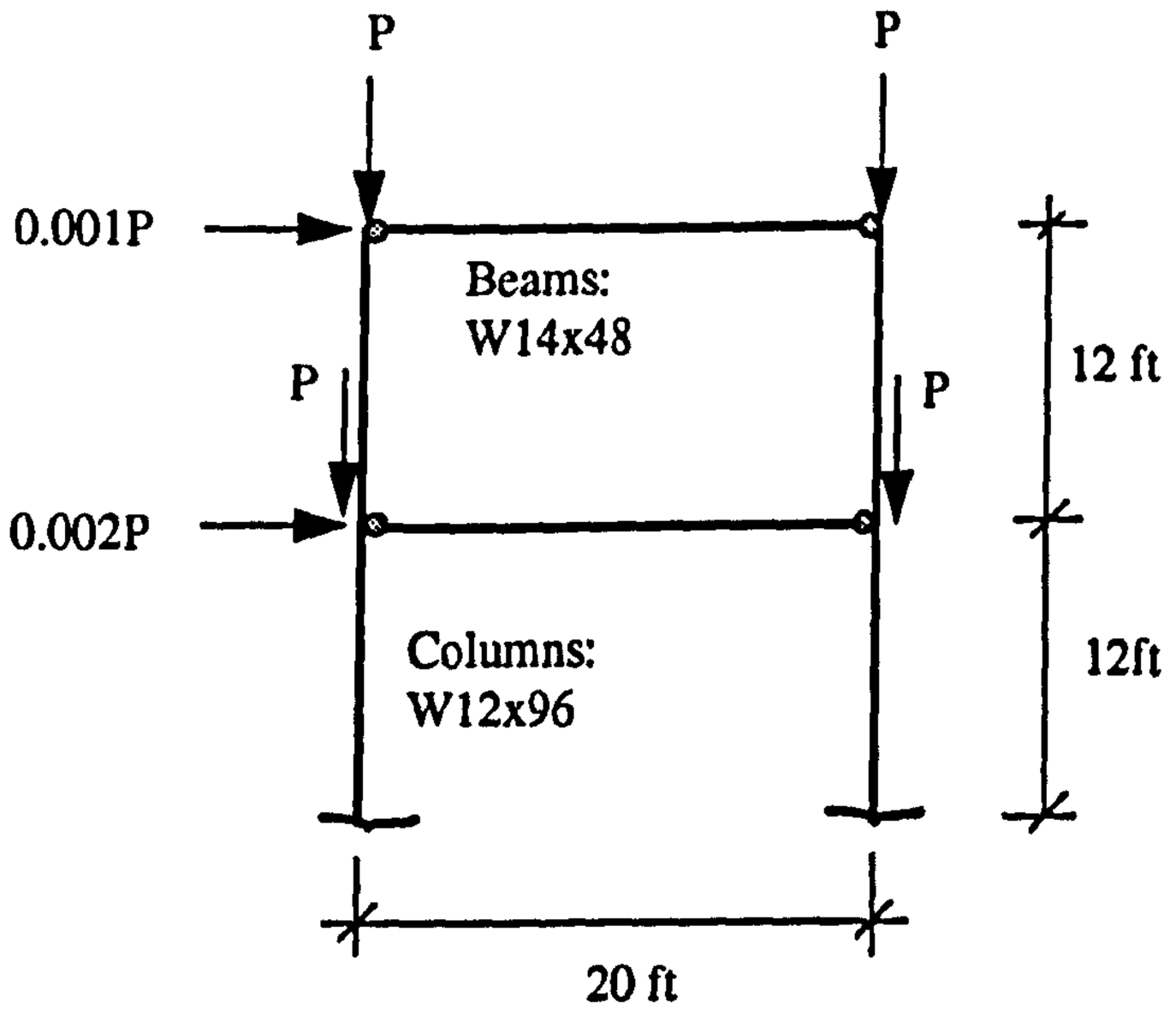

Figure 9-15(a) Frame analysed by Lui and Chen (ref. 9-7)

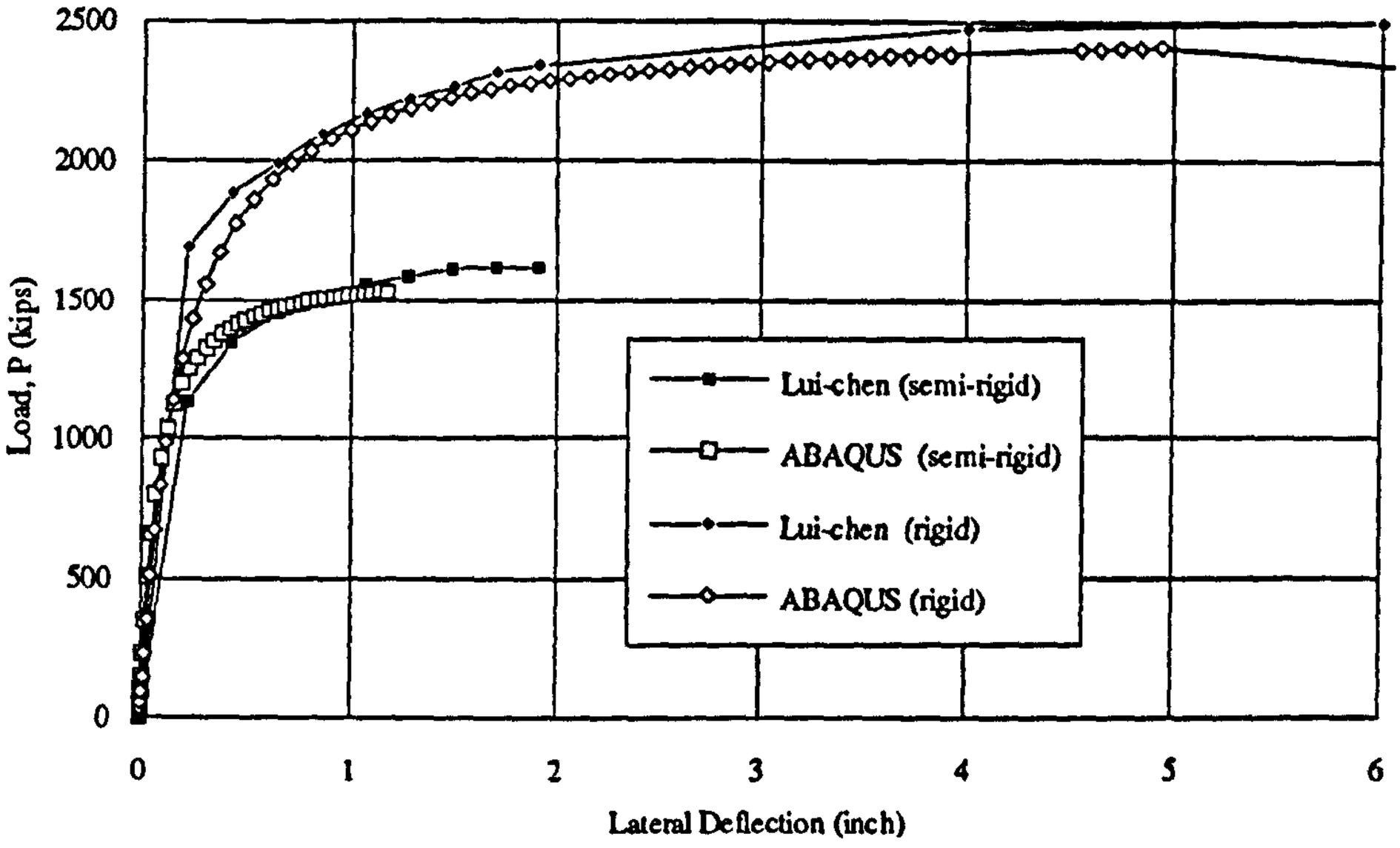

Figure 9-15(b) Comparison of elastic load deflection curves, fixed support

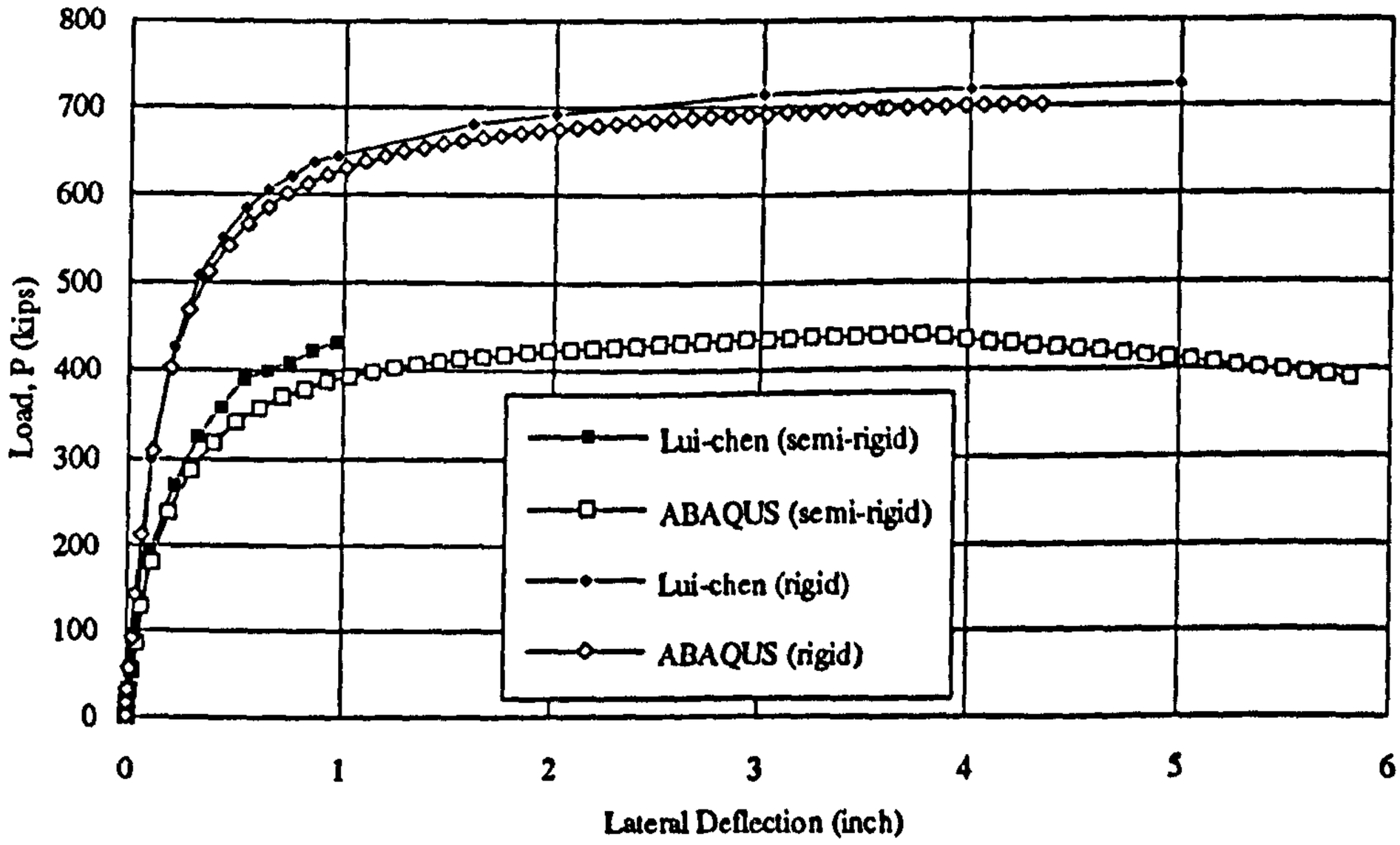

Figure 9-15(c) Comparison of elastic load deflection curves, hinged support

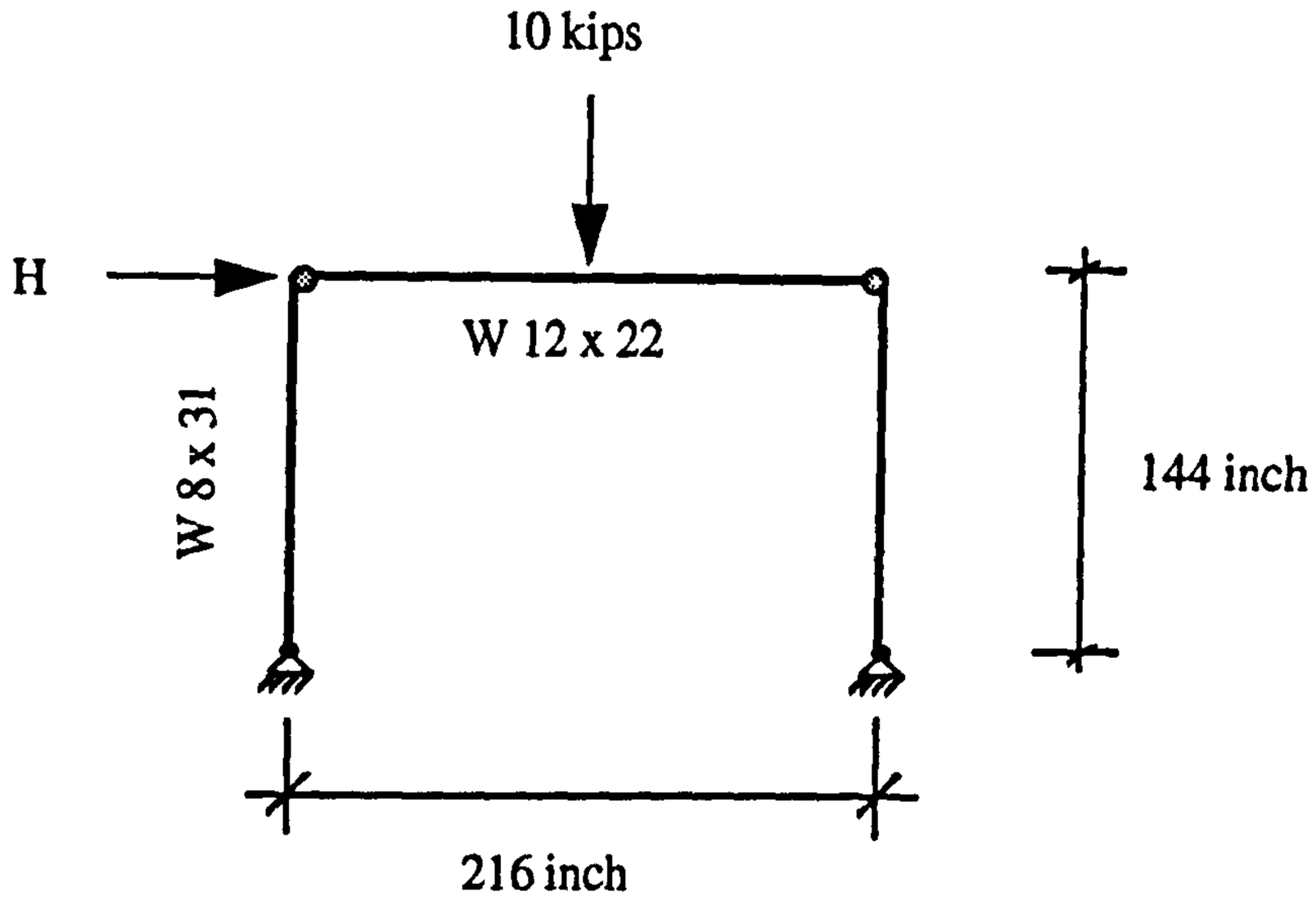

Figure 9-16(a) Frame analysed by Lui and Chen (ref. 9-8)

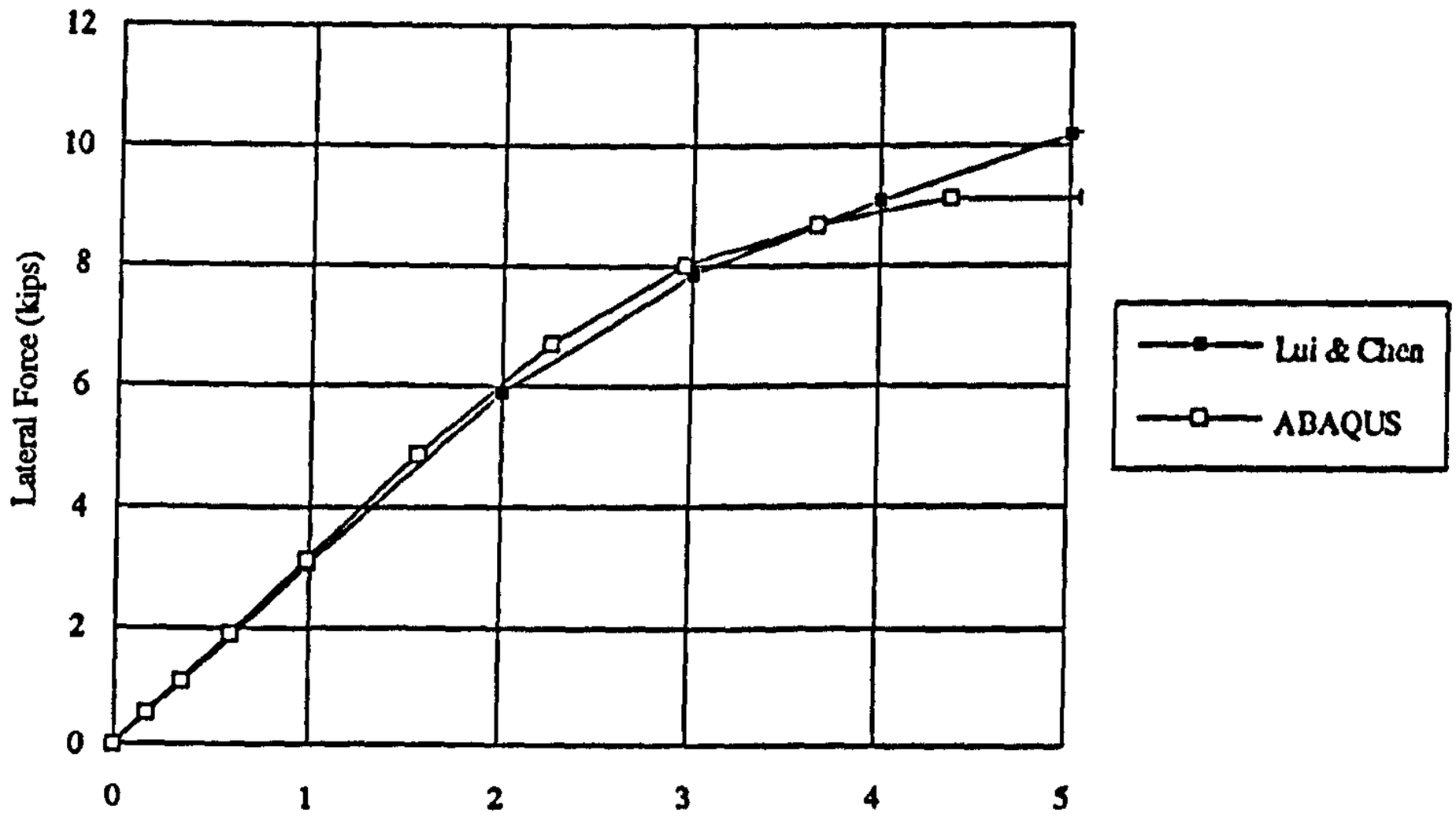

Figure 9-16(b) Comparison of load-deflection behaviour of sway frame (ref. 9-8)

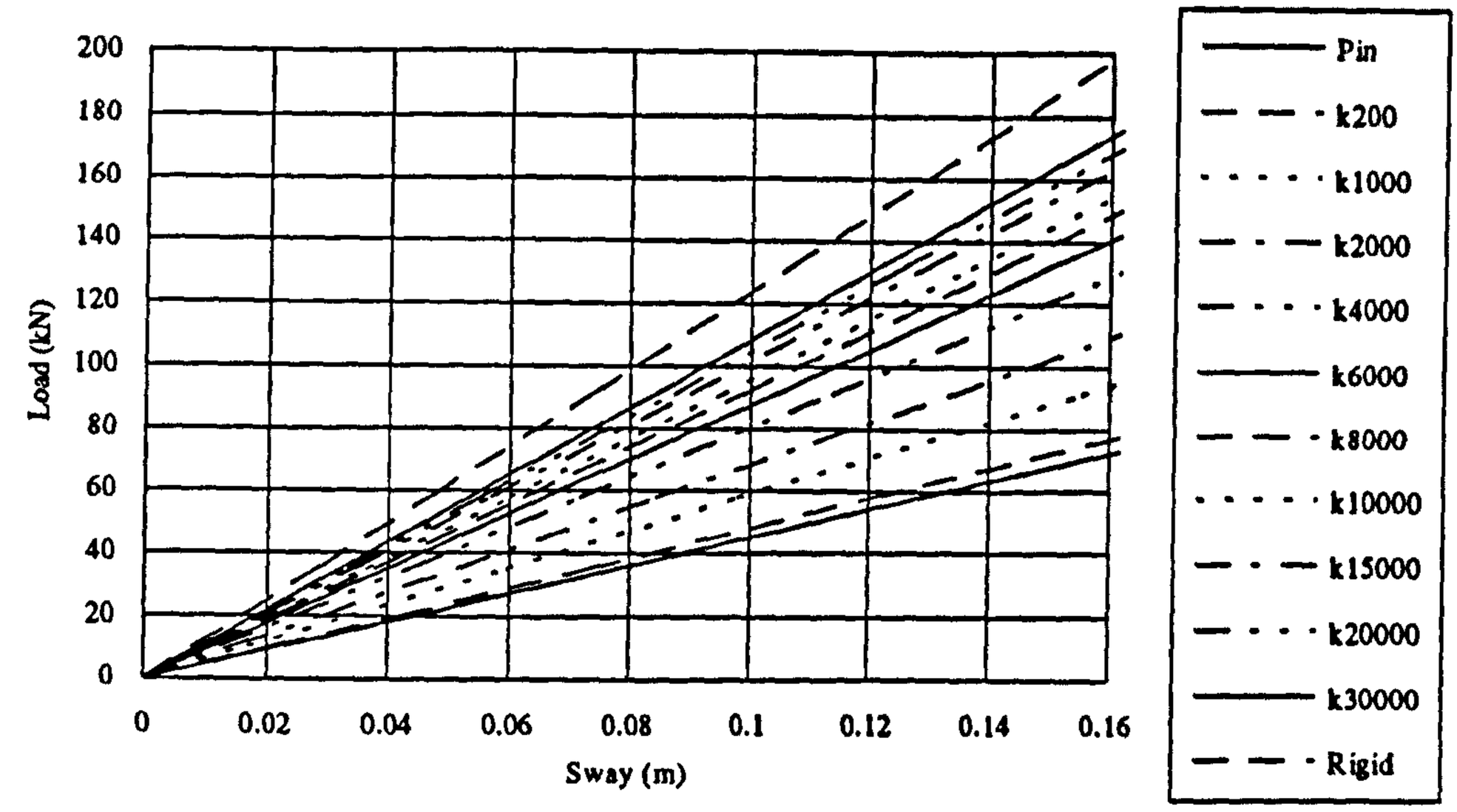

Figure 9-17 Load-displacement relation in analysis set-1

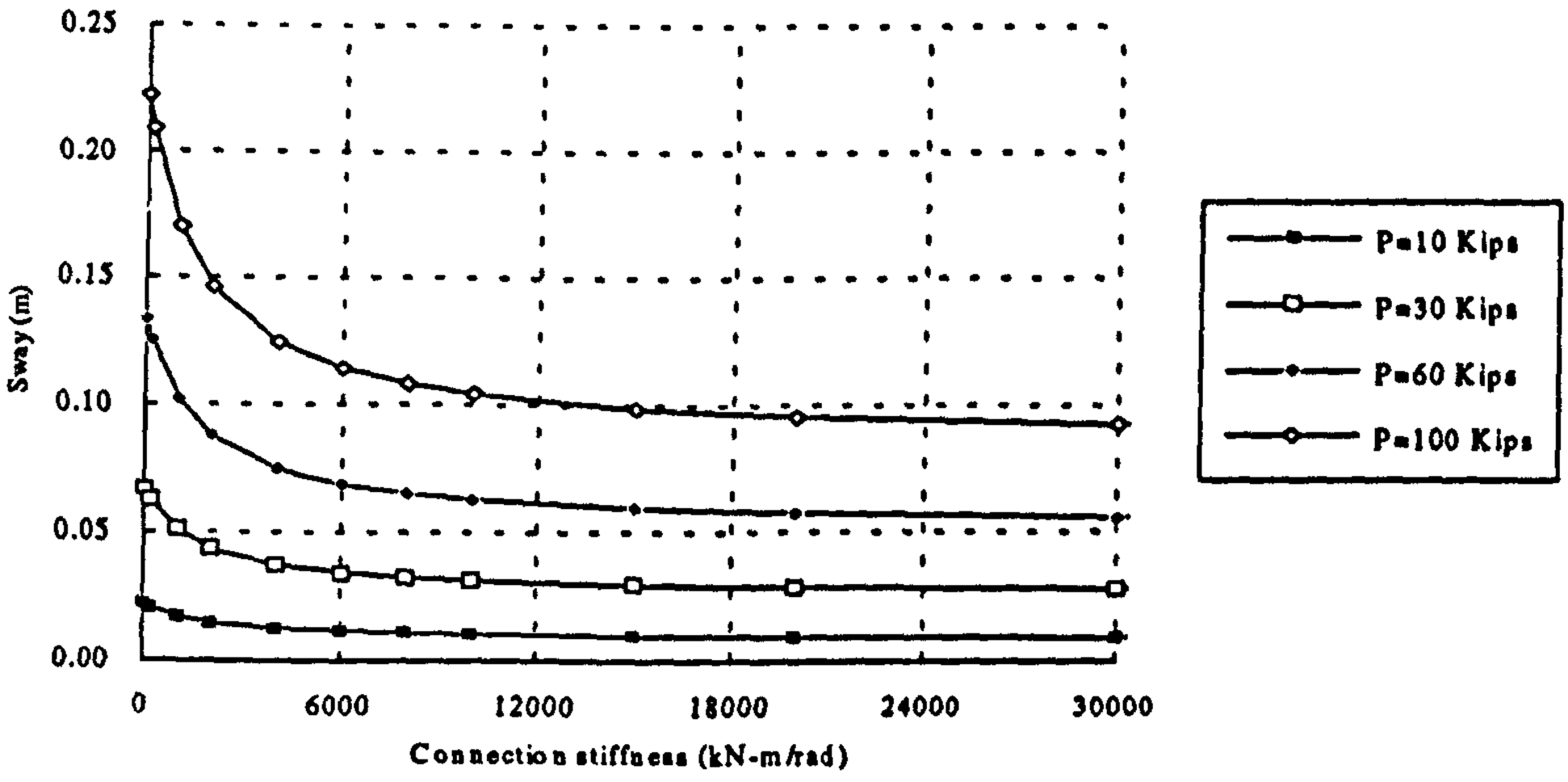

Figure 9-18 Variation of sway and connection stiffness with different loading

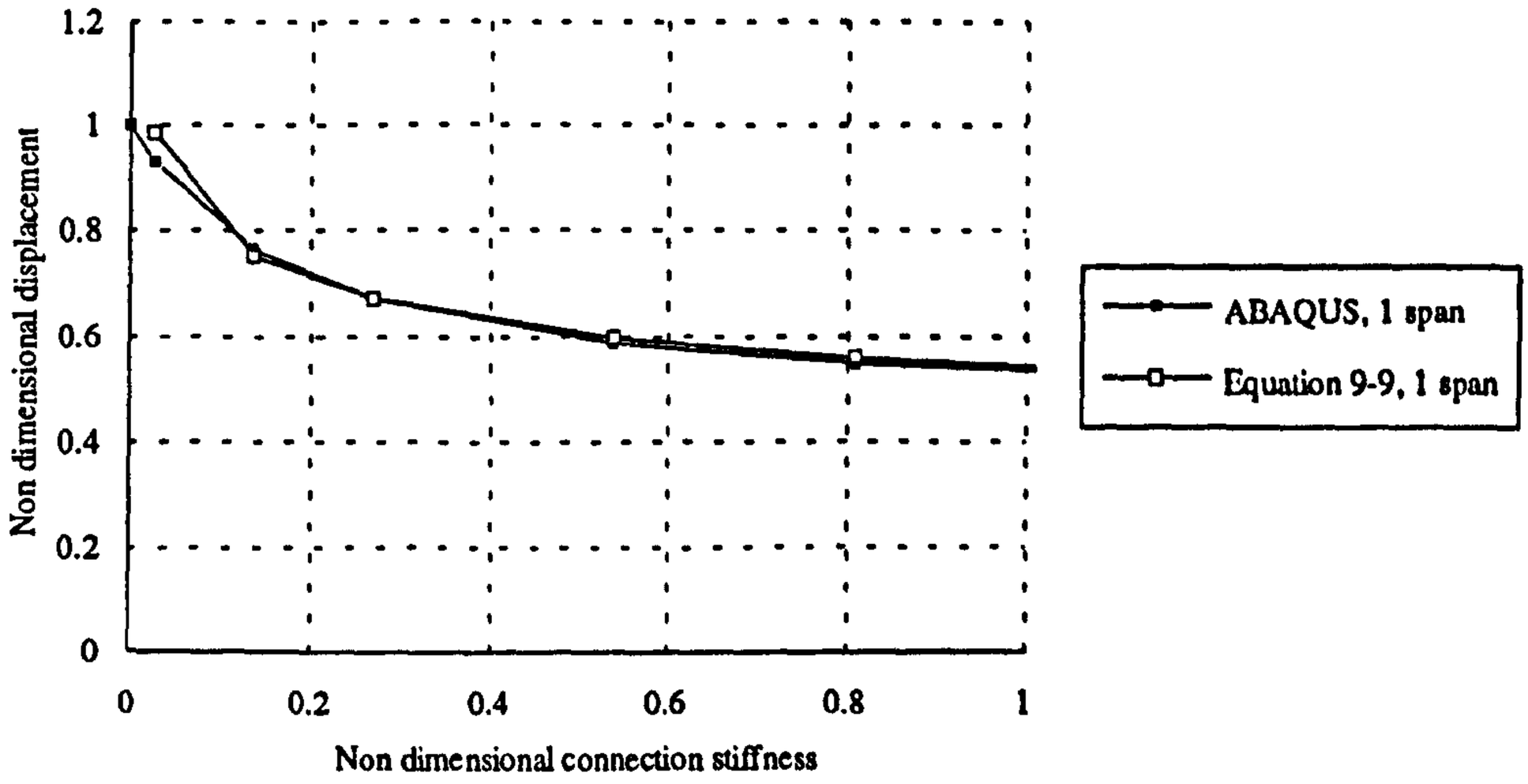

Figure 9-19 Comparison of non dimensional displacement and non dimensional connection stiffness from analysis and from equation 9-9

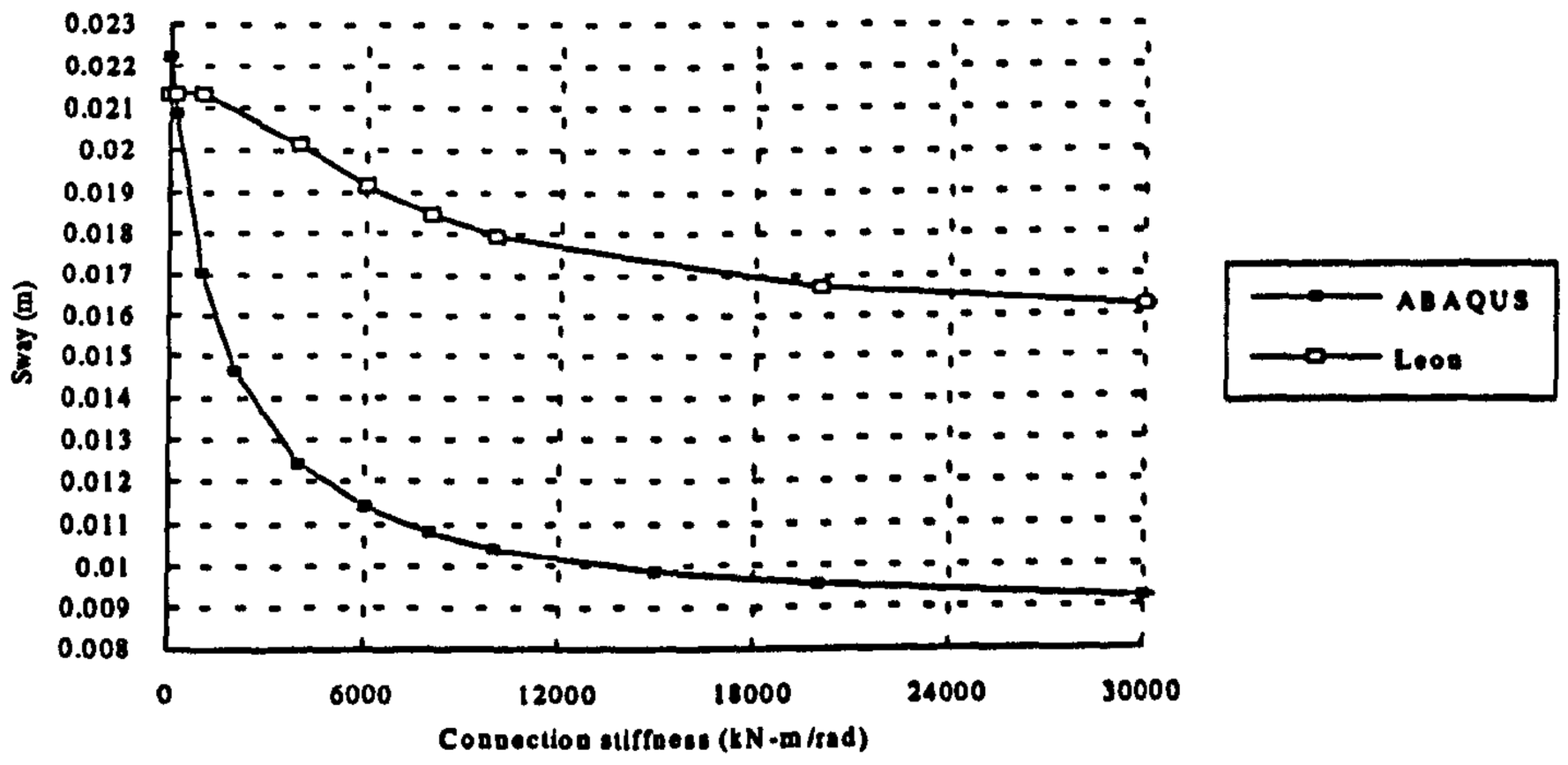

Figure 9-20 Comparison of results from FE analysis and Leon equation

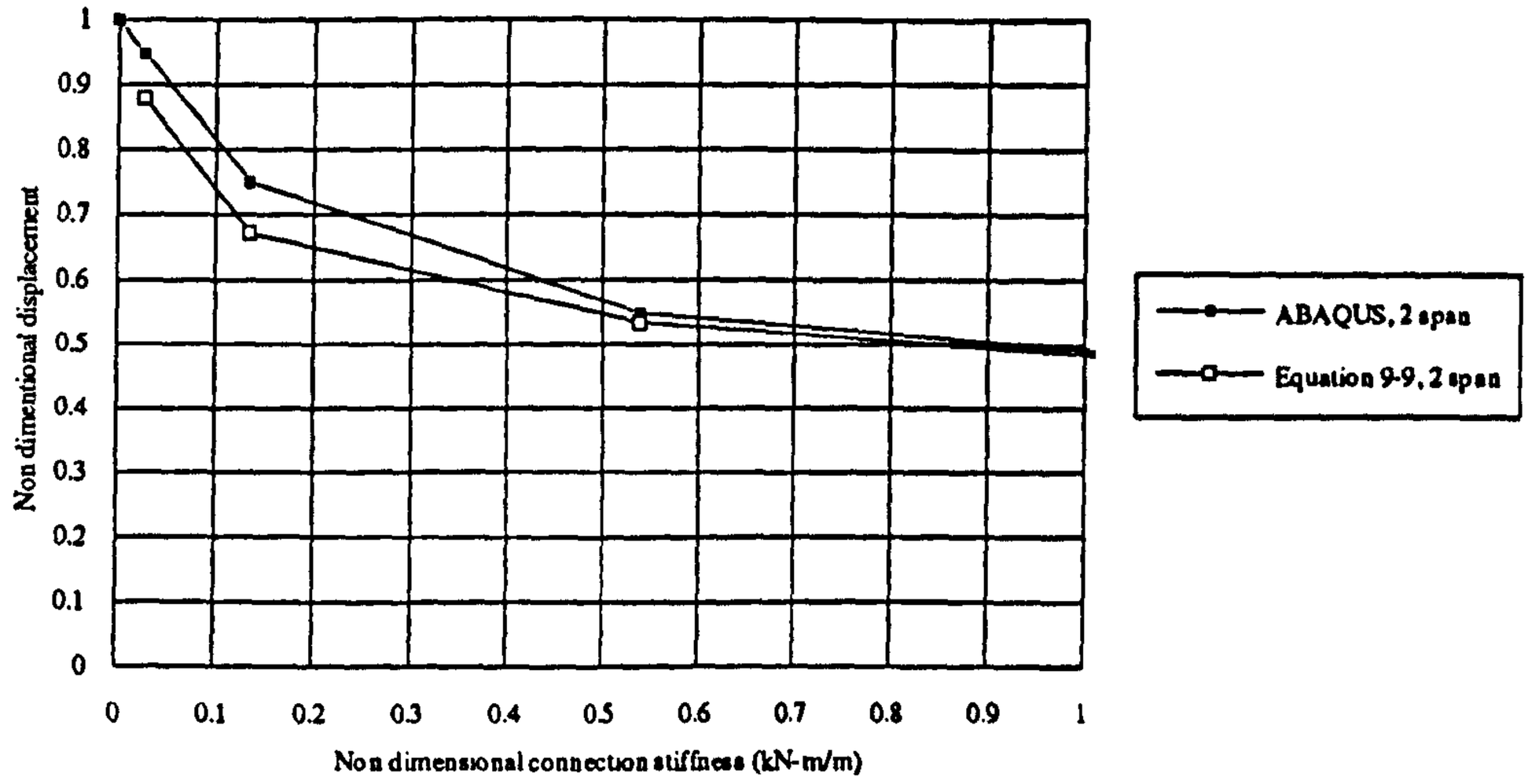

Figure 9-21 Comparison of results between equation 9-9 and FE analyses for single story single bay frame

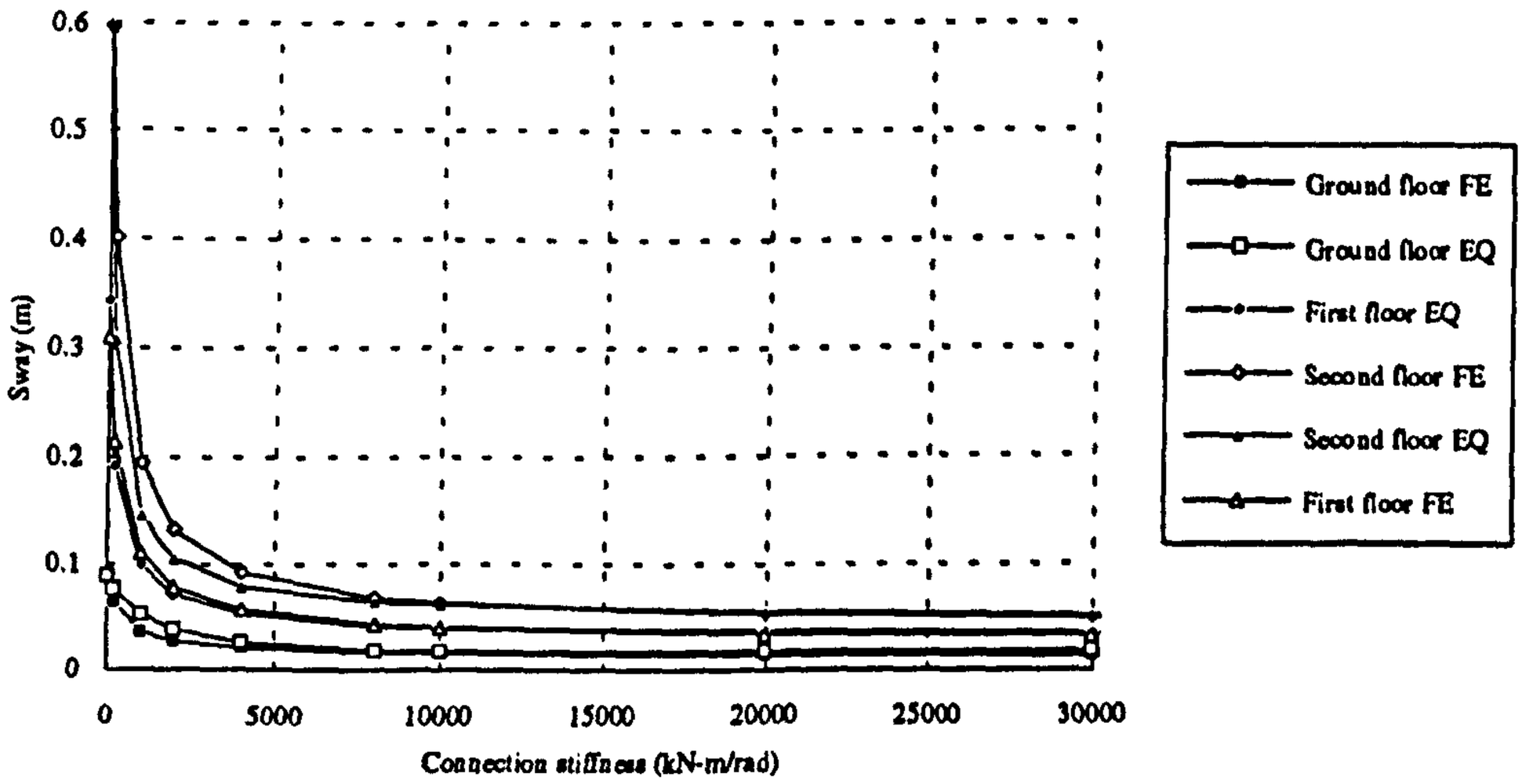

Figure 9-22 Comparison of sway from equations (9-14 and 9-15) and FE analysis for a single bay three storied frame

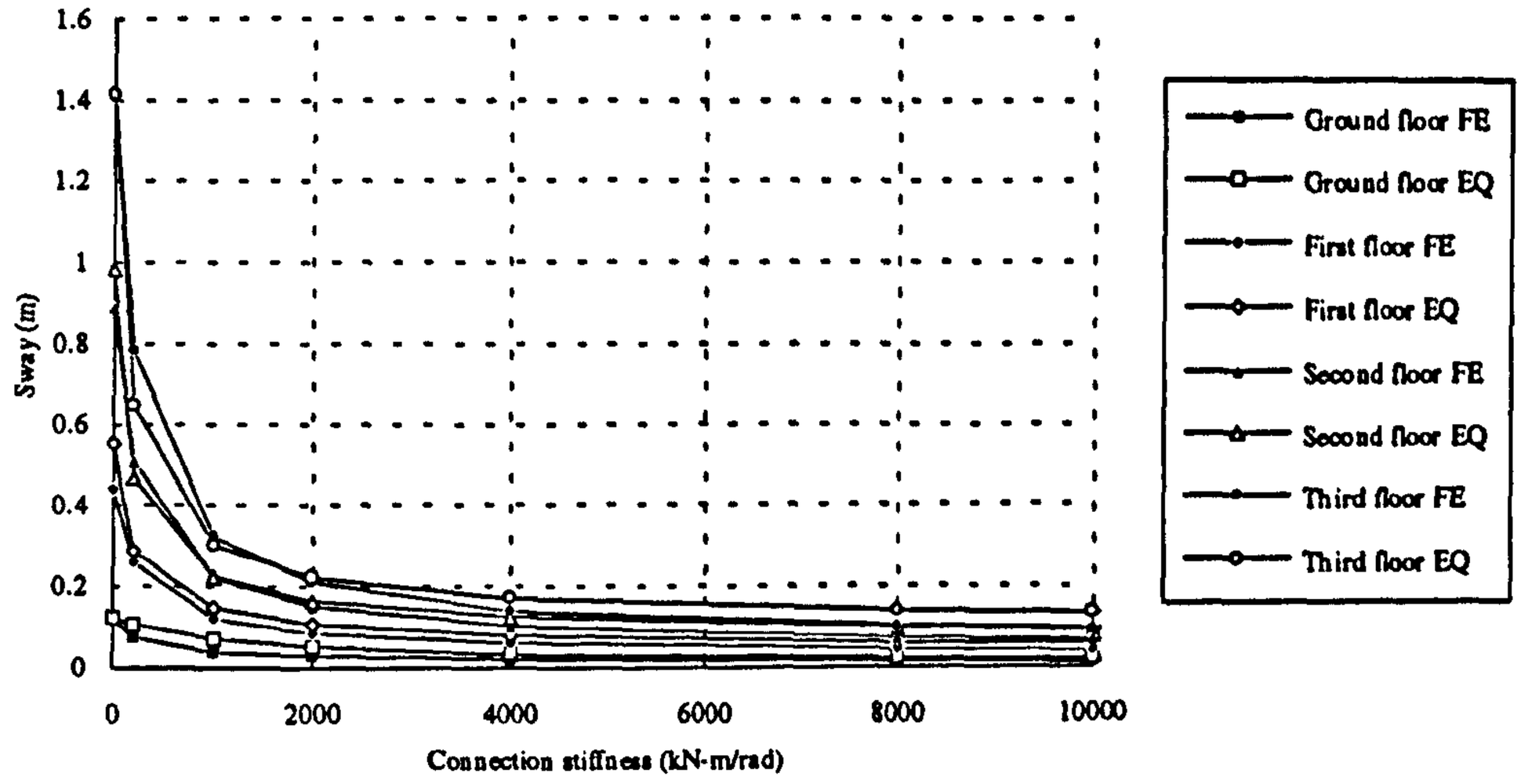

Figure 9-23 Comparison of sway from equations and FE analysis for a single bay four storied frame

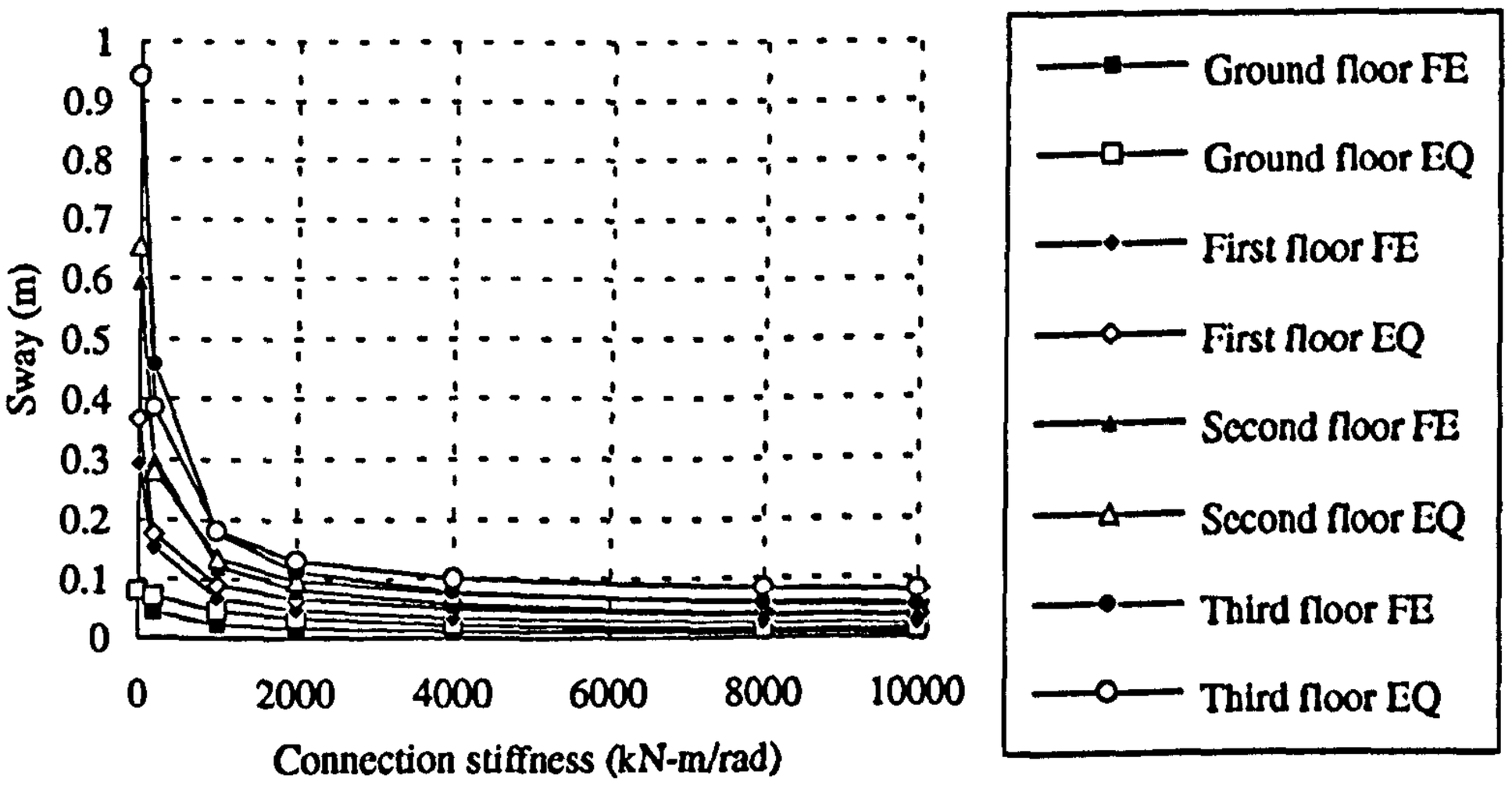

Figure 9-24 Comparison of sway from equations and FE analysis for a two bay four storied frame

Chapter 10

Conclusions and recommendations

10.1 Introduction

The thesis deals with the development of numerical models for composite connection and composite frame behaviour. The final models have been fully checked by means of verification against test results. The verified model has provided an opportunity to examine several detailed aspects of behaviour that have then formed the basis for the development of design procedures for composite connections. This chapter summarises the main findings of the study and identifies the future scope for research in this area.

10.2 Conclusions

(i) A numerical model has been developed which can represent the full structural response of several different types of composite connections. Before developing the composite connection model, important components were modelled separately and the modelling verified separately. Test measurements of response for both local and overall behaviour of composite connections were used to verify the model. It was observed that among the various different types of connections the endplate connection is the easiest to model as it does not exhibit bolt slip. The development of composite connection models are presented in chapter 3 and the preliminary modelling of various components in chapter 2. Results of parametric studies using the model described in chapter 3 are presented in chapter 4.

(ii) The results that are available from tests designed to investigate the effect of the shear to moment ratio were found to exhibit somewhat contradictory trends. Both theoretical and numerical analyses have been conducted to predict the effect of changes in the shear to moment ratio on composite connection moment capacity. Equations have been developed that incorporate these variations. A design method for cruciform flush endplate connections has been developed that relates the shear span directly with the connection moment capacity. The detailed results are presented in chapter 5.

(iii) At present no tests are reported that investigate the effect of column axial loading on composite connection moment capacity. The design equations for column web compression strength of EC3 are based on a few (bare steel) tests. It is doubted that these tests actually reflected the effect of column axial loading on the buckling resistance of the column web - not on the compression resistance of the column web. Also the column web shear strength is assumed to be constant irrespective of the level of column axial load. Both theoretical and numerical analyses have been conducted to study the effect of varying levels of column axial loading on composite connection moment capacity. It has been found that the present equation for column web compression resistance is too conservative, the equation for column web shear strength is unsafe, and that final bolt forces should be calculated from the equilibrium of the joint at the interface of the beam and the column - instead of directly using the values from equations to compute the moment capacity. New equations have been developed to predict the effect of the column loading on column web compression strength, column web shear strength and bolt force; these can be used to replace the existing EC3 equations. A design method has been developed to consider the effect of column loading on the composite flush endplate connection moment capacity. The detailed results are presented in chapter 6.

(iv) A unified design method has been developed which can consider the effect of shear to moment ratio and column axial loading for both symmetrical and non-symmetrically loaded connection. Care has been taken to include all possible modes of failure that can occur in a composite connection. The method utilises plastic theory and a simplified stress block approach, based on evidence from the numerical studies. The method is capable of determining the failure modes very accurately. It was observed that out of the 32 major axis flush endplate connections tested the proposed method predicted the correct failure mode for 27 cases. Predictions from the proposed method have been compared with a total of 53 test and finite element results. These comparisons gave an overall prediction to test ratio of 0.99 with a standard deviation of 0.14, thereby demonstrating that the proposed method can accurately predict the resistance of composite flush endplate connections under a variety of different connection arrangements and loading conditions. Detailed results are presented in chapter 7. The method is suitable as a design procedure for flush endplate connections in EC4, where, at present, there is no design procedure for connections.

(v) On the basis of the theoretical studies a method has been developed to estimate the initial stiffness of composite endplate connections. Comparison with 28 major axis flush endplate test results gave an average of 0.99 with a standard deviation of 0.21 for the proposed method. At the same time a method to predict the available connection rotation capacity has been developed that is fully compatible with the prediction method for moment capacity. Care has been taken to include the effect of the extension of the rebar and the bolts and the shear stud slip. Also, the method allows for the effect of the depth of beam web in compression during the calculation of available rotation capacity. Both methods are described in chapter 7. These two methods have been combined with the moment capacity calculation method of flush endplate composite connections to predict the overall behaviour of the connections that has also been described in chapter 7. They are

suitable for inclusion in EC4 for the computation of initial stiffness and available rotation capacity of composite connections.

(vi) Following an approach similar to that used for flush endplate connections, design procedures have been developed for composite finplate and angle cleated connections. Results are compared for 6 finplate connection tests which gave an average of 1.06 with a standard deviation of 0.18. The comparison for 16 tests on angle cleated connections gave an average of 0.98 with a standard deviation of 0.13. These have been described in detail in chapter 8 and are also suitable for inclusion in structural design codes e.g., EC4.

(vii) A numerical model has been developed for composite non-sway frames that can accurately represent behaviour observed in actual frame tests. It has been found that it is possible to model the response in terms of the frame moment distribution, connection moment rotation and the beam load displacement history very accurately. This provides an economic tool to study different aspects of the behaviour of composite non-sway frames. The frame model has been described in chapter 9.

(viii) A numerical model has been developed for unbraced bare steel frames. This model was verified against numerical results obtained by other researchers. Using this model some studies have been performed that provide basic guidance for developing equations for estimating sway. This is also reported in chapter 9.

10.3 Recommendations

Arising from the work reported herein, a number of areas for further study have been identified:

(i) There is a need for further theoretical and numerical work on the available rotation capacity of connections. In the proposed model some aspects of behaviour have been approximated. For example, the stiffness of the bolts and the length of reinforcement that is to be taken into consideration. Also, the exact way in which the extension of the rebar is to be calculated i.e., on the basis of an effective length only or by taking account of its stiffness if the rebar is not found to yield when predicting moment capacity. For medium and low levels of reinforcement the rebar is usually found to yield. Test results show the range of reinforcement strain to be 3000με to 15,000με, these will vary according to type of reinforcement (e.g., mesh or bar) and also on their diameter and spacing. This indicates that the selection of yield strain can change the rotation capacity by more than 100%. For connections with high levels of reinforcement ratio the rebar usually does not yield; for this situation it may be more appropriate to calculate the extension from force and rebar stiffness.

(ii) To experimentally investigate the moment-rotation behaviour of different types of connections when the connection is loaded in an upward direction. This will provide the data required to verify or modify the connection model with upward beam loading. These are needed to construct a complete moment rotation curve that can than be used for the composite sway frame numerical model development. Once this has been done the model can be utilised to study frame moment distribution, connection required and available rotation capacities, serviceability deflection with changes to load and member sizes. The findings can be utilised to develop a comprehensive design procedure for composite frames.

(iii) There is a further need for theoretical and numerical work on sway of steel frames which can then be extended for composite frames. It is essential to explore the sway behaviour of the composite frames experimentally. The results can be used to verify the developed numerical model for composite frames for the sway mode as described above.

(iv) The traditional approach of frame analysis assumes that the contraflexure point is located at a certain distance from the beam to column connection. Once a validated numerical model for the composite frame in the sway mode is developed the model can be used to numerically investigate the effect of horizontal load on the location of contraflexure points. Results from the numerical study can form the basis of design procedures for composite sway frames.